Fragment synthesis: pharmacophore and diversity-oriented approaches

Andrew James Peter North

Gonville and Caius College

University of Cambridge

This dissertation is submitted for the degree of Doctor of Philosophy

Department of Chemistry

September 2018

Abstract

Fragment synthesis: pharmacophore and diversity-oriented approaches

By Andrew James Peter North

This thesis explores two approaches to fragment-based drug discovery. First, protein target CK2 was chosen due to its importance in the cancer phenotype. A literature fragment, NMR154L, proved to be a promising compound for fragment development, due to its binding at the interface site of the protein rather than the highly conserved ATP pocket. Analogues were synthesised of this fragment leading to a candidate with a better IC_{50}. Additionally, computer modelling of the interface site suggested that a series of spirocyclic compounds would inhibit this protein. These were synthesised and tested *in vitro*. Results from these tests were analysed and informed the synthesis of new inhibitors with the aid of crystal structures and computer modelling.

Secondly, to address the lack of spirocyclic scaffolds in fragment screening libraries a number of diversity-orientated synthetic campaigns were undertaken. The first of these utilised glycine as starting material. Two terminal alkenes were installed. The alkenes were linked and the amino and acidic residues cyclised. This allowed for the formation of a diverse range of spirocyclic scaffolds from this one starting material.

Having established chemistry for linking amino and acidic residues a campaign with dehydroalanine was under taken. This would allow for the installation of the second ring by pericyclic chemistry as well as using chemistry previously established.

This pericyclic chemistry was also applied to synthesising spirocycles from rings with exocyclic double bonds. These being readily installed from Wittig chemistry, this allowed utilisation of starting materials which contained a cyclic ketone. Of these azetidinone was a good candidate due to the fact it was a commercially available building block and allowed access to spirocycles containing a 4-membered ring; an underrepresented ring size.

Finally, computation analysis was carried out on the library to assess it diversity and any potential biological targets which these fragments may inhibit.

For Cordelia

Declaration of Authorship

This dissertation is the result of my own work and includes nothing which is the outcome of work done in collaboration except as declared in the Preface and specified in the text.

It is not substantially the same as any that I have submitted, or, is being concurrently submitted for a degree or diploma or other qualification at the University of Cambridge or any other University or similar institution except as declared in the Preface and specified in the text. I further state that no substantial part of my dissertation has already been submitted, or, is being concurrently submitted for any such degree, diploma or other qualification at the University of Cambridge or any other University or similar institution except as declared in the Preface and specified in the text.

It does not exceed the prescribed word limit for the Physics and Chemistry Degree Committee.

Andrew North
Gonville and Caius College

Acknowledgements

Firstly, I would like to express my gratitude to Prof. David Spring for his guidance and for providing me with the opportunity to perform research in his group. It has been a fascinating and eye-opening experience and I have learnt a lot from Prof. Spring and his group. In addition, I would also like to thank the Engineering and Physical Sciences Research Council for funding this work.

I would also like to thank all members of Lab 226 for their help, support, and making the laboratory such an enjoyable place. A special mention has to go to Dr Hannah Sore who has given me help during my laboratory work and research and Dr Paul Brear in the Department of Biochemistry for running all the biological experiments on the compounds produced.

I am very grateful to all the support staff in the Department of Chemistry for enabling me to carry out my research especially the second-floor technicians, Gary Herrington and Kevin Judd, the NMR service team, the mass spectroscopy service team, and the X-ray crystallography service team.

Thank you also to my proof-readers for all their help and comments in constructing this thesis: Hannah Stewart, Dr Naomi Robertson, Dr Tommy Osberger, my wife Cordelia, and my parents.

I would like to thank my parents whose continuous help, encouragement, and support has always been forthcoming and without which I wouldn't be here today.

Finally, I would like to thank my wonderful wife Cordelia North who has been there for me throughout the whole process and has offered much need support. It is to her I dedicate this thesis.

Contents

List of Figures

List of Tables

List of Schemes

Abbreviations

%v/v	per cent by volume
{^{1}H}	NMR spectrum acquired with proton decoupling
°C	degree(s) Celsius
ΔG	change in Gibbs free energy
ΔH	change in enthalpy
ΔS	change in entropy
2D	two-dimensional
3D	three-dimensional
Å	ångström(s), 10^{-10} m
Ac	acetyl
ADME	absorption, distribution, metabolism, and excretion
anh.	anhydrous
aq.	aqueous
ATP	adenosine triphosphate
B	magnetic field
Bn	benzyl
Boc	*tert*-butyl oxycarbonyl
b.p.	boiling point
br. s	broad singlet

Bu	butyl
Bz	benzoyl
CC	chiral centres
CK2	casein kinase 2
clogP	calculated log of the partition coefficient
cm^{-1}	wavenumber(s), inverse centimetre(s)
dd	double doublet
d	doublet
DOS	diversity-oriented synthesis
dr	diastereomeric ratio
ESI	electrospray ionisation
FBDD	fragment-based drug discovery
FP	fluorescence polarisation
Fsp^3	fraction of the C sp^3 centres
g	gram(s)
GSK	GlaxoSmithKline
h	hour(s)
HBA	hydrogen bond acceptor
HBD	hydrogen bond donor
HOMO	highest occupied molecular orbital
HTS	high-throughput screening

Hz	hertz, s^{-1}
I	moment of inertia
IC_{50}	half maximal inhibitory concentration
IR	infrared spectroscopy
ITC	Isothermal titration calorimetry
K_d	dissociation constant
K_i	inhibition constant
LDA	lithium diisopropylamide
LHMDS	lithium bis(trimethylsilyl)amide
LUMO	lowest unoccupied molecular orbital
m	metre(s)
M	molarity, mol dm^{-3}
m.p.	melting point
m/z	mass-to-charge ratio
Me	methyl
min	minute(s)
mL	millilitre(s)
MOE	molecular operating environment
mol	mole(s)
mol%	mole per cent
MW	molecular weight

n	primary, unbranched alkyl chain
NMR	nuclear magnetic resonance spectroscopy
N.R.	no reaction
o/n	overnight
PCA	principle component analysis
pet.	petroleum (ether)
Pg	protecting group
PMB	*para*-methoxy benzyl
PMI	principle moment of inertia
PPI	protein-protein interaction
ppm	parts per million
PSA	polar surface area
q	quartet
quin	quintet
RBC	rotatable bond count
RCM	ring-closing metathesis
RO3	rule of three
RO5	rule of five
RT	room temperature
SAR	structure-activity relationship
sat.	saturated

SB	SmithKline Beecham
s	second(s)
	singlet
t	tertiary alkyl group, *tert*-alkyl
t	triplet
T	temperature
TBDD	target-based drug discovery
TEA	triethyl amine
TGI	tumour growth inhibition
THF	tetrahydrofuran
TLC	thin-layer chromatography
TMS	trimethylsilyl, Me_3Si-
	tetramethylsilane, Me_4Si
UV	ultraviolet
δ	NMR chemical shift
λ	wavelength
$\tilde{\nu}$	wavenumber, $1/\lambda$

Chapter 1

Introduction

1.1. Drug Discovery

1.1.1. The drug discovery pipeline

Of marketable products, pharmaceuticals are one of the most expensive to produce, time consuming to make, and heavily regulated. There is a huge burden on the drug discovery process to ensure that the drugs which are brought to market are safe and effective.[1] To this end, the drug discovery process is broken down into multiple stages: a pre-clinical stage, which sees the creation of biological agents (small molecules, proteins, antibodies, etc.) to affect a medical condition, and a clinical stage where these agents are tested in man to assess their safety and efficacy (Figure 1.1).

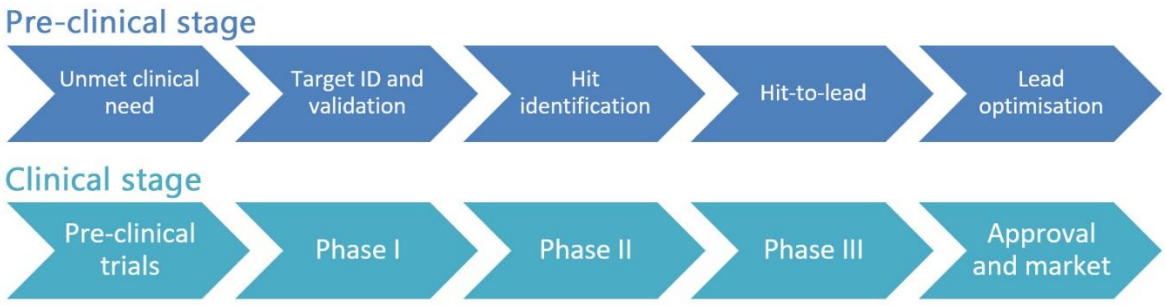

Figure 1.1 A graphic representing the drug discovery process separating out both the pre-clinical and clinical stages of the process.

Pre-clinical stage:

Unmet need: The identification of a disease for which there is little or no treatment or it is believed the treatment could be improved.

Target identification and validation: Research is carried out to identify which macromolecules are involved in a particular disease process such that their modulation will cause the desired therapeutic response. For validation, different strategies involving a wide variety of areas can be applied such as genetics, cellular or *in vivo* and *in vitro* modelling.[2]

Hit identification: A range of compound screening assays are used to identify compounds with the desired activity. This can cover a wide range of techniques from the modification of natural products with known biological effects, to screening of compound libraries to discover novel biological antagonists (this usually takes the form of high throughput screening or fragment-based drug discover, discussed later on in this introduction).

Hit development and lead optimisation: Intensive Structure-Activity Relationship (SAR) studies are conducted around each core structure. Potency and selectivity are assessed as well as detailed profiling of physico-chemical and *in vitro* absorption, distribution, metabolism, and excretion (ADME) properties.[3]

Clinical stage:

Pre-clinical trials: The clinical candidate is first tested in animals to collect information pertinent to the safety of the compound. The species chosen will have the most similar traits to humans in the part of the body which the drug is affecting.

Phase I, II & III: During these stages, the clinical candidate is tested in humans, with testing split into three phases. Phase I is the 'first-in-man' study. Usually, healthy volunteers are given the compound in increasing doses to assess the appropriate dose-range before adverse side-effects are seen. Phase II is the first time the compound is tested in humans with the disease, and as such provides the first proof-of-concept, demonstrating whether the desired clinical outcome has been achieved, whilst also continuing to monitor safety and side effects. Phase III tests the drug therapeutic effect on a larger cohort of patients over a significantly longer time frame, often years.[4]

Drug approval: The gathered data is presented to a country's licencing authority which determines whether the compound can be marketed and sold as a drug for the treatment of a specified illness.

Market: This time is also known as Phase IV as the long-term health impacts of the drug are continually monitored and assessed. A drug can be withdrawn from the market by the licencing authority if there are questions about its safety.

This process is protracted and costly. From a compound being identified as a potential therapeutic for a disease (hit identification in Figure 1.1) to a marketable drug, 10–15 years usually elapse.[5] Additionally, while it is difficult to provide a reliable estimate of the costs due

to differences in accounting practices and industry confidentiality,[6] recent research has put the cost of bringing a drug through the discovery pipeline at $1.4 billion.[7]

This astronomical figure can be mostly ascribed to the expense of carrying out Phase I, II, and III clinical trials.[8,9] The clinical phase alone can cost researchers in excess of $100 million.[5] Failed drugs also contribute to the large cost of drug discovery, with no possibility of recouping the cost of development upon failure.[10] Studies have suggested that fewer than one in five drugs progress from Phase II to Phase III, and those in Phase III only have a 50% probability of making it to the market.[11–13] Reasons for these failures are mostly attributed to the lack of safety and lack of efficacy of clinical candidates. About a third of drugs fail at Phase I for lack of safety and Phase II and III failure rates are 42% and 54% respectively for lack of efficacy.[14]

Therefore, there is a huge pressure on licensed and marketed pharmaceuticals to recoup the development costs of both successful and failed drugs. This is difficult for several reasons. The purchasers of the drugs, in most cases national governments, insurance companies, and clinics, have scarce resources.[15] On top of this is the limited life span of patents which give the producer a monopoly on the exploitation of their invention. To prohibit competitors from operating in the same areas, most compounds are patented early in the drug discovery pipeline (usually around the 'hit-to-lead' stage). However, given the life span of a patent is typically 20 years,[16] this limits the length of time for which the patent remains in place once the compound reaches the market. This significantly diminishes the time the producer has to recoup the approximately $1 billion expenditure from the drug's development. Once the patent expires, generic pharmaceutical companies can produce the same compound at a fraction of the price as they do not have to cover the large research and development costs.

Consequently, pharmaceutical companies, and researchers more generally, are searching for ways to cut down on the time and money in drug development.

1.1.2. Attrition rates and new chemical entities

The high attrition rates in the drug discovery process are an obvious place for researchers to look for a way to cut costs. If the compounds entering the clinic are more likely to succeed, costly and unsuccessful clinical trials can be avoided.

Despite advances in research methods and technology,[17] attrition rates across drug discovery have remained high,[11–14,18] and as a result, research has been carried out looking to link chemical properties with the success (or otherwise) of potential lead compounds in the clinic.

One of the first and most famous of these studies was by Lipinski *et al.* who performed a detailed study into the physico-chemical properties of orally bioavailable drugs. Their research found that:

> [P]oor absorption or permeation are more likely when: There are more than 5 H-bond donors (expressed as the sum of OHs and NHs); The MWT is over 500; The Log P is over 5 (or MLogP is over 4.15); There are more than 10 H-bond acceptors (expressed as the sum of Ns and Os) Compound classes that are substrates for biological transporters are exceptions to the rule.[19]

This was the first statement of Lipinski's 'Rule of Five' (RO5), and it has since developed as a ubiquitous rule-of-thumb in drug development and discovery.[20] Additionally, others have added to the list of physico-chemical properties which should be considered when assessing the likely oral bioavailability of a compound.

The number of rotatable bonds and the polar surface area (the surface area of all the polar atoms) were found to also be strong indicators of the oral bioavailability in rats. A rotatable bond count of less than 10 and a polar surface area of less than 140 $Å^2$ were more reliable than the molecular weight cut-off of 500 $gmol^{-1}$ as a predictor of this property.[21] Consequently, these two metrics have been added to the list of properties considered within the Rule of Five (Table 1.1).[22]

Table 1.1 Lipinski's Rule of Five.

Property	Rule of Five
Molecular Weight ($gmol^{-1}$)	< 500
clogP	≤ 5
Polar Surface Area ($Å^2$)	≤ 140
H-Bond Acceptors	≤ 10
H-Bond Donors	≤ 5
Rotatable Bond Count	≤ 10

The advantage of physico-chemical descriptors as a metric for assessing the likely attrition of a compound is that they are easily measurable before synthesis of the compound has even taken place. Thus, chemists can plan and direct their effort to maximise the chance of compounds succeeding in the clinic. In addition, physico-chemical properties are easy to analyse *en masse* from drugs and failed clinical candidates to produce helpful predictive data.

Analysis of compounds at Pfizer found that compounds with a clogP < 3 and a PSA >75 $Å^2$ were 2.5 times less likely to be toxic at 10 μM.[23] This is known as the '3/75 rule'. An additional Pfizer study has suggested that a compound with a predicted human efficacious total plasma concentration of < 250 nM was more likely to pass toxicology screening.[24]

One interesting result from meta-analysis of attrition in four major pharmaceutical companies is that molecules with a high fraction of sp^3 (Fsp^3) atoms are more likely to become marketed drugs.[25,26] This tallies with a corresponding decrease in the aromatic ring count also giving a compound greater success in making it to market.[27]

Indeed, one failing of the Rule of Five is that, although it adequately acknowledges the physico-chemical characteristics of a molecule, it makes no reference to its spatial qualities. In this way a set of compounds can obey the RO5 with a diverse set of data, but all have a very similar shape. Thus, the chance that they are going to probe a large area of chemical space is small. Research by Lovering *et al.* agrees with the above observation. They showed there was a statistically significant increase in the Fsp^3 from lead candidates entering the clinic to the marketed drug coming out (0.36 to 0.47). In addition, the number of compounds with stereocentres increased from 53% entering the clinic to 64% coming out. They hypothesise that these 3D molecules are more adapted to the inherently 3D shape of biological targets as well as conveying beneficial physical properties like increased solubility and decreased melting point, which have been shown to aid oral bioavailability.[25,28,29]

Physico-chemical descriptors are only one factor which determines a drug's success in the clinic. In fact, the early drug discovery process is similarly afflicted with challenges.

1.2. Established Methods of Drug Discovery

1.2.1. High Throughput Screening

One of the most common and powerful methods in drug discovery has been High Throughput Screening (HTS).[30–32] This method aimed to combine the vast improvement in biological assay technologies over the past 20 years[33,34] with expansive compound libraries

accrued by the pharmaceutical industry. Robots were designed and programmed to conduct millions of experiments between these libraries and biological assays in microplates of thousands of wells. The results could be quickly analysed by heat maps of the wells (Figure 1.2). The compounds which showed promise were modified in a combinatorial-type approach to improve their properties and selectivity. When these were believed to be optimal, they would progress to clinical trials.

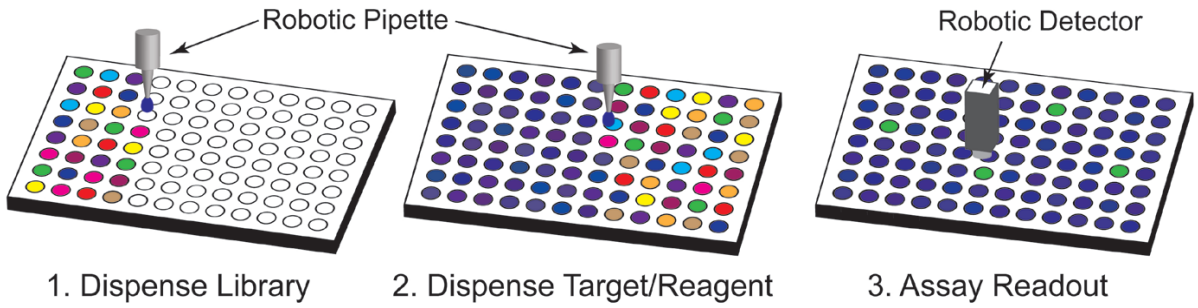

Figure 1.2 Diagram depicting an HTS method of testing a compound library against a target and assessing the outcome of the experiment. (Figure ref 35)

The driving force for industry to investigate HTS was the 'brute force' and 'enhanced serendipity' of this method. Many targets have unknown structures or ligands making a 'rational' design difficult. However, the chances that at least one molecule of the millions tested would bind to a given target was presumed reasonably high. Thus pharmaceutical companies could put their compound collection to new uses by seeing if the chemicals would bind to targets that would not have been predicted.[31]

This technique has not been unsuccessful. In the period 1991–2008, of 58 drugs for which the starting compound was known, 19 owe their existence to an HTS campaign (e.g. Figure 1.3).[30,36]

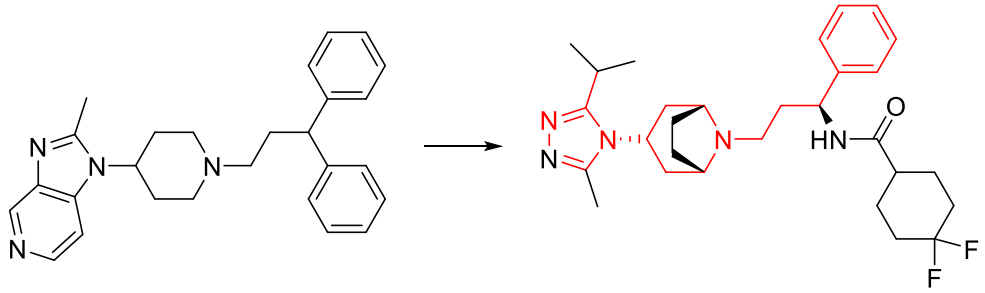

1, UK-107,543 **2, Maraviroc**

Figure 1.3 Example of a hit from HTS, UK-107,543, leading to a marketed drug, Maraviroc, used in the treatment of HIV. The red scaffold in Maraviroc shows the features maintained from the initial HTS hit.[37]

However, HTS has faced criticism for its failure to produce more drugs from such an unprecedented number of experiments.[30,31,38,39] This has been put down to weakness in the two most important factors of an HTS experiment: the nature of the compound library and the quality of the biological assays used.

Macarron *et al.* attributed the problems with the biological aspect of HTS to 'poorly validated targets,… highly artificial and non-physiological assay systems,…a severe lack of appropriate animal models, [and] unpredictable toxicities.'[30] From a chemistry perspective, libraries consisted mostly of large, impure compounds.[40] Even when the emphasis changed to single, pure-compound screening libraries, a distinct lack chemical diversity hampered the degree of chemical space which was being probed.[30,31]

One of the biggest wake-up calls for the effectiveness of HTS was the GlaxoSmithKline 7-year antibiotic discovery programme. In the face of the growing threat of antibiotic resistance,[41] SmithKline Beecham (SB) and subsequently GlaxoSmithKline (GSK) embarked on a program to test their entire compound collection for novel antibiotic activity. In total, 70 HTS were carried out using over 500,000 compounds. Only 16 hits were identified and of these only 5 became leads. Synthetic modification of these leads failed to generate any compounds to meet the desired criteria. This was incredibly disappointing considering the time and money (>$70 million) spent on the project. Analysis of the program demonstrated that the lack of chemical diversity in the compound collection inhibited the power of the screen, with many of the molecules within the same or similar areas of chemical space.

GSK were not alone in their failure to detect new antimicrobials from HTS. Between 1996 and 2004 more than 125 screens were carried out, none of which resulted in drug candidates.[42] HTS, although a powerful tool in drug discovery, still relies on serendipity and one of the best

ways to increase the chances of success is to screen as diverse a range of compounds as possible. An industry focus on combinatorial synthesis is partly to blame in this regard.[43]

1.2.2. Target-based drug discovery

Another prominent paradigm in drug discovery since the 90s has been target based drug discovery (TBDD).[17,44,45] It was hypothesised that with sufficient information regarding a disease and its mode of action, databases could be searched or drugs could be rationally designed which block its mode of action and therefore treat the disease.[17,46]

Although superficially very rational, several real-world limitations have shown this method to be less successful than first hoped. This treatment of biological systems as simple flowcharts may aid understanding in some respects, however much of the complex reality is missed. Ignoring these secondary effects at an early stage in the drug discovery process can lead to off-target activity further down the line and hence attrition.[45]

Additionally, understanding of underlying biological systems is no guarantee of success or failure in drug discovery. Effective drugs have reached the market with little understanding about their mode of action (e.g. clozapine);[17] for others, understanding has been gained during development (e.g. lyrica).[47] Conversely, despite some understanding of their mode of action, many drugs have failed to reach or pass clinical trials (e.g. beta-amyloid targeting in the treatment for Alzheimer's disease).[17] Overemphasis on this bottom-up approach has not lead to a breakthrough in drug discovery nor a lowering in attrition.[17,45]

1.3. Fragment-based drug discovery

1.3.1. Chemical space

The main challenge facing medicinal chemists is the identification of chemical entities as potential hits and developing those compounds to form the best clinical candidates. This is a vast and non-trivial problem, a contributing factor of which is the extent of chemical space (the total possible number of molecules), which is so large as to be infinite for practical purposes.

Given that medicinal chemists focus on organic 'drug-like' molecules, the size of chemical space can be limited and therefore estimated. Most commonly, medicinally-relevant chemical space is restricted to thirty non-H atoms chosen from the most common elements found in organic chemistry (C, N, O, S) which puts the estimate at 10^{63} molecules.[48]

It is not possible to synthesise even a meaningful percentage of this space to assess their pharmaceutical potential. Therefore, a strategy must be developed to effectively probe those areas of chemical space which are most likely to yield useful drugs.

Chemical space increases exponentially as the number of atoms in the molecule increases; therefore, decreasing the complexity of molecules reduces chemical space to a more manageable size. Computational research into the enumeration of smaller molecules (up to seventeen atoms of C, N, O, S, and halogens) has found the chemical space much more manageable at 166.4 billion molecules.[49]

Therefore, restricting synthesis and screening to smaller molecules allows a greater area of chemical space to be explored more efficiently. These small molecules could be regarded as 'fragments' of drugs which could be combined to form a potent lead 'drug-like' molecule.[50]

1.3.2. What is fragment based drug discovery?

Fragment based drug discovery (FBDD)[a] is a technique used to aid the discovery of potential drugs. It capitalises on restricting screening libraries to fragments (discussed in section 1.3.3) and screening these fragments against biological targets.[51] The result of these screens is both physical measurements of how well the fragment inhibits the protein (usually expressed as the half maximal inhibitory concentration, IC_{50} or dissociation constant, K_d) and crystal structures to assess the structure-activity relationship (SAR).[52] From these results, fragments are modified, grown, and linked to produce a more drug-like molecule (Figure 1.4).[53] These fragment modifications use the best available interactions with the protein as determined by SAR data, and the success of the modifications are measured by falling IC_{50}s.

[a] The term fragment-based lead discovery (FBLD) has also been used for the same process. This is because the output of this process is a lead compound for inhibiting a specific biological target. The final 'drug' being discovered after lengthy optimisation to a pre-clinical candidate, followed by clinical trials.[52] However, because this technique is used primarily as an aid to the discovery of new drugs, the term FBDD is used in this thesis.

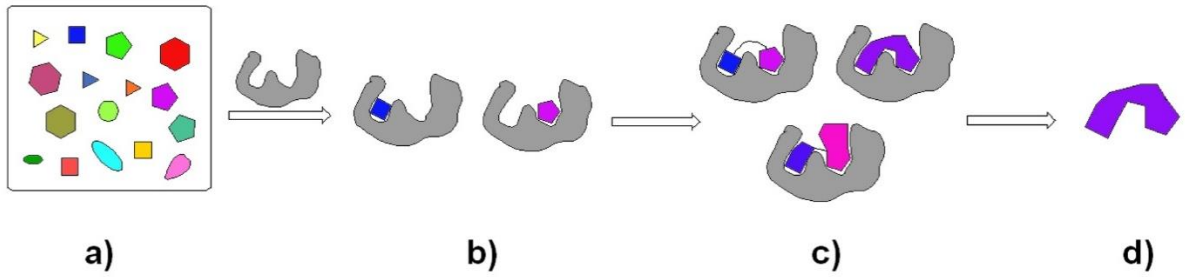

Figure 1.4 A cartoon representation of the fragment-based drug discovery process.a) A library of fragments is screened against a biological target or targets (usually a protein). b) Data is obtained from the screen of those compounds which bind. This includes physical measurement of the K_d and IC_{50}, binding modes and structure-activity relationships. c) Fragments are linked, grown, and merged to create larger molecules which should have superior biological activity and improved substrate specificity. These are then screened against the target. d) A lead compound is found and can be further optimised or taken through to the next stages of the drug discovery process.

As summarised in Figure 1.4, FBDD follows a rational framework. Firstly, a fragment library is assembled or designed (this process will be discussed in more detail in section 1.3.3). This library, typically in the region of 10^2–10^3 molecules, is then screened against a biological target. Unlike HTS, only a weak binding affinity c. 0.1–10 mM would be expected to be observed due to the small size of the fragments; however, they are found to produce better quality hits and fewer false-positive aggregations (organic molecules forming colloids in buffer solution which denature proteins and therefore causes non-specific inhibition).[53,54] A variety of techniques can be employed to assess the nature and quality of any binding found during a screen: NMR spectroscopy[55] and Mass Spectroscopy[56,57] are quick qualitative methods for gaging whether there is binding between a protein and a fragment. Fluorescence Polarisation (FP)[58] assays and Isothermal titration calorimetry (ITC)[59] are employed to gain important quantitative data about how well a fragment binds (usually as an IC_{50} or K_d respectively). Finally, X-ray crystallography gives vital structural information about where on the target the fragment binds and what non-covalent interaction(s) it utilises.[60]

Using the data gained in the screen, the most promising fragment hits are elaborated using structural data obtained from an X-ray structure. Fragment elaboration usually occurs by three methods: linking, growing, and merging. Linking is most often employed when two fragments have bound to a target at two separate sites. These fragments are then linked by a tether to produce a lead-like molecule with enhanced physico-chemical properties. Although this technique has been employed successfully in the past,[61,62] it is the most difficult strategy

within fragment elaboration due to the difficulty in optimising the length and rigidity of the tether and the limited scope for further elaboration.[53,63]

Fragment merging is most readily employed where two or more fragments have been found to occupy the same or proximal space, but structural analysis has found they interrogate different aspects of the target. In this case, structural features of the fragments are merged to give a new lead-like molecule which hopefully utilises all of the previous interactions.[64] This has been employed successfully in several cases of drug discovery.[65–67]

Finally, fragment growing is used to produce leads. This is the most common strategy and is used when only one fragment is found to have bound to a target. Using the crystal structure as a guide the fragment is grown along several vectors to explore additional interactions with the target. This gives rise to an iterative cycle where a number of compounds are screened and the resulting crystal structures used to direct further development and elaboration (Figure 1.5).[53,68,69]

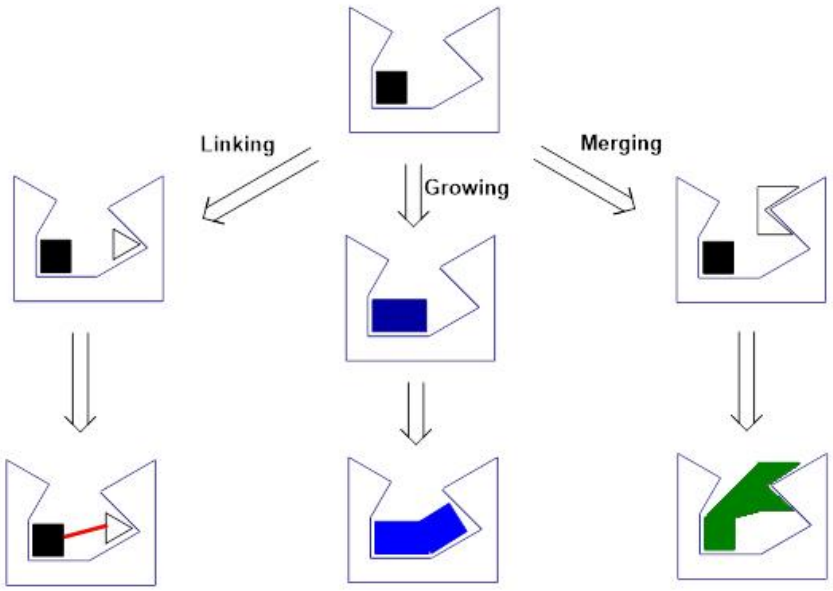

Figure 1.5 Diagram visualising the three strategies of fragment elaboration in hit-to-lead optimisation in fragment-based drug discovery.

The first example of a systematic fragment-based approach to protein inhibition was reported in 1996 by Shuker *et al.* They had discovered a method of determining the structure-activity relationship (SAR) between a ligand and a protein using NMR. A low molecular weight library was screened against a protein, FKBP, to establish which molecules, if any, would bind.

These molecules were then modified to increase their binding affinity. Finally, they were linked to give a molecule which bound to FKBP with a K_d of 19 nM (Figure 1.6).[62]

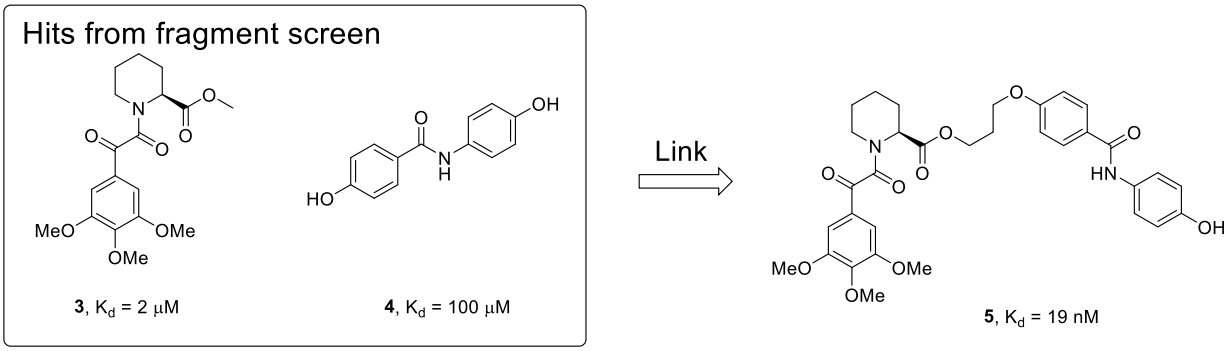

Figure 1.6 Summary of Shuker's work.A fragment library was screened against protein FKBP. Two sites of the protein were found where molecules bound. The molecules with the lowest dissociation constant (K_d) for each site were linked at various points and using a variety of tethers. This resulted in the discovery of a new compound which bound to FKBP with a K_d of 19 nM.

FBDD aids drug discovery in a number of ways. Firstly, it allows the thermodynamics of the ligand-protein interaction to be broken down in several steps. The free energy of a ligand-protein interaction is determined by the Gibbs free energy equation (1.1):

$$\Delta G = \Delta H - T\Delta S \tag{1.1}$$

The dissociation constant (K_d) is related to the Gibbs free energy by the isotherm equation (1.2):

$$\Delta G = RT\ln(K_d) \tag{1.2}$$

Thus, a small K_d, and hence large negative ΔG, will be determined by how exothermically the ligand binds to the protein (large negative ΔH) and how much entropy is lost upon binding (small positive ΔS).

Applying these principles to FBDD shows how growing, linking, and merging fragments can yield drug candidates with low K_ds.[50]

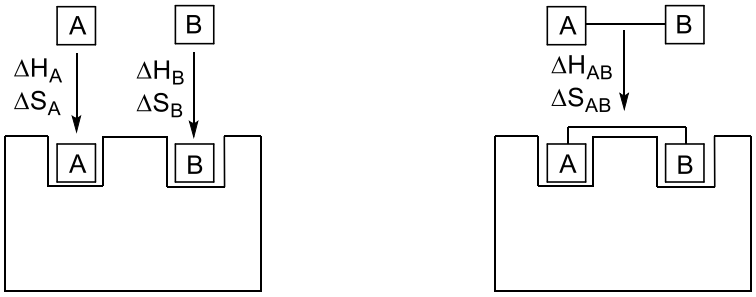

Figure 1.7 A representation of the enthalpy and entropy of molecules A, B, and AB binding to a target.

When two fragments, A and B, bind to a protein, their K_ds are determined independently of one another and are a function of their respective ΔH and ΔS (Figure 1.7). However, when A and B are combined the enthalpy of their binding will be approximately equal to the sum of the enthalpy of the binding of A and B respectively, as they are both utilising the same interactions to bind to the protein (1.3).

$$\Delta H_{AB} \approx \Delta H_A + \Delta H_B \tag{1.3}$$

Yet, the entropy penalty of AB is much less than the entropy penalty of A and B binding separately. Although there will be a greater penalty for the more complex molecule in the form of restriction on rotating and bending modes, these pale in significance compared to the reduction in entropy required for two separate entities to leave solution and bind with a protein. Thus:

$$\Delta S_{AB} \approx \Delta S_A \approx \Delta S_B \ll \Delta S_A + \Delta S_B \tag{1.4}$$

Therefore, when combining fragments to make a large drug-like molecule, the favourable enthalpic terms combine but the unfavourable entropic terms stay approximately the same. This is extremely powerful because, as detailed in equation 1.2, ΔG and K_d are related exponentially. Every time ΔG doubles, K_d is squared. This gives FBDD an advantage over HTS of large molecules which require nanomolar binding to be considered good enough for a lead, whereas fragments only need to exhibit a weaker millimolar binding as fragment development can yield high binding drugs.

Secondly, FBDD rigorously employs X-ray crystallography as well as several other techniques to ensure that the structure-activity relationships (SARs) between fragments and the target are understood. This gives FBDD fragment elaboration a rational aspect to the design of leads molecules, which can give greater success in the clinic.

Thirdly, fragments are less 'complex' than larger molecules. Complexity is desirable in drug candidates and medicines as it conveys selectivity to the target in question and minimises off-target activity which is likely to lead to increased toxicity. However, to probe biologically active chemical space it is best to have simple molecules which probe only certain interactions; an overly complex molecule is more likely to possess groups which inhibit binding (Figure 1.8). Therefore, it is possible that fragments are more promiscuous than lead-like molecules. However, the process of fragment elaboration should increase selectivity.

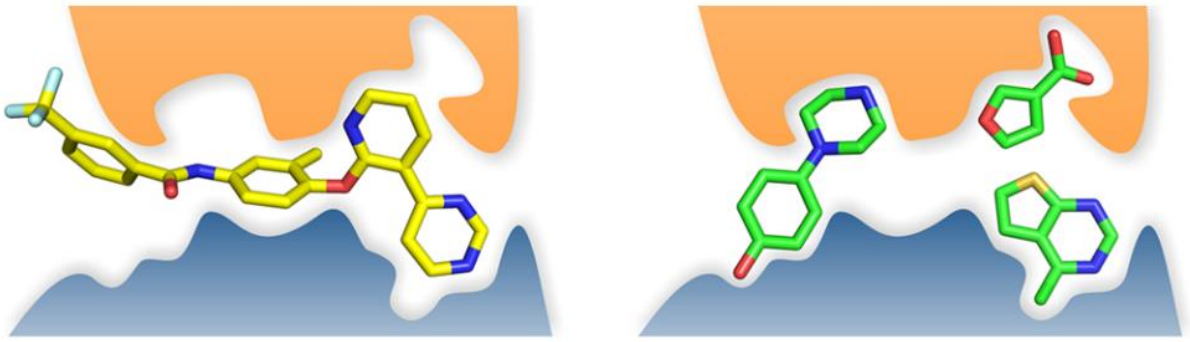

Figure 1.8 A complex molecule versus simple fragments binding on a protein.The complex molecule, although it contains groups which would interact with the target, is prohibited from doing so because of its complexity. The fragments, containing only one or two functional groups are perfectly suited to probe the target's biologic space. (Image taken from ref 53)

This proposition of less complexity leading to more biological hits has been validated statistically.[70] Hann *et al*. showed that the probability of a molecule matching a target decreases exponentially as complexity increases (Figure 1.9).

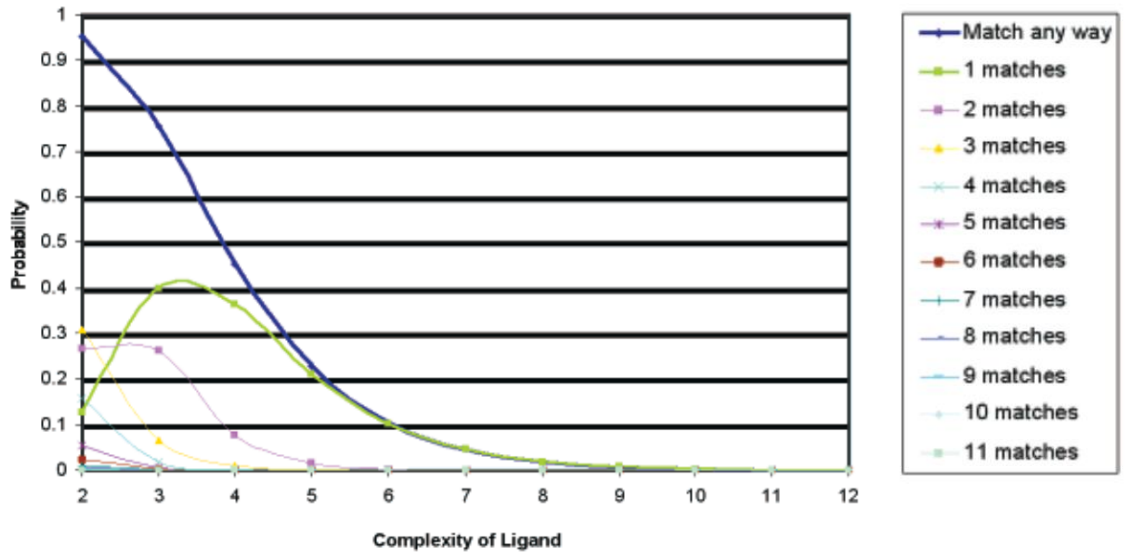

Figure 1.9 A graph showing the probability of a ligand matching a biological target compared with its complexity. The complexity was measured computationally from the length and pattern of the molecule's features. (Image adapted from ref 70)

1.3.3. Identifying fragments

Limiting chemical space to fragments can only become a reality when there is an appropriate definition to direct synthetic research. Lipinski's "Rule of Five" (RO5) (see section 1.1.2) was already well-established for highlighting the typical properties of orally bioavailable drug candidates when FBDD was first established. Since then, a number of studies have resulted in the development of similar "rules" to apply to ideal fragments.

Inspired by the RO5, Congreve *et al.* analysed the fragments used in FBDD and discovered that a 'Rule of Three' (RO3) might be a useful tool in guiding the construction of fragment libraries. Based on the criteria used by the RO5, they suggested that:

> [M]olecular weight is <300, the number of hydrogen bond donors is ≤3, the number of hydrogen bond acceptors is ≤3 and ClogP is ≤3. In addition, the results suggested NROT [number of rotatable bonds] (≤3) and PSA (≤60) might also be useful criteria for fragment selection.[71]

More recently, pharmaceutical company Astex published its internal guide for fragment synthesis. These have further restrictions compared to the RO3 and focus on other details regarding the property of fragments, including spatial and synthetic properties which are an important addition to the field of fragment synthesis.[72] Astex's rules are compared to the RO5 and RO3 in Table 1.2:

Table 1.2 Comparison of the RO5 with the RO3 and Astex's in-house fragment rules.

Property	Rule of Five[19]	Rule of Three[71]	Astex's Rules[72]
Molecular Weight ($gmol^{-1}$)	< 500	< 300	140–230
clogP	≤ 5	≤ 3	0.0–2.0
Polar Surface Area ($Å^2$)	≤ 140	≤ 60	–
H-Bond Acceptors	≤ 10	≤ 3	–
H-Bond Donors	≤ 5	≤ 3	–
Rotatable Bond Count	≤ 10	≤ 3	0–3

Astex also highlight additional properties which would be beneficial for fragments:[72]

- Diverse polar groups for protein binding
- Multiple elaboration vectors for 3D growth
- Aqueous solubility, stability, and solution and avoidance of highly reactive groups or groups which cause aggregation
- Easy to synthesise 50–100 mg in ≤ 4 steps from commercial starting materials
- A variety of 3D scaffolds
- 0–2 chiral centres

All these suggestions should be taken as good rules of thumb to aid in the design and functionality of fragment libraries.

1.3.4. Success of FBDD

Clearly the FBDD process has some notable advantages over previous drug discovery paradigms including HTS and TBDD.

More efficient sampling of chemical space: both HTS and FBDD rely on serendipity to discover novel chemical leads. However, the chances of this happening are slim unless the HTS screening libraries sample an appropriately high volume of chemical space. Given HTS chemical space, this is likely to be in the order of 10^{63} molecules. Sampling a millionth of this space would require the synthesis and screening of 10^{57} molecules; an impossible task. However, fragment space is considerably smaller at around 10^{11} molecules. A millionth of this space is only 100,000 molecules; a very achievable target. In addition, advances in computational technology mean that *in silico* screening can be readily employed to aid in the synthesis of fragments. TBDD does not rely on serendipity to find leads. However, over-

reliance on focusing on one biological system could see molecules which may inhibit other systems not being utilised to their full advantage.

Greater chances of a compound binding: Another advantage which the use of fragments gives FBDD is the molecules are less complex with fewer skeletal appendages. This allows functional groups to more efficiently probe biological space, with a lower chance of steric or electron clash related to more complex molecules.

Hit-to-lead optimisation improved: Fragments would ideally consist of multiple vectors of elaboration. This means that chemists could easily modify fragments with a hit in most spatial directions, hopefully allowing for almost any hit to be improved. The late stage nature of HTS libraries mean the number of vectors is less and elaboration would be a more laborious task.

FBDD has been successful over the past twenty years of drug discovery. Erlanson *et al.* identified 32 compounds in clinical trials which are known to have been identified from FBDD. Figure 1.10 shows two marketed drugs derived from FBDD.[73] Due to this success, this thesis focuses on the synthesis of fragments for potential use in drug discovery.

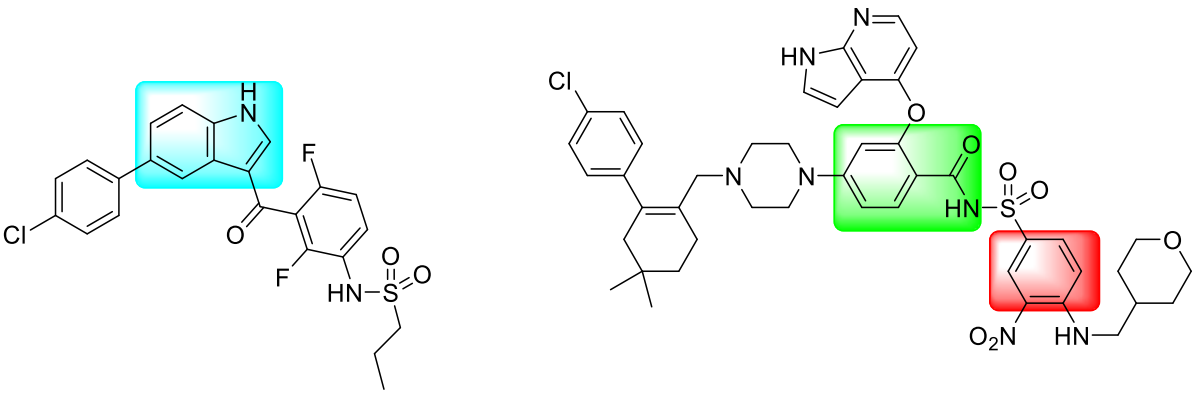

Figure 1.10 Vemurafenib and Venetoclax with the initial fragment hits highlighted.

Chapter 2

Fragment inhibitors of CK2

2.1. Introduction

2.1.1. FBDD in targeting PPIs

Biological interactions are largely governed by the interactions between proteins, called protein-protein interactions (PPIs). They modulate many key pathways in health and disease with an estimated 400,000 biological processes regulated by PPIs. Thus, they are an important target in drug discovery.[74,75] However, the often large and shallow nature of the PPI pockets has given them the reputation of being 'undruggable'.[76–78] Recently, work has begun to overcome this challenge using small molecule approaches to drug discovery which has led to PPI being examined as a potential target for discovery programmes.[79]

PPI inhibitors can be broadly sub-divided into two categories: orthosteric inhibitors, which block the interaction site between the two proteins, and allosteric inhibitors, which bind to a different site on the protein but in doing so change the shape of the protein binding site, thus inhibiting the PPI (Figure 2.1).

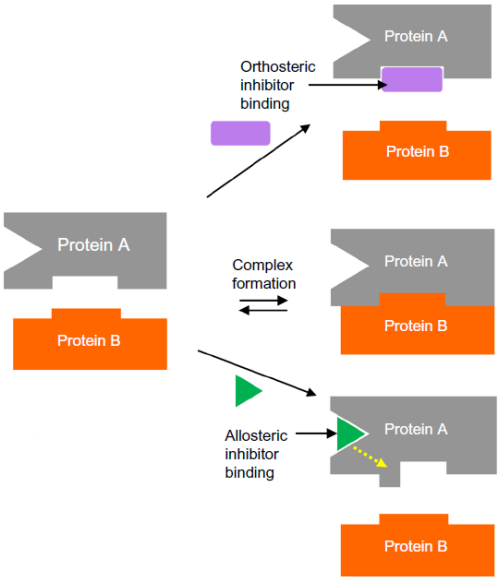

Figure 2.1 Diagram showing the mode of action for ortho- and allosteric inhibitors of PPIs.(Image take from ref 75).

Whilst traditional screening methods with larger molecules often fail to sufficiently bind these shallow pockets, the smaller nature of fragments allows them to probe these sites. This provides a way of identifying initial hits to kickstart a PPI inhibitor discovery process. Indeed, FBDD has been successful in discovering a new anticancer drug: Navitoclax was discovered from a FBDD campaign and offers potent treatment of small-cell lung cancer and chronic lymphocytic leukæmia.[80] Two fragments, a biaryl and a tetrahydronaphthalene, were discovered that bound in the PPI site and a campaign of linking and growing produced Navitoclax,[80,81] which entered the clinic in 2009 and was licenced in 2017.[82,83] Due to the highly specific nature of PPI sites, this treatment lacked the off-target effects of the previous treatment, Obatoclax, and reduced negative side-effects (Figure 2.2).[84]

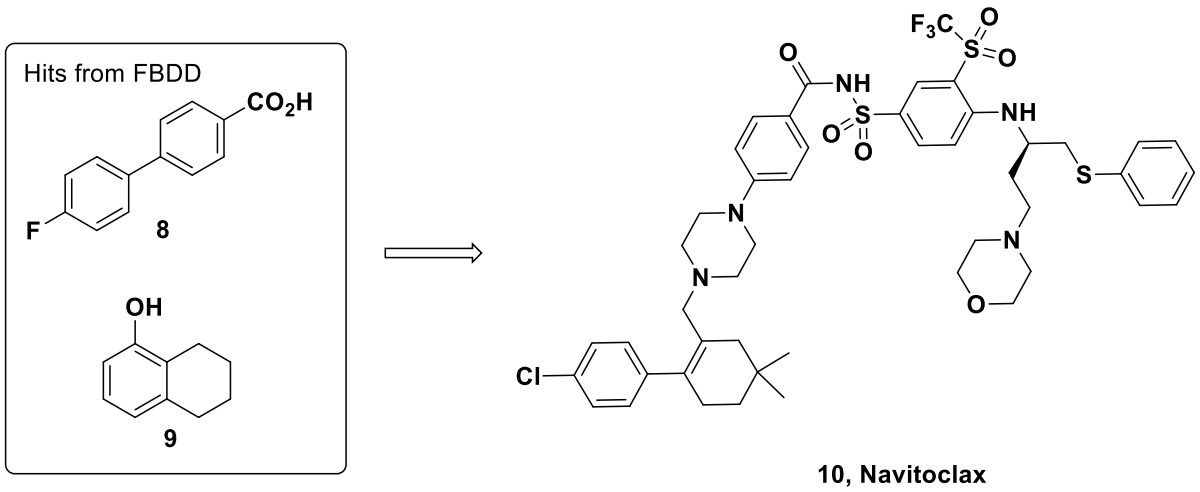

Figure 2.2 The initial fragment hits which led to the discovery of Navitoclax.

With the role FBDD can play in the discovery of PPI inhibitors in mind, the rest of this section will focus on a specific PPI interaction and how its inhibition could produce potent anti-cancer therapies.

2.1.2. Casein Kinase 2

Protein kinases were discovered serendipitously in 1954 when Kennedy and Burnett reported an enzyme catalysing the transfer of a phosphate from ATP to a protein.[85] Although the physiological significance of the discovery was not initially realised, the following six decades brought considerable knowledge and understanding to the field of protein kinases.

Since then, discoveries have demonstrated the importance of Casein Kinase 2 (CK2) in human biology. Recent research on a database of almost 11,000 naturally-occurring phosphorylated sites revealed that the unique acidic marker that identifies CK2 has been found on 2275 (>20%) of them.[86]

The pivotal role CK2 plays in controlling many other kinases and cell death has led to some calling CK2 the 'master kinase'. Indeed, the vast number of targets of CK2 signifies that almost all cellular activity is regulated in some way by CK2. The most notable of these include: stress stimulus mediation, gene expression regulation, protein synthesis and degradation, regulation of the circadian rhythm, viral infection, and counteracting apoptosis.[87]

2.1.3. Structure and activity of CK2

CK2 is a tetramer consisting of two of CK2α and CK2α' subunits and two CK2β subunits. Thorough crystallographic and structural analysis has been carried out on CK2. This has

shown that the α subunit is the catalytic subunit, the β subunit is the regulator subunit, and these form the tetrameric holoenzyme of $\alpha_2\beta_2$, $\alpha\alpha'\beta_2$, or $\alpha'_2\beta_2$ (Figure 2.3).

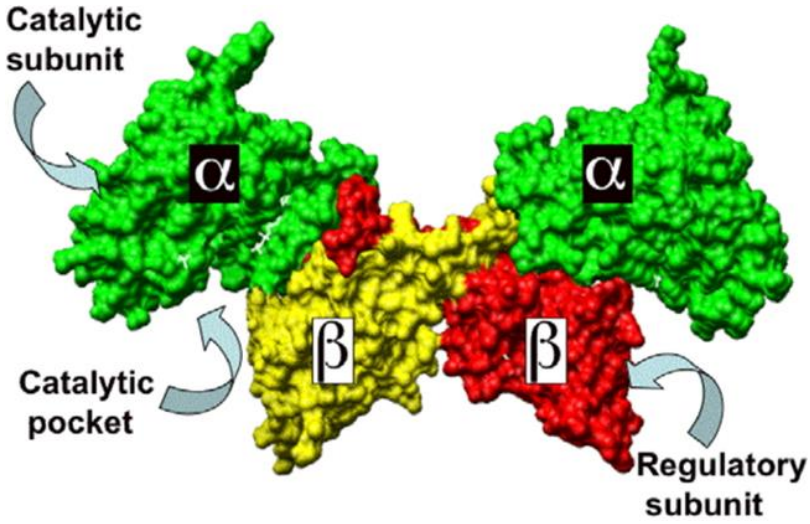

Figure 2.3 CK2 protein with the structure $\alpha_2\beta_2$ (PDB: 1JWH, Image from ref 88).

The three heterotetrameric forms of CK2 have displayed no differences in activity from one another. Analysis of the CK2α and CK2α' has shown that CK2α' lacks the *C*-terminal amino acids 330–391. In addition, comparison of the 1–329 sequence of CK2α and CK2α' has shown an 86% homology. However, they exhibit the same activity.[89]

CK2 is involved in many key cellular processes. Yet, there are two signalling pathways of particular interest especially if focus is concentrated on CK2 tumorogenisis. These are the Wnt pathway and the NF-B pathway, two signal transduction pathways that regulate important cell development events and play a role in some cancers.[90]

The CK2α subunit is always in the active conformation and possesses the key ATP binding site which is responsible for the biological activity. The CK2β subunit is a regulatory subunit. The activity of this subunit is dependent on the substrate. CK2β is also found to increase the proteolytic and thermodynamic stability of CK2α as well as providing sites for substrates to dock.[91]

2.1.4. CK2 and Cancer

As a protein kinase, CK2 phosphorylates a great many substrates involved in cell growth.[89] Being a ubiquitous protein kinase, CK2 is overexpressed in a large range of cancers.[92] Importantly, it is not mutations of CK2 which are carcinogenic, but unnaturally high quantities of CK2 and its associated activity have been observed in many tumours. In

comparison with normal cells, which sees CK2 diffused in the various cellular compartments, tumours have high levels of CK2 around the nucleus and in neoplasia and CK2 is elevated beyond what is expected for normal cells.[93] CK2, as well as being involved in cell proliferation and growth, also suppresses apoptosis, linking CK2 to the cancer phenotype.[94]

CK2 is up-regulated during cell proliferation however it readily returns to normal after proliferation has finished. Yet in cancerous cells it finds homoeostasis at this level and remains high.[95] In addition, studies on prostate cancer—forms which are both androgen sensitive and androgen independent—showed CK2 to be functional irrespective of the growth factor.[96]

Having identified CK2 as an important target, is it a viable target for cancer therapy? One reason why CK2 inhibition may be a particularly effective form of treatment is the pivotal and indispensable role it plays in the cell. If inhibited below the high critical threshold, the cancerous cell would no longer be malignant as there are no alternative signalling pathways, which could by-pass the need for CK2. Due to the role of CK2 in cell growth, proliferation, and apoptosis, its down regulation could be particularly catastrophic to cancer cells, as such down regulation of protein kinases has been researched on previous occasions.[97]

2.1.5. CK2 Inhibition

Being a protein kinase, it is not surprising that initial research into inhibiting CK2 was directed at finding competitive inhibitors at the ATP binding site of the protein. One of the challenges this presented was selectivity issues when targeting the ATP pocket due to the fact that the pocket is highly conserved among kinases. There are in excess of 500 protein kinases in the human genome, with those in the same family sharing similar structural features. Thus, finding a compound which can selectively bind in the ATP site of CK2 without affecting other protein kinases would be challenging. Another issue with targeting an ATP site is that the inhibitor in question would have to compete with the high concentration (~1–10 mM) of ATP within the cell. However, this is less of an issue when the protein in question is in an inactive form.[98]

This is not prohibitive, since there are some ATP inhibitors in clinical trials which are not completely selective.[99] A study in 2008 involving 317 kinases (over half the human kinome) showed that of the 38 kinase inhibitors tested, none were selective within the range $K_d < 3$ μM. Even the most selective ATP inhibitors, GW-2580 (primary target CSF1R, not yet in clinical trial) and lapatinib (primary target EGFR and ERBB2, approved for HER breast cancer) exhibited binding to three different kinases (Figure 2.4).[100] Therefore, when seeking an ATP

inhibitor for CK2, total selectivity may not be necessary (which may be impossible). Instead sufficient selectivity to avoid inhibiting other kinases and therefore avoid adverse side effects.

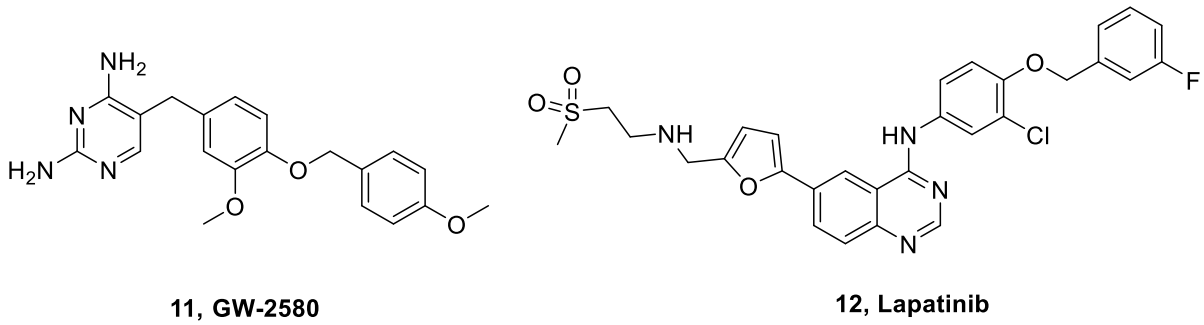

Figure 2.4 GW-2580 and Lapatinib, the most selective ATP inhibitors in the study by Karaman *et al.*

The first example of an ATP based CK2 inhibitor was found in 1986 when a compound called DRB (Figure 2.5) inhibited CK2 with an IC_{50} of 15 μM.[101] However, it was also found four years later that this compound also inhibits other kinases with similar IC_{50} values.[102]

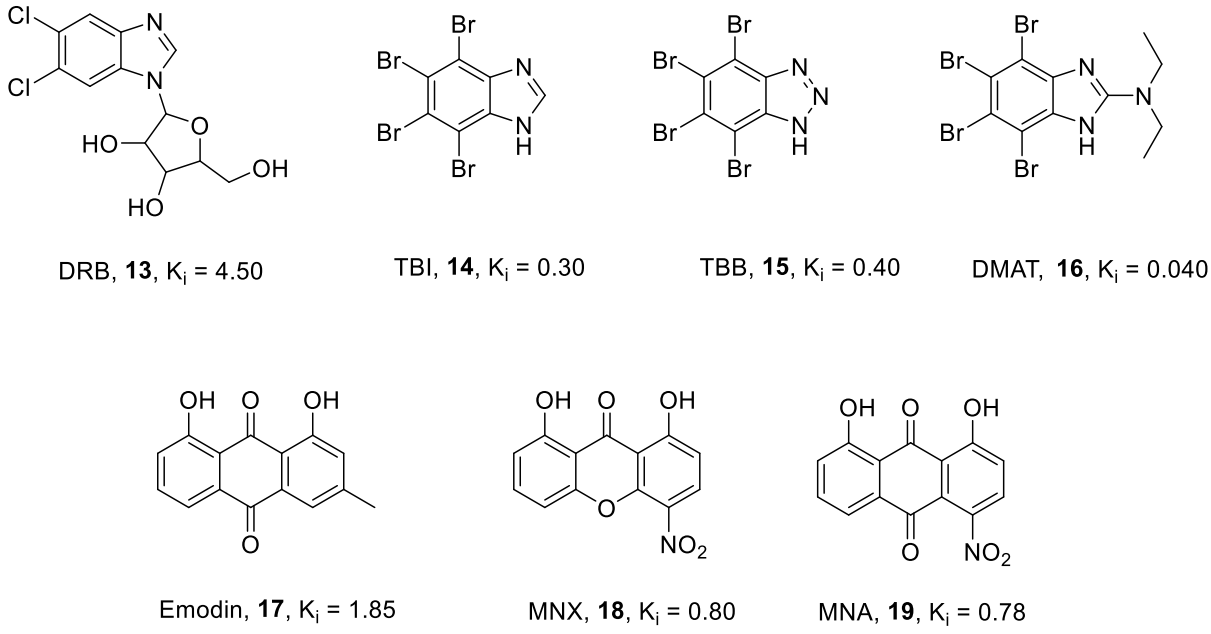

Figure 2.5 CK2 inhibitors, all K_i values are expressed in μM.

DRB also inspired a series of derivatives (Figure 2.5) to improve the potency of the original. To improve the hydrophobic interactions, all the positions on the benzene moiety were brominated and the appendant sugar was removed to form TBI. The triazole equivalent gave TBB and a diethyl amino substituted TBI produced DMAT. All of these were substantial improvements on DRB (DMAT being the most promising with a K_i of 0.040 μM compared to DRB's 4.50 μM).[103]

A range of natural products were also tested against this target. Emodin was found to be both unselective and lacking in potency. However, two unnatural analogues, MNX and MNA, where found to be an improvement on emodin.[104] Flavonoids were found to bind better than DRB, yet they lacked selectivity.[105]

The most progress made towards a drug which could inhibit CK2 through binding at the ATP site is a compound called CX4945 from Cylene Pharmaceuticals (Figure 2.6). This has been subjected to phase I clinical trials and was tested against BT-474 breast cancer cells and BxPC-3 pancreatic cells with overexpressed growth factors. It was found to suppress the PI3K/Akt signalling pathway in the cell.

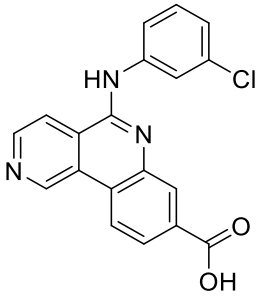

CX4945, **20**

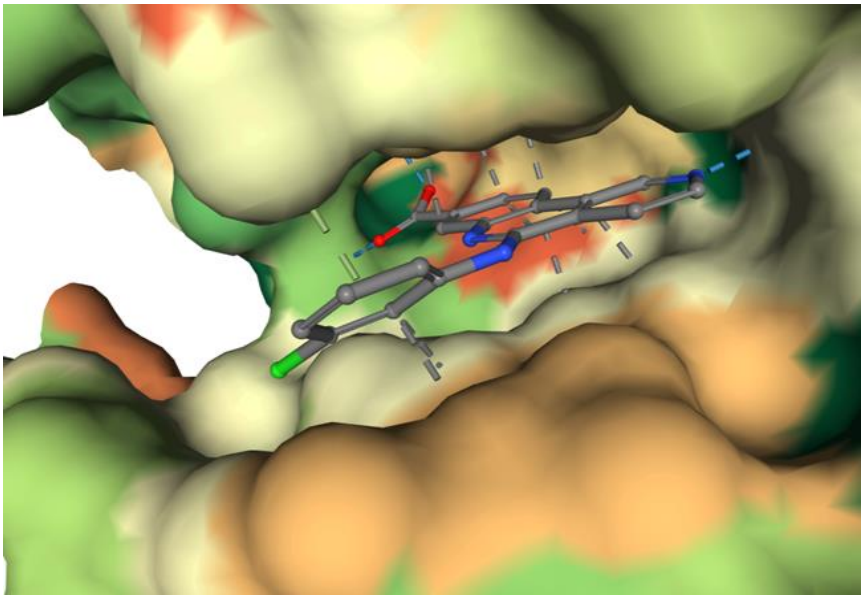

Figure 2.6 CX4945 with an image of the crystal structure of it binding in the ATP pocket of CK2 (PDB: 3PE1).

When administered orally *in vivo,* BT-474 cancer cells showed up to 97% TGI, with just over 20% showing 50% reduction in tumour size. For BxPC-3 93% TGI with about 30% showing no tumour after treatment.[106] However, due to CX4945's activity on the ATP pocket, its activity against other protein kinases may lead to adverse side effects. Studies have shown CX4945 to be a promiscuous molecule, even targeting another protein, CLK2, more potently than CK2. Indeed it targets 13 other proteins with nanomolar activity, which could present a problem in its progress through the clinic.[107]

Targeting the ATP site is not the only way to inhibit protein kinases. Research has also been directed to non-ATP competitive inhibitors which can overcome some of the disadvantages of the ATP inhibitors. Namely, they are more likely to be protein specific as there is more

variety in the shape of pockets outside the ATP site. Furthermore, because it does not have to compete with ATP for binding, they can be administered in concentrations closer to the K_i. The most commonly targeted non-ATP site in kinases is the substrate binding site.

Both small molecules and peptides have been used to bind this site.[108] Additionally, compounds have been developed which bind to both the ATP site and the substrate site simulateously.[109] Unfortunately, peptide-based inhibitors come with their own set of problems: low potency, difficult uptake, and intracellular instability. However, recent developments in drug discovery are attempting to overcome these limitations.[110] In addition, there may be other sites on the protein which can also be exploited for inhibition. As shall be seen, this is the case for CK2 at the interface of the protein-protein interaction (PPI) between the α and β subunits.

Some progress has been made in finding an inhibitor of CK2 which does not act on the ATP binding site. When a crystal structure of DRB binding in CK2 was obtained, it was noted that a second molecule of DRB bound to the interface of the α-β subunits[111] and that it has an inhibitory effect on CK2. However, when a peptide of the C-terminal 181–203 of CK2β was exposed to CK2α, it had a stimulatory effect on CK2α phosphorylation, yetr this was less than CK2β itself.[112] Continued exploration of peptide-based inhibitors of CK2 found that a cyclic peptide of CK2β 186–193 also bound in the PPI site, inhibiting the CK2 tetramer assembly.[113] In addition to this, a molecule identified as W16—as part of wider research into podophyllotoxine indolo-analogues in CK2 PPI inhibition—was found to have an IC_{50} of 20 μM (Figure 2.7).[114]

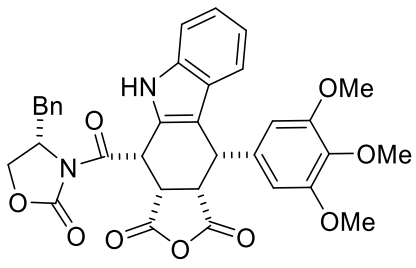

W16, **21**

Figure 2.7 Compound W16.

Recent research on a di(naphthalene) diazene core has identified a number of new compounds which exhibited inhibition of CK2. Of the 23 compounds based on this scaffold, five showed inhibition of CK2 (Figure 2.8). Of these compounds, compound **26** showed the lowest IC_{50} of

0.4 μM and analysis showed that it was inhibiting in both the ATP and PPI sites of CK2. It was further shown that against U373 cell line (cells from an aggressive form of brain tumour) compounds **24** and **26** both stopped the cell cycle and inhibited colony growth formation.[115]

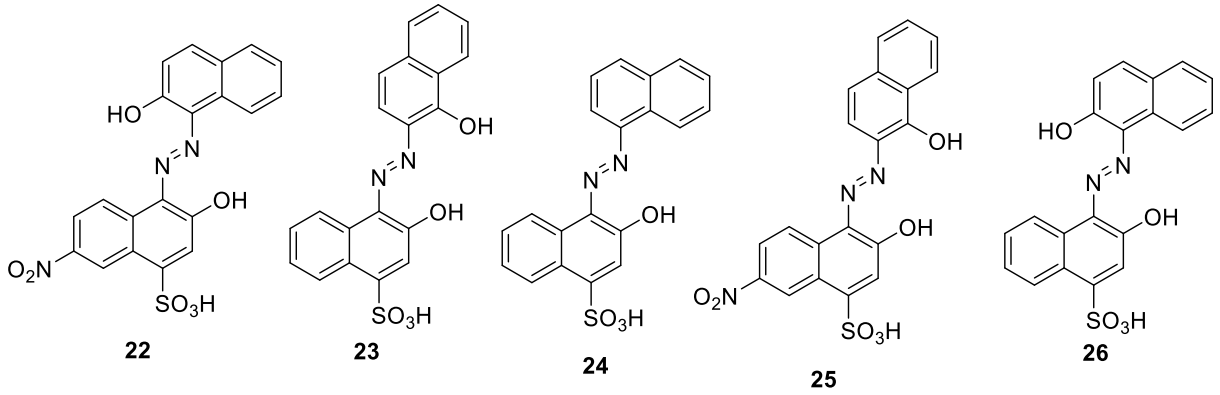

Figure 2.8 Di(naphthalene) diazene series of compounds

From all these examples, it seems that the field is developing for insights into inhibiting CK2; not just via the ATP pocket but also via allosteric inhibition of the PPI. Due to the higher specificity of a PPI inhibitor over an ATP inhibitor, the more the field of compounds is widened, the discovery of a molecule which could one day be used in a clinical setting becomes closer.

2.2. Outline of this work

Capitalising on the fact that CK2 consists of a catalytic subunit, CK2α, and a regulatory subunit, CK2β, inhibition of the protein-protein interaction may lead to molecules which selectively inhibit CK2.[116]

This is not a new strategy. Three molecules and a cyclic peptide have been identified as inhibiting CK2 at the α-β interface pocket.[117] One of these molecules, DRB (**13**), a fragment, exhibited off-target activity by binding in the ATP pocket of CK2.[111] The two other molecules, W16 (**21**) and a diazo compound (**26**), are large drug-like molecules with some undesirable physico-chemical properties, and lack crystal structure data to prove binding at the interface pocket (**Figure 2.9**).[68,114,115]

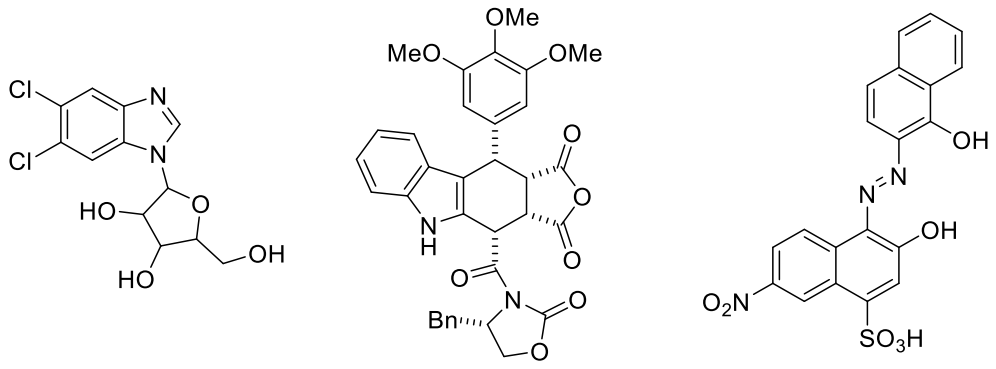

13, DRB **21, W16** **26, Diazo**

Figure 2.9 Structures of inhibitors of CK2α in the interface pocket.

A recent screen of a compound collection library produced by the Abell Group at the University of Cambridge found NMR154 (**27**), which bound in the interface pocket of CK2α (Figure 2.10).[118]

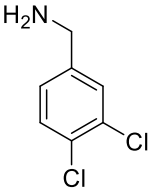

27, NMR154

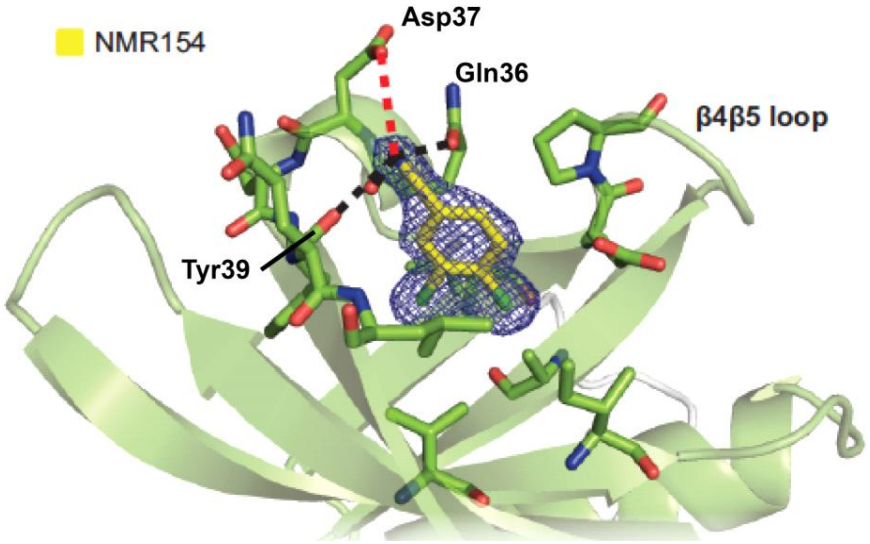

Figure 2.10 The structure of NMR154 alongside the crystal structure of NMR154 bound at the interface pocket of CK2α (image taken from ref. 118).

NMR154 had two drawbacks. Firstly, it also bound in the ATP pocket of CK2α and secondly, it had a relatively high IC_{50} of 900 μM. The Abell Group made analogues of NMR154 to improve selectivity and inhibition. Of these, only one, NMR154L (**28**, **Figure 2.11**), showed an improved inhibition of 700 μM. However, it still bound in the ATP pocket.[68]

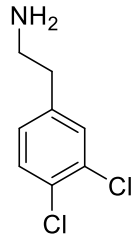

28, NMR154L

Figure 2.11 Structure of NMR154L.

Despite these failings, NMR154L has ideal features for it to be the basis of further fragment development. Firstly, its properties were well within the Rule of Three, meaning further fragment development was likely to exhibit good physico-chemical properties (Table 2.1). Secondly, NMR154L has plenty of vectors to grow and elaborate the fragment; off the aromatic ring or amine group, for example. Thirdly, the existence of a crystal structure of the molecule binding in the interface pocket allows for design of new inhibitors based on known interactions (especially that of the electrostatic interaction between the primary amine on NMR154 and Asp37, see Figure 2.10).

Table 2.1 Table comparing the physico-chemical properties of NMR154 and NMR154L with the Rule of Three. [a] MW: molecular weight in $gmol^{-1}$, clogP: calculated log of the partition coefficient, PSA: polar surface area in $Å^2$, HBA: hydrogen-bond acceptors, HBD: hydrogen-bond donors, RBC: rotatable bond count, CC: chiral centres.

Property[a]	Ideal Fragment Range (RO3)[71]	NMR154	NMR154L
MW	< 300	176.05	190.07
clogP	≤ 3	1.88	2.31
PSA	≤ 60	26.02	26.02
HBA	≤ 3	1	1
HBD	≤ 3	1	1
RBC	≤ 3	1	2
CC	0–1	0	0

This chapter will explore developments of NMR154 analogues through elaboration of the aromatic ring and the generation of a new series of fragments to inhibit the interface pocket developed by computer modelling.

2.3. NMR154(L) analogues

2.3.1. Vectors of elaboration

Previous work has seen attempted optimisation of the methylene bridge and amino group on NMR154 to improve out-of-pocket binding interactions (Figure 2.12).

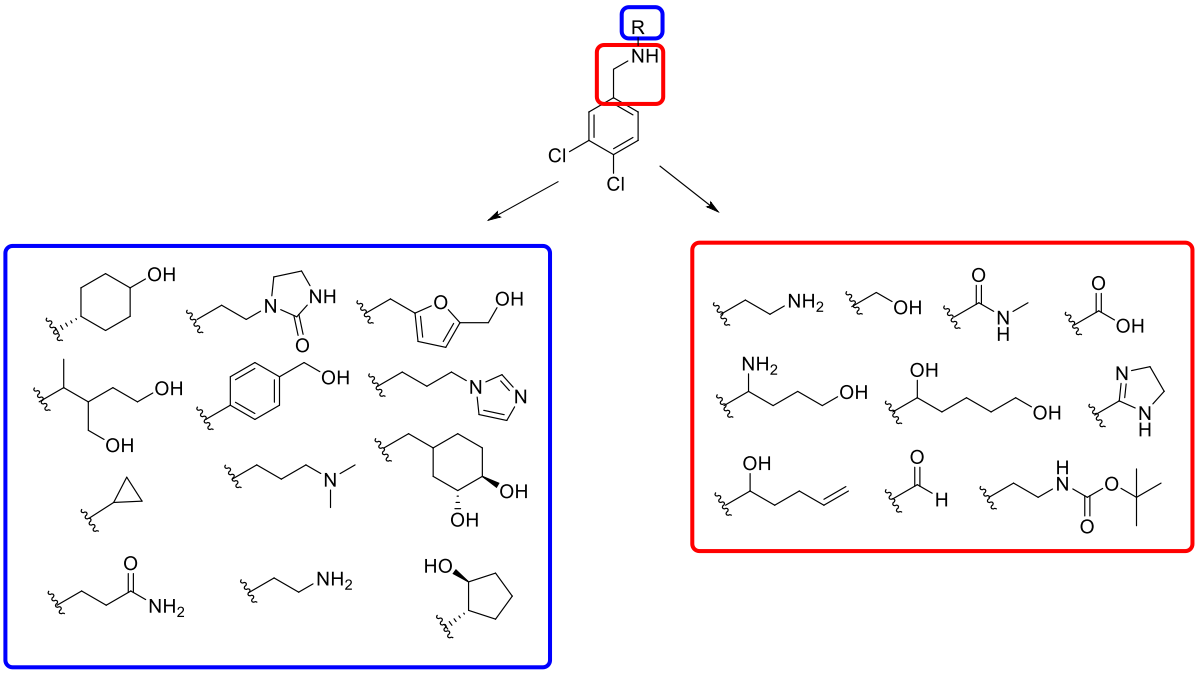

Figure 2.12 Elaboration of NMR154.Elaboration from the amino group was investigated (blue box) as well as substitution of the methylamine group (red box).

Unfortunately, varying the methylamine group only led to improved binding in one case, that of the ethyl amino group (discussed previously as NMR154L). The other functional groups evaluated: alcohol, amide, carboxylic acid, aldehyde, carbamate, and dihydroimidazole showed no improvement on NMR154(L) (Figure 2.12, red box).[68]

Thus, the methylamine group was maintained (as it was synthetically easier to synthesize than the ethyl derivative and displayed interaction with Asp37) and additional groups were grown from it. A range of functionalities were explored with the view of picking up additional electrostatic interactions outside the pocket (Figure 2.12, blue box). Again, none of these showed improvement on NMR154L.[68]

As a result, elaboration of the benzene core of NMR154 was next to be explored. The shape and structure of the α-β interaction pocket was investigated *in silico* using the computer program Maestro 10.2. As can be seen (Figure 2.13), the pocket is reasonably deep but narrow. The key to increasing the binding interactions into this pocket would be to utilise the two

aspartate residues at the top of the pocket. Suitable positioning of ammonium moieties could allow for hydrogen bonding. In addition, the breath of the pocket can also be explored.

Additionally, fragments could be synthesised elaborating at the *ortho* position of the benzene ring with regards to the ethylamino moiety on NMR154L (Figure 2.13).

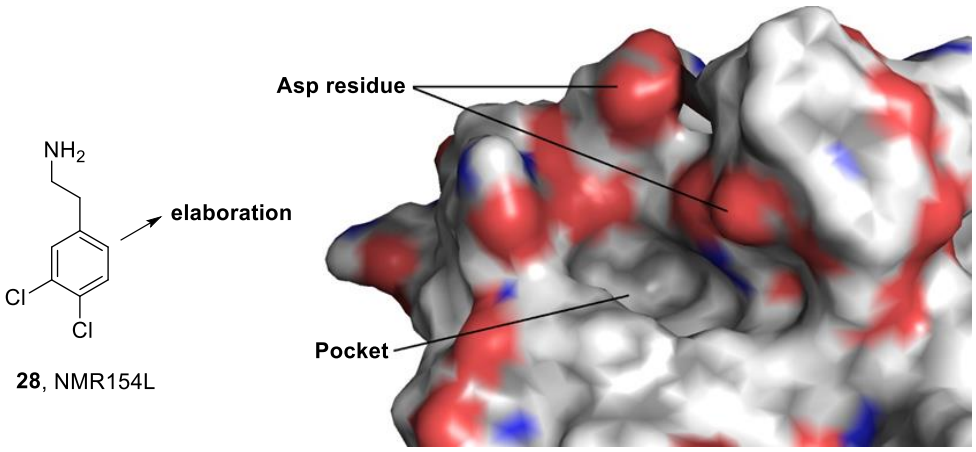

Figure 2.13 NMR154L with the elaboration vector next to the interface pocket showing the Asp residues.

The first elaboration tested was the addition of another ethyl amino group (fragment **29**) to try and mimic the success of the original ethyl amino in binding to an Asp residue. Modelling predicted that this modification would show improved binding at the interface pocket. The Maestro 10.2 program assigns a 'docking score' to aid in the prediction of how well fragments will bind. The more negative the score, better binding is predicted. NMR154L was given a docking score of –6.1 and the proposed fragment **29** was awarded a docking score of –7.0, giving a good degree of confidence in its binding (Figure 2.14).

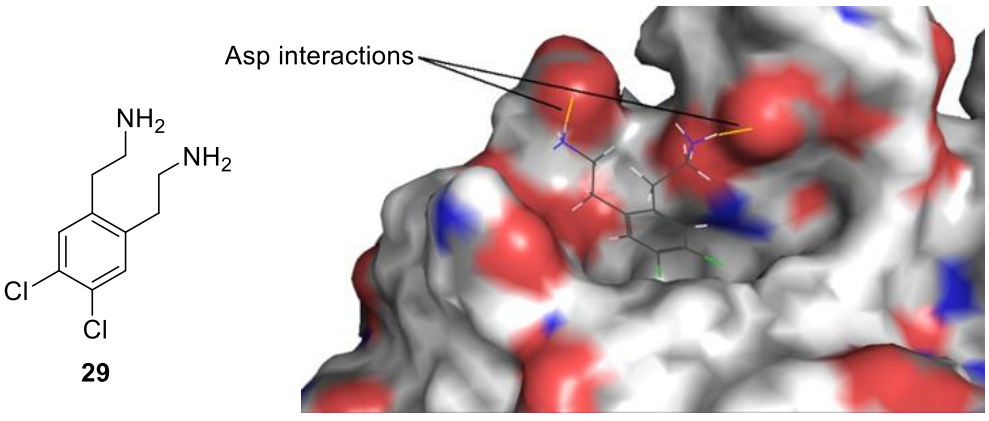

Figure 2.14 Maestro 10.2's prediction of how the proposed fragment (**29**) would bind at the interface site.This interaction was awarded a 'docking score' of –7.0 compared to NMR154L's –6.1.

2.3.2. Synthesis of fragment **29**

Due to the plane of symmetry in fragment **29** a straightforward synthesis could be proposed as all disconnections and functional group interconversions do not need to have as high a degree of regioselectivity. Looking at **29** it seemed easiest to begin from a starting material which had the dichloro functionality already present. All that would be required was an appropriate synthetic handle on the opposite side of the ring. Thus, the readily available 4,5-dichlorophthalic acid (**33**) was chosen as an ideal starting material.

The retrosynthetic plan firstly involved the primary amines being revealed from nitriles *via* reduction (**Scheme 2.1**). Nitriles may be added by S_N2 displacement of an appropriate leaving group. This is obtained from the alcohol, itself revealed from a dicarboxylic acid.

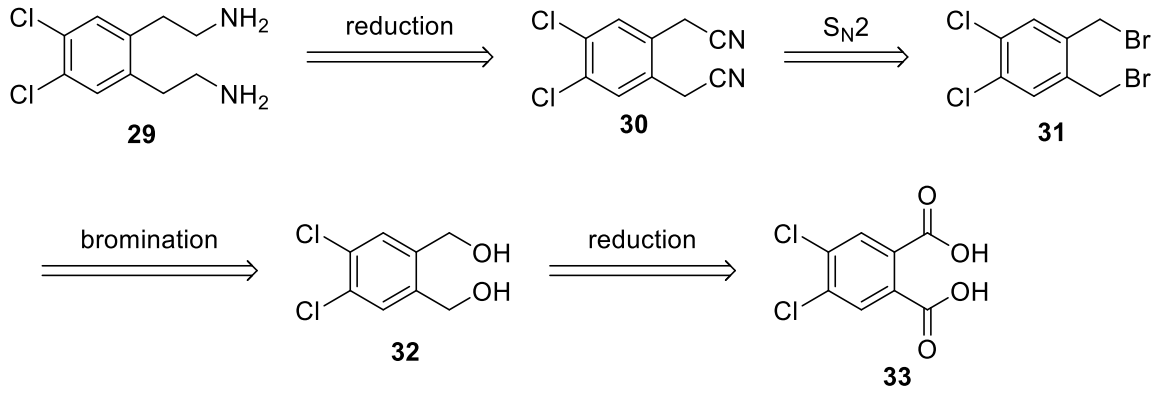

Scheme 2.1 Retrosynthetic analysis of 2,2'-(4,5-dichloro-1,2-phenylene)bis(ethan-1-amine) (**29**) from commercially available 4,5-dichlorophthalic acid (**33**).

Despite having literature precedent,[119] the product of the diacid reduction with borane in THF (Scheme 2.2) did not yield the desired product by NMR (only displaying one peak). One possible explanation of this could be that the anhydride was formed. Although borane should be strong enough to further reduce the anhydride, it could be possible that the reagent might have degraded. The reaction was repeated yielding the same results. The reduction was then attempted with lithium aluminium hydride (Scheme 2.2)—a much stronger reducing agent—which should have easily converted the carboxylic acid (**33**) to the alcohol (**32**). However, this also yielded the same, undesired, product by NMR. It would be extremely unlikely for the lithium aluminium hydride to stop reduction at the anhydride. As this strategy did not yield the desired diol, a different strategy was approached.

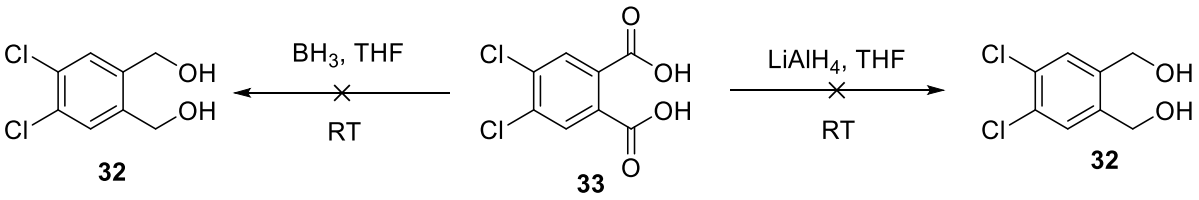

Scheme 2.2 Attempted direct reduction of **33** using borane in THF (left) and lithium aluminium hydride in THF (right).

To overcome this issue, it was postulated that direct reduction of a methyl ester would not present such a problem. The diacid was methylated by treatment with thionyl chloride in methanol (**Scheme 2.3**). This readily produced the diester (**34**) in good yields which was submitted straight for reduction with lithium aluminium hydride. The pure diol (**32**) was afforded in good yield.

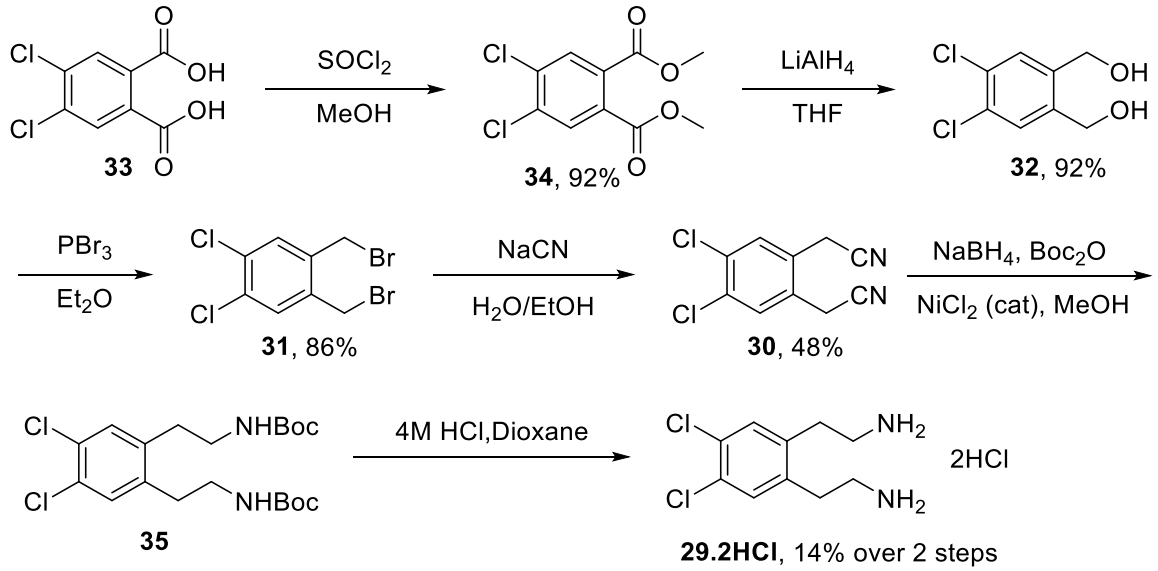

Scheme 2.3 Synthesis of fragment **29**.

With this in hand, diol **32** was submitted for bromination under phosphorous tribromide conditions. This achieved the desired effect of producing the dibromide **31**. An S_N2 reaction using sodium cyanide in refluxing ethanol transformed the dibromide into the dinitrile **30**. Finally, all that was required was reduction of the nitriles with lithium aluminium hydride. Unfortunately, this did not produce the desired product **29**. Examination of the literature showed that on a similar system (4-bromo-1,2-benzenediacetonitrile) access to the diamine was not achieved directly but *via* a Boc-protected intermediate.[120] Thus, a nickel (II) and sodium borohydride mediated reduction was performed in the presence of Boc-anhydride. This successfully produced two mono-Boc protected amines **35**. The product was carried

straight through to remove the Boc with 4M HCl/dioxane. This furnished **29** as the pure bis(HCl) salt (**Scheme 2.3**).

2.3.3. Biological testing of **29**

Compound **29** was submitted to a fluorescence polarisation (FP) assay.[b] These assays work through CK2α being soaked with a fluorescence labelled peptide which mimics the part of CK2β that binds to CK2α. If a compound binds at this interface the tumbling of the protein would be different, and this would affect the degree of polarisation of the light. In this way, the half- maximum inhibitory concentration (IC_{50}) of the compound could be measured.

The results of the experiment showed that compound **29** bound to the interface of CK2α with an IC_{50} of 250 μM (cf NMR154L IC_{50} of 700 μM). The crystal structure of CK2α with **29** bound at the interface was obtained to examine the nature of the binding and further inform design to improve the inhibition (Figure 2.15).

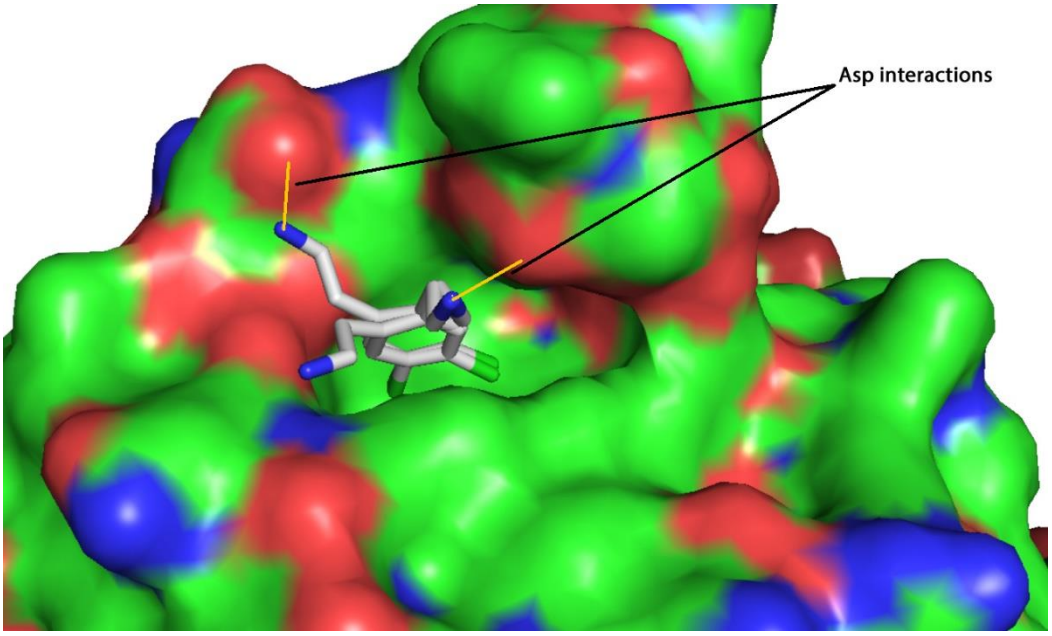

Figure 2.15 Compound **29** in interface pocket showing two binding modes.

The crystal structure confirmed the model's predictions about the nature of the binding in the pocket. Interestingly, one of the binding modes did show one of the ethylammonium moieties facing away from the aspartate residue.

[b] All biological work was carried out by Dr Paul Brear, Department of Biochemistry, University of Cambridge.

2.3.4. Methyl analogue of **29**

Due to the similarity in binding between NMR154 and NMR154L, it was investigated whether a dimethylamine analogue of **29** (fragment **38**) would display similar biological properties to **29**. If **38** could be more easily synthesised than **29** and display comparable properties, this could aid further fragment elaboration if both alkyl amino groups wish to be kept on the fragment.

Fragment **38** was readily synthesised in two steps from commercially available 1,2-dichloro-4,5-dicyanobenzene (**36**). This was submitted to the same nickel (II) mediated reduction-Boc protection to afford Boc-protected diamine **37,** which was deprotected by 4M HCl/dioxane to afford the bis(HCl) salt **38.2HCl** (Scheme 2.4).

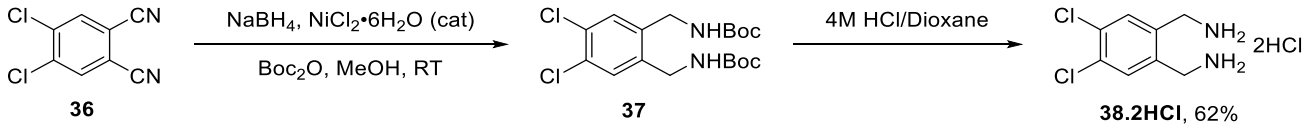

Scheme 2.4 Synthesis of **38**.

This was submitted to the same FP assay experiment as compound **29** but showed >1 mM IC_{50} meaning it was not an improvement on NMR154.

2.4. Bicyclic series

2.4.1. Exploring the pocket width

With the improvement in binding from the ethylamine moiety in mind, it was explored whether growing the benzene core of NMR154L into a fused bicyclic core would fill more of the width of the pocket and thus aid binding by anchoring the fragment in the pocket. In this way, naphthalene-based fragment **39** was conceived (Figure 2.16).

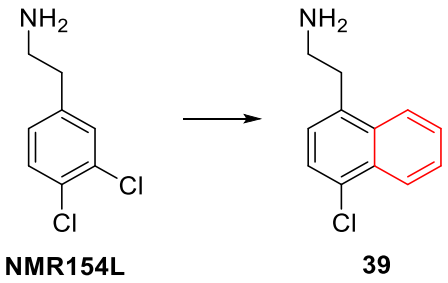

Figure 2.16 Growth of fragment NMR154L to incorporate a naphthalene core **39**.

2.4.3. Synthesis of **39**

Synthesis of this naphthalene derivative started from commercially available 1-chloronaphthalene (**40**) which was subjected to a Friedel-Crafts acetylation. The electronics of the 1-chloro substituent directs the acetyl group *para* to the chlorine (**41**).[121] Subjecting this to the iodoform reaction converted the acetyl group into a carboxylic acid (**42**).[121] Reduction then gave alcohol **43**, followed by bromination which afforded a bromomethyl species, **44**.[122] This was ripe for S_N2 displacement with cyanide to yield nitrile **45**.[120] Reduction gave **39** as the HCl salt (Scheme 2.5).

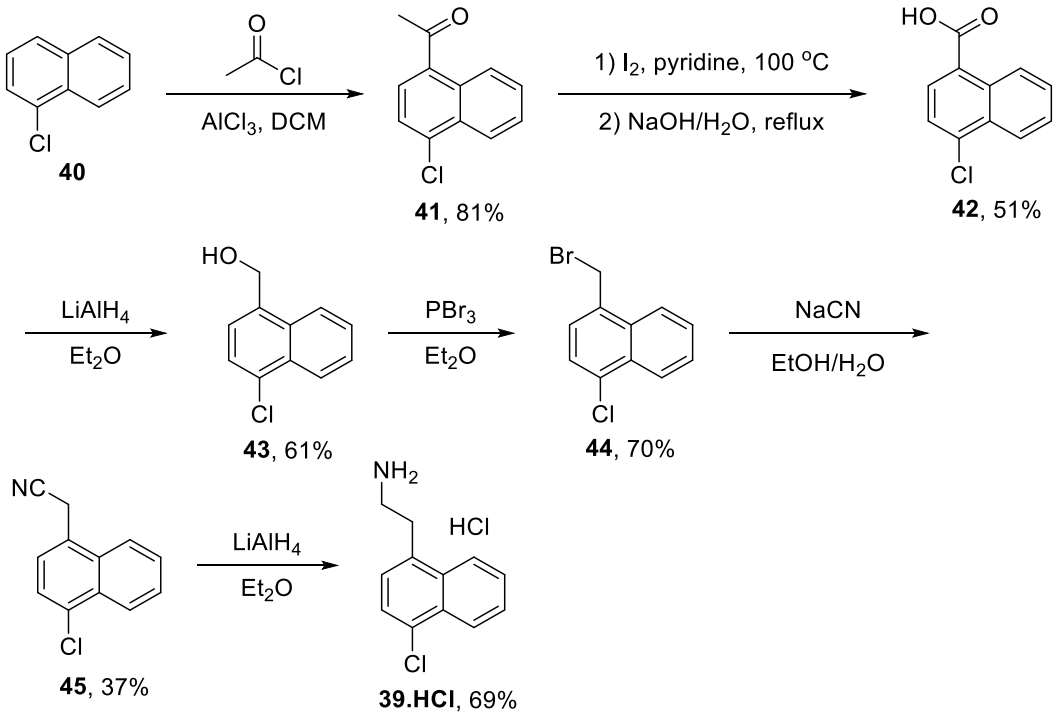

Scheme 2.5 Synthesis of naphthalene derivative **39** from commercially available starting material 1-chloronaphthalene **40**.

2.4.4. Testing of **39**

Naphthalene derivative **39** was submitted to the same fluorescence polarisation assay as previous fragments. This showed an inhibition of >500 µM, not showing an improvement.

A crystal structure was also obtained of **39** binding in the interface pocket. This was interesting as it displayed a binding mode than had not been expected (Figure 2.17).

Looking at the crystal structure of NMR154L, it was predicted that the naphthalene core would straddle the length of the pocket with the chlorine protruding into the depth of the pocket and the ethylamine making electrostatic interactions with Asp37.

However, compound **39** has turned on its side to bind into the pocket. The unsubstituted ring of the naphthalene core now explores the depth of the pocket. This leaves the ethylamine to bind with Asp37, as predicted, and the chlorine pointing into the length of the pocket (Figure 2.17). This suggests that the pocket may be able to accommodate a larger molecule into its depths as well as its length.

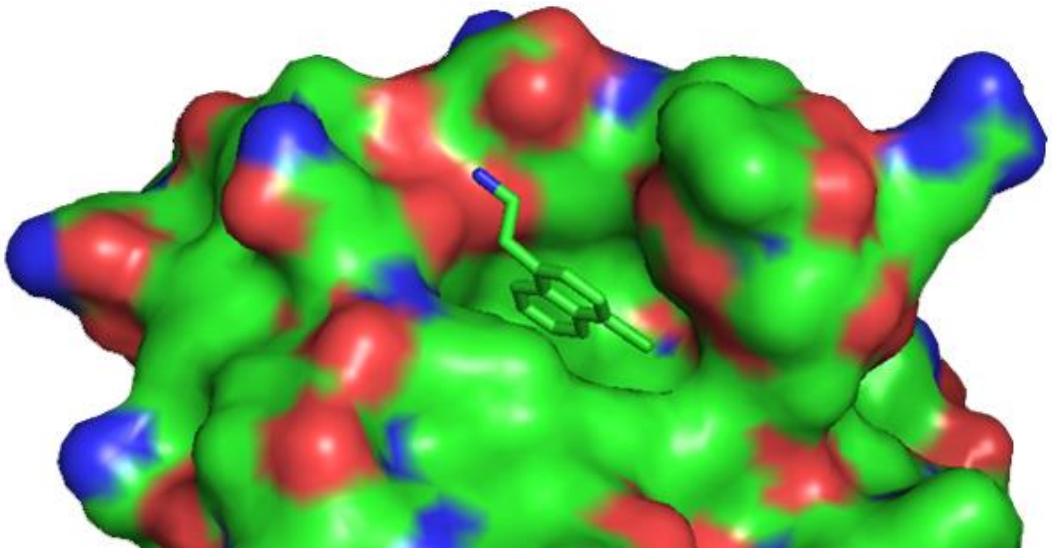

Figure 2.17 Crystal structure of compound **39** in the interface pocket of CK2α.

2.5. Expanding bis(ethylamino) fragments

2.5.1. Synthesis of precursors

With the success of adding a second ethyl amino group to NMR154L, it was investigated whether adding additional alkylamine groups to other fragments, such as naphthalene **39**, would also lead to improved binding.

This presented a challenge due to the lack of an appropriate synthetic handle on the naphthalene scaffold. A C-H activation paper by Giri and Yu offered a way of selectively installing a carboxylic acid group *ortho* to a pre-existing carboxylic acid using Pd catalysis and a CO atmosphere (Scheme 2.6).[123]

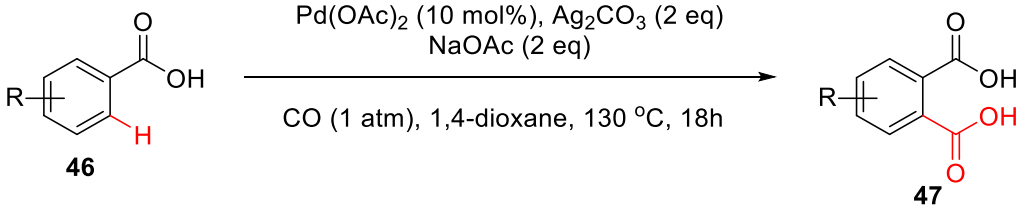

Scheme 2.6 Summary of Giri and Yu's work to install a carboxylic acid group *ortho* to a pre-existing carboxylic acid.

The advantage of using this work is that with the two carboxylic acids installed, the same chemistry to synthesise **29** can be followed.

Additionally, it was decided to pursue this methodology in tandem with further elaborations at the *ortho* position. If an acetylene moiety could be installed there, then its pluripotent functionality could be further transformed into a number of different groups.

It was hoped that the acetylene functionality could be easily installed through a Sonogashira cross coupling. The synthesis began with commercially available 2-bromo-4-chlorobenzoic acid (**48**) which was readily esterified to give methyl ester **49** for the cross-coupling. The acetylene was installed after experimenting with a few conditions. The conditions previously used by the authors did not afford the desired product (Table 2.2, Entry 1).[124] When the reaction was repeated under reflux and double concentration, the reaction proceeded with only a 5% yield (Table 2.2, Entry 2). A literature procedure from Thorand and Krause was then tried. These conditions used similar reagents to the previous one, however less base and CuI were employed, five-times the amount of $Pd(PPh_3)_2Cl_2$ used, a catalytic amount of PPh_3 added, and it was performed at a slightly higher concentration.[125] This unfortunately only returned starting material (Table 2.2, Entry 3). However, repeating the reaction under reflux gave the desired product, **50**, in good yield (Table 2.2, Entry 4).

Table 2.2 Screen of conditions to install TMS acetylene on benzene core.

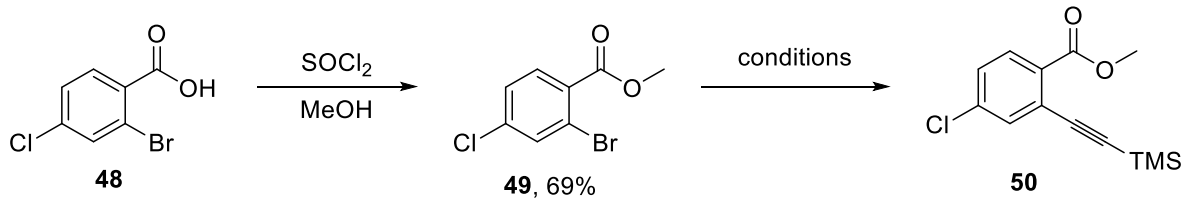

Entry	Conditions	Yield
1	NEt_3 (8 eq), CuI (10 mol%), $Pd(PPh_3)_2Cl_2$ (1 mol%), THF (0.1M), 130 °C[124]	SM Returned
2	NEt_3 (8 eq), CuI (10 mol%), $Pd(PPh_3)_2Cl_2$ (1 mol%), THF (0.2M), reflux[124]	5%
3	NEt_3 (1.5 eq), CuI (1.2 mol%), $Pd(PPh_3)_2Cl_2$ (5 mol%), PPh_3 (2.5 mol%), THF (0.25M), RT[125]	SM Returned
4	NEt_3 (1.5 eq), CuI (1.2 mol%), $Pd(PPh_3)_2Cl_2$ (5 mol%), PPh_3 (2.5 mol%), THF (0.25M), reflux[125]	79%

Ester hydrolysis and TMS deprotection were then carried out simultaneously to yield the desired 4-chloro-2-ethynylbenzoic acid (**51**, Scheme 2.7).

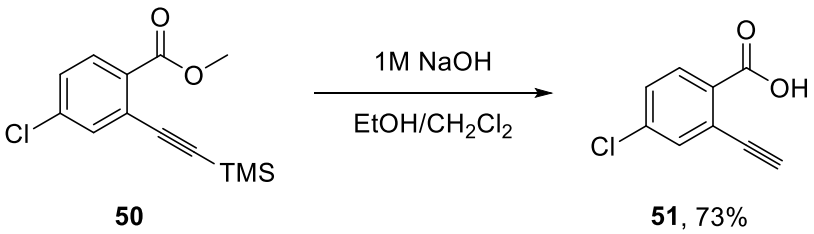

Scheme 2.7 Simultaneous ester hydrolysis and TMS deprotection to yield acid **51**.

With both **42** (chloronaphtholic acid precursor of **39** in Scheme 2.5) and **51** in hand, these were subjected to Giri and Yu's *ortho* carboxylation conditions (Table 2.3).

Table 2.3 Table summarising attempted *ortho* carboxylation of **51** and **42**.

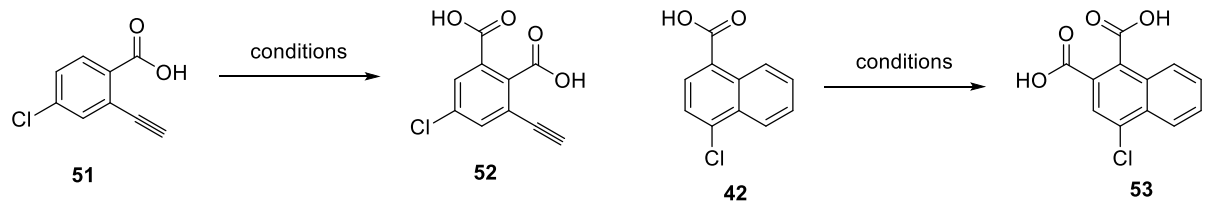

Entry	Conditions	Yield
1	$Pd(OAc)_2$ (10 mol%), Ag_2CO_3 (2 eq), NaOAc (2 eq), CO (1 atm), 1,4-dioxane, 130 °C, 18h	SM Returned
2	$Pd(OAc)_2$ (10 mol%), Ag_2CO_3 (2 eq), NaOAc (2 eq), CO (1 atm), 1,4-dioxane, 130 °C, 18h, sealed tube	Complex mixture

Despite several attempts to affect the conversion using the conditions outlined above, no pure product was isolated. Thinking this could be down to the difficulties with isolating vicinal diacids, the crude reaction mixture from the sealed tube experiment was submitted straight to methylation conditions in an attempt to form the di(methylester) which could be easier to separate. Unfortunately, the desired product was not isolated from the complex mixture that was returned (Scheme 2.8).

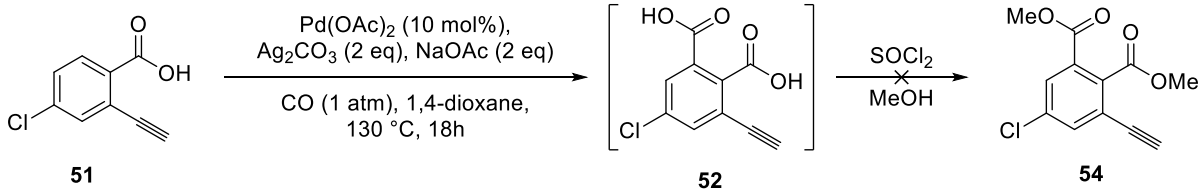

Scheme 2.8 Attempted isolation of diacid *via* diester.

2.5.2. Docking Studies

To assess qualitatively whether biaryl analogues of NMR154L would be good leads, a brief docking study was conducted with the structure of CK2. In this study, CK2β and residual water molecules were removed leaving just the CK2α subunit before energy minimisation was carried out.

From this result, a docking grid was placed over the interface site of the protein showing the area in which docking should take place. Into this model a variety of analogues of NMR154L and **39** were entered. These were transformed into 3D structures and their energy minimised.

With both the protein and compounds in hand, an SP docking glide was carried out and the program was asked to return the top 80% of hits. Each compound was returned with a 'docking score' shown in Figure 2.18. While these numbers holds little value in themselves, they can be used qualitatively against compounds known to dock to assess whether they may be worth making. As can be seen, all but compound **39** returned numbers similar to that of NMR154L.

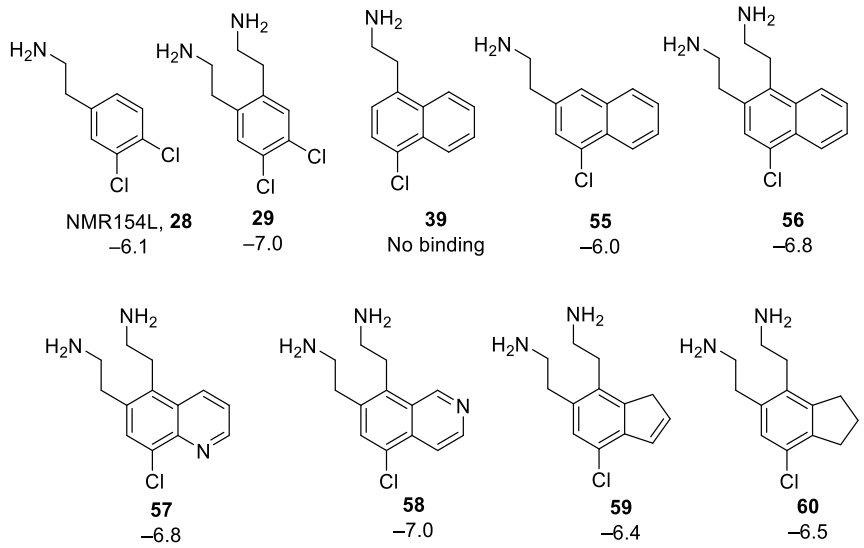

Figure 2.18 Series of molecules based on NMR154L with docking scores shown.

Interestingly, compound **39** was predicted not to bind by the computer. The reason in this case for the prediction of **39** not binding could be because the model predicted all the bicycles occupying the width of the pocket and did not explore its depth. In this way, the amine on **39** would not be able to bind with Asp37. The model perhaps underestimates the protein with regards to pocket depth or its flexibility to accommodate deeper ligands (**Figure 2.19**).

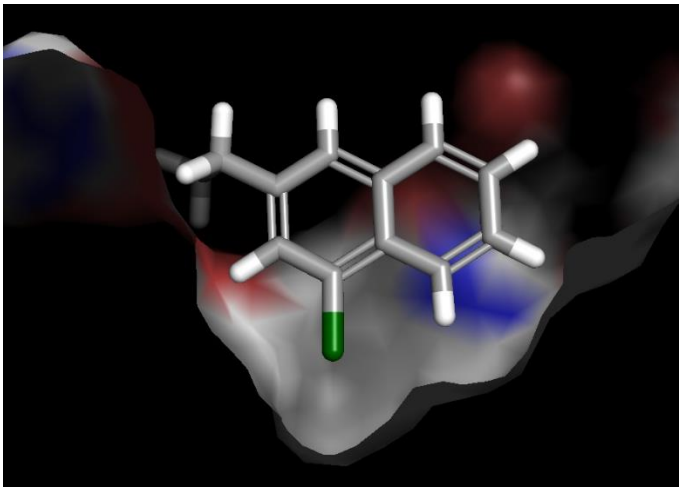

Figure 2.19 Example of how Maestro 10.2 predicted the bicycles would bind in the interface pocket (in this case compound **55**).

The bicycles with two ethyl amino groups proposed present more of a synthetic challenge than **29**. This is down to several factors: first of all, those compounds lack the symmetry seen in **29**, thus requiring a more regioselective synthesis. Secondly, due to the unusual substitution pattern of these bicycles, finding appropriate starting materials would be difficult. Thirdly, for the sake of atom economy and efficiency, a synthesis that could feature a late stage divergence to make all the structures would be desirable. However, a shorter synthesis of one compound could be achieved to test the validity of the model before embarking on a larger synthetic effort.

For the divergent synthesis, a cross-coupling reaction was the easiest to effectively introduce pyridine (for fragments **57** and **58**) and cyclopentene (for fragments **59** and **60**) into the scaffold. In this way, if a common disconnection could be found between all the structures, a common synthesis may be proposed. Work by Mamane *et al.* showed that similar aromatic systems could be synthesised by a indium (III) mediated cyclisation.[126] The reaction also has the benefit of positioning the chlorine at the desired position (Scheme 2.9). This worked by the indium coordinating to the alkyne, activating it for 6-*endo*-*dig* attack of the adjacent aromatic ring.

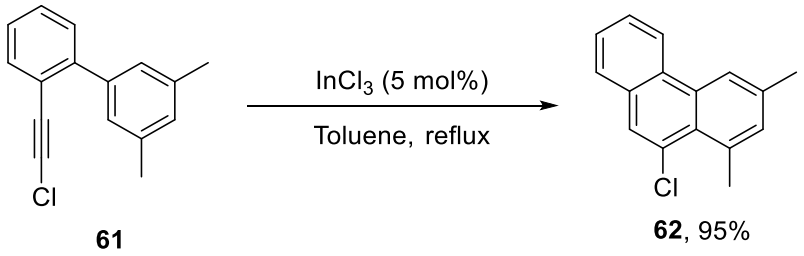

Scheme 2.9 Example of work from Mamane. Chloroacetlyene **61** is transformed into phenanthrene scaffold **62**.[126]

For our system, this would require synthesising an enyne with a pendant phenyl ring and groups which could be used later to produce the ethylamine functionality. There are established literature procedures for the synthesis of a chloroalkyne moiety from an aldehyde, and an α,β-unsaturated aldehyde from the corresponding unsaturated TBS protected alcohol.[126]

This leaves an obvious sp^2–sp^2 disconnection between the alkene and phenyl. Not only is this easily achieved through a Suzuki reaction, but it allows other rings to be added at this stage, including pyridine and furan, which form the basis for the other bicyclic systems that are to be investigated.

This leaves the key intermediate; an alkene with a bromine, methyl TBS-protected alcohol, and two groups which can be later functionalised into ethylamines (Scheme 2.10).

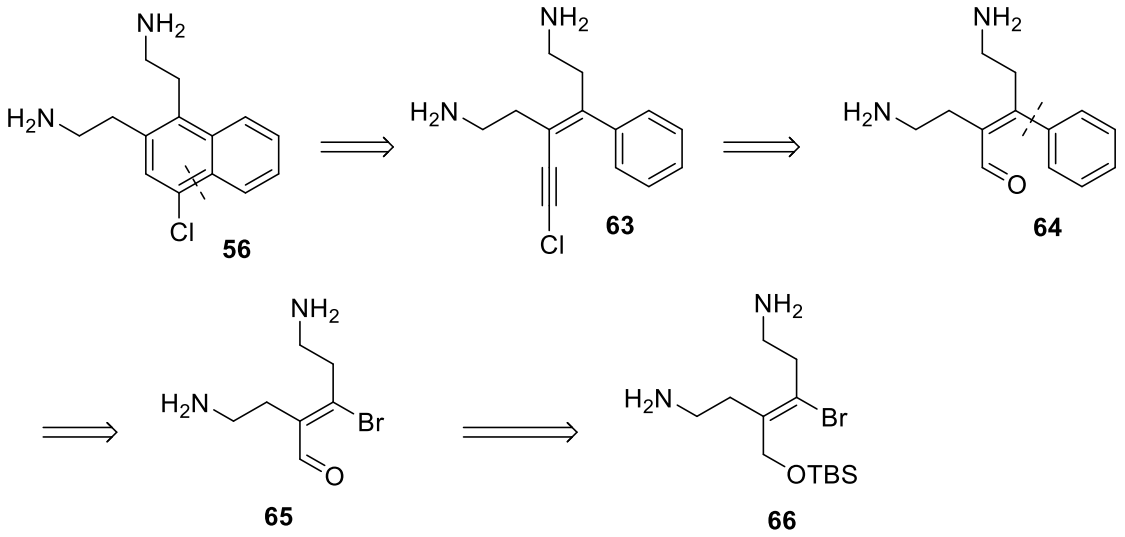

Scheme 2.10 Retrosynthesis of **66** to common intermediate.

The main challenge in synthesising this alkene is selectivity in the bond geometry. However, research from Wei-Jun *et al.* may provide an answer.[127] They showed that a cyclopropyl group at one end of an alkene may be selectively opened to install both a bromine and a tosyl-protected ethylamine in a single step (Scheme 2.11). In terms of selectivity, it was found that the bromine preferentially adds to the same side as the bulkiest substituent. The methyl TBS-protected alcohol is bulkier than a nitrile and so this should give the desired selectivity.

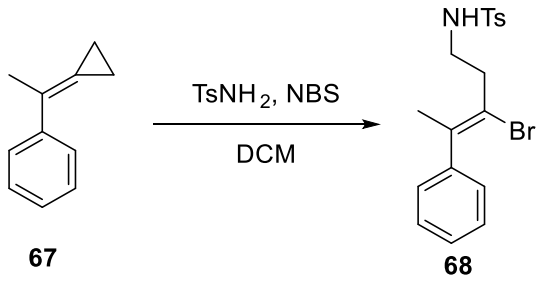

Scheme 2.11 Example of cyclopropane being opened to reveal bromine and tosyl protected ethylamine moieties.

This leaves a rather facile alkene to synthesise. The cyclopropane could be added *via* a Wittig reaction. Finally, this gives a ketone for which there is literature precedence that it can be made from a molybdenum (0) catalysed opening of an isoxazole. The total forward synthesis is summarised in Scheme 2.12.

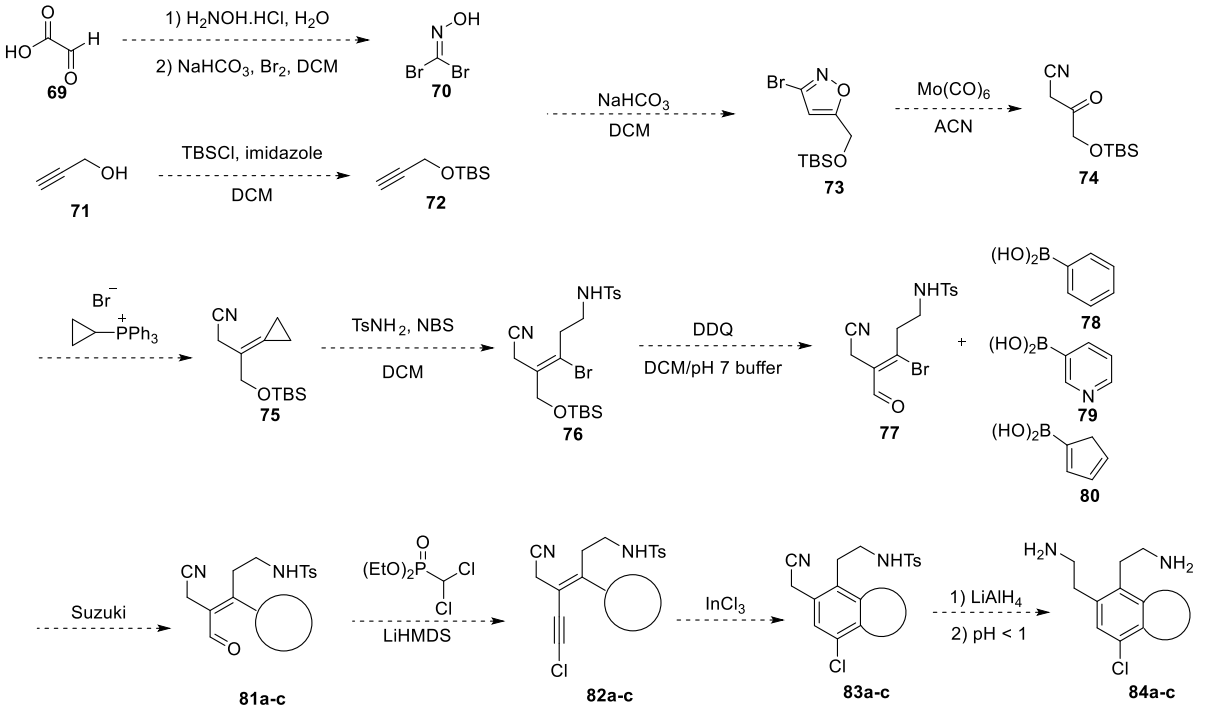

Scheme 2.12 General proposed scheme for the synthesis of the bicyclic series.

Forays were made into this synthesis to test its viability (Scheme 2.13). TBS protection of propargylic alcohol **71** is a standard procedure and proceeded without issues. 2-Oxoacetic acid (**69**) condensation with hydroxylamine followed by dropwise addition of elemental bromine, which led to the formation of dibromoformaldoxime, **70**. In the presence of base, the formaldoxime performed a 1,3-dipolar cycloaddition with the protected of propargylic alcohol to yield the bromoisoazole, **73**. Despite one example in the literature of this ring being opened with molybdenum (0), this methodology did not produce the desired result instead yielding a complex and inseparable mixture.[128]

At this point, another strand of research in the Spring Group discovered CAM187. This was derived from NMR154 and represents the best fragment inhibitor of the CK2 interface pocket with an IC_{50} of 44 μM (see Appendix D for the publication regarding this discovery).[68]

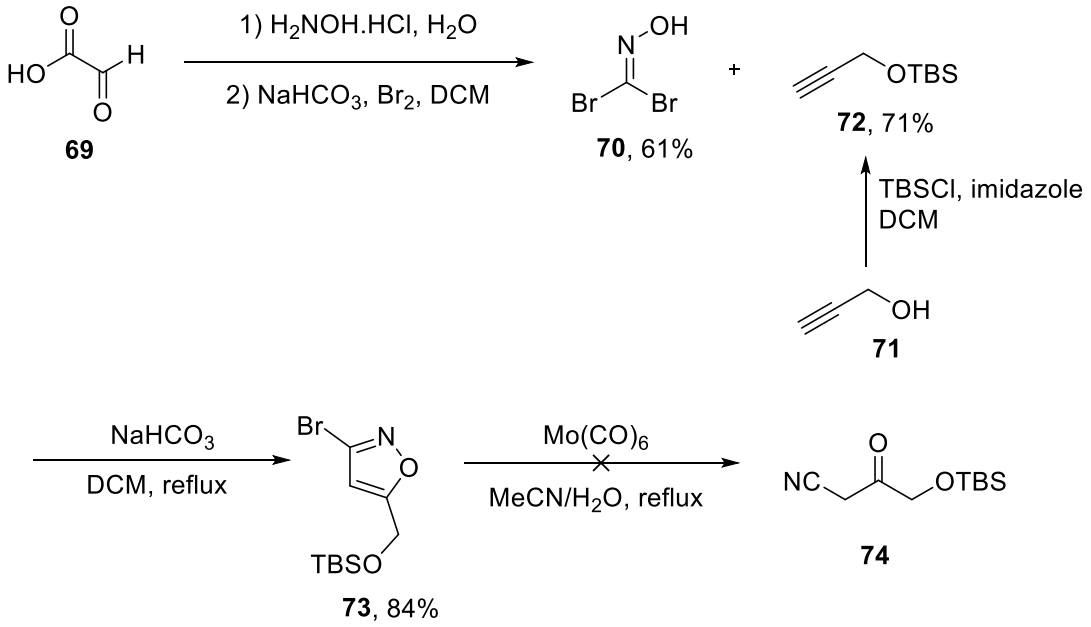

Scheme 2.13 Steps towards the synthesis of **74**.

2.6. Spirocyclic fragment series

2.6.1. Computer modelling

Work in the group had also been directed towards developing a new series of fragments based upon computer models of the interface pocket of CK2. To direct the synthesis of compounds likely to bind at this site, another member of the Spring Group, Dr Qingzhong Hu, created an *in silico* pharmacophore model.

Hu conducted the study of the pharmacophore in Molecular Operating Environment (MOE) 2014 version. In this model, the redundant protein copies in the crystal structure of CK2 holo-enzyme comprising CK2α and CK2β were removed. The CK2β subunit and water molecules were also removed. After the Amber10 force field was designated to the structure, hydrogens and partial charges were added via the Protonate3D module in MOE. A pharmocophore model was subsequently established *via* the structure-based approach. Employing this prepared structure followed the standard protocol with default parameters being adapted, which was followed by empirical manual modifications on the locations and confines of some pharmacophores. The virtual screening of the ZINC database[129] employing this pharmocophore model was performed using MOE with pharmocophores F1 and F2 being set as essential, and a spirocyclic compound **85** was identified as a hit. To further verify this hit, Hu docked compound **85** back into the prepared CK2α crystal structure with GOLD after being built and energy minimized in the Amber10 force field with MOE. The function of

automatic active site detection was switched on although amino acids composing the interface were also manually designated as the binding site, the radius of the active site was set to 19 Å and β4β5-loop was set to be flexible. The ligand was docked in 50 independent genetic algorithm (GA) iterations for each of the three GOLD-docking runs. Moreover, the GOLD score parameters were exploited, and the GA default parameters were set. The results were subsequently ranked according to fitness and compound **85** achieve a fitness score of 38.85. It was further evaluated with the LigX module in MOE and illustrated in contrast to the previously-identified fragment NMR154L as shown in Figure 2.20.

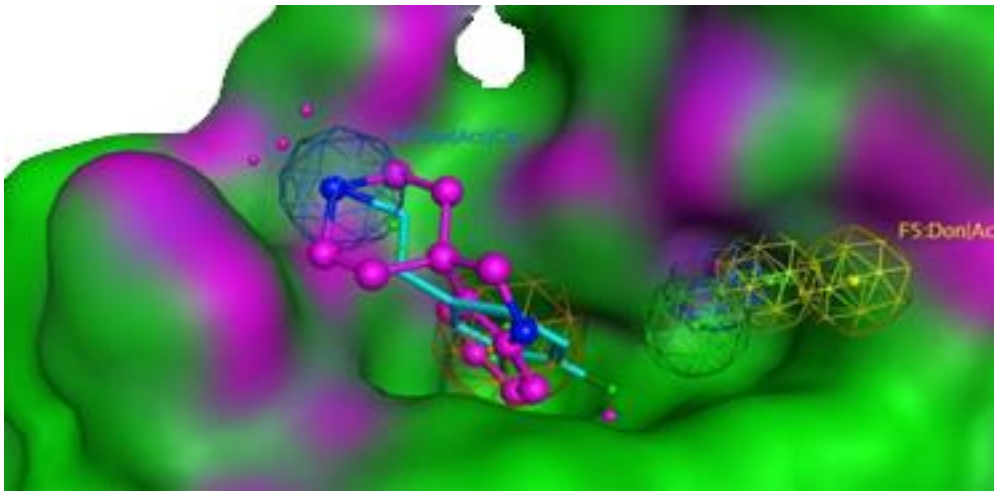

Figure 2.20 Compound **85** (in magenta) in α-β PPI pocket with previously known hit NMR154L (in cyan).

Based on the pharmacophore model producing a hit for spirocyclic compound **85,** a further library of spirocyclic compounds and fused ring compounds were proposed by Hu to see if these compounds validated the model. Through this, an inhibitor for CK2 was found (Figure 2.21).

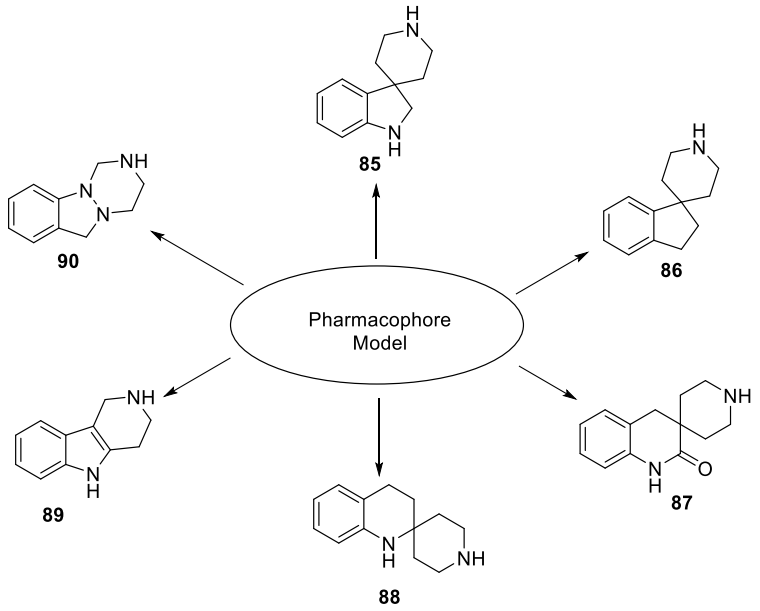

Figure 2.21 Products of the pharmacophore model.

2.6.2. Synthesis of compound **85**

Synthesis of spirocycle **85** followed the work of Zhu.[130] Bis(ethylchloro)ammonium chloride, **91**, was initially Boc protected (Scheme 2.14) to give **92** which could be used in the synthesis of three spirocyclic compounds in the series.

Initially, 2-(2-bromophenyl)acetonitrile, **93**, was reacted with sodium hydride. When compound **92** was added to the reaction this was expected to perform two S_N2 reactions at the methylene position forming a piperidine ring. Several attempts failed to yield the desired product, **94** (Scheme 2.14), returning the starting materials.

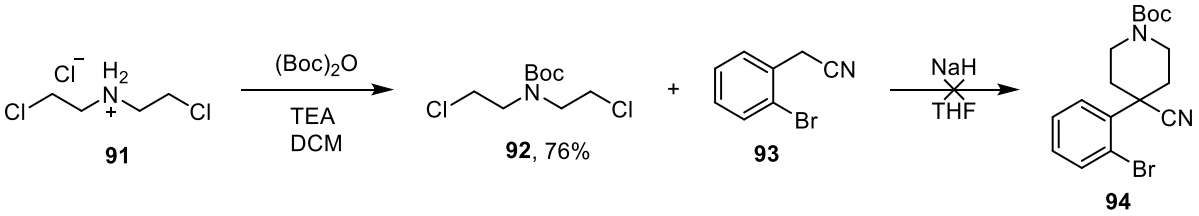

Scheme 2.14 Attempted reaction using a bromophenyl sequence.

The above procedure was repeated with the fluoro analogue, **95**. Again, base was added followed by bis(chloroethyl)amine **92** (Scheme 2.15). This formed a Boc-protected piperidine ring substituted at the 4-position with a nitrile and an *ortho*-fluorophenyl, **96**, which was deprotected to give **97**. In the presence of lithium aluminium hydride, the nitrile was reduced

to an amide anion, which performed an internal S_NAr at the fluorinated position, leading in one step to the formation of the indoline system and the spirocyclic centre, **85**.

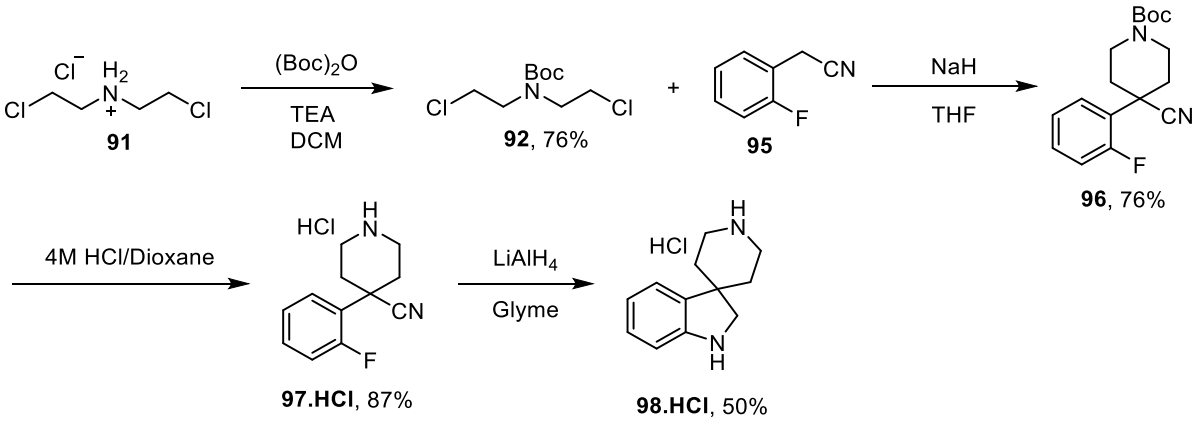

Scheme 2.15 Synthesis of compound **85**.

2.6.3. Synthesis of indane spirocycle **86**

The synthetic techniques of **85** could be employed for the synthesis of **86**. A benzyl protecting group was used on the bis(ethylchloro) amine as it was thought this could be removed in the same step as the hydrogenation of the double bond of the indene. The bis(ethylchloro)amine **91** was protected with a benzyl group to give **98** (**Scheme 2.16**). This was reacted with indene (**99**) using LHMDS in THF. The resulting spirocycle **100** was subjected to hydrogenating conditions of palladium on carbon in a hydrogen atmosphere. The alkene in the indene ring system was successfully reduced, however the benzyl remained, giving compound **101**.

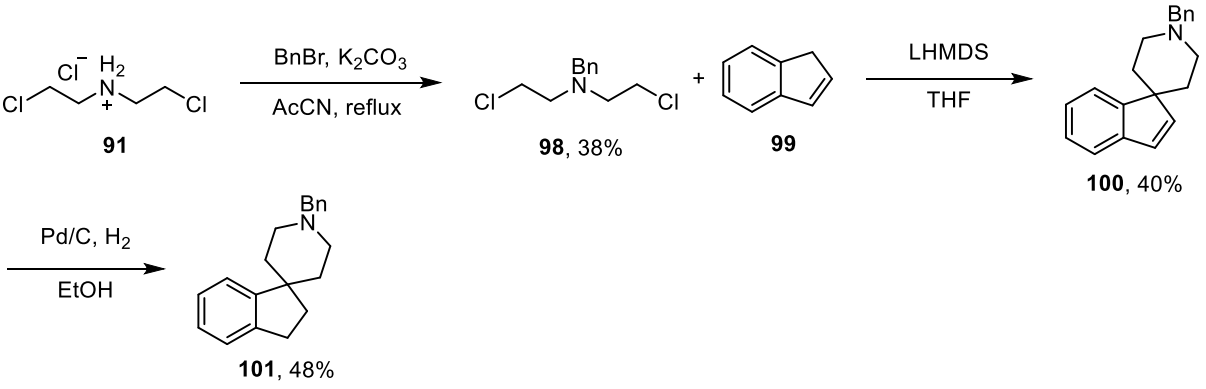

Scheme 2.16 Synthesis of benzyl protected spirocycle **101**.

Although desirable to simultaneously remove the protecting group and reduce the alkene, Boc-removal is a reliable reaction and this extra step could easily be used to reveal the desired product. Therefore **92** was reacted with indene in the presence of LHMDS to produce the Boc-

protected piperidine-indene spirocycle **102** (Scheme 2.17). Boc deprotection, giving **103**, followed in a facile and high yielding manner. Finally, **103** was hydrogenated using palladium on carbon to give **86** as the HCl salt.[131]

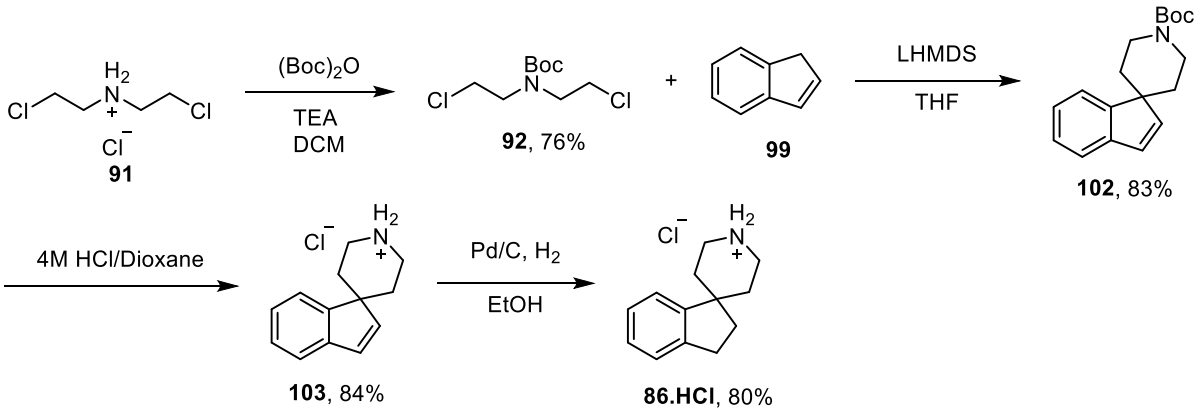

Scheme 2.17 Synthesis of **86**.HCl.

2.6.4. Synthesis toward spirocyclic amide **87**

Compound **87** has the spirocentre α to an amide. It was thought that this position could be sufficiently acidic to broadly follow the same procedure described above using two equivalents of base with **92**. To test this theory dihydroquinolone, **104**, was Boc protected, giving **105**, prior to being reacted with **92** and LHMDS. This reaction only returned starting material. Considering LHMDS may not be a strong enough base, the reaction was repeated with LDA made *in situ*. A product was isolated from this reaction. However, it was the dihydroquinolone dimer linked by a diethylamine moiety, **106**. It seems the tertiary centre was either too sterically hindered to be deprotonated or to perform the internal S_N2 (Scheme 2.18).

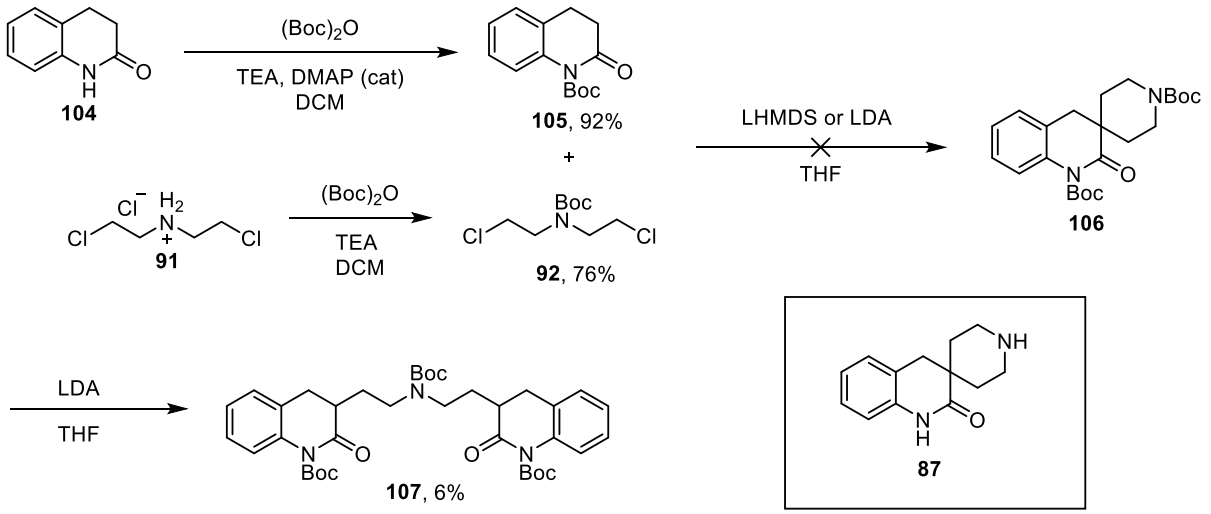

Scheme 2.18 Attempt to synthesise **87** from hydroquinolone.

A different strategy was employed to synthesise **87**. This was based on a patent by Bristol-Myers Squibb. To begin with, ethyl piperidine-4-carboxylate **108** was Boc-protected to give **109** (Scheme 2.19), which was then subjected to deprotonation at the tertiary centre. 2-Nitrobenzyl bromide **110** was added to this anion and an S_N2 occurred displacing the bromine, giving nitro-ester **111**. Hydrogenation was attempted to reduce the nitro to aniline **112**. Boc-deprotection with 4M HCl/dioxane proved to be messy, despite several attempts. Therefore, synthesis of this compound was put on hold subject to biological results from **85** and **86**.

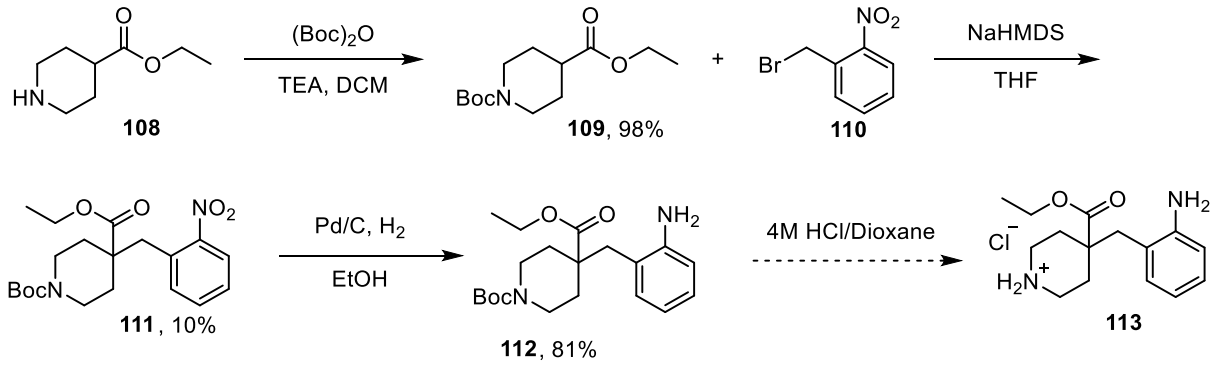

Scheme 2.19 Synthesis of **87**.

2.6.5. Initial Biological Results

Compounds **85** and **86** were submitted to a fluorescence polarisation assay. Unfortunately, neither compounds **85** nor **86** exhibited any inhibition of CK2α.

With these results in mind, work done by Dr Hu was re-evaluated. It was noted that the known hit NMR154L had a chlorine moiety protruding into the pocket. It was postulated that

this would increase the hydrophobic interactions and therefore aid in binding. Thus, a chlorine analogue of spiroindane **86** was designed (because this core was the most convenient out of **85**, **86**, and **87** to make). Additionally, instead of indole **89** a chlorine analogue of that indole was be made. It was decided not to pursue compounds **88**, **89**, or **90**.

2.6.6. Synthesis of chlorine analogue of **86**

Commercially available 6-chloroindanone **114** was easily reduced to give 6-chloroindene **115** (Scheme 2.20).[132] This was achieved by reacting 6-chloroindanone **114** with sodium borohydride, then taking the crude alcohol and heating it to reflux with *p*-toluenesulfonic acid. With chloroindene **115** in hand, the same procedure as the synthesis of **86** was used. The spirocyclic centre was formed with **92** to produce spirocycle **116.** The Boc group was removed to give salt **117**, and the alkene was reduced by hydrogenation, yielding the final chlorine analogue **118**.

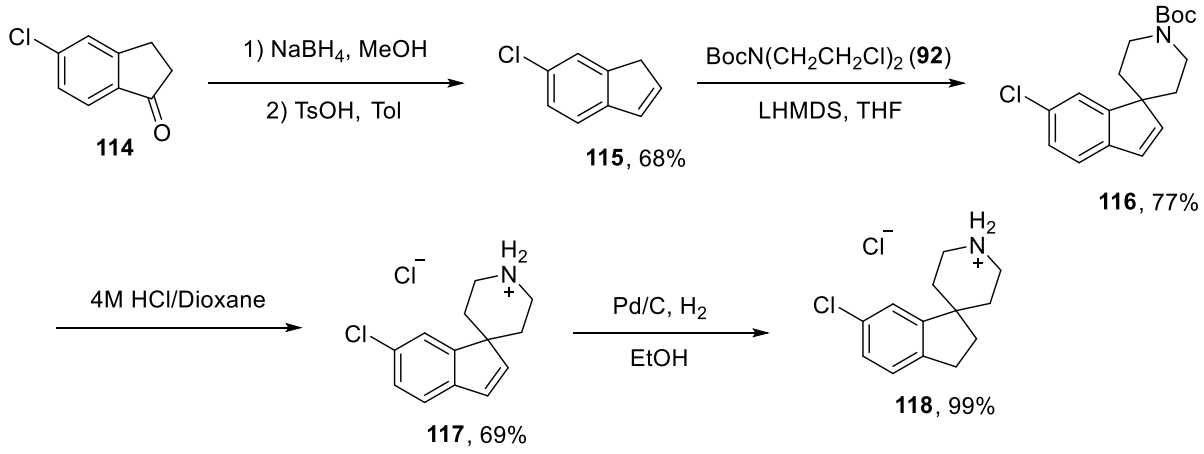

Scheme 2.20 Synthesis of **118**.

2.6.7. Synthesis of chlorine analogue of **89**

Finally, a tricyclic indole was synthesised. This was easily done *via* the Fischer indole synthesis between (4-chlorophenyl)hydrazine **119** and ethyl 4-oxopiperidine-1-carboxylate **120**. This produced indole **121,** which left only the removal of the ethyl ester by heating to reflux in base to give the desired product, **122** in two steps (Scheme 2.21).[133]

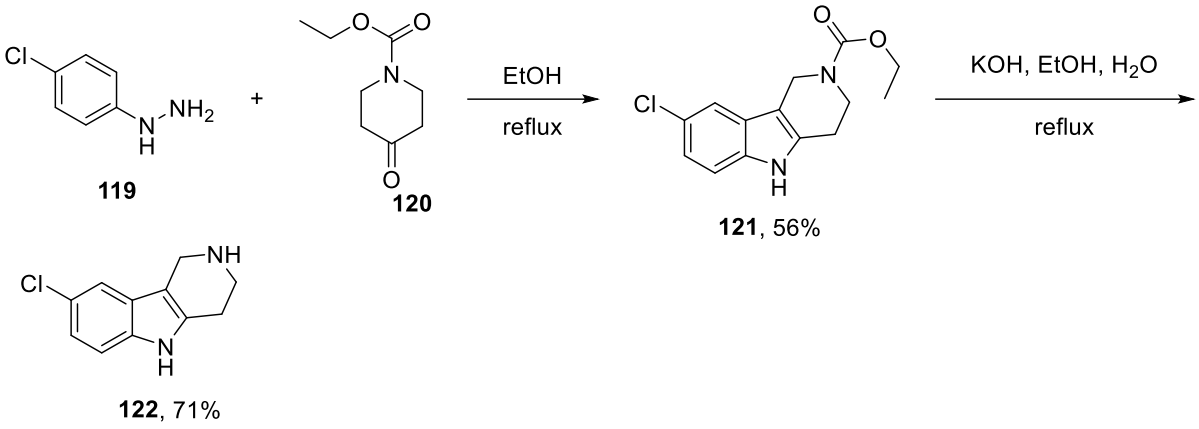

Scheme 2.21 Synthesis of **122**.

Compounds **118** and **122** were submitted to the fluorescence polarisation assay with CK2α. Unfortunately, like compounds **85** and **86,** they exhibited no binding on the interface site.

2.7. Conclusions

2.7.1. *In silico* modelling

This project produced three spirocycles and one tricycle from an *in silico* pharmacophore model. However, none of these compounds bound to the interface pocket of CK2. The model predicted that the aromatic core would anchor in the pocket while the piperidine would form an electrostatic interaction with Asp37. This is likely due to the rigidity of the spirocycle compared with the ethyl amino group of NMR154L, which did bind. The presence of aromatic chlorides may be excluded as a factor as the chloride analogues did not bind. Due to this, it would seem that a spirocycle scaffold is unsuitable for binding in the interface pocket of CK2.

2.7.2. NMR154L analogues

Elaboration of the NMR154L fragment from the *ortho* position proved more successful. With a second ethyl amino group, the IC_{50} was improved from 750 μM to 250 μM. Changing the benzene core of NMR154L to a naphthalene also produced a compound which bound at the interface. Attempts to find a facile way to install a vicinal di(ethyl amino) moiety on to the molecule proved unsuccessful.

2.7.3. Additional interface inhibitors

While the work in this chapter was being carried out, a series of other elaborations were made to NMR154 by substituting the *para* position of the benzene ring (Figure 2.22).

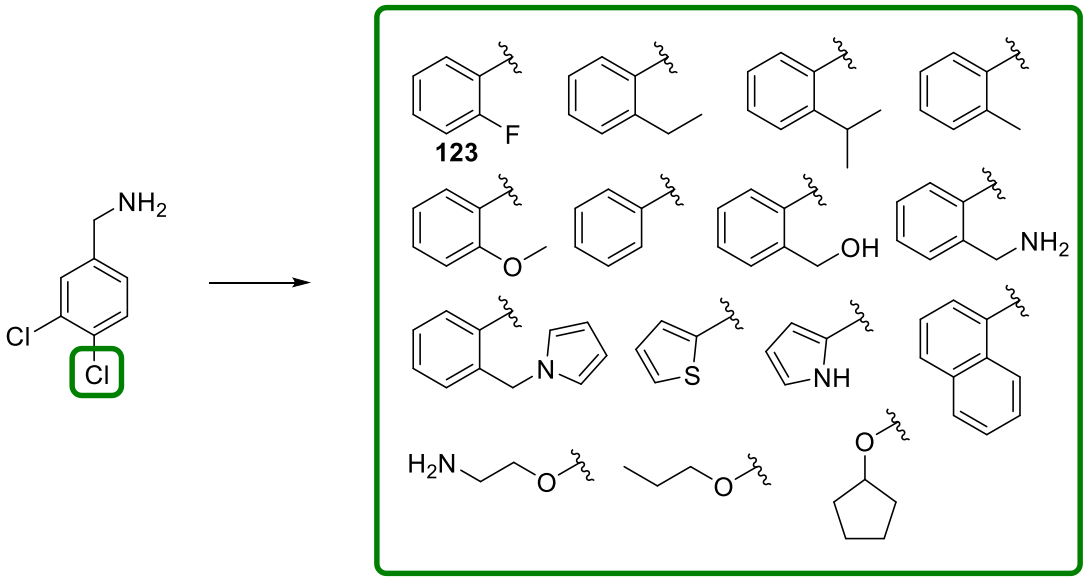

Figure 2.22 A series of mostly biaryl compounds as analogues of NMR154 by *para* substitution.

Of these, fragment **123** was the best binder at 150 µM incorporating an *ortho*-fluorophenyl moiety. Additionally, in a screen of compounds to bind in the αD pocket of CK2, the most potent inhibitor of CK2 at the interface pocket was discovered with an IC_{50} of 44 µM. This fragment was an analogue of NMR154 with an indole elaboration from the *meta* position (**124**).[68] This suggests that future work on small molecule inhibitors of CK2 at the interface pocket be directed towards development of this fragment.

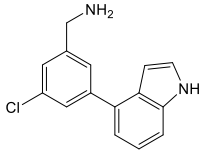

124, IC_{50} = 44 µM

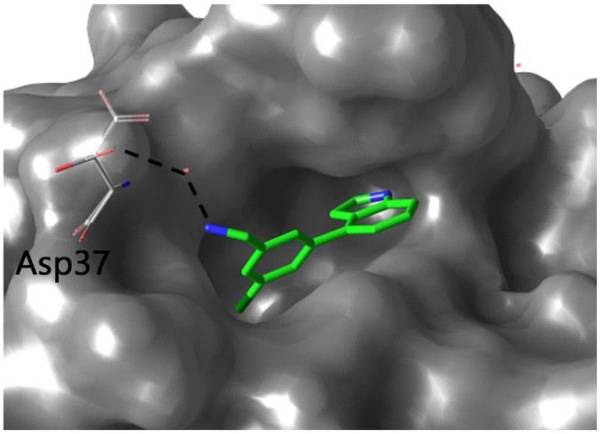

Figure 2.23 The most potent fragment inhibitor of the CK2 interface site.

Chapter 3

Spirocyclic fragment libraries

3.1. Introduction

3.1.1. The need for diversity

> An extremely important factor when searching for new drugs is the variety, or diversity, of chemicals available to screen.[43]
>
> This Essay is a call to increase chemistry research and investment into the design and synthesis of diverse fragment molecules.[72]
>
> The concept of chemical diversity is an essential component of the solution to this problem [the optimal composition of a screening collection], as it can theoretically be shown that a diverse, high-quality collection of compounds should yield more leads than, for example, a similar-sized combinatorial library of limited structural variation.[30]
>
> There are three main considerations in assembling a fragment library. Firstly, the properties of the fragments – they… should be as diverse as possible.[52]

The above quotes from the literature highlight the need for diversity in compound libraries to aid in drug discovery.

The hope was that a synthetic strategy could be devised to produce a diverse range of compounds—this strategy was developed in 2000 by Stuart Schrieber and has been term diversity oriented synthesis (DOS).[134]

This begs the questions: what is diversity? How to do we measure it? And how do we make diverse libraries? DOS is best understood when it is juxtaposed to its antithesis—target oriented synthesis (TOS). In TOS, the chemist has a specific type of compound or compounds in mind. The synthesis is usually convergent such that multiple reagents and reactants are brought together to form a single compound (or scaffold). The synthesis is usually contrived by retrosynthetic analysis with synthesis of the target as the primary goal. In DOS, a starting material is grown and modified by multiple reagents to create a collection of different molecules which are sufficiently different from one another. In this paradigm forward-

synthetic analysis is the primary driving force—there is no one target in mind but multiple. Synthetic handles and branch points are favoured to maximise the range of reactions that can be carried out (Figure 3.1).[135]

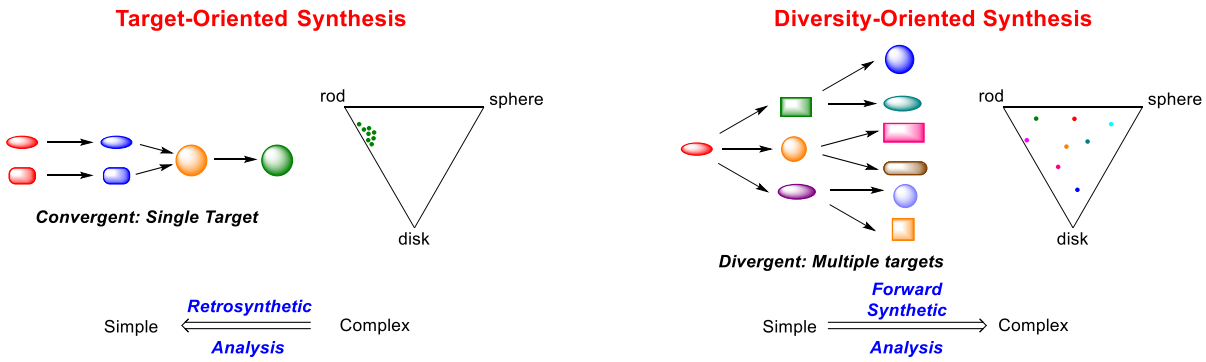

Figure 3.1 The difference between target-oriented synthesis and diversity-oriented synthesis.The grids of the right of each scheme depicting the chemical space covered by the TOS and DOS targets respectively.

TOS will often produce only one compound or a set of structurally similar compounds which only exhibit appendage diversity. DOS aims to incorporate:[136]

Structural diversity: that is the physical shape of the molecules in space are different. This requires synthesis to connect different parts of the starting material in different ways to build a variety of skeletal frameworks.

Stereochemical diversity: easy synthetic access to the different stereochemical orientations a scaffold can possess.

Functional group diversity: the molecules which occupy a wide range of physical space must also be able to display a variety of functionality (especially if their purpose be to probe biological targets). This means that it is important to incorporate a range of heteroatoms and functional groups into the molecule and its scaffold. Synthetically, this means starting materials should be selected for their ability to undergo an array of different transformations.

Appendage diversity: the scaffold of the molecules must allow for the easy addition of moieties. These are often important growth vectors in the hit-to-lead optimisation of drug discovery.

Of these scaffold diversity is perhaps the most important for a DOS library to focus on as it is the best way to maximise the three other types of diversity.[137–139]

3.1.2. Measuring diversity

With the principle of diversity established, the need arises for an appropriate way to measure diversity in compound libraries. Structural diversity can be most easily measured as numerical output of geometric properties. Advances in computer technology have made the measurement of spatial diversity easier.

One leading method for measuring the spatial diversity of compound libraries is Principle Moment of Inertia (PMI) analysis.[140–143] In this case the moment of inertia (**I**) is measured for a molecule about its three orthogonal principle axes. This gives each molecule three moments of inertia ($\mathbf{I_1}$, $\mathbf{I_2}$, and $\mathbf{I_3}$ in ascending magnitude). Since $\mathbf{I_3}$ is always greater than or equal to $\mathbf{I_1}$ and $\mathbf{I_2}$ these moments of inertia can be easily normalised by calculating $\mathbf{I_1/I_3}$ and $\mathbf{I_2/I_3}$. This also allows a spatial descriptor of the molecule to be displayed on a 2D cartesian plot of $\mathbf{I_1/I_3}$ vs $\mathbf{I_2/I_3}$.[137]

By considering the three extremes of 3D space: a rod, a disk, and a sphere, we can see that a PMI forms an isosceles triangle to represent chemical space. In one corner is (0,1) which are the coordinates for a rod (or acetylene chemically speaking), (1,1) are the coordinates for a sphere (adamentane), and (0.5,0.5) represent a disk (benzene), Figure 3.2.

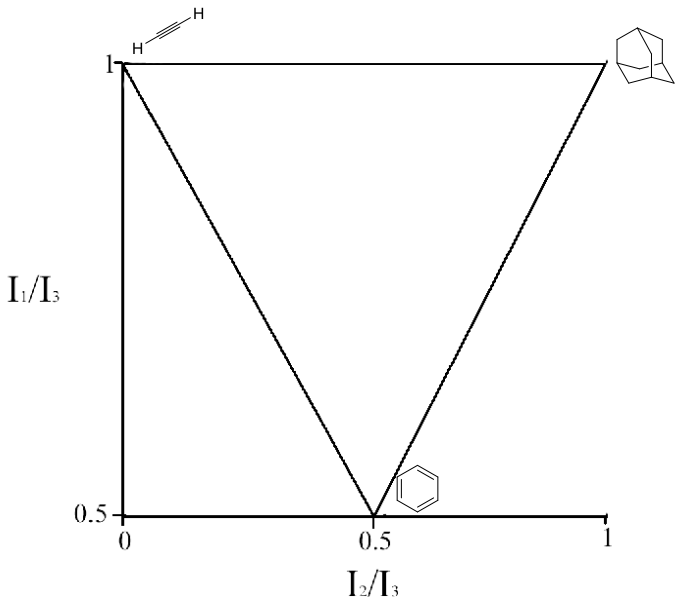

Figure 3.2 Graphical representation of a PMI plot showing acetylene, adamantane, and benzene on the three extremes of the triangle in which all molecular shapes fall.

In this way a compound library which is structurally diverse will seek to cover as much of the PMI plot as possible (Figure 3.3).

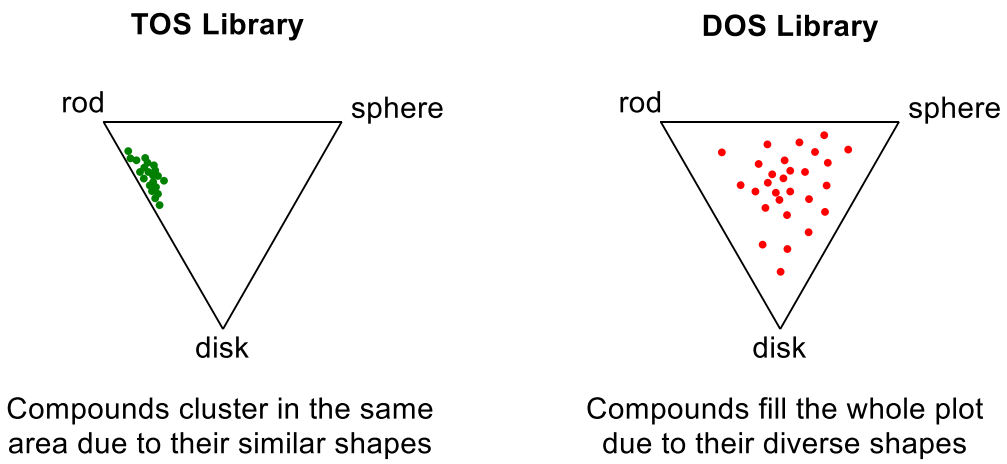

Figure 3.3 Comparison of predicted PMI plots of a non-structurally diverse TOS library and a structurally diverse DOS library.

Another useful descriptor of chemical space is the fraction of sp^3 centres (Fsp^3). This is expressed as the number of sp^3 carbons hybridised divided by the total carbon count of the molecule.[25] This is a good indicator of 3-dimensionality and the prevalence of aromatic rings. However, while molecules with a high Fsp^3 are likely to be more 3-dimensional, it does not follow that a low Fsp^3 necessarily means a flat molecule. For example, antifungal clotrimazole has a Fsp^3 count of 0.05, however because its structure is four aromatic rings around a quaternary carbon centre it is sphere-like (Figure 3.4).

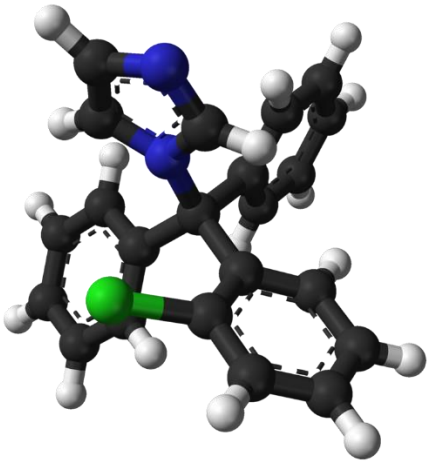

Figure 3.4 Clotrimazole: low Fsp^3 count but highly spherical in nature.

Another method of analysing diversity (or similarity) of a library is principle component analysis (PCA). This allows selection of *n* molecular descriptors, which can be anything from the physico-chemical descriptors found in the RO5 to biological descriptors like data from

protein binding studies, to be plotted on a 2D graph. The power of PCA is that by taking linear combinations of the *n*-dimensional space, vectors of the descriptors can be projected onto a 2-dimentional cartesian axis. The axes are unitless but represent the variance in the data set. PCA results will therefore always depend on both the data set and the descriptors chosen, but the plots that are produced give useful insights as to how diverse a compound library is internally and compared to other libraries (Figure 3.5).[144]

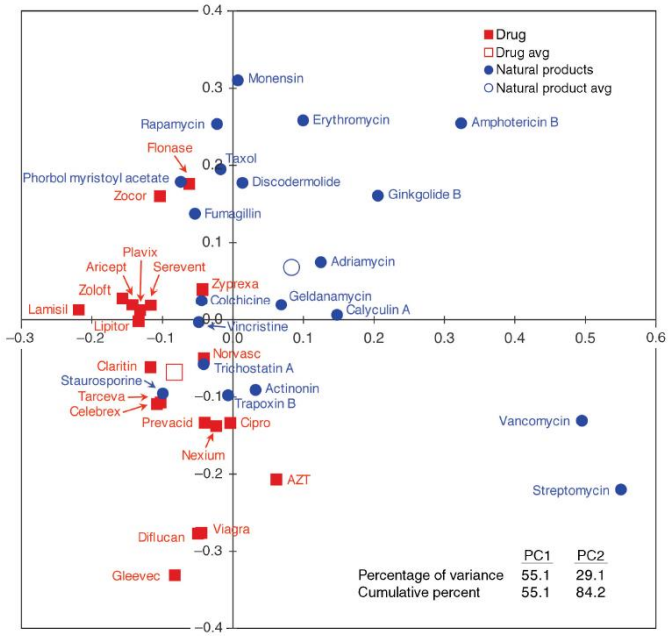

Figure 3.5 Example of PCA plot comparing a random selection of drugs (red) with a random selection of natural products. The principle components chosen were: molecular weight, clogP, hydrogen-bond donors, hydrogen-bond acceptors, rotatable bonds, polar surface area, stereogenic centres, nitrogen atoms, and oxygen atoms. There is greater variance in the natural product library then the drug library and both libraries are different from one another. (Image taken from ref 144).

3.1.3. Features of a DOS campaign

Two main synthetic strategies have been developed to enable efficient assembly of DOS libraries: a reagent-based approach and a substrate-based approach.

Reagent-based DOS sees a single starting material transformed into a diverse set of compounds by utilising both a large amount of in-built functionality, and pluripotent functional groups (i.e. a functional group that can be transformed into many others). These vectors are often folded, paired, and branched to generate the library.[145–148]

In the substrate-based approach, common reaction conditions are used on a series of starting materials which contain 'pre-encoded' skeletal information known as σ-elements which react to form a diverse array of scaffolds upon subjugation to the common reaction conditions (Figure 3.6).[145,149,150]

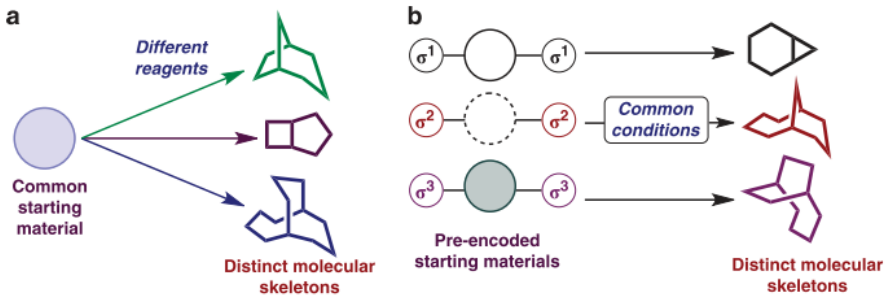

Figure 3.6 The two main strategies to generate DOS libraries: a) Reagent-based DOS wherein a common starting material for diverse scaffold from different reagents; and, b) Substrate-based DOS where pre-encoded starting materials form the DOS library from a common set of reaction conditions. (Image taken from ref 139).

Throughout most DOS strategies, however, a common synthetic plan of build, couple, pair (B/C/P) has emerged.[148] In this, initial building blocks are synthesised from commercial reagents. These are then coupled with each other or additional reagents to give a molecule appropriately furnished with orthogonal functionality. Finally, this functionality is utilised in the pair stage where different areas of the molecule are connected and folded to yield the diverse library (Figure 3.7).[139,148]

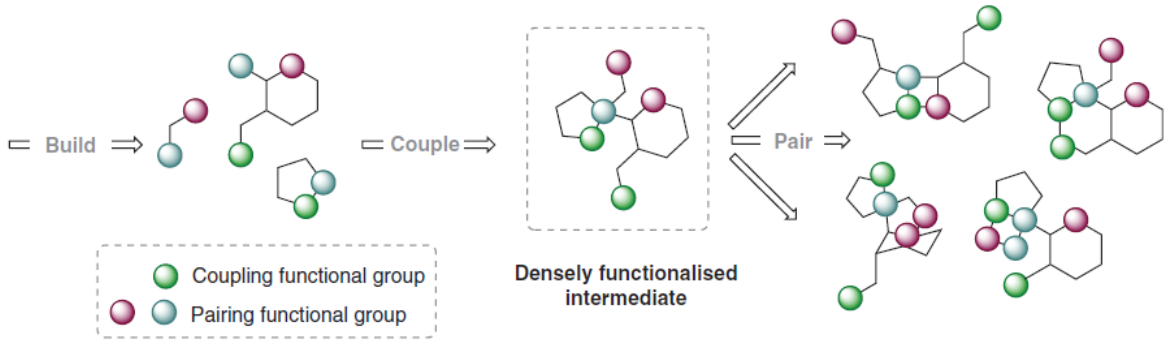

Figure 3.7 An archetypal scheme of the DOS build/couple/pair strategy (Image taken from ref 151).

3.1.4. Achievements of DOS

Despite only being conceived of around the millennium, DOS has had a number of successes in aiding drug discovery.[152–158]

For example, in the field of generating leads for novel antibacterial activity, DOS libraries have yielded some interesting compounds.

Starting from a reactive and pluripotent diazo ester Wyatt *et al*. rapidly generated a DOS library of 223 unique compounds covering 30 scaffolds.[159] Phenotypic screening revealed that 64 compounds (29% of the library) displayed growth inhibition against methicillin-resistant *Staphylococcus aureus* (MRSA). One of these compounds, Emmacin, was found to be particularly potent against methicillin-susceptible *Staphylococcus aureus* (MSSA) as well as to epidemic strains of MRSA, EMRSA-15 and EMRSA-16 (Scheme 3.1).[160]

Likewise, another reagent-based DOS campaign discovered a novel antibacterial called, Gemmacin. This DOS strategy started from a resin supported phosphoester. Using the B/C/P technique a library of 242 compounds with 18 molecular frameworks was built. Gemmacin and Gemmacin B (a benzene analogue) were discovered to also show good activity against MSSA, EMRSA-15, and EMRSA-16 (Scheme 3.1).[160,161]

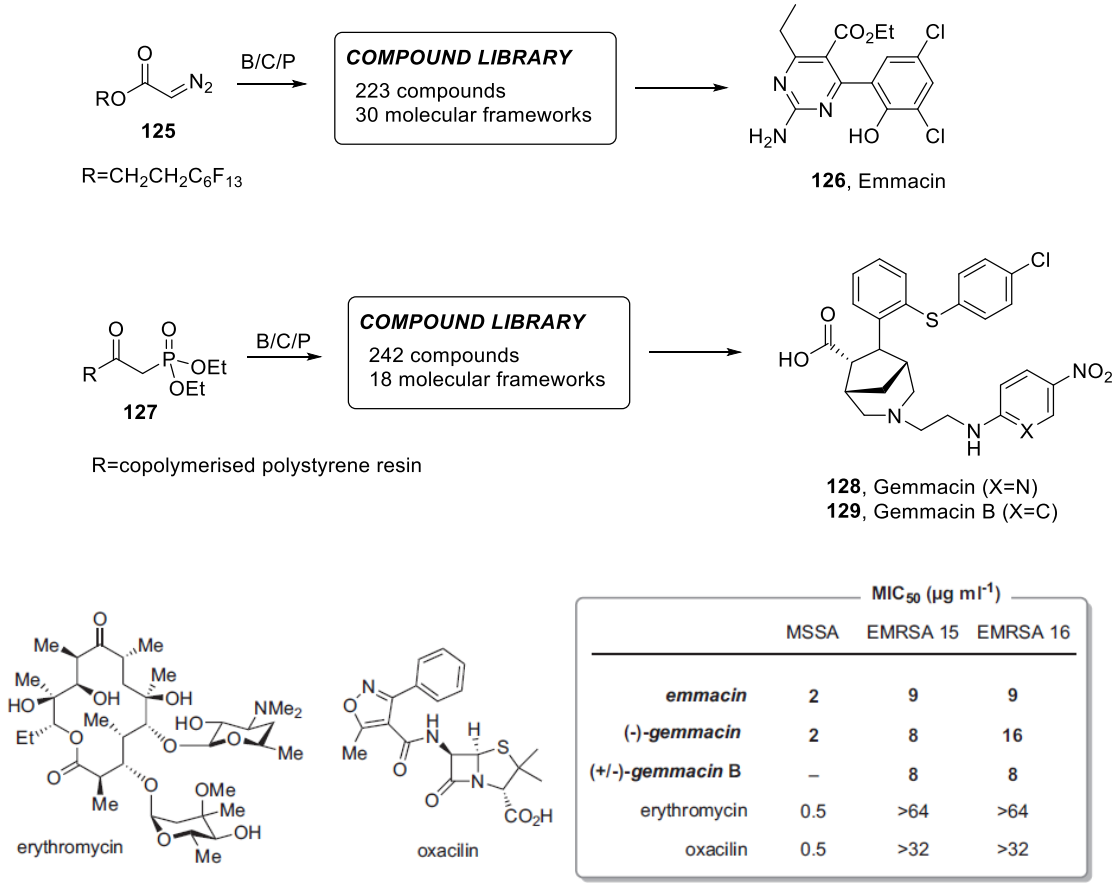

Scheme 3.1 Summary of the reagent-based DOS approaches which lead to the discovery of three novel antibacterials: emmacin, (–)-gemmacin, and (±)-gemmacin B (Image adapted from ref 151).

3.2. Gaps in fragment libraries

3.2.1. Expanding fragment space

DOS campaigns have shown the effectiveness of diversity when confronting complex biological problems (section 3.1.4). In addition, FBDD is a powerful technique to optimise the success in the hit-to-lead process (section 1.3.2). However, FBDD is only ever going to be as good as the fragments it screens. Can DOS provide FBDD with diverse fragment libraries?

Most fragment libraries lack 3D structural motifs and instead focus on sp^2-rich heteroaromatics.[162] This is not surprising given their commercial ubiquity and inherent aromatic stability. In addition, rapid growth in the field of metal-mediated cross coupling reactions have allowed researchers unprecedented access to otherwise unknown unsaturated scaffolds.[25,163] These flat libraries have led to advances in the field of drug discovery,[164,165] however, expanding the scope of fragment libraries would allow access to otherwise uncharted areas of chemical space.

3.2.2. Unsaturated rings in drug discovery

Rings are ubiquitous in pharmaceuticals with only 5% of marketed drugs not containing any kind of ring.[163]

Unsaturated ring systems are an effective way of installing complexity and 3-dimentionality into compounds. They are axiomatically more 3D than unsaturated (aromatic) ring systems and will also carry a higher Fsp^3 count. Given that 60% of drugs contain at least one sp^3 carbon in a ring, evidence exists that this area of chemical space is likely to contain biologically relevant compounds. Additionally, research from GSK has suggested that a high aromatic ring count negatively affects the prospects of drug-like compounds while hetero-aliphatic rings showed more desirable properties such as better solubility and reduced lipophilicity.[26,166] There is also a suggestion that molecules with a greater proportion of sp^3 atoms are more specific binders and so are less likely to be toxic due to off-target interactions.[167,168]

However, despite the prevalence of rings in chemistry and biology the number of structures explored remains limited. For drugs brought to the market before 2013 only 351 unique ring systems were represented across 1197 unique frameworks. However, innovation continues with, on average, 28% of new drugs containing a novel ring system.[74] The field is ripe for exploration especially focusing on 3-dimentionality in ring systems.

3.2.3. Spirocycles

Spirocycles, also known as spiranes, are an important and prominent class of unsaturated ring system which contain at least two rings joined at a vertex (via a single carbon atom). The presence of a spirocentre in organic compounds may give them some advantages when considering their application in pharmaceuticals. The spirocentre can introduce conformational rigidity, meaning that there would be a reduced conformational entropy penalty upon binding to a protein target. Furthermore, spirocycles have greater inherent three-dimensionality than fused (aromatic)ring systems which can prove advantageous over flat compounds that tend to have suboptimal physical properties.[169]

It should come a no surprise that this structural motif has been utilised in drug discovery.[170] As Figure 3.8 demonstrates, successfully marketed drugs containing spirocycles.

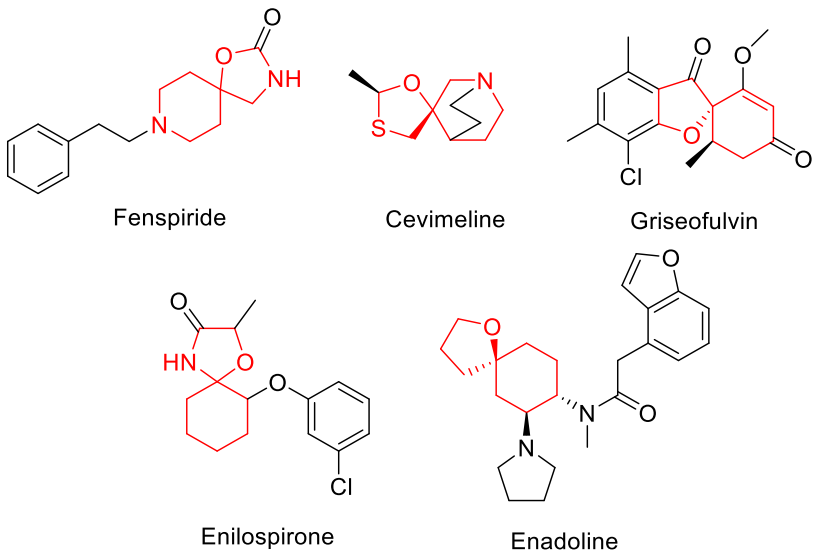

Figure 3.8 Examples of marketed drugs containing spirocycles.The spirocyclic scaffold is highlighted in red.

Spirocycles may be classified into three different classes.

Class 1: the isolated spirocyclic system where there is one or more spirocycle in a molecule and the molecule does not fall into the following two classes;

Class 2: the condensed spirocyclic system where by one or more rings containing a spirocentre is fused by an edge to another ring;

Class 3: the bridged spirocyclic system where the two rings in the spirocycle are additionally connected by bridging atoms.

These classes are demonstrated in Table 3.1. Each of these classes can be further subdivided by the number of spirocentres present.

Table 3.1 The three classes of spirocycle with example. The red bonds show the spirocycles, the green bonds show the condensed cycle and the blue bonds show the bridged cycle.

Class	Example skeleton
Class 1: isolated	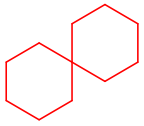
Class 2: condensed	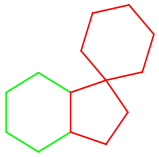
Class 3: bridged	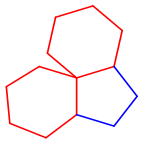

These spirocycles were analysed at their differing levels of complexity. The most basic level on which spirocycles can be analysed is their ring combination (RC). This is simply the size of the two or more rings in the spirocyclic system, ignoring all heteroatoms, multiple bonds, and appendages. The next level of complexity is the scaffold of the RC (SC[RC]), wherein the rings are furnished with their heteroatoms and multiple bonds. Above this in the hierarchy comes the scaffold of the compound as a whole (SC[CPD]) and finally the compound itself (CPD) (Table 3.2).[171]

Table 3.2 Table indicating the hierarchy of spirocyclic complexity.

RC	SC[RC]	SC[CPD]	CPD
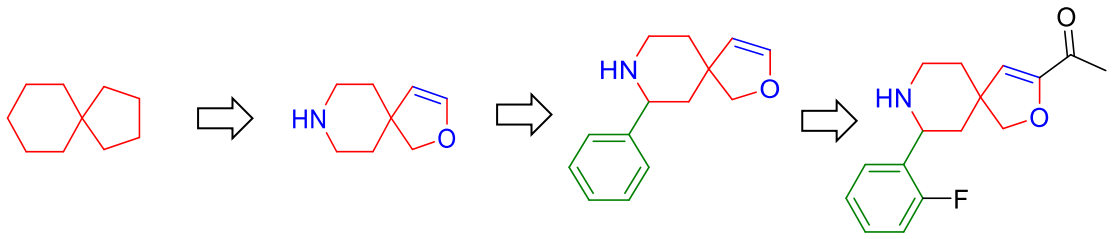			

Recent research on the ChEMBL chemical library has shown that 47,000 spirocycles are biologically active against approximately 200 targets.[171] Their distribution between the above three classes was assessed, alongside the number of spirocentres, and the size of the fused rings.

The researchers found that from their high confidence data series there were only 47 unique ring combinations which contained 1 spirocentre and 25 unique ring combinations which contained greater than 1 spirocentre. However, these had a combined activity against 548 targets (Table 3.3). Proving the field is ripe for research.

Table 3.3 Number of unique ring combinations (RC) for each class of spirocycle and the number of unique biological targets in each class.

Class	Unique RC (1 spiro atom)	Unique RC (>1 spiro atom)	Unique targets
1	20	3	219
2	18	8	240
3	9	14	89

The number of compounds targeted by the spirocycles varied from 1 to 20. These spirocycles also possess potent biological activity with over 60% showing a potency of at least 100 nM against one or more targets.

On more drug focused discovery, a range of 3-6 sized spiro rings have proved useful. For example, compound AM-5262 a spiro variant of AM-1638, a FFA1 agonist, showed a two-fold increase in potency from an EC_{50} of 0.162 μM to 0.081 μM. It also presented increased off-target selectivity against a panel of over 100 GPCRs, ion channels, transporters, and enzymes (Figure 3.9).[172]

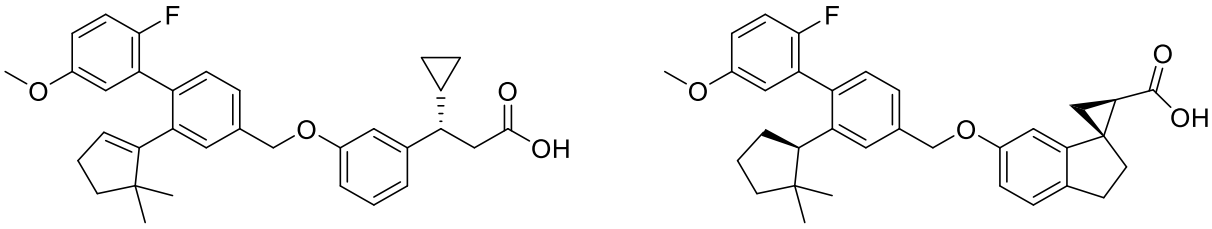

130, AM-1638 **131**, AM-5262

Figure 3.9 FFA1 agonists AM-1638 and AM-5262.

In terms of the variety of ring sizes, as to be expected, most of the spiro systems contained a six-membered ring joined to three to six-membered rings. Very few medium sized seven- or eight-membered rings were represented. This gives two interesting areas for research: one, seeing what scaffolds frequently occur in biologically active spirocycles and synthesising a diverse spirocyclic library based on these cores; and two, making entirely novel spirocyclic ring combinations in a diverse fashion.

3.3. Scope of this project

This project seeks to establish chemistry for the rapid assembly of diverse spirocyclic libraries using the divergent build/couple/pair (B/C/P) algorithm of DOS. The ideal synthetic route would allow for the greatest range of rings to be synthesised orthogonally from each other. In addition, the spirocycles synthesised should be as 'fragment-like' as possible and leave ample vectors for synthetic development.

To affect this, two synthetic routes were approached. The first installed two terminal alkene moieties onto a quaternary centre. Ring closing metathesis was used to close a ring between the alkenes and a range of other chemistry was used to produce the second ring of the spirocycle.

Secondly, cycloaddition reactions were exploited to form spirocycles. This required the synthesis of a ring wherein an *exo*-cyclic olefin can be easily installed. With this in place, a range of pericyclic coupling partners were used to furnish the second ring off the alkene, forming the spirocyclic library.

Finally, computational methods were explored to enumerate the library (finding the greatest number of compounds which could feasibly be made from the synthetic precedent) and decorate the library—finding which appendages and modifications would enhance the library's properties. A collaboration was also opened up with the Bender Group to perform

an *in silico* screen of the enumerated library, aiding any future *in vitro* biological testing of the molecules.

3.4. Glycine-based spirocycle library

3.4.1. Library strategy

The challenge in constructing a spirocyclic DOS library is finding a starting material which can be appropriately furnished to allow two separate ring forming reactions. These functional handles must be able to undergo several different reactions to form distinct scaffold ring combinations (SC[RC]), and ideally different ring combinations (RC). Hence a system which would allow easy divergence in the build stage, and a reagent-based DOS approach in the couple and pair stage, so that pluripotent functional handle can form a variety of rings.

Cheap and easy-to-handle pre-functionalised starting materials are ideal for building a DOS library. Due to this, ethyl glycinate hydrochloride (**132**) was initially selected as a starting material. This comes ideally equipped with an amino and ester group for use in the couple and pair stage. Additionally, the α-centre in **132** can be difunctionalised, meaning this carbon atom will be the vertex at which the two rings will join to form a spirocycle (Scheme 3.2).

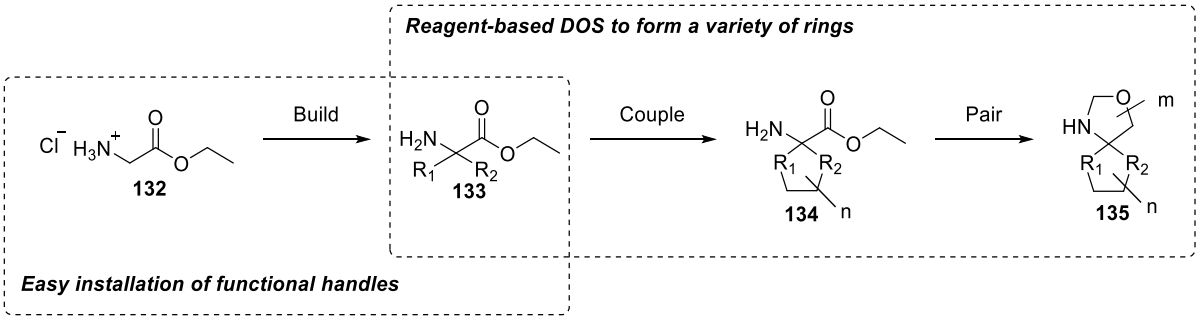

Scheme 3.2 Outline of DOS scheme to synthesise diverse spirocyclic library.

With the final pair stage requiring a form of amine and ester/ester derivative coupling, orthogonal functionalities were chosen for installation in the build stage. Ring closing metathesis (RCM) is a robust catalytic technique in the forming of small rings.[173] RCM uses a metallocarbene catalyst to connect two olefin moieties. Application to the above scheme would mean R_1 and R_2 are terminal alkenes. These were readily installed *via* S_N2 chemistry. When installed, a ring can be formed quickly by addition of a RCM catalyst, such as Grubb's second generation catalyst (Grubb's II).[174] This gives scope to vary the RC by adding a range of olefin homologues. Having two olefin functionalities to form the second ring also gives orthogonal functionality between the two ring-forming steps.

With this in mind, a broad synthetic strategy was devised. Ethyl glycinate hydrochloride (**132**) was furnished with two terminal olefins of varying length. Once installed, the first ring was formed *via* RCM, known as the tail. Then a reagent-based approach was used to form the second ring between the pendent amine and ester (Scheme 3.3), known as the warhead. This strategy allowed for sufficient scope to access a number of novel RCs and SC[RC]s.

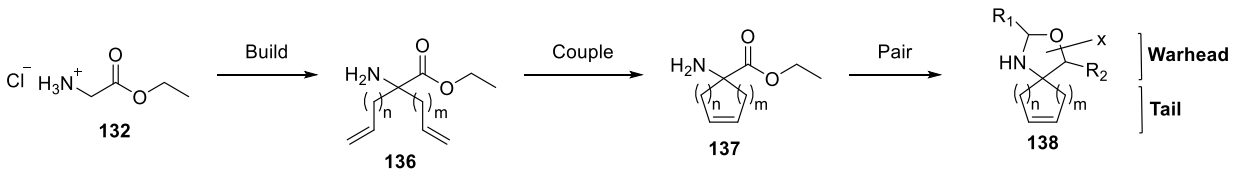

Scheme 3.3 General plan to synthesise a spirocyclic DOS library from ethyl glycinate hydrochloride (**132**) using RCM to synthesise the first ring and a variety of reagents to couple the amine and ester.

Once the spirocycles were installed, they were modified to make new SC[RC]s and explore their appendage diversity. The alkene on the bottom ring offered synthetic orthogonality to the top ring, making such processes easier.

3.4.2. Building the precursor

Established methodology allows for easy installation of the allyl moiety onto glycine.[175] Firstly, the amino group was simultaneously protected, and the α-carbon is activated, by condensation with benzophenone (**139**). The α-protons of this Schiff base (**140**) were acidic enough to be removed by base. This anion performed an S_N2 reaction, giving the alkylated product in good yield. It was chosen to install a but-1-enyl group and an allyl group. This formed a cyclohexene ring upon exposure to Grubbs II. But-1-enyl was installed first, leaving the more reactive allyl bromide electrophile to react with the tertiary anion formed from **141**. Both reactions proceeded smoothly and the acidic workup in allyl installation readily removed the benzophenone to reveal the free amine, **142** (**Scheme 3.4**).

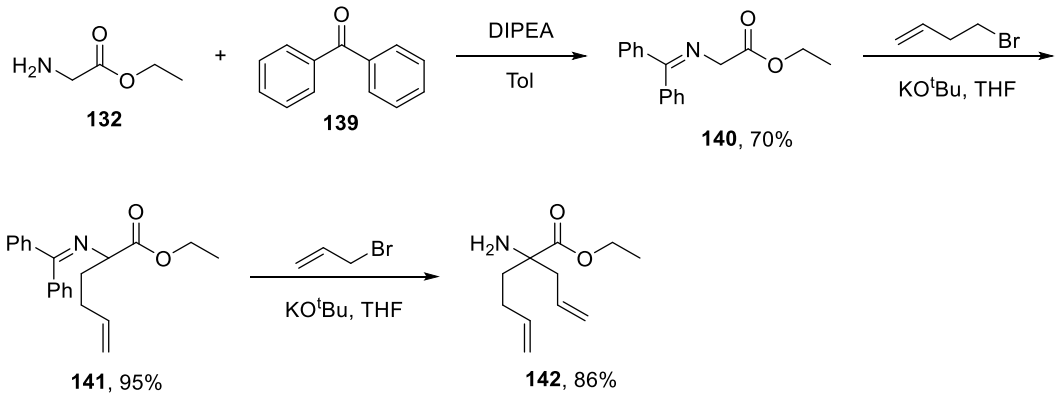

Scheme 3.4 Synthesis of glycine derivative **142**.

This strategy can be easily modified to install olefins of different length and pendent functionality onto glycinate ethyl ester.

3.4.3. Coupling and pairing to form spirocycles

With precursor **142** in hand, the warhead and tail rings were formed. As only the Grubbs II catalysed RCM is used to form the tail, whereas a variety of chemistry was to form a number of warheads, it was logical to form the tail ring first. Grubbs II, however, does not tolerate the presence of a primary amine in a reactant.[176] Therefore **142** was protected before exposure to Grubbs II. The *tert*-butyloxycarbonyl (Boc) protecting group was selected due to its ease of addition and removal, and the fact that the resulting carbamate group would tolerate Grubbs II.

Therefore, amine **142** was readily Boc-protected to give diene **143**, which was subjected to RCM with Grubbs II. This formed the tail ring as a cyclohexene derivative (**144**). While the amine was still Boc-protected, the ester was reduced to alcohol **145** for future warhead synthesis. With these reactions complete, the Boc protecting group was removed to reveal primary amine **146** as the HCl salt (Scheme 3.5).

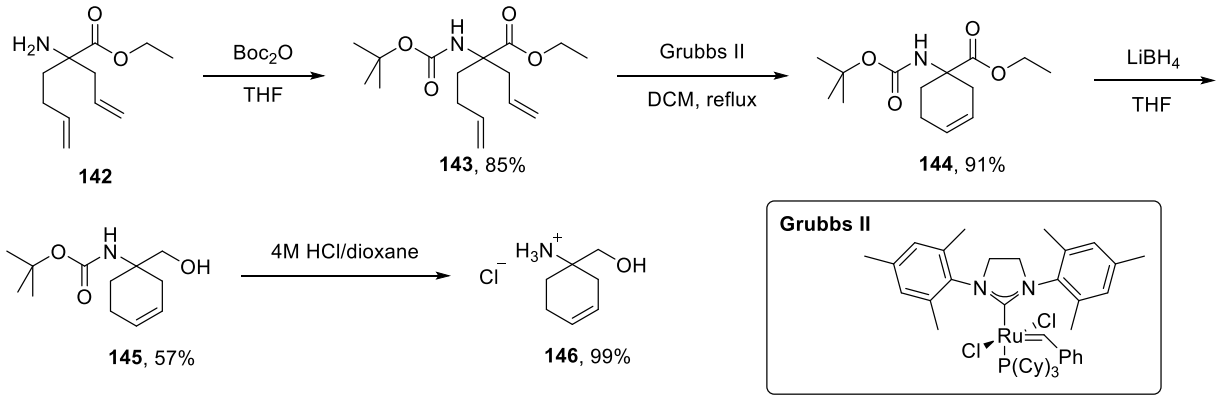

Scheme 3.5 Scheme showing the building of the cyclohexene tail of the library.

Due to the relatively low 57% yield in the reduction of ester **144** to alcohol **145**, it was seen whether reduction of diene **143** to an alcohol followed by RCM would be higher yielding. Reduction of diene **143** gave alcohol **147**, however in the more disappointing yield of 27% (Scheme 3.6). Therefore, RCM followed by reduction was used as the preferred route.

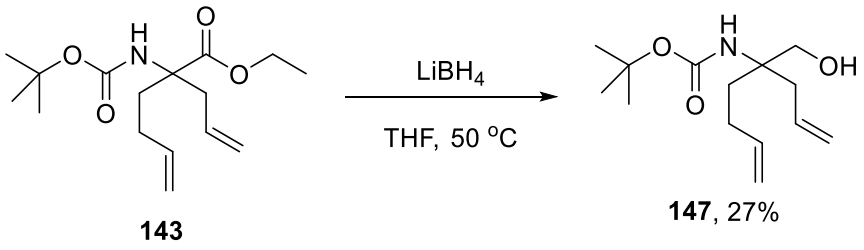

Scheme 3.6 Reduction of diene **143**.

3.4.4. Pairing to make the spirocycles

Before exploring the chemistry of amino alcohol **146**, it was noted that exposure of the Boc-protected precursor, **145**, to base caused internal displacement of the *tert*-butoxy group from the Boc, forming a oxazolidin-2-one spirocycle, **148** (Scheme 3.8).

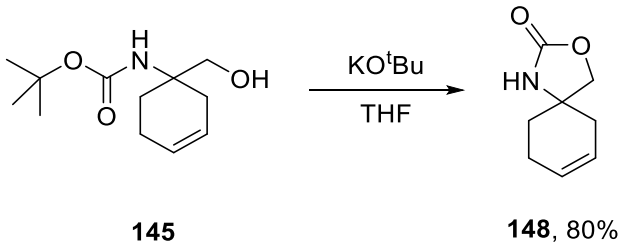

Scheme 3.7 Synthesis of oxazolidine-2-one spirocycle, **148**.

Examples of the nitrogen in **148** acting as a nucelophile are well precedented in the literature.[177] Therefore, it was explored whether cross-coupling straight to an aromatic centre would increase the scope of **148** to be grown with a variety of aromatics. The Goldberg reaction was first tried. Although its scope was originally confined to aniline derivatives, this has recently been expanded to amides, and carbamates.[178,179] Thus, it was seen whether the nitrogen carbamate on spirocycle **148** would be tolerated. Unfortunately, no product was obtained from this reaction; an inseparable complex mixture was returned. A literature procedure[180] was tried to couple a *meta*-acetyl phenyl to spirocycle **148**; this only returned starting material. Finally, conditions were tried to couple *para*-nitrile bromobenzene to **148** (Table 3.4).[181] One possibility for the failure of these reactions could be steric hindrance due to the adjacent spirocentre. Although there is literature for these reactions to be carried out next to a quaternary centre,[182] there is no precedent for the reaction next to a 3–7 membered spirocycle.

Table 3.4 Table of conditions for Cu mediated arylation of the carbamate nitrogen.

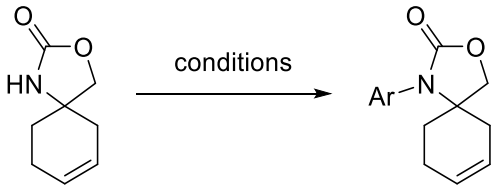

148

Entry	Coupling partner	Conditions	Yield
1	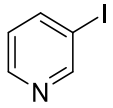	CuI (50 mol%), *N*^{1},*N*^{2}-dimethylethane-1,2-diamine, Cs_2CO_3, dioxane, 90 °C, 16 h	Complex mixture
2	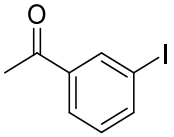	CuI (10 mol%), trishydroxymethyl ethane, K_3PO_4, dioxane, DMF, 110 °C, 72 h	SM
3	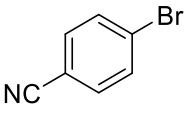	CuI (5 mol%), *N*,*N*-dimethylglycine, K_2CO_3, DMF, 120 °C, 16 h	SM

Warheads derived from amino alcohol **146** were subsequently explored. Multiple reactions can be carried out with vicinal amino alcohols to form rings as well as other precursors in the synthetic steps to make **146**. First of all, **146** was condensed with imidate **150** to give spirocycle

151 containing a dihydrooxazole ring (Scheme 3.8). This procedure allows for ready substitution of phenyl in **151** or other groups due to the ease of the imidate synthesis from nitriles.

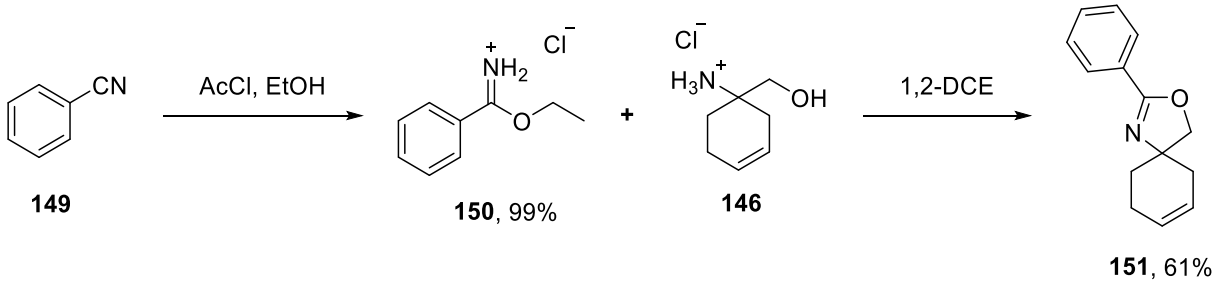

149 **150**, 99% **146** **151**, 61%

Scheme 3.8 Synthesis of dihydrooxazole spirocycle.

In a similar manner, an amine substituted dihydrooxazole spirocycle was synthesised by exposing amino alcohol **146** to cyanogen bromide. This afforded spirocycle **152** (Scheme 3.9). This is an interesting motif containing an H-bond donor/acceptor pair similar to DNA base adenine, perhaps privileging it in biological interactions.

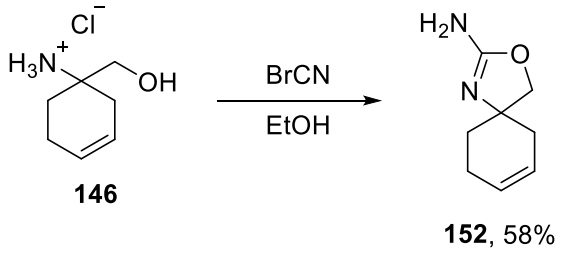

146 **152**, 58%

Scheme 3.9 Synthesis of amino-dihydrooxazole spirocycle **152**.

An X-ray structure of **152** was taken to confirm the desired product was made.

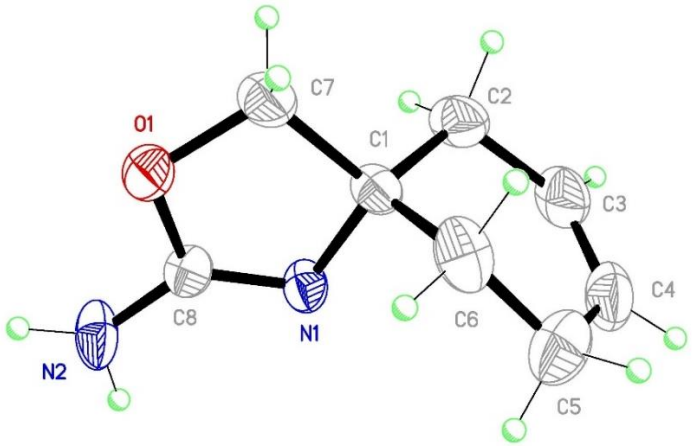

Figure 3.10 Crystal structure of the (*S*)–**152**.

It was assessed whether the exocyclic NH_2 group on **152** could be readily used as a synthetic handle. A patent was adapted to see if the biologically-relevant morpholine could be installed on the amino group.[110] A quick microwave experiment produced a complex mixture from which no discernible product was obtained (Scheme 3.10).

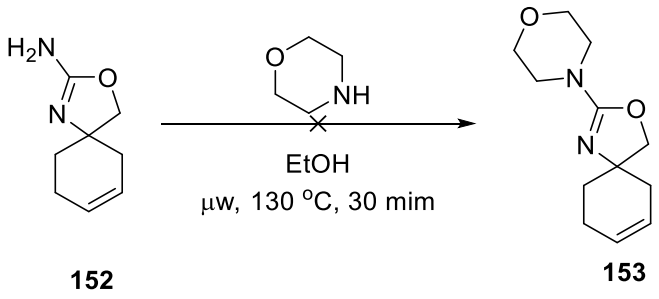

Scheme 3.10 Attempted installation of morpholine moiety onto **152**.

Following this, 6-membered rings synthesis of morpholine-derivatives was explored. Firstly, a few microwave reactions were tested. Amino alcohol **146** was subjected to microwave reaction with ethyl benzoylformate and α-chloroacetophenone to form dihydrooxazine-2-one (**154**) and dihydrooxazine (**155**) rings respectively. These would give an imine and/or ester functionality which could be a useful tool for further fragment growth. Unfortunately, neither of these techniques proved successful, even with increasing the number of molecular sieves used (Scheme 3.11).

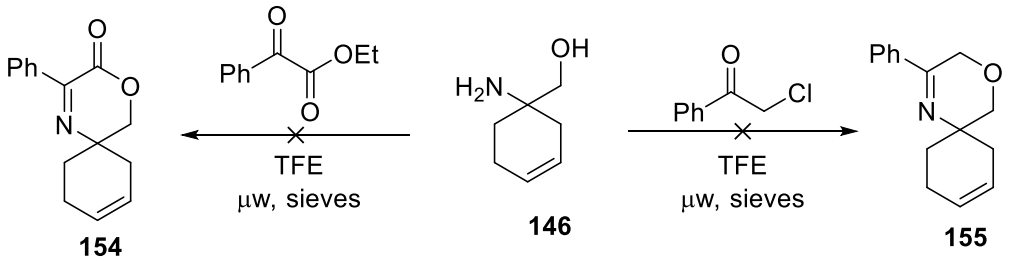

Scheme 3.11 Attempted microwave condensations to form spirocycles.

A stepwise approach was then tried; either first an imine condensation followed by an S_N2, or an S_N2 followed by an internal imine condensation. Starting from Boc-protected amino alcohol **145**, exposure to base and α-chloroacetophenone failed to yield the desired product; the fractions isolated by column chromatography being complex mixtures. Reaction of **146** with α-chloroacetophenone under Dean-Stark conditions also failed to yield the imine (Scheme 3.12).

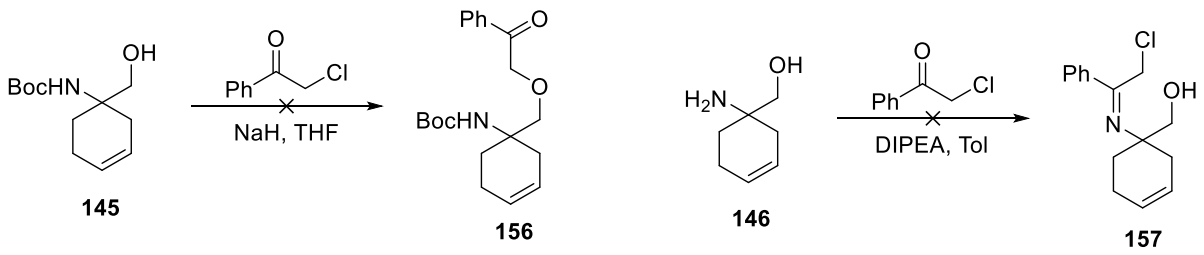

Scheme 3.12 Failed stepwise reactions to give spirocycle **155**.

Finally, it was postulated that synthesising the morpholin-2-one ring could be more fruitful. Following a literature procedure,[183] **146** was submitted to basic conditions and phenyl 2-bromoacetate. This gave spirocycle **158** with a morpholin-2-one warhead. With **158** in hand, this could be transformed in the desired dihydrooxazine-2-one warhead as well as a morpholine *via* reduction. Exposure of **158** to $Pb(OAc)_4$ readily oxidised it to dihydrooxazine-2-one spirocycle **159**. This has the advantage over similar spirocycle **154** in that it lacks the phenyl group and so allows greater scope in Cu-mediated nucleophilic addition into the imine (Scheme 3.13).

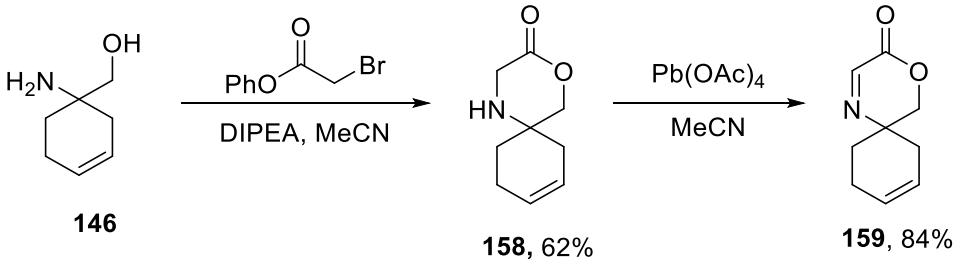

Scheme 3.13 Synthesis of morpholin-2-one spirocycle **158** and its subsequent transformation into spirocycles **159**.

Additionally, the regio-isomer of **158**, a morpholin-3-one spirocycle, was prepared by reacting **146** initially with chloroacetyl chloride. The more reactive primary amine formed an amide bond with the acid chloride, making compound **160**. Subsequent exposure to base allowed for an S_N2 reaction between the deprotonated alcohol and the chloride forming morpholin-3-one spirocycle **161** (Scheme 3.14).

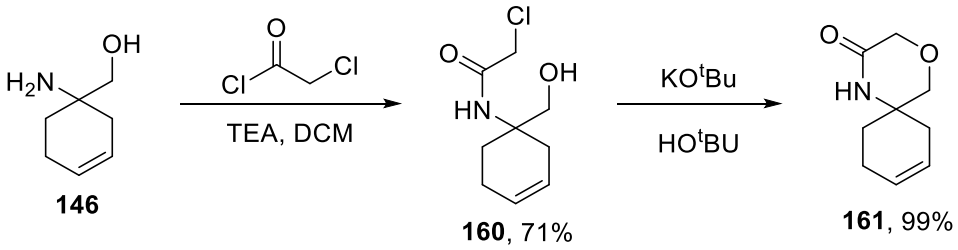

Scheme 3.14 Synthesis of morpholin-3-one spirocycle **161**.

Attempted reduction of the amide group in **161** to form the morpholine ring was unsuccessful, despite literature precedent.[184] Spirocycle **161** was reacted with lithium aluminium hydride at room temperature overnight. When TLC showed only starting material, the reaction was heated under reflux for another day; starting material was returned (Scheme 3.15).

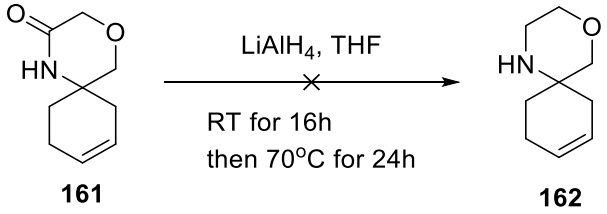

Scheme 3.15 Attempted reduction of morpholin-3-one spirocycle **161** to morpholine spirocycle **162**.

It was also explored whether the amide could be transformed into the dihydrooxazin-3-amine, **164**, to imitate the same imine-amine functional motif as in **152**. A literature procedure was followed,[185] first reacting **161** with phosphorous (V) sulphide to form morpholin-3-thione intermediate (**163**) which, upon exposure to aqueous ammonia, should form the desired dihydrooxazin-3-amine, **164**. Unfortunately, NMR after the first sulphonation step showed only starting material returned. Therefore, it was seen whether Lawesson's Reagent would affect sulphonation. Again, this failed to produce the desired product (Scheme 3.16).

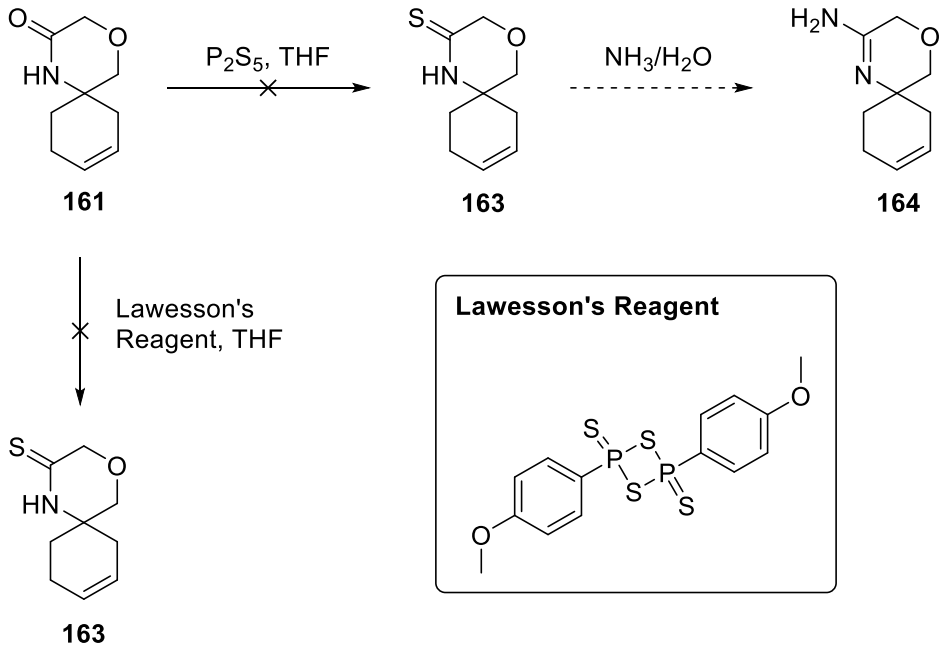

Scheme 3.16 Attempted sulphonation of spirocycle **161** in order to form dihydrooxazin-3-amine spirocycle **164**.

Although there was a need to protect the primary amine before RCM, this need not be done with a Boc-protecting group. A group could be installed in the amino moiety of precursor **142** which itself could be used to produce a ring. In this way, **142** was reacted with ethyl malonyl chloride to form diester **165**. Exposure to base cyclised this species to form tetramic acid derivative **166**, which in turn underwent ester hydrolysis-decarboxylation to give tetramic acid diene **167**. With no offending primary amine present, the two terminal alkenes were readily cyclised using Grubbs II to give tetramic acid spirocycle **168** (Scheme 3.17).

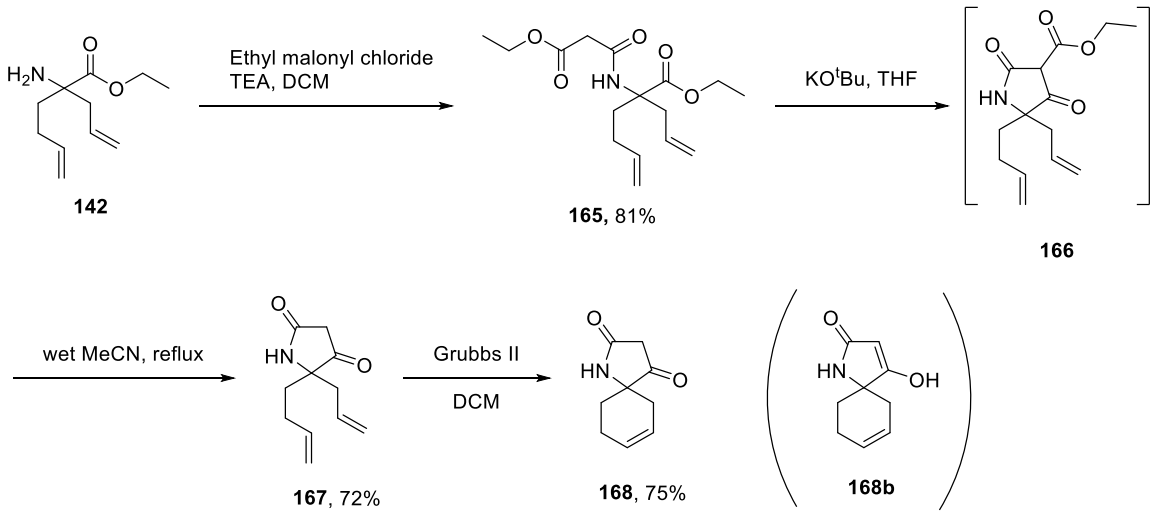

Scheme 3.17 Synthesis of tetramic acid spirocycle **168** from amino ester **142**.

Tetramic acid is known to exist in two tautomeric forms: the keto form as in **168**, or the enol form **168b**.[186] NMR confirmed the more common form of tetramic acid (**168**) was isolated due to the presence of two protons between the ketone and amide. This tetramic acid spirocycle gives several vectors for elaboration and derivation into new spirocycles.

It was investigated whether the oxo-group on the tetramic acid ring would undergo Wittig chemistry to form a substituted exocyclic olefin. Stabilised Wittig Reagent (**169**) was initially tried. However, no reaction took place, with the reagents re-isolated. It was examined whether the reaction would proceed if **169** were made *in situ*. Unfortunately, starting material was returned (Scheme 3.18).

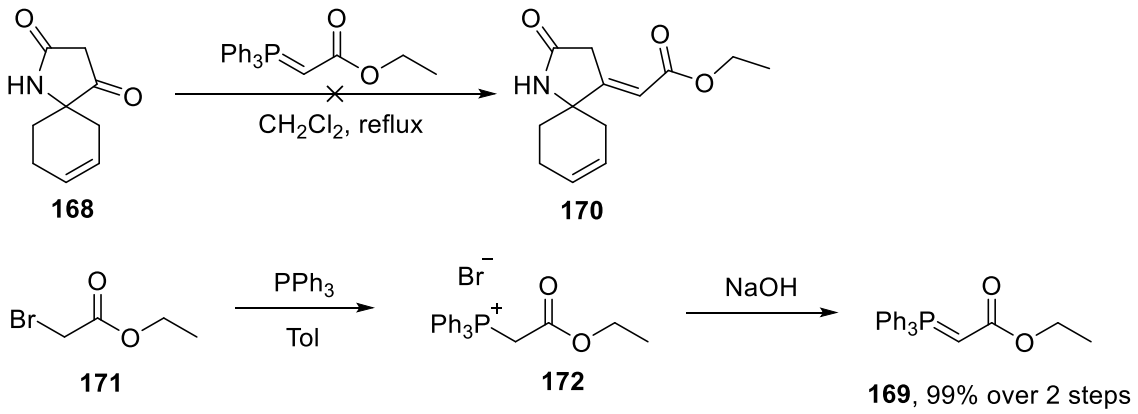

Scheme 3.18 Attempted reaction of **168** with stabilised Wittig reagent **169**.

It was postulated that **169** might be too stable to react with **168**, as the literature example showed reaction with an unstablilised ylide.[182] Therefore, the reaction was repeated with unstabilised ylide, methylenetriphenylphosphorane. The methylene group had much less steric bulk than the methylene ethyl ester of **169**, also hopefully discounting any steric factors. Again, starting material was returned (Scheme 3.19).

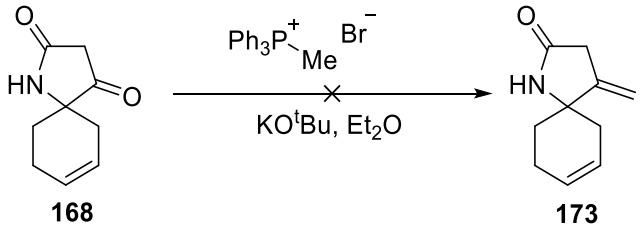

Scheme 3.19 Attempted functionalisation of **168** using unstabilised ylide methylenetriphenylphosphorane.

With both these failures, it was postulated whether tetramic acid exists in the enol tautomer (**168b**) under the basic reaction conditions, rendering it unable to perform Wittig chemistry.

This enol form of the tetramic acid was trapped out and isolated as an ethyl ether (**174**).[187] This 'protected' version of **168** could be used to explore functionalisation on the nitrogen (Scheme 3.20).

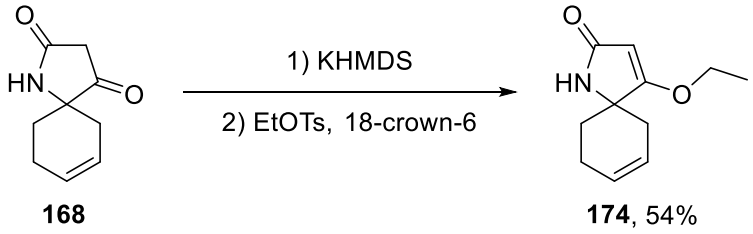

Scheme 3.20 Synthesis of **174**.

The extent to which **168** could be transformed into a γ-lactam or α,β-unsaturated-γ-lactam was then explored. First, exploiting the enol tautomer of **168**, triflic anhydride formed the triflate enol **175**. This triflate functionality could be exploited in cross-coupling reactions as a pseudo-halogen. This was demonstrated by Suzuki-Miyaura coupling **175** with *para*-methoxyphenyl boronic acid to give β-functionalised α,β-unsaturated-γ-lactam **176**. This is a very useful functional handle to install a variety of sp^2-sp^2 or sp^2-sp coupled centres (Scheme 3.21).

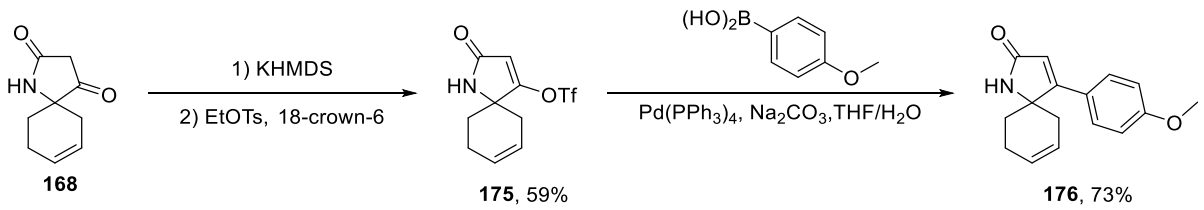

Scheme 3.21 Transformation of **168** into β-functionalised α,β-unsaturated-γ-lactam **176**.

X-ray crystallography was used to produce a crystal structure of **176** to assess its geometry (Figure 3.11). This showed that the α,β-unsaturated-γ-lactam and the aromatic ring were in the same plane and flat with respect to one another.

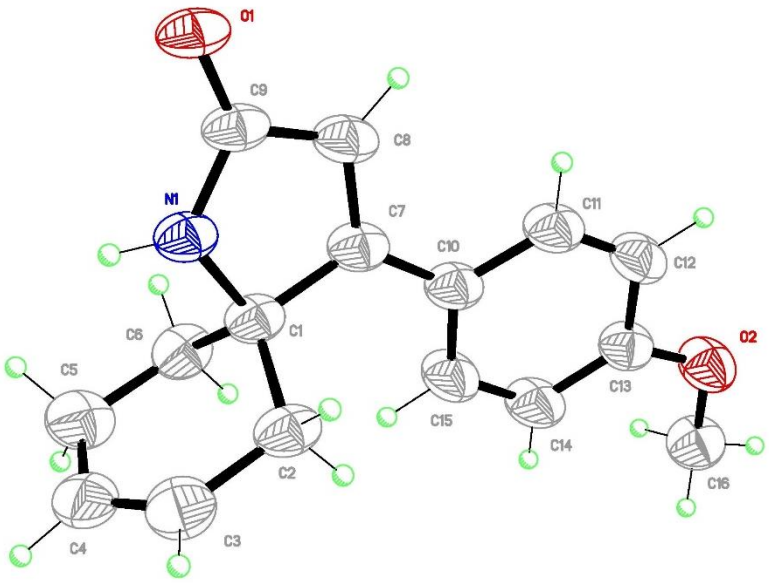

Figure 3.11 Crystal structure of (*R*)-**176**.

In addition to the substituted α,β-unsaturated-γ-lactam, it was seen whether an unsubstituted α,β-unsaturated-γ-lactam could be synthesised *via* elimination. Firstly, conditions were repeated that were used in the similar reduction-elimination of 6-chloroindanone (entry 1 in Table 3.5). The initial reduction to form alcohol **177** proceeded without issue however elimination was not observed. Next, a literature procedure was tried,[188] in which the authors performed a reduction followed by elimination on a spirocyclic tetramic acid. Unfortunately, when this was tried carrying **177** through crude, only 10% of **168** was returned after purification. Therefore, the reactions were repeated step-wise as described in the literature. Reduction worked smoothly, followed by high-yielding mesylation of the alcohol to give **178**. Alas, upon subjection to the final elimination conditions, **178** was consumed but no discernible product was detected. Finally, conditions were tried from a paper which performed the same reduction on a α-N-*gem*-dimethyl tetramic acid.[189] After reduction trifluoroacetic anhydride was used to trifluroacetylate both the alcohol and the amide. Exposure to TEA eliminated trifluroacetate and reaction with $KHCO_3$ revealed the amide giving **179** in 30% yield (Table 3.5).

Table 3.5 List of conditions to transform tetramic acid spirocycle **168** into α,β-unsaturated-γ-lactam **179**.

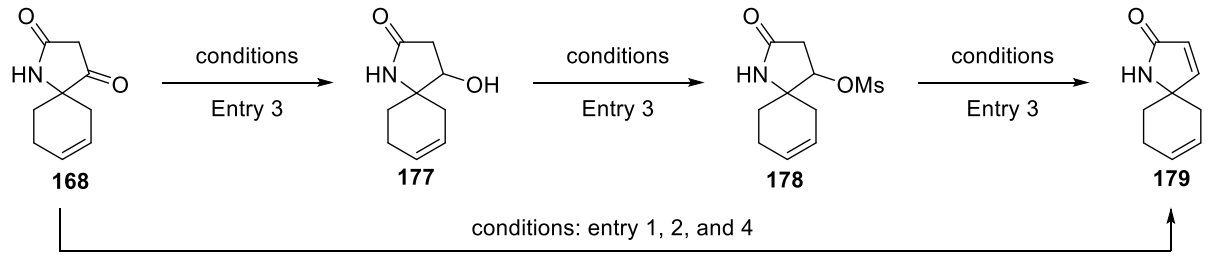

Entry	Conditions	Yield
1	1) $NaBH_4$, MeOH, RT, 1h. 2) TsOH, Tol, reflux, 2h	Alcohol returned
2	1) $NaBH_4$, MeOH, RT, 1h. 2) MsCl, TEA, DBU, DCM, RT, 3h	10% of SM returned
3	$NaBH_4$, MeOH, RT, 1h, gave **177** in 86% yield; then MsCl, TEA, DCM, gave **178** in 99% yield; then TEA, THF, reflux	No product
4	1) $NaBH_4$, MeOH, RT, 1h. 2) TFA anhydride, reflux, 12 h. 3) TEA, DCM, RT, 12 h. 4) $KHCO_3$, MeOH, RT, 2 h.	30%

Although conditions in entry 3 failed to achieve the desired α,β-unsaturated-γ-lactam, **179**, it did allow access to γ-lactams **177** and **178**.

The crystal structure of **179** was also obtained for future comparisons with the spatial properties of derivative **176** (Figure 3.12).

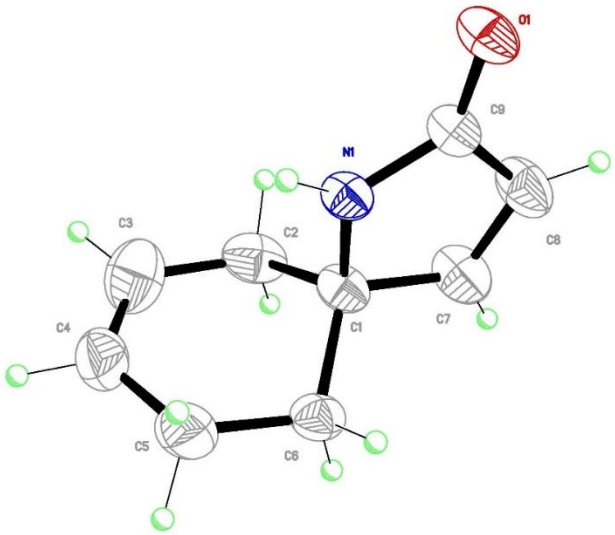

Figure 3.12 Crystal structure of (*S*)-**179**.

It was explored whether the amino and ester groups of precursor **142** could be linked in such a way so as to form rarer 4- and 3-membered rings. It was decided to pursue these linking strategies before RCM of the terminal alkenes, as having the cyclohexene ring may limit gyration of the amino and ester appendages in forming rings with bond angles less than the preferred 109.5°.

The synthesis of 4-membered β-lactam was explored. For this to be synthesised it would require the homologue of amine or ester to be initially synthesised. Homologation of carboxylic acids is known *via* the Arndt-Eistert reaction.[190] This sees a carboxylic acid activated to the acid chloride before reaction with diazomethane to form a diazoketone. Exposure to silver (I) causes this to undergo the Wolff-rearrangement and form the homologous carboxylic acid (Scheme 3.22).

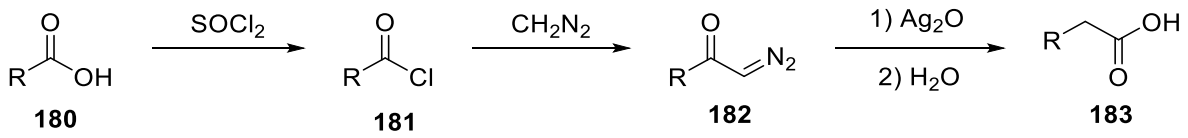

Scheme 3.22 General scheme for the Arndt-Eistert reaction for homologation of carboxylic acids.

Once the homologous carboxylic acid has been obtained, intra-molecular amide coupling reactions may couple the carboxylic acid with the amine to yield a β-lactam.

Hydrolysis of ester **143** proceeded without issue, giving carboxylic acid **184** (Scheme 3.23). Next, it was decided not to use diazomethane as the reagent in the Arndt-Eistert reaction due to the high explosion risk. Therefore the more stable analogue, TMS-diazomethane, was used.[191] The crude result of the Arndt-Eistert reaction (**185**) was carried through to a DCC mediated amide coupling.[192] Unfortunately, no product could be isolated.

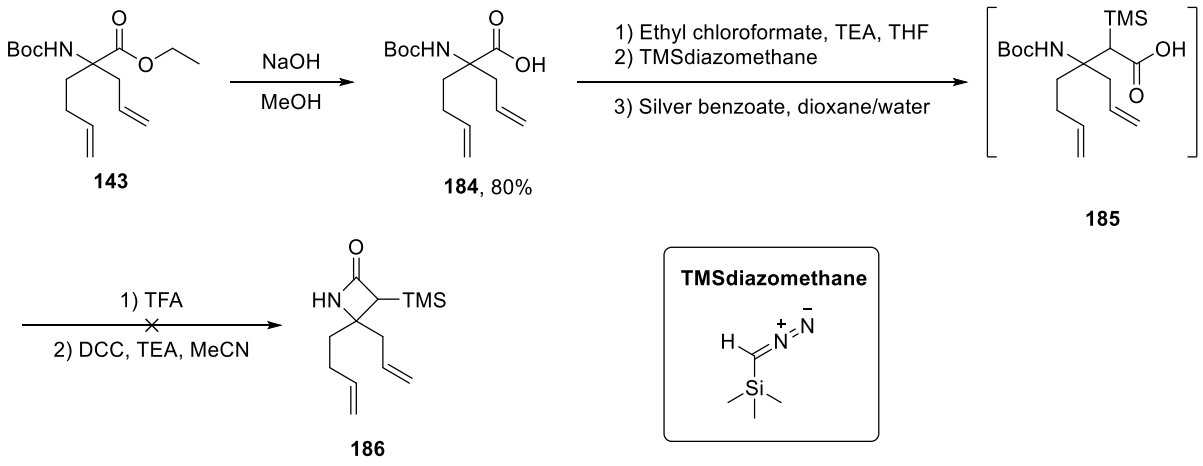

Scheme 3.23 Attempted synthesis of β-lactam **186**.

Finally, it was seen whether a 3-membered aziridine ring could be synthesised. Starting from alcohol **147**, a literature sequential alcohol-activation, then internal S_N2, was tried.[193] This activated the alcohol by tosylation, however the presence of base did not result in internal cyclisation. Unfortunately, only a crude mixture of alcohol **147** and tosylated alcohol **187** was returned (Scheme 3.24).

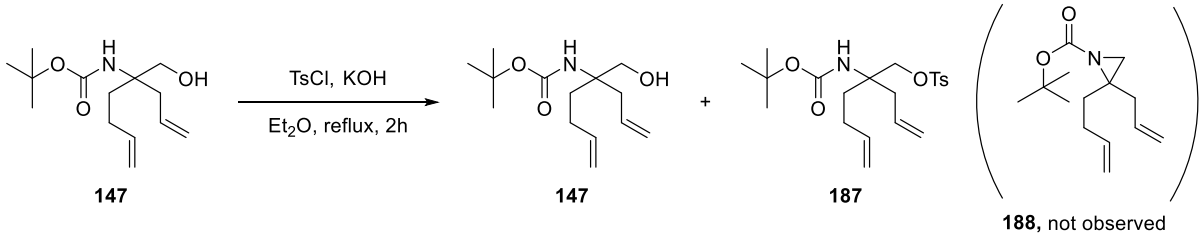

Scheme 3.24 Attempted synthesis of **188** from **147**.

3.4.5. Summary

In summary, this strategy (to synthesise a spirocyclic library from ethyl glycinate hydrochloride (**132**) by furnishing it with two terminal olefins to allow orthogonal ring formation between these and the amino and ester moieties) has yielded 13 novel spirocycles comprising 2 RCs, and 10 SC[RC]s (Scheme 3.25). The longest linear sequence in making a spirocycle was 9 steps (synthesis of **161**). These fragment scaffolds give ample chemical handle for further fragment growth. The warheads are appropriately furnished to allow a variety of chemistry to be installed at various points (only a fraction of the possible elaborations are shown here). In addition, the tail section of the spirocycle could be modified to allow for 5- or 7- or larger membered rings. The olefin synthetic handle in the tail is orthogonal to the functionality in the warheads allowing for easier synthetic development of this species.

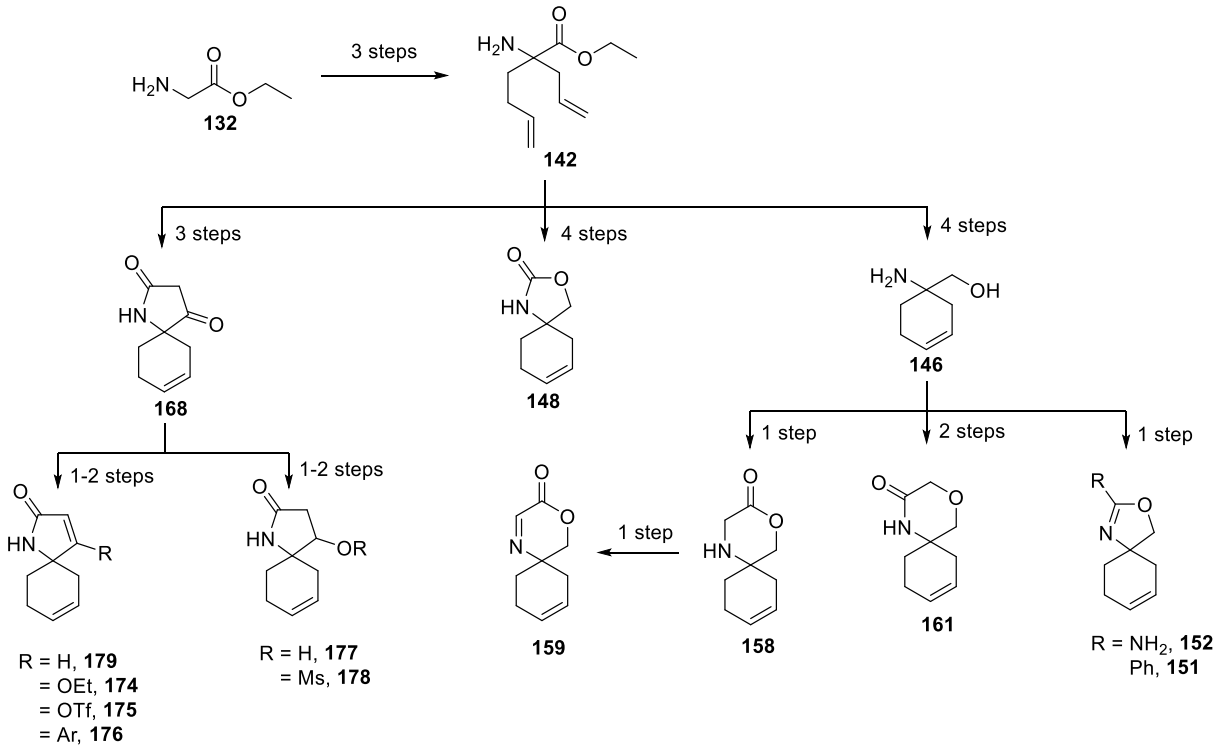

Scheme 3.25 Scheme summarising the spirocyclic derivatives of ethyl glycinate **132**.

3.5. Pericyclic spirocycle libraries

3.5.1. Pericyclic reactions

Pericyclic reactions proceed *via* a cyclic aromatic transition state and are a powerful and versatile method of forming carbon-carbon bonds. Transformations are often regio-and diastereiospecific because of the frontier orbital control of this reaction class.

The cycloaddition class of pericyclic reactions is defined as:[194]

> A reaction in which two or more unsaturated molecules (or parts of the same molecule) combine with the formation of a cyclic adduct.

For the synthesis of spirocycles, this requires unsaturation in both coupling partners to form the spirocyclic adduct. Practically, this means a ring should be furnished with an *exo*-cyclic double bond and the coupling partner would be a diene or 1,3-dipole. As the interaction is controlled by frontier orbitals, this means the reactions are under electronic control.

The two types of cycloaddition explored in this section will be a [4+2] Diels-Alder cycloaddition and a [3+2] 1,3-dipolar cycloaddition. Because these reactions are under orbital control, there must be the right electronic match between the coupling partners to ensure the reaction proceeds.

Diels-Alder reactions can be split into two categories: normal-electron-demand and inverse-electron-demand. In a normal-demand reaction, an electron-rich diene's frontier orbital's HOMO is the most similar in energy to a dieneophile's LUMO. Using a frontier molecular orbital (FMO) approach, it can be seen that the molecules combine suprafacially (Figure 3.13).

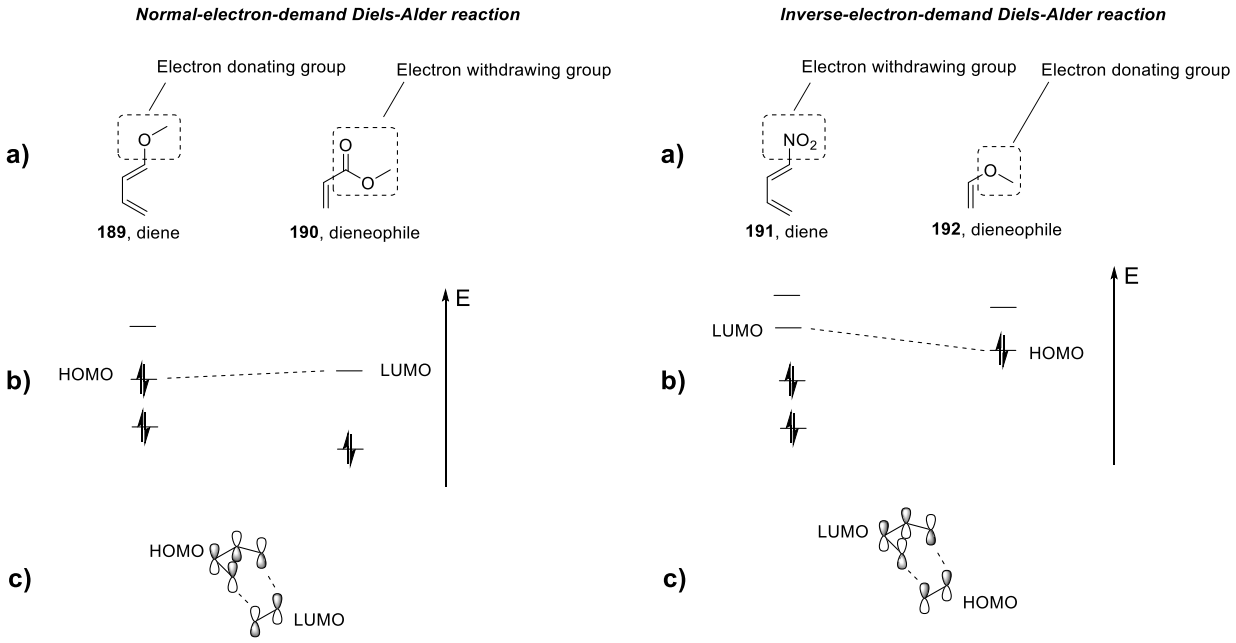

Figure 3.13 Examples of normal-electron-demand and inverse-electron-demand Diels-Alder reactions. a) Examples of electron-rich diene **189** with electron-poor species dieneophile **190** in a normal-demand interaction and electron-poor diene **191** with electron-rich dieneophile **192** in an inverse-demand interaction, b) Orbital energy diagram of the HOMOs and LUMOs interacting, c) a frontier diagram showing the orbital overlap of the HOMOs and LUMOs showing the symmetry dictating the suprafacial nature of the interactions.

Additionally, due to the orbital control of the reaction there is high regiocontrol on the arrangements of the pendent functionality in the adduct. The orbitals with the largest coefficients will have the better overlap and so will interact preferentially. Drawing the resonance structures can aid in the prediction of which orbitals are likely to interact (Figure 3.14).

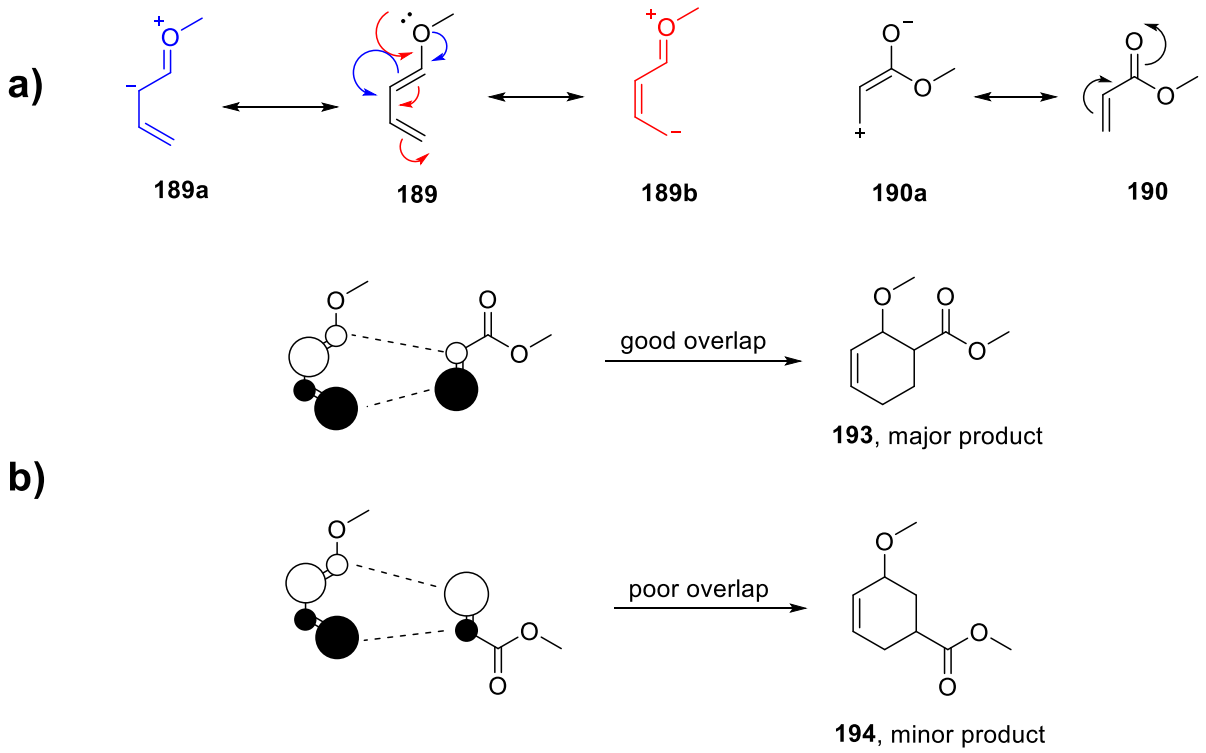

Figure 3.14 Diagram showing the origin of selectivity in the Diels Alder reaction: a) the two resonance structures of electron-rich diene **189** (**189a** in blue formed from the blue curly arrows and above **189b** in red from the red curly arrows). The location of the negative charge shows the location of the orbitals with the greatest coefficient in the HOMO. The positive charge on the resonance structure of electron-poor dieneophile **190** (**190a**) shows the location of the largest orbital coefficient on the LUMO; b) the major product (**193**) of the reaction is formed when the orbitals with the most similar coefficient overlap and the minor product (**194**) is formed by the disfavoured dissimilar interaction.

The same theory can equally be applied to 1,3-dipolar cycloadditions. A 1,3-dipole is a functional group with a pair of delocalised electrons shared over three atoms, giving resonance structures where one atom has a formal positive charge, and another has a formal negative charge.

An FMO approach of the interaction of 1,3-dipoles with dipolarphiles can also be used to see which interactions are favoured. In this case 1,3-dipoles can be divided in three categories: Type I, Type II, and Type III (Figure 3.15).

Type I: This dipole has a high lying HOMO (as most closely resembles an electron-rich diene). This mean it will quickly react with electron-poor alkenes but react slowly or not at all with electron-rich alkene.[195]

Type II: In this case the HOMO and LUMO of the dipole are so placed that they could readily overlap with both electron-rich and electron-poor alkenes.[196]

Type III: This dipole has a low energy LUMO (just as the electron-poor diene in the Diels Alder reaction) which is positioned to react best with electron-rich alkenes.[197]

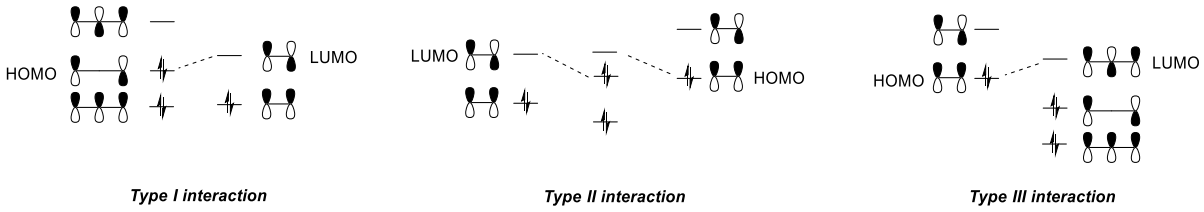

Figure 3.15 Diagram of the three dipole types interacting with dipolarphiles. A Type I dipole interacts best with a low energy LUMO from an electron-poor dipolarphile. Type II dipoles have HOMO and LUMO so placed that interaction can be made with both electron-rich and electron-poor dipolarphile. Type III dipoles have a low lying LUMO which can best interact with a high-energy HOMO from an election-rich dipolarphile.

3.5.2. Dehydroalanine derived spirocycles

In the synthesis of the ethyl glycinate series, a variety of chemistry was established to link the amine group with ester, or in its reduced form, the alcohol. It was proposed that this chemistry could be coupled with another way of making rings other than by RCM of installed terminal alkenes. A library could be built from a dehydroalanine derivative. This has the amine group and ester group to be exploited as before, but these are *gem*-disposed on a double bond meaning pericyclic reactions at this olefin would produce spirocycles. Thus, a general scheme was proposed where L-serine ethyl ester (**195**) could be transformed into dehydroalanine derivative (**196**) which in turn could be coupled and paired to make a spirocyclic library (Scheme 3.26). The order of the coupling and pairing is variable in this case depending on the functionality involved and the group which can be synthesised.

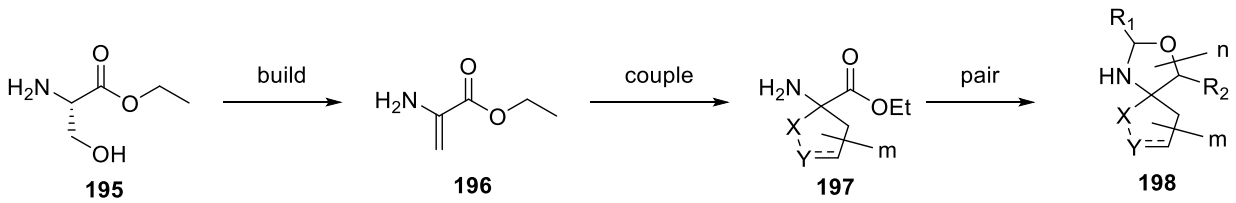

Scheme 3.26 An outline of the proposed spirocyclic library constructed from dehydroalanine.

Additionally, considering **195** has both alcoholic and ester functionalities, a ring can be constructed from this molecule before an alkene is revealed. This could then be subject to pericyclic chemistry, constructing the library (Scheme 3.27).

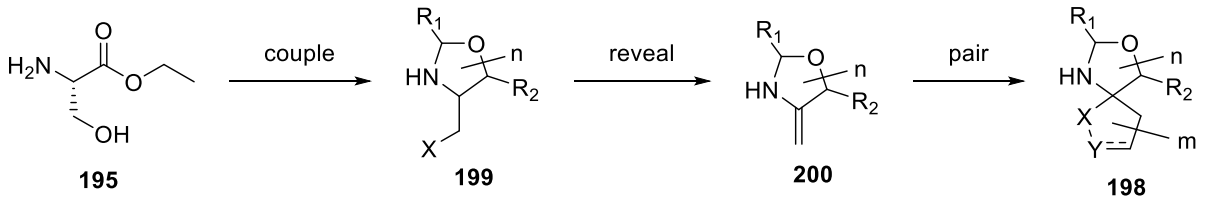

Scheme 3.27 A second approach to constructing the pericyclic libraries starting from L-serine.

This allows for flexibility in the construction of these libraries which may prove useful if certain synthetic paths become fruitless.

Starting along the dehydroalanine path, L-serinate ethyl ester hydrochloride (**195**) was readily Boc-protected (**201**) and then eliminated to form *N*-Boc-dehydroalanate ethyl ester (**202**). Reduction of **202** to alcohol **203** was explored as a potential route to 4-methyleneoxazolidin-2-one (**205**). With this in hand it was hoped a variety of pericyclic reactions could be explored. The reduction of **202** proved challenging, with alcohol **203** proving unstable (a ^{1}H NMR of **203** was obtained however by the time ^{13}C and 2D NMR were obtained, the sample had decomposed). Thus, alcohol **203** was reacted immediately with KO^{t}Bu in an effort to yield **205**. However, the endo-cyclic alkene isomer **204** was obtained. This was even the case when base was limited (Scheme 3.28).

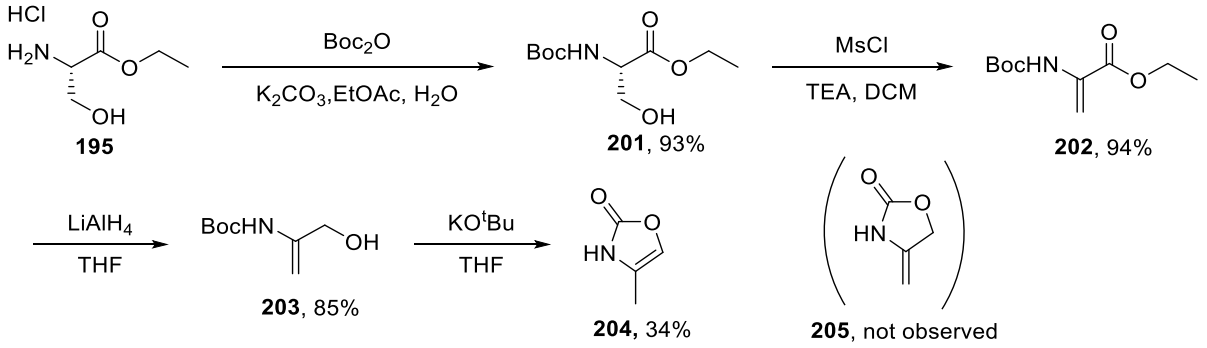

Scheme 3.28 Summary of work to make key intermediate **202** and attempted synthesis of 4-methyleneoxazolidin-2-one **205**.

Although it was disappointing that **205** could not be made, the intermediate **202** could be used in pericyclic chemistry to generate a ring before the amine and ester are coupled to form the spirocycle.

With the carbamate group being an electron donor into the alkene and the ester group being an electron withdrawing from the alkene, the electronic state of the alkene in **202** was established by ^{13}C NMR. The chemical shift of a magnetic nucleus (δ) is related to the effective

magnetic field it experiences ($\mathbf{B_{eff}}$). This is the product of the external applied field from the machine's magnet ($\mathbf{B_0}$) and any induced field from the electronic structure of the molecule ($\mathbf{B_{ind}}$). The induced field is opposed to the applied field and is larger the greater the electron density around the nucleus. The induced field can be calculated around a given atom from its chemical shift.

Table 3.6 shows clearly that **202** is an electron rich alkene. The molecule was split into its two components as an ethyl acrylate moiety (**206**) and a *tert*-butyl vinylcarbamate moiety (**207**). The difference in the induced fields about the α and β carbons of each molecule was calculated. The results clearly show that **202** is electron-rich at the β carbon (being more similar to *tert*-butyl vinylcarbamate electronically).

Table 3.6 Table calculating the difference in the induced magnetic field (B_{ind}) between the α and β carbons on ethyl acrylate, *tert*-butyl vinyl carbamate and **202**. δ = chemical shift, $\nu_{nucleus}$ = resonance frequency of the ^{13}C nucleus, B_{eff} = effective magnetic field experienced by the nucleus, B_{ind} = magnitude of the induced magnetic field around the nucleus, $C_\alpha - C_\beta$ = the difference in the induced magnetic field between the α and β nucleus.

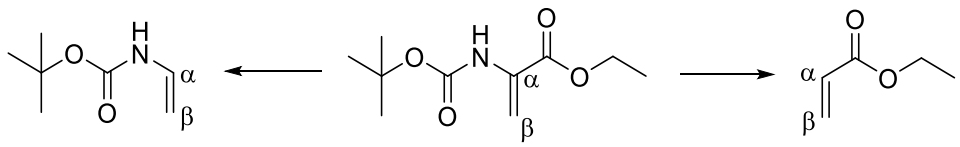

tert-butyl vinylcarbamate, **207** **202** ethyl acrylate, **206**

Compound	Nucleus	δ/ppm	$\nu_{nucleus}$/MHz	B_{eff}/T	B_{ind}/T	C_α–C_β/μT
206	C_α	128.8	100.6257	9.39689	0.034957	
	C_β	131.3	100.6260	9.39692	0.034928	29.13
207	C_α	128.6	100.6257	9.39689	0.034953	
	C_β	95.5	100.6224	9.39658	0.035264	-311.00
202	C_α	131.5	100.6260	9.39692	0.034926	
	C_β	104.8	100.6233	9.39667	0.035177	-250.86

Knowing that **202** is an electron rich alkene, it would most likely perform cycloadditions with Type II and Type III dipoles as well as inverse-demand dienes.

Compound **202** was first reacted with a nitrile oxide dipole formed *in situ* from hydroxylimidoyl chloride . Because of the electron-rich nature of the alkene in **202**, the

reaction was expected to proceed *via* transition state **TS** , forming the regioisomer . This was confirmed by NOESY NMR (Figure 3.16) showing spatial proximity between the *ortho*-aromatic protons (H11) and the methylene protons in the isooxazole ring (H8). Compound was reduced, giving alcohol which was cyclised to give spirocycle (Scheme 3.29). A crystal structure was taken of to confirm the regiochemical assignment of (Figure 3.17).

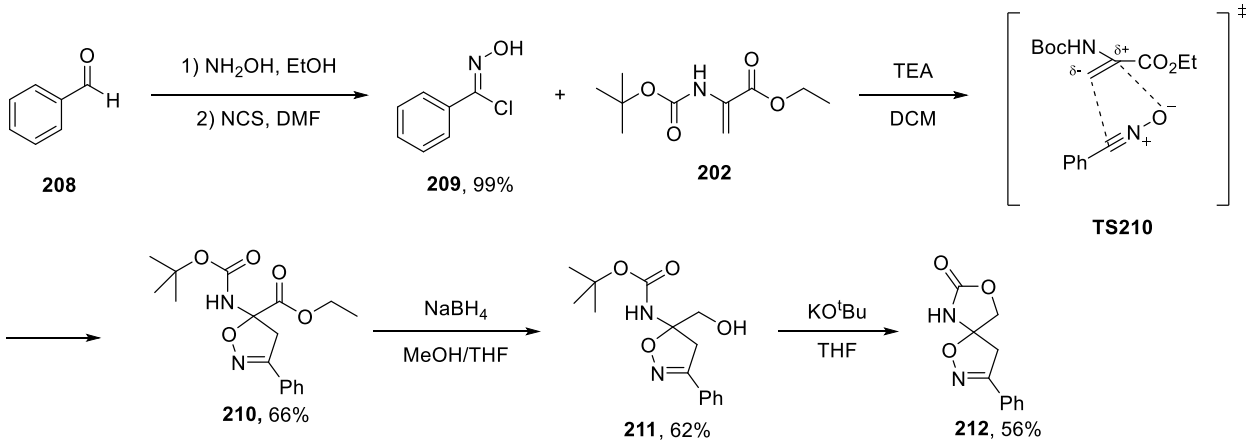

Scheme 3.29 Synthesis of spirocycle **212**.

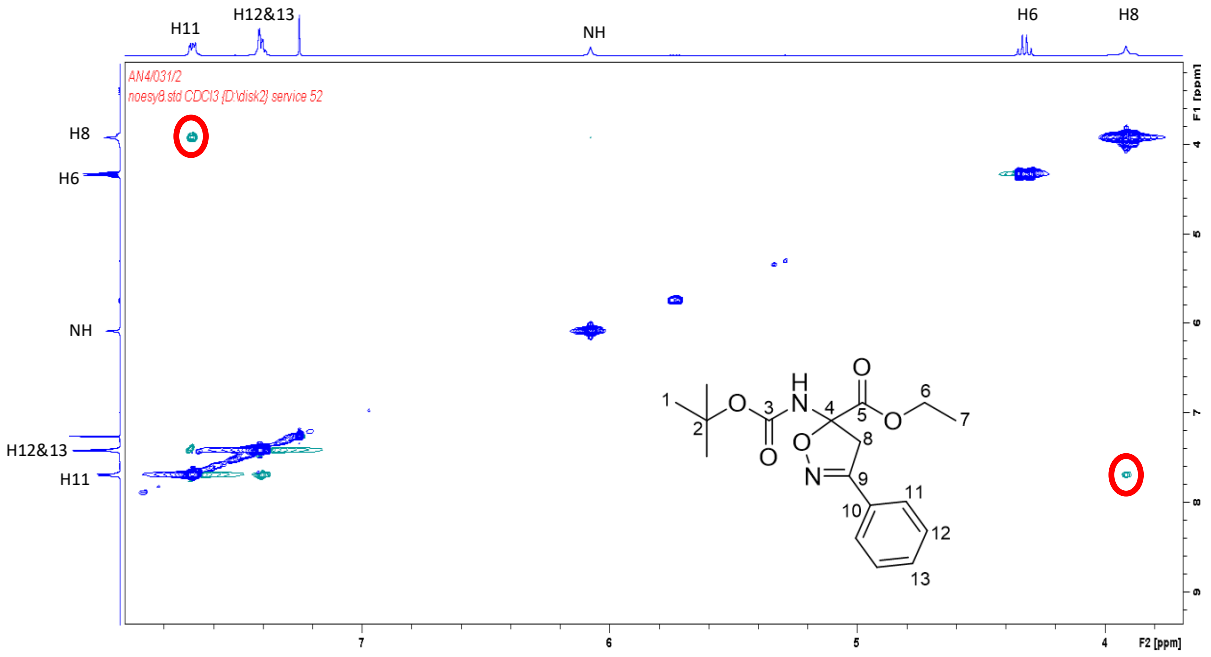

Figure 3.16 NOESY NMR of compound **210** showing correlation between protons 11 and 8.

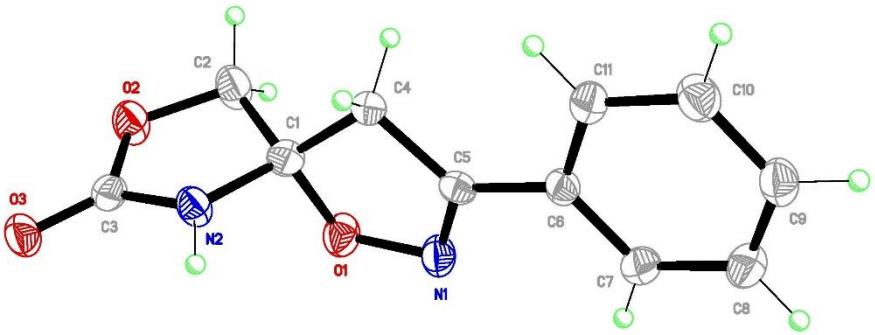

Figure 3.17 Crystal structure of spirocycle **212** confirming the isomer synthesised.

Benzyl azide was also reacted with **202** in an attempt to form a dihydro-1,2,3-triazole spirocycle. Initially, following a literature procedure,[198] heating the reaction under reflux for 6 h only gave a mixture of benzyl azide and **202**. Repeating the reaction by heating under reflux overnight seemed to produce the desired product; however, despite the NMR losing the olefin peaks of **202** and gaining aromatic peaks to integral 5, the benzyl methylene peak was absent and a valid structure could not be proposed to support the data. Finally, a more forcing condition of heating to 100 °C in a sealed vessel for 48 h was tried yet no identifiable product was isolated from this reaction (Scheme 3.30).

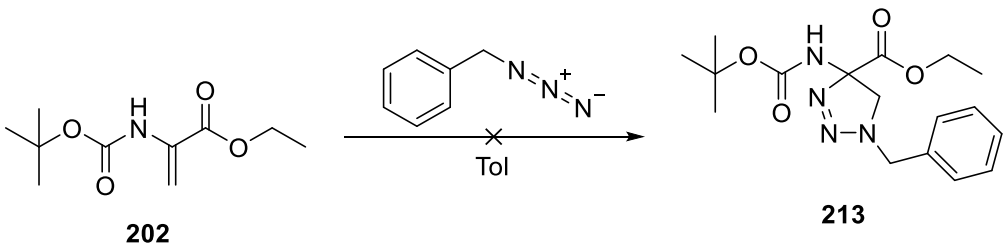

Scheme 3.30 Attempted synthesis of dihydro-1,2,3-triazole **213**.

The second proposed strategy was then explored: forming a ring, revealing the alkene, and then performing the cycloaddition. To minimise the use of protecting groups, it was first tried to construct the ring using the already present amine and alcohol functionality in L-serinate ethyl ester **195**.

Firstly, a morpholin-3-one was the synthetic target, using similar chemistry as in the synthesis of **161**. Amino alcohol **195** was reacted with chloroacetyl chloride giving amide **214**. Only a small amount of the difunctionalised by-product **215** was observed. It was hoped that the facile S_N2 ring closing between the alcohol and the chloride could produce morpholin-3-one **216**, yet unfortunately this was not the case. Reaction with KO^{t}Bu in THF gave an insoluble

jelly, suggesting polymerisation had taken place. Switching the solvent to HO^{t}Bu produced the same product, as did IPA. However, this product was submitted for reduction in the hope that some of alcohol **217** could be recovered post-purification. No reaction took place. NMR analysis of the jelly seemed to suggest alkene **218** had been the product of the reaction (Scheme 3.31).

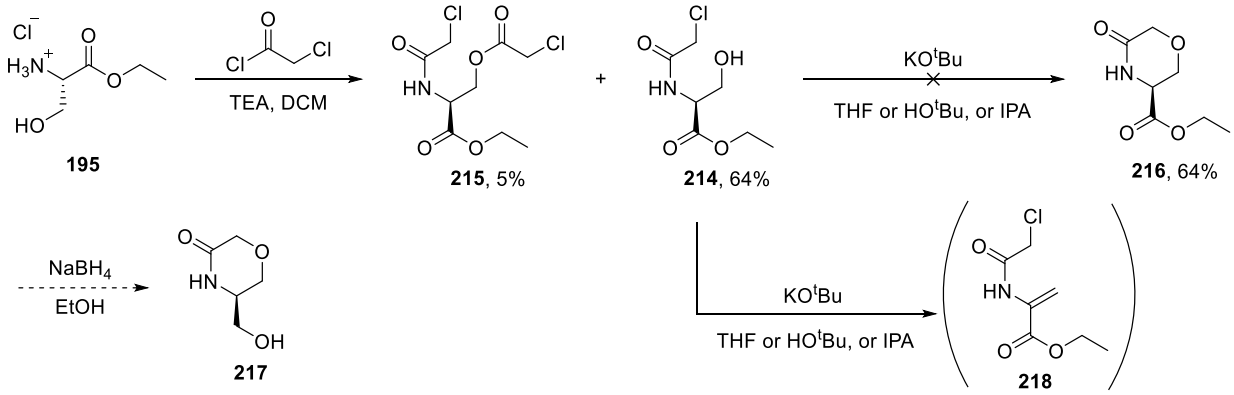

Scheme 3.31 Attempted synthesis of morpholin-3-one precursor for cycloadditions.

The pre-furnished amino alcohol in **195** allows quicker synthesis of the oxazolidin-2-one ring than previously. Reacting **195** with triphosgene joins the amine and the alcohol to form oxazolidin-2-one **219**. However, despite literature precedent,[199] the reduction to **220** could not be affected. Despite multiple attempts and the TLC in each case showing a spot-to-spot reaction, no material was left post work-up. Thus, this synthetic strategy was abandoned (Scheme 3.32).

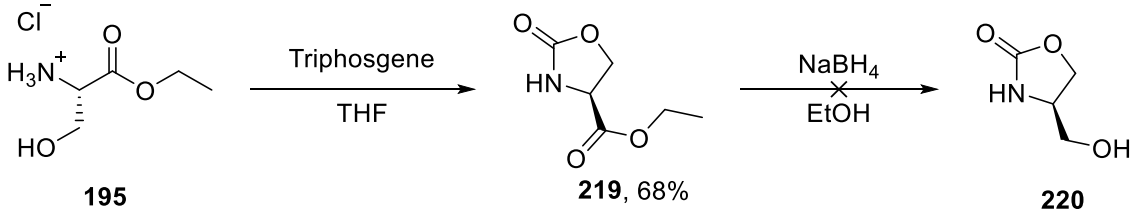

Scheme 3.32 Synthesis of oxazolidin-2-one ring and attempted reduction.

Finally, reaction of **195** with ethyl benzimidate (**150**) yielded dihydrooxazole **221** which was subsequently reduced to alcohol **222**. In spite of several attempts to eliminate this alcohol it was returned by the reaction (Scheme 3.33).

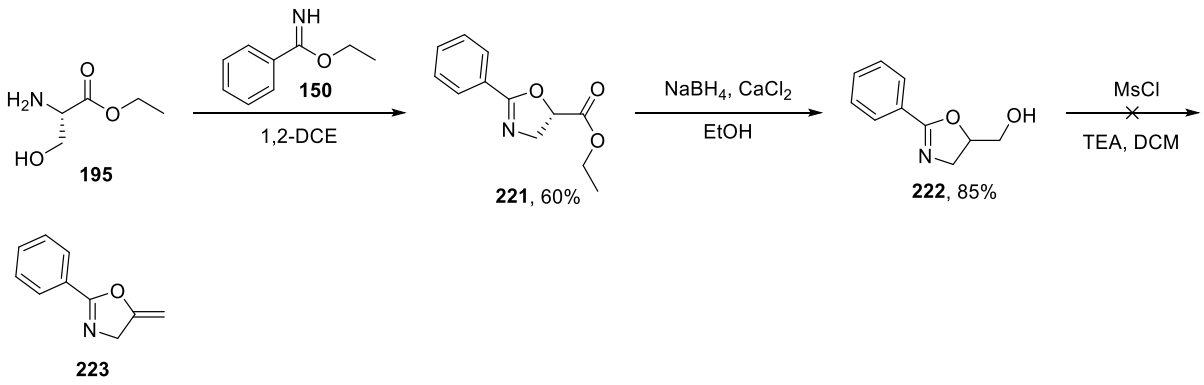

Scheme 3.33 Formation of dihydrooxazole ring but failed elimination.

A second approach to forming the ring and revealing the alkene was tried. This time, the free alcohol on **195** would be TBS-protected before ring forming reactions then a deprotection-elimination could reveal the olefin.

Compound **195** was readily TBS protected (**224**). Firstly, synthesis of the morpholin-3-one ring was re-examined. Chloroacetyl chloride acetylated the free amine giving compound **225** which was reduced to give alcohol **226** (Scheme 3.34). Again a 6-*exo*-tet ring closure was attempted using the previous conditions to produce morpholin-3-one **227**. This produced a clean product by NMR, however this was not the desired product (**Figure 3.18**). The TBS group was present however it was one CH_2 group short of **227**. No structure or reaction mechanism could be proposed which satisfied the given NMR.

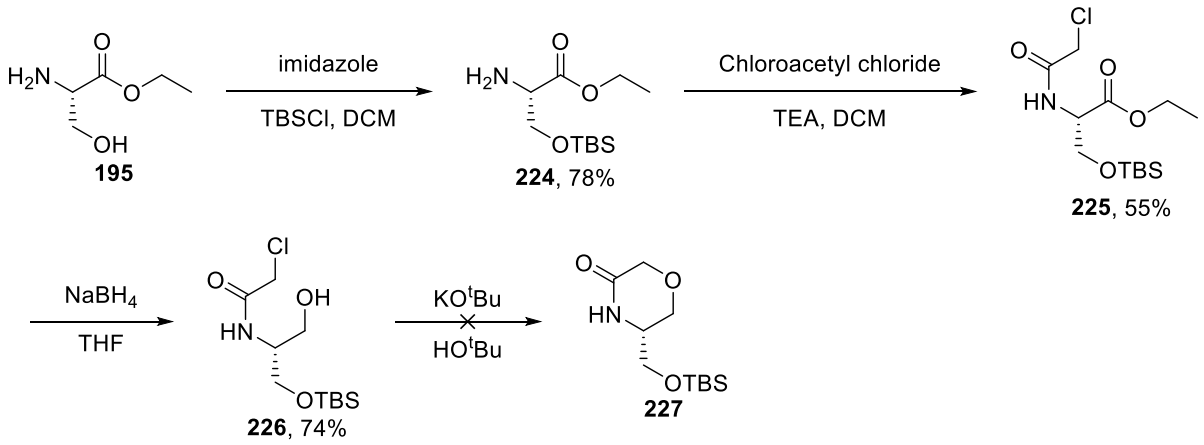

Scheme 3.34 Synthesis of morpholin-3-one precursor **226**.

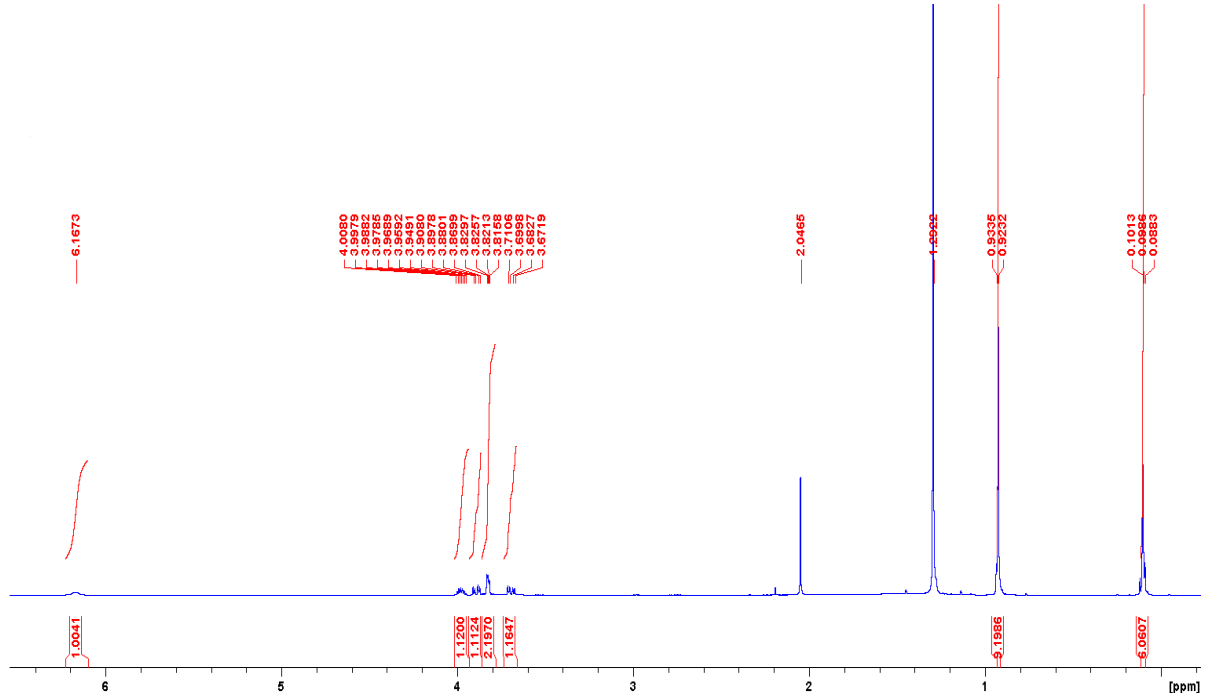

Figure 3.18 ^{1}H NMR of reaction of **226** with base.

Further, the synthesis of the tetramic acid warhead was explored. The same process in the synthesis of **168** was repeated. Reaction of TBS-protected serine ethyl ester **224** with ethyl malonyl chloride gave compound **228**. However, several attempts at repeating the ring closure-hydroylsis-decarboxylation to afford tetramic acid derivative **229** failed (Scheme 3.35).

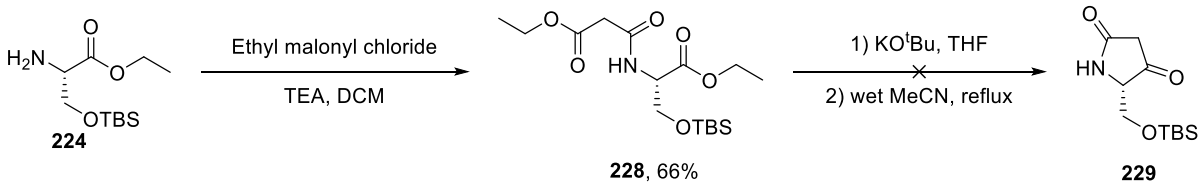

Scheme 3.35 Successful reaction of **224** to give diester **228** however cyclisation to form tetramic acid derivative failed.

With this in mind, a different approach was taken. The literature showed that reaction of compound **224** with Bestmann's ylide formed the enol ether of tetramic acid *via* internal Wittig reaction.[200] When this reaction was performed, the expected tetramic acid enol ether with TBS protected alcohol was not observed. Instead the more desirable elimination product, **230**, was isolated. This avoided additional steps to reveal the olefin *via* elimination. The presence of the catalytic amount benzoic acid aided in the deprotection-elimination. The eliminated enol was observed as a by-product previously,[200] however in this case it was major product of the reaction (Scheme 3.36).

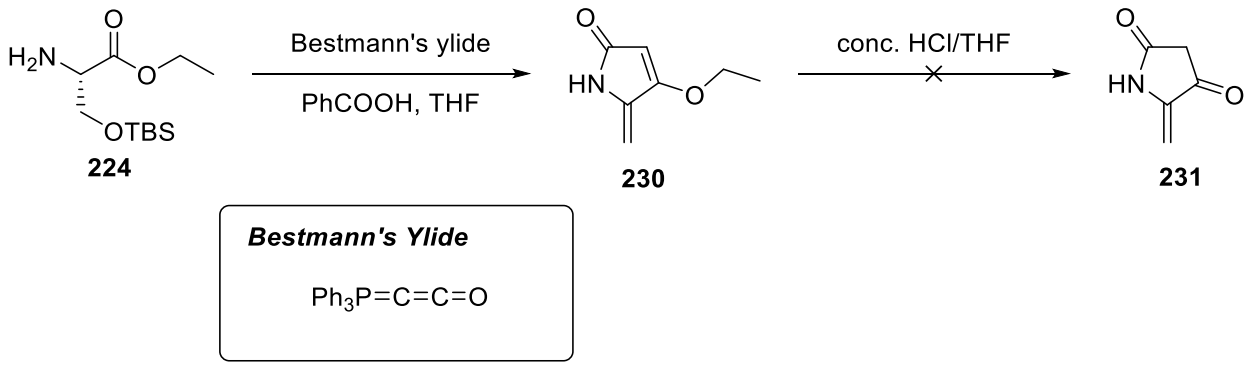

Scheme 3.36 Synthesis of enol ether tetramic acid derivate **230** *via* Bestmann's ylide.

Due to the presence of two alkene moieties in **230**, it was decided that deprotection of the enol ether to reveal the tetramic acid in ketone form was necessary before the pericyclic reaction to ensure selectivity on the olefin. This was initially tried with conc. HCl in THF but the reaction returned a complex mixture. However, due to literature precedent of this transformation, it is expected to work in slightly different solvents e.g. ether or dioxane.[190]

In summary, despite difficulty in forming the *exo*-cyclic olefin from elimination, a spirocycle was formed by pericyclic reaction with *N*-Boc-dehydroalanine ethyl ester and forays have been made toward synthesising tetramic acid with an exocyclic double bond.

3.5.3. 3-Azetidinone derived spirocycles

Alongside the synthesis of *exo*-cyclic olefins from L-serinate ethyl ester hydrochloride, **195**, pericyclic chemistry was also explored to investigate its application to a range of other *exo*-cyclic olefins.

In this case, the ease of transforming ketones into alkenes *via* the Wittig reaction was used. The 'build' stage would see the construction of a ring which possesses a ketone. The 'couple' stage reacted this ketone with a Wittig reagent to form an alkene. Depending on the Wittig reagent used, the subsequent alkene can be furnished with various groups which may change its reactivity in the 'pair' step. In pairing, various pericyclic coupling partners could be used to form the spirocycle.

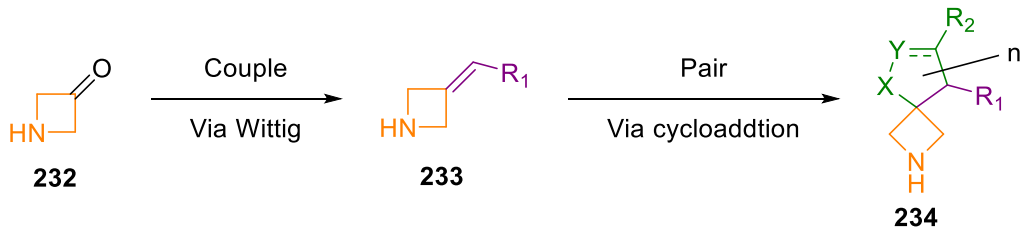

Scheme 3.37 Outline of B/C/P strategy for azetidin-3-one based spirocyclic library.

Due to the wide commercial availability of rings possessing ketone functionality, it was decided that the 'build' stage could be by-passed by purchasing the desired ring. *N*-Boc-azetidin-3-one (**235**) was selected as a starting material. Firstly, due to its commercial availability, and secondly, despite effort being directed towards their synthesis[201], four membered aza-spiro rings are under-represented in spirocyclic space.[171] Thirdly, the nitrogen in the ring is a useful vector for further elaboration. Therefore, a general scheme was proposed; *N*-Boc-azetidin-3-one (**235**) would be furnished with an *exo*-cyclic olefin *via* the Wittig reaction, and then the spirocycle would be formed *via* a pericyclic reaction using a similar method as outlined in section 3.5.2 (Scheme 3.37).

N-Boc-azetidin-3-one (**235**) was appropriately furnished with an ethyl acetate substituted olefin by Wittig reaction to give compound **236**. The ethyl acetate substitution was chosen as a versatile synthetic handle for future modification and to ensure the olefin was electron-deficient to allow for a greater range of pericyclic reactions (**Scheme 3.38**).

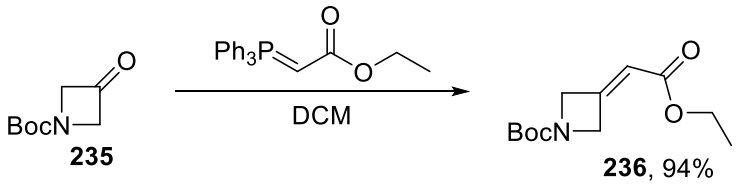

Scheme 3.38 Wittig reaction forming α-β unsaturated ester **236**.

Compound **236** was first reacted with previously synthesised nitrile oxide precursor **209** and gave spirocycle **237**. In contrast to the synthesis of **210**, which took an hour to complete, this reaction was complete within minutes and the yield of the product diminished if the reaction was left for a long time (Scheme 3.39).

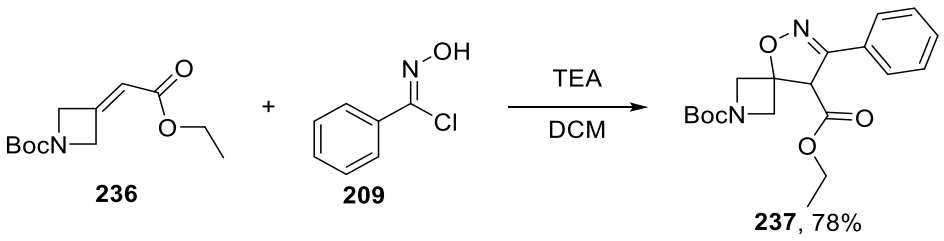

Scheme 3.39 Cycloaddition with nitrile oxide forming isoazole **237**.

Compound **236** was also reacted with benzyl azide, a reaction which **202** was unable to perform. An initial attempt following a literature procedure[202] by stirring at 45 °C for 12 h without solvent simply returned **236**. However, the procedure was adapted, and the mixture was heated to 100 °C in a sealed vessel for 48 h. This did produce the desired dihydro-1,2,3-triazole spirocycle product, **238** (Scheme 3.40).

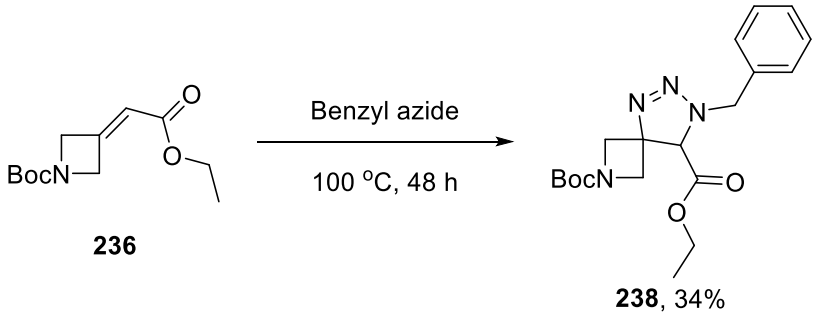

Scheme 3.40 Cycloaddition with azide forming 1,2,3-triazole **238**.

Next, being an electron deficient alkene, **236** should also be able to perform cycloaddition reactions with Type I dipoles and 'normal demand' electron-rich dienes. An attempt was made to form some bridged cyclic structures using the Diels-alder reaction. Firstly, it was attempted to react **236** with furan using a Lewis acid catalyst of zinc iodide.[203] After refluxing overnight at 40 °C, all of the starting material was returned unreacted. The same result occurred when the reaction was repeated in a sealed tube at 50 °C. Therefore, another set of conditions was tried. These saw the reaction repeated with Lewis acid catalysis from niobium (V) chloride and the reaction carried out –20 °C.[204] Again, the starting material was returned and spirocycle **239** was not isolated (Scheme 3.41).

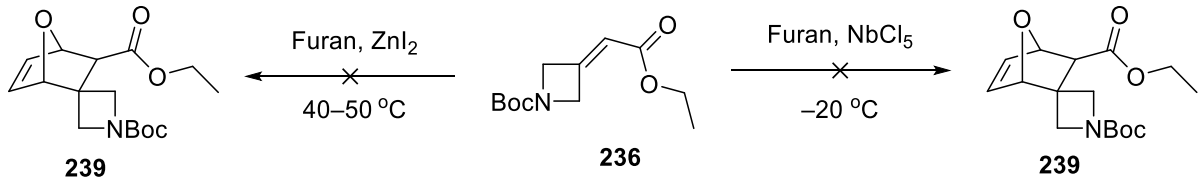

Scheme 3.41 Diels-Alder reactions between furan and **236**.

Another attempt was made at a Diels-Alder reaction using 2-(trimethylsiloxy)-1,3-cyclohexadiene with stoichiometric amounts of titanium tetrachloride. Following the literature, this was performed at –40 °C.[205] Despite the TLC indicating a product had been formed, nothing could be isolated from column chromatography (Scheme 3.42).

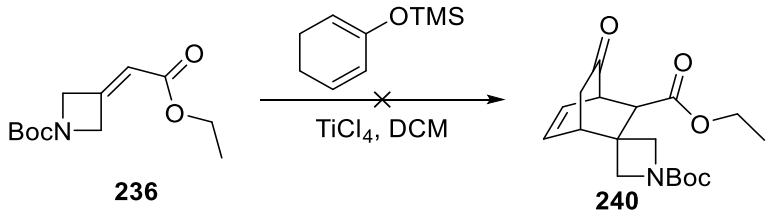

Scheme 3.42 Attempted Diels-Alder reaction with 2-(trimethylsiloxy)-1,3-cyclohexadiene.

Moving to Type I dipoles, it was decided to move beyond standard 1,3-dipoles and try an oxypyrylium zwitterion which could undergo [5+2] cycloaddition with a dipolarphile. The precursor to this zwitterion was readily synthesised using literature procedure.[206] Furan **241** was expanded into six-membered hemi-acetal **242** which was acetylated to give oxypyrylium zwitterion precursor **243** (Scheme 3.43).

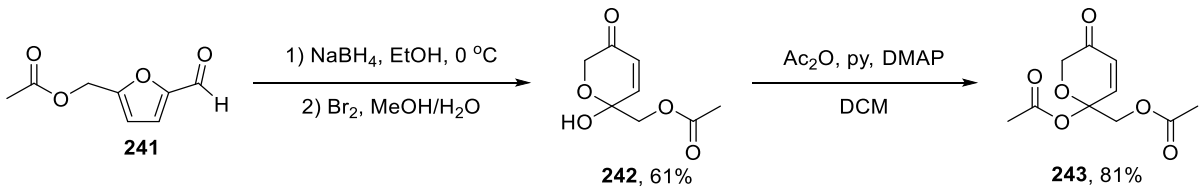

Scheme 3.43 Transformation of (5-formylfuran-2-yl)methyl acetate into oxypyrylium precursor.

This was submitted to cycloaddition with **236**. Unfortunately, in this case only the oxypyrylium dimer (**244**) was observed (Scheme 3.44).

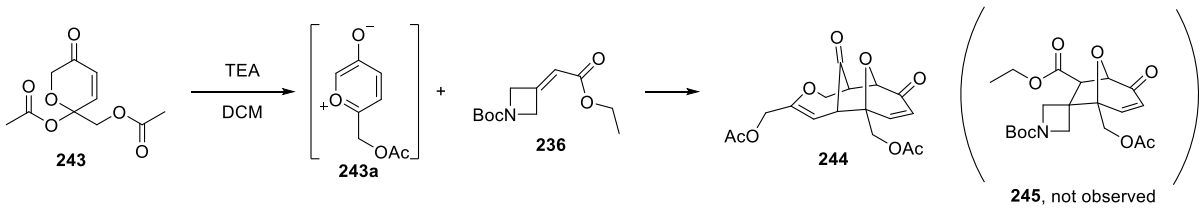

Scheme 3.44 Reaction of oxypyrylium zwitterion with **236**.

3.5.4. 1,4-Oxazepane based library

7-Membered rings are underrepresented in spirocyclic libraries.[171] Therefore increasing their representation in these libraries would hopefully allow a greater probing of biologically relevant chemical space. 1,4-Oxazepanes were chosen as a 7-membered ring to build a library around because of their potential to be synthesised from amino acids. Additionally, they are a privileged structure, having many biological effects including antifungal,[207] anti-viral,[208] anti-congestive heart failure,[209] and acting as apoptotic agents (Figure 3.19).[208]

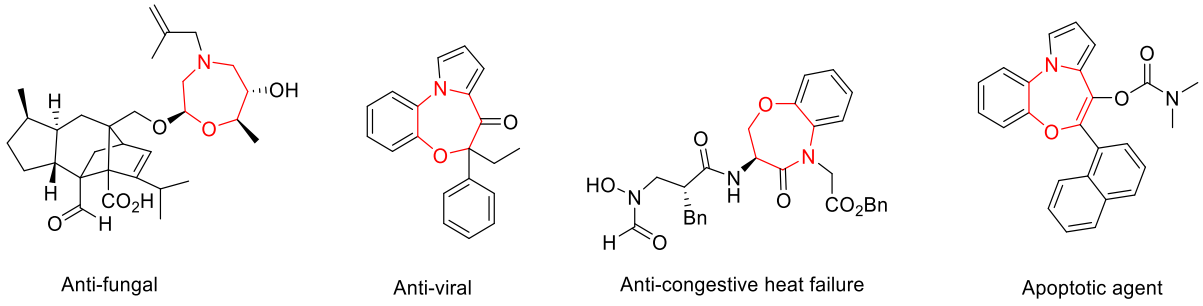

Figure 3.19 A selection of biologically active compounds containing a 1,4-oxazepane ring (highlighted in red).

Amino alcohols were chosen as a good starting material for 1,4-oxazepane synthesis as they are easily derived from the large amino acid pool and can carry intrinsic stereochemistry. The 1,4-oxazepane could then be built by reacting an amino alcohol with a three-carbon linker. This could then be furnished with an exo-cyclic olefin on which a range of pericyclic reactions could be paired to create the spirocycle library (Scheme 3.45).

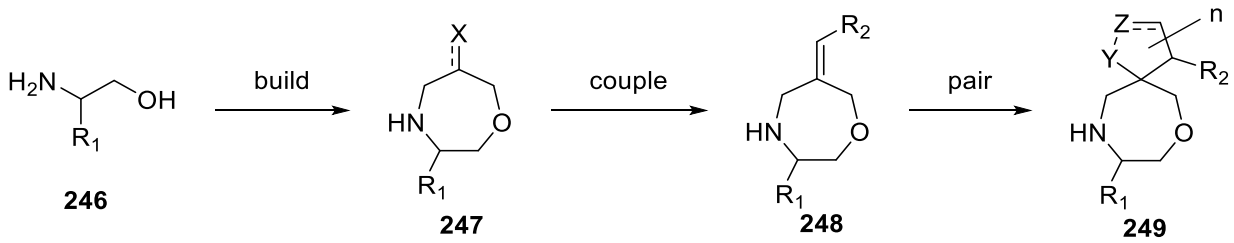

Scheme 3.45 Outline of DOS 1,4-oxazepane spirocyclic library. R_1 represents a range of functionality from commercially available amino acids and amino alcohols. X is a functionality that can be manipulated during the couple stage to reveal an exo-cyclic olefin. Finally, the range of dienes and dipoles can be used to form the spirocycles in the pair stage.

Initially *N*-Boc-ethanolamine (**250**) was chosen as a starting material as it lacked the α-pendent group found in all other amino alcohols derived from the naturally occurring amino acids. This was pre-treated with exactly two equivalents of sodium hydride before reaction to 1,3-dichloroacetone (**251**); however, NMR of the crude reaction mixture did not show the desired product (**252, Scheme 3.46**).

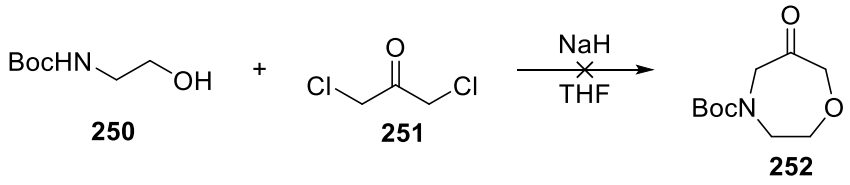

Scheme 3.46 Attempted formation of 1,4-oxazepane ring with 1,3-dichloroacetone.

The same reaction was repeated with L-prolinol (**254**) to form a condensed spirocycle and to explore the amino acid pool as a source for 1,4-oxazepane formation. The prolinol (**254**) was easily synthesised from L-proline (**253**) *via* literature reduction.[210] Again the 1,4-oxapene synthesis was repeated, however this failed to yield the desired product in either DMF or THF as solvents (Scheme 3.47).

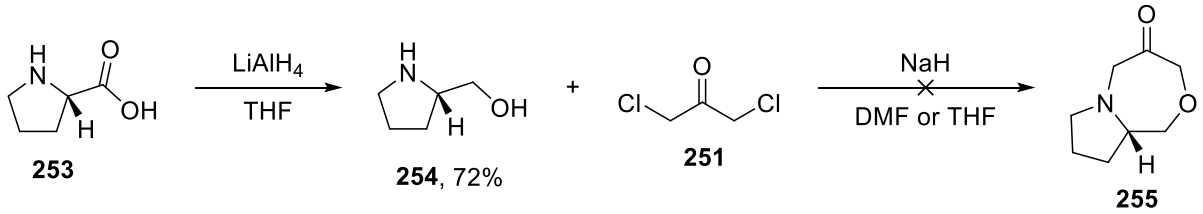

Scheme 3.47 Repeat of 1,4-oxazepane synthesis with prolinol.

Wondering whether the 1,3-dichloroacetone was active enough to react with the amino alcohol, it was iodinated to 1,3-diiodoacetone (**256**) *via* the Finkelstein reaction. This was then reacted with prolinol and *N*-benzyl-ethanolamine, as the fluorescent benzene ring may aid in detection during reaction monitoring and purification. In this case a weaker base, potassium carbonate, was used as it was thought that sodium hydride may have been too strong and causing enolization of 1,3-dichloroacetone. The reaction with prolinol did not produce the desired product (**257**). However, the reaction with *N*-benzyl-ethanolamine produced an NMR spectrum of the crude product seemed to suggest 1,4-oxazepane **258** had been produced. Attempted purification could not get the small quantity of material clean enough to confirm its synthesis (Scheme 3.48).

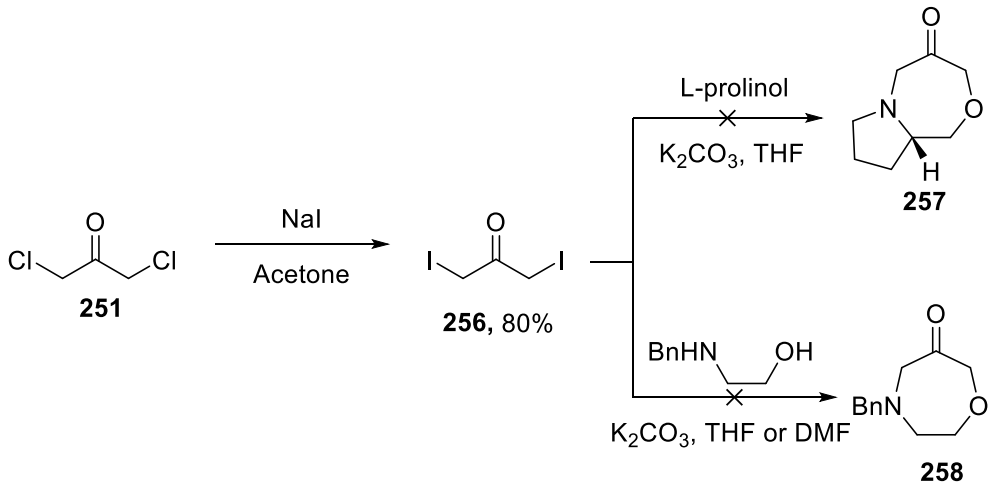

Scheme 3.48 1,4-Oxazepane synthesis with 1,3-diiodoacetone, showing the attempted reaction been prolinol and *N*-Boc-ethanolamine.

Removal of the ketone from the coupling partner was considered for two reasons. One, the presence of base and/or deprotonated alcohols and amines may cause competing enolization; two, the ketone itself it susceptible to nucleophilic attack. Therefore, the haloacetones were replaced with 1,3-dichloropropanol (**259**). Upon reaction with *N*-benzyl-ethanolamine no discernible product (**260**) was seen. However, a small amount (<5%) of 1,4-oxazepane **261** was believed to have been identified by NMR spectroscopy; however, like before, this couldn't be isolated cleanly enough or in high enough yield to progress further in the chemistry (Scheme 3.49).

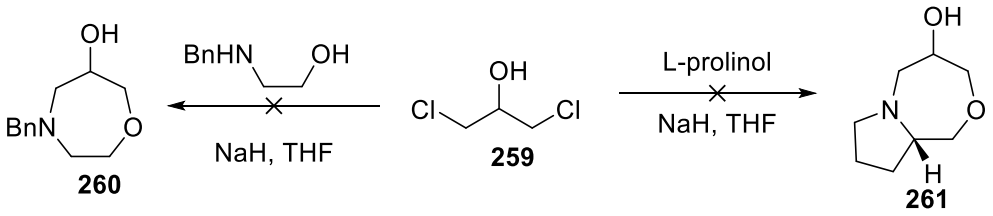

Scheme 3.49 1,4-Oxazepane synthesis with 1,3-dichloroisopropanol, showing the attempted reaction been prolinol and *N*-Boc-ethanolamine.

Additionally, a TBS-protected analogue of 1,3-dichloropropanol, compound **262**, was submitted to the same coupling conditions with *N*-benzyl-ethanolamine in case the presence of the free alcohol in **259** prevented coupling. However, this did not yield **263** (Scheme 3.50).

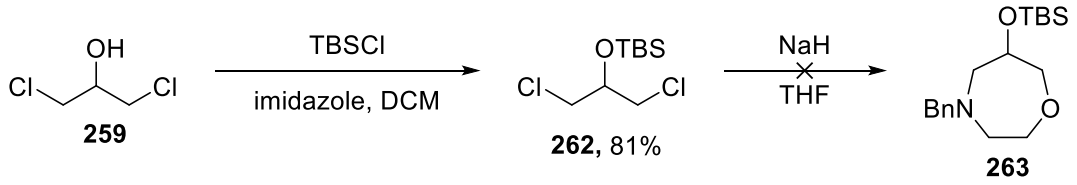

Scheme 3.50 TBS-protection of 1,3-dichloroisopropanol before attempted 1,4-oxazepane.

It was then examined whether a functional group other than a ketone or alcohol could be used in the coupling partners. A terminal alkene could also be used. This might be transformed into a ketone *via* the Lemieux–Johnson oxidation or submitted for pericyclic reactions itself.

Therefore 1,3-dichloroisobutene (**264**) was selected as a coupling partner. This was reacted with *N*-Boc-ethanolamine (**250**) under sodium hydride as a base and DMF solvent. This did produce a 1,4-oxazepane ring however, in the process, the nitrogen had its Boc-group removed and the olefin isomerised to an *endo* position within the ring (**265, Scheme 3.51**).

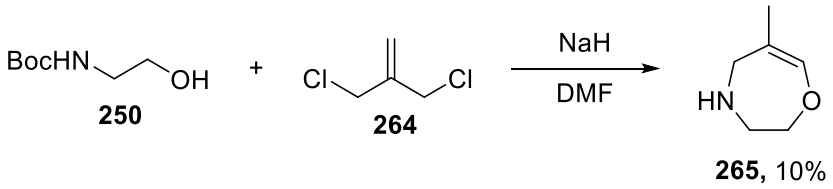

Scheme 3.51 Synthesis of 1,4-oxazepane with *endo*-cyclic olefin.

The reaction was repeated with prolinol under similar conditions with THF as solvent. This time a 1,4-oxazepane ring was formed with the desired *exo*-cyclic olefin (**266**) albeit in a disappointing 38% yield (Scheme 3.52).

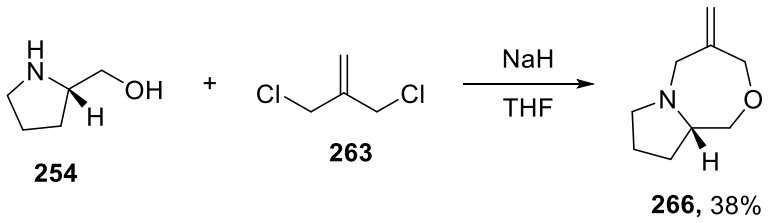

Scheme 3.52 Synthsis of 1,4-oxazepane, **266**, from prolinol and 1,3-dichloroisobutene.

With the first 1,4-oxazepane in hand, its oxidation was explored to transform the alkene into a ketone so that the Wittig reaction could be exploited to allow functionalised alkenes. Initially a Lemieux-Johnson oxidation was tried. Unfortunately, this reaction only returned 15% of the starting material and no product (Entry 1, Table 3.7). Therefore, the reaction was repeated with 20% more catalyst and at a slightly lower concentration. Again, none of the desired product (**267**) was produced (Entry 2, Table 3.7). Finally, the sodium metaperiodate equivalents were doubled so that this key oxidising agent was in excess. This did not yield the product either (Entry 3, Table 3.7). As can be seen from the ^{1}H NMRs (Figure 3.20), entries 2 and 3 gave the same product. In both cases, the alkene CH_2 peaks were still present as well as the other peaks found in the starting material. The new peaks could not be assigned, but all appeared in the region of the peaks for the 1,4-oxazepane ring.

Therefore, a different metallic oxidising agent was tried. A literature-based ruthenium (III) chloride oxidation was tried with Oxone acting the co-oxidising agent.[211] Finally, the ruthenium (III) chloride oxidation was repeated with sodium metaperiodate as the co-oxidant, but to no avail.

Table 3.7 Conditions for attempted oxidation of temrinal alkene to ketone.

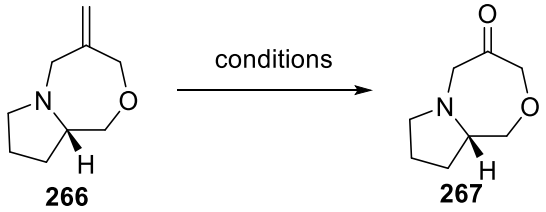

Entry	Conditions	Yield
1	OsO_4 (2.5% in ^tBuOH, 0.5 mol%), $NaIO_4$ (2.0 eq), Dioxane (0.3 M), H_2O (0.3 M), 18 h, RT	15% SM retuned
2	OsO_4 (2.5% in ^tBuOH, 0.6 mol%), $NaIO_4$ (2.0 eq), Dioxane (0.25 M), H_2O (0.25 M), 18 h, RT	21% by mass of by-product
3	OsO_4 (2.5% in ^tBuOH, 0.6 mol%), $NaIO_4$ (4.0 eq), Dioxane (0.25 M), H_2O (0.25 M), 18 h, RT	27% by mass of by-product
4	$RuCl_3$ (3.5 mol%), Oxone (2.5 eq), $NaHCO_3$ (7.8 eq), MeCN/H_2O (5:3, 0.02 M), 30 min, RT	Complex mixture
5	$RuCl_3$ (3.5 mol%), $NaIO_4$ (2.0 eq), DCE/H_2O (5:4, 0.1 M), 2H, RT	Complex mixture

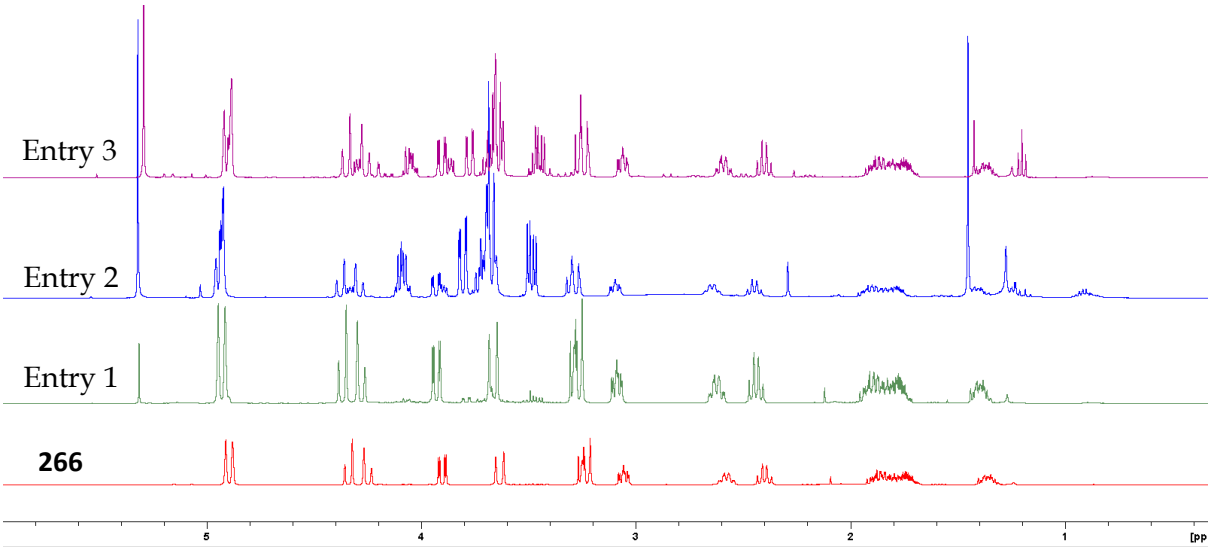

Figure 3.20 ^1H NMR from attempted Lemieux-Johnson oxidation of **266**. The red spectrum is the ^1H NMR of purified **266**. The green, blue, and purple spectra are the purified product of entries 1, 2, and 3 respectively in Table 3.7.

Finally, in an attempt to form a spirocycle with 1,4-oxazepane **266**, and questioning the reactivity of the alkene through the attempted oxidations, it was decided to react **266** with a carbene to undergo a [1+2] carbene insertion into a double bond. Thus, a literature procedure of rhodium (II) acetate mediated ethyl diazo acetate carbene generation was used to cyclopropanate the olefin in **266**. Despite a couple of attempts, only the carbene dimer (diethyl maleate) was isolated cleanly enough.

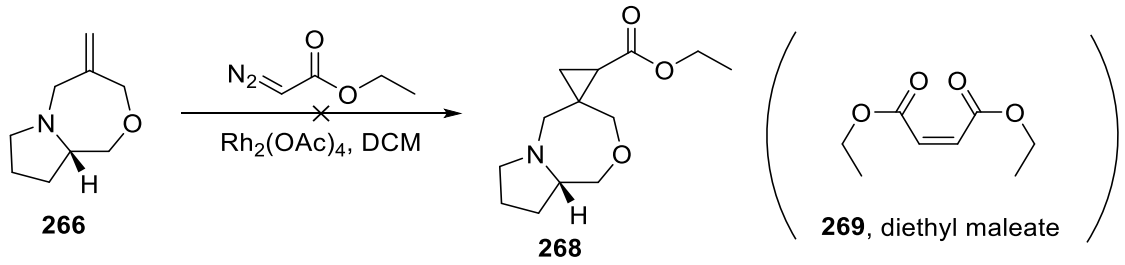

Scheme 3.53 Reaction between **266** and ethyl diazo acetate.

Due to the difficulties in constructing the 1,4-oxazepane ring and the problems in functionalising the ring when constructed, it was decided to abandon this line of research and focus on analysing the libraries already constructed.

3.6. Expansion and analysis of libraries

3.6.1. Enumeration and decoration libraries

The synthesis of the libraries above only represents a proportion of the scope of the chemical space the chemistry could probe. The full extent of this space can be appreciated by enumerating and decorating the libraries synthesised. In this context, enumeration means the combination of chemistry to form different scaffolds. This would be regarded as the SC[CPD] in Table 3.2. Decoration is the addition of appendages onto the SC[CPD] after it has been synthesised.

In the glycine-based spirocyclic library, only the six-membered cyclohexene tail ring was used. However, work by Attila Sveiczer also synthesised cyclopentene and cycloheptene tail rings. Additionally, he performed some double bond modifications (Figure 3.21).

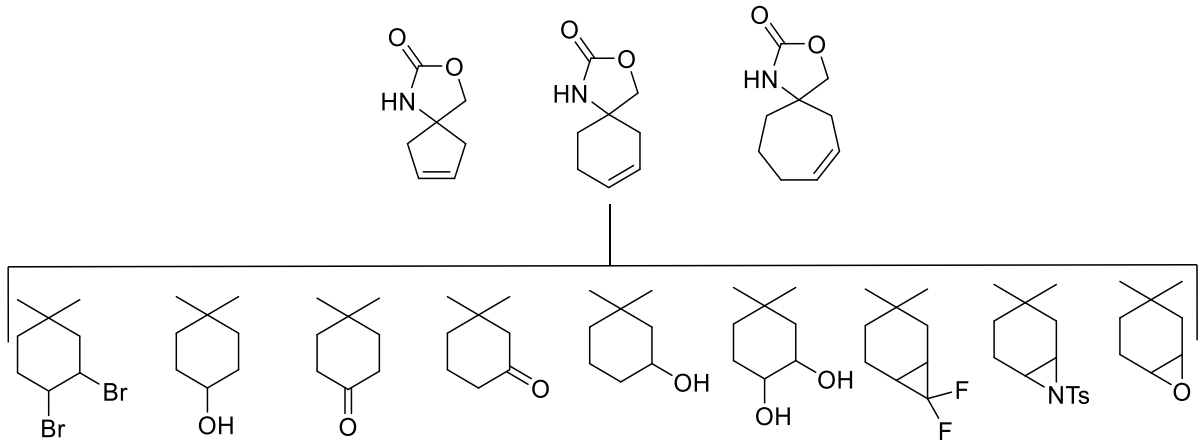

Figure 3.21 Summary of the tails and modifications synthesised by Sveiczer.

It is not necessary to synthesise each of these tails with each of the warheads as the modular nature of the chemistry means each can be made independently of one another. Therefore, a library can be constructed wherein all the spirocycles could be synthesised.

A first-generation library (1GLY) was computationally enumerated combining all the synthesised warheads (as detailed in section 3.4), with all the tails synthesised by Sveiczer (Figure 3.21). This is the library with the highest synthetic confidence.

A second-generation library was also enumerated (2GLY). This extended the scope of the tails by predicting that all the alkene modifications made to the cyclohexene ring would also be successful on the cyclopentene and cycloheptene rings. Additionally, a cycloheptene isomer with modification was also included in this library (Figure 3.22).

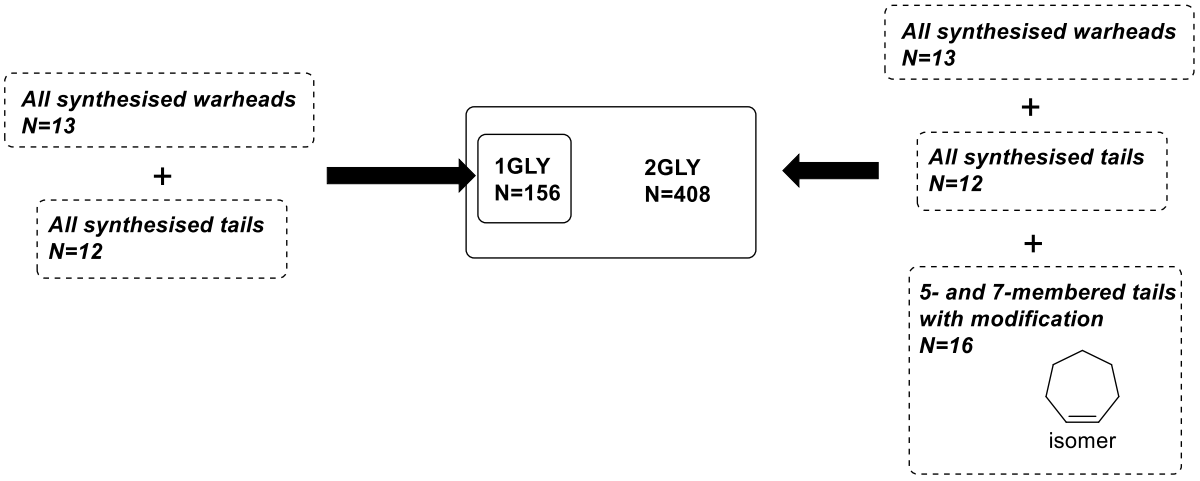

Figure 3.22 A diagram showing the component parts of libraries 1GLY and 2GLY. 1GLY is necessarily a sub-library of 2GLY.

The properties of these two libraries were analysed and compared to indicators of fragment-likeness (RO3) and likely success in biological screening.

Table 3.8 Comparison of the two enumerated libraries, 1GLY and 2GLY , showing the average value of the properties with the standard deviation in parenthesis. The 3/75 Rule finds that a compound with a clogP < 3, and a PSA of < 75 Å^2 ia 2.5 times less likely to be toxic at 10 µM. The value in the table is the percentage of the library which obey the rule.

Property	Rule of Three[71]	1GLY	2GLY
Molecular Weight (gmol^{-1})	< 300	231.42 (73)	242.77 (75.6)
clogP	≤ 3	0.53 (1.0)	0.52 (1.1)
Polar Surface Area (Å^2)	≤ 60	57.7 (23)	60.7 (23)
H-Bond Acceptors	≤ 3	3.9 (1.2)	4.1 (1.3)
H-Bond Donors	≤ 3	1.3 (0.8)	1.3 (0.8)
Rotatable Bond Count	≤ 3	0.80 (1.1)	0.81 (1.1)
3/75 Rule[23]	—	74%	70%

As can been seen from Table 3.8, the mean properties of the libraries broadly fall within the RO3. As expected, the mean value of the molecular weight is higher for 2GLY because two types of cycloheptene ring were allowed in the enumeration. The two properties which may cause some concern are the PSA and H-bond acceptors. These are only just in range or slightly violate the RO3. The high PSA is due to the presence of bromides and tosyl groups in some compounds. The presence of the tosyl groups also explains the high mean of H-bond acceptors. However, as can be seen from Figure 3.23, most of the compound which contributes to the high PSA fall outside the RO3 limits on molecular weight and clogP. This indicates that the compounds in the libraries either have properties which all generally fall into the RO3 or all fall outside the RO3.

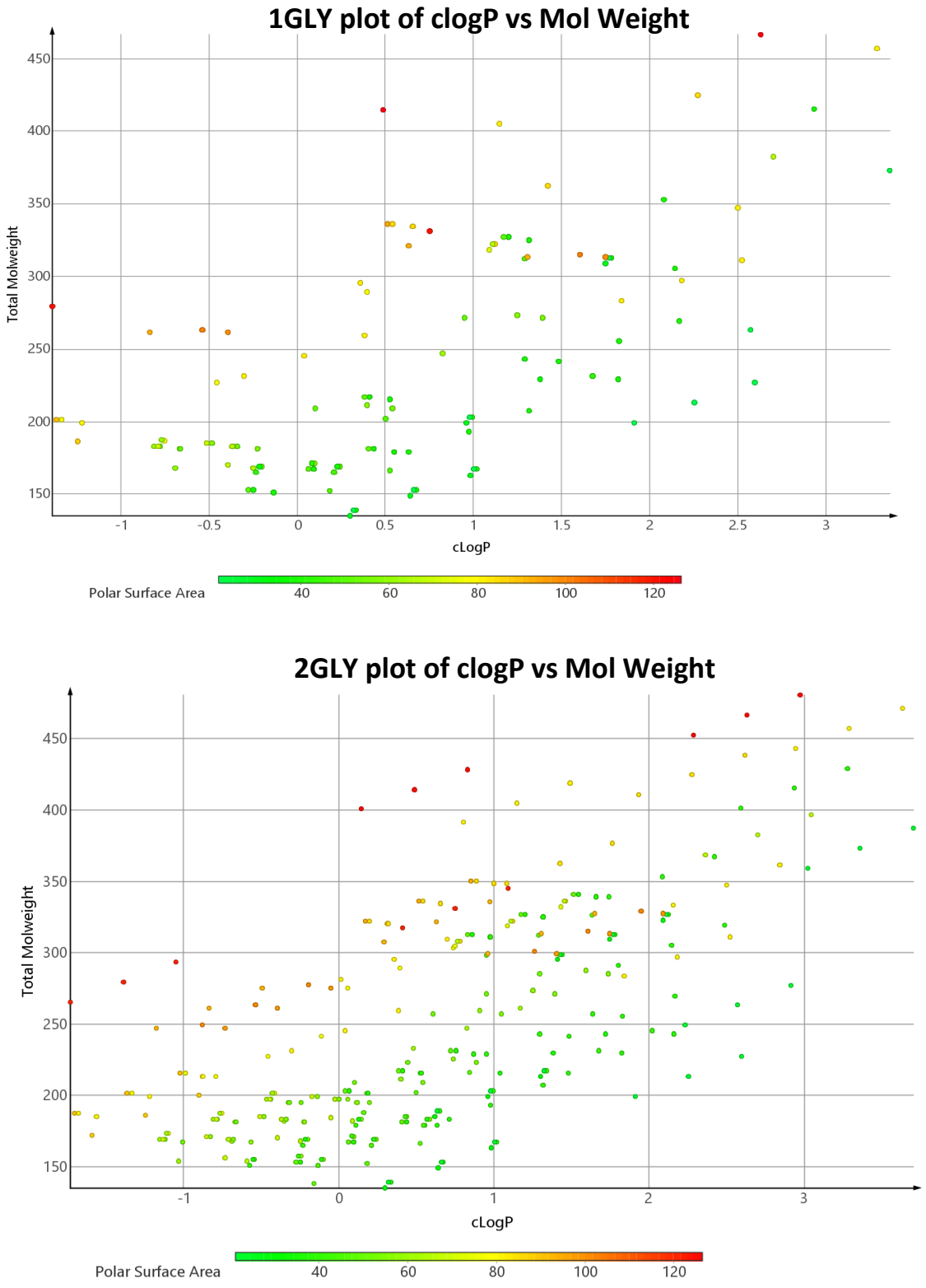

Figure 3.23 Plot of clogP against molecular weight for libraries 1GLY and 2GLY. The shading of the points also indicates the value of the PSA.

For the next level of enumeration of the glycine-based library, different reagents can be explored at key points in the synthesis. This will have a lower confidence level as the proposed reactions will not have been tried on the substrates in the laboratory, however, use of the literature can guide the viability of the reactions. Examination of the synthesis of glycine library can show where enumeration points occur.

The advantages of this synthetic approach are evident in the multiple vectors of elaboration. The modular installation of the terminal alkene moieties allows early substitution on the tail ring (Figure 3.24). Consideration here would have to be given to the compatibility of the groups with the S_N2 installation, acidic removal the benzophenone, and Grubbs II RCM.

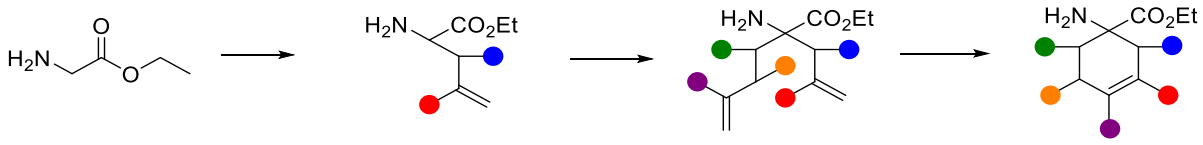

Figure 3.24 Installation of five possible vectors for further fragment development by modular installation of the alkene moieties.

Additionally, the warheads leave ample vectors for decoration and elaboration (Figure 3.25).

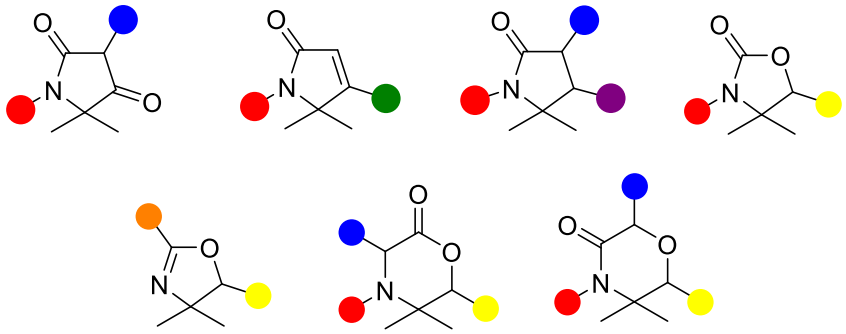

Figure 3.25 Elaboration vectors on the warheads. The colours represent the possible reactions to elaborate the vectors. Red: alkylation/acylation by nucleophilic N. Blue: Addition from nucleophilic enolate formation. Green: Metal-mediated cross coupling. Purple: S_N2. Yellow: Grignard-type nucleophilic-reduction of ester to alcohol. Orange: Imidate condensation.

A sample of the possible decoration vectors can be explored and assessed computationally. Using the open access LLAMA programme,[212] the synthesised warheads with a cyclohexene tail were decorated with a variety of reliable reactions (see appendix). This gave a decorated library GLY-DEC1. This can give an indication about the properties of the chemical space around 1GLY and 2GLY.

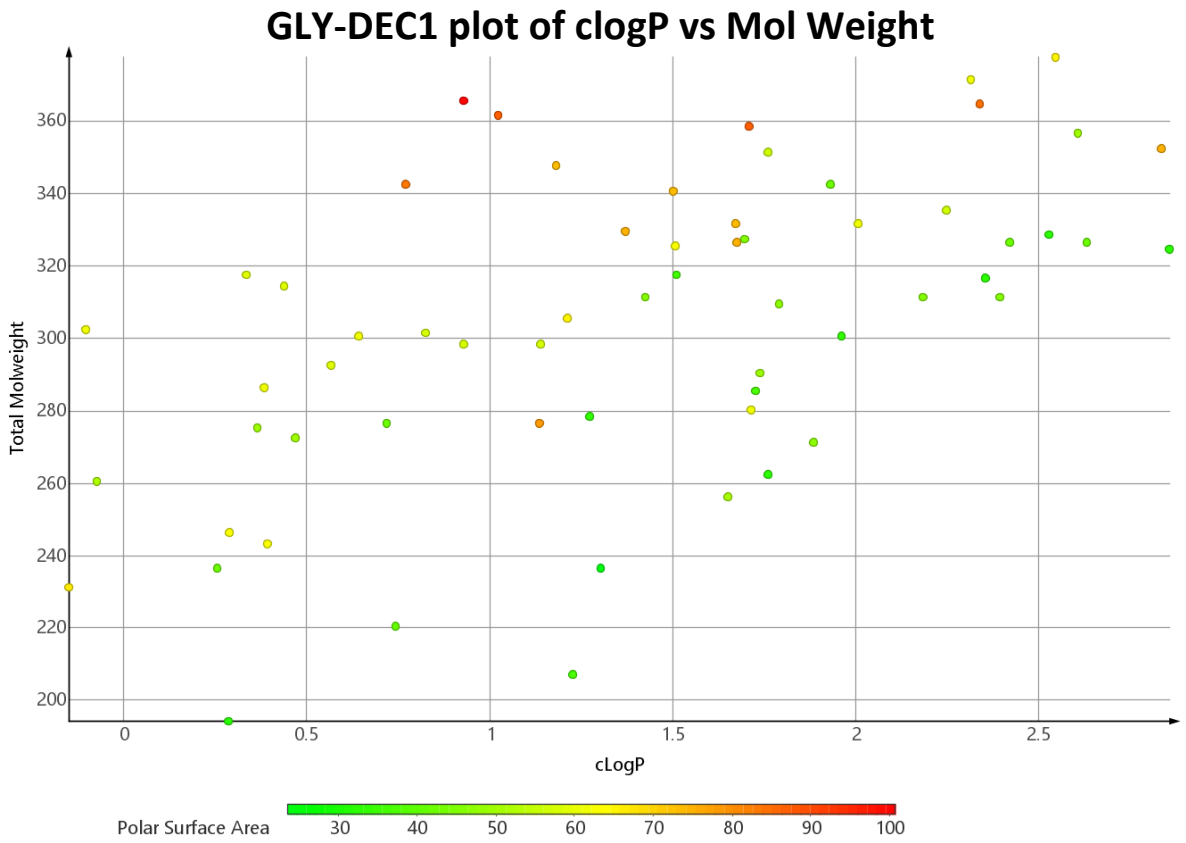

Figure 3.26 Plot of clogP against molecular weight GLY-DEC1 library. The shading of the points also indicated the value of the PSA.

As can be seen from Figure 3.26, the library still has favourable physico-chemical properties and most of the molecules are either in RO3 limits or are moving more into lead-like RO5 space. This is promising for further development of the library.

Next, the dehydroalanine library was enumerated. This involved the synthesis of intermediate **202**. This was successfully reacted with a nitrile oxide to form a dihydroisoxazole ring, and the Boc-protected N and ester were closed to give a carbamate warhead (Scheme 3.54).

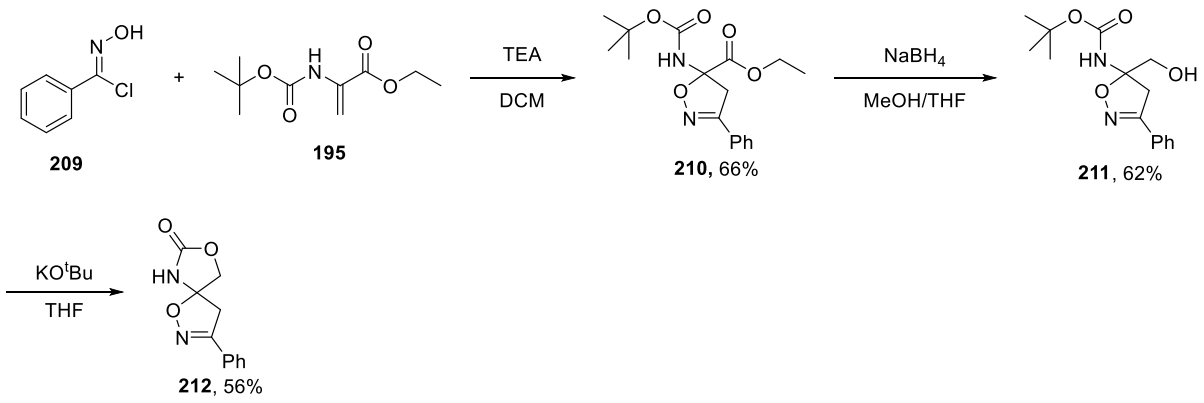

Scheme 3.54 Formation of dehydroalanine spirocycle **212**.

This allows for two areas of elaboration: the amino and ester closure, and the pendent group on the nitrile oxide. The existence in the literature[213] of the dihydroisoxazole ring with a geminally disposed primary amine and ester (**270**) means that there is reasonable confidence that the warheads enumerated in the 1GLY library could also be enumerated here (Figure 3.27).

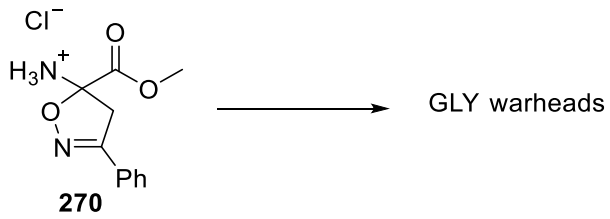

Figure 3.27 Literature compound **270** gives reasonable confidence to enumerating the warheads from the glycine library.

To complement this, a small range of imidates were chosen as nitrile oxide precursors for dihydroisoazole ring formation. These were selected to represent a range of functionalities: aromatic, heterocyclic, cyclic, and aliphatic.

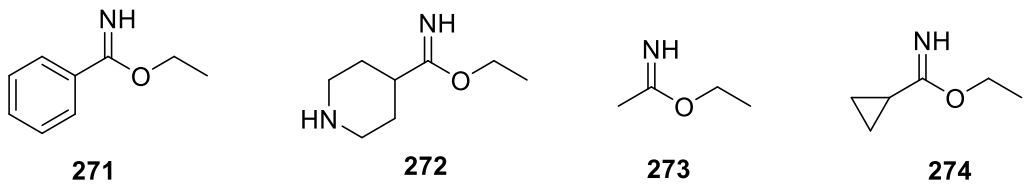

Figure 3.28 Chosen imidates as nitrile oxide precursors.

Therefore, a library was enumerated combining the warheads with an isoazole ring substituted with the four groups in Figure 3.28. This gave library DEHAL (Figure 3.29).

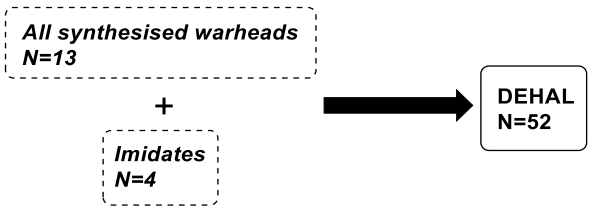

Figure 3.29 Construction of DEHAL library.

The physico-chemical properties of this library are summarised in Table 3.9 and Figure 3.30. Pleasingly, this library seems to be reasonably fragment-like. Unfortunately, this library suffers from high PSA and H-bond donors for a fragment collection. This is down to the isoazole ring containing two heteroatoms which increases both metrics.

Table 3.9 Comparison of DEHAL library, showing the average value of the properties with the standard deviation in parenthesis.

Property	Rule of Three[71]	DEHAL
Molecular Weight ($gmol^{-1}$)	< 300	233.88 (54)
clogP	≤ 3	1.20 (0.9)
Polar Surface Area ($Å^2$)	≤ 60	69.7 (17.7)
H-Bond Acceptors	≤ 3	5.4 (1.0)
H-Bond Donors	≤ 3	1.2 (0.6)
Rotatable Bond Count	≤ 3	1.5 (1.1)
3/75 Rule[23]	–	75%

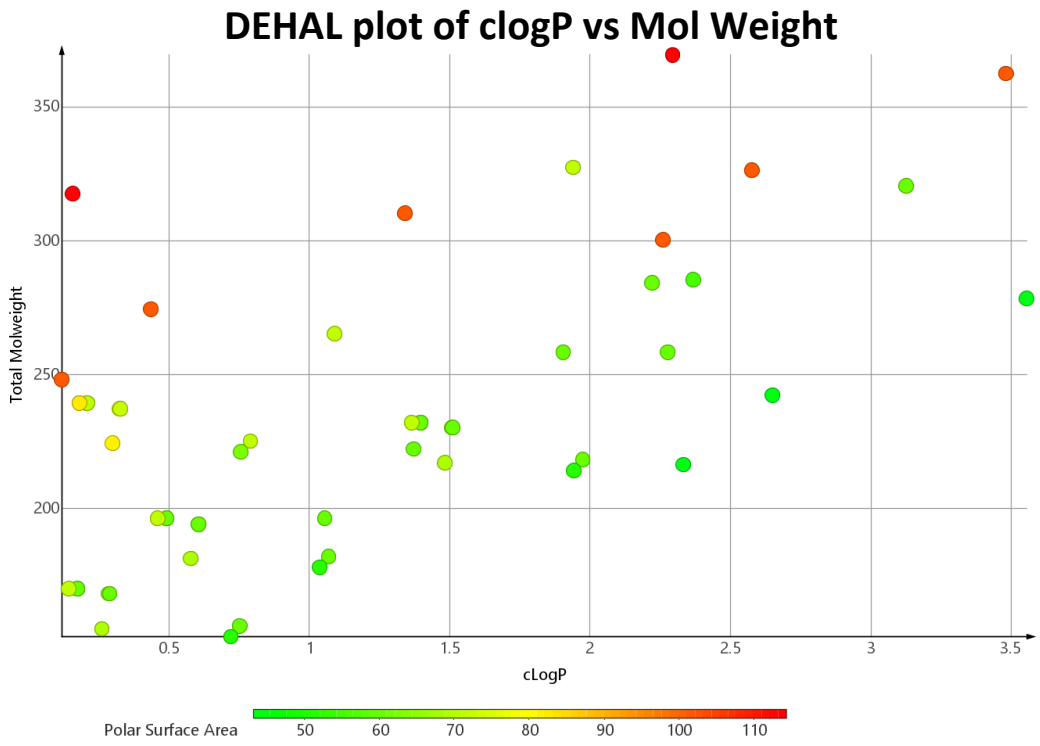

Figure 3.30 Plot of clogP against molecular weight GLY-DEC1 library. The shading of the points also indicates the value of the PSA.

Finally, a small compound library was constructed from the azetidinone series. This took the two key reactions established in the research (the nitrile oxide cycloaddition and the azide cycloaddition) and extended them for four nitrile oxide (the ones given in Figure 3.28) and four azides (again the same appendages as in Figure 3.28 but a benzyl group in lieu of the phenyl one). These were computationally-coupled with two azetidinone derivatives: the α,β-unsaturated ethyl ester as used in the chemistry, above and the electronically similar α,β-unsaturated nitrile. This gave the AZE library.

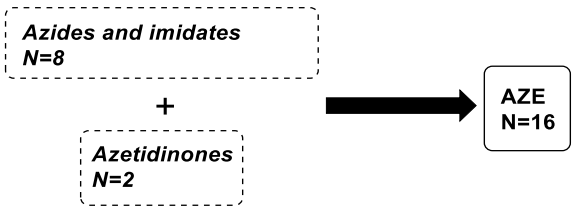

Figure 3.31 construction of the AZE library.

As with the DEHAL library, most of the properties are fragment-like yet there is the slight problem of the high PSA and number of H-bond acceptors. Perhaps a way to minimise this in

these libraries would be to use 1,3-dipoles or dienes with fewer heteroatoms (Table 3.10 and Figure 3.32).

Table 3.10 Comparison of AZE library, showing the average value of the properties with the standard deviation in parenthesis.

Property	Rule of Three[71]	DEHAL
Molecular Weight ($gmol^{-1}$)	< 300	214.00 (38)
clogP	≤ 3	-0.03 (1.1)
Polar Surface Area ($Å^2$)	≤ 60	64.86 (6.4)
H-Bond Acceptors	≤ 3	5.3 (1.0)
H-Bond Donors	≤ 3	1.3 (0.9)
Rotatable Bond Count	≤ 3	2.3 (1.6)
3/75 Rule[23]	–	88%

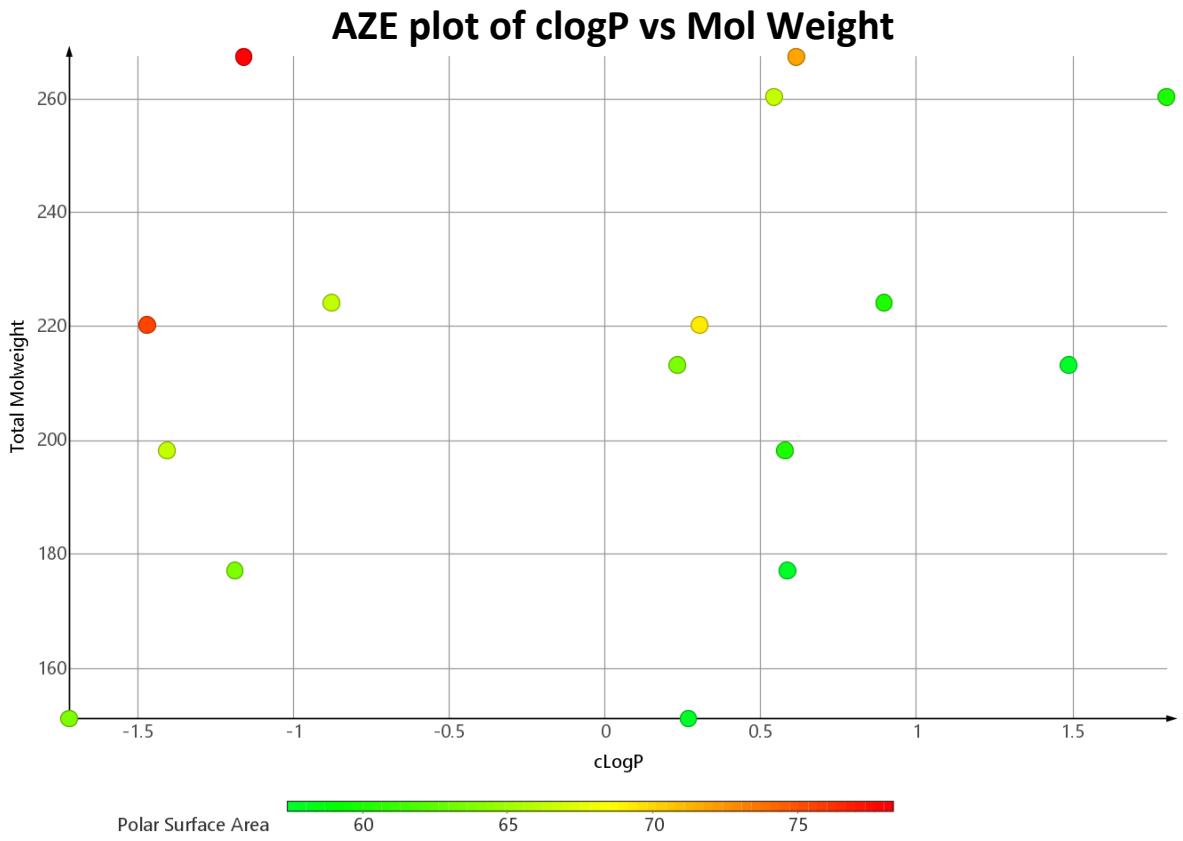

Figure 3.32 Plot of clogP against molecular weight GLY-DEC1 library. The shading of the points also indicates the value of the PSA.

3.6.2. Spatial diversity of libraries

As well as analysing the raw physico-chemical properties of these libraries, the spatial diversity can also be measured by plotting PMI graphs and the diversity of the physico-chemical data can be measure by PCA graphs.

Computational analysis of the above libraries was performed using Molecular Operating Environment (MOE) software version 2016.0802 from the Chemical Computing Group.

The computational parameters of the PMI analysis and PCA are given in Appendix C.[c]

The above libraries (1GLY, 2GLY, GLY-DEC1, DEHAL, and AZE) were evaluated and compared to small molecules in the top 50 selling pharmaceuticals of 2013[214] (Structures in Appendix C).

Merck molecular force field 94X (MMFF94x), an all-atom force field parameterised for small organic molecules with the Generalised Born solvation model, was used to minimise the energy potential of the library members. A Low Mode MD search was employed for the conformation generation.

Since crystal structures were obtained for four of the spirocycles, a visual comparison was first performed. The structures are shown in **Table 3.11** and are seen to be visually similar. The conformationally constrained nature of spirocycles means that computational models are more likely to be reliable in predicting conformation.

[c] The procedure followed to carry out PMI analysis and PCA is based on the procedure developed by Dr Feilin Nie

Table 3.11 Comparison of the computational lowest energy conformation and crystal structures.

Structure	Lowest Energy Confirmation	Crystal structure
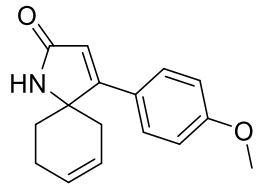	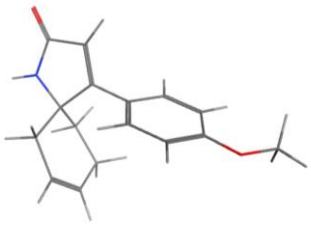	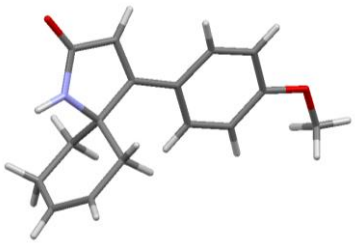
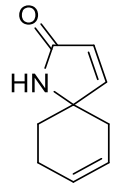	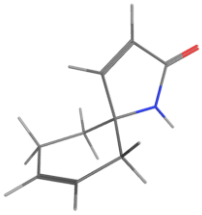	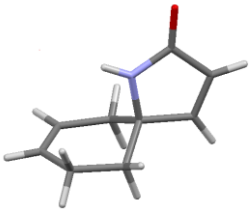
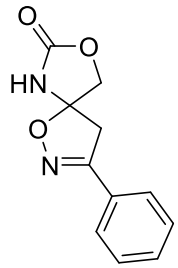	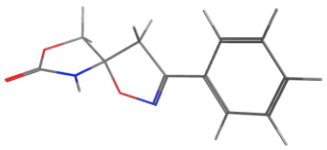	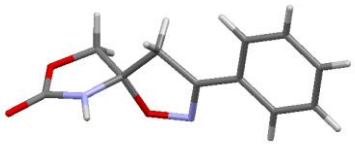
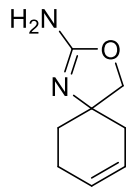	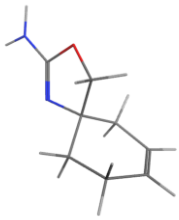	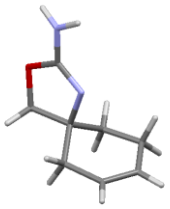

The conformers of each library member were calculated, with the lowest energy conformer assigned a relative energy value of 0 kJmol^{-1}. For each conformer, the principle moments of inertia ($\mathbf{I_1}$, $\mathbf{I_2}$, $\mathbf{I_3}$) were calculated and then normalised to ($\mathbf{I_1/I_3}$) and ($\mathbf{I_2/I_3}$). These values were then plotted on a triangle graph, with the three vertices at (0,1), (0.5,0.5), and (1,1) representing the three 3D extremes of rod-like, disk-like, and sphere-like respectively. The lowest energy conformation is plotted in Figure 3.33.

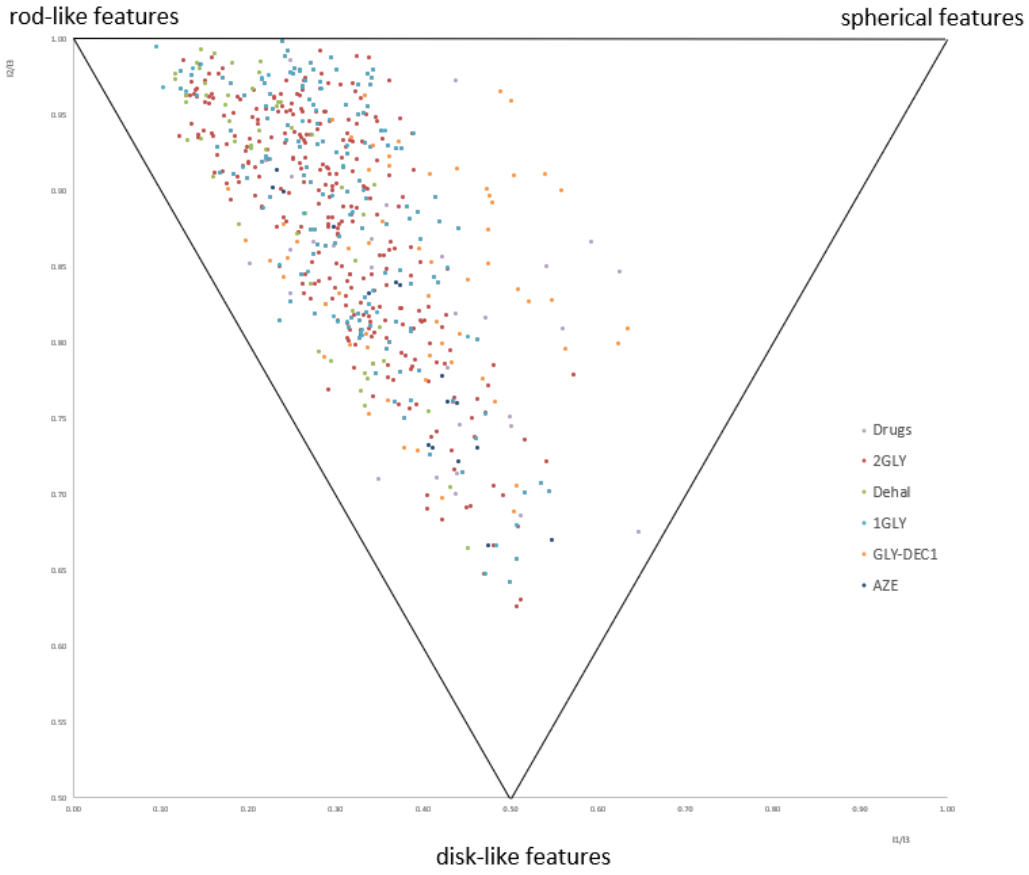

Figure 3.33 PMI plot showing the spatial diversity of compound libraries. Each point on the plot represents a compound in the library at its lowest energy conformation as calculated by MOE. 30 top selling drugs (purple), 168 1GLY library (light blue), 408 2GLY library (red), 61 GLY-DEC1 library (orange), 52 DEHAL library (green), 16 AZE library (dark blue). x-azis $\mathbf{I_1/I_3}$, y-axis $\mathbf{I_2/I_3}$.

As can be expected, the spirocycles predominantly possess rod-like features, with most clustering around the top-left of the PMI plot. Pleasingly, the range of compounds seem to have escaped 'flat-land', the rod-disk line. By inspection of the plot it seems that the appendage decorated library, GLY-1DEC, increased the spatial spread of the spirocycles incorporating more sphere properties.

Fortunately, the cumulative frequency of the compounds can be measured as a function of their distance from the rod-disk axis. This allows for easier inspection of how 'flat' the library is and how much of the chemical space it covers (Figure 3.34).

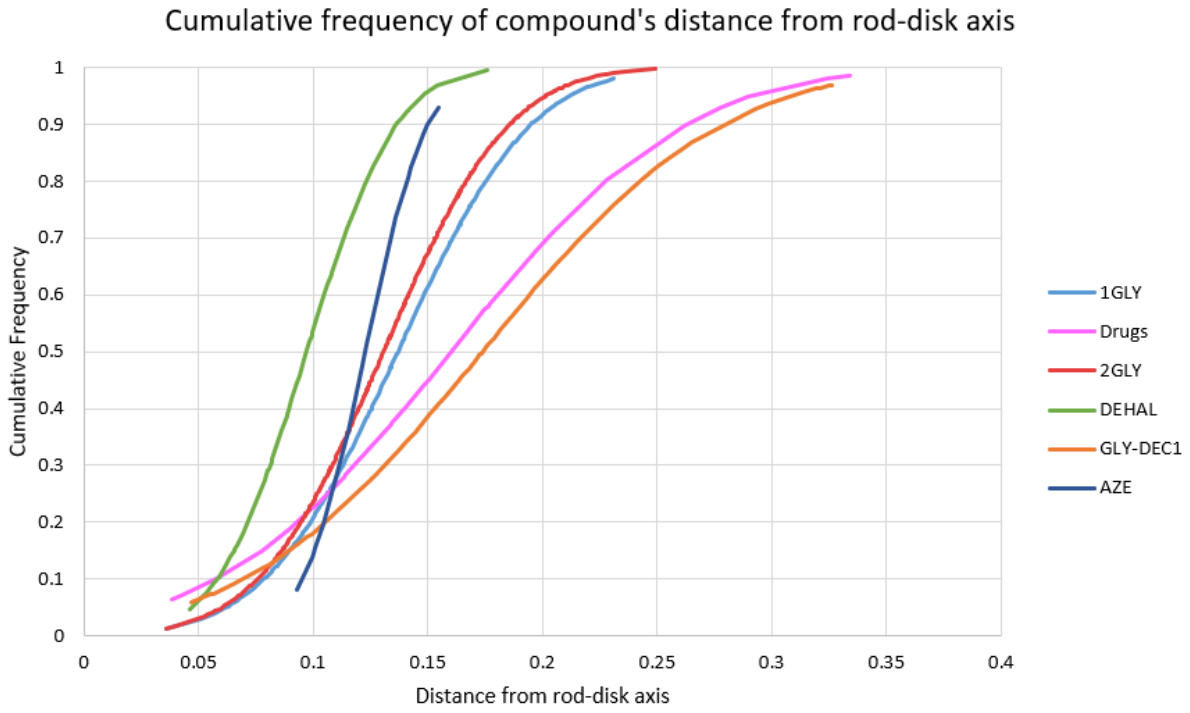

Figure 3.34 Cumulative frequency graph of compound distance from rod-disk axis. This allows easy visualisation of the diversity of compound libraries on the PMI plot. The steeper the gradient of the lines, the less chemical space the library explores. The maximum distance a compound can be form the rod-disk axis is $1/\sqrt{2} \approx 0.71$.

The least spatially diverse library is AZE, probably due to the second ring being limited to either an isoazole to 1,2,3-triazole. Despite allowing for more possible ring combinations between 1GLY and 2GLY, the libraries occupy a broadly similar chemical space. The AZE library is slightly further from flat land, however the steeper gradient of the line indicates it displays less spatial diversity. Finally, and most interestingly, there is a strong similarity between the chemical space occupied by GLY-DEC1 and the marketed drugs. The core fragment scaffolds being small, appendages can make a large difference to the spatial diversity of the library. This simple modification of the library is likely to bring it into biologically relevant space.

The lowest energy conformer is only part of the picture because a molecule's conformation can change in solution or find favourable interactions on a biologically target. Therefore, the energy window was expanded to 3 $kJmol^{-1}$. Since $\Delta G = -RTln(k)$ with an energy window of $\Delta G = 3\ kJmol^{-1}$ $k \approx 0.3$, so the top 70% lowest energy conformers are included.

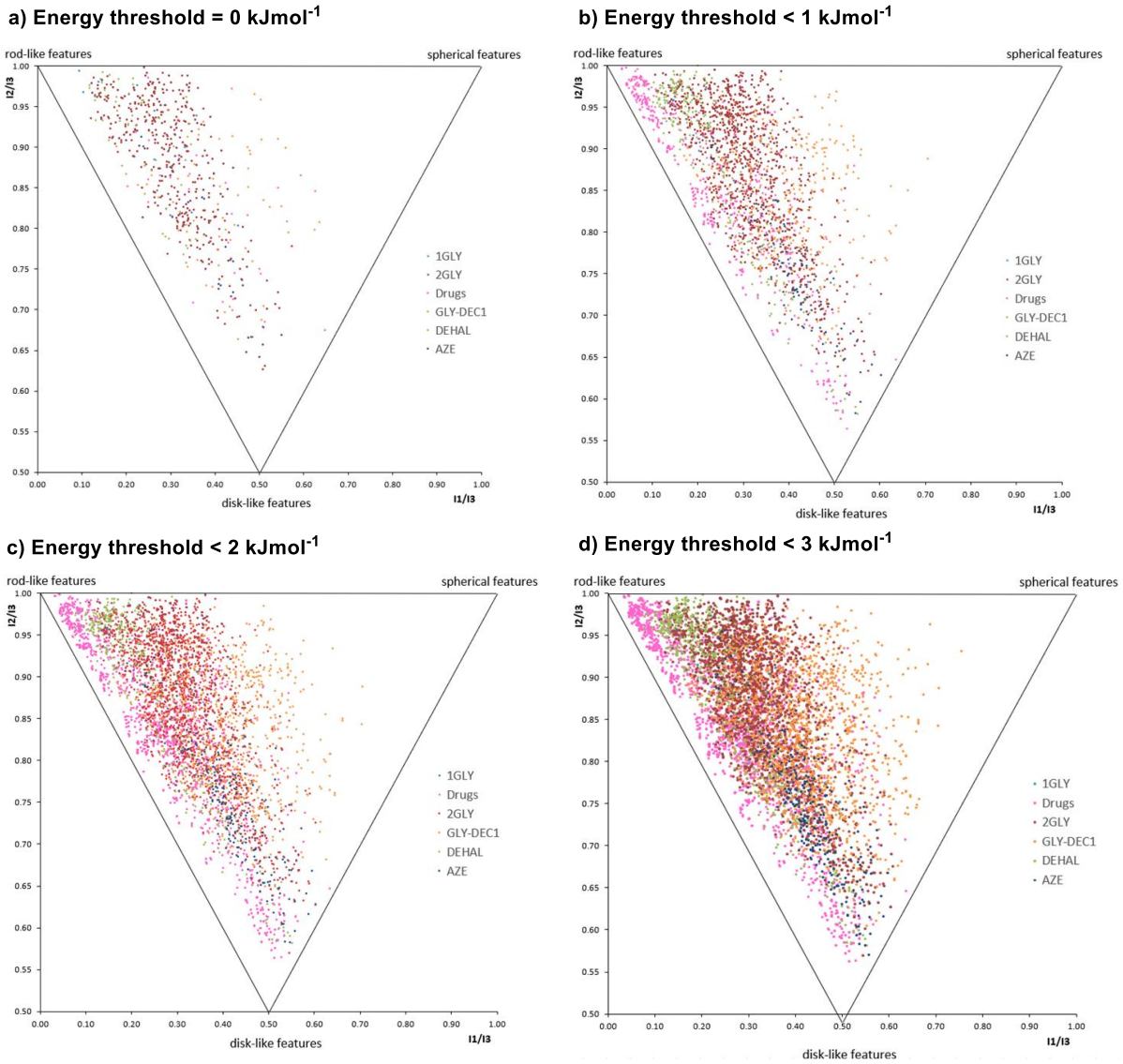

Figure 3.35 PMI plots of the conformers of the five compound libraries compared to the drugs reference set. a) Energy level cut of at 0 kJmol^{-1} (lowest energy conformer); b) energy level cut of at 1 kJmol^{-1}; c) energy level cut of at 2 kJmol^{-1}; d) energy level cut of at 3 kJmol^{-1}.

As can be seen in Figure 3.35, as the energy threshold is increased the marketed drugs start to cluster along the rod-disk axis, whereas the GLY-DEC1 library pleasingly spreads out and occupies more chemical space. The DEHAL and AZE libraries begin to cluster; DEHAL into the top left rod-like area and AZE trending more towards disk-like features. The 1GLY and 2GLY library spread out a reasonable distance from the rod-disk axis. A clearer illustration of this comparison can be seen in Figure 3.36 where each component of Figure 3.35d is separated.

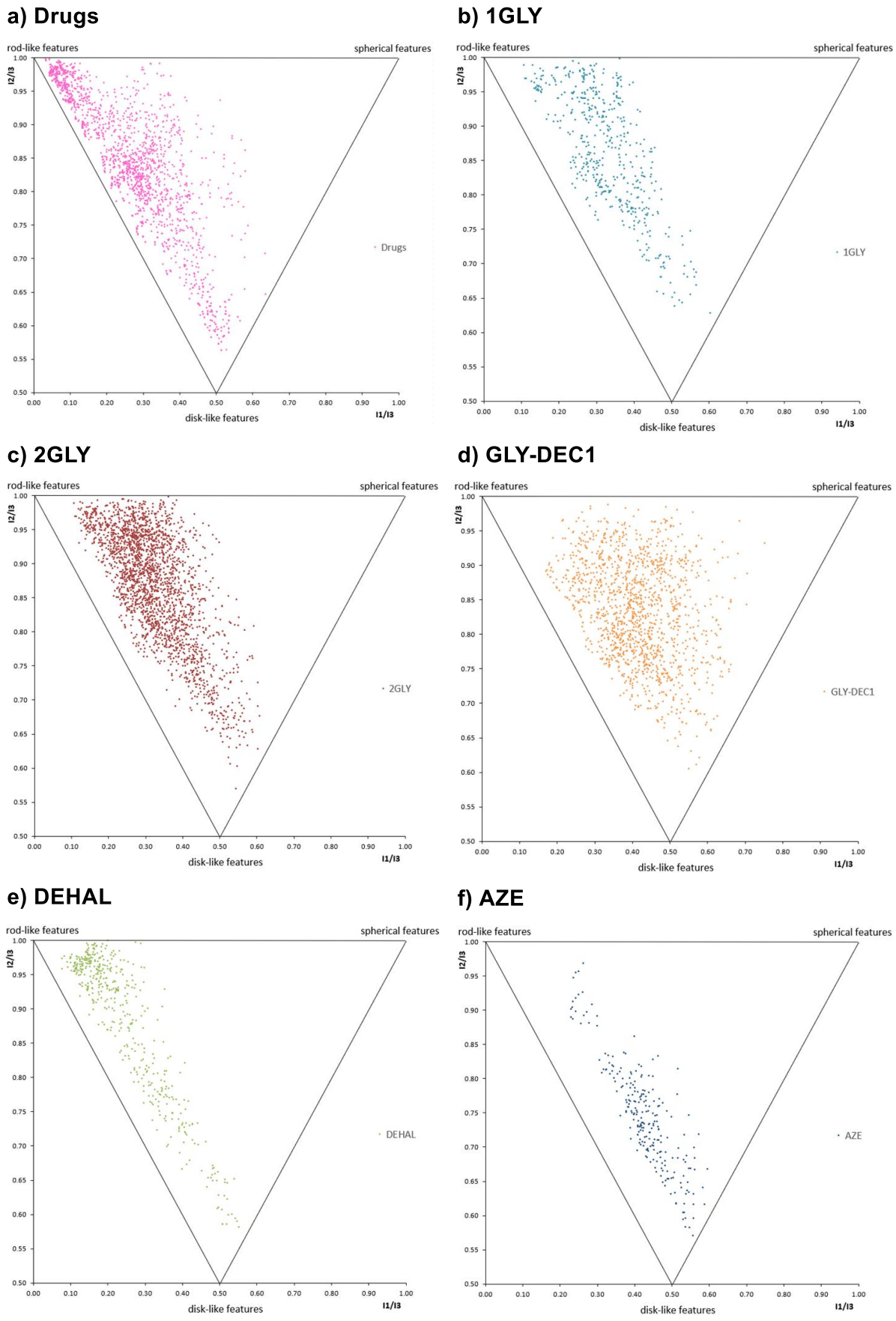

Figure 3.36 PMI plot of each DOS library at 3 kJmol^{-1} threshold.

Overall, the different spirocyclic libraries integrated a large range of chemical space. Most interesting was the GLY-DEC1 library which showed that appendage growth from these scaffolds creates spatially diverse compounds. All the libraries avoided 'flat land', the region of chemical space which seems to be exhausted for novel chemical leads. This gives confidence that these libraries possess the necessary spatial qualities for further exploration.

3.6.3. Principle component analysis of libraries

For each compound based on its lowest energy conformation, seventeen structural and physico-chemical descriptors were selected. These ranged from solubility, weight, H-bond acceptors, PSA, etc. Due to the impossibility of visualising these data in 17-dimensions, principle component analysis was employed. Each of the 17-dimensional vectors were reduced to 2-dimensional vectors by linear transformation. A linear combination of the descriptors was calculated to represent as much of the variance in the data as possible. This gave seventeen unitless principle components. Each compound represented by a 2-dimensional vector was plotted on a scatter chart to visualise the extent of chemical space spanned by the libraries. To keep 95% of the variance original data set, seven principle components were retained (Table 3.12).

Table 3.12 Standard deviation and contribution of each principle component of variant. [a] The standard deviation of the data along the principle component vector. [b] Condition number of the covariance matrix if the principle component list were terminated at that row. [c] Percentage of the variance retained if the component list were truncated at that row.

PC#	Deviation[a]	Condition[b]	Proportion of Variance	% Variance[c]
PC1	2.798	1.000	46.037	46.037
PC2	1.899	2.170	21.214	67.251
PC3	1.300	4.629	9.944	77.195
PC4	1.049	7.116	6.47	83.665
PC5	0.914	9.378	4.909	88.574
PC6	0.888	9.916	4.643	93.217
PC7	0.682	16.810	2.738	95.955

The first three principle components, accounting for 77% of the variance of the data set, were plotted onto three scatter graphs (Figure 3.37).

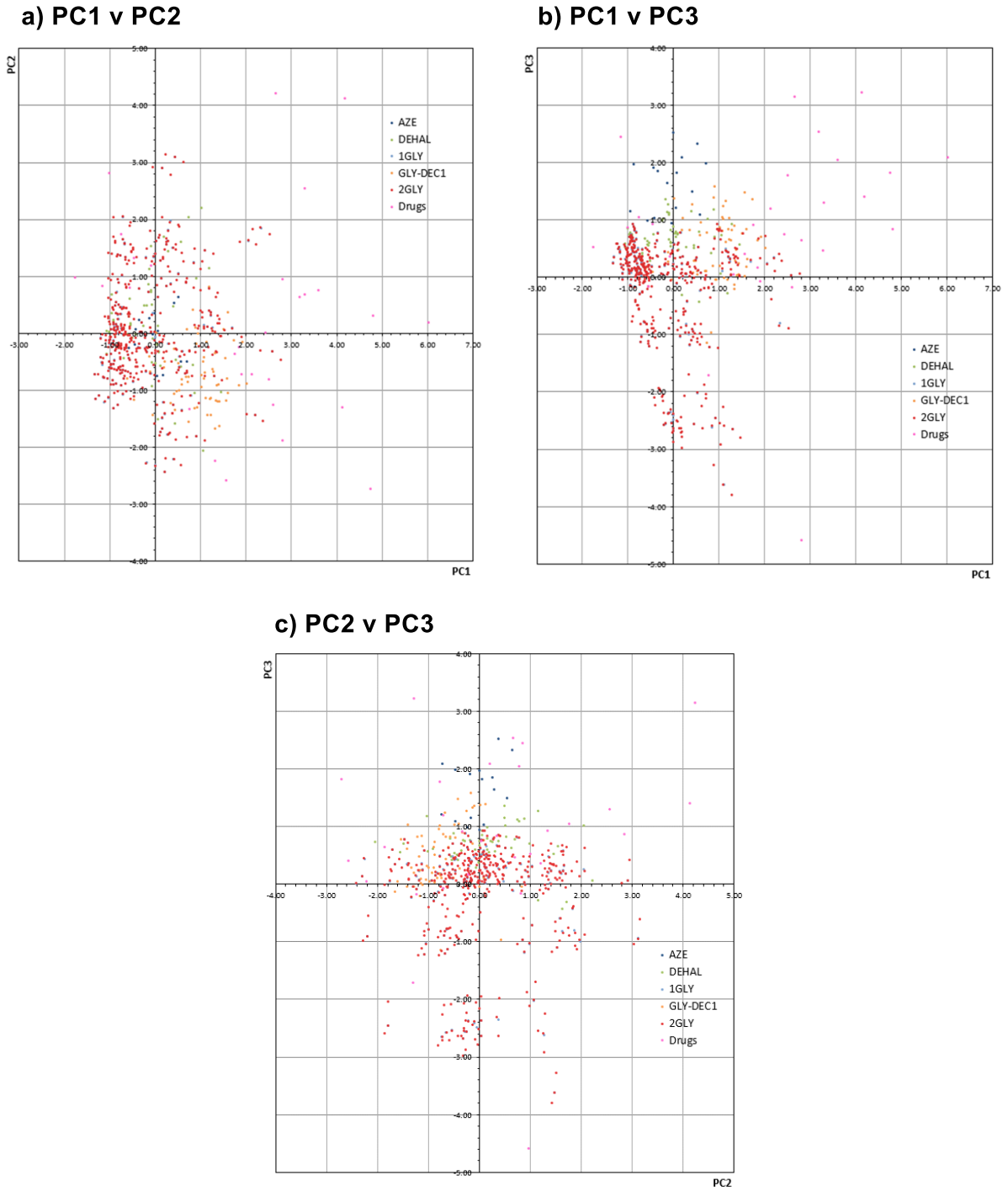

Figure 3.37 PCA plots of each spirocyclic library against the drugs data set. a) PC1 v PC2, b) PC1 vPC3, c) PC2 v PC3.

Figure 3.37a shows the 'Drugs' library occupying a very broad and different range of chemical space compared to the spirocyclic libraries. The difference in breadth is likely down to the fact that the spirocyclic libraries were restricted to a spirocyclic core and were only fragment-like. Again, the differences are highlighted between the 1GLY, 2GLY, and GLY-DEC1 with different areas of the grid occupied.

In Figure 3.37b, the 1GLY and 2GLY libraries seem to cover approximately the same chemical space as in Figure 3.37a. However, this time the libraries are more differentiated. Moving from left to right along the x-axis 2GLY gives way to DEHAL and AZE, with AZE further up the y-axis. Next comes GLY-DEC1, most of whose members are in the positive region of the x-axis. Finally, the drugs represent their diversity by scattering about the first quadrant.

Figure 3.37c again shows the range of chemical space explored by the spirocycles with each library integrating different areas of space. 2GLY also demonstrates its larger physcio-chemical diversity by being represented below the x-axis. Interestingly the DEHAL library is quite diverse under these conditions, having components in quadrants I, II, and IV.

The transformation matrix of the first seven principle components (95% of the total variance) is shown in Table 3.13. This suggests that increasing the number of rings and the number of nitrogens the molecular flexibility would shift the molecules in a positive direction along the x-axis (more into the chemical space occupied by the drugs).

The most important contributors to PC2 were the number of H-bond donors and acceptors and the number of oxygen atoms. Increasingly these should shift the libraries positively along the PC2 axis, whereas increasing the number of rings would have the opposite effect.

Finally, PC3 indicates that the number of nitrogen atoms, the solubility in water, and the number of H-bond acceptors would move the spirocyclic libraries up along the PC3 axis.

Table 3.13 Component loadings for the PCA of the six compound libraries. The top six contributing parameters to each principle component are highlighted in grey. All values are normalised.

Descriptor	PC1	PC2	PC3	PC4	PC5	PC6	PC7
ASA_H	0.0011	-0.0011	0.0020	-0.0020	-0.0020	0.0015	0.0030
ASA_P	0.0004	0.0033	-0.0059	0.0048	0.0059	-0.0051	-0.0076
KierFlex	0.0708	0.0568	-0.1725	0.1722	-0.0880	0.1523	0.4722
SlogP	0.0680	-0.1347	-0.1280	0.1404	-0.0639	0.0846	-0.0863
TPSA	0.0023	0.0108	0.0079	-0.0003	-0.0001	-0.0044	-0.0113
Weight	0.0015	0.0005	-0.0024	0.0006	0.0005	-0.0009	0.0004
a_acc	0.0523	0.1495	0.1231	-0.0949	-0.0891	-0.1786	0.1970
a_aro	0.0280	-0.0229	0.0413	-0.0104	-0.0260	0.0332	-0.1695
a_don	-0.0092	0.1924	0.1552	0.0816	0.1762	0.9748	-0.5035
a_nN	0.0712	-0.0065	0.3321	0.3013	0.7741	-0.2422	0.2015
a_nO	0.0326	0.1818	0.0188	-0.1776	-0.3656	-0.1868	-0.1056
b_rotN	0.0523	0.0192	0.0522	0.1314	-0.0406	0.0575	0.1366
chiral	0.0261	0.0624	-0.2553	-0.5431	0.4069	0.2576	0.2794
logS	-0.0752	0.0440	0.1579	-0.0122	0.0867	0.0335	0.4598
mr	0.0633	-0.0119	0.0080	-0.0067	-0.0079	0.0329	0.0467
rings	0.1077	-0.1095	0.1183	-0.4540	0.3349	-0.3067	-0.3722
vol	0.0019	-0.0002	0.0000	-0.0002	0.0002	0.0012	0.0027

Principle component analysis has shown that the different libraries integrate different areas of physico-chemical space, with the 2GLY library having the broadest reach. This analysis can also aid in the further refinement of the libraries to ensure the greatest amount of diversity.

3.7. Conclusions

Herein, four synthetic strategies have been employed to synthesise diverse fragment libraries based on spirocyclic compounds. The first of these was based upon a tetra-functionalised glycine derivative which was subjected to the B/C/P paradigm. A range of chemistry was employed to join the amino and ester functionalities to form a 'warhead' ring, while RCM formed a cyclohexene tail. This approach yielded thirteen novel spirocyclic scaffolds.

Next, pericyclic chemistry was explored to form spirocycles. Trying to utilise the same amino-ester couplings as previously, a dehydroalanine derivative was synthesised. A range of approaches were used in trying to synthesise spirocycles from this compound. Forming the warhead first and then using pericyclic chemistry proved unsuccessful, but direct formation of the pericyclic ring on the dehydroalanine did work. This establishing the possibility of

using electron deficient 1,3-dipoles or dienes to form the 'tail' and using the established amino-ester couplings to form the warhead.

The use of pericyclic reactions was further explored by attempted Wittig installation of *exo*-cyclic olefins onto rare or privileged scaffolds. Azetidinone proved a good starting material for the installation of an electron deficient alkene which performed pericyclic reactions. On the other hand, 1,4-oxazepanes proved a synthetic challenge to make.

These libraries were enumerated computationally giving five libraries. The spatical and physico-chemical diversity of these libraries were measured and pleasingly they were found to possess descriptors which favour successful clinical candidates.

Chapter 4

Conclusions and future work

4.1. Conclusions

This project has focused on two key areas of the fragment-based drug discovery (FBDD) process: the design of fragments, and the elaboration of fragments to increase potency of potential inhibitors of CK2.

As part of the ongoing research to discover novel non-ATP competitive inhibitors of CK2, a lead fragment NMR154L emerged in the literature. Using NMR154L as a lead, this project has utilised novel chemistry, X-ray crystallography and computational analysis to improve the binding and specificity of the fragment which, in turn, could lead to improved CK2 inhibitors.

Screening libraries of fragments have historically failed to incorporate sufficient spatial diversity in their collections and this could be leading to higher attrition rates along the drug-discovery process. Methods were developed for the rapid assembly of novel spirocyclic fragments. Spirocycles—being two rings joined at a quaternary carbon—are inherently more 3-dimensional when compared to sp^2-rich aromatic ring dominated libraries.

In the first line of investigation, two terminal alkenes were installed on to glycine ethyl ester. Combining ring-closing metathesis and a range of amine and ester coupling, it was demonstrated that an initial library of 14 novel spirocycles could be synthesised. Expanding this methodology to different ring sizes could lead to a spirocyclic library of 168 novel compounds. A second approach demonstrated how pericyclic reactions could be used to make spirocycles. This used both amino acids as building blocks as well as rare and privileged heterocycles to expand the chemical space. Computational analysis of these libraries showed that they possessed the required spatial and physico-chemical properties to make them promising fragment libraries for future drug discovery.

Overall, this work has expanded novel fragment space by demonstrating how fragment hits can be improved by analysis of structure activity relationships, and how novel sp^3-rich diverse spirocyclic libraries can be quickly assembled with promising structural and physical properties.

4.2. Future work

4.2.1. CK2 inhibition

Work in this project and in the wider Spring Group has led to the discovery of the led to the discovery CAM187, currently the most active fragment-like interface specific CK2 inhibitor. Due to the fragment nature of this molecule, there is ample room for development to improve on the compound's 44 μM IC_{50}.

4.2.2. Progressing spirocycle libraries

The novel spirocyclic libraries resulting from these investigations will be screened to determine whether there are any promising leads against biological targets.

Hence, a collaboration has been initiated with the Bender Group at the University of Cambridge. They has developed computational methods for screening large libraries against a myriad of known biological targets *in silico*. The libraries 1GLY and 2GLY have already been submitted for computational analysis. It is hoped that any leads from this can be tested against the biological targets *in vitro* to establish any tractable leads. These could be developed into potent inhibitors.

In addition to the *in silico* analysis, the synthesised compounds may be screened against a large number of protein crystals at the Diamond synchrotron. This would give crystal structures of the spirocycles binding in protein pockets. These data could be applied to the identification of new active compounds with the potential of being developed into new medicines.

4.2.3. α-Allyl serine ethyl ester spirocycles

There is excellent scope to apply synthetic methods employed in the synthesis of the glycine-based cyclohexene spirocycles and the dehydroalanine spirocycles. Again, this would start from the serine ethyl ester. However, instead of using elimination chemistry to install an exo-cyclic double bond, a fourth orthogonal functionality can be added onto the α-carbon; in this case an allyl group. There is established literature chemistry for the diastereoselective insertion of the allyl group onto serine (Scheme 4.1).[215]

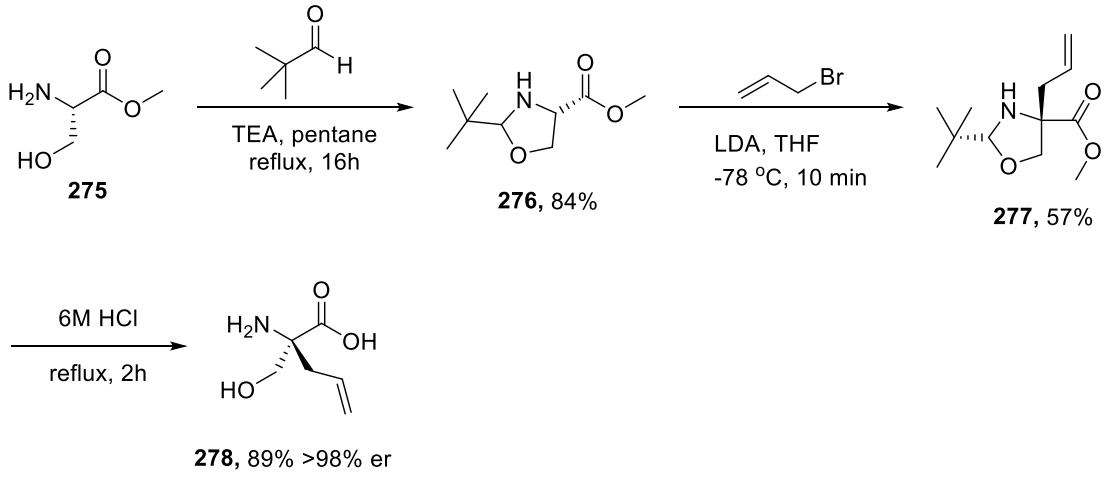

Scheme 4.1 Previous work installing an allyl group onto L-serine.

This work could be repeated to form compound **278**, or the pivaldehyde could be substituted with acetaldehyde to decrease the selectivity of the allyl addition so that both enantiomers can be synthesised simultaneously.

With compound **278** in hand, there are three different pairs of combinations of functional groups which could be used to make spirocycles (Figure 4.1).

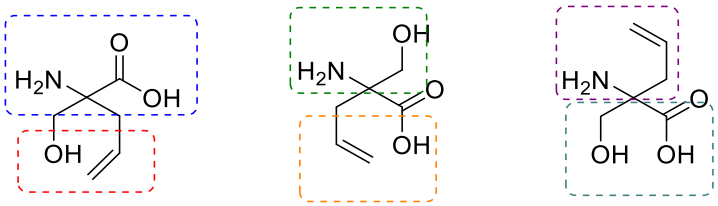

Figure 4.1 The functional groups in **278** may be combined in three pairs to produce novel spirocycles.

This could lead to the synthesis of a new spirocyclic library exploring more coupling chemistry, different ring sizes, and diverse functionality.

Chapter 5

Experimental

Reactions For reactions requiring anhydrous conditions, experiments were carried out in oven-dried glassware. Unless otherwise stated, all reactions were carried out under nitrogen atmosphere. Room temperature (RT) refers to ambient temperature. All temperatures below 0 °C are that of the external bath. Temperatures of 0 °C were maintained using an ice-water bath. Temperatures of –15 °C were maintained using a salt and ice-water bath. Temperatures of –78 °C were maintained using an acetone-cardice bath.

Solvents and reagents Solvents and commercially available reagents were dried and purified before use, where appropriate using standard procedures. Toluene, hexane, diethyl ether, ethyl acetate, methanol, THF, and dichloromethane were dried and distilled using standard methods from oxygen free from solvent dispenser units under an argon atmosphere.

Chromatography Analytical thin layer chromatography (TLC) was performed using pre-coated Merck glass backed silica gel plates (Silica gel 60 F254). Flash column chromatography was undertaken on Fluka or Material Harvest silica gel (230–400 mesh) under a positive pressure of nitrogen unless otherwise stated. Visualization was achieved using ultraviolet light (254 nm) and chemical staining with basic potassium permanganate solution as appropriate. Retention factors (R_f) are quoted to 0.01.

Infrared spectra Infrared (IR) spectra were recorded on a Perkin Elmer 1FT-IR Spectrometer fitted with an ATR sampling accessory as either solids or neat films, either through direct application or deposited in $CDCl_3$. Absorption maxima (ν_{max}) are reported in wavenumbers (cm^{-1}) with the following abbreviations: w, weak; m, medium; s, strong; br, broad.

NMR spectra Magnetic resonance spectra were processed using TopSpin v. 3.5 (Bruker). An aryl, quaternary, or two or more possible assignments were given when signals could not be distinguished by any means. Measured coupling constants (*J*) are reported for mutually coupled signals; coupling constants are labelled apparent in the absence of an observed mutual coupling, or multiplet when none can be determined.

Proton magnetic resonance spectra were recorded using an internal deuterium lock (at 298 K unless stated otherwise) on Bruker DPX (400 MHz; 1H-13C DUL probe), Bruker Avance III HD (400 MHz; Smart probe), Bruker Avance III HD (500 MHz; Smart probe) and Bruker Avance III HD (500 MHz; DCH Cryoprobe) spectrometers. Proton assignments are supported by ^{1}H–^{1}H COSY, ^{1}H–^{13}C HSQC or ^{1}H–^{13}C HMBC spectra, or by analogy. Chemical shifts (δ_H) are quoted in ppm to the nearest 0.01 ppm and are referenced to the residual non-deuterated solvent peak. Discernible coupling constants for mutually coupled protons are reported as measured values in Hertz, rounded to the nearest 0.5 Hz. Data are reported as: chemical shift, multiplicity (br = broad; s = singlet; d = doublet; t = triplet; q = quartet; qn = quintet; sp = septet; m = multiplet; or a combination thereof), coupling constants, number of nuclei, and assignment. Diastereotopic protons are assigned as Xa and Xb, where Xb designates the lower-field proton.

Carbon magnetic resonance spectra were recorded using an internal deuterium lock (at 298 K unless stated otherwise) on Bruker DPX (101 MHz), Bruker Avance III HD (101 MHz) and Bruker Avance III HD (126 MHz) spectrometers with broadband proton decoupling. Carbon spectra assignments are supported by DEPT editing, ^{1}H–^{13}C HSQC or ^{1}H–^{13}C HMBC spectra, or by analogy. Chemical shifts (δ_C) are quoted in ppm to the nearest 0.1 ppm and are referenced to the deuterated solvent peak. Data are reported as: chemical shift, number of nuclei (if not one), multiplicity (if not a singlet), coupling constants, and assignment.

Fluorine magnetic resonance spectra were recorded on Bruker Avance III (376 MHz; QNP Cryoprobe) or Bruker Avance III HD (376 MHz; Smart probe) spectrometers. Chemical shifts (δ_F) are quoted in ppm to the nearest 0.1 ppm. Data are reported as: chemical shift, number of nuclei (if not one), multiplicity (if not a singlet), coupling constants and assignment.

The numbering of molecules used for ^{13}C and ^{1}H NMR assignments does not conform to IUPAC standards.

Mass spectra High-resolution mass spectra (HRMS) were measured on a Micromass LCT Premier spectrometer using electron spray ionization (ESI) techniques. Masses are quoted within the 5 ppm error limit.

Melting points Melting points were obtained on a Buchi B-545 melting point apparatus and are uncorrected.

Optical rotations Chiral products had their optical rotation recorded on an Anton-Paar MCP 100 polarimeter. $[\alpha]_D^{20}$ values are reported in $°g^{-1}cm^{-2}10^{-1}$ at the sodium D-line of 598 nm, concentration (*c*) is given in $g(100\ mL)^{-1}$ in the solvent stated.

2,2′-(4,5-Dichloro-1,2-phenylene)bis(ethan-1-aminium) dichloride, 29

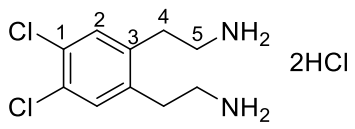

Compound **35** (60.6 mg, 0.14 mmol) was stirred in HCl/dioxane (4M, 5 mL) for 1 h. The mixture was filtered and the filtrate was washed with cold diethyl ether (5 mL). The isolated white crystals were placed in a desiccator overnight to yield the pure white crystalline product (39.0 mg, 0.13 mmol, 14% over two steps); **IR (thin film)** $\tilde{\nu}$/cm^{-1}: 2936 (C-H, m), 1760 (C=O, s), 1499 (C=C, m). **^{1}H NMR (400MHz, $(CD_3)_2SO$)** δ/ppm: 8.26 (s, 6H, NH3) 7.57 (s, 2H, H1) 3.00 (s, 8H, H4,5). **^{13}C NMR (101 MHz, $(CD_3)_2SO$)** δ/ppm: 137.3 (C1×2) 131.8 (C2×2) 129.5 (C3×2) 66.4 (C5×2) 29.2 (C4×2). **HRMS (ESI)** $C_{10}H_{15}N_2Cl_2$ *m/z*: $[M+H]^+$ 233.0600 (*calc.* 233.0607). **m.p.** 349-350 °C.

2,2′-(4,5-dichloro-1,2-phenylene)diacetonitrile, 30

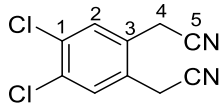

To a solution of dibromide **31** (1.08 g, 3.24 mmol, 1.0 eq) in ethanol (21 mL) was added sodium cyanide (3.98 mg, 8.11 mmol, 2.5 eq) in water (7 mL) at 0 °C. The reaction was refluxed overnight. The excess solvent was removed *in vacuo* before being diluted with ethyl acetate (20 mL) and washed with water (20 mL × 2). The aqueous layer was extracted with ethyl acetate (30 mL × 3) and the combined organics were washed with brine (50 mL). This was dried over $MgSO_4$, filtered, concentrated and purified by column chromatography (25% EtOAc in Hexane) to give the pure product as a colourless oil (631 mg, 2.80 mmol, 86%); **R_f** 0.50 (40% EtOAc in Hexane); **IR (thin film)** $\tilde{\nu}$/cm^{-1}: 3029 (C-H, w), 2859 (C-H, w), 2252 (C≡N, m), 1481 (C=C, s), 682 (C-Cl, s). **^{1}H NMR (400 MHz, $CDCl_3$)** δ/ppm: 7.58 (s, 2H, H2), 3.74 (s, 4H, H4). **^{13}C NMR (101 MHz, $CDCl_3$)** δ/ppm: 133.8 (C1×2), 131.7 (C2×2), 128.1 (C3×2), 115.5 (C5×2), 21.1 (C4×2). **HRMS (ESI)** $C_{10}H_6N_2Cl_2Na$ *m/z*: $[M+Na]^+$ 246.9793 (*calc.* 246.9800).

The physical and spectroscopic data was found to be in agreement with Rosowsky *et al.*[216]

1,2-Bis(bromomethyl)-4,5-dichlorobenzene, 31

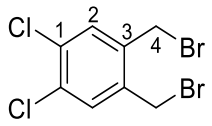

Dialcohol **32** (550 mg, 2.65 mmol, 1.0 eq) was dissolved in diethyl ether (5 mL). Phosphorous tribromide (0.6 mL, 6.36 mmol, 2.4 eq) was added dropwise at 0 °C and the reaction was stirred overnight at RT. The reaction was poured into ice water (5 mL), the organic phase was separated and washed with brine (5 mL). This was dried over $MgSO_4$, filtered, concentrated and purified by column chromatography (10% CH_2Cl_2 in Hexane) to give the pure product as off white crystals (761 mg, 2.29 mmol, 86%); $\mathbf{R_f}$ 0.39 (10% CH_2Cl_2 in Hexane); **IR (thin film)** $\tilde{\nu}$/cm^{-1}: 1588 (C=C, w), 1473 (C-H, m), 951 (C-Br, s), 683 (C-Cl, s). **^{1}H NMR (400 MHz, $CDCl_3$)** δ/ppm: 7.82 (s, 2H, H2), 4.80 (s, 4H, H4). **^{13}C NMR (101 MHz, $CDCl_3$)** δ/ppm: 138.0 (C1×2), 133.3 (C2×2), 131.8 (C3×2), 29.6 (C4×2). **HRMS (ESI)** $C_8H_6Cl_2Br_2Na$ *m/z*: $[M+Na]^+$ 354.8099 (*calc.* 354.8088). **m.p.** 65–66 °C.

The physical and spectroscopic data was found to be in agreement with Levy *et al.*[217]

(4,5-Dichloro-1,2-phenylene)dimethanol, 32

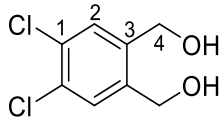

To a suspension of lithium aluminium hydride (600 mg, 15.7 mmol, 2.0 eq) in THF (10 mL) was added **34** (2.07 g, 7.9 mmol, 1.0 eq) dissolved in THF at 0 °C. The reaction was warmed to RT and stirred for 24 h. Following this, the reaction was cooled to 0 °C and water (0.6 mL), 15% NaOH (0.6 mL), and water (1.8 mL) were added and the mixture was stirred for 30 min. This mixture was filtered and washed with THF (10 mL). The excess solvent of the filtrate was removed *in vacuo* to yield the pure product (1.5043 g, 7.25 mmol, 92%); $\mathbf{R_f}$ 0.21 (20% diethyl ether/pet. ether); **IR (thin film)** $\tilde{\nu}$/cm^{-1}: 3265 (O-H, br s), 2901 (C-H, w), 1483 (C=C, m), 1050 (C-O, s), 732 (C-Cl, s). **^{1}H NMR (400 MHz, $CDCl_3$)** δ/ppm: 7.46 (s, 2H, H2), 4.68 (s, 4H, H4), 2.65 (s, 2H, H5). **^{13}C NMR (101 MHz, $CDCl_3$)** δ/ppm: 139.0 (C1×2), 132.0 (C3×2), 131.1 (C2×2), 62.9 (C4×2). **HRMS (ESI)** $C_8H_8O_2Cl_2Na$ *m/z*: $[M+Na]^+$ 228.9786 (*calc.* 228.9794).

The physical and spectroscopic data was found to be in agreement with Di Lauro *et al.*[218]

Dimethyl 4,5-dichlorophthalate, 34

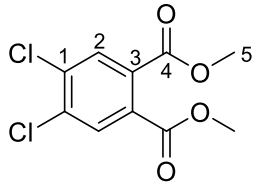

To a solution of 4,5-dichlorophthalic acid (3 g, 12.76 mmol, 1.0 eq) in methanol (25 mL) cooled to 0 °C thionyl chloride (2.33 mL, 31.90, 2.5 eq) was added dropwise. The reaction was warmed to RT and stirred for 3 days. The mixture was quenched with sat. aq. $NaHCO_3$ and extracted with CH_2Cl_2. The organic layer was dried over $MgSO_4$, filtered and concentrated *in vacuo*. The crude material was purified by column chromatography (50% diethyl ether in pet. ether) to give the pure product as a translucent crystal (3.0838 g, 11.7 mmol, 92%); **IR (thin film)** $\tilde{\nu}$/cm^{-1}: 3097 (C-H, w), 2957 (C-H, w), 1719 (C=O, s), 1592 (C=C, m), 1551 (C=C, m), 1430 (C=C, m), 1290 (C-O, s), 781 (CCl, s). **^{1}H NMR (400 MHz, $CDCl_3$)** δ/ppm: 7.81 (s, 2H, H2) 3.90 (s, 6H, H5). **^{13}C NMR (101 MHz, $CDCl_3$)** δ/ppm: 161.0 (C4×2), 135.8 (C1×2), 131.3 (C3×2), 131.0 (C2×2), 52.3 (C5×2). **HRMS (ESI)** $C_{10}H_9O_4Cl_2$ *m/z*: $[M+H]^+$ 262.9866 (*calc.* 262.9872). **m.p.** 48–49 °C.

The physical and spectroscopic data was found to be in agreement with Hennessy *et al.*[219]

Di-*tert*-butyl ((4,5-dichloro-1,2-phenylene)bis(ethane-2,1-diyl))dicarbamate, 35

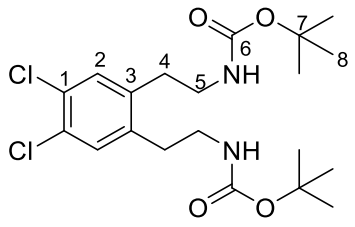

Sodium borohydride (470.6 mg, 12.44 mmol, 14.0 eq) was added portion wise at 0 °C to a mixture of **30** (200 mg, 0.89 mmol, 1.0 eq), $NiCl_2$.6H2O (42.2 mg, 0.18 mmol, 0.2 eq), and di-*tert*-butyl dicarbonate (0.82 mL, 3.55 mmol, 4.0 eq) in methanol (10 mL). The reaction was stirred at RT for 6 h. The reaction mixture was poured into ice water and the excess solvent

was removed *in vacuo*. This was diluted with ethyl acetate (20 mL) and washed with $NaHCO_3$ (20 mL). The aqueous was extracted with ethyl acetate (20 mL × 3). The combined organics were washed with brine, dried over $MgSO_4$, filtered, concentrated and purified by column chromatography (15% ethyl acetate in hexane) to give the pure product which was carried straight over to the next reaction; **R_f** 0.21 (50% Et_2O in pet. ether); **IR (thin film)** $\tilde{\nu}$/cm^{-1}: 3326 (N-H, m), 2978 (C-H, w), 1678 (C=O, s), 1524 (C=C, s), 1136 (C-O, s), 780 (C-Cl, s). **^{1}H NMR (400 MHz, $CDCl_3$)** δ/ppm: 7.24 (s, 2H, H2) 3.30 (q, *J* = 7.0 Hz, 4H, H5) 2.80 (t, *J* = 7.0 Hz, 4H, H4) 1.43 (s, 18H, H8). **^{13}C NMR (101 MHz, $CDCl_3$)** δ/ppm: 155.9 (C6×2), 137.6 (C1×2), 131.6 (C2×2), 130.3 (C3×2), 79.5 (C7×6), 41.1 (C5×2), 32.7 (C4×2), 28.3 (C8×2). **HRMS (ESI)** $C_{20}H_{31}N_2O_4Cl_2$ *m/z*: $[M+H]^+$ 433.1644 (*calc.* 433.1661).

(4,5-Dichloro-1,2-phenylene)dimethanaminium dichloride, 38

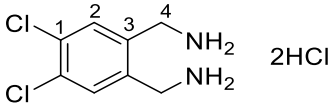

Sodium borohydride (1.34 g, 35.353 mmol, 14.0 eq) was added portion wise at 0 °C to a mixture of dichlorodicyanobenzene (500 mg, 2.54 mmol, 1.0 eq), $NiCl_2$.6H2O (120.6 mg, 0.51 mmol, 0.2 eq), and di-*tert*-butyl dicarbonate (2.33 mL, 10.15 mmol, 4.0 eq) in methanol (25 mL). The reaction was stirred at RT for 6h before the reaction was poured into ice. The mixture was extracted with ethyl acetate (3 × 20 mL) and washed with sat. aq. $NaHCO_3$ (20 mL) and brine (20 mL). This was dried over anh. $MgSO_4$, filtered and concentrated *in vacuo*. The crude oil was dissolved in 4M HCl/Dioxane (5 mL) and stirred for 1h. The reaction was filtered and the residue was washed with cold acetone to give the product as white crystals (241.3 mg, 0.87 mmol, 34%); **IR (thin film)** $\tilde{\nu}$/cm^{-1}: 2847 (N-H, br s), 1498 (C=C, s), 1116 (C-N, s), 683 (C-Cl, m). **^{1}H NMR (400 MHz, $(CD_3)_2SO$)** δ/ppm: 8.45 (br s, 6H, NH), 8.08–8.07 (m, 2H, H2), 4.21 (s, 4H, H4). **^{13}C NMR (101 MHz, $(CD_3)_2SO$)** δ/ppm: 136.7 (C1), 134.6 (C3), 132.0 (C2), 39.9 (C4). **HRMS (ESI)** $C_8H_{11}Cl_2$ *m/z*: $[M+H]^+$ 205.0290 (*calc.* 205.0294). **m.p.** 277–278 °C.

2-(4-Chloronaphthalen-1-yl)ethan-1-aminium chloride, 39

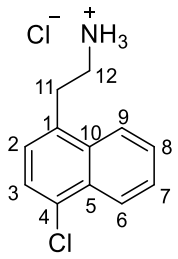

To a suspension of lithium aluminium hydride (11 mg, 2.5 mmol, 2.0 eq) in diethyl ether (3 mL) under N_2 was added **45** (25 mg, 0.12 mmol, 1.0 eq) dissolved in diethyl ether (2 mL) dropwise. The reaction was stirred overnight. Water (25 µL) was added dropwise at 0 °C followed by 15% aq. NaOH (25 µL) and water (75 µL). This was warmed to RT and stirred for 15 min. The resulting mixture was diluted with diethyl ether (5 mL) and washed with brine (10 mL). The organics were dried over anh. $MgSO_4$, filtered and concentrated *in vacuo* to give the crude oil. This was stirred with 4M HCl in dioxane (5 mL) for 15 min and then filtered giving the residue as pure white-yellow crystalline product (20.1 mg, 0.08 mmol, 69%); **IR (thin film)** $\tilde{\nu}$/cm^{-1}: 3382 (N-H, m), 3029 (C-H, m), 1500 (C=C, m), 758 (C-Cl, s). **^{1}H NMR (400 MHz, $(CD_3)_2SO$)** δ/ppm: 8.27–8.21 (m, 2H, H6&9), 7.95 (br s, 3H, NH_3^+), 7.76–7.71 (m, 2H, H7&8), 7.68 (d, J = 7.5 Hz, 1H, H2), 7.43 (d, J = 7.5 Hz, 1H, H3), 3.38–3.34 (m, 2H, H11), 3.10 (br s, 2H, H12). **^{13}C NMR (101 MHz, $(CD_3)_2SO$)** δ/ppm: 133.4 (C4), 132.6 (C1), 130.3 (C5), 130.0 (C10), 127.6 (C7/8), 127.5 (C7/8), 127.4 (C3), 126.2 (C2), 124.6 (C6/9), 124.4 (C6/9), 39.5 (C12), 30.1 (C11). **HRMS (ESI)** $C_{12}H_{13}ClN$ *m/z*: $[M]^+$ 206.0735 (*calc.* 206.0737). **m.p.** 270–271 °C.

1-Acetyl-4-chloronaphthalene, 41

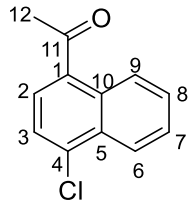

Acetyl chloride (2.80 mL, 40.4 mmol, 1.1 eq) was dissolved in CH_2Cl_2 (150 mL) under N_2. Aluminium trichloride (5.68 g, 42.6 mmol, 1.16 eq) was added and stirred for 5 min before 1-chloronaphthalene (5 mL, 36.7 mmol, 1.0 eq) was added dropwise over 10 min. The reaction was refluxed for 1 h. The reaction was poured into a mixture of ice and conc. HCl. This was

extracted with diethyl ether (3 × 50 mL) and the ethereal layer was washed with brine. The combined organics were dried over $MgSO_4$. The mixture was filtered and concentrated *in vacuo*. The crude was purified by column chromatography (10% diethyl ether in pet. ether) to give the pure product as a yellow oil (6.0849 g, 29.73 mmol, 81%); **R_f** 0.28 (20% diethyl ether in pet. ether); **IR (thin film)** $\tilde{\nu}$/cm^{-1}: 3005 (C-H, w), 1674 (C=O, s), 1565 (C=C, s), 1505 (C=C, s) 758 (C-Cl, s). **^{1}H NMR (400 MHz, $CDCl_3$)** δ/ppm: 8.78–8.75 (m, 1H, H6), 8.36–8.33 (m, 1H, H9), 7.64 (d, *J* = 8.0 Hz, 1H, H2), 7.68–7.63 (m, 2H, H7&8), 7.59 (d, *J* = 8.0 Hz, 1H, H3), 2.73 (s, 3H, H12). **^{13}C NMR (101 MHz, $CDCl_3$)** δ/ppm: 201.0 (C11), 136.9 (C1), 134.6 (C4), 131.3 (C10), 131.1 (C5), 128.8 (C8), 128.3 (C2), 127.6 (C7), 126.5 (C6), 124.8 (C3), 124.8 (C9), 30.0 (C12). **HRMS (ESI)** $C_{12}H_{10}ClO$ *m/z*: $[M+H]^+$ 205.0412 (*calc.* 205.0415).

The physical and spectroscopic data was found to be in agreement with Wiley *et al.*[121]

4-Chloro-1-naphthoic acid, 42

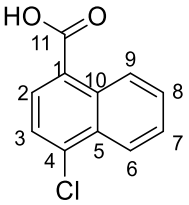

Compound **41** (6.00 g, 29.32 mmol, 1.0 eq) was dissolved in pyridine (25 mL). To this iodine (4.09 g, 32.25 mmol, 1.1 eq) dissolved in pyridine (25 mL) was added dropwise and the reaction was refluxed for 40 min. The mixture was cooled to RT and diluted with diethyl ether until a brown precipitate formed. The precipitate was filtered and suspended in 6M NaOH. The mixture was refluxed for 2 h. Afterwards, it was cooled to RT and acidified with 3M HCl. This was extracted with diethyl ether (3 × 30 mL) and the combined organics where washed with brine (30 mL). The organics were dried over anh. $MgSO_4$ and the mixture was filtered and concentrated *in vacuo*. This give the pure product as white crystals (3.08 g, 14.90 mmol, 51%); **IR (thin film)** $\tilde{\nu}$/cm^{-1}: 2926 (O-H, br s), 1682 (C=O, s), 1509 (C=C, m), 1249 (C-O, s) 761 (C-Cl, s). **^{1}H NMR (400 MHz, $(CD_3)_2SO$)** δ/ppm: 13.40 (br s, 1H, OH), 8.97–8.93 (m, 1H, H6), 8.36–8.28 (m, 1H, H9), 8.11 (d, *J* = 8.0 Hz, 1H, H2), 7.89 (d, *J* = 8.0 Hz, 1H, H3), 7.78 (m, 2H, H7&8). **^{13}C NMR (101 MHz, $(CD_3)_2SO$)** δ/ppm: 168.1 (C11), 135.3 (C1), 131.9 (C4), 130.2 (C10), 129.9 (C2), 128.6 (C8), 127.9 (C7), 127.8 (C5), 126.4 (C6), 125.7 (C3), 124.3 (C9). **HRMS (ESI)** $C_{11}H_6ClO_2$ *m/z*: $[M-H]^-$ 205.0062 (*calc.* 205.0062). **m.p.** 220-221 °C.

The physical and spectroscopic data was found to be in agreement with Wiley *et al.*[121]

(4-Chloronaphthalen-1-yl)methanol, 43

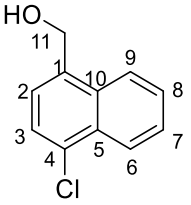

Lithium Aluminium Hydride (264 mg, 6.97 mmol, 7.2 eq) was suspended in diethyl ether (2 mL) under nitrogen. Compound **42** (200 mg, 0.97 mmol, 1.0 eq) dissolved in diethyl ether (4 mL) was added dropwise. The reaction was refluxed for 3 h then returned to RT and stirred for 14 h. Following this water (0.26 mL), 15% aq. NaOH (0.26 mL), and water (0.78 mL) was added dropwise. The resulting suspension was filtered and the filtrate was extracted with diethyl ether (3 × 10 mL). This was dried over anh. $MgSO_4$ and the mixture was filtered and concentrated *in vacuo*. This give the pure product as white crystals (114.5 g, 0.59 mmol, 61%); **R_f** 0.24 (50% diethyl ether in pet. ether); **IR (thin film)** $\tilde{\nu}$/cm^{-1}: 3261 (O-H, br s), 2971 (C-H, w), 2860 (C-H, w), 1508 (C=C, m), 1076 (C-O, m), 752 (C-Cl, m). **^{1}H NMR (400 MHz, $CDCl_3$)** δ/ppm: 8.36–8.32 (m, 1H, H6), 8.16–8.12 (m, 1H, H9), 7.65–7.60 (m, 2H, H7&8), 7.55 (d, *J* = 7.5 Hz, 1H, H2), 7.45 (d, *J* = 7.5 Hz, 1H, H3), 5.14 (s, 2H, H11). **^{13}C NMR (101 MHz, $CDCl_3$)** δ/ppm: 135.6 (C1), 132.3 (C4), 131.0 (C10), 128.7 (C5), 127.1 (C7/8), 127.0 (C7/8), 125.6 (C2), 125.2 (C3&6), 124.0 (C9), 63.3 (C11). **HRMS (ESI)** $C_{11}H_{10}ClO$ *m/z*: $[M+H]^+$ 193.0420 (*calc.* 193.0415). **m.p.** 71–72 °C.

The physical and spectroscopic data was found to be in agreement with Wiley *et al.*[122]

1-(Bromomethyl)-4-chloronaphthalene, 44

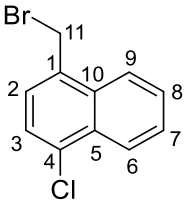

Phosphorus tribromide (58.5 µL, 0.62 mmol, 1.2 eq) was added dropwise at 0 °C to a solution of **43** (100 mg, 0.52 mmol, 1.0 eq) in diethyl ether (1 mL). The reaction was stirred overnight at RT, before being poured into ice water. The organic layer was separated and washed with brine (10 mL), then dried over anh. $MgSO_4$. This was filtered and the filtrate was concentrated *in vacuo* to give a crude oil. This was purified by column chromatography (10% diethyl ether in pet. ether) to yield the product as white crystals (93.0 mg, 0.36mmol, 70%); $\mathbf{R_f}$ 0.63 (20% diethyl ether in pet. ether); **IR (thin film)** $\tilde{\nu}$/cm^{-1}: 2987 (C-H, s), 2901 (C-H, s), 1568 (C=C, m). **^{1}H NMR (400 MHz, $CDCl_3$)** δ/ppm: 8.36–8.34 (m, 1H, H6), 8.18–8.16 (m, 1H, H9), 7.71–7.64 (m, 2H, H7&8), 7.52 (d, *J* = 7.5 Hz, 1H, H2), 7.47 (d, *J* = 7.5 Hz, 1H, H3), 4.93 (s, 2H, H11). **^{13}C NMR (101 MHz, $CDCl_3$)** δ/ppm: 133.5 (C4), 132.6 (C1), 132.1 (C5), 131.3 (C10), 127.5 (C3), 127.4 (C7/8), 127.3 (C7/8), 125.7 (C2), 125.4 (C6), 124.2 (C9), 31.0 (C11). **HRMS (ESI)** $C_{11}H_9BrCl$ *m/z*: $[M+H]^+$ 254.9559 (*calc.* 254.9571). **m.p.** 90–91 °C.

The physical and spectroscopic data was found to be in agreement with Dixon *et al.*[122]

2-(4-Chloronaphthalen-1-yl)acetonitrile, 45

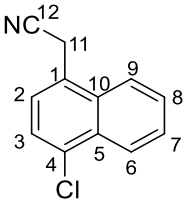

Sodium cyanide (23 mg, 0.47 mmol, 1.3 eq) was dissolved in water (0.7 mL) and added dropwise at 0 °C to a solution of **44** (92 mg, 0.36 mmol, 1.0 eq) in ethanol (2.4 mL). The reaction mixture was refluxed overnight. It was then concentrated *in vacuo* and diluted with ethyl acetate (10 mL). This was washed with water (3 × 10 mL), the aqueous was extracted with ethyl acetate (2 × 10 mL), and the combined organics were washed with brine (30 mL). The organic layer was dried over anh. $MgSO_4$, filtered and concentrated *in vacuo* to give the crude

product. This was puried by column chromatography (20% diethyl ether in pet. ether) to yield the pure product as white crystals (26.7 mg, 0.13 mmol, 37%); $\mathbf{R_f}$ 0.21 (20% diethyl ether in pet. ether); **IR (thin film)** $\tilde{\nu}$/cm^{-1}: 2247 (C≡N, w), 1511 (C=C, m), 751 (C-Cl, s). **^{1}H NMR (400 MHz, $CDCl_3$)** δ/ppm: 8.40–8.37 (m, 1H, H6), 7.91–7.88 (m, 1H, H9), 7.71–7.67 (m, 2H, H7&8), 7.59 (d, *J* = 7.5 Hz, 1H, H3), 7.53 (d, *J* = 7.5 Hz, 1H, H2), 4.13 (s, 2H, H11). **^{13}C NMR (101 MHz, $CDCl_3$)** δ/ppm: 133.1 (C4), 131.8 (C10), 131.0 (C5), 127.9 (C7/8), 127.5 (C7/8), 126.4 (C2), 125.7 (C3), 125.7 (C6), 125.1 (C1), 122.9 (C9), 117.2 (C12), 21.7 (C11). **HRMS (ESI)** $C_{12}H_7ClN$ *m/z*: [M-H]$^-$ 200.0275 (*calc.* 200.0272). **m.p.** 71–72 °C.

Methyl 2-bromo-4-chlorobenzoate, 49

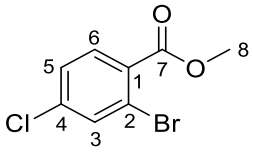

2-Bromo-4-chlorobenzoic acid (2 g, 8.49 mmol, 1.0 eq) was dissolved in methanol (25 mL) and cooled to 0 °C before thionyl chloride (2.30 mL, 32.82 mmol, 3.8 eq) was added dropwise. The reaction was refluxed for 4 h. The mixture was concentrated *in vacuo* and was diluted with dichloromethane (25 mL). This was washed with water (20 mL), sat. aq. $NaHCO_3$ (20 mL), and brine (20 mL). The organic layer wad dried over anh. Na_2SO_4, filtered and concentrated *in vacuo* to give the crude product. This was purified by column chromatography (15% diethyl ether in pet. ether) to give the pure product as a colourless oil (1.46 g, 5.87 mmol, 69%); $\mathbf{R_f}$ 0.50

(15% diethyl ether in pet. ether) **IR (thin film)** $\tilde{\nu}$/cm^{-1}: 2952 (C-H, w), 1732 (C=O, s), 1581 (C=C, s), 1100 (C-O, s), 763 (C-Cl, s). **^{1}H NMR (400 MHz, $CDCl_3$)** δ/ppm: 7.76 (d, *J* = 8.5 Hz, 1H, H6), 7.67 (d, *J* = 2.0 Hz, 1H, H3), 7.33 (dd, *J* = 2.0, 8.5 Hz, 1H, H5), 3.91 (s, 3H, H8). **^{13}C NMR (101 MHz, $CDCl_3$)** δ/ppm: 165.6 (C7), 138.3 (C4), 134.2 (C6), 132.4 (C3), 130.2 (C1), 127.5 (C5), 122.6 (C2), 52.6 (C8). **HRMS (ESI)** $C_8H_7BrClO_2$ *m/z*: $[M+H]^+$ 248.9315 (*calc.* 248.9318).

The physical and spectroscopic data was found to be in agreement with Sun *et al.*[220]

Methyl 4-chloro-2-((trimethylsilyl)ethynyl)benzoate, 50

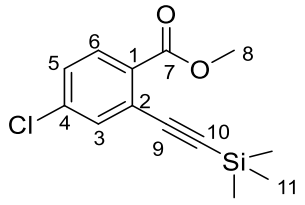

Trimethylsilylacetylene (0.42 mL, 3.01 mmol, 1.5 eq), **49** (500 mg, 2.00 mmol, 1.0 eq), bis(triphenylphosphine)palladium(II) dichloride (70.2 mg, 0.10 mmol, 5 mol%), triphenylphosphine (13.1 mg, 0.05 mmol, 2.5 mol%), triethylamine (0.42 mL, 3.01 mmol, 1.5 eq) were dissolved in tetrahydrofuran (8mL) and stirred at RT for 20 min. Copper (I) iodide (4.6 mg, 0.024 mmol, 1.2 mol%) was added and the reaction was refluxed for a further 16 h. This was concentrated *in vacuo* and diluted with dichloromethane and was filtered through celite. The filtrate was concentrated *in vacuo* to give the crude product. This was purified by column chromatography (6.25% ethyl acetate in hexane) to gie the pure product as a yellow oil (420.5 mg, 1.58 mmol, 79%); **Rf** 0.31 (6.25% ethyl acetate in hexane); **IR (thin film)** $\tilde{\nu}/\mathrm{cm}^{-1}$: 2955 (C-H, w), 2163 (C≡C, w), 1736 (C=O, s), 1247 (C-O, s). **^{1}H NMR (400 MHz, $CDCl_3$)** δ/ppm: 7.86 (d, *J* = 8.5 Hz, 1H, H6), 7.57 (d, *J* = 2.0 Hz, 1H, H3), 7.33 (dd, *J* = 2.0, 8.5 Hz, 1H, H5), 3.91 (s, 3H, H8), 0.27 (s, 9H, H11). **^{13}C NMR (101 MHz, $CDCl_3$)** δ/ppm: 165.9 (C7), 137.8 (C2), 134.2 (C3), 131.7(C6), 130.7 (C4), 128.5 (C5), 125.0 (C1), 101.9 (C9/10), 101.5 (C9/10), 52.1 (C8), –0.2 (C11). **HRMS (ESI)** $C_{13}H_{16}ClO_2Si$ *m/z*: $[M+H]^+$ 267.0619 (*calc.* 267.0608).

4-Chloro-2-ethynyl benzoic acid, 51

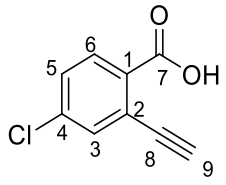

Compound **50** (200 mg, 0.75 mmol, 1.0 eq) was dissolved 3:2 ethanol:dichloromethane (2mL) and cooled to 0 °C when 1M NaOH (3 mL, 3.00 mmol, 4.0 eq) was added dropwise over 10 min. The reaction was warmed to RT and stirred for 4h. The solution was washed with diethyl ether (5 mL) and 1M HCl was added dropwise until a precipitate appeared. The precipitate was collected by filtration, dissolved in diethyl ether (5 mL) and washed with water (5 mL). The organic layer was dried over Na_2SO_4 and the excess solvent was removed *in vacuo* to yield

the pure product as yellow crystals (98.6 mg, 0.55 mmol, 73%); **IR (thin film)** $\tilde{\nu}$/cm^{-1}: 3304 (C≡C-H, w), 3282 (O-H, m), 2952 (C-H, m), 2113 (C≡C, m), 1686 (C=O, s), 1586 (C=C, s), 1271 (C-O, s), 777 (C-Cl, s). **^{1}H NMR (400 MHz, $CDCl_3$)** δ/ppm: 13.29 (s, 1H, OH), 7.85 (d, *J* = 8.5 Hz, 1H, H6), 7.67 (d, *J* = 2.0 Hz, 1H, H3), 7.57 (dd, *J* = 2.0, 8.5 Hz, 1H, H5), 4.51 (s, 1H, H9). **^{13}C NMR (101 MHz, $CDCl_3$)** δ/ppm: 166.2 (C7), 136.3 (C2), 133.7 (C3), 132.6 (C4), 131.8 (C6), 129.1 (C5), 123.6 (C1), 87.0 (C9), 80.8 (C8). **HRMS (ESI)** $C_9H_4ClO_2$ *m/z*: $[M-H]^-$ 178.9903 (*calc.* 178.9905).

Hydroxycarbonimidic dibromide, 70

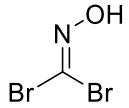

Glyoxylic acid (5.00 g, 54.32 mmol, 1.0 eq) and hydroxylamine hydrochloride (3.77 g, 54.32 mmol, 1.0 eq) were stirred in water (150mL) for 24 h. $NaHCO_3$ (9.13 g, 108.60mmol, 2.0 eq) was added and stirred with CH_2Cl_2 (200 mL). The mixture was cooled to 6 °C and stirred vigorously. Bromine (5.43 mL, 108.60 mmol, 2.0 eq) was added dropwise over 20 min and stirred for 3 h. The organic layer was separated, the aqueous was extracted with CH_2Cl_2 (100 mL × 3), and the combined organic layers were dried over $MgSO_4$. The salt was filtered and the remaining organic layer was concentrated *in vacuo* to give the product as a white crystal (6.7510 g, 33.29 mmol, 61%): $\mathbf{R_f}$ 0.45 (20% Et_2O in pet. ether); **IR (thin film)** $\tilde{\nu}$/cm^{-1}: 3290 (O-H, br s), 1580 (C=N, m), 890 (C-Br, s). **^{1}H NMR (400 MHz, $(CD_3)_2SO$)** δ/ppm: 12.74 (s, 1H, OH). **^{13}C NMR (101 MHz, $CDCl_3$)** δ/ppm: 96.7. **HRMS (ESI)** CH_2NOBr_2 *m/z*: $[M+H]^+$ 200.8425 (*calc.* 200.8433).

The physical and spectroscopic data was found to be in agreement with Soleimani *et al.*[221]

tert-Butyldimethyl(prop-2-yn-1-yloxy)silane, 72

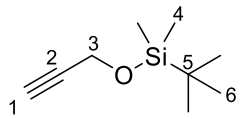

Propargylic alcohol (3.00 mL, 51.5 mmol, 1.0 eq) and imidazole (5.26 g, 77.3 mmol, 1.5 eq) were dissolved in CH_2Cl_2 (150 mL). The mixture was cooled to 0 °C TBSCl (11.7 g, 77.3 mmol, 1.5 eq) was added and stirred for 90 min. The reaction was quenched with sat. aq. NH_4Cl (50 mL), extracted with diethyl ether (20 mL × 3), and washed with brine (50 mL). The organic layer was dried over $MgSO_4$, the salt was filtered and the remaining organic layer was concentrated *in vacuo*. The crude oil was purified by column chromatography (20% diethyl ether in pet. ether) to give the product as a colourless oil (6.2657 g, 36.79 mmol, 71%); $\mathbf{R_f}$ 0.70 (20% diethyl ether in pet. ether); **IR (thin film)** $\tilde{\nu}$/cm^{-1}: 2970 (C-H, s), 2901 (C-H, s), 2125 (C≡C, w), 1253 (C-Si, m), 1087 (C-O, s). **^{1}H NMR (400 MHz, $CDCl_3$)** δ/ppm: 4.29 (d, J = 2.5 Hz, 2H, H3), 2.36 (t, J = 2.5 Hz, 1H, H1), 0.89 (s, 9H, H6), 0.10 (s, 6H, H4). **^{13}C NMR (101 MHz, $CDCl_3$)** δ/ppm: 82.4 (C2), 72.8 (C1), 51.5 (C3), 25.8 (C6×2), 18.3 (C5), –5.2 (C4×3). **HRMS (ESI)** $C_9H_{19}OSi$ *m/z*: $[M+H]^+$ 171.1195 (*calc.* 171.1200).

The physical and spectroscopic data was found to be in agreement with Yatvin *et al.*[222]

3-Bromo-5-(((*tert*-butyldimethylsilyl)oxy)methyl)isoxazole, 73

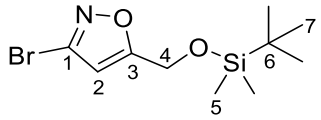

Alkyne **72** (5.00 g, 29.4 mmol, 4.0 eq) and oxime **70** (1.49 g, 7.34 mmol, 1.0 eq) were dissolved in CH_2Cl_2 (10 mL) refluxed for 18 h. The reaction was cooled to room temperature and poured into 1M HCl (10 mL). The organic layer was separated and dried over anh. $NaHSO_4$. This mixture was filtered and the excess solvent of the filtrate was removed *in vacuo*. The crude was purified by column chromatography (40% diethyl ether in pet. ether) to give the pure product as a yellow oil (1.7948 g, 6.14 mmol, 84%); $\mathbf{R_f}$ 0.28 (40% diethyl ether in pet. ether); **IR (thin film)** $\tilde{\nu}$/cm^{-1}: 2955 (C-H, w), 2858 (C-H, w), 1594 (C=C, m), 1258 (N-O, m), 1124 (C-O, m). **^{1}H NMR (400 MHz, $CDCl_3$)** δ/ppm: 6.30 (t, J = 1.0 Hz, 2H, H4), 4.78 (d, J = 1.0 Hz, 1H, H2), 0.94 (s, 9H, H5), 0.14 (s, 6H, H7). **^{13}C NMR (101 MHz, $CDCl_3$)** δ/ppm: 174.0 (C1), 140.3

(C3), 105.1 (C2), 57.3 (C4), 25.7 (C7×3), 18.2 (C6), –5.5 (C5×2). **HRMS (ESI)** $C_{10}H_{19}O_2NBrSi$ *m/z*: $[M+H]^+$ 292.0351 (*calc.* 292.0363).

Spiro[indoline-3,4′-piperidin]-1′-ium chloride, 85

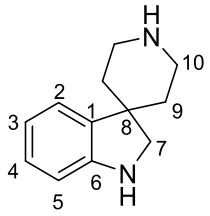

A suspension of lithium aluminium hydride (749 mg, 19.7 mmol, 4.75 eq) in glyme (20 mL) was cooled to 0 °C and ethanol (1.7 mL) added. The mixture was heated to reflux and compound **96** (1.00 g, 4.15 mmol, 1.0 eq) dissolved in glyme (10 mL) was added followed by continuing reflux for 72 h. Subsequently the reaction was cooled to 0 °C and water (20 mL) was added slowly. Added to this was a conc. solution of Rochelle's salt (20 mL) and extracted with CH_2Cl_2 (50 mL). The organic layers were dried over anh. $MgSO_4$ which was removed by filtration and the excess solvent was evaporated *in vacuo*. To the residual oil was added 4M HCl/Dioxane (5 mL). The insoluble salt produced was isolated by filtration and washed with cold acetone (10 mL) to give the product as white crystals (546 mg, 2.09 mmol, 50%); **IR (thin film)** $\tilde{\nu}$/cm^{-1}: 2923 (C-H, s), 2714 (C-H, s), 1596 (C=C, m). **^{1}H NMR (400 MHz, $(CD_3)_2SO$)** δ/ppm: 9.21 (br. s, 2H, NH_2), 7.59–7.54 (m, 2H, H3&4), 7.44–7.36 (m, 2H, H2&5), 3.55 (d, *J* = 13.5 Hz, 2H, H10a), 3.36 (s, 2H, H7), 3.18 (t, *J* = 13.5 Hz, 2H, H10b), 2.56–2.51 (m, 2H, H9a), 2.40–2.33 (m, 2H, H9b). **^{13}C NMR (101 MHz, $(CD_3)_2SO$)** δ/ppm: 159.2 (C6), 131.3 (C3), 127.2 (C4), 125.5 (C2), 119.9 (C1), 117.0 (C5), 40.9 (C10×2), 38.9 (C8), 36.9 (C7), 30.2 (C9×2). **HRMS (ESI)** $C_{12}H_{17}N_2$ *m/z*: $[M+H]^+$ 188.1313 (*calc.* 188.1319). **m.p.** 264–265 °C.

2,3-Dihydrospiro[indene-1,4′-piperidin]-1′-ium chloride, 86

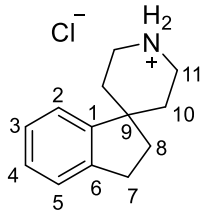

The 10% Pd on C (384 mg, 0.36 mmol, 0.1 eq) was suspended in ethanol (10 mL) and hydrogen gas was bubbled through the mixture. Compound **103** (500 mg, 2.25 mmol, 1.0 eq) was added to the reaction and it was stirred for 2 h in an atmosphere of hydrogen. The catalyst was remove by filtering through celite and the ethanol was removed *in vacuo*. The crystals were washed with cold acetone (10 mL) to yield product as white crystals (402 mg, 1.80 mmol, 80%); **IR (thin film)** $\tilde{\nu}$/cm^{-1}: 2943 (C-H, s), 2730 (C-H, s), 1595 (C=C, m). **^{1}H NMR (400MHz, (CD$_3$)$_2$SO)** δ/ppm: 9.71 (d, *J* = 64.0 Hz, 2H, NH$_2$), 7.30–7.20 (m, 4H, H2–5), 3.55 (d, *J* = 12.5 Hz, 2H, H11a), 3.11 (q, *J* = 11.5 Hz, 2H, H11b), 2.97 (t, *J* = 7.5 Hz, 2H, H7), 2.35 (td, *J* = 14.0, 4.0 Hz, 2H, H10a), 2.07 (t, *J* = 7.5 Hz, 2H, H8), 1.75 (d, *J* = 14.0 Hz, 2H, H10b). **^{13}C NMR (101 MHz, (CD$_3$)$_2$SO)** δ/ppm: 148.5 (C6), 142.4 (C1), 127.6 (C2), 127.0 (C4), 124.8 (C5), 122.7 (C3), 45.2 (C9), 41.8 (C11×2), 34.6 (C8), 33.2 (C10×2), 29.8 (C7). **HRMS (ESI)** $C_{13}H_{17}N$ *m/z*: $[M+H]^+$ 188.1447 (*calc.* 188.1439). **m.p.** 289–290 °C.

The physical and spectroscopic data was found to be in agreement with Chambers *et al.*[131]

tert-Butyl bis(2-chloroethyl)carbamate, 92

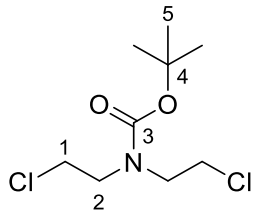

Di-*tert*-butyl dicarbonate (4.6 mL, 20.0 mmol, 1.2 eq) and bis(2-chloroethyl)amine (3.0 g, 16.8 mmol, 1.0 eq) were dissolved in CH_2Cl_2 (20 mL). Triethylamine (2.6 mL, 20.1 mmol, 1.2 eq) was added dropwise. The mixture was left to stir for an hour before more triethylamine (0.2 mL, 1.4 mmol, 0.08 eq) was added. The reaction was stirred overnight before TLC showed it had gone to completion. Excess solvent was removed *in vacuo*. The residue was dissolved in

diethyl ether (30 mL) and extracted with water (30 mL). The combined ethereal layers were dried over anh. $MgSO_4$ and the excess solvent was removed *in vacuo*. the residue was purified via column chromatography (pet. ether/diethyl ether 20%) to give the product as a colourless oil (3.10 g, 12.8 mmol, 76%); $\mathbf{R_f}$ 0.31 (pet. ether / Et_2O (20%)); **IR (thin film)** $\tilde{\nu}$/cm^{-1}: 2977 (C-H, m), 1693 (C=O, s), 1465 (C-H, m), 1405 (C-H, m), 775 (C-Cl, m). **^{1}H NMR (400 MHz, $CDCl_3$)** δ/ppm: 3.66–3.59 (m, 8H, H1&2), 1.47 (s, 9H, H5). **^{13}C NMR (101 MHz, $CDCl_3$)** δ/ppm: 154.9 (C3), 80.7 (C4), 51.0 (C2x2), 42.1 (C1x2), 28.3 (C5x3). **HRMS (ESI)** $C_5H_{10}NO_2Cl_2$ *m/z*: [M+H–*t*-butyl]$^+$ 186.0089 (*calc.* 186.0094).

The physical and spectroscopic data was found to be in agreement with Tantry *et al.*[223]

4-Cyano-4-(2-fluorophenyl)piperidin-1-ium chloride, 95

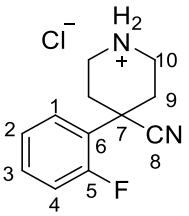

Compound **96** (476 mg, 1.57 mmol) was stirred in HCl/dioxane (4M, 5 mL) for 1 h. The mixture was filtered and the filtrate was washed with cold diethyl ether (10 mL). The isolated white crystals were placed in a desiccator overnight to yield the pure white crystalline product (183 mg, 0.76 mmol, 48%); **IR (thin film)** $\tilde{\nu}$/cm^{-1}: 2925 (C-H, m), 2712 (C-H, m), 2241 (C≡N, w), 1597 (C=C, m). **1H NMR (400 MHz, $(CD_3)_2SO$)** δ/ppm: 9.26–9.20 (m, 2H, NH_2), 7.55–7.50 (m, 2H, H3&5), 7.40–7.25 (m, 2H, H2,4), 3.51 (d, *J* = 13.5 Hz, 2H, H10), 3.17–3.09 (m, 2H, H10), 2.52–2.48 (m, 2H, H9), 2.33 (td, *J* = 13.5, 3.5 Hz, 2H, H9). **^{13}C NMR (101 MHz, $(CD_3)_2SO$)** δ/ppm: 161.8 (C6), 159.4 (C1), 131.7 (C3), 127.5 (C5), 125.9 (C2), 120.3 (C8), 117.3 (C4), 41.2 (C10×2), 37.3 (C7), 30.6 (C9×2). **HRMS (ESI)** $C_{12}H_{14}FN_2$ *m/z*: [M+H]$^+$ 205.1130 (*calc.* 205.1136). **m.p.** 276–277 °C.

tert-Butyl 4-cyano-4-(2-fluorophenyl)piperidine-1-carboxylate, 96

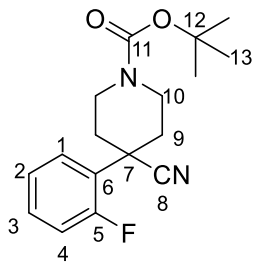

2-(2-Fluorophenyl)acetonitrile (1.6 mL, 12.39 mmol, 1.5 eq) was added to a suspension of sodium hydride (50% in mineral oil, 3.2 g, 80.95 mmol, 9.8 eq) in dry THF (20 mL) at 5 °C. The mixture was warmed to RT and stirred for 30 min. The reaction was cooled to 0 °C and compound **92** (2.0 g, 8.26 mmol, 1.0 eq) was added before being heated to reflux for 3 h. After the reaction had finished, as shown by TLC, the excess solvent was removed *in vacuo*, ice water (10 mL) was added slowly to the residue before being extracted with diethyl ether (20 mL x 3). The combined organic layers were dried over $MgSO_4$ and the excess solvent was removed *in vacuo*. The resulting substance was purified by column chromatography (40% diethyl ether in pet. ether) to give the product as a white amorphous solid (2.09 g, 6.87 mmol, 83%); $\mathbf{R_f}$ 0.34 (40% diethyl ether in pet. ether); **IR (thin film)** $\tilde{\nu}$/cm^{-1}: 2979 (C-H, s), 2251 (C≡N, m), 1694 (C=O, s), 1605 (C=C, m). **^{1}H NMR (400 MHz, $CDCl_3$)** δ/ppm: 7.46 (td, J = 8.0, 2.0 Hz, 1H, H4), 7.37–7.34 (m, 1H, H2), 7.19 (td, J = 7.5, 1.5 Hz, 1H, H3), 7.13 (ddd, J = 12.0, 8.0, 1.0 Hz, 1H, H1), 4.28 (br. s, 2H, H10a), 3.23 (br. s, 2H, H10b), 2.21–2.06 (m, 4H, H9), 1.48 (s, 9H, H13). **^{13}C NMR (101 MHz, $CDCl_3$)** δ/ppm: 161.7 (C11), 159.7 (C5×3), 154.4 (C6), 130.4 (C4), 127.0 (C2), 124.7 (C3), 120.2 (C8), 117.0 (C1), 80.1 (C12), 41.3 (C7), 40.2 (C9×2), 33.8 (C10×2), 28.4 (C13). **HRMS (ESI)** $C_{17}H_{21}N_2O_2FNa$ *m/z*: $[M+Na]^+$ 327.1479 (*calc.* 327.1470).

The physical and spectroscopic data was found to be in agreement with Xie *et al.*[130]

N-Benzyl-2-chloro-*N*-(2-chloroethyl)ethan-1-amine, 98

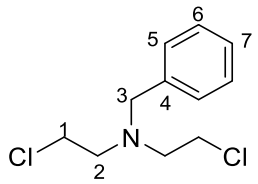

Benzyl bromide (0.80 mL, 6.75 mmol, 1.0 eq) was added dropwise to a suspension of K_2CO_3 (0.93 g, 6.72 mmol, 1.2 eq) and bis(2-chloroethyl)ammonium chloride (1.00 g, 5.60 mmol, 1.0 eq) in acetonitrile (7 mL). The reaction was refluxed overnight. Afterwards the excess solvent was removed *in vacuo* and the remaining mixture was re-dissolved in diethyl ether (20 mL) and extracted with water (20 mL) and brine (20 mL) and the combined aqueous layers were extracted with diethyl ether (20 mL × 3). The combined ethereal layers were dried over $MgSO_4$ and the excess solvent was removed *in vacuo*. The product was purified *via* column chromatography (100% pet. ether) to give the pure product as a colourless oil (500 mg, 2.15 mmol, 38%); $\mathbf{R_f}$ 0.17 (pet. ether); **IR (thin film)** $\tilde{\nu}$/cm^{-1}: 2961 (C-H, m), 2809 (C-H, m), 1610 (C=C, w), 1453 (C-H, m), 742 (C-Cl, s). **^{1}H NMR (400 MHz, $CDCl_3$)** δ/ppm: 7.34–7.25 (m, 5H, Ar), 3.75 (s, 2H, H3), 3.50–3.33 (m, 4H, H1), 3.01–2.91 (m, 4H, H2). **^{13}C NMR (101 MHz, $CDCl_3$)** δ/ppm: 138.8 (C4), 128.6 (C5/6×2), 128.4 (C5/6×2), 127.4 (C7), 59.2 (C3), 56.3 (C2×2), 42.0 (C1×2). **HRMS (ESI)** $C_{11}H_{16}NCl_2$ *m/z*: $[M+H]^+$ 232.0668 (*calc.* 232.0660).

The physical and spectroscopic data was found to be in agreement with Chan *et al.*[224]

1′-Benzylspiro[indene-1,4′-piperidine], 100

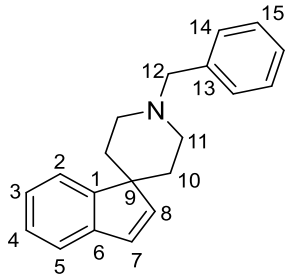

Indene (0.50 mL, 4.31 mmol, 1.0 eq) was dissolved in THF (10 mL) and cooled to 0 °C and LHMDS (1M in THF, 8.62 mL, 8.62 mmol, 2.0 eq) was added over 15 min. The mixture was stirred for 30 min before compound **98** (1.00 g, 4.31 mmol, 1.0 eq) was added dropwise. The reaction was heated to RT and stirred for 2 h. When the reaction had concluded, the solvent

was removed *in vacuo* and the residue was diluted with diethyl ether (20 mL) and washed with sat. aq. NH_4Cl (20 mL) and brine (20 mL). The combined aqueous layers were extracted with diethyl ether (20 mL × 3). The combined ethereal layers were dried over $MgSO_4$ and the excess solvent was removed *in vacuo*. The given oil was purified *via* column chromatography (20% diethyl ether in pet. ether) to give the product as a golden oil (809 mg, 2.94 mmol, 68%); $\mathbf{R_f}$ 0.11 (20% diethyl ether in pet. ether); **IR (thin film)** $\tilde{\nu}$/cm^{-1}: 3065 (C-H, m), 2945 (C-H, m), 2804 (C-H, m), 1454 (C=C, m), 698 (C-H, s). **^{1}H NMR (400 MHz, $CDCl_3$)** δ/ppm: 7.42–7.19 (m, 9H, Ar), 6.87 (d, *J* = 5.5 Hz, 1H, H8), 6.75 (d, *J* = 5.5 Hz, 1H, H7), 3.67 (s, 2H, H12), 3.00 (dt, *J* = 12.0, 3.0 Hz, 2H, H10a), 2.39 (td, *J* = 12.0, 2.5 Hz, 2H, H10b), 2.22 (td, *J* = 12.5, 3.5 Hz, 2H, H11a), 1.36 (d, *J* = 12.0 Hz, 2H, H11b). **^{13}C NMR (101 MHz, $CDCl_3$)** δ/ppm: 152.4 (C1), 142.9 (C6), 141.7 (C8), 138.3 (C13), 129.4 (C14/15/16), 129.3 (C7), 128.3 (C14/15/16), 127.1 (C14/15/16), 126.8 (C2/3/4/5), 125.2 (C2/3/4/5), 121.8 (C2/3/4/5), 121.3 (C2/3/4/5), 63.7 (C12), 52.2 (C11×2), 52.1 (C9), 33.9 (C10×2),. **HRMS (ESI)** $C_{20}H_{22}N$ *m/z*: $[M+H]^+$ 276.1739 (*calc.* 276.1747).

1′-Benzyl-2,3-dihydrospiro[indene-1,4′-piperidine], 101

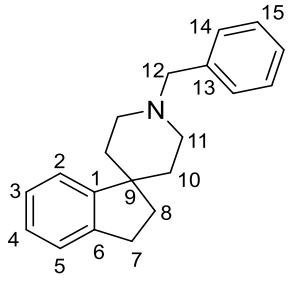

The 10% Pd on C (142 mg, 0.13 mmol, 0.1 eq) was suspended in ethanol (10 mL) and hydrogen gas was bubbled through the mixture. Compound **100** (230 mg, 0.84 mmol, 1.0 eq) was added to the reaction as a solution in ethanol (5 mL) and it was stirred for 2 h in an atmosphere of hydrogen. The catalyst was removed by filtering through celite and the ethanol was removed *in vacuo*. The given oil was purified *via* column chromatography (5 % methanol in CH_2Cl_2) to give the product as a colourless oil (110 mg, 0.40 mmol, 48%); $\mathbf{R_f}$ 0.26 (5 % methanol in dichloromethane); **IR (thin film)** $\tilde{\nu}$/cm^{-1}: 3021 (C-H, m), 2924 (C-H, s), 1602 (C=C, w), 1494 (C=C, w). **^{1}H NMR (400 MHz, $CDCl_3$)** δ/ppm: 7.38–7.13 (m, 9H, Ar), 3.57 (s, 2H, H12), 2.91–2.85 (m, 4H, H7,11a), 2.20 (t, *J* = 10.5 Hz, 2H, H11b), 2.02–1.92 (m, 4H, H8,10a), 1.53 (d, *J* = 13.0 Hz, 2H, H10b). **^{13}C NMR (101 MHz, $CDCl_3$)** δ/ppm: 151.5 (C1), 143.2 (C6), 138.4 (C13), 129.4 (C2/3/4/5), 128.3 (C2/3/4/5), 127.1 (C2/3/4/5), 126.7 (C2/3/4/5), 126.5 (C14/15/16), 124.6

(C14/15/16), 122.7 (C14/15/16), 63.7 (C12), 51.3 (C11), 46.5 (C9), 36.9 (C10), 35.1 (C8), 30.0 (C7). **HRMS (ESI)** $C_{20}H_{24}N$ *m/z*: $[M+H]^+$ 278.1891 (*calc.* 278.1903).

tert-Butyl spiro[indene-1,4′-piperidine]-1′-carboxylate, 102

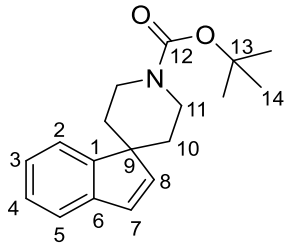

Indene (0.10 mL, 0.86 mmol, 1.0 eq) was dissolved in dry THF (2 mL) and cooled to 0 °C. LHMDS (288 mg, 1.72 mmol, 2.0 eq) was added dropwise over 15 min. This was left to stir for 30 min before compound **92** (208 mg, 0.86 mmol, 1.0 eq) was added at 0 °C and stirred for 2 h. After the reaction had gone to completion excess solvent was removed *in vacuo*. This was purified via column chromatography (20% diethyl ether in pet. ether) to give the product as a yellow oil (203 mg, 0.712 mmol, 83%); $\mathbf{R_f}$ 0.28 (20% diethyl ether in pet. ether); **IR (thin film)** $\tilde{\nu}$/cm^{-1}: 3057 (C-H, m), 2976 (C-H, m), 2935 (C-H, m), 2865 (C-H, m), 1687 (C=O, s). **^{1}H NMR (400 MHz, $CDCl_3$)** δ/ppm: 7.36–7.19 (m, 4H, H2–5), 6.85 (d, *J* = 5.5 Hz, 1H, H8), 6.79 (d, *J* = 5.5 Hz, 1H, H7), 4.20–4.18 (m, 2H, H11a), 3.13 (t, *J* = 12.5 Hz, 2H, H11b), 2.01 (td, *J* = 12.5, 4.5 Hz, 2H, H10a), 1.51 (s, 9H, H14), 1.34 (d, *J* = 13.0 Hz, 2H, H10b). **^{13}C NMR (101 MHz, $CDCl_3$)** δ/ppm: 155.1 (C12), 151.7 (C1), 142.8 (C6), 140.4 (C8), 130.3 (C7), 127.0 (C2/3/4/5), 125.4 (C2/3/4/5), 121.7 (C2/3/4/5), 121.5 (C2/3/4/5), 79.6 (C13), 77.2 (C11), 52.1 (C9), 33.4 (C10), 28.5 (C14). **HRMS (ESI)** $C_{18}H_{24}NO_2$ *m/z*: $[M+H]^+$ 286.1812 (*calc.* 286.1811).

The physical and spectroscopic data was found to be in agreement with Tantry *et al*.[223]

Spiro[indene-1,4′-piperidin]-1′-ium chloride, 103

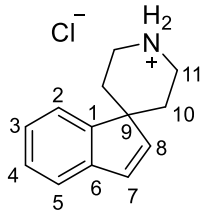

Compound **102** (1.78 g, 6.24 mmol) was stirred in HCl/dioxane (4M, 5.00 mL) for 1 h. The mixture was filtered and the filtrate was washed with cold diethyl ether (10 mL). The isolated white crystals were placed in a desiccator overnight to yield the pure white crystalline product (405 mg, 5.23 mmol, 84%); **IR (thin film)** $\tilde{\nu}$/cm^{-1}: 3361 (N-H, m), 2936 (C-H, m), 2801 (C-H, m), 1644 (C=C, m), 1600 (C=C, m). **^{1}H NMR (400 MHz, (CD$_3$)$_2$SO)** δ/ppm: 9.92 (d, *J* = 33.5 Hz, 2H, NH2), 7.48 (d, *J* = 7.0 Hz, 1H, H5), 7.37–7.24 (m, 3H, H2–4), 6.87 (d, *J* = 5.5 Hz, 1H, H7), 6.74 (d, *J* = 5.5 Hz, 1H, H8), 3.69 (d, *J* = 13.0 Hz, 2H, H11a), 3.26 (q, *J* = 13.0 Hz, 2H, H11b), 2.58 (td, *J* = 13.0, 4.0 Hz, 1H, H10a) 1.60 (d, *J* = 13.0 Hz, 2H, H10b). **^{13}C NMR (101 MHz, (CD$_3$)$_2$SO)** δ/ppm: 150.0 (C1), 142.3 (C6), 138.1 (C8), 132.1 (C7), 127.7 (C2/3/4), 126.1 (C2/3/4), 122.0 (C2/3/4), 121.9 (C5), 50.1 (C9), 42.81 (C11×2), 30.4 (C10×2). **HRMS (ESI)** $C_{13}H_{17}N$ *m/z*: $[M+H]^+$ 186.1275 (*calc.* 186.1277). **m.p.** 309–310 °C.

tert-Butyl 2-oxo-3,4-dihydroquinoline-1(2*H*)-carboxylate, 105

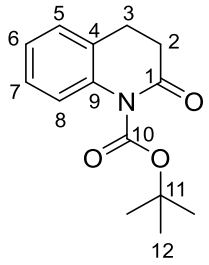

3,4-Dihydroquinolin-2(1*H*)-one (100 mg, 0.68 mmol, 1.0 eq) was dissolved in dry CH_2Cl_2 (5 mL) before triethylamine (0.095 mL, 0.68 mmol, 1.0 eq), di-*tert*-butyl decarbonate (0.19 mL, 0.82 mmol, 1.2 eq), and 4-dimethylaminopyridine (8.50 mg, 0.07 mmol, 0.1 eq) were added to the mixture. The mixture was stirred for 18 h at RT. After the reaction had finished the excess solvent was removed *in vacuo*. To the mixture water (20 mL) was added and the mixture was extracted with diethyl ether (10 mL × 3). The combined ethereal layers were washed with 1 M $KHSO_4$ (20 mL), sat. $NaHCO_3$ (20 mL), and brine (20 mL). The organic layers were dried

over Na_2SO_4 and the excess solvent was removed *in vacuo*. The resulting substance was purified by column chromatography (20% diethyl ether in pet. ether) to give the product as a white crystalline solid (154 mg, 0.62 mmol, 92%); $\mathbf{R_f}$ 0.17 (20% diethyl ether in pet. ether); **IR (thin film)** $\tilde{\nu}$/cm^{-1}: 2981 (C-H, w), 1755 (C=O, s), 1692 (C=O, s), 1605 (C=C, m). **^{1}H NMR (400 MHz, CDCl3)** δ/ppm: 7.23–7.17 (m, 2H, H6,7), 7.06 (td, *J* = 7.5,1.0 Hz, 1H, H5), 6.94 (d, *J* = 8.0 Hz, 1H, H8), 2.95 (t, *J* = 7.0 Hz, 2H, H3), 2.68–2.64 (m, 2H, H2), 1.60 (s, 9H, H12). **^{13}C NMR (101 MHz, CDCl3)** δ/ppm: 169.3 (C1), 151.8 (C10), 137.1 (C9), 128.0 (C7), 127.3 (C6), 125.9 (C4), 124.1 (C5), 117.0 (C8), 85.0 (C11), 32.3 (C2), 27.7 (C12×3), 25.5 (C3). **HRMS (ESI)** $C_{14}H_{17}NO_3Na$ *m/z*: $[M+Na]^+$ 270.1063 (*calc.* 270.1063). **m.p.** 68–69 °C.

The physical and spectroscopic data was found to be in agreement with Evans *et al.*[225]

1-(*tert*-Butyl) 4-ethyl piperidine-1,4-dicarboxylate, 109

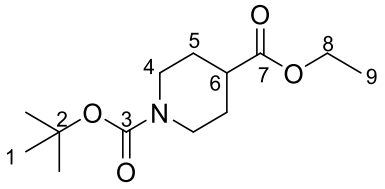

Di-*tert*-butyl dicarbonate (0.17 mL, 0.76 mmol, 1.2 eq) and ethyl piperidine-4-carboxylate (0.10 mL, 0.64 mmol, 1.0 eq) were dissolved in CH_2Cl_2 (5 mL). Triethylamine (0.11 mL, 0.76 mmol, 1.2 eq) was added dropwise and the mixture was left to stir overnight. The excess solvent was removed *in vacuo* and the residue was dissolved in diethyl ether (20 mL) before being extracted with water (20 mL × 3). The ethereal layers were dried over $MgSO_4$ and the excess solvent was removed *in vacuo*. The remaining solid was purified *via* column chromatography (20% diethyl ether in pet. ether) to give the product as a colourless oil (162 mg, 0.63 mmol, 98%); $\mathbf{R_f}$ 0.18 (20% diethyl ether in pet. ether); **IR (thin film)** $\tilde{\nu}$/cm^{-1}: 2978 (C-H, m), 1732 (C=O, s), 1692 (C=O, s). **^{1}H NMR (400 MHz, $CDCl_3$)** δ/ppm: 4.14 (q, *J* = 7.0 Hz, 2H, H8), 4.01 (d, *J* = 13.0 Hz, 2H, H4), 2.83 (t, *J* = 12.5 Hz, 2H, H4), 2.43 (tt, *J* = 11.0, 4.0 Hz, 1H, H6), 1.87 (d, *J* = 13.5 Hz, 2H, H5), 1.67–1.57 (m, 2H, H5), 1.45 (s, 9H, H1), 1.25 (t, *J* = 7.0 Hz, 3H, H9). **^{13}C NMR (101 MHz, $CDCl_3$)** δ/ppm: 174.6 (C7), 154.7 (C3), 79.6 (C2), 60.5 (C8), 43.2 (C4×2), 41.2 (C6), 28.4 (C1×3), 28.0 (C5×2), 14.2 (C9). **HRMS (ESI)** $C_{13}H_{23}NO_4Na$ *m/z*: $[M+Na]^+$ 280.1535 (*calc.* 280.1525).

The physical and spectroscopic data was found to be in agreement with Ueno *et al.*[226]

1-(*tert*-Butyl) 4-ethyl 4-(2-nitrobenzyl)piperidine-1,4-dicarboxylate, 111

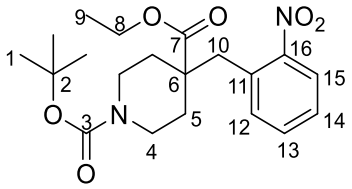

A solution of **109** (1.21 g, 4.70 mmol, 1.0 eq) in THF (10 mL) was cooled to –78 °C and NaHMDS (1M in THF, 6.58 mL, 6.58 mmol, 1.4 eq) was added dropwise. The reaction was stirred at this temperature for 1 h, before 2-nitrobenzyl bromide (1.22 g, 5.64 mmol, 1.2 eq) was added and the reaction was warmed to RT and stirred overnight. At completion, the excess solvent was removed *in vacuo* and the residue was extracted between water and ethyl acetate and the organic washed with brine. The organic layer was dried over $MgSO_4$ and the solvent was removed *in vacuo*. The crude oil produced was purified *via* column chromatography (20% ethyl acetate in hexane) to give the product as a brown oil (184.6 mg, 0.47 mmol, 10%); $\mathbf{R_f}$ 0.26 (20% ethyl acetate in hexane); **IR (thin film)** $\tilde{\nu}$/cm^{-1}: 2913 (C-H, w), 2713 (C-H, w), 1652 (C=O, s), 1596 (N=O, s), 1401 (N=O, s). **^{1}H NMR (400 MHz, $CDCl_3$)** δ/ppm: 7.86 (d, *J* = 8.0 Hz, 1H, H15), 7.48 (td, *J* = 1.5,11.5 Hz, 1H, H13), 7.40–7.37 (m, 1H, H14), 7.20 (dd, *J* = 1.5,7.5 Hz, 1H, H12) 4.07 (q, *J* = 7.0 Hz, 2H, H8), 3.67 (br. s, 2H, H4a), 3.31–3.29 (m, 2H, H4b), 2.69 (br. s, 2H, H10), 2.07–2.05 (m, 2H, H5a), 1.56 (s, 2H, H5b), 1.42 (s, 9H, H1), 1.18 (t, *J* = 7.0 Hz, 3H, H9). **^{13}C NMR (101MHz, $CDCl_3$)** δ/ppm: 174.0 (C7), 154.7 (C3), 150.4 (C16), 133.2 (C12), 132.8 (C13), 132.2 (C11), 128.0 (C14), 127.9 (C15), 79.6 (C6), 61.0 (C8), 47.6 (C2), 41.7 (C4), 38.4 (C10) 33.3 (C5), 28.4 (C1), 14.0 (C9). **HRMS (ESI)** $C_{20}H_{29}N_2O_6$ *m/z*: $[M+H]^+$ 393.2042 (*calc.* 393.2026).

1-(*tert*-Butyl) 4-ethyl 4-(2-aminobenzyl)piperidine-1,4-dicarboxylate, 112

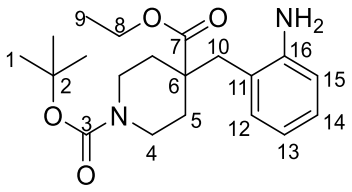

Hydrogen gas was bubbled through a suspension of palladium on carbon (10%, 112 mg, 0.10 mmol, 20 mol %) in ethanol (10 mL) to which **111** (179 mg, 0.46 mmol, 1.0 eq) was added. After completion, the reaction was filter through celite and the excess solvent was removed *in vacuo*. The product was purified by column chromatography (10% methanol in CH_2Cl_2) to give the

product as a colourless oil (146 mg, 0.37 mmol, 81%) $\mathbf{R_f}$ 0.21 (10% methanol in CH_2Cl_2); **IR (thin film)** $\tilde{\nu}$/cm^{-1}: 2913 (C-H, w), 2713 (C-H, w), 1652 (C=O, s), 1620 (C=O, s), 1225 (C-N, m). **^{1}H NMR (400 MHz, $CDCl_3$)** δ/ppm: 7.20–7.15 (m, 2H, H12,14) 7.01–6.98 (m, 1H, H13) 6.73 (d, *J* = 8.0 Hz, 1H, H15) 3.72 (q, *J* = 7.0 Hz, 2H, H8) 3.66–3.61 (m, 2H, H4a) 3.47–3.42 (m, 2H, H4b) 2.87 (s, 2H, H10) 2.62 (s, 2H, H5) 1.94 (s, 2H, H5) 1.45 (s, 9H, H1) 1.24 (t, *J* = 3.5 Hz, 3H, H9). **^{13}C NMR (101 MHz, $CDCl_3$)** δ/ppm: 174.7 (C7) 154.8 (C3) 136.3 (C16) 128.6 (C12) 127.7 (C14) 123.2 (C13) 122.2 (C11) 114.5 (C15) 79.5 (C6) 58.5 (C8) 45.7 (C2) 41.0 (C4) 38.5 (C5) 36.5 (C10) 28.4 (C1) 18.4 (C9). **HRMS (ESI)** $C_{20}H_{31}N_2O_4$ *m/z*: $[M+H]^+$ 363.2268 (*calc.* 363.2278).

6-Chloro-1H-indene, 115

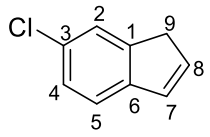

To a solution of 5-chloro-1-indanone (1.00 g, 6.00 mmol, 1.0 eq) in methanol (30 mL) was added sodium borohydride (613mg, 16.21mmol, 2.7 eq). The mixture was warmed to RT and stirred for 1 h. Next water (10 mL) was added and the reaction was extracted with CH_2Cl_2 (30 mL × 3). The organic layer was dried over $MgSO_4$ which was subsequently filtered off and the filtrated was concentrated *in vacuo* to give the crude alcohol. This alcohol was dissolved in toluene (30 mL) and *p*-toluenesulfonic acid monohydrate (34.2 mg, 0.18 mmol, 0.03 eq) was added before the reaction was refluxed for 2 h. The reaction was cooled to RT and sat. aq. $NaHCO_3$ (30 mL) was added before extraction with ethyl acetate (20 mL × 3). The organic layers were washed with brine (50 mL) and dried over $MgSO_4$. This was filtered off and the filtrate was concentrated *in vacuo*. The crude oil was purified *via* column chromatography (100%hexane) to yield the pure product as a colourless oil (615 mg, 4.09 mmol, 68%); $\mathbf{R_f}$ 0.45 (100% hexane); **IR (thin film)** $\tilde{\nu}$/cm^{-1}: 2988 (C-H, m), 1583 (C=C, m), 818 (C-Cl, s). **^{1}H NMR (400 MHz, $CDCl_3$)** δ/ppm: 7.47 (s, 1H, H2), 7.33 (d, *J* = 8.0 Hz, 1H, H5), 7.28–7.26 (m, 1H, H4), 6.87 (d, *J* = 5.5 Hz, 1H, H7), 6.58 (dt, *J* = 5.5,2.0 Hz, 1H, H8), 3.42 (s, 2H, H9). **^{13}C NMR (101 MHz, $CDCl_3$)** δ/ppm: 145.4 (C6), 143.3 (C1), 134.6 (C8), 131.4 (C7), 130.6 (C3), 126.4 (C4), 124.1 (C5), 121.6 (C2), 39.0 (C9). **HRMS (ESI)** C_9H_8Cl *m/z*: $[M+H]^+$ 151.0309 (*calc.* 151.0315).

The physical and spectroscopic data was found to be in agreement with Capkova *et al.*[132]

tert-Butyl 6-chlorospiro[indene-1,4′-piperidine]-1′-carboxylate, 116

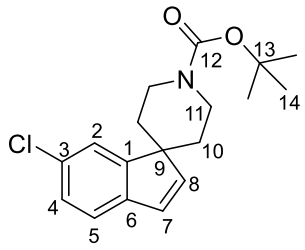

To a solution of **115** (615 mg, 4.08 mmol, 1.0 eq) dissolved in THF (10 mL) cooled to 0 °C was added LiHMDS (1M in THF, 8.16 mL, 8.16 mmol, 2.0 eq) over 15 min. The reaction was stirred for 30 min before **92** (988 mg, 4.08 mmol, 1.0 eq) was added dropwise. The mixture was stirred for 2 h at RT. The excess solvent was removed *in vacuo*. The residue was diluted with diethyl ether (20 mL) and washed with sat. aq. NH4Cl (20 mL). The aqueous was extracted with diethyl ether (20 mL × 3). The organic layers were dried over $MgSO_4$ and the excess solvent was removed *in vacuo* to give a crude oil. This was purified by column chromatography (20% diethyl ether in pet. ether) to give the pure product as a colourless oil (1.0022 g, 3.13 mmol, 77%); $\mathbf{R_f}$ 0.24 (20% diethyl ether in pet. ether); **IR (thin film)** $\tilde{\nu}$/cm^{-1}: 2974 (C-H, m), 1686 (C=O, s), 1601 C=C, m), 733 (C-Cl, s). **^{1}H NMR (400 MHz, $CDCl_3$)** δ/ppm: 7.30–7.28 (m, 1H, H2), 7.23–7.16 (m, 1H, H4,5), 6.87 (dd, *J* = 22.0, 5.5 Hz, 1H, H8), 6.73 (dd, *J* = 5.5,4.0 Hz, 1H, H7), 4.18 (br. s, 2H, H11a), 3.10 (t, *J* = 12.5 Hz, 2H, H11b), 1.97 (td, *J* = 12.5, 4.5 Hz, 2H, H10a), 1.51 (s, 9H, H14) 1.35–1.30 (m, 2H, H10b). **^{13}C NMR (101 MHz, $CDCl_3$)** δ/ppm: 154.9 (C12), 153.5 (C6), 149.9 (C3), 144.4 (C1), 141.2 (C8), 129.6 (C7), 127.2 (C5), 125.2 (C4), 122.4 (C2), 79.7 (C13), 52.4 (C9), 42.1 (C11×2), 33.3 (C10×2), 28.5 (C14). **HRMS (ESI)** $C_{18}H_{22}NO_2ClNa$ *m/z*: $[M+Na]^+$ 342.1225 (*calc.* 342.1231).

6-Chlorospiro[indene-1,4′-piperidin]-1′-ium chloride, 117

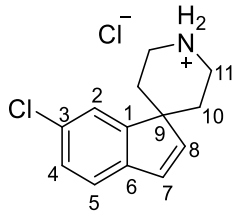

A solution of **116** (1.0 g, 3.13 mmol, 1.0 eq) was stirred in 4M HCl/dioxane (10 mL) for 30 min. The mixture was filtered and the residue was desiccated to give the product as a white crystal

(552 mg, 2.15 mmol, 69%); **IR (thin film)** $\tilde{\nu}$/cm^{-1}: 2944 (C-H, s), 2730 (C-H, s), 1595 (C=C, m), 1457 (C=C, m), 1428 (C-H, m), 1072 (C-N, m), 734 (C-Cl, s). **^{1}H NMR (400 MHz, (CD$_3$)$_2$SO)** δ/ppm: 8.89 (br. s, 2H, NH$_2$), 7.45–7.27 (m, 3H, H2,4,5), 7.20 (dd, *J* = 24.0, 5.5 Hz, 1H, H7), 6.86 (t, *J* = 5.5 Hz, 1H, H8), 3.41–3.38 (m, 2H, H11a), 3.22 (td, *J* = 3.0,13.0 Hz, 2H, H11b), 2.33–2.22 (m, 2H, H10a), 1.36–1.30 (m, 2H, H10b). **^{13}C NMR (101 MHz, (CD$_3$)$_2$SO)** δ/ppm: 153.6 (C1), 149.6 (C6), 144.6 (C7), 141.9 (C3), 129.6 (C8), 127.4 (C2/4/5), 125.3 (C2/4/5), 123.0 (C2/4/5), 50.7 (C9), 41.8 (C11×2), 29.7 (C10×2). **HRMS (ESI)** $C_{13}H_{15}NCl$ *m/z*: $[M+H]^+$ 220.0879 (*calc.* 220.0888). **m.p.** 294–296 °C.

6-Chloro-2,3-dihydrospiro[indene-1,4′-piperidin]-1′-ium chloride, 118

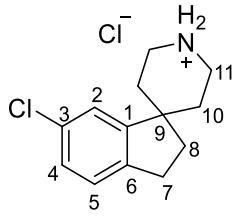

Hyrdrogen gas was bubbled through a suspension of Pd on C (10% w/w, 200 mg, 0.19 mmol, 0.16) in ethanol (10 mL). To this **117** was added and the reaction was stirred for 1 h. The catalyst was removed by filtration through celite. The excess solvent of the filtrate was removed *in vacuo* to give the product as white crystals (299 mg, 1.16 mmol, 99%); **IR (thin film)** $\tilde{\nu}$/cm^{-1}: 2953 (C-H, s), 1475 (C=C, m), 1439 (C-H, m), 1073 (C-N, s), 815 (C-Cl, m). **^{1}H NMR (400 MHz, (CD$_3$)$_2$SO)** δ/ppm: 8.83 (br. s, 2H, NH$_2$), 7.29–7.11 (m, 3H, H2,4,5), 3.27 (d, *J* = 13.0 Hz, 2H, H11a), 3.00 (t, *J* = 13.0 Hz, 2H, H11b), 2.87 (q, *J* = 8.0 Hz, 2H, H7), 2.10–1.93 (m, 4H, H8,10a), 1.62–1.60 (m, 2H, H10b). **^{13}C NMR (101 MHz, (CD$_3$)$_2$SO)** δ/ppm: 152.3 (C1), 141.9 (C6), 131.1 (C3), 127.2 (C2/4/5), 126.5 (C2/4/5), 122.2 (C2/4/5), 45.3 (C9), 41.0 (C11×2), 34.3 (C8), 32.6 (C10×2), 29.0 (C7). **HRMS (ESI)** $C_{13}H_{17}NCl$ *m/z*: $[M+H]^+$ 222.1036 (*calc.* 222.1044). **m.p.** 300–301 °C.

8-Chloro-2-(ethoxycarbonyl)-2,3,4,5-tetrahydro-1H-pyrido[4,3-b]indol-5-ium chloride, 121

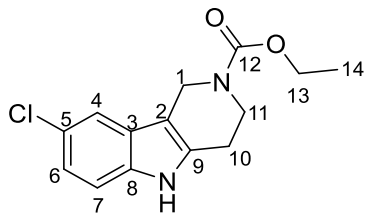

Ethyl 4-oxopiperidine-1-carboxylate (0.84 mL, 5.59 mmol, 1.0 eq) and (4-chlorophenyl) hydrazine (1 g, 5.59 mmol, 1.0 eq) were dissolved in ethanol (10 mL) and refluxed for 3 h before being left to stir at room temperature overnight. The residual solid was collected by filtration and washed with 1:1 mixture of H_2O:EtOH to give the product as a white amorphous solid (872.6 mg, 3.14 mmol, 56%); **IR (thin film)** $\tilde{\nu}$/cm^{-1}: 3414 (N-H, br. s), 2988 (C-H, m), 1658 (C=O, m), 1050 (C-N, s), 823 (C-Cl, m). **^{1}H NMR (400 MHz, $CDCl_3$)** δ/ppm: 11.13 (s, 2H, NH_2), 7.48 (d, *J* = 2.0 Hz, 1H, H7), 7.29 (d, *J* = 8.5 Hz, 1H, H4), 7.02 (dd, *J* = 8.5,2.0 Hz, 1H, H6), 4.56 (s, 2H, H1), 4.09 (q, *J* = 7.0 Hz, 2H, H13), 3.74 (t, *J* = 5.5 Hz, 2H, H11), 2.79 (t, *J* = 5.5 Hz, 2H, H10), 1.21 (t, *J* = 7.0 Hz, 3H, H14). **^{13}C NMR (101 MHz, $CDCl_3$)** δ/ppm: 155.2 (C12), 134.6 (C3), 134.3 (C8), 126.3 (C9), 123.2 (C5), 120.5 (C6), 116.8 (C7), 112.4 (C4), 105.7 (C2), 61.0 (C13), 40.9 (C1), 40.2 (C11), 23.0 (C10), 14.7 (C14). **HRMS (ESI)** $C_{14}H_{16}ClN_2O_2$ *m/z*: $[M+H]^+$ 279.0904 (*calc.* 279.0895).

The physical and spectroscopic data was found to be in agreement with Yin *et al.*[133]

8-Chloro-2,3,4,5-tetrahydro-1H-pyrido[4,3-b]indol-2-ium chloride, 122

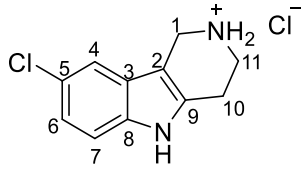

A mixture of **121** (340 mg, 1.22 mmol, 1.0 eq), 0.8M potassium hydroxide (5 mL, 6.10 mmol, 5.0 eq) and ethanol (10 mL) was refluxed overnight. After the reaction was cooled to RT it was stirred with 4M HCl/dioxane. The mixture was filtered and the residue dried in a desiccator to achieve the product as a white crystalline solid (207 mg, 0.85 mmol, 71%); **IR (thin film)** $\tilde{\nu}$/cm^{-1}: 2919 (C-H, m), 2727 (C-H, m), 1441 (C=C, m), 790 (C-Cl, s). **^{1}H NMR (400 MHz,**

$(CD_3)_2SO$) δ/ppm: 10.9 (s, 2H, NH_2), 7.37 (d, J = 2.0 Hz, 1H, H7), 7.21 (d, J = 8.5 Hz, 1H, H4), 7.08 (dd, J = 8.5,2.0 Hz, 1H, H6), 4.02 (t, J = 1.5 Hz, 2H, H11), 3.22 (t, J = 5.5 Hz, 2H, H1), 2.77 (t, J = 5.5 Hz, 2H, H10). **^{13}C NMR (101 MHz, $(CD_3)_2SO$)** δ/ppm: 135.5 (C3), 133.9 (C8), 126.8 (C9), 122.8 (C5), 119.9 (C6), 116.5 (C7), 112.1 (C4), 108.3 (C2), 42.9 (C1), 41.5 (C11), 24.1 (C10). **HRMS (ESI)** $C_{11}H_{12}N_2Cl$ *m/z*: $[M+H]^+$ 207.0676 (*calc.* 207.0684). **m.p.** 277-279 °C.

The physical and spectroscopic data was found to be in agreement with Yin *et al.*[133]

Ethyl (diphenylmethylene)glycinate, 140

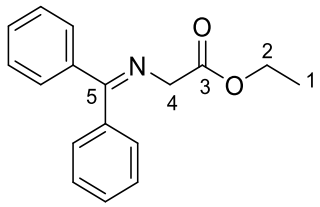

Ethyl glycinate hydrochloride (20 g, 143.3 mmol, 1.0 eq), benzophenone (26.11 g, 143.3 mmol, 1.0 eq), and diisopropylethylamine (25 mL, 143.3 mmol, 1.0 eq) were dissolved in toluene (90 mL) and heated with Dean-Stark apparatus until one equivalent of water was observed in the trap. The reaction was cooled to RT and diluted with water (50 mL). The aqueous was extracted with ethyl acetate (3 × 25 mL) and the combined organics were washed with water (50 mL), sat. aq. $NaHCO_3$ (50 mL), and brine (50 mL). The organics were dried over anh. $MgSO_4$, filtered, and concentrated *in vacuo* to give the crude product. This was purified by column chromatography (10% ethyl acetate in pet. ether) to yield the pure product as white crystals (16.61 g, 62.13 mmol, 43%); **R_f** 0.14 (10% ethyl acetate in pet. ether); **IR (thin film)** $\tilde{\nu}$/cm^{-1}: 2981 (C-H, w), 1749 (C=O, s), 1620 (C=N, m), 1188 (C-O, s). **^{1}H NMR (400 MHz, $CDCl_3$)** δ/ppm: 7.68–7.65 (m, 2H, Ar), 7.49–7.31 (m, 6H, Ar), 7.20–7.17 (m, 2H, Ar), 4.21 (q, J = 7.0 Hz, 2H, H2), 4.20 (s, 2H, H4), 1.27 (t, J = 7.0 Hz, 3H, H1). **^{13}C NMR (101 MHz, $CDCl_3$)** δ/ppm: 171.9 (C5), 170.7 (C3), 139.3 (Ar C), 136.0 (Ar C), 130.5 (Ar C), 128.8 (Ar C), 128.8 (Ar C×2), 128.7 (Ar C×2), 128.1 (Ar C×2), 127.7 (Ar C×2), 60.9 (C2), 55.7 (C4), 14.2 (C1). **HRMS (ESI)** $C_{17}H_{17}NO_2Na$ *m/z*: $[M+Na]^+$ 290.1160 (*calc.* 290.1157). **m.p.** 51–52 °C.

The physical and spectroscopic data were found to be in agreement with Mukherjee *et al.*[227]

Ethyl 2-((diphenylmethylene)amino)hex-5-enoate, 141

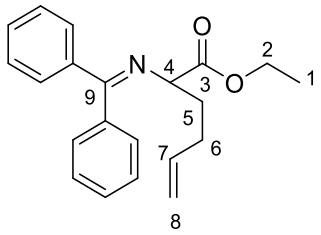

Potassium *tert*-butoxide (3.15 g, 28.06 mmol, 1.5 eq) was dissolved in THF (150 mL) under nitrogen at 0 °C. To the mixture was added **140** (5 g, 18.70 mmol, 1.0 eq) and this was stirred for 10 min. 4-bromo-1-butene (5.7mL, 56.11 mmol, 3.0 eq) was added to the reaction dropwise before it was warmed to RT and left to stir overnight. The excess solvent was removed *via* a rotary evaporator and the residue was diluted with ethyl acetate (50 mL). This was washed with sat. aq. $NaHCO_3$ (50 mL). The organic layer was extracted with ethyl acetate (3 × 20 mL) before the combined organics were washed with brine (50 mL). The organic layer was dried over anh. $MgSO_4$. This was filtered and concentrated *in vacuo* to yield the pure product as a yellow oil (5.7169 g, 17.8 mmol, 95%); **IR (thin film)** $\tilde{\nu}$/cm^{-1}: 2979 (C-H, w), 1735 (C=O, s), 1622 (C=C, m), 1238 (C-O, s). **^{1}H NMR (400 MHz, $CDCl_3$)** δ/ppm: 7.66–7.64 (m, 2H, Ar), 7.45–7.31 (m, 6H, Ar), 7.19–7.16 (m, 2H, Ar), 5.77–5.67 (m, 1H, H7), 4.98–4.88 (m, 2H, H8), 4.19–4.04 (m, 3H, H2&4), 2.10–1.96 (m, 4H, H5&6), 1.26 (t, J = 7.0 Hz, 3H, H1). **^{13}C NMR (101 MHz, $CDCl_3$)** δ/ppm: 172.3 (C9), 170.6 (C3), 139.6 (Ar), 137.8 (C7), 136.5 (Ar), 130.9 (Ar), 128.8 (Ar×2), 128.6 (Ar), 128.5 (Ar×2), 128.1 (Ar×2), 127.9 (Ar×2), 115.0 (C8), 64.9 (C4), 60.9 (C2), 33.0 (C5/6), 30.2 (C5/6), 14.2 (C1). **HRMS (ESI)** $C_{21}H_{23}NO_2Na$ *m/z*: $[M+Na]^+$ 344.1624 (*calc.* 344.1626).

The physical and spectroscopic data were found to be in agreement with Andrei *et al*.[228]

Ethyl 2-allyl-2-aminohex-5-enoate, 142

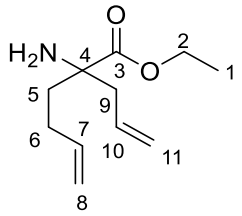

Potassium *tert*-butoxide (6.47 g, 57.76 mmol, 1.5 eq) was dissolved in THF (100 mL) under nitrogen at 0 °C. To the mixture was added **141** (12.36 g, 38.4 mmol, 1.0 eq) and was stirred for 10 min. Allyl bromide (10.0 mL, 115.32 mmol, 3.0 eq) was added dropwise before the reaction was warmed to RT and stirred overnight. This was quenched with 3M HCl (38.4 mL, 1 mL $mmol^{-1}$ of **141**) and stirred for 5 min. This mixture was diluted with dichloromethane (50 mL) and water (20 mL). This was extracted with dichloromethane (3 × 30 mL). The combined aqueous was basified was Na_2CO_3 and was extracted with ethyl acetate (3 × 30 mL). These organic extractions were dried over $MgSO_4$, filtered and concentrated *in vacuo* to yield the pure product as a yellow oil (6.5392 g, 33.15 mmol, 86%); **IR (thin film)** $\tilde{\nu}/cm^{-1}$: 3078 (C-H, w), 1727 (C=O, s), 1640 (C=C, m), 1199 (C-O, s). **^{1}H NMR (400 MHz, $CDCl_3$)** δ/ppm: 5.82–5.74 (m, 1H, H7), 5.73–5.64 (m, 1H, H10), 5.15–5.12 (m, 2H, H11), 5.04–4.93 (m, 2H, H8), 4.20–4.15 (m, 2H, H2), 2.58–2.54 (m, 1H, H9a), 2.28–2.23 (m, 1H, H9b), 2.17–2.09 (m, 1H, H6a), 1.99–1.91 (m, 1H, H6b), 1.88–1.82 (m, 1H, H5a), 1.67–1.61 (m, 3H, H5b&NH_2), 1.29–1.26 (m, 3H, H1). **^{13}C NMR (101 MHz, $CDCl_3$)** δ/ppm: 176.5 (C3), 137.9 (C7), 132.6 (C10), 119.5 (C11), 114.9 (C8), 61.0 (C2), 60.4 (C4), 44.3 (C9), 39.1 (C5), 28.4 (C6), 14.8 (C1). **HRMS (ESI)** $C_{11}H_{19}NO_2Na$ *m/z*: $[M+Na]^+$ 220.1313 (*calc.* 220.1313).

Ethyl 2-allyl-2-((tert-butoxycarbonyl)amino)hex-5-enoate, 143

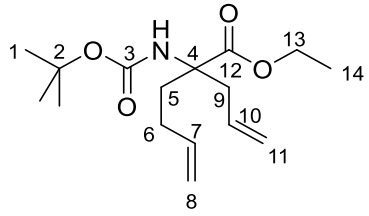

Compound **142** (4 g, 20.28 mmol, 1.0 eq) was dissolved in THF (100 mL). Boc_2O (7 mL, 30.41 mmol, 1.5 eq) was added dropwise and the reaction was refluxed at 70 °C for 3 hours. The excess solvent was removed *in vacuo* and the crude oil was purified *via* column

chromatography (100% dichloromethane) to yield the product as a colourless oil (5.1314 g, 17.25 mmol, 85%); **IR (thin film)** $\tilde{\nu}$/cm^{-1}: 3430 (N-H, w), 3076 (C-H, w), 1714 (C=O, s), 1642 (C=C, w). **^{1}H NMR (400 MHz, CDCl$_3$)** δ/ppm: 5.80–5.70 (m, 1H, H7), 5.67–5.56 (m, 1H, H10), 5.51 (br s, 1H, NH$_2$), 5.08–5.05 (m, 2H, H11), 5.01–4.91 (m, 2H, H8), 4.20 (q, *J* = 7.0 Hz, 2H, H13), 3.07 (m, 1H, H9a), 2.51–2.45 (m, 1H, H9b), 2.40 (m, 1H, H5a), 2.11–2.01 (m, 1H, H6a), 1.88–1.78 (m, 2H, H5b&6b), 1.43 (s, 9H, H1), 1.28 (t, *J* = 7.0 Hz, 3H, H14). **^{13}C NMR (101 MHz, CDCl$_3$)** δ/ppm: 173.3 (C12), 146.7 (C3), 137.6 (C7), 132.5 (C10), 118.8 (C11), 115.0 (C8), 85.2 (C2), 63.2 (C4), 61.7 (C13), 39.8 (C9), 34.4 (C5), 28.4 (C6), 27.4 (C1), 14.2 (C14). **HRMS (ESI)** $C_{16}H_{28}NO_4$ *m/z*: $[M+H]^+$ 298.2007 (*calc.* 298.2018).

Ethyl 1-((tert-butoxycarbonyl)amino)cyclohex-3-ene-1-carboxylate, 144

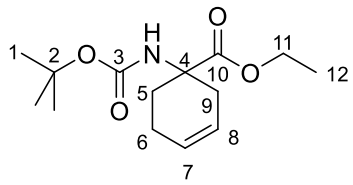

Compound **143** (1 g, 3.36 mmol, 1.0 eq) was dissolved in dichloromethane (170 mL) and Grubbs second generation catalyst (285 mg, 0.34 mmol, 10 mol%) was added. The reaction was refluxed at 50 °C for 1 hour under nitrogen. When the reaction had gone to completion the excess solvent was removed *in vacuo* to give the crude product. The was purified *via* column chromatography (50 % ethyl acetate in pet. ether) to yield the pure product as a brown oil (709.6 mg, 2.63 mmol, 78%); **IR (thin film)** $\tilde{\nu}$/cm^{-1}: 3379 (n-H, w), 2975 (C-H, w), 1708 (C=O, s), 1163 (C-O, s). **^{1}H NMR (400 MHz, CDCl$_3$)** δ/ppm: 5.74—5.71 (m, 1H, H7), 5.59—5.55 (m, 1H, H8), 4.78 (br s, 1H, NH), 4.22—4.12 (m, 2H, H11), 2.59—2.53 (m, 1H, H9a), 2.28—2.18 (m, 2H, H9b&5a), 2.13—2.04 (m, 2H, H6), 1.93—1.86 (m, 1H, H5b), 1.42 (s, 9H, H1), 1.25 (t, *J* = 2.0 Hz, 3H, H12). **^{13}C NMR (101 MHz, CDCl$_3$)** δ/ppm: 174.1 (C10), 154.9 (C3), 127.1 (C7), 122.5 (C8), 79.8 (C2), 61.1 (C11), 56.8 (C4), 34.1 (C9), 28.3 (C1), 27.5 (C5), 21.8 (C6), 14.2 (C12). **HRMS (ESI)** $C_{14}H_{23}NO_4Na$ *m/z*: $[M+Na]^+$ 292.1515 (*calc.* 292.1519).

The physical and spectroscopic data were found to be in agreement with Fariba *et al*.[229]

tert-Butyl (1-(hydroxymethyl)cyclohex-3-en-1-yl)carbamate, 145

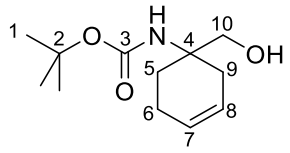

Compound **144** (660 mg, 2.45 mmol, 1.0 eq) was dissolved in THF (25 mL) and cooled to 0 °C before lithium borohydride (267 mg, 12.25 mmol, 5.0 eq) was added and the reaction was stirred overnight. This was quenched with sat. aq. NH_4Cl (25 mL) and stirred for 10 min. The layers were separated and the aqueous was extracted with ethyl acetate (3 × 20 mL). The combined organics were washed with sat. aq. $NaHCO_3$ (30 mL) and brine (30 mL) and dried over $MgSO_4$ before being filtered and concentrated *in vacuo* to give a crude oil. This was purified *via* column chromatography (20% ethyl acetate in pet. ether) to yield the product as white crystals (319.4 mg, 1.41 mmol, 57%); $\mathbf{R_f}$ 0.18 (20% ethyl acetate in pet. ether); **IR (thin film)** $\tilde{\nu}$/cm^{-1}: 3423 (O-H, m), 2889 (C-H, w), 1681 (C=O, s), 1528 (C=C, s). **^{1}H NMR (400 MHz, $CDCl_3$)** δ/ppm: 5.76–5.74 (m, 1H, H7), 5.59–5.56 (m, 1H, H8), 4.65 (br s, 1H, NH), 4.22 (br s, 1H, OH), 3.70 (d, J = 6.5 Hz, H10), 2.17–2.00 (m, 5H, H5a&6&9), 1.74–1.69 (m, 1H, H5b), 1.44 (s, 9H, H1). **^{13}C NMR (101 MHz, $CDCl_3$)** δ/ppm: 156.6 (C3), 127.4 (C7), 123.1 (C8), 80.0 (C2), 69.2 (C10), 55.0 (C4), 34.0 (C9), 28.3 (C1), 27.3 (C5), 22.1 (C6). **HRMS (ESI)** $C_{12}H_{21}NO_3Na$ *m/z*: $[M+Na]^+$ 250.1403 (*calc.* 250.1414). **m.p.** 77–78 °C.

1-(Hydroxymethyl)cyclohex-3-en-1-aminium chloride, 146

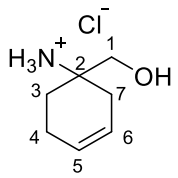

Compound **145** (151.6 mg, 0.67 mmol) was dissolved in hydrochloric acid (4M in dioxane, 10 mL) and was left for 1 h. The reaction was concentrated *in vacuo* to give off white crystals. These were washed with cold acetone to yield the pure product as white crystals (108.3 mg, 0.66 mmol, 99%); **IR (thin film)** $\tilde{\nu}$/cm^{-1}: 3217 (O-H, m), 2837 (C-H, s), 1628 (C=C, m), 1048 (C-O, s). **^{1}H NMR (400 MHz, $CDCl_3$)** δ/ppm: 7.95 (br s, 3H, NH_3^+), 5.69–5.66 (m, 1H, H6), 5.57–5.54 (m, 1H, H5), 5.47 (t, J = 5.0 Hz, 1H, OH), 3.42 (d, J = 5.0 Hz, 2H, H1), 2.14 (br s, 2H, H7), 2.08–2.06 (m, 2H, H4), 1.81–1.66 (m, 2H, H3). **^{13}C NMR (101 MHz, $CDCl_3$)** δ/ppm: 126.2 (C6),

122.9 (C5), 62.7 (C1), 55.1 (C2), 30.3 (C7), 26.5 (C3), 21.4 (C4). **HRMS (ESI)** $C_7H_{14}NO$ *m/z*: [M-Cl-]$^+$ 128.1071 (*calc.* 128.1070). **m.p.** 222–223 °C.

3-Oxa-1-azaspiro[4.5]dec-7-en-2-one, 148

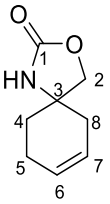

Compound **145** (200 mg, 0.88 mmol, 1.0 eq) was dissolved in THF (10 mL). The mixture was cooled to 0°C and potassium *tert*-butoxide (197 mg, 1.76 mmol, 2.0 eq) was added and the reaction was warmed to RT and stirred for 1 h. The reaction was then diluted with sat. aq. NH_4Cl (10 mL), extracted with dichloromethane (3 × 10 mL), dried over anh. $MgSO_4$, before the mixture was filtered and concentrated *in vacuo*. The crude was purified by column chromatography (40% ethyl acetate in pet. ether) to give the product as white crystals (108.0 mg, 0.71 mmol, 80%); $\mathbf{R_f}$ 0.11 (40% ethyl acetate in pet. ether); **IR (thin film)** $\tilde{\nu}$/cm^{-1}: 3240 (N-H, w), 2924 (C-H, w), 1730 (C=O, s). **^{1}H NMR (400 MHz, $CDCl_3$)** δ/ppm: 5.76–5.71 (m, 1H, H6), 5.65–5.61 (m, 1H, H7), 5.28 (br s, 1H, NH), 4.15 (d, *J* = 8.5 Hz, 1H, H2a), 4.12 (d, *J* = 8.5 Hz, 1H, H2b), 2.32–2.21 (m, 4H, H5&8), 1.89–1.84 (m, 1H, H4a), 1.74–1.72 (m, 1H, H4b). **^{13}C NMR (101 MHz, $CDCl_3$)** δ/ppm: 158.5 (C1), 127.0 (C6), 123.7 (C7), 75.5 (C2), 55.9 (C3), 36.8 (C5/8), 32.2 (C4), 22.5 (C5/8). **HRMS (ESI)** $C_8H_{11}NO_2Na$ *m/z*: [M+Na]$^+$ 176.0690 (*calc.* 176.0682). **m.p.** 107–108°C.

tert-Butyl (4-(hydroxymethyl)octa-1,7-dien-4-yl)carbamate, 147

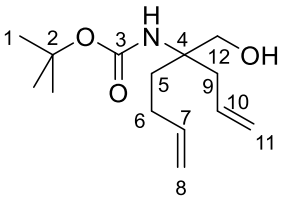

Compound **143** (2 g, 6.72 mmol, 1.0 eq) was dissolved in THF (50 mL) and cooled to 0 °C under nitrogen. Lithium borohydride (2M in THF, 10.1 mL, 20.17 mmol, 3eq) was added dropwise.

The reaction was warned to RT and stirred overnight. The reaction was quenched by slow addition of sat. aq. NH_4Cl. This was extracted with ethyl acetate (3 × 25 mL). The combined organics were dried over anh. Na_2SO_4, filtered and the excess solvent removed *in vacuo* to give the crude product. This was purified *via* column chromatography (25 % ethyl acetate in pet. ether) to yield the product as a colourless oil (463.2 mg, 1.81 mmol, 27%); $\mathbf{R_f}$ 0.24 (25% ethyl acetate in pet. ether); **IR (thin film)** $\tilde{\nu}$/cm^{-1}: 3404 (O-H, br w), 2978 (C-H, w), 1683 (C=O, s), 1640 (C=C, m), 1164 (C-O, s), 1053 (C-OH, s). **^{1}H NMR (400 MHz, $CDCl_3$)** δ/ppm: 5.83–5.72 (m, 2H, H7&10), 5.15–5.11 (m, 2H, H11), 5.04–4.93 (m, 2H, H8), 4.66 (br s, 1H, OH), 4.22 (br s, 1H, NH_2), 3.69–3.60 (m, 2H, H12), 2.38–2.27 (m, 2H, H9), 2.14–1.96 (m, 2H, H6), 1.74–1.59 (m, 2H, H5), 1.41 (s, 9H, H1). **^{13}C NMR (101 MHz, $CDCl_3$)** δ/ppm: 156.2 (C3), 138.1 (C7), 132.8 (C10), 119.4 (C11), 11408 (C8), 79.9 (C2), 67.8 (C12), 58.7 (C4), 39.0 (C9), 33.6 (C5), 28.3 (C1), 27.7 (C6). **HRMS (ESI)** $C_{14}H_{26}NO_3$ *m/z*: $[M+H]^+$ 256.1908 (*calc.* 256.1913).

Ethyl benzimidate hydrochloride, 150

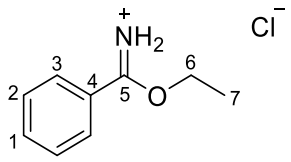

To a solution on benzonitrile (5.00 g, 48.49 mmol, 1.0 eq) in ethanol (34 mL, 581.85 mmol, 12.0 eq), acetyl chloride (27.68 mL, 387.90 mmol, 8.0 eq) was added dropwise. The reaction was stirred overnight then concentrated *in vacuo* to yield the product as white crystals (8.0401 g, 43.31 mmol, 89%); **IR (thin film)** $\tilde{\nu}$/cm^{-1}: 2828 (C-H, br s), 1626 (C=N, s), 1451 (C=C, s), 1059 (C-O, s). **^{1}H NMR (400 MHz, $CDCl_3$)** δ/ppm: 12.60 (br s, 1H, NH), 11.91 (br s, 1H, NH), 8.40–8.38 (m, 2H, H3), 7.76–7.67 (m, 1H, H1), 7.58–7.54 (m, 2H, H2), 4.93 (q, J = 7.0 Hz, 2H, H6), 1.61 (t, J = 7.0 Hz, 3H, H7). **^{13}C NMR (101 MHz, $CDCl_3$)** δ/ppm: 170.9 (C5), 135.6 (C1), 129.7 (C3), 129.3 (C2), 125.3 (C4), 71.3 (C6), 13.9 (C7). **HRMS (ESI)** $C_9H_{12}NO$ *m/z*: $[M\text{-}Cl^-]^+$ 150.0913 (*calc.* 150.0913). **m.p.** 120–121 °C.

The physical and spectroscopic data were found to be in agreement with Berger *et al.*[230]

2-Phenyl-3-oxa-1-azaspiro[4.5]deca-1,7-diene, 151

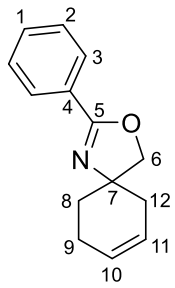

Compound **146** (50 mg, 0.31 mmol, 1.1 eq) and **150** (41.4 mg, 0.28 mmol, 1.0 eq) were dissolved in 1,2-dichloroethane (1 mL) and refluxed overnight. The reaction was cooled to RT and filtered. The filtrate was concentrated *in vacuo* and the crude was purified by column chromatography (30% ethyl acetate in hexane) to yield the product was white crystals (34.0 mg, 0.16 mmol, 57%); $\mathbf{R_f}$ 0.44 (30% ethyl acetate in hexane); **IR (thin film)** $\tilde{\nu}$/cm^{-1}: 2905 (C-H, w), 1648 (C=N, s), 1581 (C=C, m), 1059 (C-O, m). **^{1}H NMR (400 MHz, $CDCl_3$)** δ/ppm: 7.96–7.92 (m, 2H, H3), 7.48–7.44 (m, 1H, H1), 7.41–7.37 (m, 2H, H2), 5.77–5.73 (m, 1H, H10), 5.69–5.63 (m, 1H, H11), 4.16 (d, *J* = 8.5 Hz, 1H, H6a), 4.11 (d, *J* = 8.5 Hz, 1H, H6b), 2.48–2.43 (m, 1H, H12a), 2.36–2.29 (m, 1H, H9a), 2.17–2.08 (m, 2H, H9b&12b), 2.05–1.98 (m, 1H, H8a), 1.75–1.69 (m, 1H, H8b). **^{13}C NMR (101 MHz, $CDCl_3$)** δ/ppm: 162.5 (C5), 131.2 (C1), 128.28 (C3), 128.26 (C2), 128.1 (C4), 127.2 (C10), 124.4 (C11), 77.6(C6), 69.4 (C7), 37.3 (C12), 33.0 (C8), 22.8 (C9). **HRMS (ESI)** $C_{14}H_{16}NO$ *m/z*: $[M+H]^+$ 214.1222 (*calc.* 214.1226).

3-Oxa-1-azaspiro[4.5]deca-1,7-dien-2-amine, 152

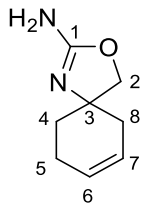

Cyanobromide (175 mg, 1.65 mmol, 1.2 eq) was added to a solution of **146** (175 mg, 1.38 mmol, 1.0 eq) as a free base in ethanol (5 mL) and refluxed overnight. This was concentrated *in vacuo* and dissolved in dichloromethane (10 mL). This was washed with 1M NaOH (10 mL) and the aqueous was extracted with dichloromethane (10 mL). The combined organics were concentrated *in vacuo* to yield the product as off-white crystals (122.2 mg, 0.80 mmol, 58%); **IR (thin film)** $\tilde{\nu}$/cm^{-1}: 3437 (N-H, m), 2903 (C-H, m), 1666 (C=N, s), 1650 (C=C, m), 1010 (C-O, s).

^{1}H NMR (400 MHz, $CDCl_3$) δ/ppm: 5.72–5.68 (m, 1H, H6), 5.64–5.60 (m, 1H, H7), 4.01 (d, *J* = 8.0 Hz, 1H, H2a), 3.97 (d, *J* = 8.0 Hz, 1H H2b), 2.31–2.21 (m, 2H, H5a&8a), 2.12–2.02 (m, 2H, H5b&8b), 1.83–1.78 (m, 1H, H4a), 1.67–1.62 (m, 1H, H4b). **^{13}C NMR (101 MHz, $CDCl_3$)** δ/ppm: 159.2 (C1), 127.0 (C6), 124.6 (C7), 78.6 (C2), 66.6 (C3), 37.9 (C5/8), 33.4 (C4), 23.1 (C5//8). **HRMS (ESI)** $C_8H_{13}N_2O$ *m/z*: $[M+H]^+$ 153.1025 (*calc.* 153.1028). **m.p.** 198–199 °C

Crystallographic data for this compound is in Appendix B.

4-Oxa-1-azaspiro[5.5]undec-8-en-3-one, 158

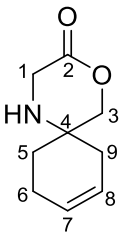

Compound **146** as a free base (150 mg, 0.92 mmol, 1.0 eq) was dissolved in acetonitrile before phenyl bromoacetate (216.5 mg, 1.00 mmol, 1.1 eq) and diisopropylethylamine (0.4 mL, 2.29 mmol, 2.5 eq) were added. The reaction was stirred at RT for 4 h before being concentrated *in vacuo* to give the crude product. This was purified by column chromatography (100% ethyl acetate) to yield the pure product as white crystals (20 mg, 0.12 mmol, 13%); **IR (thin film)** $\tilde{\nu}$/cm^{-1}: 3317 (N-H, w), 2921 (C-H, w), 1730 (C=O, s), 1215 (C-N, s), 1040 (C-O, s). **^{1}H NMR (400 MHz, $CDCl_3$)** δ/ppm: 5.74–5.70 (m, 1H, H7), 5.62–5.57 (m, 1H, H8), 4.20 (d, *J* = 11.0 Hz, 1H, H3a), 4.13 (d, *J* = 11.0 Hz, 1H, H3b), 3.68 (s, 2H, H1), 2.17–1.97 (m, 5H, H6&9&NH), 1.80–1.74 (m, 1H, H5a), 1.67–1.61 (m, 1H, H5b). **^{13}C NMR (101 MHz, $CDCl_3$)** δ/ppm: 169.1 (C2), 126.7 (C7), 123.3 (C8), 76.2 (C3), 48.2 (C4), 44.0 (C1), 33.2 (C6/9), 28.6 (C5), 22.0 (C6/9). **HRMS (ESI)** $C_9H_{14}NO_2$ *m/z*: $[M+H]^+$ 168.1017 (*calc.* 168.1019).

4-Oxa-1-azaspiro[5.5]undeca-1,8-dien-3-one, 159

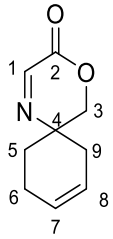

Compound **158** (100 mg, 0.60 mmol, 1.0 eq), was dissolved in acetonitrile (6 mL) and lead (IV) acetate (345 mg, 0.78 mmol, 1.3 eq) was added before the reaction was allowed to stir for 30 min at RT. This was then diluted with ethyl acetate (10 mL) and filtered through Celite. The filtrate was washed with sat. aq. $NaHCO_3$ solution (20 mL) and brine (20 mL) before being dried over anh. $MgSO_4$, filtered and concentrated *in vacuo*. The crude oil was purified by column chromatography (20% ethyl acetate in hexane) to give the pure product as a yellow oil (91.1 mg, 0.55 mmol, 92%); $\mathbf{R_f}$ 0.25 (20% ethyl acetate in hexane); **IR (thin film)** $\tilde{\nu}$/cm^{-1}: 2923 (C-H, w), 1737 (C=O, s), 1622 (C=N, m), 1038 (C-O, s). **^{1}H NMR (400 MHz, $CDCl_3$)** δ/ppm: 7.82 (s, 1H, H1), 5.83–5.77 (m, 1H, H7), 5.71–5.65 (m, 1H, H8), 4.29 (d, J = 11.5 Hz, 1H, H3a), 4.25 (d, J = 11.5 Hz, 1H, H3b), 2.31–2.21 (m, 2H, H6a&9a), 2.15–2.03 (m, 2H, H6b&9b), 2.02–1.95 (m, 1H, H5a), 1.70–1.64 (m, 1H, H5b). **^{13}C NMR (101 MHz, $CDCl_3$)** δ/ppm: 154.6 (C2), 151.0 (C1), 127.0 (C7), 122.9 (C8), 72.0 (C3), 55.8 (C4), 32.6 (C6/9), 30.1 (C5), 22.0 (C6/9). **HRMS (ESI)** $C_9H_{11}NO_2Na$ *m/z*: $[M+H]^+$ 188.0681 (*calc* 188.0682).

2-Chloro-*N*-(1-(hydroxymethyl)cyclohex-3-en-1-yl)acetamide, 160

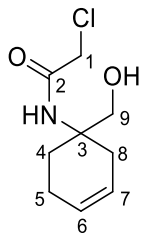

Compound **145** (1.19 g, 5.24 mmol, 1.0 eq) was dissolved in THF (50 mL). 3M HCl (17.5 mL, 0.3M) was added and the mixture was refluxed for 3 h. This was concentrated *in vauco* and the residue was dissolved in dichloromethane (50 mL) before triethylamine (2.2 mL, 15.7 mmol, 3.0 eq), and chloroacetyl chloride (0.42 mL, 5.24 mmol, 1.0 eq) were added dropwise at 0 °C. This was stirred for 90 min. The reaction was then diluted with sat. aq. NH_4Cl

(25 mL) and stirred for 10 min. This was extracted with dichloromethane (3 × 20 mL) and the organics were dried over anh. $MgSO_4$ before being filtered and concentrated *in vacuo*. This crude was purified *via* column chromatography (dichloromethane to 10% diethyl ether in dichloromethane) to give the pure product as white crystals (261.2 mg, 1.28 mmol, 24%); **R_f** 0.14 (10% diethyl ether in dichloromethane); **IR (thin film)** $\tilde{\nu}$/cm^{-1}: 3352 (O-H, br m), 3271 (N-H, m), 3070 (C-H alkene, w), 2938 (C-H, w), 1654 (C=O, s), 1549 (C=C, s), 656 (C-Cl, s). **^{1}H NMR (400 MHz, $CDCl_3$)** δ/ppm: 6.67 (br s, 1H, N-H), 5.81–5.77 (m, 1H, H6), 5.64–5.60 (m, 1H, H7), 4.30 (t, *J* = 6.5 Hz, 1H, OH), 4.04 (s, 2H, H1), 3.75 (d, *J* = 6.5 Hz, 2H, H9), 2.27–2.18 (m, 3H, H8&5a), 2.11–2.03 (m, 2H, H5b&4a), 1.79–1.73 (m, 1H, H4b). **^{13}C NMR (101 MHz, $CDCl_3$)** δ/ppm: 166.9 (C2), 127.4 (C6), 122.8 (C7), 68.3 (C9), 57.4 (C3), 42.9 (C1), 33.4 (C8), 27.2 (C4), 21.8 (C5). **HRMS (ESI)** $C_9H_{15}ClNO_2$ *m/z*: $[M+H]^+$ 204.0776 (*calc.* 204.0786). **m.p.** 86–87 °C.

4-Oxa-1-azaspiro[5.5]undec-8-en-2-one, 161

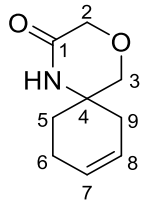

Compound **145** (260 mg, 1.28 mmol, 1.0 eq) was dissolved in *tert*-butanol (25 mL) and heated to 30 °C before potassium *tert*-butoxide (158 mg, 1.40 mmol, 1.1 eq) was added and the reaction was left to stir for 5 h. It was then diluted with sat. aq. NH_4Cl (20 mL) and stirred for 10 min. This was extracted with dichloromethane (3 × 20 mL). The organics were dried over anh. $MgSO_4$. This was filtered and concentrated *in vacuo* to yield the pure product as off-white crystals (211.9 mg, 1.27 mmol, 99%); **R_f** 0.28 (10% diethyl ether in dichloromethane); **IR (thin film)** $\tilde{\nu}$/cm^{-1}: 3169 (N-H, m), 3070 (C-H alkene, w), 2924 (C-H alkane, w), 1661 (C=O, s), 1098 (C-O, s). **^{1}H NMR (400 MHz, $CDCl_3$)** δ/ppm: 6.13 (br s, 1H, NH), 5.76–5.73 (m, 1H, H7), 5.62–5.58 (m, 1H, H8), 4.16 (d, *J* = 4.5 Hz, 2H, H2), 3.60 (s, 2H, H3), 2.27–2.21 (m, 1H, H9a), 2.18–2.16 (m, 2H, H6), 2.05–1.99 (m, 1H, H9b), 1.93–1.86 (m, 1H, H5a), 1.70–1.63 (m, 1H, H5b). **^{13}C NMR (101 MHz, $CDCl_3$)** δ/ppm: 168.7 (C1), 126.9 (C7), 123.0 (C8), 71.8 (C3), 67.2 (C2), 52.4 (C4), 34.7 (C9), 31.0 (C5), 21.9 (C6). **HRMS (ESI)** $C_9H_{13}NO_2Na$ *m/z*: $[M+Na]^+$ 190.0831 (*calc.* 190.0839). **m.p.** 128–129 °C.

Ethyl 2-allyl-2-(3-ethoxy-3-oxopropanamido)hex-5-enoate, 165

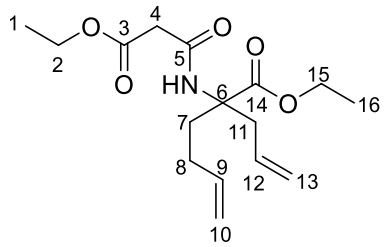

Compound **142** (1.0 g, 5.07 mmol, 1.0 eq) was dissolved in dichloromethane (50 mL) at 0 °C under nitrogen. Triethylamine (1.52 mL, 10.90 mmol, 2.15 eq) and ethyl malonyl chloride (1.04 mL, 8.11 mmol, 1.6 eq) were added dropwise. The reaction was warmed to RT and stirred for 30 min. This was quench with sat. aq. NH_4Cl (25 mL) and stirred for a further 10 min. The layers were separated and the aqueous was extracted with dichloromethane (2 × 20 mL). The combined organics were dried over anh. $MgSO_4$, filtered and concentrated *in vacuo* to give the crude product. This was purified by column chromatography (20% ethyl acetate in pet. ether) to yield the pure product as a yellow oil (1.2711 g, 4.08 mmol, 81%); $\mathbf{R_f}$ 0.23 (20% ethyl acetate in pet. ether); **IR (thin film)** $\tilde{\nu}$/cm^{-1}: 3337 (N-H, w), 2980 (C-H, w), 1732 (C=O ester, s), 1681 (C=O amide, m), 1650 (C=C, m), 1221 (C-O, s). **^{1}H NMR (400 MHz, $CDCl_3$)** δ/ppm: 7.66 (br s, 1H, NH), 5.77–5.67 (m, 1H, H9), 5.63–5.52 (m, 1H, H12), 5.10–4.90 (m, 4H, H10&13), 4.25–4.18 (m, 4H, H2&15), 3.28 (s, 2H, H4), 3.24–3.18 (m, 1H, H11a), 2.59–2.47 (m, 2H, H8a&11b), 2.07–1.99 (m, 1H, H7a), 1.90–1.74 (m, 2H, H8b&7b), 1.30–1.26 (m, 6H, H1&16). **^{13}C NMR (101 MHz, $CDCl_3$)** δ/ppm: 173.1 (C14), 168.8 (C3), 163.8 (C5), 137.3 (C9), 132.2 (C12), 118.9 (C13), 115.1 (C10), 64.5 (C6), 61.9 (C2/5), 61.6 (C2/5), 42.6 (C4), 39.4 (C11), 34.0 (C7), 28.5 (C8), 14.2 (C1/16), 14.1 (C1/16). **HRMS (ESI)** $C_{16}H_{26}NO_5$ *m/z*: $[M+H]^+$ 312.1820 (*calc.* 312.1811).

5-Allyl-5-(but-3-en-1-yl)pyrrolidine-2,4-dione, 167

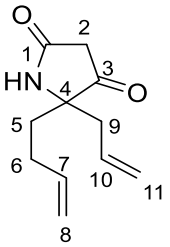

Potassium *tert*-butoxide (691.9 mg, 6.17 mmol, 1.6 eq) was dissolved in THF (35 mL) and **165** (1.2 g, 3.85, 1.0 eq) was added dropwise. The reaction was refluxed for 2 hours. It was then cooled to RT and diluted with ethyl acetate (20 mL) and 1M HCl (20 mL) before stirred for 5 min. The layers were separated and the aqueous was washed with ethyl acetate (10 mL). The combined organics were dried over $MgSO_4$, filtered, and concentrated *in vacuo*. This crude yellow oil was dissolved in acetonitrile-water mixture (10:1, total volume 35 mL). This was refluxed at 100 °C for 1 hour. The reaction was cooled to RT, dried over $MgSO_4$, filtered, and concentrated *in vacuo*. The crude oil was purified *via* column chromatography (50% ethyl acetate in pet. ether) to yield the product as white crystals (147.0 mg, 0.76 mmol, 20%); $\mathbf{R_f}$ 0.28 (50% ethyl acetate in pet. ether); **IR (thin film)** $\tilde{\nu}/\mathrm{cm^{-1}}$: 3197 (N-H, m), 2980 (C-H, w), 1642 (C=O, s), 1574 (C=C, s). **^{1}H NMR (400 MHz, $CDCl_3$)** δ/ppm: 6.34 (br s, 1H, NH), 5.74–5.66 (m, 2H, H7&10), 5.22–5.14 (m, 2H, H11), 5.06–4.98 (m, 2H, H8), 2.87 (d, J = 3.5 Hz, 2H, H2), 2.45–2.34 (m, 2H, H9), 2.22–2.14 (m, 1H, H6a), 2.02–1.92 (m, 2H, H6b&5a), 1.75–1.66 (m, 1H, H5b). **^{13}C NMR (101 MHz, $CDCl_3$)** δ/ppm: 209.5 (C3), 170.3 (C1), 136.8 (C7), 130.2 (C10), 121.5 (C11), 116.1 (C8), 71.2 (C4), 42.1 (C9), 41.5 (C2), 35.6 (C5), 28.3 (C6). **HRMS (ESI)** $C_{11}H_{15}NO_2$ *m/z*: $[M]^+$ 193.1099 (*calc.* 193.1103). **m.p.** 99–100 °C.

1-Azaspiro[4.5]dec-7-ene-2,4-dione, 168

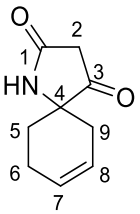

Compound **167** (119 mg, 0.62 mmol, 1.0 eq) was dissolved in dichloromethane (31 mL) and degassed with nitrogen for 5 min. Grubbs second generation catalyst (52.3 mg, 0.06 mmol, 10

mol%) was added and the reaction was refluxed for 1 hour. The reaction was cooled to RT and concentrated *in vacuo*. This was purified *via* column chromatography (dichloromethane then ethyl acetate) to yield the pure product as white crystals (60 mg, 0.36 mmol, 59%); $\mathbf{R_f}$ 0.14 (100% diethyl ether); **IR (thin film)** $\tilde{\nu}$/cm^{-1}: 3185 (N-H, w), 3035 (C-H, w), 1651 (C=C, s), 1588 (N-H, s). **^{1}H NMR (400 MHz, $CDCl_3$)** δ/ppm: 6.27 (br s, 1H, NH), 5.81–5.78 (m, 1H, H7), 5.72–5.68 (m, 1H, H8), 3.16 (d, *J* = 22.0 Hz, 1H, H2a), 3.07 (d, *J* = 22.0 Hz, 1H, H2b), 2.62–2.54 (m, 1H, H9a), 2.34–2.29 (m, 1H, H6a), 2.21–2.09 (m, 1H, H6b), 2.06–2.00 (m, 1H, H9b), 1.93–1.85 (m, 1H, H5a), 1.74–1.68 (m, 1H, H5b) . **^{13}C NMR (101 MHz, $CDCl_3$)** δ/ppm: 209.0 (C3), 169.6 (C1), 126.5 (C7), 123.2 (C8), 66.0 (C4), 40.1 (C2), 33.3 (C9), 29.3 (C5), 21.3 (C6). **HRMS (ESI)** $C_9H_{12}NO_2$ *m/z*: $[M+H]^+$ 166.0866 (*calc.* 166.0863). **m.p.** 187–188°C.

4-Ethoxy-1-azaspiro[4.5]deca-3,7-dien-2-one, 174

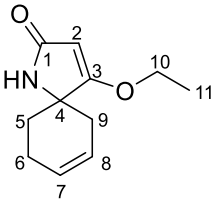

Compound **168** (100 mg, 0.61 mmol, 1.0 eq) was dissolved in THF (10 mL) at 0 °C. To this was added Potassium bis(trimethylsilyl)amide (0.5 M in toluene, 1.22 mL, 0.61 mmol, 1.0 eq) and the reaction was left to stir for 10 min before ethyl bromide (0.09 mL, 0.73 mmol, 1.2 eq) and 18-crown-6 (176 mg, 0.66 mmol, 1.1 eq) was added. The reaction was warmed to RT and left to stir overnight. The reaction was concentrated *in vacuo* and purified *via* column chromatography (ethyl acetate) to give the product as yellow-white crystals (64.1 mg, 0.33 mmol, 54%); $\mathbf{R_f}$ 0.24 (ethyl acetate); **IR (thin film)** $\tilde{\nu}$/cm^{-1}: 3188 (N-H, w), 3060 (C-H alkene, w), 2933 (C-H alkane, w), 1672 (C=O, s), 1026 (C-O, s). **^{1}H NMR (400 MHz, $CDCl_3$)** δ/ppm: 5.82–5.80 (m, 1H, H7), 5.72–5.68 (m, 1H, H8), 4.91 (d, *J* = 1.5 Hz, 1H, H2), 4.01 (q, *J* = 7.0 Hz, 2H, H10), 2.64 (m, 1H, H9a), 2.32–2.12 (m, 2H, H6), 1.97–1.85 (m, 2H, H9b&5a), 1.60–1.55 (m, 1H, H5b), 1.39 (t, *J* = 7.0 Hz, 3H, H11). **^{13}C NMR (101 MHz, $CDCl_3$)** δ/ppm: 180.4 (C1), 173.2 (C3), 126.5 (C7), 124.1 (C8), 92.1 (C2), 67.1 (C10), 59.9 (C4), 33.6 (C9), 29.2 (C5), 22.5 (C6), 14.1 (C11). **HRMS (ESI)** $C_{11}H_{16}NO_2$ *m/z*: $[M+H]^+$ 194.1181 (*calc.* 194.1176). **m.p.** 145–146 °C.

2-Oxo-1-azaspiro[4.5]deca-3,7-dien-4-yl trifluoromethanesulfonate, 175

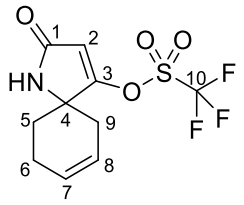

Compound **168** (100mg, 0.61 mmol, 1.0 eq) was dissolved in dichloromethane (5 mL), triethylamine (0.25 mL, 1.82 mmol, 3.0 eq) and triflic anhydride (0.3 mL, 1.82 mmol, 3.0 eq) were added dropwise at 0 °C, and the reaction was stirred for 1 h. The reaction was concentrated *in vacuo*. This was purified by column chromatography (70% to 90% diethyl ether in pet. ether) to give the pure product as white crystals (107.0 mg, 0.36 mmol, 59%); $\mathbf{R_f}$ 0.18 (70% diethyl ether in pet. ether); **IR (thin film)** $\tilde{\nu}$/cm^{-1}: 3164 (N-H, w), 2926 (C-H, w), 1698 (C=O, s), 1634 (C=C, s), 1332 (S=O, m), 1131 (C-F, s). **^{1}H NMR (400 MHz, $CDCl_3$)** δ/ppm: 6.44 (br s, 1H, NH), 5.93 (d, *J* = 2.0 Hz, 1H, H2), 5.86–5.83 (m, 1H, H7), 5.77–5.73 (m, 1H, H8), 2.67–2.60 (m, 1H, H9a), 2.41–2.33 (m, 1H, H6a), 2.28–2.17 (m, 1H, H6b), 2.02–1.94 (m, 2H, H9a&5a), 1.71–1.67 (m, 1H, H5b). **^{13}C NMR (101 MHz, $CDCl_3$)** δ/ppm: 168.5 (C1/3), 167.9 (C1/3), 126.7 (C7), 123.1 (C8), 120.0 (C10), 107.3 (C2), 60.8 (C4), 32.6 (C9), 28.6 (C5), 22.4 (C6). **^{19}F NMR (376 MHz, $CDCl_3$)** δ/ppm: -72.5. **HRMS (ESI)** $C_{10}H_{11}F_3NO_4S$ *m/z*: $[M+H]^+$ 298.0361 (*calc.* 298.0355). **m.p.** 119–120 °C.

4-(4-Methoxyphenyl)-1-azaspiro[4.5]deca-3,7-dien-2-one, 176

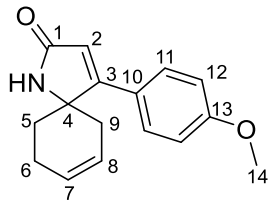

Compound **175** (50 mg, 0.17 mmol, 1.0 eq) was dissolved in THF (1.7 mL). (4-methoxyphenyl)boronic acid (38.3 mg, 0.25 mmol, 1.5 eq) was added and stirred until it was dissolved. Tetrakis(triphenylphosphine)palladium(0) (9.7 mg, 0.008 mmol, 5 mol%) was added as well as sodium carbonate (39.2 mg, 0.37 mmol, 2.2 eq) dissolved in water (0.2 mL). The reaction was stirred for 40 min before being refluxed for 3 h. It was then called to RT, filtered through Celite, washed with ethyl acetate, and concentrated *in vacuo*. The crude was

purified *via* column chromatography (diethyl ether to 50% diethyl ether in ethyl acetate to ethyl acetate) to give the pure product as yellow-white crystals (31.5 mg, 0.12 mmol, 73%); $\mathbf{R_f}$ 0.11 (diethyl ether); **IR (thin film)** $\tilde{\nu}$/cm^{-1}: 3160 (N-H, w), 3035 (alkene C-H, w), 2924 (C-H, w), 1680 (C=O, s), 1607 (C=C, m), 1511 (C=C aromatic, m), 1181 (C-O, s). **^{1}H NMR (400 MHz, $CDCl_3$)** δ/ppm: 7.43 (d, *J* = 9.0 Hz, 2H, H11), 6.93 (d, *J* = 9.0 Hz, 2H, H12), 6.35 (br s, 1H, NH), 6.17 (d, *J* = 2.0 Hz, 1H, H2), 5.89–5.84 (m, 1H, H7), 5.80–5.75 (m, 1H, H8), 3.84 (s, 3H, H14), 2.82–2.77 (m, 1H, H9a), 2.35–2.18 (m, 3H, H6&5a), 1.98–1.94 (m, 1H, H9b), 1.73–1.71 (m, 1H, H5b). **^{13}C NMR (101 MHz, $CDCl_3$)** δ/ppm: 171.9 (C1), 165.4 (C3), 160.6 (C13), 132.1 (C10), 129.0 (C11), 126.7 (C7), 124.7 (C8), 120.4 (C2), 114.2 (C12), 63.5 (C4), 55.4 (C14), 34.8 (C9), 30.4 (C5), 23.1 (C6). **HRMS (ESI)** $C_{16}H_{18}NO_2$ *m/z*: $[M+H]^+$ 256.1331 (*calc.* 256.1338). **m.p.** 196–197 °C.

4-Hydroxy-1-azaspiro[4.5]dec-7-en-2-one, 177

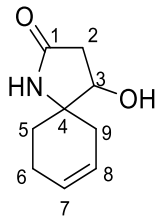

Compound **168** (200 mg, 1.21 mmol, 1.0 eq) was added to a suspension of sodium borohydride (77.9 mg, 2.06 mmol, 1.7 eq) in methanol (5 mL) at 0 °C. The reaction was warmed to RT and stirred for 1 h. Water (5 mL) was added dropwise and the mixture was extracted with dichloromethane (3 × 10 mL). the combined organic layers were dried over anh. $MgSO_4$, filtered, and concentrated *in vacuo*. The product was purified by column chromatography (ethyl acetate) to yield the pure product as white crystals (32 mg, 0.19 mmol, 16%); $\mathbf{R_f}$ 0.06 (ethyl acetate); **IR (thin film)** $\tilde{\nu}$/cm^{-1}: 3368 (N-H, m), 3194 (O-H, br m), 2950 (C-H, w), 1698 (C=O, s), 1662 (C=C, s), 1058 (C-O, s). **^{1}H NMR (400 MHz, $CDCl_3$)** δ/ppm: 5.87–5.73 (m, 3H, NH, OH, H7), 5.64–5.60 (m, 1H, H8), 4.19 (q, *J* = 5.55 Hz, 1H, H3), 2.75 (dd, *J* = 17.0, 7.0 Hz, 1H, H2a), 2.39 (dd, 1H, *J* = 17.0, 5.0 Hz, 1H, H2b), 2.31–2.28 (m, 1H, H6a), 2.23–2.09 (m, 2H, H6b&9a), 2.03–1.97 (m, 1H, H9b), 1.88–1.82 (m, 1H, H5a), 1.78–1.73 (m, 1H, H5b). **^{13}C NMR (101 MHz, $CDCl_3$)** δ/ppm: 173.9 (C1), 127.5 (C7), 123.9 (C8), 73.6 (C3), 61.0 (C4), 39.2 (C2), 36.3 (C9), 26.4 (C5), 22.5 (C6). **HRMS (ESI)** $C_9H_{13}NO_2Na$ *m/z*: $[M+Na]^+$ 190.0841 (*calc.* 190.0844). **m.p.** 130–131 °C.

2-Oxo-1-azaspiro[4.5]dec-7-en-4-yl methanesulfonate, 178

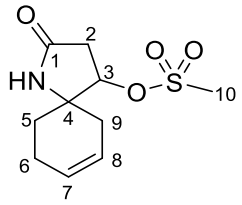

Compound **177** (30 mg, 0.18 mmol, 1.0 eq) was dissolved in dichloromethane (1 mL) before mesyl chloride (16 µL, 0.22 mmol, 1.2 eq) and triethylamine (35 µL, 0.25 mmol, 1.4 eq) were added dropwise at 0 °C. The reaction was stirred at this temperature for 1 h, before being quenched with sat. aq. $NaHCO_3$ (5 mL) and extracted with dicholormethane (3 × 5 mL). The combined organics were concentrated *in vacuo* and the crude was purified by column chromatography (ethyl acetate) to give the pure product as a white amorphous solid (54.0 mg, 0.17 mmol, 94%); $\mathbf{R_f}$ 0.24 (ethyl acetate); **IR (thin film)** $\tilde{\nu}$/cm^{-1}: 3352 (N-H, w), , 2929 (C-H, w), 1692 (C=O, s), 1643 (C=C, s), 1302 (S=O, m). **^{1}H NMR (400 MHz, $CDCl_3$)** δ/ppm: 5.97 (br s, 1H, Nh), 5.80–5.77 (m, 1H, H7), 5.64–5.61 (m, 1H, H8), 5.02 (dd, J = 7.0, 5.0 Hz, 1H, H3), 3.08 (s, 3H, H10), 2.92–2.83 (m, 1H, H2a), 2.72–2.60 (m, 1H, H2b), 2.47–2.30 (m, 2H, H6a&9a), 2.20–2.04 (m, 2H, H6b&9b), 1.90–1.76 (m, 2H, H5). **^{13}C NMR (101 MHz, $CDCl_3$)** δ/ppm: 171.9 (C1), 127.5 (C7), 123.1 (C8), 79.8 (C3), 60.2 (C4), 38.7 (C2), 37.0 (C10), 36.1 (C9), 26.9 (C5), 22.1 (C6). **HRMS (ESI)** $C_{10}H_{16}NO_4S$ *m/z*: $[M+H]^+$ 245.0732 (*calc.* 245.0722).

1-Azaspiro[4.5]deca-3,7-dien-2-one, 179

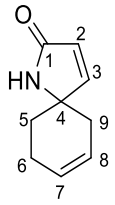

Compound **177** (23 mg, 0.14 mmol, 1.0 eq) was dissolved in trifluoroacetic anhydride (67 µL, 0.48 mmol, 3.5 eq) and refluxed for 12 h. Excess solvent was removed *in vacuo* and the residue was dissolved in dichloromethane (0.25 mL). Triethylamine (24 µL, 0.17 mmol, 1.26 eq) was added and the reaction was stirred for a further 12 h. Potassium hydrogen carbonate (36 mg, 0.36 mmol, 2.63 eq) in methanol (0.25 mL) was added to the reaction and it was allowed to stir for a further 2 h. Chloroform (5 mL) was added and the mixture was washed with 1M HCl (5

mL), water (5 mL), and brine (5 mL). The organic layer was then dried over anh. $MgSO_4$. The mixture was filtered and the filtrated was concentrated *in vacuo* to give a crude product. This was then purified by column chromatography (ethyl acetate) to give the pure product as off-white crystals (6.3 mg, 0.04 mmol, 30%); $\mathbf{R_f}$ 0.18 (ethyl acetate); **IR (thin film)** $\tilde{\nu}$/cm^{-1}: 3170 (N-H, m), 3030 (C-H alkene, w), 2926 (C-H alkane, w), 1682 (C=O, s), 1655 (C=C, s). **^{1}H NMR (400 MHz, $CDCl_3$)** δ/ppm: 7.08 (d, *J* = 5.0 Hz, 1H, H3), 6.15 (br s, 1H, NH), 6.03 (d, *J* = 5.0 Hz, 1H, H2), 5.84–5.79 (m, 1H, H7), 5.76–5.71 (m, 1H, H8), 2.38–2.32 (m, 1H, H9a), 2.27–2.21 (m, 2H, H6), 2.10–2.04 (m, 1H, H9b), 1.84–1.77 (m, 1H, H5a), 1.73–1.67 (m, 1H, H5b). **^{13}C NMR (101 MHz, $CDCl_3$)** δ/ppm: 154.6 (C3), 129.1 (C2), 126.7 (C7), 124.2 (C8), 62.2 (C4), 34.3 (C9), 30.9 (C5), 23.6 (C6). **HRMS (ESI)** $C_9H_{12}NO$ *m/z*: $[M+H]^+$ 150.0918 (*calc.* 150.0919). **m.p.** 75–76 °C.

2-Allyl-2-((tert-butoxycarbonyl)amino)hex-5-enoic acid, 184

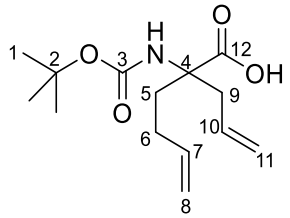

Compound **143** (1g, 3.36 mmol, 1.0 eq) was dissolved in methanol (67.25 mL) and 1M NaOH (67.25 mL, 67.25 mmol, 20.0 eq) was added dropwise. The reaction was refluxed at 75 °C for 24 hours. The solvent was removed *in vacuo* and the residue was diluted with water (20 mL). Ice and 0.5 M HCl (135 mL) was added. The precipitate was filtered and washed with cold water to yield the product as a colourless oil (383.7 mg, 1.42 mmol, 42%); **IR (thin film)** $\tilde{\nu}$/cm^{-1}: 2979 (C-H, w), 1707 (C=O, s), 1642 (C=C, s). **^{1}H NMR (400 MHz, $CDCl_3$)** δ/ppm: 10.57 (br s, 1H, COOH), 5.82–5.74 (m, 1H, H7), 5.72–5.64 (m, 1H, H10), 5.16–5.11 (m, 2H, H11), 5.04–4.95 (m, 2H, H8) 3.01 (br s, 1H, H9a), 2.64–2.56 (m, 1H, H9b), 2.36 (br s, 1H, H5a), 2.12–2.05 (m, 1H, H6a), 1.95–1.89 (m, 2H, H5b&6b), 1.44 (s, 9H, H1). **^{13}C NMR (101 MHz, $CDCl_3$)** δ/ppm: 178.0 (C12), 154.2 (C3), 137.3 (C7), 132.0 (C10), 119.4 (C11), 115.2 (C8), 79.8 (C2), 63.1 (C4), 39.7 (C9), 34.3 (C5), 28.3 (C1&6). **HRMS (ESI)** $C_{14}H_{23}NO_4Na$ *m/z*: $[M+Na]^+$ 292.1523 (*calc.* 292.1519).

Ethyl (*tert*-butoxycarbonyl)-L-serinate, 201

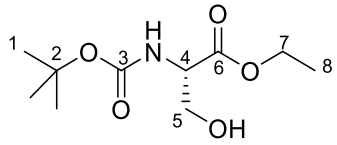

L-serine ethyl ester hydrochloride (5 g, 29.48 mmol, 1.0 eq) and di-*tert*-butyl decarbonate (6.43 mL, 28.01 eq, 0.95 mmol) were dissolved in ethyl acetate (40 mL) and water (40 mL). Potassium carbonate (6.11 g, 44.22 mmol, 1.5 eq) was added to the reaction and it was left to stir overnight at RT. The layers were then separated and the aqueous extracted with ethyl acetate (2 × 30 mL) and the combined organics were washed with brine (50 mL). This was then dried over anh. $MgSO_4$. This mixture was filtered and the filtrate was concentrated *in vacuo* to give the product as a pure colourless oil (6.41 g, 27.49 mmol, 93%); $\mathbf{R_f}$ 0.07 (20% ethyl acetate in pet. ether); **IR (thin film)** $\tilde{\nu}/cm^{-1}$: 3383 (O-H, br s), 2978 (C-H, w), 1714 (C=O ester, s), 1692 (C=O carbamide, s), 1158 (C-O, s). **^{1}H NMR (400 MHz, $CDCl_3$)** δ/ppm: 5.44 (br s, 1H, NH), 4.36 (br s, 1H, H4), 4.24 (q, *J* = 7.0 Hz, 2H, H7), 3.98–3.89 (m, 2H, H5), 2.30 (br s, 1H, OH), 1.46 (s, 9H, H1), 1.30 (t, *J* = 7.0 Hz, 3H, H8). **^{13}C NMR (101 MHz, $CDCl_3$)** δ/ppm: 170.7 (C6), 155.8 (C3), 80.3 (C2), 63.8 (C5), 61.8 (C7), 55.8 (C4), 28.3 (C1), 14.1 (C8). **HRMS (ESI)** $C_{10}H_{19}NO_5Na$ *m/z*: $[M+Na]^+$ 256.1151 (*calc.* 256.1155). $[\boldsymbol{\alpha}]_{\mathbf{D}}^{\mathbf{20}}$ –17.2 (c = 1.0, $CHCl_3$).

The physical and spectroscopic data were found to be in agreement with Tang *et al*.[231]

Ethyl 2-((*tert*-butoxycarbonyl)amino)acrylate, 202

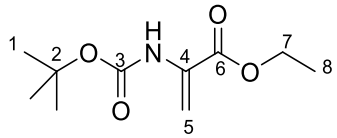

Compound **201** (6.4 g, 27.44 mmol, 1.0 eq) was dissolved in dichloromethane (70 mL) at -15 °C. Mesyl chloride (2.65 mL, 34.30 mmol, 1.25 eq) was added dropwise followed by triethylamine (11.41 mL, 82.31 mmol, 3.0 eq). The reaction was stirred for 30 min before being warmed to RT and stirred for a further 2 h. Then one third molar HCl (30 mL) was added. The mixture was washed with water and the combined organics were dried over anh. $MgSO_4$. This mixture was filtered, and the filtrate was concentrated *in vacuo* to give the crude product. This was filtered through Celite with dichloromethane to afford the pure product as a yellow oil

(5.5667 g, 25.86 mmol, 94%); **R_f** 0.60 (20% ethyl acetate in pet. ether); **IR (thin film)** $\tilde{\nu}$/cm^{-1}: 3420 (N-H, w), 2980 (C-H, w), 1733 (C=O carbamate, m), 1707 (C=O ester, s), 1638 (C=C, w), 1152 (C-O, s). **^{1}H NMR (400 MHz, $CDCl_3$)** δ/ppm: 7.02 (br s, 1H, NH), 6.14 (br s, 1H, H5a), 5.72 (d, *J* = 1.5 Hz, 1H, H5b), 4.28 (q, *J* = 7.0 Hz, 2H, H7), 1.48 (s, 9H, H1), 1.33 (t, *J* = 7.0 Hz, 3H, H8). **^{13}C NMR (101 MHz, $CDCl_3$)** δ/ppm: 164.0 (C6), 152.6 (C3), 131.5 (C4), 104.8 (C5), 80.6 (C2), 62.0 (C7), 28.2 (C1), 14.1 (C8). **HRMS (ESI)** $C_{10}H_{17}NO_4Na$ *m/z*: $[M+Na]^+$ 238.1046 (*calc*. 238.1050).

The physical and spectroscopic data were found to be in agreement with Ramesh *et al*.[232]

4-Methyloxazol-2(3H)-one, 204

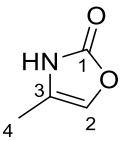

To a solution of potassium *tert*-butoxide (181.4 mg, 1.62 mmol, 1.0 eq) in THF (15 mL) was added **203** (280 mg, 1.62 mmol, 1.0 eq) at 0 °C and the reaction was stirred for 1h. The reaction was diluted with sat. aq. NH_4Cl (10 mL) and extracted with dichloromethane (3 × 10 mL). The combined organics were dried over anh. $MgSO_4$, filtered, and concentrated *in vacuo* to give the pure product as a white crystalline solid (57.2 mg, 0.58 mmol, 36%); **IR (thin film)** $\tilde{\nu}$/cm^{-1}: 3163 (N-H, br s), 1706 (C=O, s). **^{1}H NMR (400 MHz, $CDCl_3$)** δ/ppm: 9.14 (br s, 1H, NH), 6.53 (s, 1H, H2), 2.02 (d, *J* = 1.5 Hz, 3H, H4). **^{13}C NMR (101 MHz, $CDCl_3$)** δ/ppm: 157.7 (C1), 124.6 (C2), 122.7 (C3), 9.2 (C4). **HRMS (ESI)** $C_4H_6NO_2$ *m/z*: $[M+H]^+$ 100.0397 (*calc* 100.0393). m.p. 50–51°C.

N-Hydroxybenzimidoyl chloride, 209

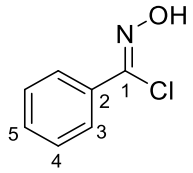

Benzaldehyde (1.5 g, 14.13 mmol, 1.0eq) was dissolved in diethyl ether (12 mL) and hydroxylamine (50% in H_2O, 1.73 mL, 28.27 mmol, 2.0 eq) was added. The reaction was stirred for 10 min. The reaction was dried with direct addition of anh. $MgSO_4$. The mixture was filtered and the filtrate was concentrated *in vacuo*. The residual oil was dissolved in DMF (12 mL) and *N*-chlorosuccinimide (2.08 g, 15.55 mmol, 1.1 eq) was added and the reaction was stirred for 30 min. The reaction was diluted with water (10 mL), and extracted with ethyl acetate (2 × 10 mL). The combined organics were washed with water (20 mL) and brine (20 mL) before being dried over anh. Na_2SO_4. The mixture was filtered and the filtrate was concentrated *in vacuo* to give the crude product as a yellow oil. This was carried through crude to the following reactions. (2.17 g, 13.95 mmol, 99%); **^{1}H NMR (400 MHz, $CDCl_3$)** δ/ppm: 8.94 (br s, 1H, OH), 7.89–7.86 (m, 2H, H3), 7.47–7.41 (m, 3H, H4&5).

The physical and spectroscopic data were found to be in agreement with Castellano *et al.*[233]

Ethyl 4-((*tert*-butoxycarbonyl)amino)-3-phenyl-4,5-dihydroisoxazole-4-carboxylate, 210

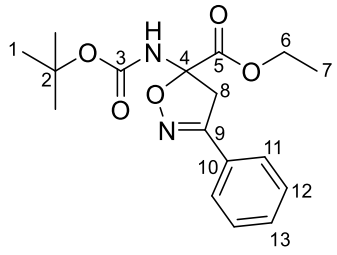

Triethylamine (2.2 mL, 15.80 mmol, 6.8 eq) was added to a mixture of **202** (500 mg, 2.32 mmol, 1.0 eq) an **209** (2.17 g, 13.94 mmol, 6.0 eq) in dichloromthane (40 mL) and the reaction was stirred at RT for 1 h. Water (30 mL) was added and the organic layer was washed with water (30 mL) and brine (30 mL). The combined organics were dried over anh. $MgSO_4$. This mixture was filtered, and the filtrate was concentrated *in vacuo* to give the crude product. This was

purified by column chromatography (20% diethyl ether in pet. ether) to give the pure product as off-white amorphous solid (448.6 mg, 1.34 mmol, 58%); $\mathbf{R_f}$ 0.12 (20% diethyl ether in pet. ether); **IR (thin film)** $\tilde{\nu}$/cm^{-1}: 3410 (N-H, m), 2976 (C-H, w), 1741 (C=O, m), 1721 (C=N, s), 1484 (C=C, s), 1308 (N-O, s). **^{1}H NMR (400 MHz, $CDCl_3$)** δ/ppm: 7.70–7.66 (m, 2H, H11), 7.43–7.38 (m, 3H, H12&13), 6.08 (br s, 1H, NH), 4.32 (q, J = 7.0 Hz, 2H, H6), 3.91 (br s, 2H, H8), 1.40 (s, 9H, H1), 1.32 (t, J = 7.0 Hz, 3H, H7). **^{13}C NMR (101 MHz, $CDCl_3$)** δ/ppm: 167.6 (C5), 156.3 (C9), 153.3 (C3), 130.4 (C12), 129.8 (C10), 128.7 (C13), 126.9 (C11), 92.4 (C4), 81.2 (C2), 63.4 (C6), 42.7 (C8), 28.2 (C1), 14.0 (C7). **HRMS (ESI)** $C_{17}H_{23}N_2O_5$ *m/z*: $[M+H]^+$ 335.1591 (*calc.* 335.1607).

tert-Butyl (4-(hydroxymethyl)-3-phenyl-4,5-dihydroisoxazol-4-yl)carbamate, 211

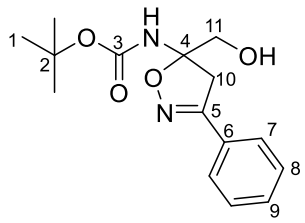

Compound **210** (100 mg, 0.30 mmol, 1.0 eq), was dissolved in an 8:1 THF/methanol mixture (1.8 mL). This was colled to 0 °C and sodium borohydride (2.83 mg, 0.07 mmol, 0.25 eq) were added. The reaction was stirred for 4 h before further sodium borohydride (8.49 mmol, 0.21 mmol, 0.75 eq) was added. The reaction was stirred overnight. It was quenched with sat. aq. NH_4Cl (2 mL), and extracted with dichloromethane (3 × 5 mL). The combined organics were then dried over anh. $MgSO_4$. This mixture was filtered, and the filtrate was concentrated *in vacuo* to give the crude product. This was purified *via* column chromatography (55% ethyl acetate in hexane) to give the pure product as a white powder (54.0 mg, 0.18 mmol, 62%); $\mathbf{R_f}$ 0.29 (55% ethyl acetate in hexane); **IR (thin film)** $\tilde{\nu}$/cm^{-1}: 3408 (N-H, w), 3278 (O-H, w), 2970 (C-H, w), 1717 (C=O, s), 1545 (C=C, s). **^{1}H NMR (400 MHz, $CDCl_3$)** δ/ppm: 7.66–7.64 (m, 2H, H7), 7.40–7.37 (m, 3H, H8&9), 5.74 (br s, 1H, NH), 3.90–3.86 (m, 2H, H10a&11a), 3.77–3.73 (m, 1H, H11b), 3.30 (d, J = 17.5 Hz, 1H, H10b), 3.05 (br s, 1H, OH), 1.40 (s, 9H, H1). **^{13}C NMR (101 MHz, $CDCl_3$)** δ/ppm: 157.3 (C5), 154.1 (C3), 130.3 (C8), 129.6 (C6), 128.7 (C9), 126.7 (C7), 95.4 (C4), 80.9 (C2), 66.2 (C11), 40.4 (C10), 28.2 (C1). **HRMS (ESI)** $C_{15}H_{21}N_2O_4$ *m/z*: $[M+H]^+$ 293.1498 (*calc.* 293.1501).

3-Phenyl-1,8-dioxa-2,6-diazaspiro[4.4]non-2-en-7-one, 212

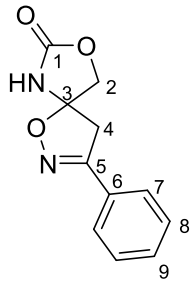

To a solution of potassium *tert*-butoxide (30.7 mg, 0.27 mmol, 2.0 eq) in THF (1.4 mL) at 0 °C was added **211** (40 mg, 0.14 mmol, 1.0 eq) and the reaction was stirred for 1 h. This was then diluted with sat. aq. NH_4Cl (5 mL) and extracted with dichloromethane (3 × 5 mL). The combined organics were dried over anh. $MgSO_4$, filtered and concentrated *in vacuo* to give the crude product. This was purified by column chromatography (60% ethyl acetate in hexane) to give the pure product as a white powder (17 mg, 0.08 mmol, 56%); $\mathbf{R_f}$ 0.16 (60% ethyl acetate in hexane); **IR (thin film)** $\tilde{\nu}$/cm^{-1}: 3226 (N-H, w), 1765 (C=O, s), 1048 (C-O, s). **^{1}H NMR (400 MHz, $CDCl_3$)** δ/ppm: 7.64–7.62 (m, 2H, H7), 7.48–7.41 (m, 3H, H8&9), 5.97 (br s, 1H, NH), 4.77 (d, *J* = 10.0 Hz, 1H, H2a), 4.59 (d, *J* = 10.0 Hz, 1H, H2b), 3.59 (d, *J* = 18.0 Hz, 1H, H4a), 3.49 (d, *J* = 18.0 Hz, 1H, H4b). **^{13}C NMR (101 MHz, $CDCl_3$)** δ/ppm: 156.3 (C5), 156.2 (C1), 131.1 (C8), 129.1 (C9), 128.2 (C6), 126.6 (C7), 96.1 (C3), 73.9 (C2), 42.8 (C4). **HRMS (ESI)** $C_{11}H_{10}N_2O_3Na$ *m/z*: $[M+H]^+$ 241.0576 (*calc* 241.0584). **m.p.** 178–179 °C

Crystallographic data for this compound is in Appendix B.

Ethyl (2-chloroacetyl)-L-serinate, 214

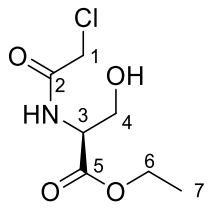

L-Serinate ethyl ester hydrochloride (1 g, 5.90 mmol, 1.0 eq), was dissolved in dichloromethane (60 mL) and triethylamine (1.73 mL, 12.38 mmol, 2.1 eq) was added to the solution. This was cooled to 0 °C before chloroacetyl chloride (0.47 mL, 5.90 mmol, 1.0 eq) was added dropwise and the reaction was stirred for 90 min. After this it was diluted with aq. sat.

NH_4Cl and stirred for 10 min. The mixture was extracted with dichloromethane. The combined organics were dried over anh. $MgSO_4$, filtered and concentrated *in vacuo* to give the crude product. This was purified *via* column chromatography (80% ethyl acetate in hexane) to yield the pure product as a white crystalline solid (673.8 mg, 3.21 mmol, 54%); $\mathbf{R_f}$ 0.31 (80% ethyl acetate in hexane); **IR (thin film)** $\tilde{\nu}/cm^{-1}$: 3500 (O-H, m), 3276 (N-H, m), 2957 (C-H, w), 1712 (C=O ester, s), 1664 (C=O amide, s), 1555 (N-H, s), 1035 (C-O, s), 781 (C-Cl, m). **^{1}H NMR (400 MHz, $CDCl_3$)** δ/ppm: 7.43 (br s, 1H, NH), 4.65 (dt, *J* = 7.5, 3.5 Hz, 1H, H3), 4.28 (q, *J* = 7.0 Hz, 2H, H6), 4.10 (s, 2H, H1), 4.07–3.94 (m, 2H, H4), 2.26 (t, *J* = 5.5 Hz, 1H, OH), 1.32 (t, *J* = 7.0 Hz, 3H, H7). **^{13}C NMR (101 MHz, $CDCl_3$)** δ/ppm: 169.7 (C5), 166.5 (C2), 63.2 (C4), 62.3 (C6), 42.4 (C1), 14.1 (C7). **HRMS (ESI)** $C_7H_{13}ClNO_4Si$ *m/z*: $[M+H]^+$ 210.0524 (*calc.* 210.0528). $[\alpha]_D^{20}$ +41.3 (c = 1.00, $CHCl_3$).

The physical and spectroscopic data were found to be in agreement with Yoshimura *et al.*[234]

Ethyl *N*,*O*-bis(2-chloroacetyl)-L-serinate, 215

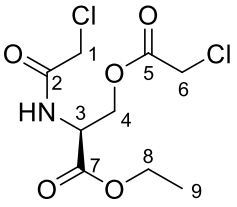

The title compound was isolated as a by-product from the reaction to synthesise **214**. White crystalline solid (87.5 mg, 0.42 mmol, 5.2%); $\mathbf{R_f}$ 0.13 (60% ethyl acetate in hexane); **IR (thin film)** $\tilde{\nu}/cm^{-1}$: 3268 (O-H, s), 2957 (C-H, w), 1744 (C=O ester, s), 1679 (C=O amide, s), 1540 (N-H, s), 1194 (C-Cl, s). **^{1}H NMR (400 MHz, $CDCl_3$)** δ/ppm: 7.31 (d, *J* = 6.5 Hz, 1H, NH), 4.86–4.82 (m. 1H, H3), 4.60–4.53 (m, 2H, H4), 4.27 (q, *J* = 7.0 Hz, 2H, H8), 4.08 (s, 2H, H1), 4.06 (s, 2H, H6), 1.30 (t, *J* = 7.0 Hz, 3H, H9). **^{13}C NMR (101 MHz, $CDCl_3$)** δ/ppm: 168.4 (C7), 166.9 (C5), 166.1 (C2), 64.9 (C4), 62.6 (C8), 52.0 (C3), 42.3 (C1), 40.4 (C6), 14.1 (C9). **HRMS (ESI)** $C_9H_{13}Cl_2NO_5$ *m/z*: $[M+H]^+$ 232.0356 (*calc.* 232.0353). $[\alpha]_D^{20}$ +45.0 (c = 1.00, $CHCl_3$).

Ethyl (*S*)-2-oxooxazolidine-4-carboxylate, 219

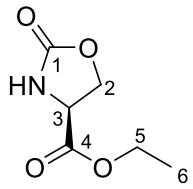

Triphosgene (2.73 g, 9.20 mmol, 0.5 eq) and L-serine ethyl ester hydrochloride (3.00 g, 17.69 mmol, 1.0 eq) were dissolved in THF (180 mL) and refluxed for 1h. The reaction was concentrated *in vacuo* and submitted to column chromatography (80% ethyl acetate in hexane) to yield the pure product as off-white crystals (2.7054 g, 17.00 mmol, 96%); **R_f** 0.27 (80% ethyl acetate in hexane); **IR (thin film)** $\tilde{\nu}$/cm^{-1}: 3264 (N-H, br w), 2998 (C-H, w), 1739 (C=O ester, s), 1714 (C=O carbamide, s), 1204 (C-O, s). **^{1}H NMR (400 MHz, $CDCl_3$)** δ/ppm: 6.03 (br s, 1H, NH), 4.64–4.59 (m, 1H, H2a), 4.54–4.51 (m, 1H, H2b), 4.41–4.38 (m, 1H, H3), 4.27 (q, *J* = 7.0 Hz, 2H, H5), 1.31 (t, *J* = 7.0 Hz, 3H, H6). **^{13}C NMR (101 MHz, $CDCl_3$)** δ/ppm: 170.0 (C4), 158.7 (C1), 66.7 (C2), 62.4 (C5), 53.3 (C3), 14.1 (C6). **HRMS (ESI)** $C_6H_{10}NO_4$ *m/z*: $[M+H]^+$ 160.0603 (*calc.* 160.0604). $[\alpha]_D^{20}$ –14.8 (c = 1.00, $CHCl_3$).

The physical and spectroscopic data were found to be in agreement with Paz *et al.*[235]

Ethyl (*S*)-2-phenyl-4,5-dihydrooxazole-4-carboxylate, 221

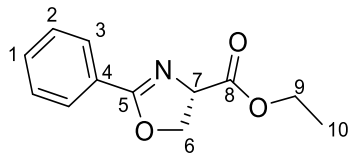

Compound **150** (1.6 g, 10.72 mmol, 1.0 eq) as a free base was dissolved in 1,2-dichloroethane (20 mL) and L-serine ethyl ester hydrochloride (2.00 g, 11.79 mmol, 1.1 eq) was added. The reaction was refluxed overnight. This was cooled to RT and filtered. The filtrate was concentrated *in vacuo* and the crude oil was purified by column chromatography (30% ethyl acetate in hexane) to yield the pure product as a white amorphous solid (1.4862 g, 6.78 mmol, 63%); **R_f** 0.33 (30% ethyl acetate in hexane); **IR (thin film)** $\tilde{\nu}$/cm^{-1}: 2984 (C-H, w), 1726 (C=O, s), 1631 (C=N, s), 1201 (C-O, s). **^{1}H NMR (400 MHz, $CDCl_3$)** δ/ppm: 7.98–7.96 (m, 2H, H3), 7.50–7.46 (m, 1H, H1), 7.41–7.37 (m, 2H, H2), 4.91 (dd, *J* = 10.5, 8.0 Hz, 1H, H7), 4.68–4.64 (m, 1H, H6a), 4.60–4.55 (m, 1H, H6b), 4.30–4.21 (m, 2H, H9), 1.31 (t, *J* = 7.0 Hz, 3H, H10). **^{13}C NMR**

(101 MHz, $CDCl_3$) δ/ppm: 171.2 (C8), 166.2 (C5), 131.8 (C1), 128.6 (C3), 128.3 (C2), 127.0 (C4), 69.6 (C6), 68.8 (C7), 61.8 (C9), 14.2 (C10). **HRMS (ESI)** $C_{12}H_{14}NO_3$ *m/z*: $[M+H]^+$ 220.0909 (*calc.* 220.0974). $[\alpha]_D^{20}$ +122.0 (c = 1.00, $CHCl_3$).

The physical and spectroscopic data were found to be in agreement with Robertson *et al*.[236]

(*R*)-(2-Phenyl-4,5-dihydrooxazol-4-yl)methanol, 222

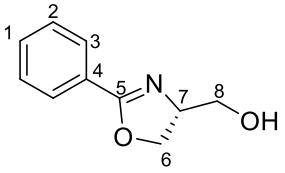

Calcium chloride (3.14 g, 28.28 mmol, 4.0 eq) and **221** (1.55 g, 7.07 mmol, 1.0 eq) were dissolved in ethanol (125 mL). The mixture was cooled to 0 °C and sodium borohydride (2.14 g, 56.56 mmol, 8.0 eq) was added portion-wise. The reaction was stirred at 0 °C for a further 5 h. Water (100 mL) was added and stirred for 1 h. The resulting mixture was filtered, and the filtrate concentrated *in vacuo*. This was diluted with ethyl acetate (50 mL) and washed with brine (50 mL), dried over anh. Na_2SO_4, filtered, and contracted *in vacuo*. This give the pure product as an amorphous white solid (882.6 mg, 4.98 mmol, 70%); **IR (thin film)** $\tilde{\nu}$/cm^{-1}: 3235 (O-H, br w), 2899 (C-H, w), 1644 (C=N, s). **^{1}H NMR (400 MHz, $CDCl_3$)** δ/ppm: 7.85 (d, *J* = 7.5 Hz, 2H, H1), 7.45 (t, *J* = 7.5 Hz, 1H, H2), 7.35 (t, *J* = 7.5 Hz, 2H, H3), 4.50–4.32 (m, 3H, H7&8), 3.97 (d, *J* = 9.0 Hz, 1H, H6a), 3.66 (d, *J* = 9.0 Hz, 1H, H6b), 2.92 (br s, 1H, OH). **^{13}C NMR (101 MHz, $CDCl_3$)** δ/ppm: 165.6 (C5), 131.6 (C2), 128.3 (C1&3), 127.1 (C4), 69.3 (C8), 68.0 (C7), 63.9 (C6). **HRMS (ESI)** $C_{10}H_{12}NO_2$ *m/z*: $[M+H]^+$ 178.0861 (*calc.* 178.0863).

The physical and spectroscopic data were found to be in agreement with Braga *et al*.[237]

Ethyl *O*-(tert-butyldimethylsilyl)-L-serinate, 224

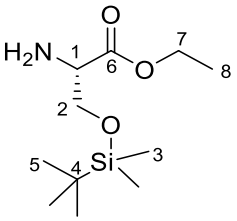

L-serinate ethyl ester hydrochloride (2 g, 11.79 mmol, 1.0 eq) and *tert*-butyldimethylsilyl chloride (3.55 g, 23.58 mmol, 2.0 eq) were dissolved in dichloromethane (150 mL). Imidazole (2.41 g, 35.38 mmol, 3.0 eq) was added at 0 °C and the reaction was warmed to RT and stirred overnight. This was quenched by the addition of water (100 mL) and extracted with dichloromethane (3 × 100 mL) to give the pure product as a colourless oil (2.2867 g, 9.24 mmol, 78%); **IR (thin film)** $\tilde{\nu}$/cm^{-1}: 2930 (C-H, w), 1739 (C=O, s), 1095 (C-O, s). **^{1}H NMR (400 MHz, $CDCl_3$)** δ/ppm: 4.20 (q, *J* = 7.0 Hz, 2H, H7), 3.94 (dd, *J* = 9.5, 4.0 Hz, 1H, H2a), 3.83 (dd, *J* = 9.5, 4.0 Hz, 1H, H2b), 3.51 (t, *J* = 4.0 Hz, 1H, H1), 1.70 (br s, 2H, NH_2), 1.30 (t, *J* = 7.0 Hz, 3H, H8), 0.89 (s, 9H, H5), 0.07 (s, 3H, H3a), 0.06 (s, 3H, H3b). **^{13}C NMR (101 MHz, $CDCl_3$)** δ/ppm: 174.1 (C6), 65.4 (C2), 60.9 (C7), 56.5 (C1), 25.7 (C5), 18.2 (C4), 14.2 (C8), –5.5 (C3a), –5.6 (C3b). **HRMS (ESI)** $C_{11}H_{25}NO_3SiNa$ *m/z*: $[M+Na]^+$ 270.1493 (*calc.* 270.1501). $[\alpha]_D^{20}$ –6.1 (c = 1.00, $CHCl_3$).

The physical and spectroscopic data were found to be in agreement with Hakimelahi *et al.*[238]

Ethyl *O*-(*tert*-butyldimethylsilyl)-*N*-(2-chloroacetyl)-L-serinate, 225

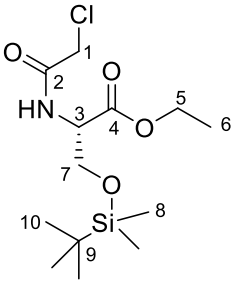

Triethylamine (1.18 mL, 8.49 mmol, 2.1 eq) was added to a solution of **224** (1.00 g, 4.04 mmol, 1.0 eq) in dichloromethane (40 mL). This was cooled to 0 °C and chloroacetyl chloride (0.32 mL, 4.04 mmol, 1.0 eq) was added dropwise. The reaction was warmed to RT and stirred for 90 min. The reaction was then quenched with sat. aq. NH_4Cl (20 mL), and stirred for 10 min. This mixture was extracted with dichloromethane (2 × 10 mL). The combined organics were

dried over anh. $MgSO_4$, filtered and concentrated *in vacuo* to give the crude product. This was purified by column chromatography (20% ethyl acetate in hexane) to yield the pure product as a colourless oil (723.6 mg, 2.23 mmol, 55%); $\mathbf{R_f}$ 0.20 (20% ethyl acetate in hexane); **IR (thin film)** $\tilde{\nu}$/cm^{-1}: 2932 (C-H, w), 1745 (C=O ester, m), 1679 (C=O amide, s), 1110 (C-O, s), 776 (C-Cl, s). **^{1}H NMR (400 MHz, $CDCl_3$)** δ/ppm: 7.38 (d, *J* = 8.0 Hz, 1H, NH), 4.61 (dt, *J* = 8.0, 3.0 Hz, 1H, H3), 4.22 (q, *J* = 7.0 Hz, 2H, H5), 4.12–4.04 (m, 3H, H1&7a), 3.84 (dd, *J* = 10.0, 3.0 Hz, 1H, H7b), 1.28 (t, *J* = 7.0 Hz, 3H, H6), 0.86 (s, 9H, H6), 0.04 (s, 3H, H8a), 0.02 (s, 3H, H8b). **^{13}C NMR (101 MHz, $CDCl_3$)** δ/ppm: 169.7 (C4), 165.7 (C2), 63.1 (C7), 61.7 (C5), 54.5 (C3), 42.5 (C1), 25.6 (C10), 18.1 (C9), 14.2 (C6), –5.6 (C8a), –5.7 (C8b). **HRMS (ESI)** $C_{13}H_{26}ClNO_4SiNa$ *m/z*: $[M+Na]^+$ 346.1203 (*calc.* 346.1212). $[\alpha]_D^{20}$ +29.2 (c = 1.00, $CHCl_3$).

(*R*)-*N*-(1-((*tert*-Butyldimethylsilyl)oxy)-3-hydroxypropan-2-yl)-2-chloroacetamide, 226

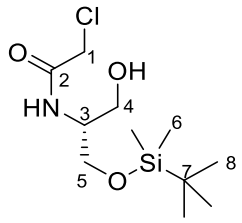

Powdered sodium borohydride (37.4 mg, 2.34 mmol, 1.05 eq) was added to a solution of **225** (305 mg, 2.22 mmol, 1.0 eq) and the reaction was stirred at RT for 2 h. Sat. aq. NH_4Cl solution was added dropwise and the mixture was stirred for 30 min. This was filtered and the filtrate was dried over anh. $MgSO_4$ and filtered and concentrated *in vacuo*. The crude oil was purified by column chromatography (80% ethyl acetate in hexane) to give the pure product as a colourless oil (27 mg, 0.10 mmol, 43%); $\mathbf{R_f}$ 0.29 (80% ethyl acetate in hexane); **IR (thin film)** $\tilde{\nu}$/cm^{-1}: 3243 (O-H, br m), 2927 (C-H, w), 1645 (C=O, s), 1053 (C-O, m), 720 (C-Cl, s). **^{1}H NMR (400 MHz, $CDCl_3$)** δ/ppm: 7.26 (br s, 1H, NH), 4.09 (d, *J* = 15.5 Hz, 1H, H1a), 4.05 (d, *J* = 15.5 Hz, 1H, H1b), 3.98 (sp, *J* = 4.0 Hz, 1H, H3), 3.87–3.84 (m, 2H, H4a&5a), 3.78 (dd, *J* = 10.5, 4.5 Hz, 1H, H5b), 3.70 (dd, *J* = 10.5, 4.5 Hz, 1H, H4b), 2.85 (br s, 1H, OH), 0.90 (s, 9H, H8), 0.08 (s, 6H, H6). **^{13}C NMR (101 MHz, $CDCl_3$)** δ/ppm: 166.2 (C2), 63.3 (C4/5), 63.2 (C4/5), 52.0 (C3), 42.6 (C1), 25.7 (C8), 18.1 (C7), –5.6 (C6). **HRMS (ESI)** $C_{11}H_{25}CLNO_3Si$ *m/z*: $[M+H]^+$ 281.1210 (*calc.* 281.1214). $[\alpha]_D^{20}$ +18.7 (c = 1.00, $CHCl_3$).

Ethyl *O*-(*tert*-butyldimethylsilyl)-*N*-(3-ethoxy-3-oxopropanoyl)-L-serinate, 228

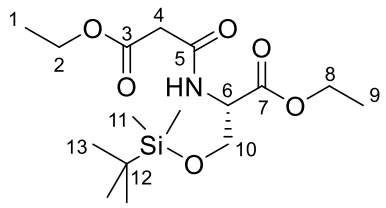

Compound **224** (500 mg, 2.02 mmol, 1.0 eq) was dissolved in dichloromethane (20 mL) at 0 °C. Triethylamine (0.61 mL, 4.35 mmol, 2.15 eq) and ethyl malonyl chloride (0.41 mL, 3.23 mmol, 1.6 eq) were added dropwise to the reaction which was subsequently warmed to RT and stirred for 4h. this was quenched with sat. aq. NH_4Cl (20 mL) and stirred for 10 min. This mixture was separated and the aqueous was extracted with dichloromethane (2 × 20 mL). The combined organics were dried over $MgSO_4$, filtered, and the filtrate was concentrated *in vacuo* to give a crude oil. This was purified *via* column chromatography (40% ethyl acetate in hexane) to give the pure product as a yellow oil (482.8 mg, 1.34 mmol, 66%); $\mathbf{R_f}$ 0.29 (40% ethyl acetate in hexane); **IR (thin film)** $\tilde{\nu}$/cm^{-1}: 3337 (N-H, w), 2932 (C-H, w), 1739 (C=O ester, s), 1679 (C=O amide, m), 1109 (C-O, s). **^{1}H NMR (400 MHz, $CDCl_3$)** δ/ppm: 7.77 (d, *J* = 7.5 Hz, 1H, NH), 4.65 (dt, *J* = 7.5, 3.0 Hz, 1H, H6), 4.21 (qd, *J* = 7.0, 3.0 Hz, 4H, H2&8), 4.08 (dd, *J* = 10.0, 3.0 Hz, 1H, H10a), 3.84 (dd, *J* = 10.0, 3.0 Hz, 1H, H10b), 3.35 (s, 2H, H4), 1.28 (td, *J* = 7.0, 5.5 Hz, 6H, H1&9), 0.87 (s, 9H, H13), 0.03 (s, 3H, H11a), 0.02 (s, 3H, H11b). **^{13}C NMR (101 MHz, $CDCl_3$)** δ/ppm: 170.0 (C7), 168.7 (C3), 164.9 (C5), 63.3 (C10), 61.6 (C2/8), 61.5 (C2/8), 54.5 (C6), 41.4 (C4), 25.7 (C13), 18.1 (C12), 14.2 (C1/9), 14.1 (C1/9), –5.6 (C11a), –5.7 (C11b). **HRMS (ESI)** $C_{16}H_{31}NO_6SiNa$ *m/z*: $[M+Na]^+$ 384.1812 (*calc.* 384.1818). $[\boldsymbol{\alpha}]_{\mathbf{D}}^{\mathbf{20}}$ +32.1 (c = 1.00, $CHCl_3$).

4-Ethoxy-5-methylene-1,5-dihydro-2H-pyrrol-2-one, 230

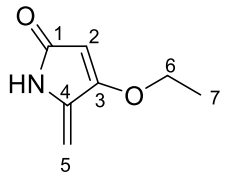

Compound **224** (400 mg, 1.62 mmol, 1.0 eq), Bestmann's Ylide (489 mg, 1.62 mmol, 1.0 eq), benzoic acid (39.5 mg, 0.32 mmol, 0.2 eq) were dissolved in THF (8 mL) and refluxed overnight at 65 °C in the dark. The reaction mixture was concentrated *in vacuo* and purified *via* column

chromatography (diethyl ether) to give the pure product as a yellow oil (139.2 mg, 1.00 mmol, 62%); $\mathbf{R_f}$ 0.28 (diethyl ether) **IR (thin film)** $\tilde{\nu}$/cm^{-1}: 2980 (C-H, w), 1686 (C=O, s), 1652 (C=C, s), 1593 (C-O, s). **^{1}H NMR (400 MHz, $CDCl_3$)** δ/ppm: 6.90 (br s, 1H, NH), 5.09 (s, 1H, H2), 5.00 (d, J = 1.0 Hz, 1H, H5a), 4.74 (t, J = 1.5 Hz, 1H, H5b), 4.05 (q, J = 7.0 Hz, 2H, H6), 1.42 (t, J = 7.0 Hz, 3H, H7). **^{13}C NMR (101 MHz, $CDCl_3$)** δ/ppm: 171.4 (C1), 165.2 (C4), 139.4 (C3), 93.7 (C2), 91.8 9C5), 67.1 (C6), 14.1 (C7). **HRMS (ESI)** $C_7H_{10}NO_2$ *m/z*: $[M+H]^+$ 140.0705 (*calc.* 140.0705).

tert-Butyl 3-(2-ethoxy-2-oxoethylidene)azetidine-1-carboxylate, 236

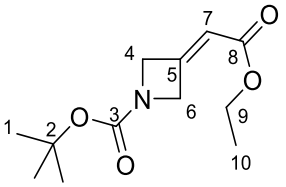

Tert-butyl 3-oxoazetidine-1-carboxylate (2.90 g, 16.93 mmol, 1.0 eq) and ethyl (triphenylphosphoranylidene)acetate (6.49 g, 18.62 mmol, 1.1 eq) were dissolved in dichloromethane (56 mL) and refluxed for 6 h. The reaction was concentrated *in vacuo* and submitted to column chromatography (20% ethyl acetate in hexane) to yield the pure product as colourless crystals (3.8496 g, 15.95 mmol, 94%); $\mathbf{R_f}$ 0.29 (20% ethyl acetate in hexane); **IR (thin film)** $\tilde{\nu}$/cm^{-1}: 2978 (C-H, w), 1725 (C=O carbamide, s), 1704 (C=O ester, s), 1197 (C-O, s). **^{1}H NMR (400 MHz, $CDCl_3$)** δ/ppm: 5.75 (s, 1H, H7), 4.79 (s, 2H, H6), 4.57 (s, 2H, H4), 4.15 (q, J = 7.0 Hz, 2H, H9), 1.43 (s, 9H, H1), 1.26 (t, J = 7.0 Hz, 3H, H10). **^{13}C NMR (101 MHz, $CDCl_3$)** δ/ppm: 165.2 (C8), 156.2 (C3), 152.6 (C5), 113.7 (C7), 80.0 (C2), 60.4 (C6&9), 57.8 (C4), 28.3 (C1), 14.3 (C10). **HRMS (ESI)** $C_{12}H_{19}NO_4Na$ *m/z*: $[M+Na]^+$ 264.1215 (*calc.* 264.1212).

The physical and spectroscopic data were found to be in agreement with Collier.[239]

2-(*tert*-Butyl) 8-ethyl 7-phenyl-5-oxa-2,6-diazaspiro[3.4]oct-6-ene-2,8-dicarboxylate, 237

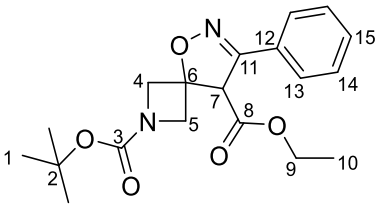

Compound **236** (300 mg, 1.24 mmol, 1.0 eq) and **209** (1.16 g, 7.46 mmol, 6.0 eq) were dissolved in dichloromethane (20 mL). Triethylamine (1.17 mL, 8.43 mmol, 6.8 eq) was added dropwise and the reaction was stirred at RT for 1 h. Water (10 mL) was added and the reaction was washed with brine (10 mL). The combined organics were concentrated *in vacuo* and purified by column chromatography (30% ethyl acetate in hexane) to yield the product as an orange oil (349.6 mg, 0.97 mmol, 78%); $\mathbf{R_f}$ 0.38 (30% ethyl acetate in hexane) **IR (thin film)** $\tilde{\nu}$/cm^{-1}: 2978 (C-H, w), 1736 (C=O, s), 1698 (C=N, s), 1392 (N-O, s), 1153 (C-O, s). **^{1}H NMR (400 MHz, $CDCl_3$)** δ/ppm: 7.68–7.66 (m, 2H, H14), 7.43–7.38 (m, 3H, H15&13), 4.45 (s, 1H, H7), 4.33 (dd, *J* = 10.5, 1.0 Hz, 1H, H4/5a), 4.25–4.14 (m, 4H, H9&4/5b), 4.05 (dd, *J* = 10.0, 1.0 Hz, 1H, H4b), 1.45 (s, 9H, H1), 1.19 (t, *J* = 7.0 Hz, 3H, H10). **^{13}C NMR (101 MHz, $CDCl_3$)** δ/ppm:167.0 (C8), 155.9 (C3), 154.8 9C11), 130.8 (C15), 128.9 (C13), 128.0 (C12), 126.8 (C14), 83.4 (C5), 80.3 (C2), 64.7 (C4/5), 62.4 9C9), 60.5 (C7), 57.3 (C4/5), 28.3 (C1), 14.0 (C10). **HRMS (ESI)** $C_{19}H_{25}N_2O_5$ *m/z*: $[M+H]^+$ 360.6087 (*calc.* 360.6085).

2-(*tert*-Butyl) 8-ethyl 7-benzyl-2,5,6,7-tetraazaspiro[3.4]oct-5-ene-2,8-dicarboxylate, 238

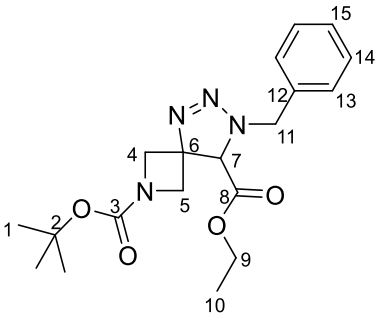

Compound **236** (386 mg, 1.60 mmol, 1.0 eq) was dissolved in benzyl azide (2 mL, 16.0, 10.0 eq) and heated in a sealed tube at 100 °C for 48 h. This was purified *via* column chromatography

(30% ethyl acetate in pet. ether) to give the pure compound as a yellow oil (204 mg, 0.54 mmol, 34%); $\mathbf{R_f}$ 0.49 (30% ethyl acetate in pet. ether) **IR (thin film)** $\tilde{\nu}$/cm^{-1}: 2988 (C-H, w), 1726 (C=O, s), 1631 (C=C, m), 1115 (C-O, s). **^{1}H NMR (400 MHz, $CDCl_3$)** δ/ppm: 7.30–7.17 (m, 5H, H13,14,15), 5.68 (br s, 2H, H4a&5a), 4.89 (br s, 2H, H4b&5b), 4.41 (q, *J* = 7.0 Hz, 2H, H9), 2.65 (br s, 3H, H7&11), 1.42–1.38 (m, 12H, H1&10). **^{13}C NMR (101 MHz, $CDCl_3$)** δ/ppm: 154.3 (C8), 138.1 (C3), 128.9 (C12), 128.2 (C14), 127.6 (C13), 126.8 (C15), 89.5 (c7), 79.8 (C2), 59.0 (C9), 54.8 (C6), 51.1 (d, *J* = 12.0 Hz, C4/5), 50.3 (d, *J* = 20.0 Hz, C4/5), 48.4 (C11), 28.4 (C1), 14.6 (C10). **HRMS (ESI)** $C_{19}H_{26}N_4O_4Na$ *m/z*: $[M+Na]^+$ 397.1840 (*calc.* 397.1846).

(2-Hydroxy-5-oxo-5,6-dihydro-2*H*-pyran-2-yl)methyl acetate, 242

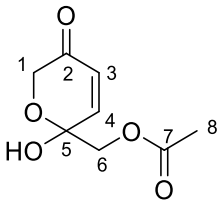

To a suspension of sodium borohydride (225 mg, 5.95 mmol, 0.5 eq) in ethanol (26 mL) was added at 0 °C a solution of (5-acetylfuran-2-yl)methyl acetate (2 g, 11.89 mmol, 1.0 eq) in ethanol (34 mL) and the reaction was stirred for 10 min at 0 °C. Acetic acid was added dropwise until the sodium borohydride had been quenched. The resulting mixture was concentrated *in vacuo* and dissolved in water (80 mL). To this a solution of bromine (1.9 g, 11.89 mmol, 1.0 eq) in methanol (6 mL) was added dropwise and the reaction was stirred for 2 h. Sat. aq. NH_4Cl was added dropwise until the mixture had reach pH 5. Brine was added and the mixture was extracted with ethyl acetate (3 × 50 mL). The combined organics were dried over anh. $MgSO_4$, filtered, and concentrated *in vacuo* to give the pure product as an orange oil (1.3491 g, 7.25 mmol, 61%); **IR (thin film)** $\tilde{\nu}$/cm^{-1}: 3375 (O-H, br s), 1740 (C=O ester, s), 1699 (C=O ketone, s), 1044 (C-O, s). **^{1}H NMR (400 MHz, $CDCl_3$)** δ/ppm: 6.90 (d, *J* = 10.5 Hz, 1H, H4), 6.18 (d, *J* = 10.5 Hz, 1H, H3), 4.61 (d, *J* = 17.0 Hz, 1H, H1a), 4.46 (d, *J* = 12.0 Hz, 1H, H6a), 4.19 (d, *J* = 17.0 Hz, 1H, H1b), 4.08 (d, *J* = 12.0 Hz, 1H, H6b), 3.37 (br s, 1H, OH), 2.16 (s, 3H, H8). **^{13}C NMR (101 MHz, $CDCl_3$)** δ/ppm: 194.0 (C2), 171.1 (C7), 144.5 (C4), 128.2 (C3), 92.2 (C5), 67.6 (C6), 66.5 (C1), 20.8 (C8). **HRMS (ESI)** $C_8H_{10}O_5Na$ *m/z*: $[M+Na]^+$ 209.0416 (*calc* 209.0420).

The physical and spectroscopic data were found to be in agreement with Snider *et al.*[206]

(2-Acetoxy-5-oxo-5,6-dihydro-2*H*-pyran-2-yl)methyl acetate, 243

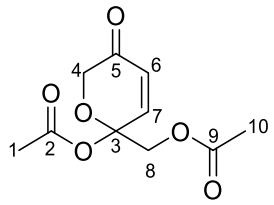

To a solution of **242** (1.34 g, 7.20 mmol, 1.0 eq) in dichloromethane (85 mL) was added acetic anhydride (14.4 mL, 152.3 mmol 20.0 eq), 4-dimethylaminopyridine (0.09 mL, 0.72 mmol, 0.1 eq), and pyridine (7.2 mL, 89.4 mmol, 12.5 eq) at 0 °C. The reaction was stirred for 30 min at 0 °C. This was then washed with 10% aq. $CuSO_4$ (50 mL), water (50 mL), sat. aq. $NaHCO_3$ (50 mL), and brine (50 mL). The organic layer was dried over anh. $MgSO_4$, filtered and concentrated *in vacuo* to give the pure product as an amorphous blood-red solid (1.3357 g, 5.85 mmol, 81%); **IR (thin film)** $\tilde{\nu}$/cm^{-1}: 1736 (C=O ester ,s), 1699 (c=O ketone, m), 1211 (C-O, s). **^{1}H NMR (400 MHz, $CDCl_3$)** δ/ppm: 7.22 (d, *J* = 10.5 Hz, 1H, H7), 6.21 (d, *J* = 10.5 Hz, 1H, H6), 4.59 (d, *J* = 17.0 Hz, 1H, H4a), 4.54 (d, *J* = 11.5 Hz, 1H, H8a), 4.42 (d, *J* = 11.5 Hz, 1H, H8b), 4.29 (d, *J* = 17.0 Hz, 1H, H4b), 2.09 (s, 3H, H1/10), 2.07 (s, 3H, H1/10). **^{13}C NMR (101 MHz, $CDCl_3$)** δ/ppm: 193.2 (C5), 170.1 (C2/9), 169.3 (C2/9), 143.3 (C7), 128.1 (C6), 97.3 (C3), 68.0 (C4), 65.0 (C8), 21.2 (C1/10), 20.7 (C1/10). **HRMS (ESI)** $C_{10}H_{12}O_6$ *m/z*: $[M+Na]^+$ 251.0519 (*calc.* 251.0526).

The physical and spectroscopic data were found to be in agreement with Snider *et al.*[206]

10,12-Dioxo-3,11-dioxatricyclo[5.3.1.1^{2,6}]dodeca-4,8-diene-4,7-diyl)bis(methylene) diacetate, 244

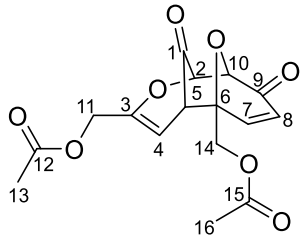

The title compound was isolated as a by-product from the reaction to synthesise **245**. Dark orange oil (30.1 mg, 0.09 mmol, 5%); **R_f** 0.12 (40% ethyl acetate in hexane); **IR (thin film)** $\tilde{\nu}$/cm^{-1}: 2977 (C-H, w), 1742 (C=O ester, s), 1698 (C=O ketone, s), 1223 (C-O, s). **^{1}H NMR (400 MHz, $CDCl_3$)** δ/ppm: 6.83 (d, *J* = 10.5 Hz, 1H, H7), 6.30 (d, *J* = 10.5 Hz, 1H, H8), 4.91 (d, *J* = 9.0 Hz,

1H, H4), 4.80–4.76 (m, 2H, H2&10), 4.44–4.25 (m, 4H, H11&14), 3.27 (dd, *J* = 7.5, 2.5 Hz, 1H, H5), 2.21 (s, 3H, H16), 2.09 (s, 3H, H13). **^{13}C NMR (101 MHz, $CDCl_3$)** δ/ppm: 198.3 (C1), 189.0 (C9), 170.4 (C15), 170.3 (C12), 150.8 (C3), 147.9 (C7), 129.6 (C8), 101.0 (C2), 81.5 (C4), 81.4 (C6), 75.9 (C10), 66.7 (C14), 61.7 (C11), 48.5 (C5), 20.8 (C13), 20.6 (C16). **HRMS (ESI)** $C_{16}H_{16}O_8Na$ *m/z*: $[M+Na]^+$ 359.0743 (*calc.* 359.0743).

The physical and spectroscopic data were found to be in agreement with Lee *et al*.[240]

L-(+)-Prolinol, 254

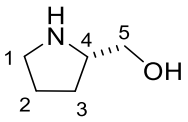

To a suspension of lithium aluminium hydride (2.47 g, 65.14 mmol, 15 eq) in THF (65 mL) was added portion-wise L-proline (5 g, 43.43 mmol, 1.0 eq) at 0 °C. The reaction was refluxed under nitrogen for 2h. This was cooled to RT and quenched with 20% aq. KOH (6.5 mL) the mixture was filtered and the residue was refluxed in THF for 45 min. This was filtered and combined to the previous filtrate and dried over $MgSO_4$. This was filtered and concentrated *in vacuo* to give the crude product. This was purified by vacuum distillation (77–78 °C, 5 mbar) to give the pure product as a colourless oil (3.95 g, 39.09 mmol, 90%); **IR (thin film)** $\tilde{\nu}$/cm^{-1}: 3294 (O-H, br s), 2869 (C-H, s), 1457 (C-H, m), 1047 (C-O, s). **^{1}H NMR (400 MHz, $(CD_3)_2SO$)** δ/ppm: 4.40 (br s, 1H, OH), 3.23 (d, *J* = 6.0 Hz, 2H, H5), 2.99 (qn, *J* = 6.0 Hz, 1H, H4), 2.80–2.75 (m, 1H, H1a), 2.72–2.66 (m, 1H, H1b), 1.71–1.54 (m, 3H, H3a&2), 1.35–1.27 (m, 1H, H3b). **^{13}C NMR (101 MHz, $(CD_3)_2SO$)** δ/ppm: 64.7 (C5), 59.7 (C4), 46.0 (C1), 27.9 (C3), 25.2 (C2). **HRMS (ESI)** $C_9H_4ClO_2$ *m/z*: $[M+H]^+$ 102.0913 (*calc.* 102.0913).

The physical and spectroscopic data was found to be in agreement with Widianti *et al*.[210]

1,3-Diiodoacetone, 256

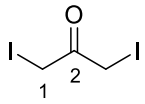

Sodium iodide (260.0 mg, 0.87 mmol, 2.2 eq) was dissolved in acetone (5 mL) and 1,3-dichloroacetone (100 mg, 0.79 mmol, 1.0 eq) was added. The reaction was stirred at RT for 1h before being filtered and concentrated to give the pure product as a pure yellow solid (197 mg, 0.64 mmol, 80%); **IR (thin film)** $\tilde{\nu}$/cm^{-1}: 1710 (C=O, s). **^{1}H NMR (400 MHz, $CDCl_3$)** δ/ppm: 4.11 (s, 4H, H1). **^{13}C NMR (101 MHz, $CDCl_3$)** δ/ppm: 195.6 (C2), 1.3 (C1).

The physical and spectroscopic data was found to be in agreement with Voronkov *et al.*[110]

tert-Butyl((1,3-dichloropropan-2-yl)oxy)dimethylsilane, 262

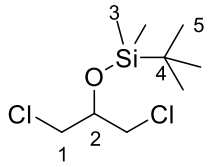

1,3-Dichloroisopropanol (2 mL, 11.48 mmol, 1.0 eq) and imidazole (1.17 g, 17.22 mmol, 1.5 eq) were dissolved in dichloromethane (35 mL). The mixture was cooled to 0 °C, *tert*-butyldimethylsilyl chloride (2.59 g, 17.22 mmol, 1.5 eq) was added, and the reaction was stirred overnight at RT. This was quenched by addition of sat. aq. NH_4Cl (30 mL). The layers were separated and the aqueous was extracted with diethyl ether (3 × 10 mL). The combind organics were washed with brine (30 mL), dried over anh. $MgSO_4$, filtered, and the excess solvent was removed *in vacuo* to give the crude product. This was purified by column chromatography (10% diethyl ether in pet. ether) to yield the pure product as a colourless oil (2.25 g, 9.29 mmol, 81%); **R_f** 0.76 (10% diethyl ether in pet. ether); **IR (thin film)** $\tilde{\nu}$/cm^{-1}: 2931 (C-H, w), 1107 (C-O, m), 775 (C-Cl, s). **^{1}H NMR (400 MHz, $CDCl_3$)** δ/ppm: 4.03 (qn, J = 5.5 Hz, 1H, H2), 3.62 (dd, J = 11.0, 5.5 Hz, 2H, H1a), 3.56 (dd, J = 11.0, 5.5 Hz, 2H, H1b), 0.91 (s, 9H, H5), 0.12 (s, 9H, H3). **^{13}C NMR (101 MHz, $CDCl_3$)** δ/ppm: 72.2 (C2), 45.9 (C1), 25.7 (C5), 18.1 (C4), –4.7 (C3). **HRMS (ESI)** $C_9H_{21}Cl_2SiO$ *m/z*: $[M+H]^+$ 243.0730 (*calc.* 243.0739).

The physical and spectroscopic data was found to be in agreement with Axenrod *et al.*[241]

(S)-(+)-4-Methylenehexahydro-1H,3H-pyrrolo[2,1-c][1,4]oxazepane, 266

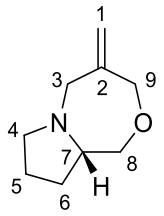

To a suspension of NaH (53% suspension in mineral oil, 1.86 g, 40.97 mmol, 2.0 eq) in THF (100 mL) at 0 °C under nitrogen L-prolinol (2 mL, 20.48 mmol, 1.0) was added dropwise. This was warmed to RT and stirred for 1 h. 3-Chloro-2-(chloromethyl)prop-1-ene (2.37 mL, 20.48 mmol, 1.0 eq) was added dropwise and reaction was stirred for 2 h at 60 °C. Afterwards it was cooled to RT and the excess solvent was removed *in vacuo*. This was diluted with ethyl acetate (50 mL) and washed sat. aq. NH_4Cl (30 mL). The aqueous was extracted with ethyl acetate (20 mL). The combined organics were dried over $MgSO_4$, filtered and concentrated *in vacuo* to give the crude product. This was purified by column chromatography (10% methanol in dichloromethane) to give the pure product as a colourless oil (1.1813 g, 7.71 mmol, 38%); $\mathbf{R_f}$ 0.35 (10% methanol in dichloromethane); **IR (thin film)** $\tilde{\nu}/cm^{-1}$: 2935 (C-H, m), 1643 (C=C, w), 1102 (C-O, s). **^{1}H NMR (400 MHz, $CDCl_3$)** δ/ppm: 4.89 (d, *J* = 14.0 Hz, 2H, H1), 4.34 (d, *J* = 14.0 Hz, 1H, H3a), 4.25 (d, *J* = 14.0 Hz, 1H, H3b), 3.90 (dd, *J* = 12.0, 2.5 Hz, 1H, H8a), 3.63 (d, *J* = 15.0 Hz, 1H, H9a), 3.27–3.21 (m, 2H, H8b&9b), 3.08–3.03 (m, 1H, H4a), 2.61–2.54 (m, 1H, H7), 2.43–2.37 (m, 1H, H4b), 1.92–1.68 (m, 3H, H6a&5), 1.40–1.31 (m, 1H, H6b). **^{13}C NMR (101 MHz, $CDCl_3$)** δ/ppm: 146.9 (C2), 111.8 (C1), 76.5 (C8), 74.9 (C3), 67.8 (C7), 58.5 (C9), 56.2 (C4), 27.2 (C6), 22.6 (C5). **HRMS (ESI)** $C_9H_{16}NO$ *m/z*: $[M+H]^+$ 154.1221 (*calc.* 154.1226). $[\boldsymbol{\alpha}]_{\mathbf{D}}^{\mathbf{20}}$ +110.0 (c = 1.00, $CHCl_3$).

References

1. Development & Approval Process (Drugs). at <https://www.fda.gov/Drugs/DevelopmentApprovalProcess/default.htm>

2. Hughes, J., Rees, S., Kalindjian, S. & Philpott, K. Principles of early drug discovery. *Br. J. Pharmacol.* **162,** 1239–1249 (2011).

3. Pickett, S. D., McLay, I. M. & Clark, D. E. Enhancing the Hit-to-Lead Properties of Lead Optimization Libraries. *J. Chem. Inf. Model.* **40,** 263–272 (2000).

4. Clinical trial phases | GSK UK. at <http://uk.gsk.com/en-gb/research/trials-in-people/clinical-trial-phases/>

5. Van Norman, G. A. Drugs, Devices, and the FDA: Part 1: An Overview of Approval Processes for Drugs. *JACC Basic to Transl. Sci.* **1,** 170–179 (2016).

6. Morgan, S., Grootendorst, P., Lexchin, J., Cunningham, C. & Greyson, D. The cost of drug development: A systematic review. *Health Policy (New. York).* **100,** 4–17 (2011).

7. DiMasi, J. A., Grabowski, H. G. & Hansen, R. W. Innovation in the pharmaceutical industry: New estimates of R&D costs. *J. Health Econ.* **47,** 20–33 (2016).

8. Martin, L., Hutchens, M., Hawkins, C. & Radnov, A. How much do clinical trials cost? *Nat. Rev. Drug Discov.* **16,** 381–382 (2017).

9. Collier, R. Rapidly rising clinical trial costs worry researchers. *CMAJ* **180,** 277–8 (2009).

10. Lo, C. Counting the cost of failure in drug development - Pharmaceutical Technology. *Pharmaceutical Technology* (2017). at <https://www.pharmaceutical-technology.com/features/featurecounting-the-cost-of-failure-in-drug-development-5813046/>

11. Arrowsmith, J. & Miller, P. Phase II and Phase III attrition rates 2011–2012. *Nat. Rev. Drug Discov.* **12,** 569–569 (2013).

12. Arrowsmith, J. Phase II failures: 2008–2010. *Nat. Rev. Drug Discov.* **10,** 328–329 (2011).

13. Arrowsmith, J. Phase III and submission failures: 2007–2010. *Nat. Rev. Drug Discov.* **10,**

87–87 (2011).

14. Hay, M., Thomas, D. W., Craighead, J. L., Economides, C. & Rosenthal, J. Clinical development success rates for investigational drugs. *Nat. Biotechnol.* **32,** 40–51 (2014).

15. Drummond, M. *Methods for the economic evaluation of health care programmes*. at <https://www.oupjapan.co.jp/en/node/8281>

16. Patents Act 1977. at <https://www.legislation.gov.uk/ukpga/1977/37>

17. Sams-Dodd, F. Is poor research the cause of the declining productivity of the pharmaceutical industry? An industry in need of a paradigm shift. *Drug Discov. Today* **18,** 211–217 (2013).

18. Bunnage, M. E. Getting pharmaceutical R&D back on target. *Nat. Chem. Biol.* **7,** 335–339 (2011).

19. Lipinski, C. A., Lombardo, F., Dominy, B. W. & Feeney, P. J. Experimental and computational approaches to estimate solubility and permeability in drug discovery and development settings. *Adv. Drug Deliv. Rev.* **46,** 3–26 (2001).

20. Lipinski, C. A. Lead- and drug-like compounds: the rule-of-five revolution. *Drug Discov. Today Technol.* **1,** 337–341 (2004).

21. Veber, D. F. *et al.* Molecular Properties That Influence the Oral Bioavailability of Drug Candidates. *J. Med. Chem.* **45,** 2615–2623 (2002).

22. Leeson, P. D. & Springthorpe, B. The influence of drug-like concepts on decision-making in medicinal chemistry. *Nat. Rev. Drug Discov.* **6,** 881–890 (2007).

23. Hughes, J. D. *et al.* Physiochemical drug properties associated with in vivo toxicological outcomes. *Bioorg. Med. Chem. Lett.* **18,** 4872–4875 (2008).

24. Wager, T. T. *et al.* Improving the Odds of Success in Drug Discovery: Choosing the Best Compounds for in Vivo Toxicology Studies. *J. Med. Chem.* **56,** 9771–9779 (2013).

25. Lovering, F., Bikker, J. & Humblet, C. Escape from Flatland: Increasing Saturation as an Approach to Improving Clinical Success. *J. Med. Chem.* **52,** 6752–6756 (2009).

26. Ritchie, T. J., Macdonald, S. J. F., Young, R. J. & Pickett, S. D. The impact of aromatic ring count on compound developability: further insights by examining carbo- and

hetero-aromatic and -aliphatic ring types. *Drug Discov. Today* **16,** 164–171 (2011).

27. Waring, M. J. *et al.* An analysis of the attrition of drug candidates from four major pharmaceutical companies. *Nat. Rev. Drug Discov.* **14,** 475–486 (2015).

28. Chu, K. A. & Yalkowsky, S. H. An interesting relationship between drug absorption and melting point. *Int. J. Pharm.* **373,** 24–40 (2009).

29. Thomas, V. H. *et al.* The road map to oral bioavailability: an industrial perspective. *Expert Opin. Drug Metab. Toxicol.* **2,** 591–608 (2006).

30. Macarron, R. *et al.* Impact of high-throughput screening in biomedical research. *Nat. Rev. Drug Discov.* **10,** 188–195 (2011).

31. Macarron, R. Critical review of the role of HTS in drug discovery. *Drug Discov. Today* **11,** 277–279 (2006).

32. Broach, J. R. & Thorner, J. High-throughput screening for drug discovery. *Nature* **384,** 14–6 (1996).

33. Eggeling, C., Brand, L., Ullmann, D. & Jäger, S. Highly sensitive fluorescence detection technology currently available for HTS. *Drug Discov. Today* **8,** 632–641 (2003).

34. Haber, C., Boillat, M. & Schoot, B. van der. Precise Nanoliter Fluid Handling System with Integrated High-Speed Flow Sensor. *Assay Drug Dev. Technol.* **3,** 203–212 (2005).

35. Basu, A. S. B. A. S. High Throughput Screening in Droplet Microreactors (Microfluidics at Interfaces). (2016). at <https://nanohub.org/resources/23770/about>

36. Perola, E. An Analysis of the Binding Efficiencies of Drugs and Their Leads in Successful Drug Discovery Programs. *J. Med. Chem.* **53,** 2986–2997 (2010).

37. Dorr, P. *et al.* Maraviroc (UK-427,857), a potent, orally bioavailable, and selective small-molecule inhibitor of chemokine receptor CCR5 with broad-spectrum anti-human immunodeficiency virus type 1 activity. *Antimicrob. Agents Chemother.* **49,** 4721–32 (2005).

38. Lahana, R. Who wants to be irrational? *Drug Discov. Today* **8,** 655–656 (2003).

39. Ashburn, T. T. & Thor, K. B. Drug repositioning: identifying and developing new uses for existing drugs. *Nat. Rev. Drug Discov.* **3,** 673–683 (2004).

40. Gribbon, P. & Andreas, S. High-throughput drug discovery: What can we expect from HTS? *Drug Discov. Today* **10,** 17–22 (2005).

41. Antibiotic resistance. at <http://www.who.int/en/news-room/fact-sheets/detail/antibiotic-resistance>

42. Chan, P. F., Holmes, D. J. & Payne, D. J. Finding the gems using genomic discovery: antibacterial drug discovery strategies – the successes and the challenges. *Drug Discov. Today Ther. Strateg.* **1,** 519–527 (2004).

43. Payne, D. J., Gwynn, M. N., Holmes, D. J. & Pompliano, D. L. Drugs for bad bugs: confronting the challenges of antibacterial discovery. *Nat. Rev. Drug Discov.* **6,** 29–40 (2007).

44. Weisbach, J. A. & Moos, W. H. Diagnosing the decline of major pharmaceutical research laboratories: A prescription for drug companies. *Drug Dev. Res.* **34,** 243–259 (1995).

45. Sams-Dodd, F. Target-based drug discovery: is something wrong? *Drug Discov. Today* **10,** 139–147 (2005).

46. Drews, J. & Ryser, S. Innovation Deficit in the Pharmaceutical Industry. *Drug Inf. J.* **30,** 97–108 (1996).

47. Silverman, R. B. From Basic Science to Blockbuster Drug: The Discovery of Lyrica. *Angew. Chemie Int. Ed.* **47,** 3500–3504 (2008).

48. Bohacek, R. S., McMartin, C. & Guida, W. C. The art and practice of structure-based drug design: A molecular modeling perspective. *Med. Res. Rev.* **16,** 3–50 (1996).

49. Ruddigkeit, L., van Deursen, R., Blum, L. C. & Reymond, J.-L. Enumeration of 166 Billion Organic Small Molecules in the Chemical Universe Database GDB-17. *J. Chem. Inf. Model.* **52,** 2864–2875 (2012).

50. Jencks, W. P. On the attribution and additivity of binding energies. *Proc. Natl. Acad. Sci. U. S. A.* **78,** 4046–50 (1981).

51. Price, A. J., Howard, S. & Cons, B. D. Fragment-based drug discovery and its application to challenging drug targets. *Essays Biochem.* **61,** 475–484 (2017).

52. Lamoree, B. & Hubbard, R. E. Current perspectives in fragment-based lead discovery

(FBLD). *Essays Biochem.* **61,** 453–464 (2017).

53. Scott, D. E., Coyne, A. G., Hudson, S. A. & Abell, C. Fragment-Based Approaches in Drug Discovery and Chemical Biology. *Biochemistry* **51,** 4990–5003 (2012).

54. Irwin, J. J. *et al.* An Aggregation Advisor for Ligand Discovery. *J. Med. Chem.* **58,** 7076–7087 (2015).

55. Klages, J., Coles, M. & Kessler, H. NMR-based screening: a powerful tool in fragment-based drug discovery. *Analyst* **132,** 692–705 (2007).

56. Hofstadler, S. A. & Sannes-Lowery, K. A. Applications of ESI-MS in drug discovery: interrogation of noncovalent complexes. *Nat. Rev. Drug Discov.* **5,** 585–595 (2006).

57. Vivat Hannah, V., Atmanene, C., Zeyer, D., Van Dorsselaer, A. & Sanglier-Cianférani, S. Native MS: an ESI, way to support structure- and fragment-based drug discovery. *Future Med. Chem.* **2,** 35–50 (2010).

58. Lea, W. A. & Simeonov, A. Fluorescence polarization assays in small molecule screening. *Expert Opin. Drug Discov.* **6,** 17–32 (2011).

59. Drinkwater, N. *et al.* Fragment-based screening by X-ray crystallography, MS and isothermal titration calorimetry to identify PNMT (phenylethanolamine N-methyltransferase) inhibitors. *Biochem. J.* **431,** 51–61 (2010).

60. Erlanson, D. A. in *Fragment-Based Drug Discovery and X-Ray Crystallography* (eds. Davies, T. G. & Hyvönen, M.) 1–32 (Springer, 2011). doi:10.1007/128_2011_180

61. Howard, N. *et al.* Application of Fragment Screening and Fragment Linking to the Discovery of Novel Thrombin Inhibitors. *J. Med. Chem.* **49,** 1346–1355 (2006).

62. Shuker, S. B., Hajduk, P. J., Meadows, R. P. & Fesik, S. W. Discovering High-Affinity Ligands for Proteins: SAR by NMR. *Science* **274,** 1531–1534 (1996).

63. Hung, A. W. *et al.* Application of Fragment Growing and Fragment Linking to the Discovery of Inhibitors of *Mycobacterium tuberculosis* Pantothenate Synthetase. *Angew. Chemie Int. Ed.* **48,** 8452–8456 (2009).

64. Erlanson, D. A., McDowell, R. S. & O'Brien, T. Fragment-Based Drug Discovery. *J. Med. Chem.* **47,** 3463–3482 (2004).

65. Hughes, S. J. *et al.* Fragment based discovery of a novel and selective PI3 kinase inhibitor. *Bioorg. Med. Chem. Lett.* **21,** 6586–6590 (2011).

66. Erlanson, D. A. *et al.* Site-directed ligand discovery. *Proc. Natl. Acad. Sci. U. S. A.* **97,** 9367–72 (2000).

67. Brough, P. A. *et al.* Combining Hit Identification Strategies: Fragment-Based and in Silico Approaches to Orally Active 2-Aminothieno[2,3-d]pyrimidine Inhibitors of the Hsp90 Molecular Chaperone. *J. Med. Chem.* **52,** 4794–4809 (2009).

68. Brear, P. *et al.* Novel non-ATP competitive small molecules targeting the CK2 α/β interface. *Bioorg. Med. Chem.* **26,** 3016–3020 (2018).

69. Potter, A. *et al.* Discovery of cell-active phenyl-imidazole Pin1 inhibitors by structure-guided fragment evolution. *Bioorg. Med. Chem. Lett.* **20,** 6483–6488 (2010).

70. Hann, M. M., Leach, A. R. & Harper, G. Molecular Complexity and Its Impact on the Probability of Finding Leads for Drug Discovery. *J. Chem. Inf. Model.* **41,** 856–864 (2001).

71. Congreve, M., Carr, R., Murray, C. & Jhoti, H. A 'Rule of Three' for fragment-based lead discovery? *Drug Discov. Today* **8,** 876–877 (2003).

72. Murray, C. W. & Rees, D. C. Opportunity Knocks: Organic Chemistry for Fragment-Based Drug Discovery (FBDD). *Angew. Chemie Int. Ed.* **55,** 488–492 (2016).

73. Erlanson, D. A., Fesik, S. W., Hubbard, R. E., Jahnke, W. & Jhoti, H. Twenty years on: the impact of fragments on drug discovery. *Nat. Rev. Drug Discov.* **15,** 605–619 (2016).

74. Taylor, R. D., MacCoss, M. & Lawson, A. D. G. Rings in Drugs. *J. Med. Chem.* **57,** 5845–5859 (2014).

75. Turnbull, A., Boyd, S. & Walse, B. Fragment-based drug discovery and protein-protein interactions. *Res. Reports Biochem.* **4,** 13 (2014).

76. Dang, C. V., Reddy, E. P., Shokat, K. M. & Soucek, L. Drugging the 'undruggable' cancer targets. *Nat. Rev. Cancer* **17,** 502–508 (2017).

77. McCormick, F. KRAS as a Therapeutic Target. *Clin. Cancer Res.* **21,** 1797–1801 (2015).

78. Whitfield, J. R., Beaulieu, M.-E. & Soucek, L. Strategies to Inhibit Myc and Their Clinical Applicability. *Front. Cell Dev. Biol.* **5,** 10 (2017).

79. Toogood, P. L. Inhibition of Protein−Protein Association by Small Molecules: Approaches and Progress. *J. Med. Chem.* **45,** 1543–1558 (2002).

80. Tse, C. *et al.* ABT-263: a potent and orally bioavailable Bcl-2 family inhibitor. *Cancer Res.* **68,** 3421–3428 (2008).

81. Petros, A. M. *et al.* Discovery of a Potent Inhibitor of the Antiapoptotic Protein Bcl-xL from NMR and Parallel Synthesis. *J. Med. Chem.* **49,** 656–663 (2006).

82. Trametinib and Navitoclax in Treating Patients With Advanced or Metastatic Solid Tumors - Full Text View - ClinicalTrials.gov. at <https://clinicaltrials.gov/ct2/show/NCT02079740>

83. Krystal, G. W., Sulanke, G., Litz, J. & Krystal, G. W. Inhibition of phosphatidylinositol 3-kinase-Akt signaling blocks growth, promotes apoptosis, and enhances sensitivity of small cell lung cancer cells to chemotherapy. *Mol. Cancer Ther.* **1,** 913–922 (2002).

84. Gandhi, L. *et al.* Phase I study of Navitoclax (ABT-263), a novel Bcl-2 family inhibitor, in patients with small-cell lung cancer and other solid tumors. *J. Clin. Oncol.* **29,** 909–916 (2011).

85. Burnett, G. & Kennedy, E. P. The enzymatic phosphorylation of proteins. *J. Biol. Chem.* **211,** 969–980 (1954).

86. Salvi, M., Sarno, S., Cesaro, L., Nakamura, H. & Pinna, L. A. Extraordinary pleiotropy of protein kinase CK2 revealed by weblogo phosphoproteome analysis. *Biochim. Biophys. Acta* **1793,** 847–859 (2009).

87. Pinna, L. A. & Allende, J. E. Protein Kinase CK2 in Health and Disease. *Cell. Mol. Life Sci.* **66,** 1795–1799 (2009).

88. CEA. CK2 Holoenzyme. (2015). at <https://www.google.com/url?sa=i&source=images&cd=&ved=2ahUKEwipjvL2nujfAhVyUBUIHV3RCFkQjRx6BAgBEAU&url=http%3A%2F%2Fbig.cea.fr%2Fdrf%2Fbig%2Fenglish%2FPages%2FBCI%2FKIN%2FResearch-activities.aspx&psig=AOvVaw0Kfo3_QZTGCOaZ-QYdEK6m&ust=1547382418388361>

89. Guerra, B. & Issinger, O.-G. Protein kinase CK2 and its role in cellular proliferation,

development and pathology. *Electrophoresis* **20,** 391–408 (1999).

90. Dominguez, I., Sonenshein, G. E. & Seldin, D. C. Protein Kinase CK2 in Health and Disease. *Cell. Mol. Life Sci.* **66,** 1850–1857 (2009).

91. Raaf, J., Brunstein, E., Issinger, O.-G. & Niefind, K. The interaction of CK2alpha and CK2beta, the subunits of protein kinase CK2, requires CK2beta in a preformed conformation and is enthalpically driven. *Protein Sci.* **17,** 2180–2186 (2008).

92. Guerra, B. & Issinger, O.-G. Protein Kinase CK2 in Human Diseases. *Curr. Med. Chem.* **15,** (2016).

93. Faust, R. A. *et al.* Subcellular immunolocalization of protein kinase CK2 in normal and carcinoma cells. *Int. J. Biochem. Cell Biol.* **31,** 941–949 (1999).

94. Ahmed, K., Gerber, D. A. & Cochet, C. Joining the cell survival squad: an emerging role for protein kinase CK2. *Trends Cell Biol.* **12,** 226–230 (2002).

95. Gapany, M. *et al.* Association of elevated protein kinase CK2 activity with aggressive behavior of squamous cell carcinoma of the head and neck. *Mol. Med.* **1,** 659–666 (1995).

96. Guo, C., Yu, S., Davis, A. T. & Ahmed, K. Nuclear matrix targeting of the protein kinase CK2 signal as a common downstream response to androgen or growth factor stimulation of prostate cancer cells. *Cancer Res.* **59,** 1146–1151 (1999).

97. Gleave, M. E. & Monia, B. P. Antisense therapy for cancer. *Nat. Rev. Cancer* **5,** 468–479 (2005).

98. Battistutta, R. Protein Kinase CK2 in Health and Disease. *Cell. Mol. Life Sci.* **66,** 1868–1889 (2009).

99. Fabian, M. A. *et al.* A small molecule–kinase interaction map for clinical kinase inhibitors. *Nat. Biotechnol.* **23,** 329–336 (2005).

100. Karaman, M. W. *et al.* A quantitative analysis of kinase inhibitor selectivity. *Nat. Biotechnol.* **26,** 127–132 (2008).

101. Zandomeni, R., Zandomeni, M. C., Shugar, D. & Weinmann, R. Casein kinase type II is involved in the inhibition by 5,6-dichloro-1-beta-D-ribofuranosylbenzimidazole of specific RNA polymerase II transcription. *J. Biol. Chem.* **261,** 3414–3419 (1986).

102. Meggio, F., Shugar, D. & Pinna, L. A. Ribofuranosyl-benzimidazole derivatives as inhibitors of casein kinase-2 and casein kinase-1. *Eur. J. Biochem.* **187,** 89–94 (1990).

103. Mishra, S. *et al.* Treatment of P190 Bcr/Abl lymphoblastic leukemia cells with inhibitors of the serine/threonine kinase CK2. *Leukemia* **21,** 178–180 (2007).

104. Meggio, F. *et al.* Inhibition of Protein Kinase CK2 by Condensed Polyphenolic Derivatives. An in Vitro and in Vivo Study. *Biochemistry* **43,** 12931–12936 (2004).

105. Pagano, M. A. *et al.* The selectivity of inhibitors of protein kinase CK2: an update. *Biochem. J.* **415,** 353–365 (2008).

106. Siddiqui-Jain, A. *et al.* CX-4945, an orally bioavailable selective inhibitor of protein kinase CK2, inhibits prosurvival and angiogenic signaling and exhibits antitumor efficacy. *Cancer Res.* **70,** 10288–10298 (2010).

107. Brear, P. *et al.* Specific inhibition of CK2α from an anchor outside the active site. *Chem. Sci.* **7,** 6839–6845 (2016).

108. Bogoyevitch, M. A. & Fairlie, D. P. A new paradigm for protein kinase inhibition: blocking phosphorylation without directly targeting ATP binding. *Drug Discov. Today* **12,** 622–633 (2007).

109. Parang, K. & Cole, P. A. Designing bisubstrate analog inhibitors for protein kinases. *Pharmacol. Ther.* **93,** 145–157 (2002).

110. Wójcik, P. & Berlicki, Ł. Peptide-based inhibitors of protein–protein interactions. *Bioorg. Med. Chem. Lett.* **26,** 707–713 (2016).

111. Raaf, J., Brunstein, E., Issinger, O.-G. & Niefind, K. The CK2α/CK2β Interface of Human Protein Kinase CK2 Harbors a Binding Pocket for Small Molecules. *Chem. Biol.* **15,** 111–117 (2008).

112. Pagano, M. A. *et al.* Modulation of Protein Kinase CK2 Activity by Fragments of CFTR Encompassing F508 May Reflect Functional Links with Cystic Fibrosis Pathogenesis. *Biochemistry* **47,** 7925–7936 (2008).

113. Laudet, B. *et al.* Structure-based design of small peptide inhibitors of protein kinase CK2 subunit interaction. *Biochem. J.* **408,** 363–73 (2007).

114. Laudet, B. *et al.* Identification of chemical inhibitors of protein-kinase CK2 subunit interaction. *Mol. Cell. Biochem.* **316,** 63–69 (2008).

115. Moucadel, V. *et al.* Antitumoral activity of allosteric inhibitors of Protein kinase CK2. *Oncotarget* **2,** 997–1010 (2011).

116. Pinna, L. A. Protein kinase CK2: a challenge to canons. *J. Cell Sci.* **115,** 3873–8 (2002).

117. Zhou, Y., Zhang, N., Chen, W., Zhao, L. & Zhong, R. Underlying mechanisms of cyclic peptide inhibitors interrupting the interaction of CK2α/CK2β: comparative molecular dynamics simulation studies. *Phys. Chem. Chem. Phys.* **18,** 9202–9210 (2016).

118. Seetoh, W., Stubbs, C., Dickson, C., Hyvönen, M., Matak-Vinković, D., & Abell, C. Research Data Supporting 'Achieving small–molecule disruption of the CK2α/CK2β protein–protein interaction within the protein kinase CK2 heterotetramer' https://doi.org/10.17863/CAM.189. at <https://www.repository.cam.ac.uk/handle/1810/256247>

119. Montavon, T. J. *et al.* [2+2+2] Cycloadditions of Siloxy Alkynes with 1,2-Diazines: From Reaction Discovery to Identification of an Antiglycolytic Chemotype. *Angew. Chemie Int. Ed.* **52,** 13576–13579 (2013).

120. Suzuki, N. *et al.* Immobilized 1,2-Bis(guanidinoalkyl)benzenes: Potentially Useful for the Purification of Arsenic-Polluted Water. *Synlett* **24,** 2510–2514 (2013).

121. Wiley, J. L., Smith, V. J., Chen, J., Martin, B. R. & Huffman, J. W. Synthesis and pharmacology of 1-alkyl-3-(1-naphthoyl)indoles: Steric and electronic effects of 4- and 8-halogenated naphthoyl substituents. *Bioorg. Med. Chem.* **20,** 2067–2081 (2012).

122. Dixon, E. A., Fischer, A. & Robinson, F. P. Preparation of a series of substituted fluoromethylnaphthalenes. *Can. J. Chem.* **59,** 2629–2641 (1981).

123. Giri, R. & Yu, J.-Q. Synthesis of 1,2- and 1,3-Dicarboxylic Acids via Pd(II)-Catalyzed Carboxylation of Aryl and Vinyl C−H Bonds. *J. Am. Chem. Soc.* **130,** 14082–14083 (2008).

124. North, A. Towards the total synthesis of Heronamide F. (University of Oxford, 2015).

125. Thorand, S. & Krause, N. Improved Procedures for the Palladium-Catalyzed Coupling of Terminal Alkynes with Aryl Bromides (Sonogashira Coupling). *J. Org. Chem.* **63,** 8551–8553 (1998).

126. Mamane, V., Hannen, P. & Fürstner, A. Synthesis of Phenanthrenes and Polycyclic Heteroarenes by Transition-Metal Catalyzed Cycloisomerization Reactions. *Chemistry* **10,** 4556–75 (2004).

127. Huang, X. & Fu, W.-J. Stereoselective Aminobromination of Alkylidenecyclopropanes with TsNH2 and NBS as Nitrogen and Bromine Sources: A Simple Access to γ-Bromohomoallylic Sulfonamides. *Synthesis (Stuttg).* **2006,** 1016–1020 (2006).

128. Kociolek, M., Straub, N. & Marton, E. Synthesis of β -Ketonitriles from 3-Bromoisoxazoles. *Lett. Org. Chem.* **2,** 280–282 (2005).

129. Irwin, J. J., Sterling, T., Mysinger, M. M., Bolstad, E. S. & Coleman, R. G. ZINC: A Free Tool to Discover Chemistry for Biology. *J. Chem. Inf. Model.* **52,** 1757–1768 (2012).

130. Xie, J.-S., Huang, C. Q., Fang, Y.-Y. & Zhu, Y.-F. A convenient synthesis of 1′-H-spiro-(indoline-3,4′-piperidine) and its derivatives. *Tetrahedron* **60,** 4875–4878 (2004).

131. Chambers, M. S. *et al.* Spiropiperidines as high-affinity, selective .sigma. ligands. *J. Med. Chem.* **35,** 2033–2039 (1992).

132. Čapková, K., Yoneda, Y., Dickerson, T. J. & Janda, K. D. Synthesis and structure–activity relationships of second-generation hydroxamate botulinum neurotoxin A protease inhibitors. *Bioorg. Med. Chem. Lett.* **17,** 6463–6466 (2007).

133. Yin, Z. *et al.* Discovery of Lead Compounds Targeting the Bacterial Sliding Clamp Using a Fragment-Based Approach. *J. Med. Chem.* **57,** 2799–2806 (2014).

134. Schreiber, S. L. Target-Oriented and Diversity-Oriented Organic Synthesis in Drug Discovery. *Science (80-.).* **287,** 1964–1969 (2000).

135. Spring, D. R. Diversity-oriented synthesis; a challenge for synthetic chemists. *Org. Biomol. Chem.* **1,** 3867 (2003).

136. Bender, A. *et al.* in *Chemical Genomics: Small Molecule Probes to Study Cellular Function* 47–60 (2006).

137. Sauer, W. H. B. & Schwarz, M. K. Molecular Shape Diversity of Combinatorial Libraries: A Prerequisite for Broad Bioactivity. *J. Chem. Inf. Model.* **43,** 987–1003 (2003).

138. Waldmann, H. & Janning, P. *Concepts and Case Studies in Chemical Biology*. (Wiley-VCH

Verlag, 2014).

139. Galloway, W. R. J. D., Isidro-Llobet, A. & Spring, D. R. Diversity-oriented synthesis as a tool for the discovery of novel biologically active small molecules. *Nat. Commun.* **1,** 1–13 (2010).

140. Collins, S., Bartlett, S., Nie, F., Sore, H. & Spring, D. Diversity-Oriented Synthesis of Macrocycle Libraries for Drug Discovery and Chemical Biology. *Synthesis (Stuttg).* **48,** 1457–1473 (2016).

141. Nie, F. *et al.* A Multidimensional Diversity-Oriented Synthesis Strategy for Structurally Diverse and Complex Macrocycles. *Angew. Chemie Int. Ed.* **55,** 11139–11143 (2016).

142. Guarnieri-Ibáñez, A. *et al.* Diversity-oriented synthesis of heterocycles and macrocycles by controlled reactions of oxetanes with α-iminocarbenes. *Chem. Sci.* **8,** 5713–5720 (2017).

143. Ciardiello, J. J., Stewart, H. L., Sore, H. F., Galloway, W. R. J. D. & Spring, D. R. A novel complexity-to-diversity strategy for the diversity-oriented synthesis of structurally diverse and complex macrocycles from quinine. *Bioorg. Med. Chem.* **25,** 2825–2843 (2017).

144. Tan, D. S. Diversity-oriented synthesis: exploring the intersections between chemistry and biology. *Nat. Chem. Biol.* **1,** 74–84 (2005).

145. Spandl, R. J., Bender, A. & Spring, D. R. Diversity-oriented synthesis; a spectrum of approaches and results. *Org. Biomol. Chem.* **6,** 1149 (2008).

146. Isidro-Llobet, A. *et al.* Diversity-oriented synthesis of macrocyclic peptidomimetics. *Proc. Natl. Acad. Sci. U. S. A.* **108,** 6793–8 (2011).

147. Galloway, W. R. J. D., Bender, A., Welch, M. & Spring, D. R. The discovery of antibacterial agents using diversity-oriented synthesis. *Chem. Commun.* 2446 (2009). doi:10.1039/b816852k

148. Burke, M. D. & Schreiber, S. L. A Planning Strategy for Diversity-Oriented Synthesis. *Angew. Chemie Int. Ed.* **43,** 46–58 (2004).

149. Oguri, H. & Schreiber, S. L. Skeletal Diversity via a Folding Pathway: Synthesis of Indole Alkaloid-Like Skeletons. *Org. Lett.* **7,** 47–50 (2005).

150. Burke, M. D., Berger, E. M. & Schreiber, S. L. A Synthesis Strategy Yielding Skeletally Diverse Small Molecules Combinatorially. *J. Am. Chem. Soc.* **126,** 14095–140104 (2004).

151. Mateu, N. *et al.* in *Chemical Biology No. 10* (eds. Westwood, N. J. & Nelson, A.) 6–42 (Royal Society of Chemistry, 2018).

152. Ibbeson, B. M. *et al.* Diversity-oriented synthesis as a tool for identifying new modulators of mitosis. *Nat. Commun.* **5,** 3155 (2014).

153. Lenci, E., Menchi, G., Guarna, A. & Trabocchi, A. Skeletal Diversity from Carbohydrates: Use of Mannose for the Diversity-Oriented Synthesis of Polyhydroxylated Compounds. *J. Org. Chem.* **80,** 2182–2191 (2015).

154. Kim, J. *et al.* Diversity-oriented synthetic strategy for developing a chemical modulator of protein–protein interaction. *Nat. Commun.* **7,** 13196 (2016).

155. Aldrich, L. N. *et al.* Discovery of a Small-Molecule Probe for V-ATPase Function. *J. Am. Chem. Soc.* **137,** 5563–5568 (2015).

156. Kuo, S.-Y. *et al.* Small-molecule enhancers of autophagy modulate cellular disease phenotypes suggested by human genetics. *Proc. Natl. Acad. Sci.* **112,** E4281–E4287 (2015).

157. Kato, N. *et al.* Diversity-oriented synthesis yields novel multistage antimalarial inhibitors. *Nature* **538,** 344–349 (2016).

158. Heidebrecht, R. W. *et al.* Diversity-Oriented Synthesis Yields a Novel Lead for the Treatment of Malaria. *ACS Med. Chem. Lett.* **3,** 112–117 (2012).

159. Wyatt, E. E. *et al.* Skeletal diversity construction via a branching synthetic strategy. *Chem. Commun.* 3296 (2006). doi:10.1039/b607710b

160. Wyatt, E. E. *et al.* Identification of an anti-MRSA dihydrofolate reductase inhibitor from a diversity-oriented synthesis. *Chem. Commun.* 4962 (2008). doi:10.1039/b812901k

161. Robinson, A., Thomas, G. L., Spandl, R. J., Welch, M. & Spring, D. R. Gemmacin B: bringing diversity back into focus. *Org. Biomol. Chem.* **6,** 2978 (2008).

162. Hajduk, P. J., Galloway, W. R. J. D. & Spring, D. R. Drug discovery: A question of library design. *Nature* **470,** 42–43 (2011).

163. Aldeghi, M., Malhotra, S., Selwood, D. L. & Chan, A. W. E. Two- and Three-dimensional Rings in Drugs. *Chem. Biol. Drug Des.* **83,** 450–461 (2014).

164. Hajduk, P. J. & Greer, J. A decade of fragment-based drug design: strategic advances and lessons learned. *Nat. Rev. Drug Discov.* **6,** 211–219 (2007).

165. Murray, C. W. & Rees, D. C. The rise of fragment-based drug discovery. *Nat. Chem.* **1,** 187–192 (2009).

166. Ritchie, T. J. & Macdonald, S. J. F. The impact of aromatic ring count on compound developability – are too many aromatic rings a liability in drug design? *Drug Discov. Today* **14,** 1011–1020 (2009).

167. Clemons, P. A. *et al.* Small molecules of different origins have distinct distributions of structural complexity that correlate with protein-binding profiles. *Proc. Natl. Acad. Sci. U. S. A.* **107,** 18787–92 (2010).

168. Clemons, P. A. *et al.* Quantifying structure and performance diversity for sets of small molecules comprising small-molecule screening collections. *Proc. Natl. Acad. Sci. U. S. A.* **108,** 6817–22 (2011).

169. Zheng, Y., Tice, C. M. & Singh, S. B. The use of spirocyclic scaffolds in drug discovery. *Bioorg. Med. Chem. Lett.* **24,** 3673–82 (2014).

170. Marson, C. M. New and unusual scaffolds in medicinal chemistry. *Chem. Soc. Rev.* **40,** 5514–33 (2011).

171. Müller, G., Berkenbosch, T., Benningshof, J. C. J., Stumpfe, D. & Bajorath, J. Charting Biologically Relevant Spirocyclic Compound Space. *Chem. - A Eur. J.* **23,** 703–710 (2017).

172. Wang, Y. *et al.* Discovery and Optimization of Potent GPR40 Full Agonists Containing Tricyclic Spirocycles. *ACS Med. Chem. Lett.* **4,** 551–555 (2013).

173. Grubbs, R. H., Miller, S. J. & Fu, G. C. Ring-Closing Metathesis and Related Processes in Organic Synthesis. *Acc. Chem. Res.* **28,** 446–452 (1995).

174. Scholl, M., Ding, S., Lee, C. W. & Grubbs, R. H. Synthesis and Activity of a New Generation of Ruthenium-Based Olefin Metathesis Catalysts Coordinated with 1,3-Dimesityl-4,5-dihydroimidazol-2-ylidene Ligands. *Org. Lett.* **1,** 953–956 (1999).

175. Nun, P., Pérez, V., Calmès, M., Martinez, J. & Lamaty, F. Preparation of Chiral Amino Esters by Asymmetric Phase-Transfer Catalyzed Alkylations of Schiff Bases in a Ball Mill. *Chem. - A Eur. J.* **18,** 3773–3779 (2012).

176. Wilson, G. O. *et al.* Stability of Second Generation Grubbs' Alkylidenes to Primary Amines: Formation of Novel Ruthenium-Amine Complexes. *Adv. Synth. Catal.* **351,** 1817–1825 (2009).

177. Heravi, M. M., Zadsirjan, V. & Farajpour, B. Applications of oxazolidinones as chiral auxiliaries in the asymmetric alkylation reaction applied to total synthesis. *RSC Adv.* **6,** 30498–30551 (2016).

178. Monnier, F. & Taillefer, M. Catalytic C-C, C-N, and C-O Ullmann-Type Coupling Reactions. *Angew. Chemie Int. Ed.* **48,** 6954–6971 (2009).

179. Klapars, A., Huang, X. & Buchwald, S. L. A General and Efficient Copper Catalyst for the Amidation of Aryl Halides. *J. Am. Chem. Soc.* **124,** 7421–7428 (2002).

180. Chen, Y.-J. & Chen, H.-H. 1,1,1-Tris(hydroxymethyl)ethane as a New, Efficient, and Versatile Tripod Ligand for Copper-Catalyzed Cross-Coupling Reactions of Aryl Iodides with Amides, Thiols, and Phenols. *Org. Lett.* **8,** 5609–5612 (2006).

181. Li, J., Zhang, Y., Jiang, Y. & Ma, D. CuI/N,N-dimethylglycine-catalyzed synthesis of N-aryloxazolidinones from aryl bromides. *Tetrahedron Lett.* **53,** 3981–3983 (2012).

182. McNulty, J. & Calzavara, J. Tandem oxidative radical fragmentation–rearrangement of 2-amino-1,3-benzylidene acetals: a short entry to densely functionalised fully differentiated oxazolidinones. *RSC Adv.* **3,** 6771 (2013).

183. Chen, X., Chen, J. & Zhu, J. Synthetic Studies on Ecteinascidin 743 (Et 743): Asymmetric Synthesis of a Highly Oxygenated Tetrahydroisoquinoline via a Key Phenolic Mannich Reaction. *Synthesis (Stuttg).* **2006,** 4081–4086 (2006).

184. Dugar, S. *et al.* A Concise and Efficient Synthesis of Substituted Morpholines. *Synthesis (Stuttg).* **47,** 712–720 (2014).

185. Rombouts, F. J. R. *et al.* 1,4-Oxazine β-Secretase 1 (BACE1) Inhibitors: From Hit Generation to Orally Bioavailable Brain Penetrant Leads. *J. Med. Chem.* **58,** 8216–8235 (2015).

186. Mo, X., Li, Q. & Ju, J. Naturally occurring tetramic acid products: isolation, structure elucidation and biological activity. *RSC Adv.* **4,** 50566–50593 (2014).

187. Hosseini, M., Kringelum, H., Murray, A. & Tønder, J. E. Dipeptide Analogues Containing 4-Ethoxy-3-pyrrolin-2-ones. *Org. Lett.* **8,** 2103–2106 (2006).

188. Lee, C.-W. *et al.* Stereoselective Synthesis of Spiropiperidines as BACE-1 Aspartyl Protease Inhibitors via Late Stage *N* -Arylation of a 1,8-Diazaspiro[4.5]dec-3-en-2-one Pharmacophore. *J. Org. Chem.* **78,** 2661–2669 (2013).

189. Ihlefeld, A. & Margaretha, P. Synthesis and Photochemistry of 5,5-Dimethyl-1H-pyrrol-2(5H)-one and of SomeN-Substituted Derivatives. *Helv. Chim. Acta* **75,** 1333–1340 (1992).

190. Jeffries, D. E. & Lindsley, C. W. Total Synthesis and Biological Evaluation of Hybrubin A. *J. Org. Chem.* **82,** 431–437 (2017).

191. Cesar, J. & Sollner Dolenc, M. Trimethylsilyldiazomethane in the preparation of diazoketones via mixed anhydride and coupling reagent methods: a new approach to the Arndt–Eistert synthesis. *Tetrahedron Lett.* **42,** 7099–7102 (2001).

192. Jacobi, P. A., Murphree, S., Rupprecht, F. & Zheng, W. Formal Total Syntheses of the β-Lactam Antibiotics Thienamycin and PS-5. *J. Org. Chem.* **61,** 2413–2427 (1996).

193. Wessig, P. & Schwarz, J. A Convenient One-Pot Conversion of N-Boc-β-Aminoalcohols into N-Boc-Aziridines. *Synlett* **8,** 893–894 (1997).

194. IUPAC Gold Book. *IUPAC Compendium of Chemical Terminology* doi:10.1351/goldbook.C01496

195. Geittner, J., Huisgen, R. & Sustmann, R. Kinetics of 1,3-dipolar cycloaddition reactions of diazomethane; A correlation with homo-lumo energies. *Tetrahedron Lett.* **18,** 881–884 (1977).

196. Huisgen, R., Szeimies, G. & Möbius, L. 1,3-Dipolare Cycloadditionen, XXXII. Kinetik der Additionen organischer Azide an CC-Mehrfachbindungen. *Chem. Ber.* **100,** 2494–2507 (1967).

197. Williamson, D. G. & Cvetanovic, R. J. Rates of ozone-olefin reactions in carbon tetrachloride solutions. *J. Am. Chem. Soc.* **90,** 3668–3672 (1968).

198. Bateson, J. H., Southgate, R., Tyler, J. W. & Fell, S. C. M. Olivanic acid analogues. Part 4. Cycloaddition reactions of p-nitrobenzyl 7-oxo-1-azabicyclo[3.2.0]hept-2-ene-2-carboxylate, and synthesis of the 8-oxo-1-azatricyclo[4.2.0.02,4]octane-2-carboxylate system. *J. Chem. Soc. Perkin Trans. 1* 973 (1986). doi:10.1039/p19860000973

199. Bégis, G., Cladingboel, D. E., Jerome, L., Motherwell, W. B. & Sheppard, T. D. Asymmetric Synthesis of Aminocyclopropanes and *N* -Cyclopropylamino Alcohols Through Direct Amidocyclopropanation of Alkenes Using Chiral Organozinc Carbenoids. *European J. Org. Chem.* **2009,** 1532–1548 (2009).

200. Loke, I. *et al.* Influence of steric parameters on the synthesis of tetramates from α-amino-β-alkoxy-esters and Ph3PCCO. *Tetrahedron* **68,** 697–704 (2012).

201. Li, D. B., Rogers-Evans, M. & Carreira, E. M. Construction of Multifunctional Modules for Drug Discovery: Synthesis of Novel Thia/Oxa-Azaspiro[3.4]octanes. *Org. Lett.* **15,** 4766–4769 (2013).

202. Troyer, T. L., Muchalski, H., Hong, K. B. & Johnston, J. N. Origins of Selectivity in Brønsted Acid-Promoted Diazoalkane−Azomethine Reactions (The Aza-Darzens Aziridine Synthesis). *Org. Lett.* **13,** 1790–1792 (2011).

203. Wathier, M. *et al.* A Large-Molecular-Weight Polyanion, Synthesized via Ring-Opening Metathesis Polymerization, as a Lubricant for Human Articular Cartilage. *J. Am. Chem. Soc.* **135,** 4930–4933 (2013).

204. Santos, D. A. dos *et al.* Niobium(V) Chloride as Catalyst in Diels-Alder Reaction of Furan Ring. *J. Braz. Chem. Soc.* **25,** 882–886 (2014).

205. Asaoka, M., Ishibashi, K., Takahashi, W. & Takei, H. Synthesis of Sterically Hindered Bicyclo[2.2.2]octanes by Lewis Acid Catalyzed Reaction of 2-(Trimethylsiloxy)-1,3-cyclohexadienes with 4-Methyl-3-penten-2-one. *Bull. Chem. Soc. Jpn.* **60,** 2259–2260 (1987).

206. Snider, B. B. & Grabowski, J. F. Synthesis of the 5-hydroxymethyl-6-aryl-8-oxabicyclo[3.2.1]oct-3-en-2-one natural products descurainin and cartorimine. *Tetrahedron* **62,** 5171–5177 (2006).

207. Kaneko, S. *et al.* Synthesis and evaluation of N-substituted 1,4-oxazepanyl sordaricins

as selective fungal EF-2 inhibitors. *Bioorg. Med. Chem. Lett.* **12,** 1705–1708 (2002).

208. Campiani, G. *et al.* Pyrrolobenzothiazepinones and Pyrrolobenzoxazepinones: Novel and Specific Non-Nucleoside HIV-1 Reverse Transcriptase Inhibitors with Antiviral Activity. *J. Med. Chem.* **39,** 2672–2680 (1996).

209. Robl, J. A., Simpkins, L. M. & Asaad, M. M. N-Formyl hydroxylamine containing dipeptides: generation of a new class of vasopeptidase inhibitors. *Bioorg. Med. Chem. Lett.* **10,** 257–260 (2000).

210. Widianti, T., Hiraga, Y., Kojima, S. & Abe, M. Novel cyclic β-aminophosphonate derivatives as efficient organocatalysts for the asymmetric Michael addition reactions of ketones to nitrostyrenes. *Tetrahedron: Asymmetry* **21,** 1861–1868 (2010).

211. Yang, D. & Zhang, C. Ruthenium-Catalyzed Oxidative Cleavage of Olefins to Aldehydes. *J. Org. Chem.* **66,** 4814–4818 (2001).

212. Colomer, I. *et al.* A divergent synthetic approach to diverse molecular scaffolds: assessment of lead-likeness using LLAMA, an open-access computational tool. *Chem. Commun.* **52,** 7209–7212 (2016).

213. Balsamini, C. *et al.* 4,5-Dihydroisoxazole and 4,5-dihydro-1,2,4-oxadiazole derivatives from cycloaddition reactions of nitrile oxides to alkyl *N* -(diphenylmethylene)-α,β-dehydroamino acids. *J. Heterocycl. Chem.* **29,** 1593–1598 (1992).

214. Top 200 Drugs | Fabian Weber. at <http://fabian-weber.eu/top-200-drugs/>

215. Seebach, D., Aebi, J. D., Gander-Coquoz, M. & Naef, R. Stereoselektive Alkylierung an C von Serin, Glycerinsure, Threonin und Weinsure ber heterocyclische Enolate mit exocyclischer Doppelbindung. *Helv. Chim. Acta* **70,** 1194–1216 (1987).

216. Rosowsky, A., Dey, A. S., Battaglia, J. & Modest, E. J. Synthesis of 2,4-diamino-9 *H* -indeno[2,1- *d*]pyrimidines. *J. Heterocycl. Chem.* **6,** 613–622 (1969).

217. Levy, L. A. The Synthesis Of 2,3,6,7-Tetrasubstituted Naphthalenes: 2,3,6,7-Tetrachloronaphthalene. *Synth. Commun.* **13,** 639–648 (2006).

218. DiLauro, A. M., Lewis, G. G. & Phillips, S. T. Self-Immolative Poly(4,5-dichlorophthalaldehyde) and its Applications in Multi-Stimuli-Responsive Macroscopic Plastics. *Angew. Chemie Int. Ed.* **54,** 6200–6205 (2015).

219. Hennessy, E. J. & Buchwald, S. L. Synthesis of 4,5-Dianilinophthalimide and Related Analogues for Potential Treatment of Alzheimer's Disease via Palladium-Catalyzed Amination. *J. Org. Chem.* **70,** 7371–7375 (2005).

220. Sun, X., Shan, G., Sun, Y. & Rao, Y. Regio- and Chemoselective C□H Chlorination/Bromination of Electron-Deficient Arenes by Weak Coordination and Study of Relative Directing-Group Abilities. *Angew. Chemie Int. Ed.* **52,** 4440–4444 (2013).

221. Soleimani, E., Yazdani, H. & Saei, P. *Synthesis of spiro 3-bromo-4,5-dihydroisoxazoles via [1,3]dipolar cycloaddition reactions*. *Tetrahedron Letters* **56,** (2015).

222. Yatvin, J., Brooks, K. & Locklin, J. SuFEx on the Surface: A Flexible Platform for Postpolymerization Modification of Polymer Brushes. *Angew. Chemie Int. Ed.* **54,** 13370–13373 (2015).

223. Tantry, S. J. *et al. Whole cell screen based identification of spiropiperidines with potent antitubercular properties*. *Bioorganic & Medicinal Chemistry Letters* **25,** (2015).

224. Chan, C. Y. & Barnard, P. J. Rhenium complexes of bidentate, bis-bidentate and tridentate N-heterocyclic carbene ligands. *Dalt. Trans.* **44,** 19126–19140 (2015).

225. Evans, V., Mahon, M. F. & Webster, R. L. A mild, copper-catalysed amide deprotection strategy: use of tert-butyl as a protecting group. *Tetrahedron* **70,** 7593–7597 (2014).

226. Hiroshi Ueno *et al.* Synthesis and Structure−Activity Relationships of Novel Selective Factor Xa Inhibitors with a Tetrahydroisoquinoline Ring. *J. Med. Chem.* **48,** 3586–3604 (2005).

227. Mukherjee, D. K. & Ghosh, N. Enantioselective phase transfer alkylation using orthopalladated complex in chiral ionic liquid. *Catal. Commun.* **9,** 40–44 (2008).

228. Andrei, D. & Wnuk, S. F. S-Adenosylhomocysteine Analogues with the Carbon-5′ and Sulfur Atoms Replaced by a Vinyl Unit. *Org. Lett.* **8,** 5093–5096 (2006).

229. Jam, F., Tullberg, M., Luthman, K. & Grøtli, M. Microwave assisted synthesis of spiro-2,5-diketopiperazines. *Tetrahedron* **63,** 9881–9889 (2007).

230. Berger, O. *et al.* Reverse-benzamidine antimalarial agents: Design, synthesis, and biological evaluation. *Bioorg. Med. Chem. Lett.* **20,** 5815–5817 (2010).

231. Tang, R., Yan, Z. & Luo, Y. Synthesis of o-L-α-glycerylphosphoryl-L-serine. *J. Cent. South Univ. Technol.* **12,** 693–698 (2005).

232. Ramesh, R., De, K. & Chandrasekaran, S. An efficient synthesis of dehydroamino acids and dehydropeptides from O-Cbz and O-Eoc derivatives of serine and threonine. *Tetrahedron* **63,** 10534–10542 (2007).

233. Castellano, S. *et al.* Synthesis and Biochemical Evaluation of Δ^2-Isoxazoline Derivatives as DNA Methyltransferase 1 Inhibitors. *J. Med. Chem.* **54,** 7663–7677 (2011).

234. Yoshimura, M., Shibata, N., Kawakami, M. & Sakaguchi, S. Ligand design for dual enantioselective control in Cu-catalyzed asymmetric conjugate addition of R2Zn to cyclic enone. *Tetrahedron* **68,** 3512–3518 (2012).

235. Paz, J., Pérez-Balado, C., Iglesias, B. & Muñoz, L. Carbon Dioxide as a Carbonylating Agent in the Synthesis of 2-Oxazolidinones, 2-Oxazinones, and Cyclic Ureas: Scope and Limitations. *J. Org. Chem.* **75,** 3037–3046 (2010).

236. Robertson, J. *et al.* Radical 1,4-aryl transfer in arylcarboxamides leading to phthalimides, biaryls and enantiomerically enriched β-arylethylamines. *Tetrahedron* **64,** 11896–11907 (2008).

237. Braga, A. L., Lüdtke, D. S., Sehnem, J. A. & Alberto, E. E. Modular chiral selenium-containing oxazolines: synthesis and application in the palladium-catalyzed asymmetric allylic alkylation. *Tetrahedron* **61,** 11664–11671 (2005).

238. Hakimelahi, G. H. & Jarrahpour, A. A. Synthesis of ethylcis 2-[(Diethoxyphosphoryl)methyl]-7-oxo-3-phenyl-6-phthalimido-l-azabicyclo[3.2.0]hept-3-ene-2-carboxylate and Methylcis-2-Bromo-3-methyl-8-oxo-7-phthalimido-4-oxa-1-azabicyclo[4.2.0]octane-2-carboxylate. *Helv. Chim. Acta* **72,** 1501–1505 (1989).

239. Collier, P. N. The synthesis of 3-aryl-3-azetidinyl acetic acid esters by rhodium(I)-catalysed conjugate addition of organoboron reagents. *Tetrahedron Lett.* **50,** 3909–3911 (2009).

240. Lee, H.-Y., Kim, H., Kim, B. & Kee, J. The Stereoselective Dimerization Reaction of Oxidopyrylium Ions. *Synthesis (Stuttg).* **2007,** 2360–2364 (2007).

241. Axenrod, T., Watnick, C., Yazdekhasti, H. & Dave, P. R. Synthesis of 1,3,3-

Trinitroazetidine via the Oxidative Nitrolysis of N-p-Tosyl-3-azetidinone Oxime. *J. Org. Chem.* **60,** 1959–1964 (1995).

Appendix A

Spectra

2,2′-(4,5-Dichloro-1,2-phenylene)bis(ethan-1-aminium) dichloride, 29

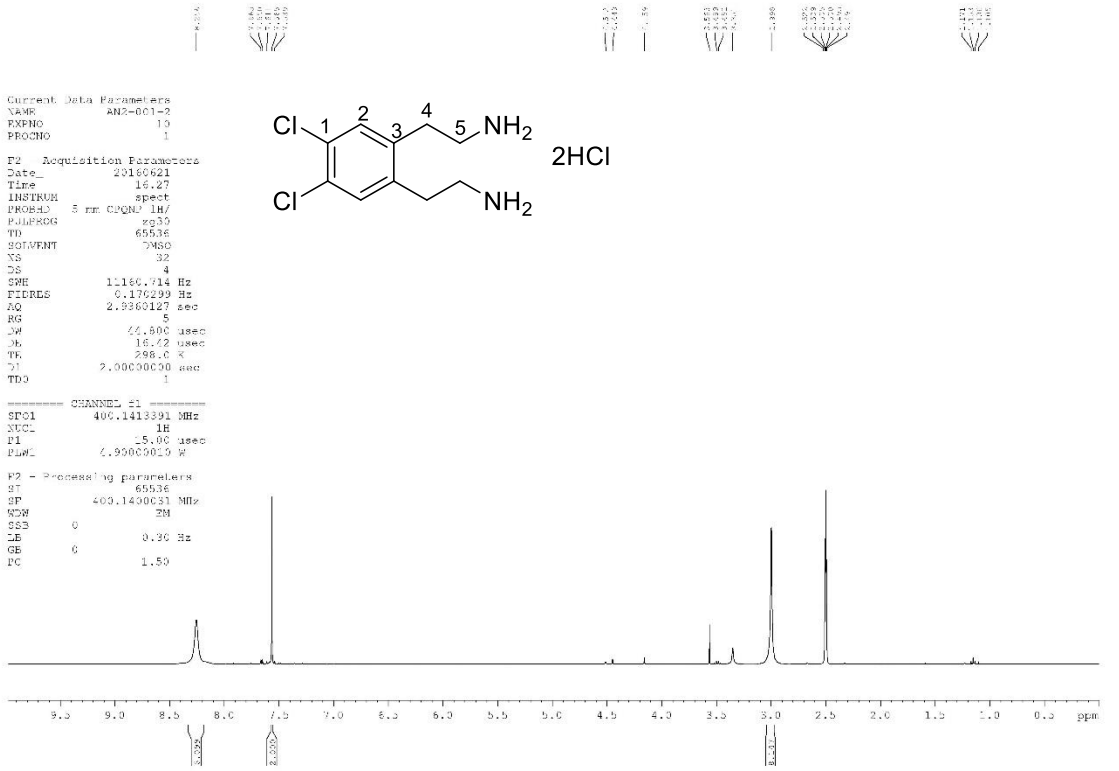

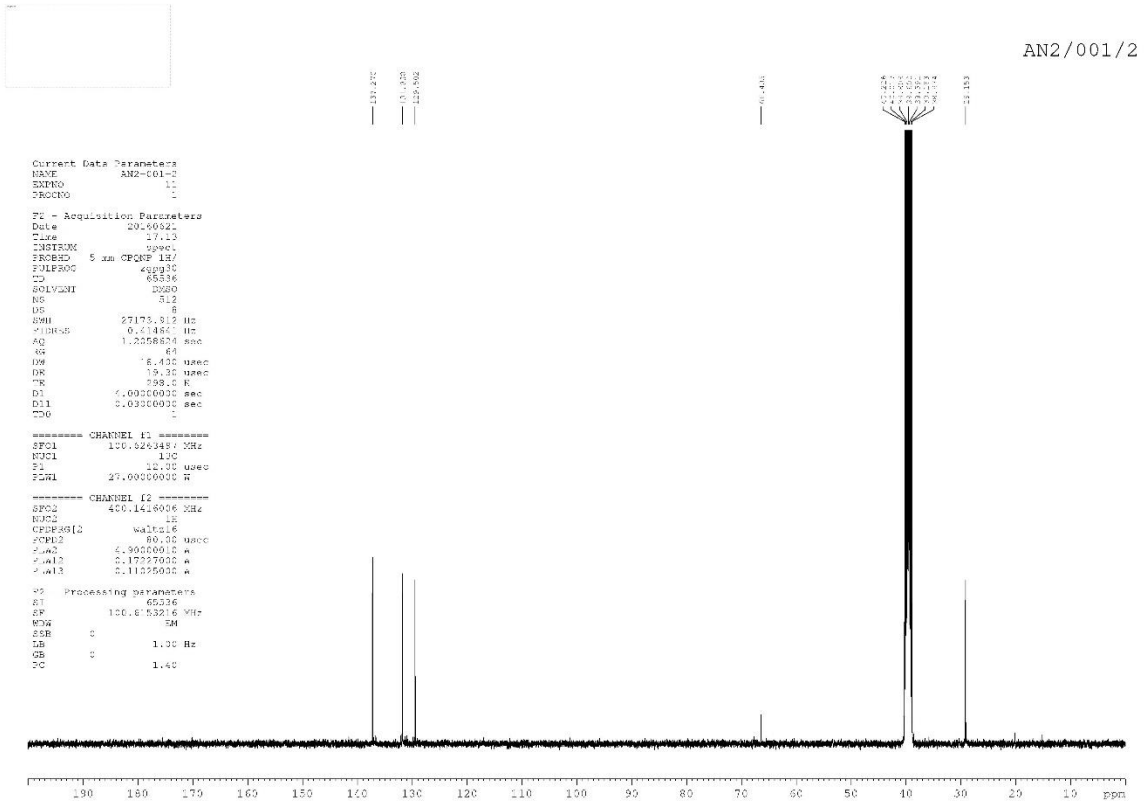

2,2′-(4,5-Dichloro-1,2-phenylene)diacetonitrile, 30

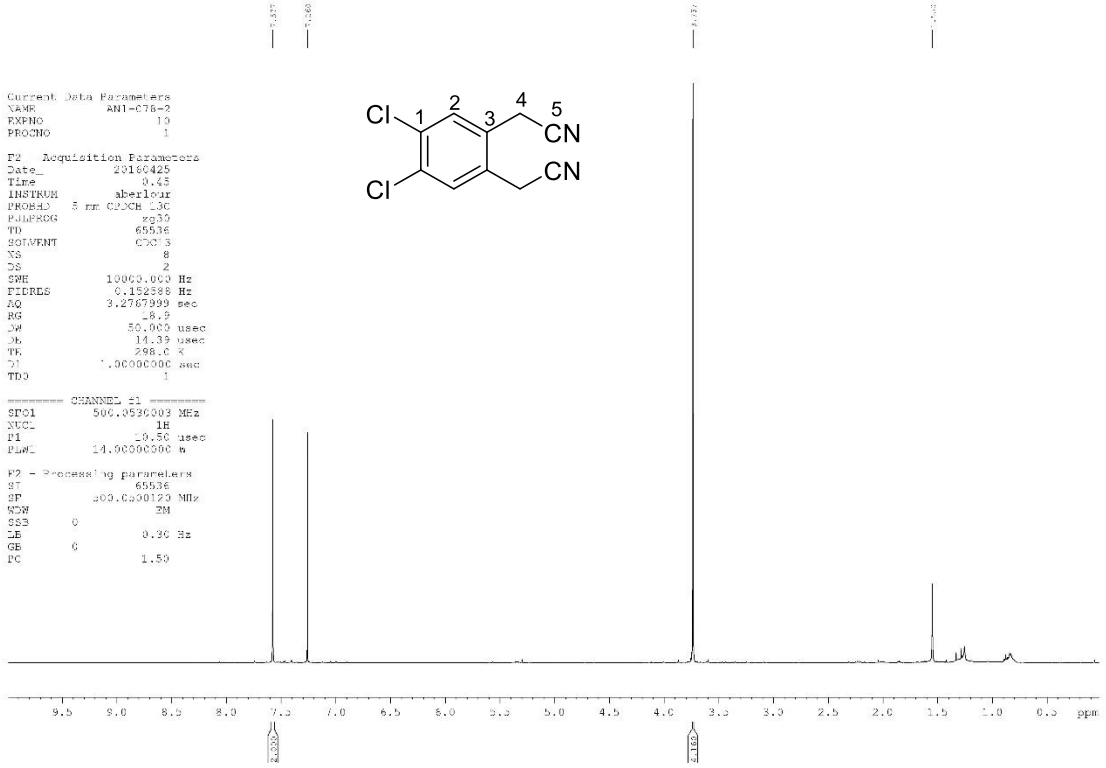

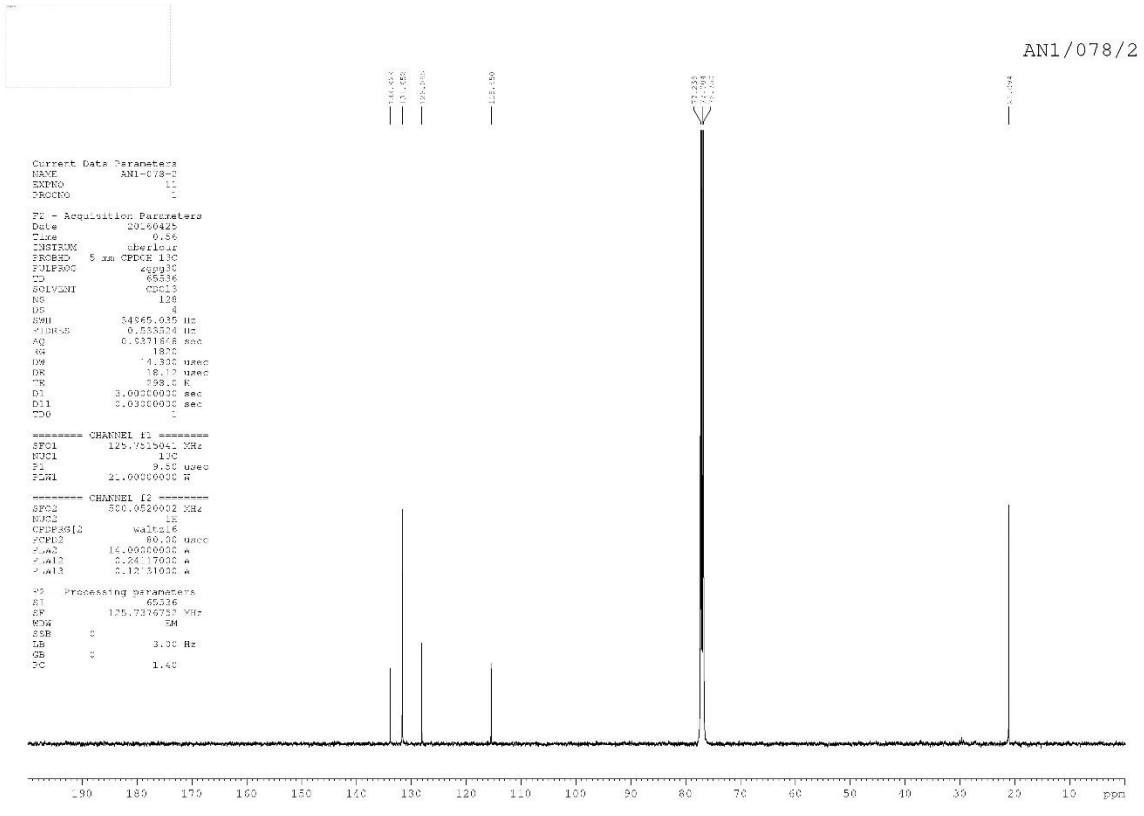

1,2-Bis(bromomethyl)-4,5-dichlorobenzene, 31

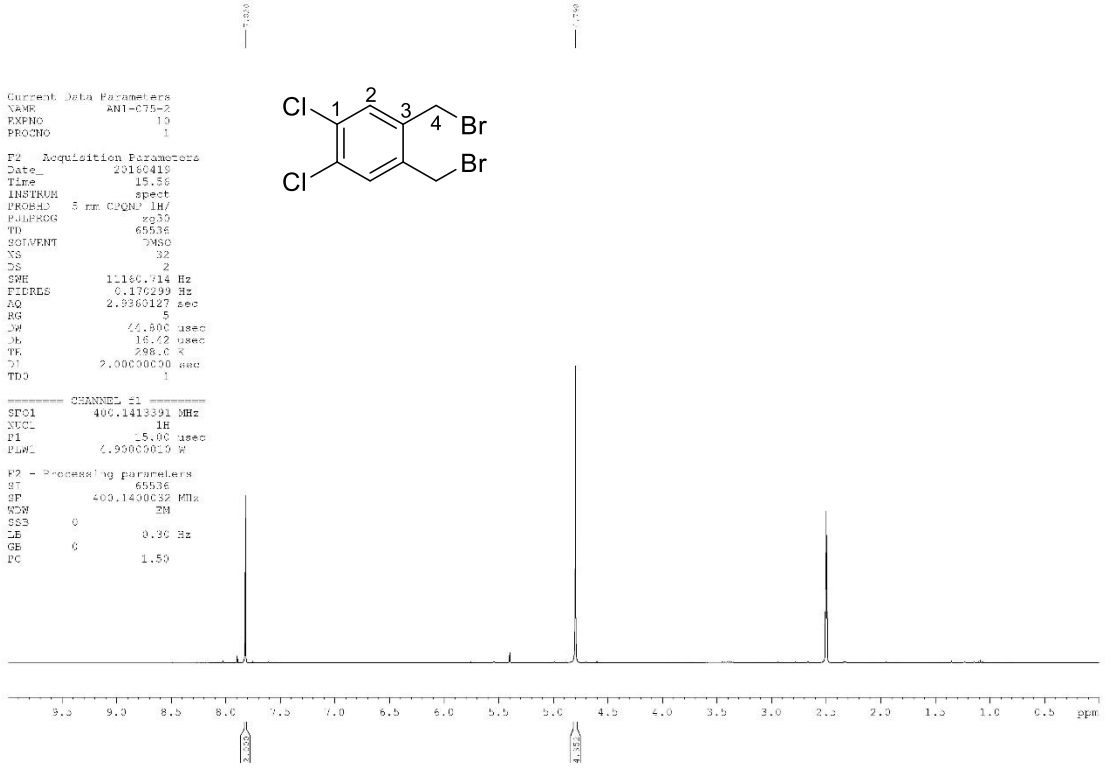

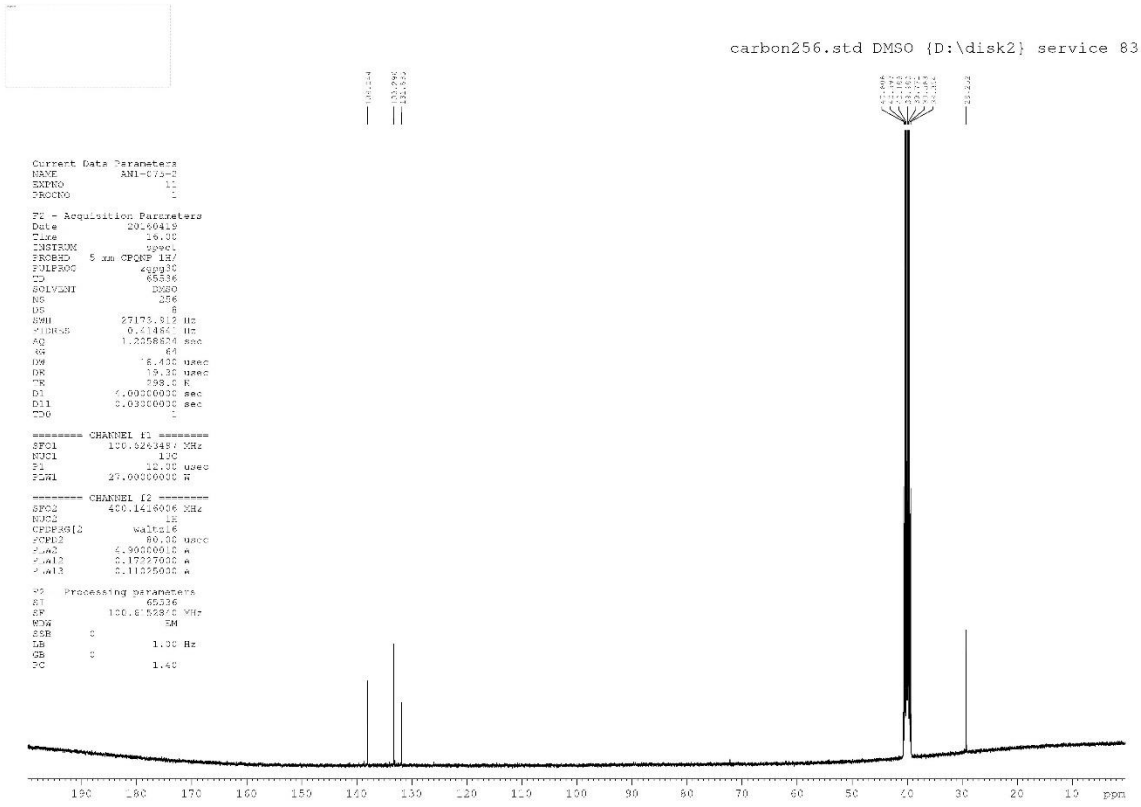

(4,5-Dichloro-1,2-phenylene)dimethanol, 32

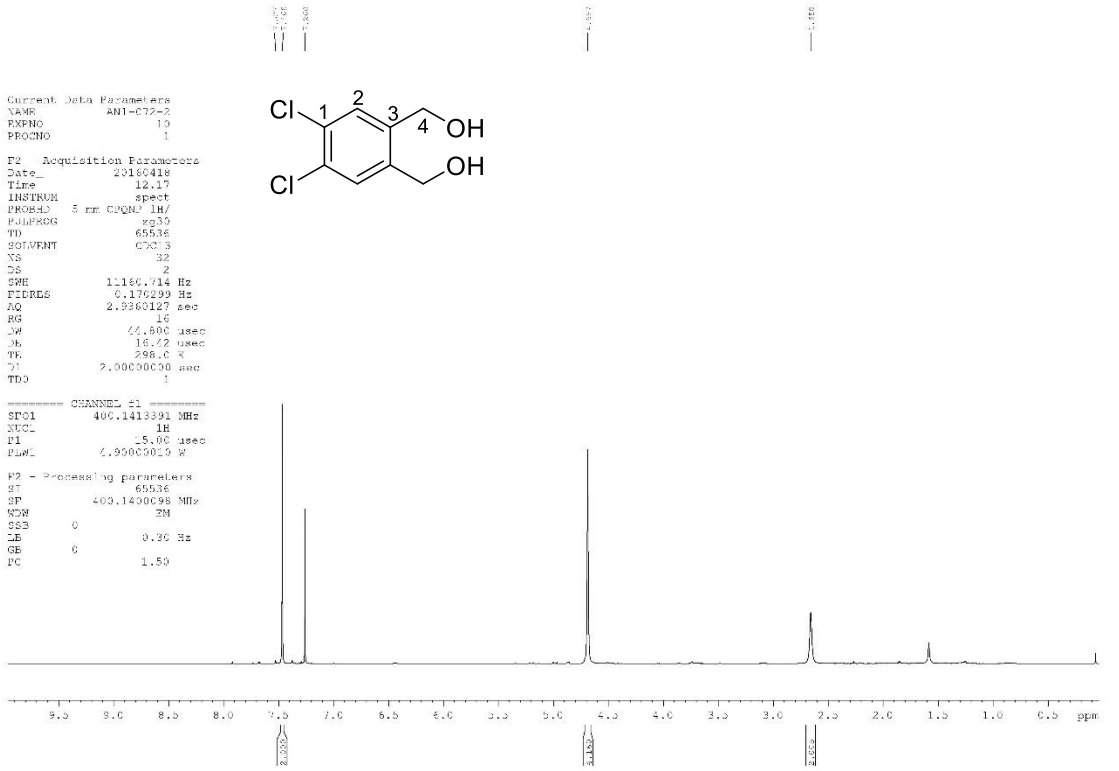

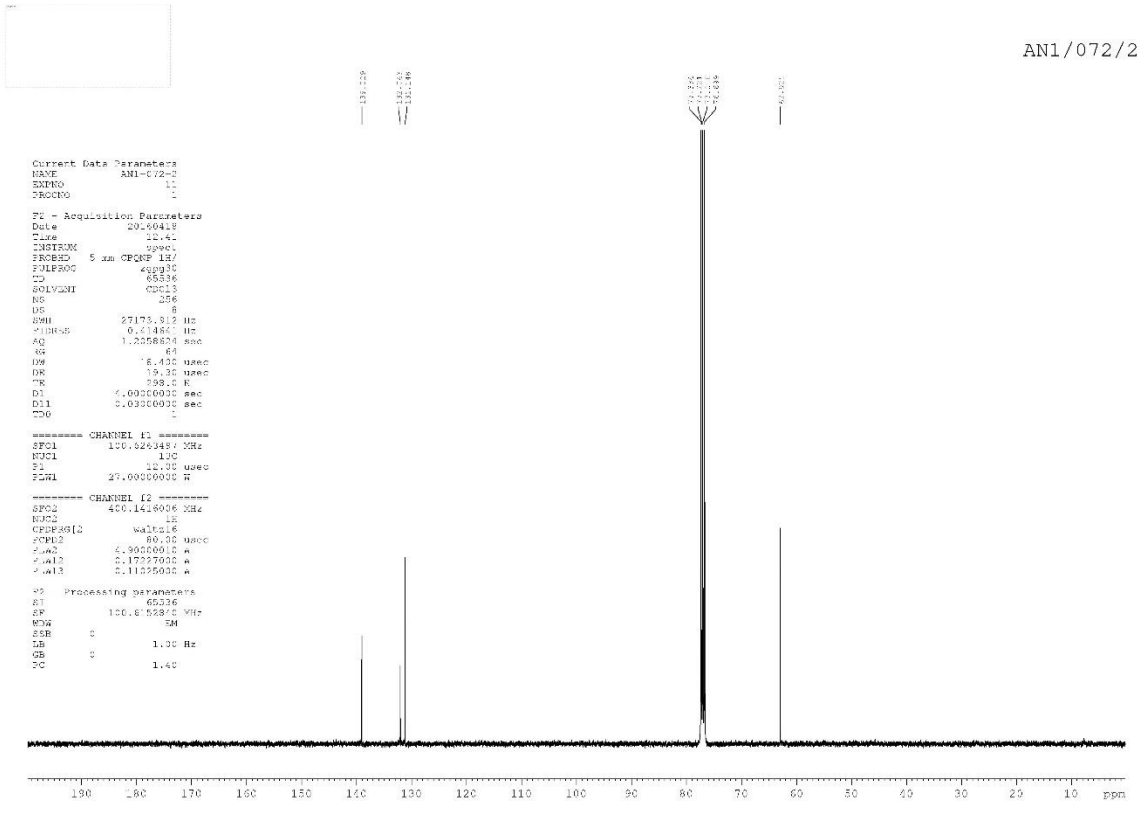

Dimethyl 4,5-dichlorophthalate, 34

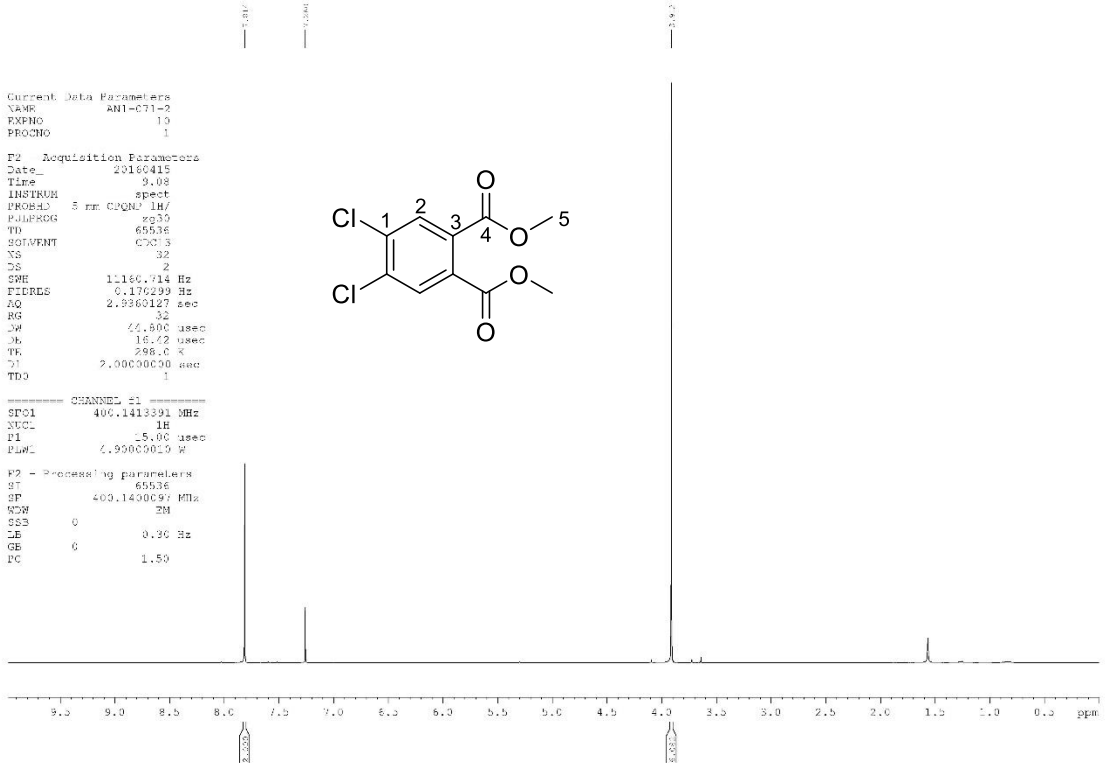

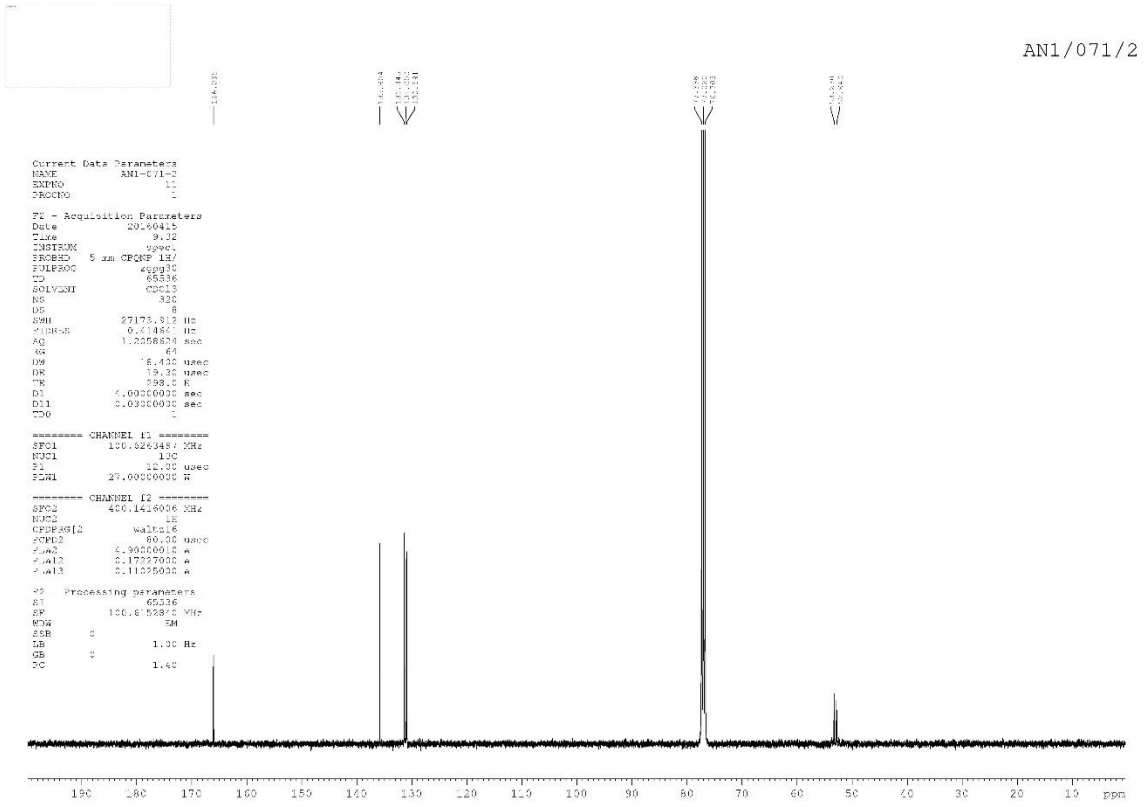

Di-*tert*-butyl ((4,5-dichloro-1,2-phenylene)bis(ethane-2,1-diyl))dicarbamate, 35

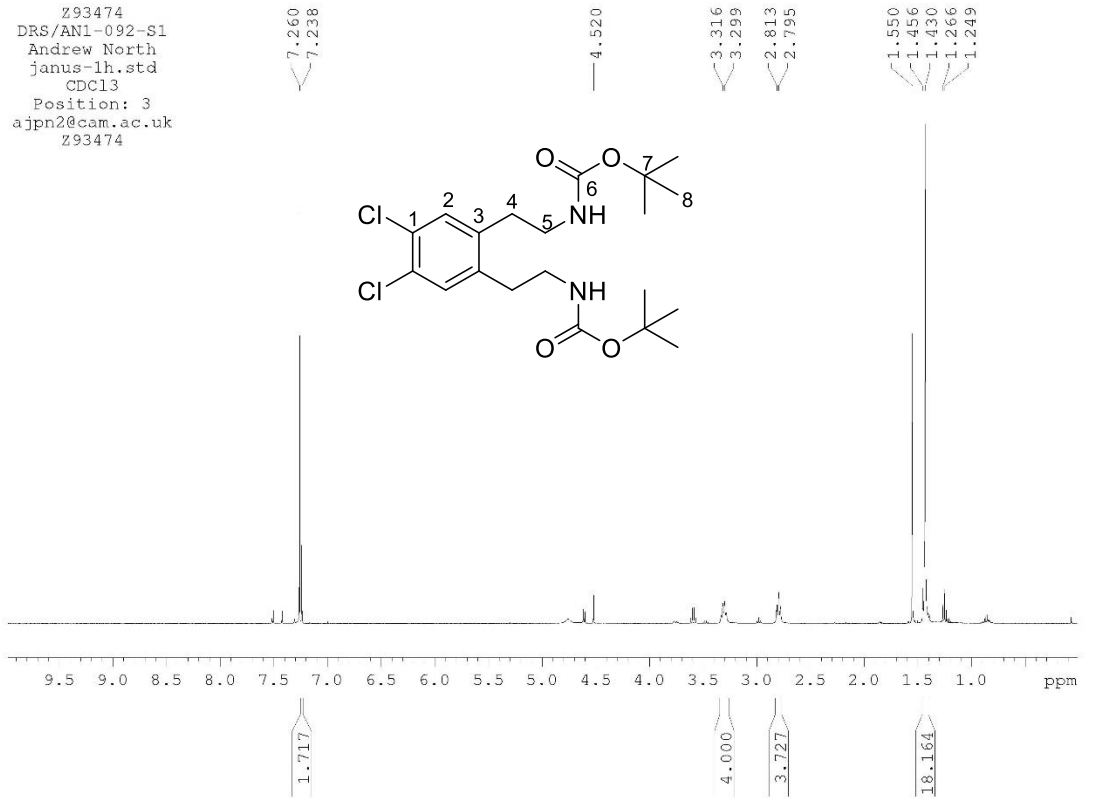

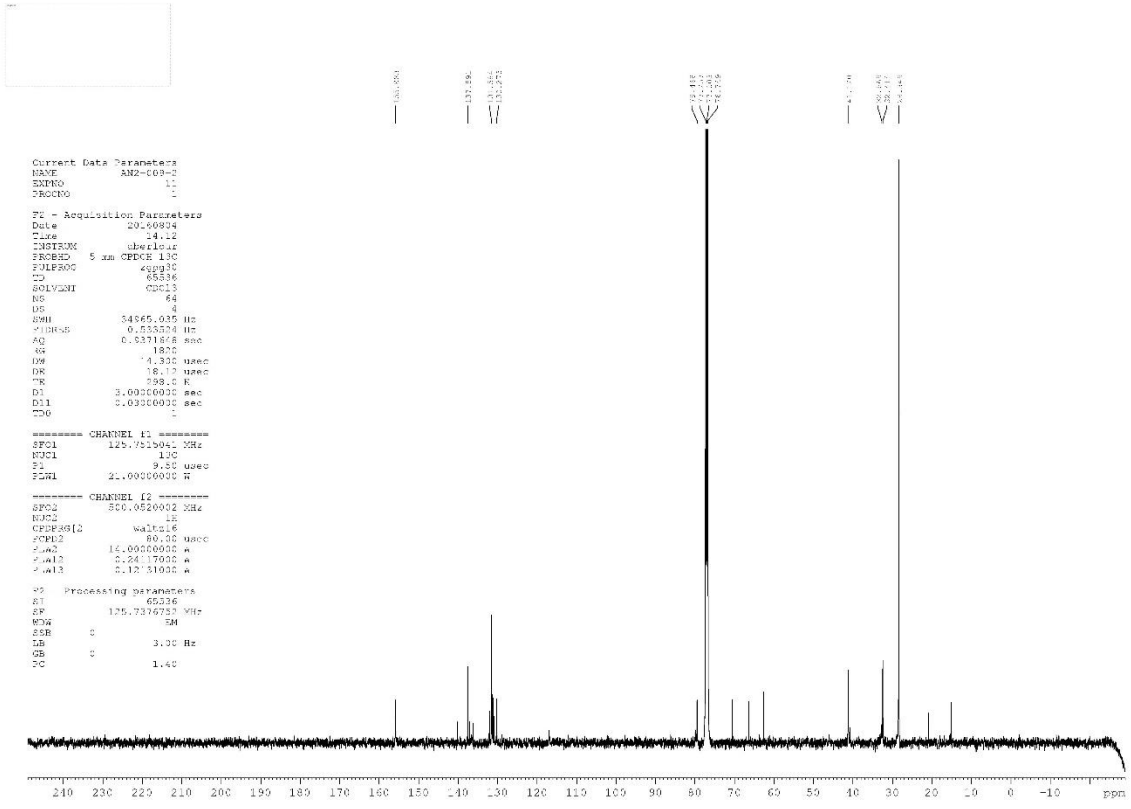

(4,5-Dichloro-1,2-phenylene)dimethanaminium dichloride, 38

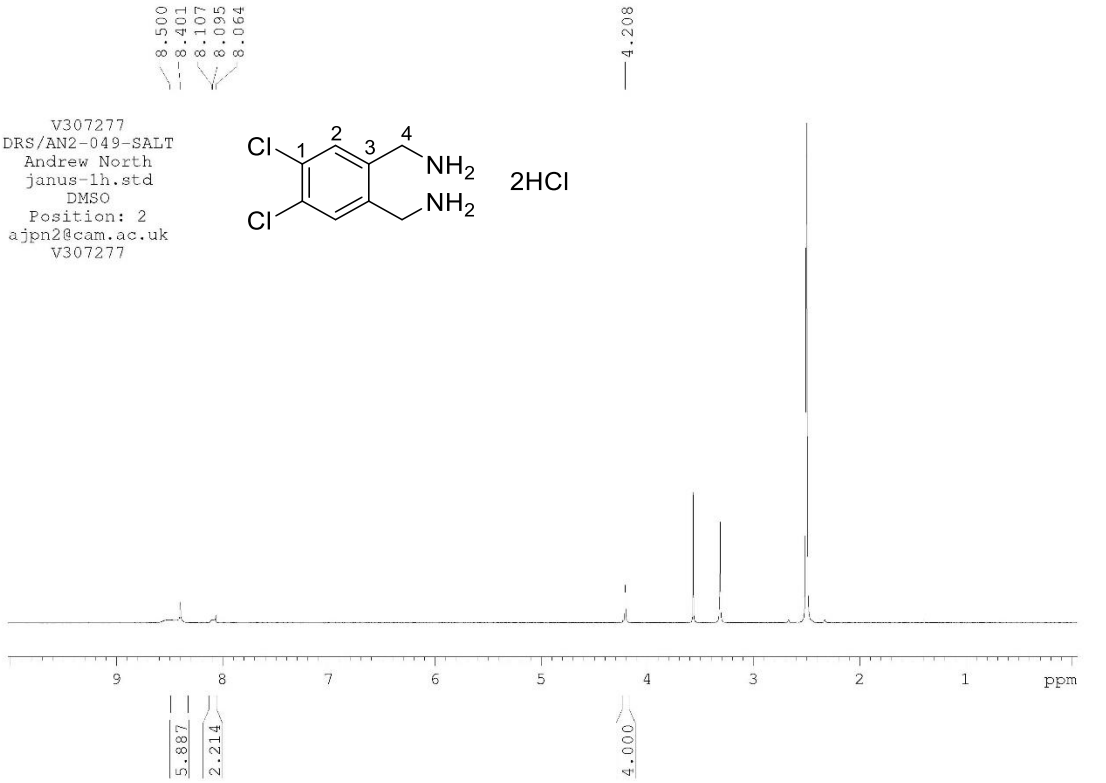

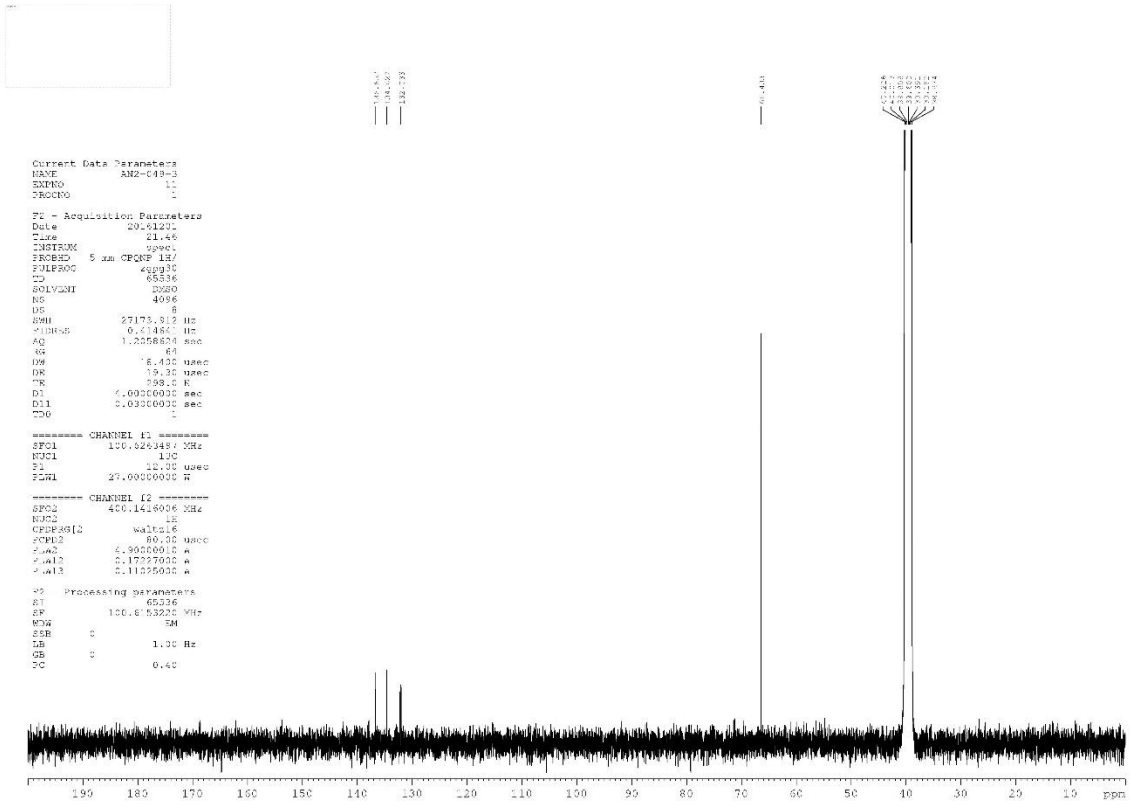

2-(4-Chloronaphthalen-1-yl)ethan-1-aminium chloride, 39

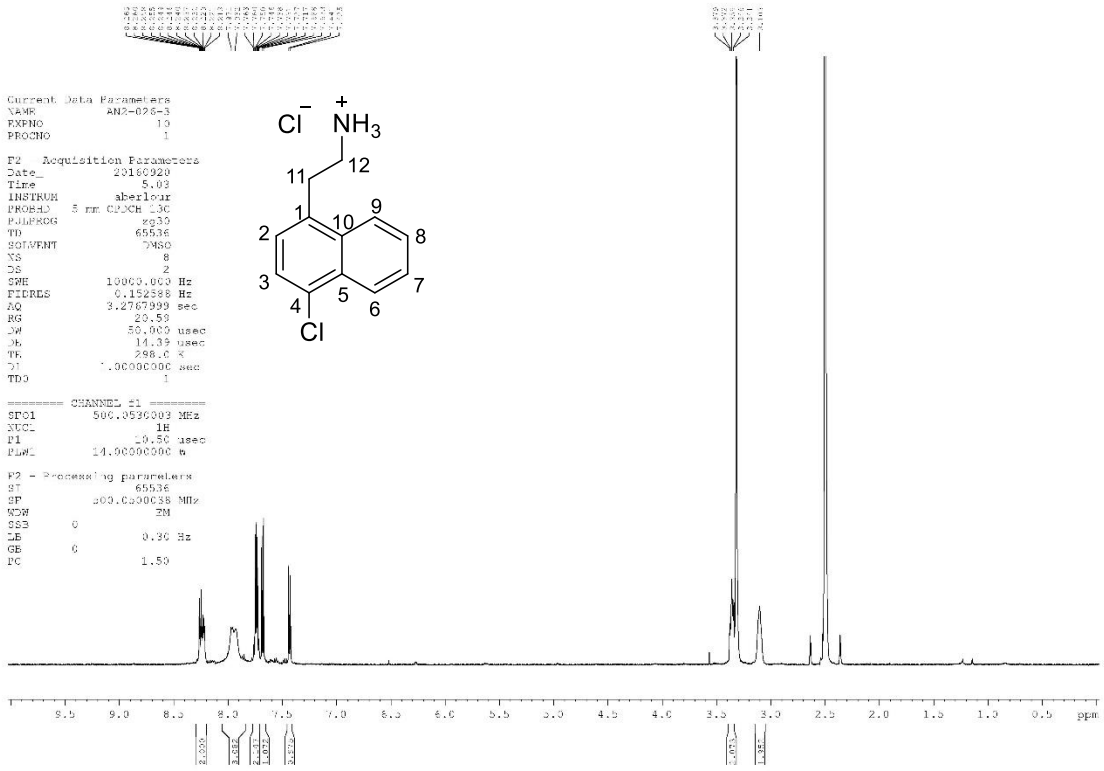

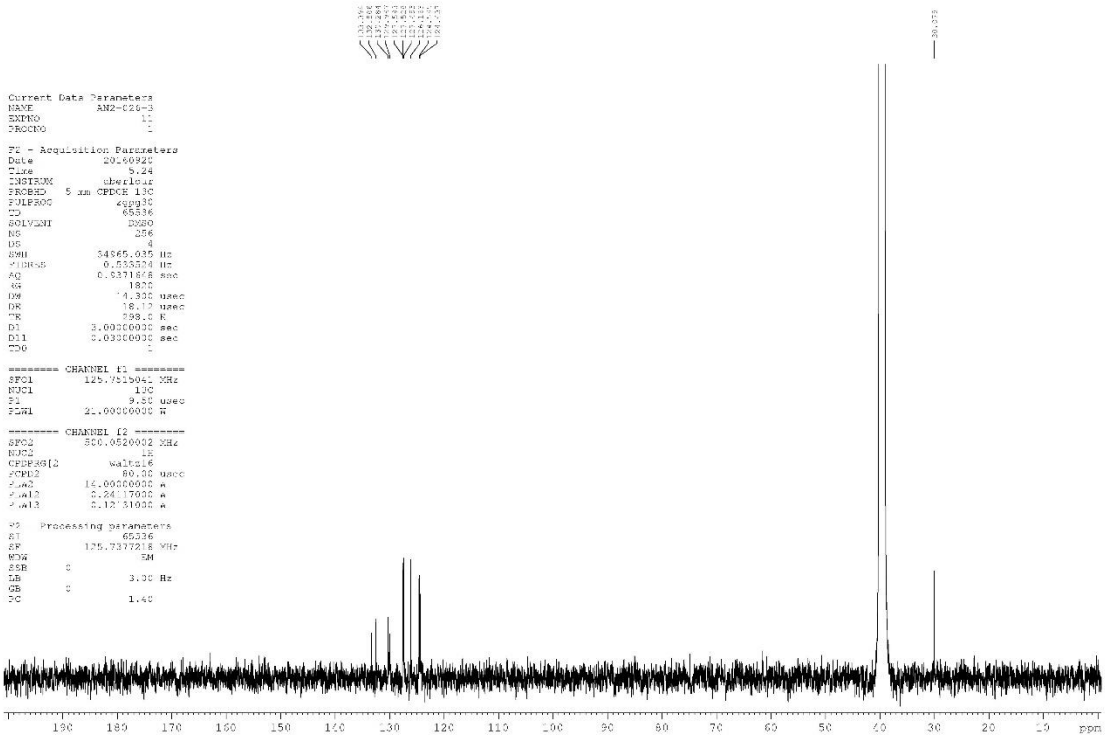

1-Acetyl-4-chloronaphthalene, 41

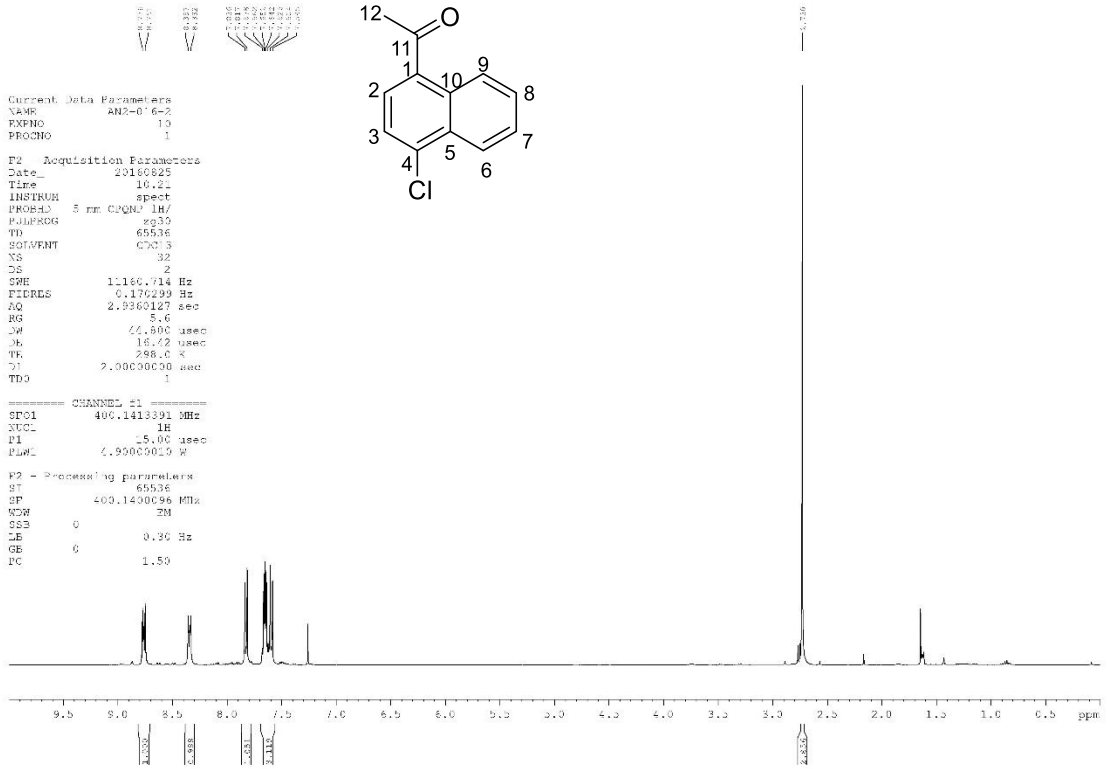

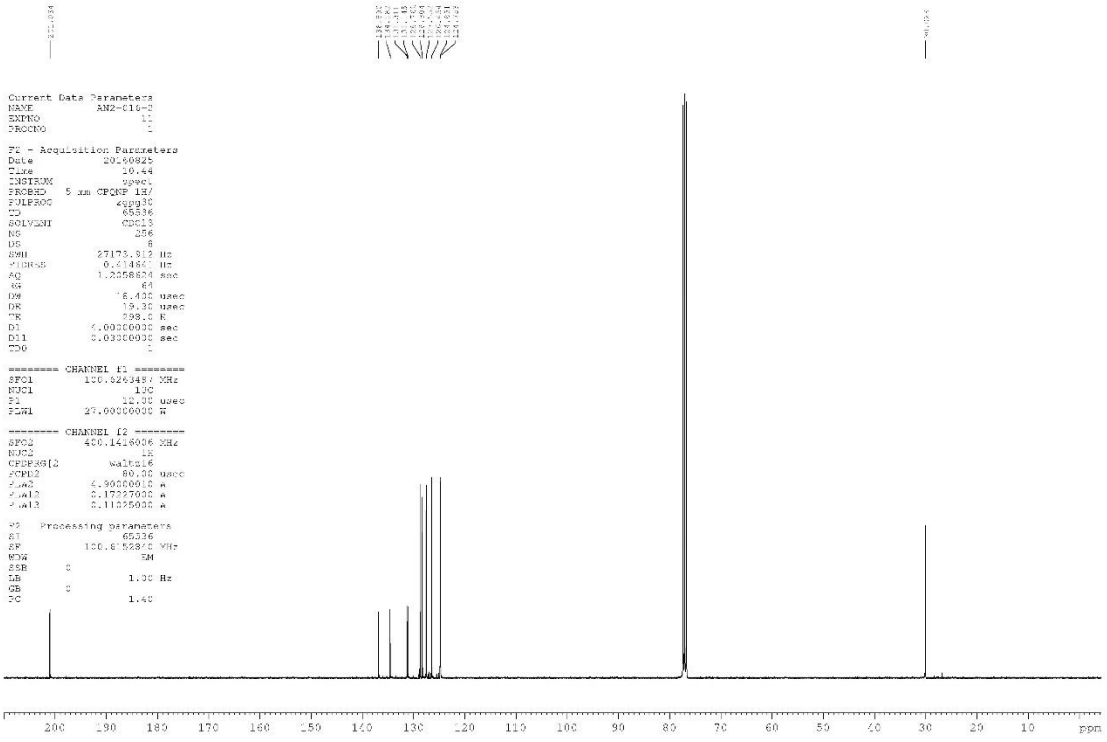

4-Chloro-1-naphthoic acid, 42

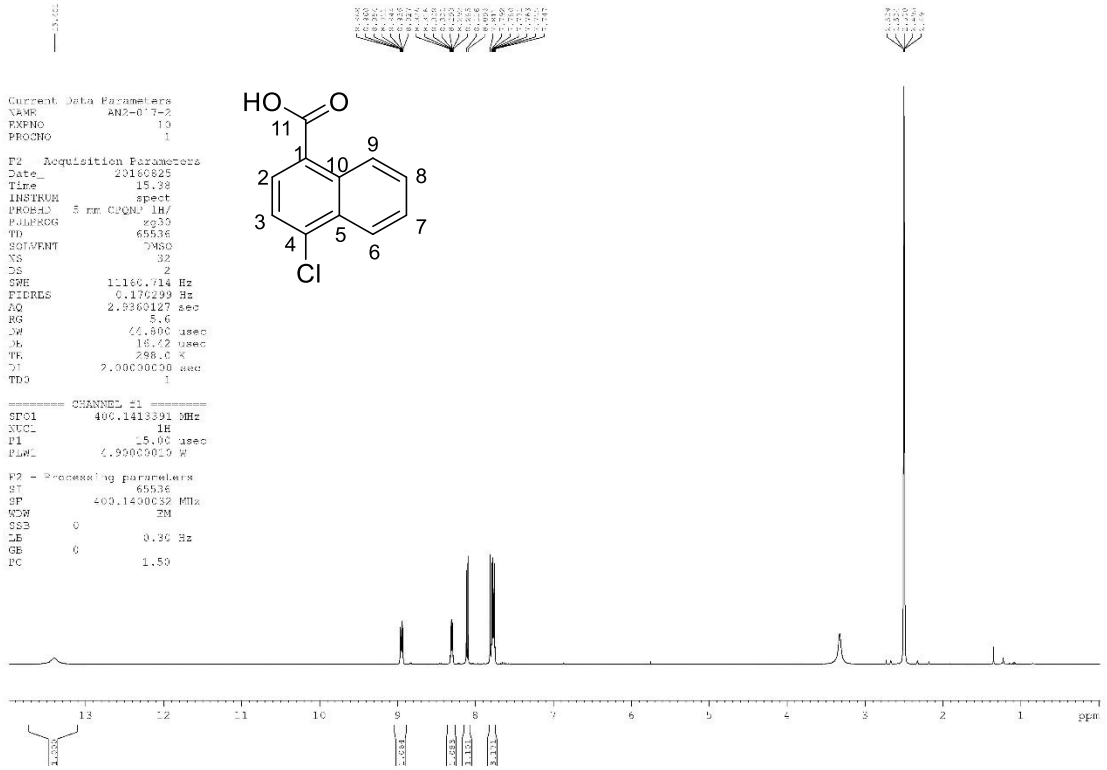

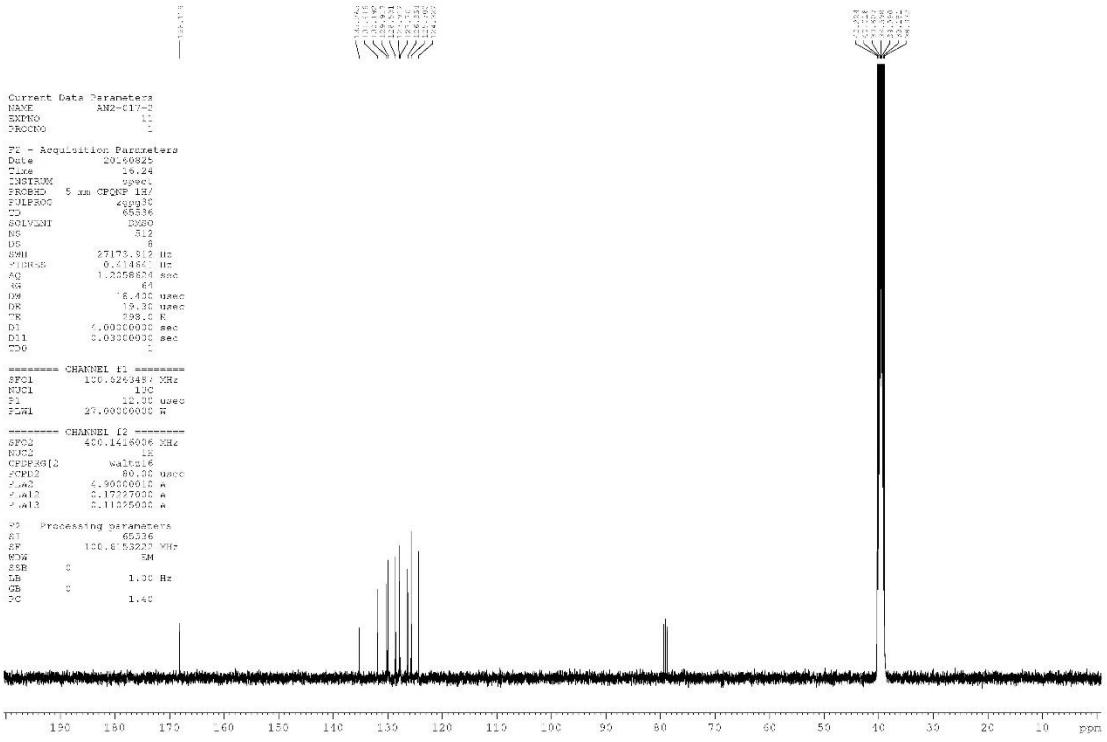

(4-Chloronaphthalen-1-yl)methanol, 43

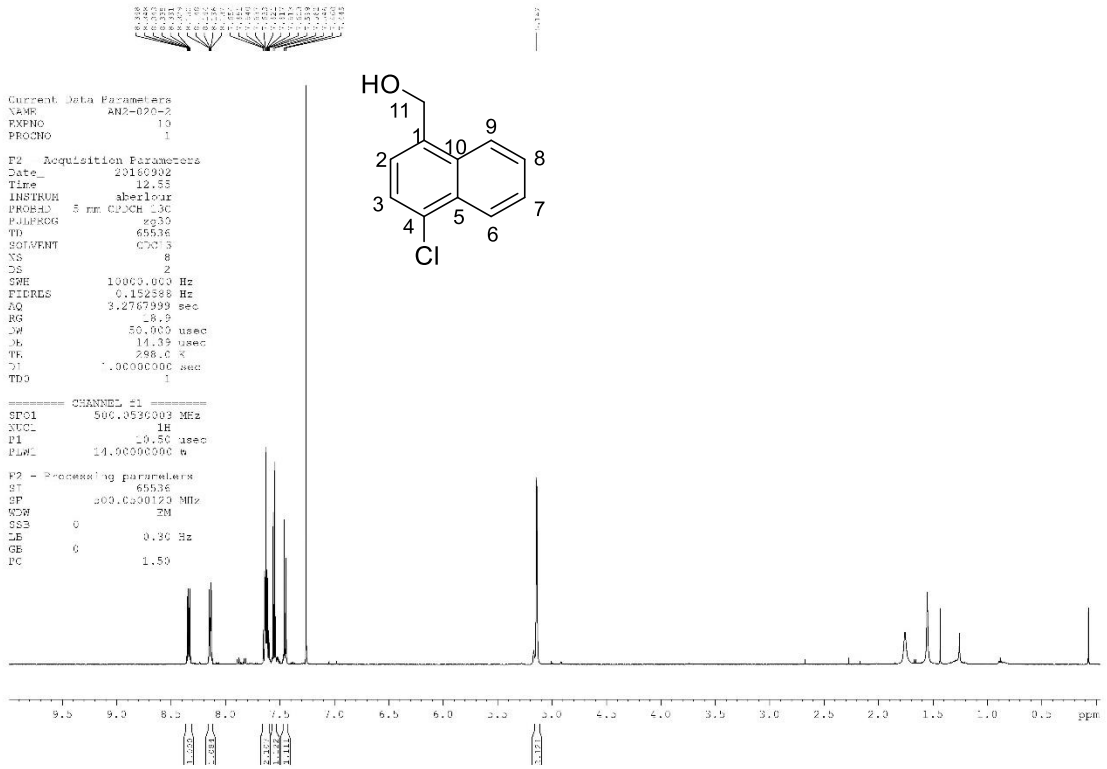

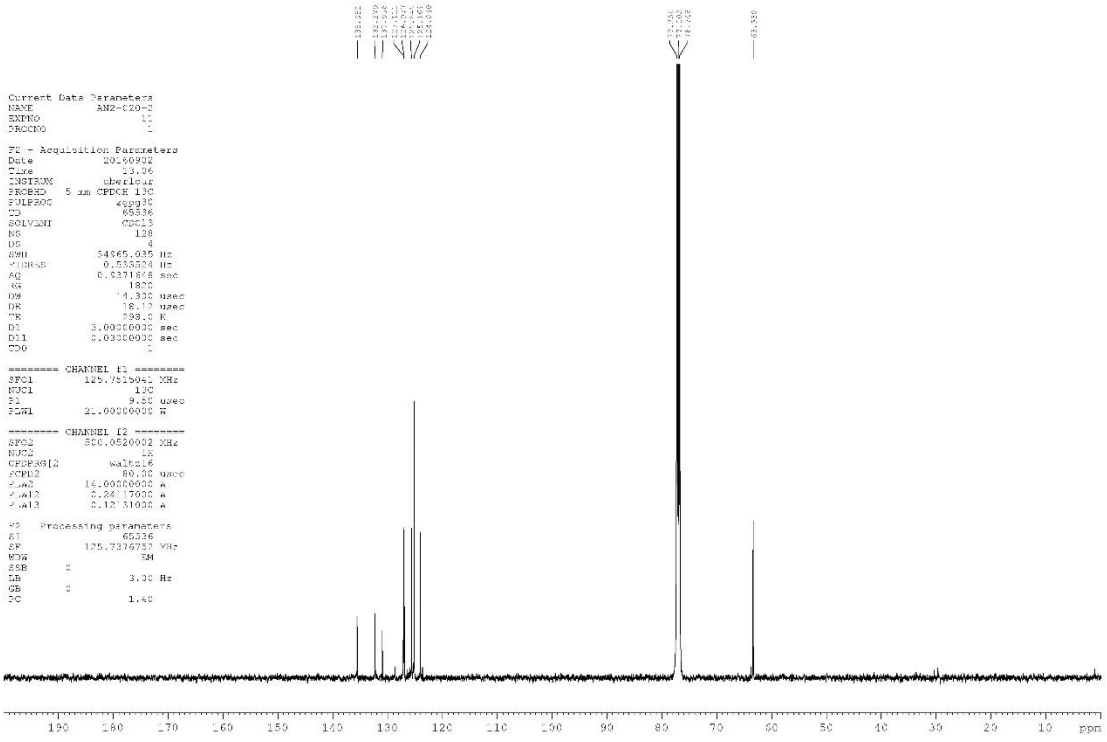

1-(Bromomethyl)-4-chloronaphthalene, 44

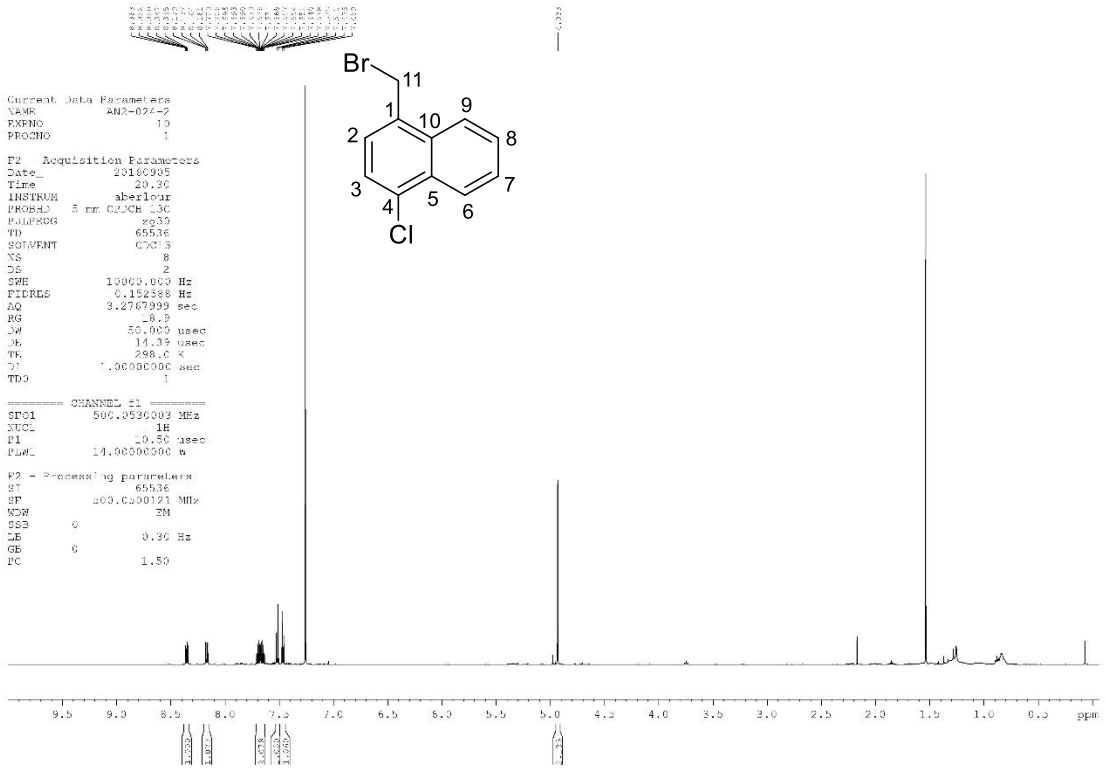

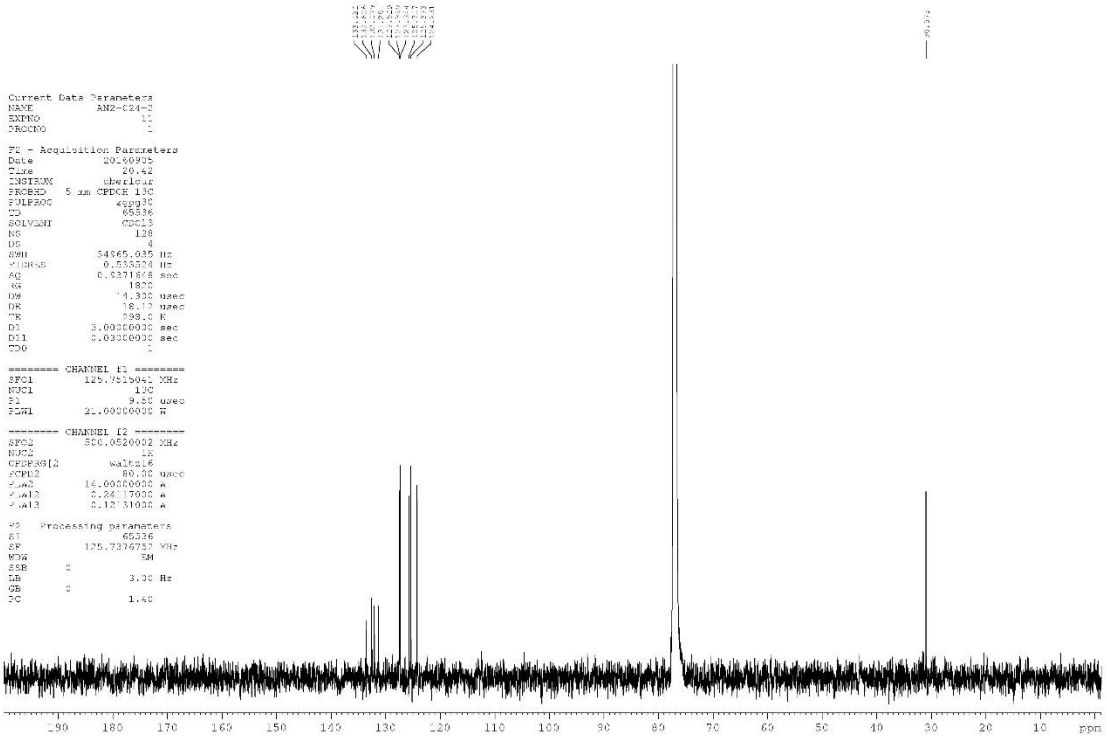

2-(4-Chloronaphthalen-1-yl)acetonitrile, 45

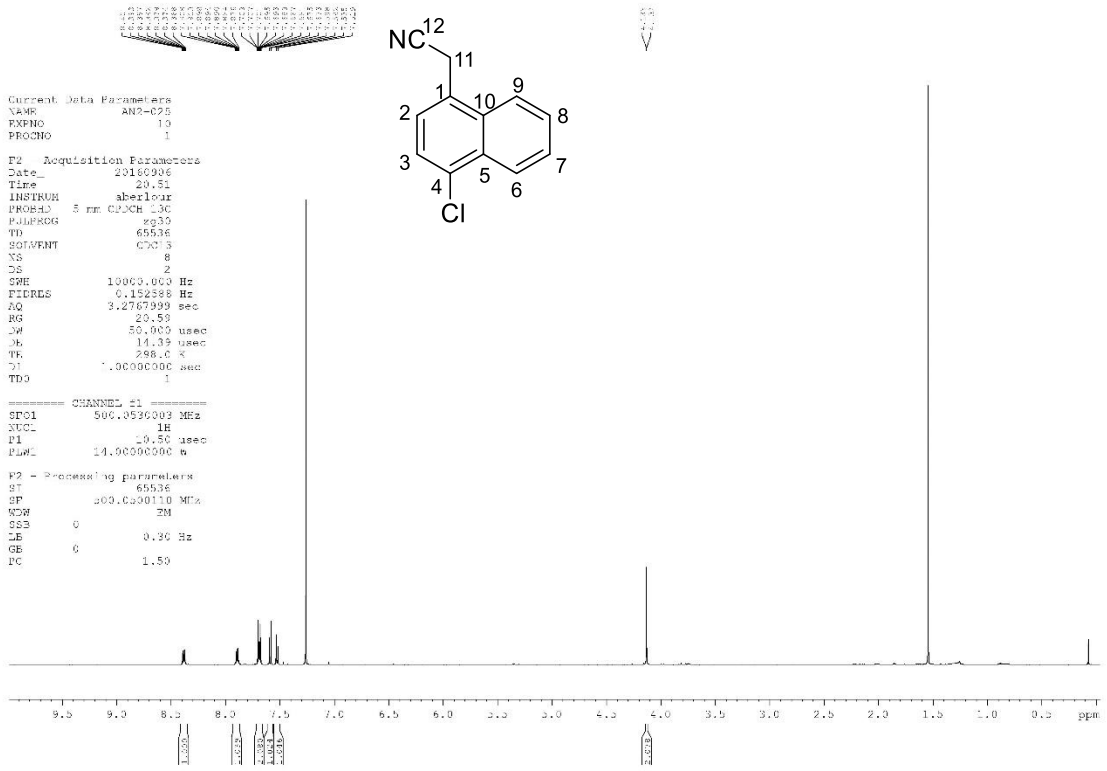

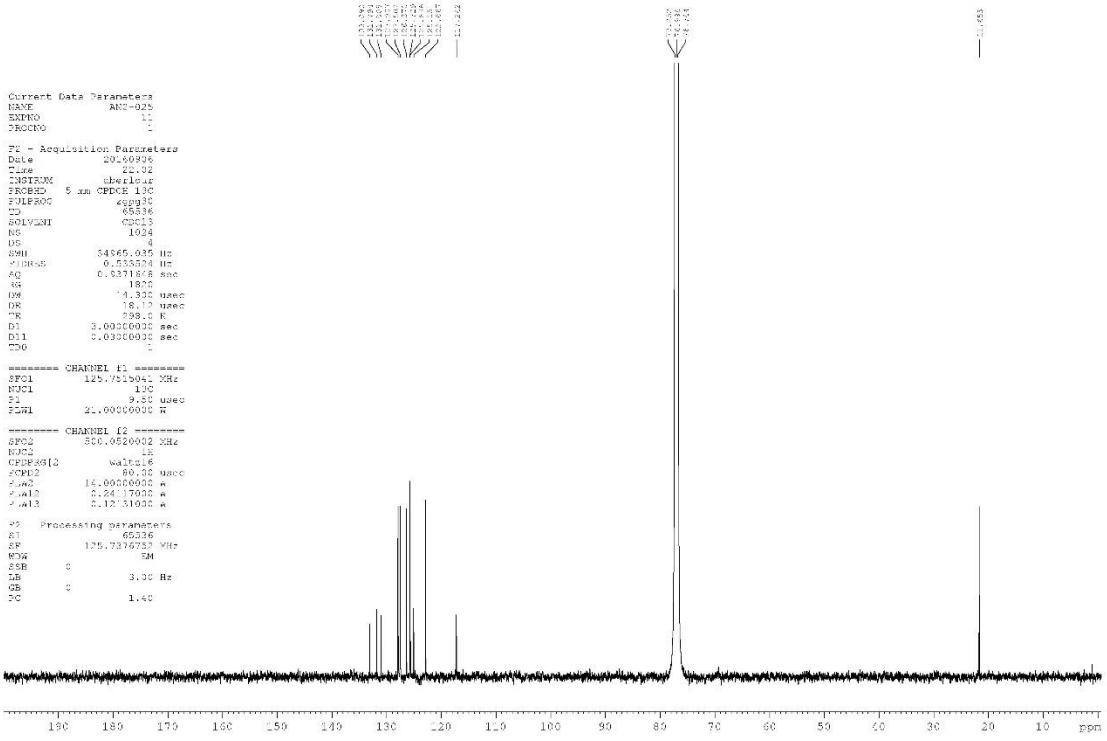

Methyl 2-bromo-4-chlorobenzoate, 49

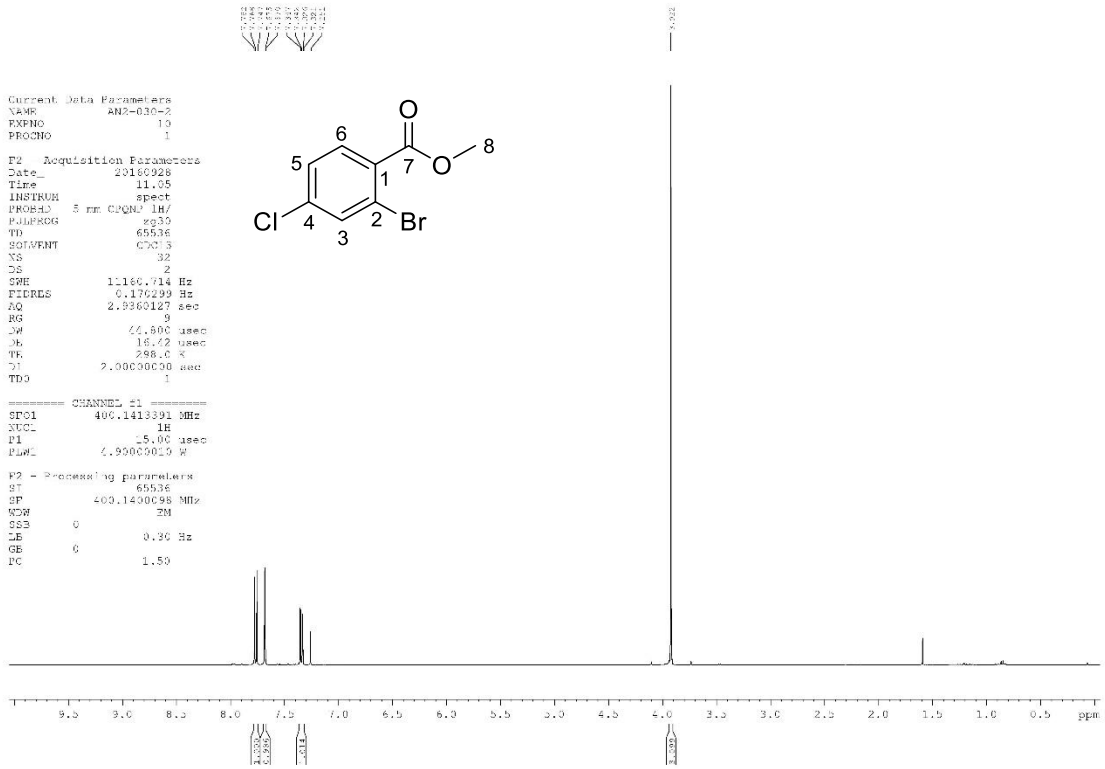

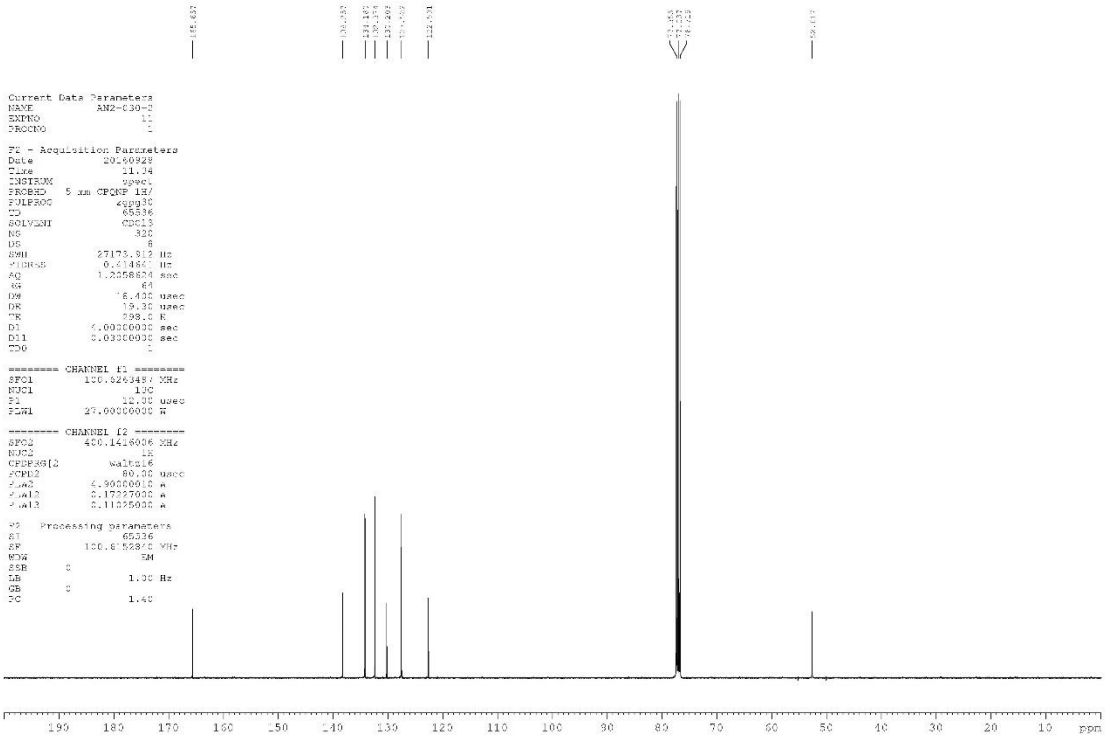

Methyl 4-chloro-2-((trimethylsilyl)ethynyl)benzoate, 50

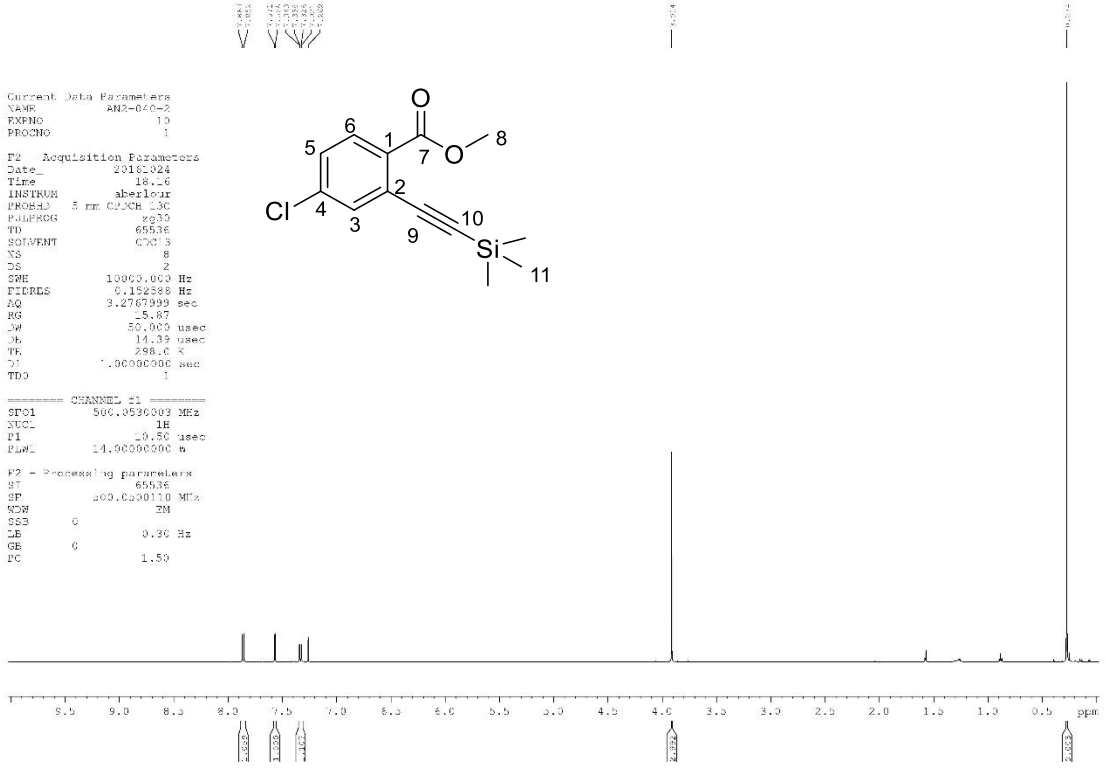

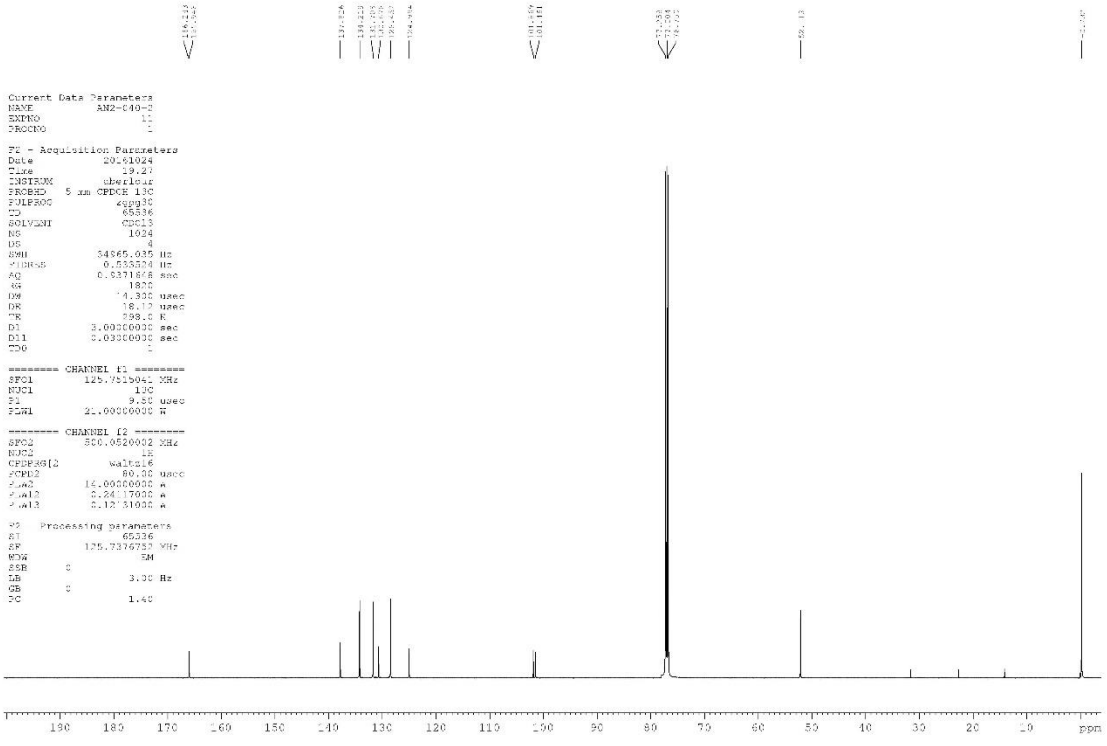

4-Chloro-2-ethynyl benzoic acid, 51

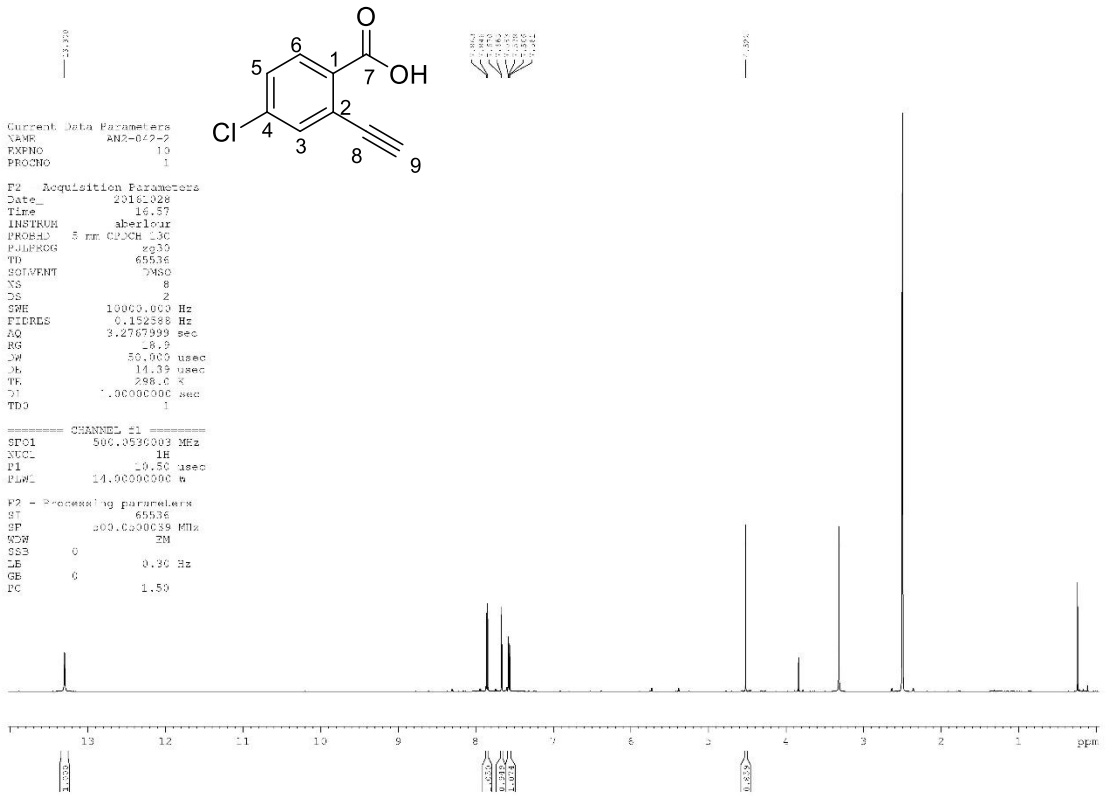

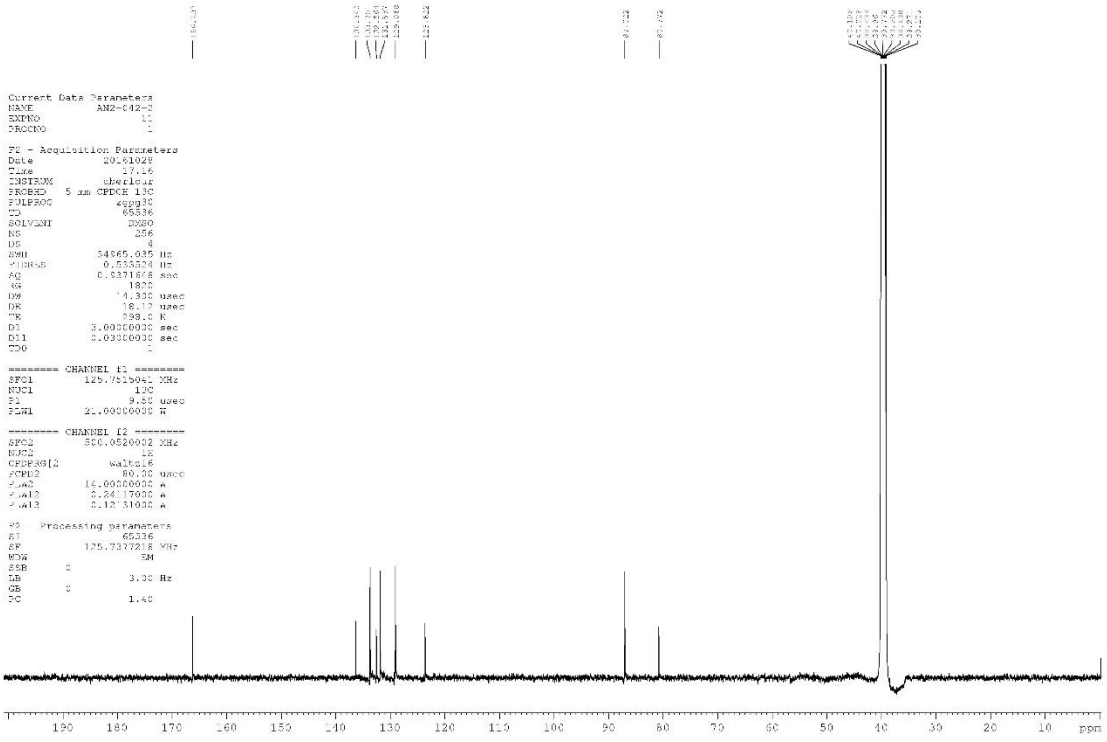

Hydroxycarbonimidic dibromide, 70

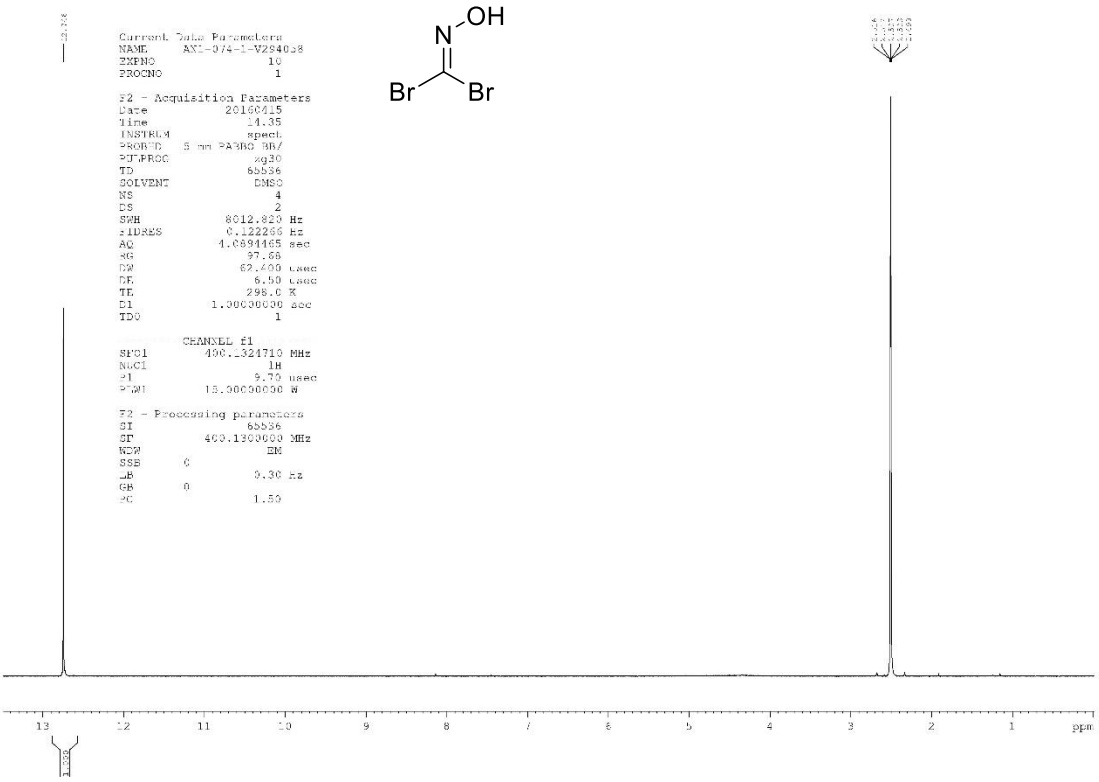

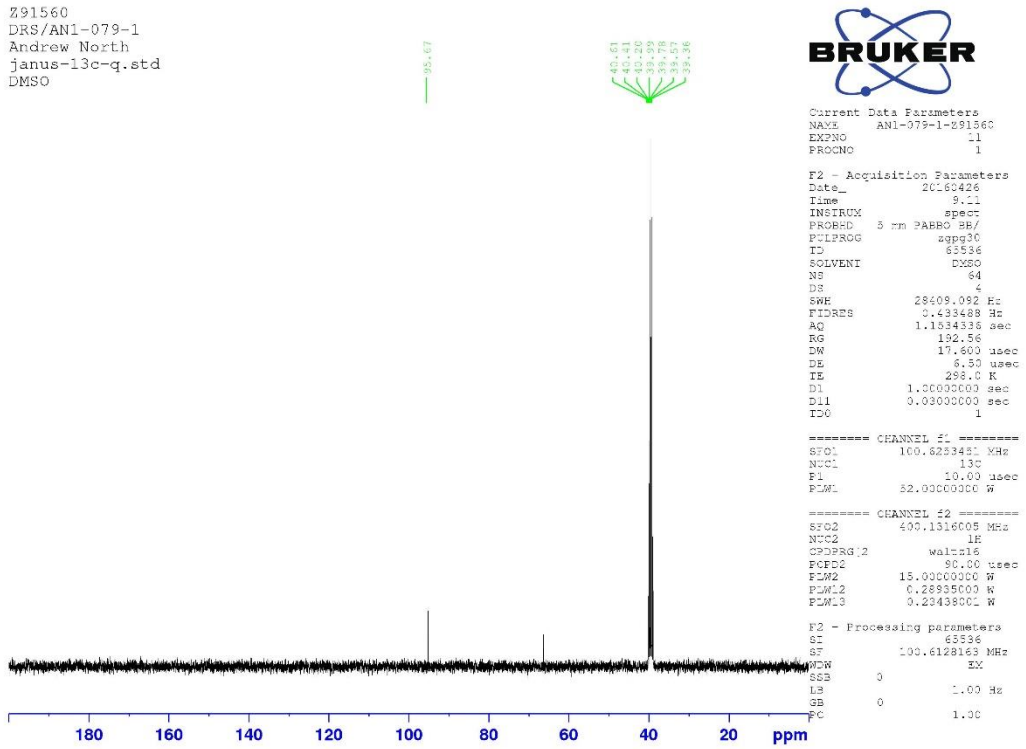

tert-Butyldimethyl(prop-2-yn-1-yloxy)silane, 72

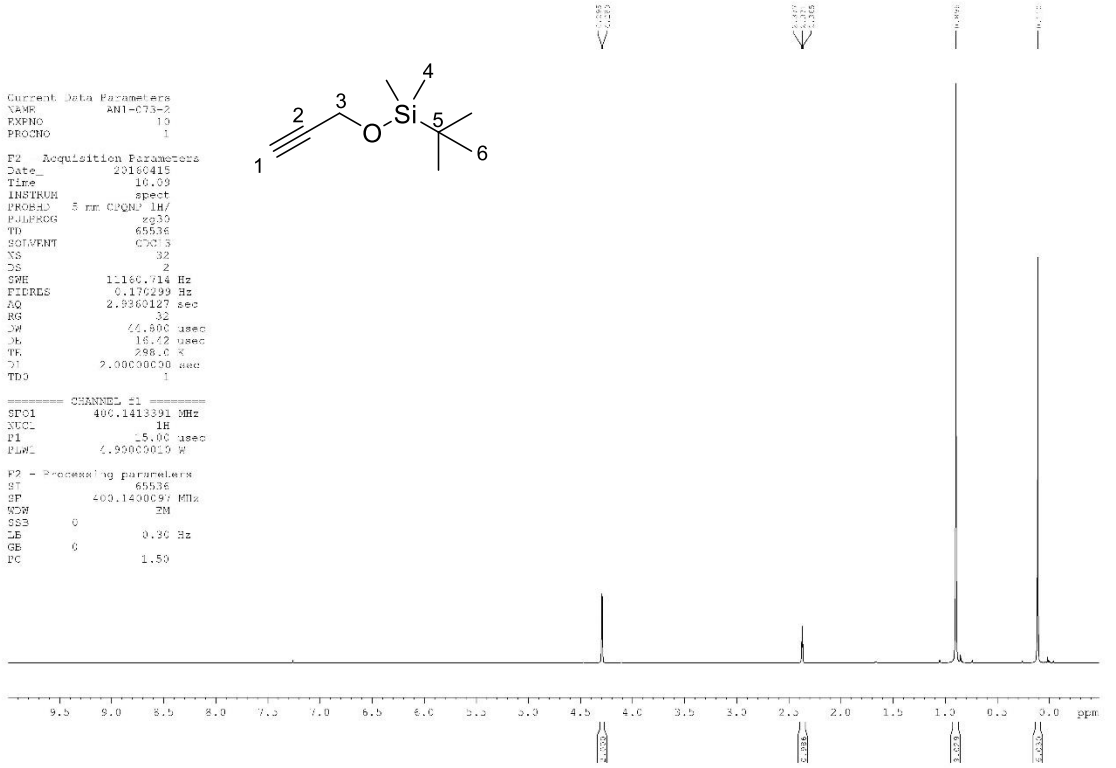

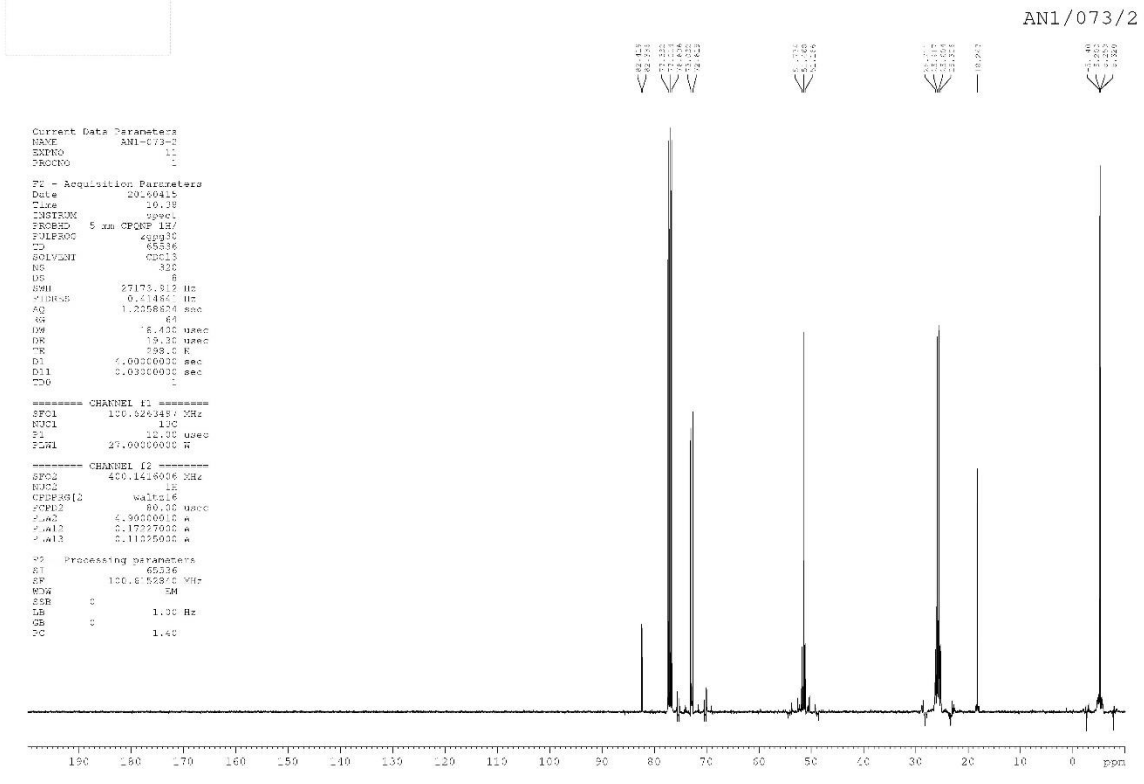

3-Bromo-5-(((tert-butyldimethylsilyl)oxy)methyl)isoxazole, 73

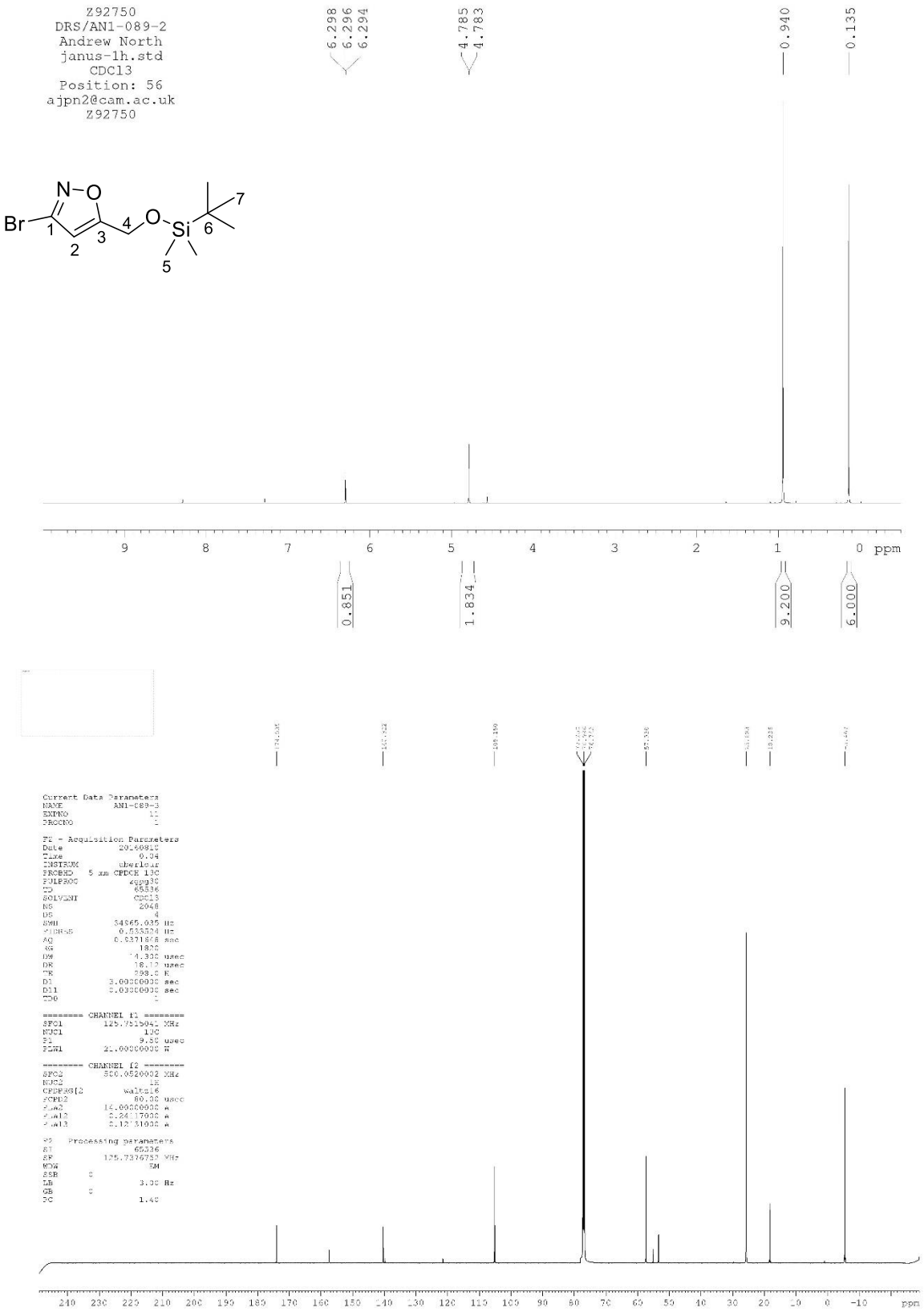

Spiro[indoline-3,4′-piperidin]-1′-ium chloride, 85

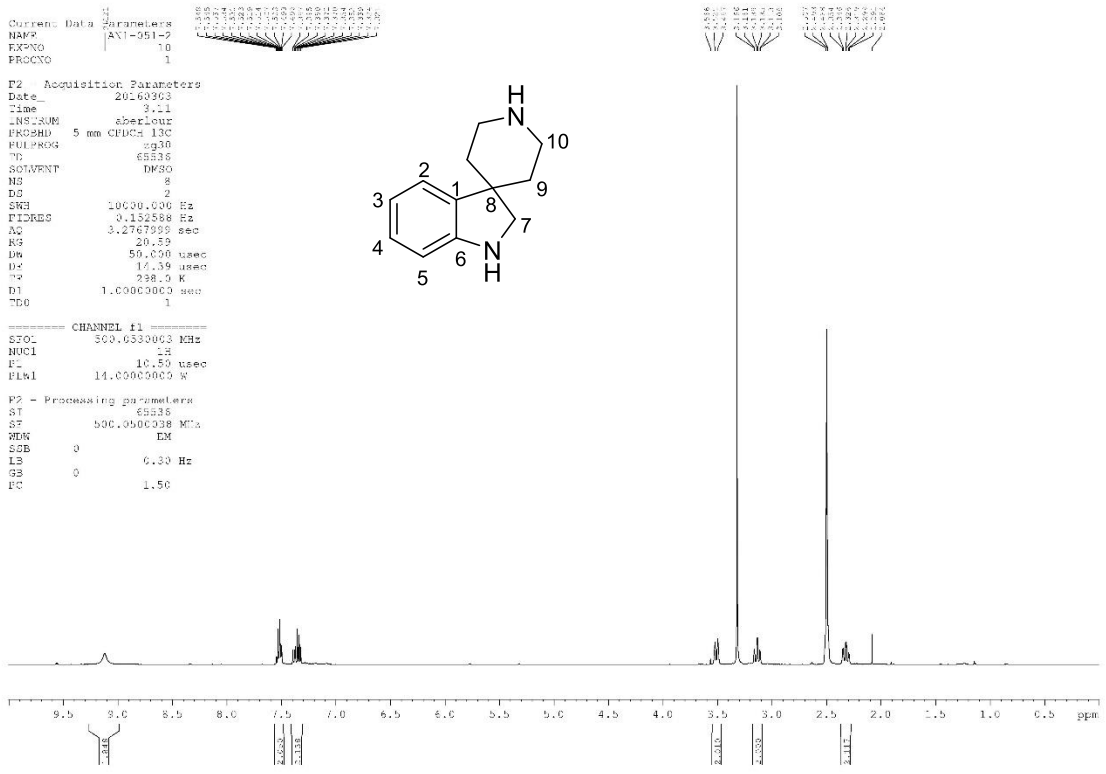

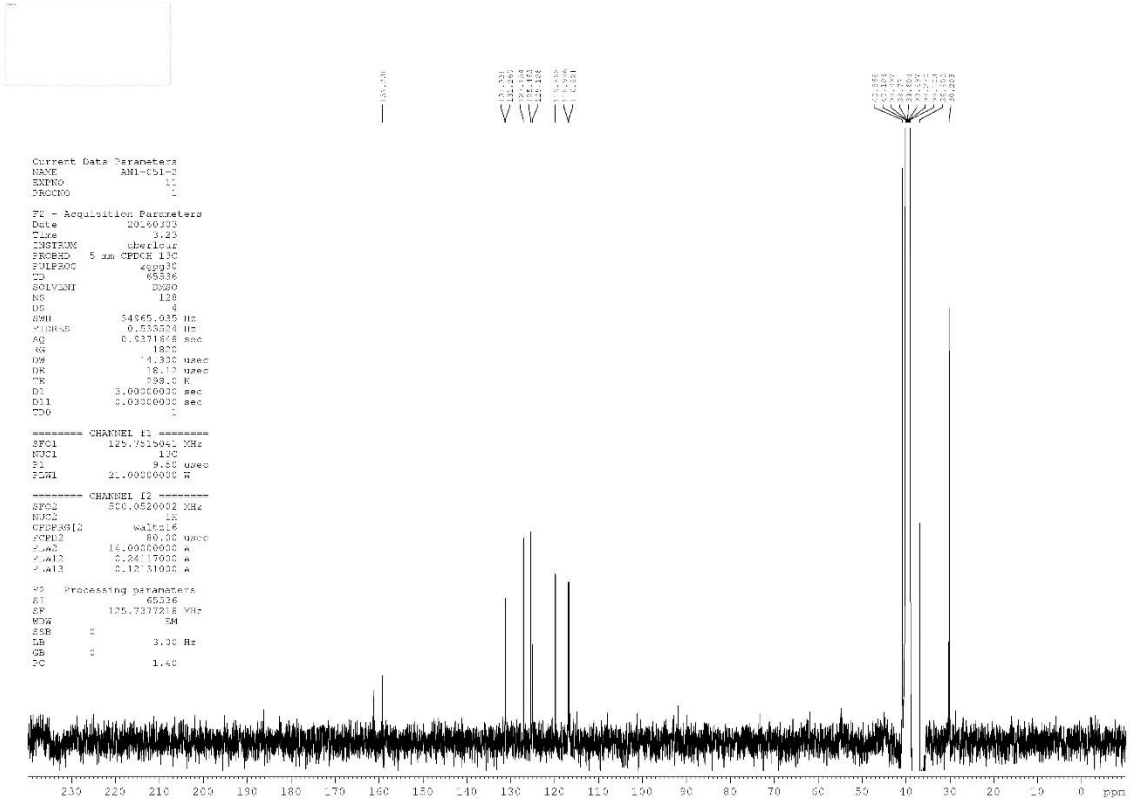

2,3-Dihydrospiro[indene-1,4′-piperidin]-1′-ium chloride, 86

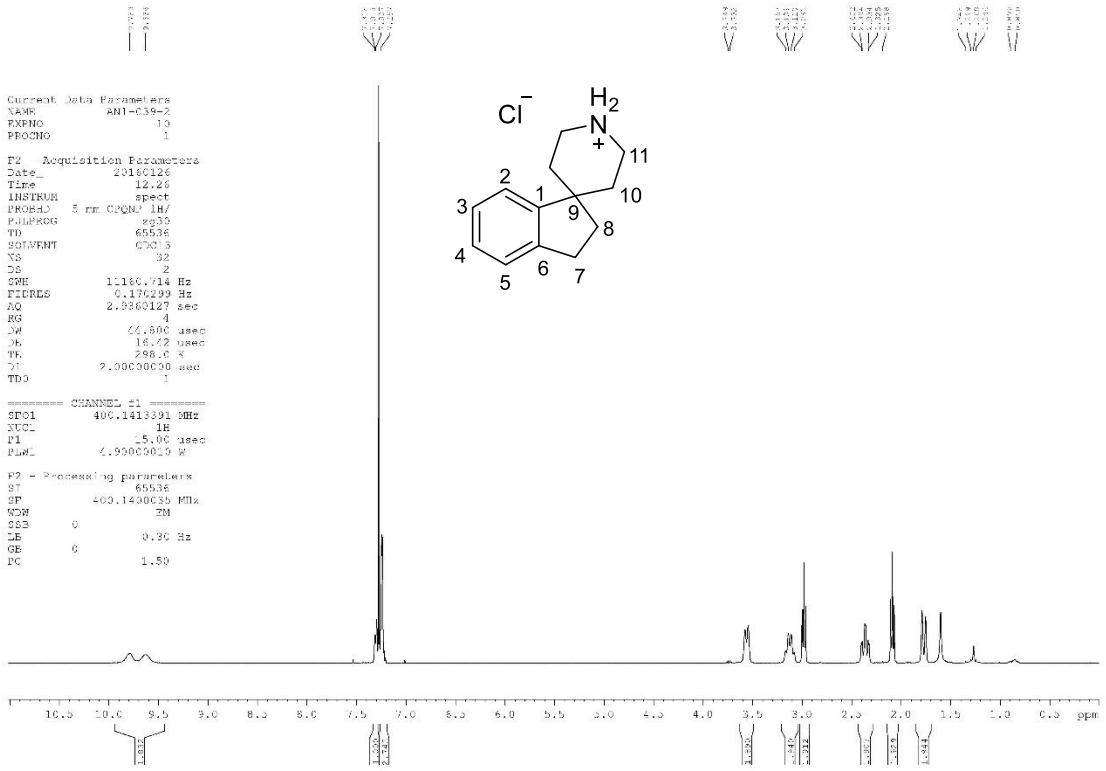

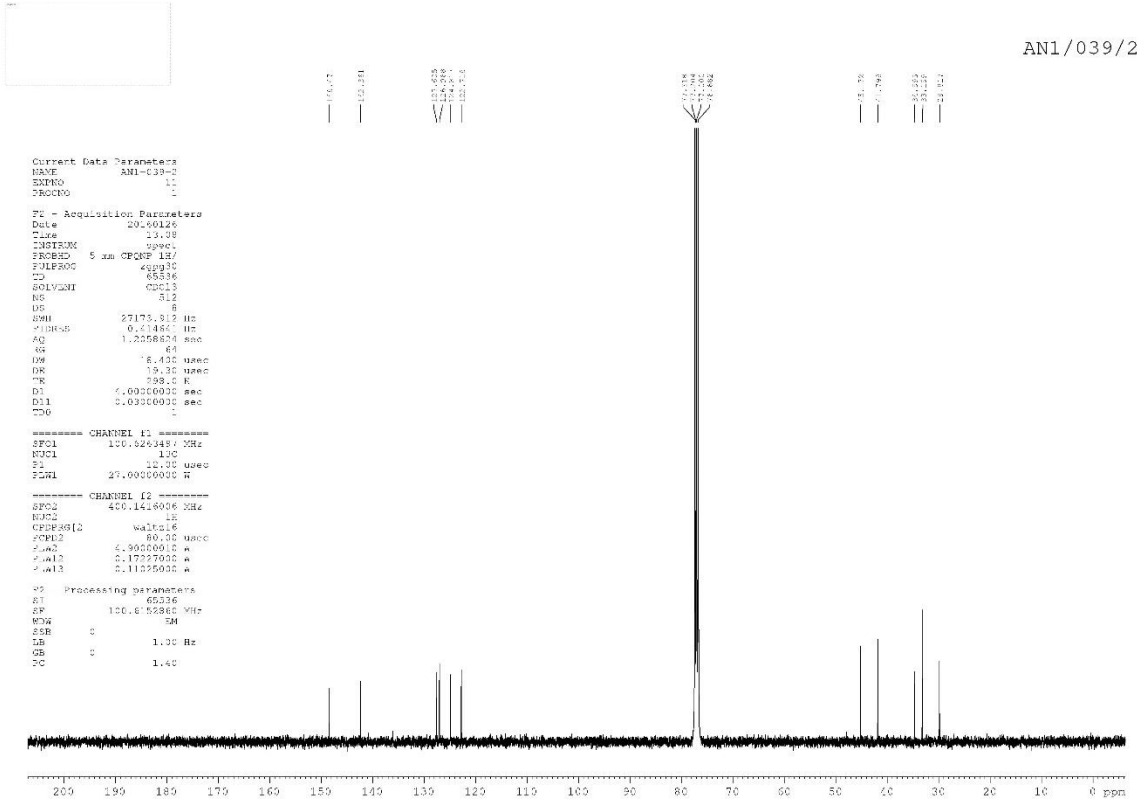

tert-Butyl bis(2-chloroethyl)carbamate, 92

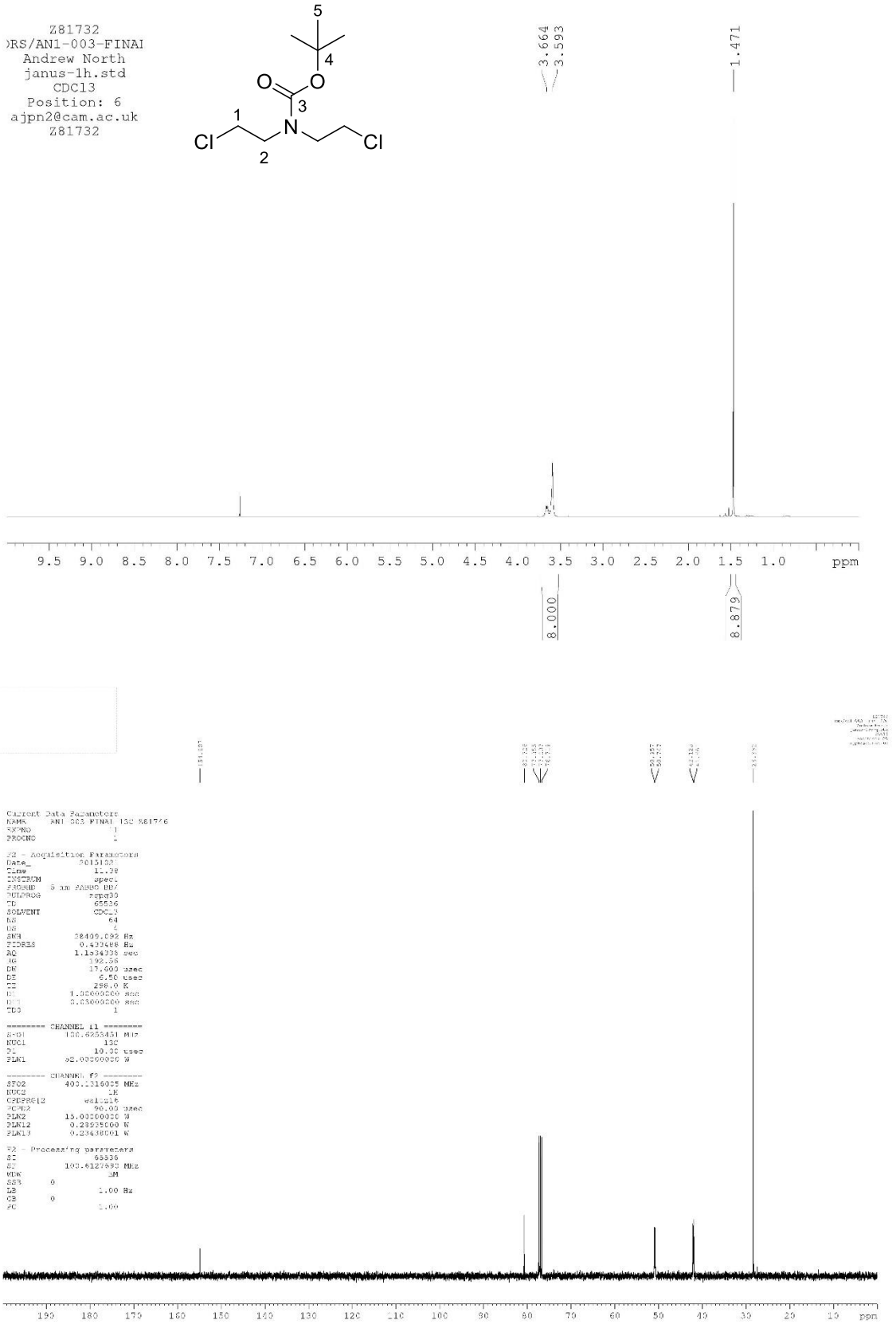

4-Cyano-4-(2-fluorophenyl)piperidin-1-ium chloride, 95

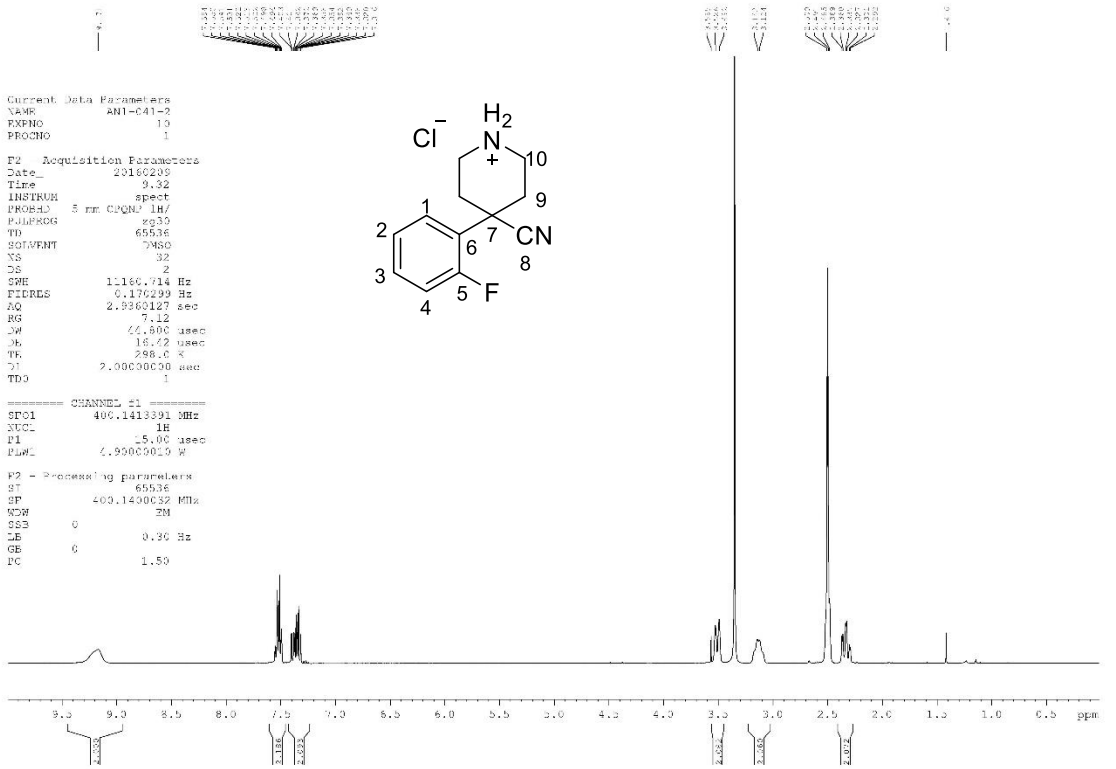

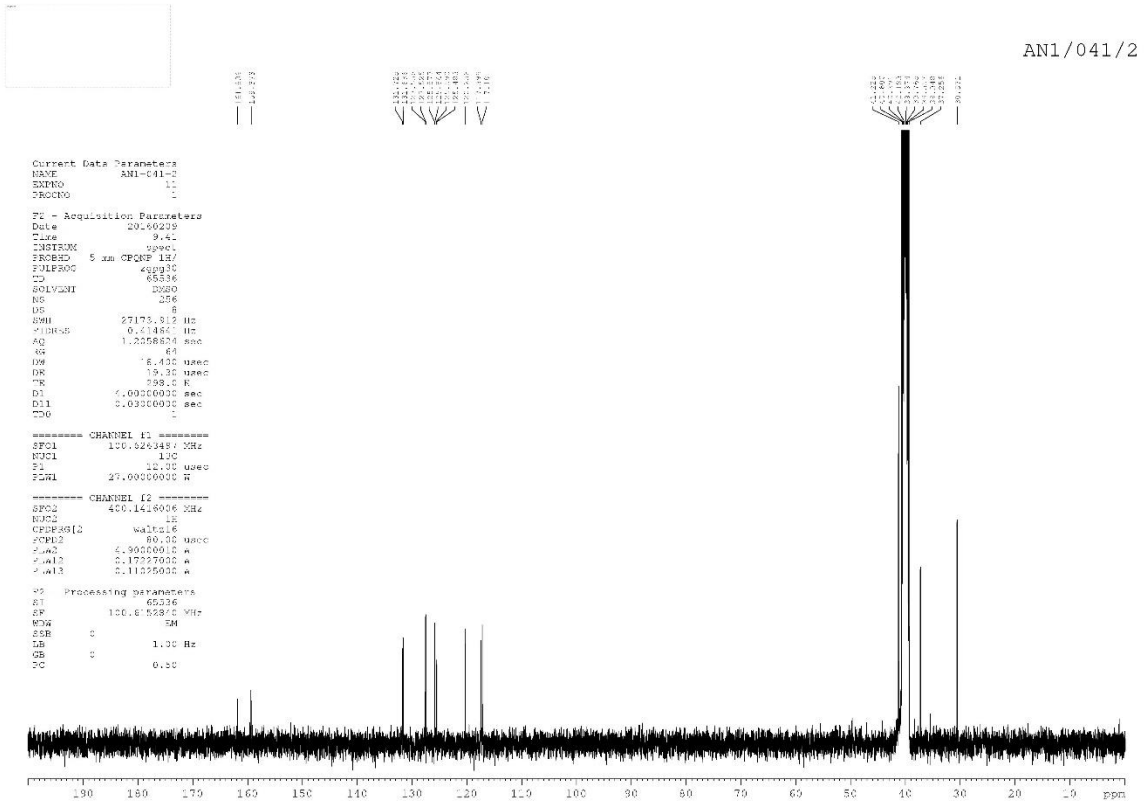

tert-Butyl 4-cyano-4-(2-fluorophenyl)piperidine-1-carboxylate, 96

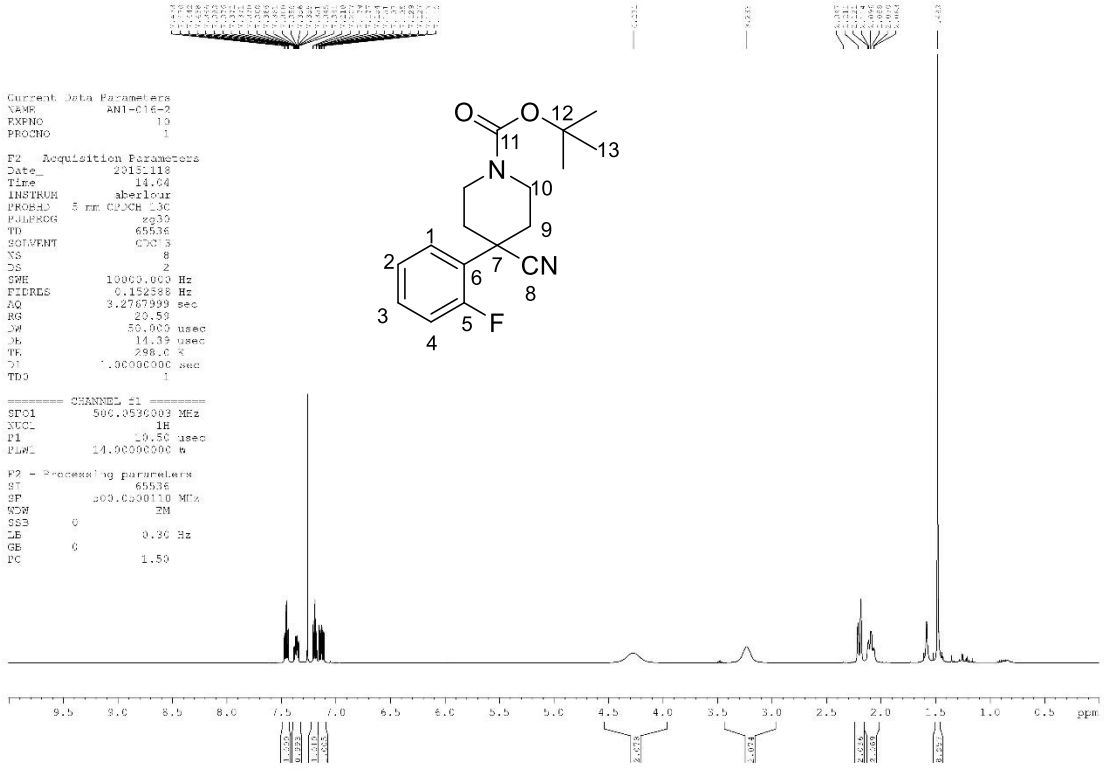

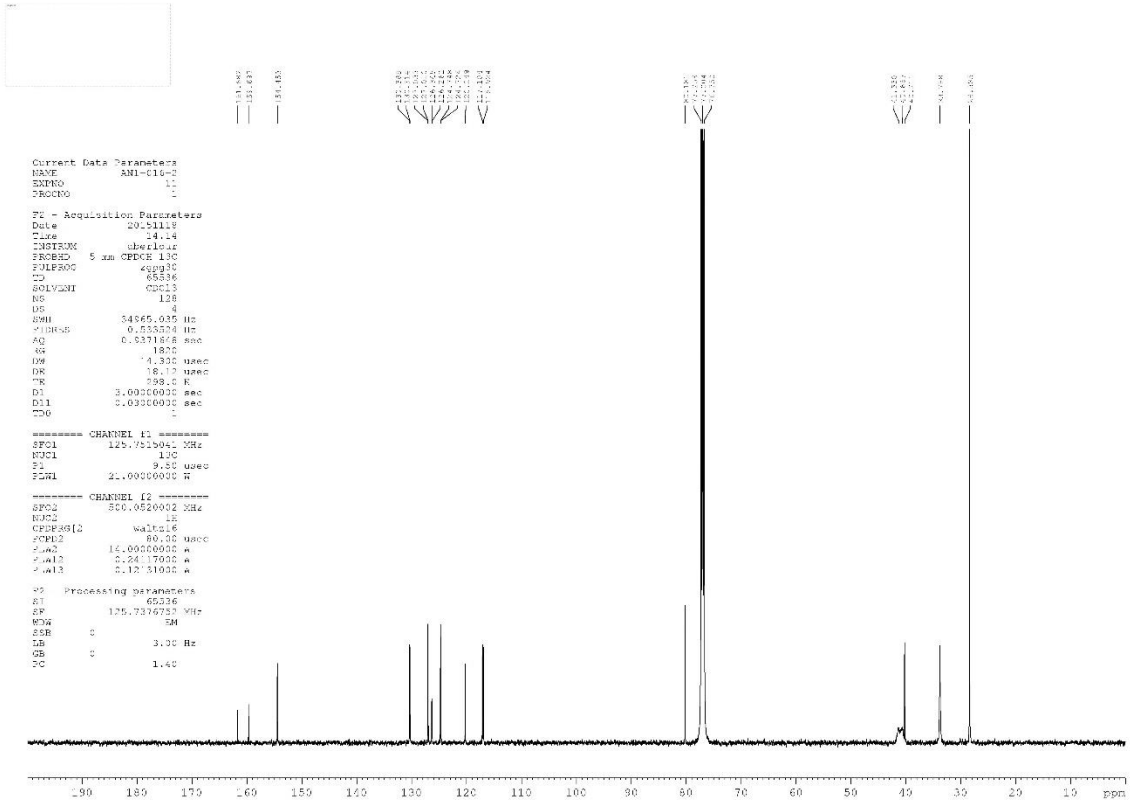

N-Benzyl-2-chloro-N-(2-chloroethyl)ethan-1-amine, 98

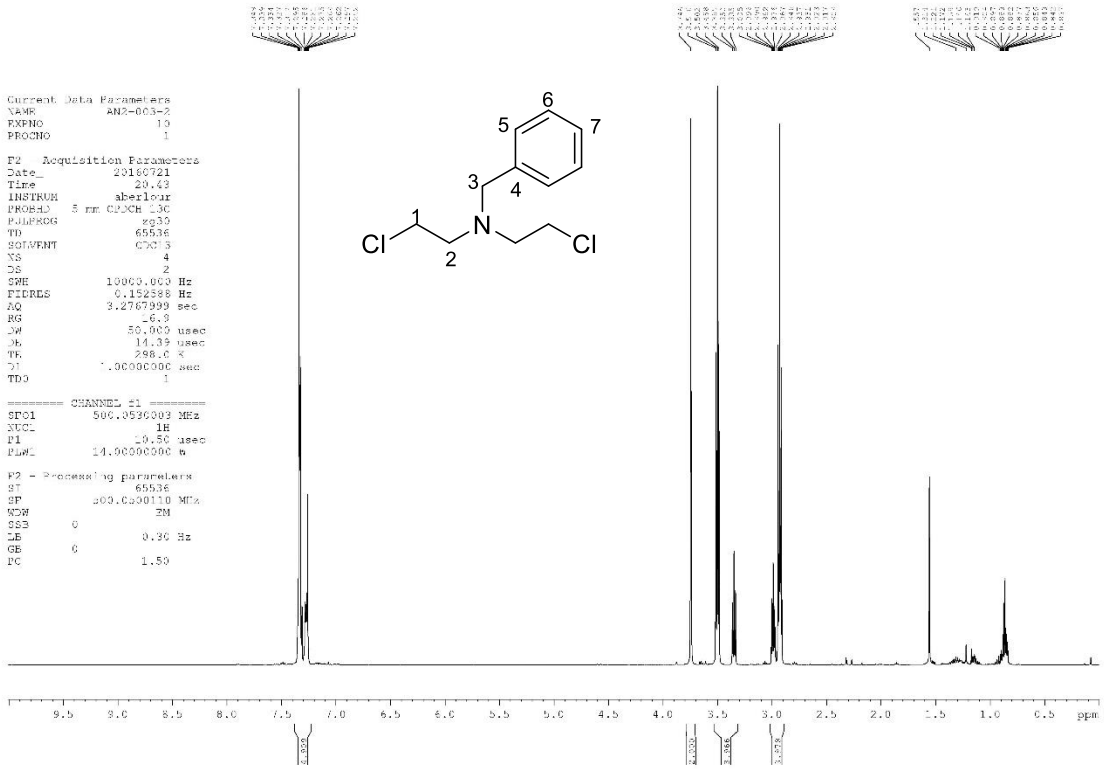

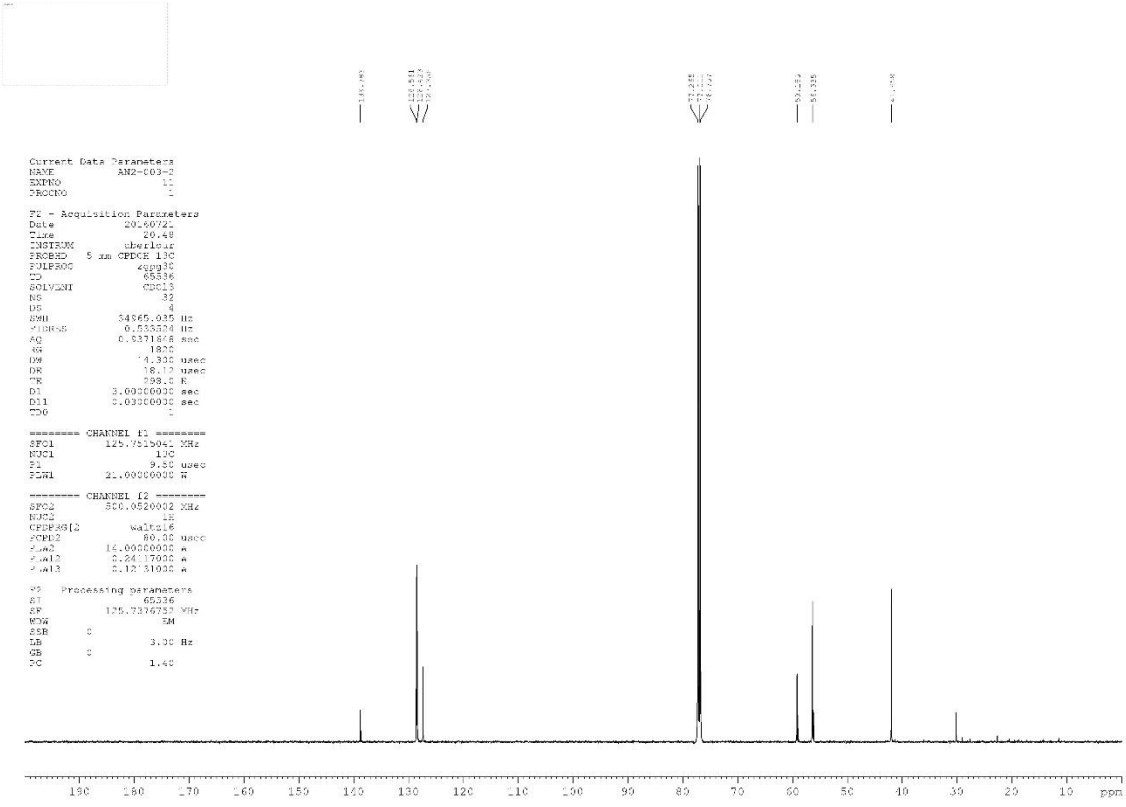

1′-Benzylspiro[indene-1,4′-piperidine], 100

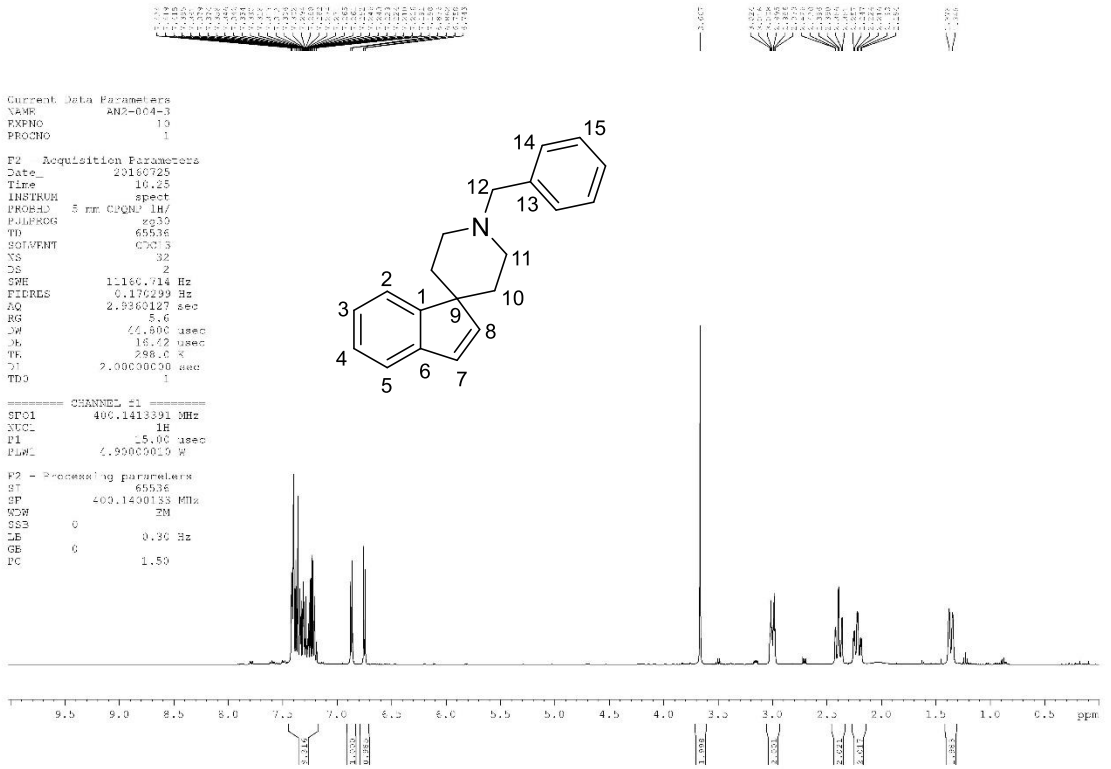

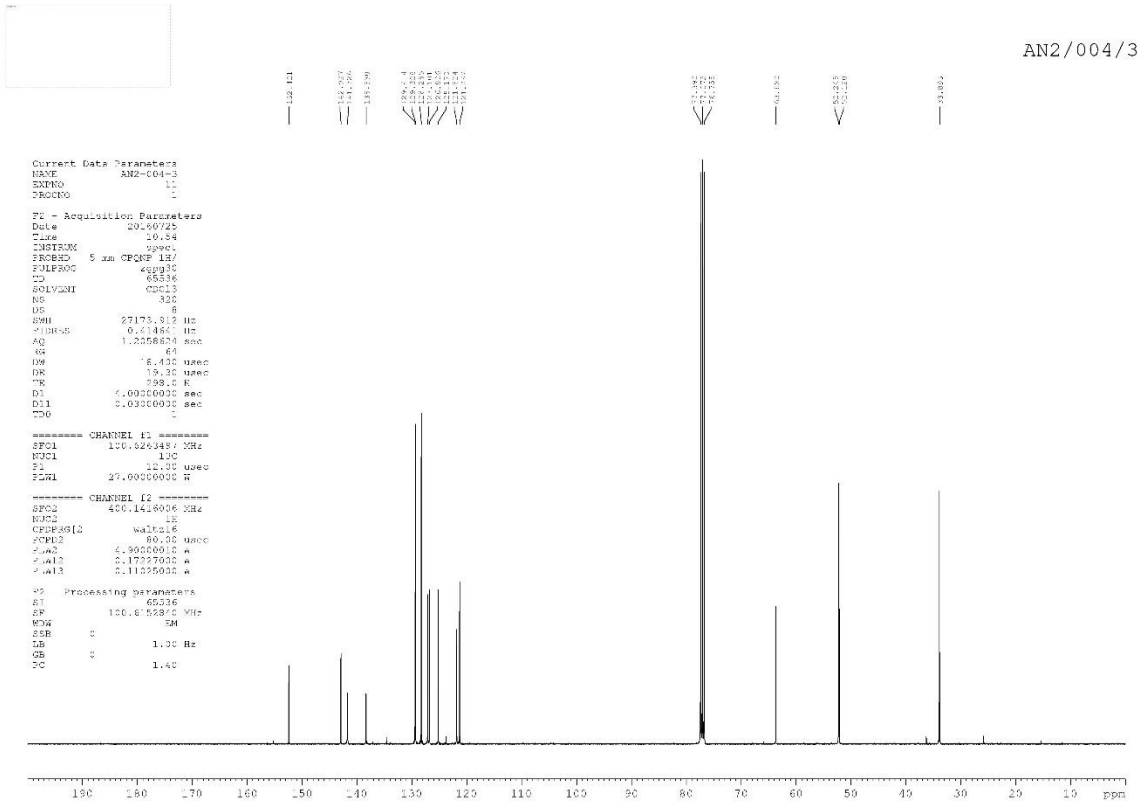

1′-Benzyl-2,3-dihydrospiro[indene-1,4′-piperidine], 101

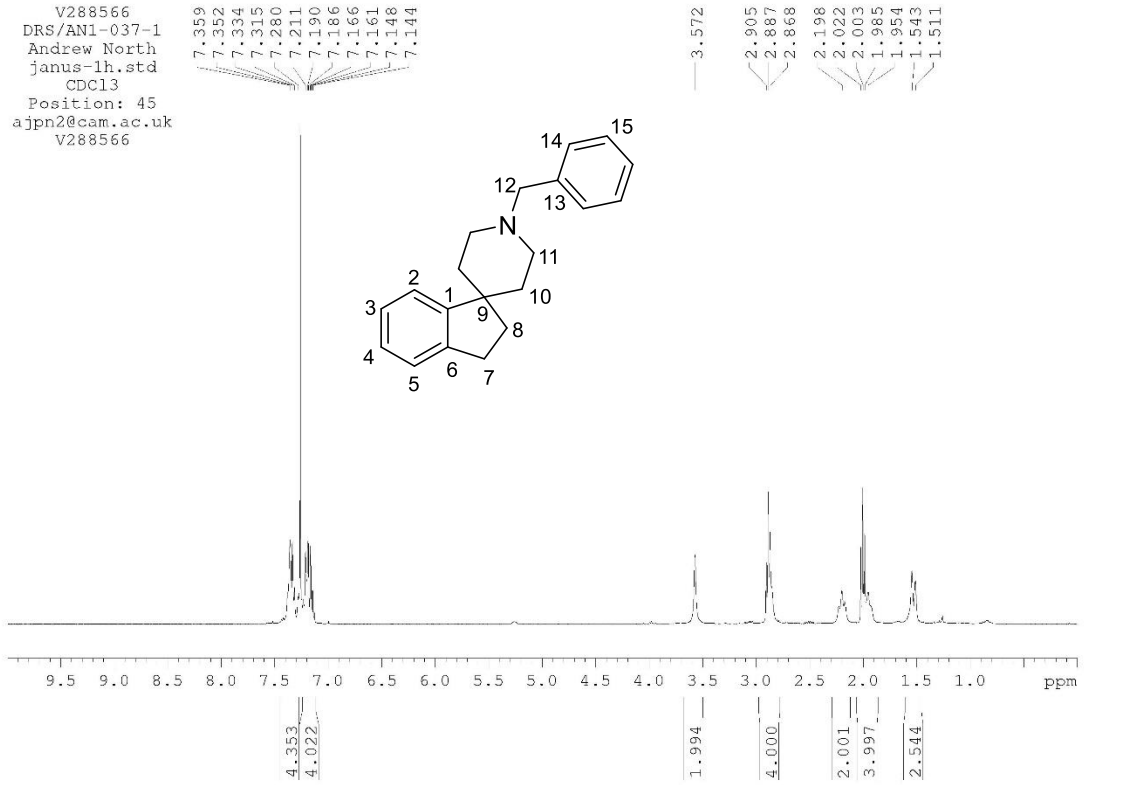

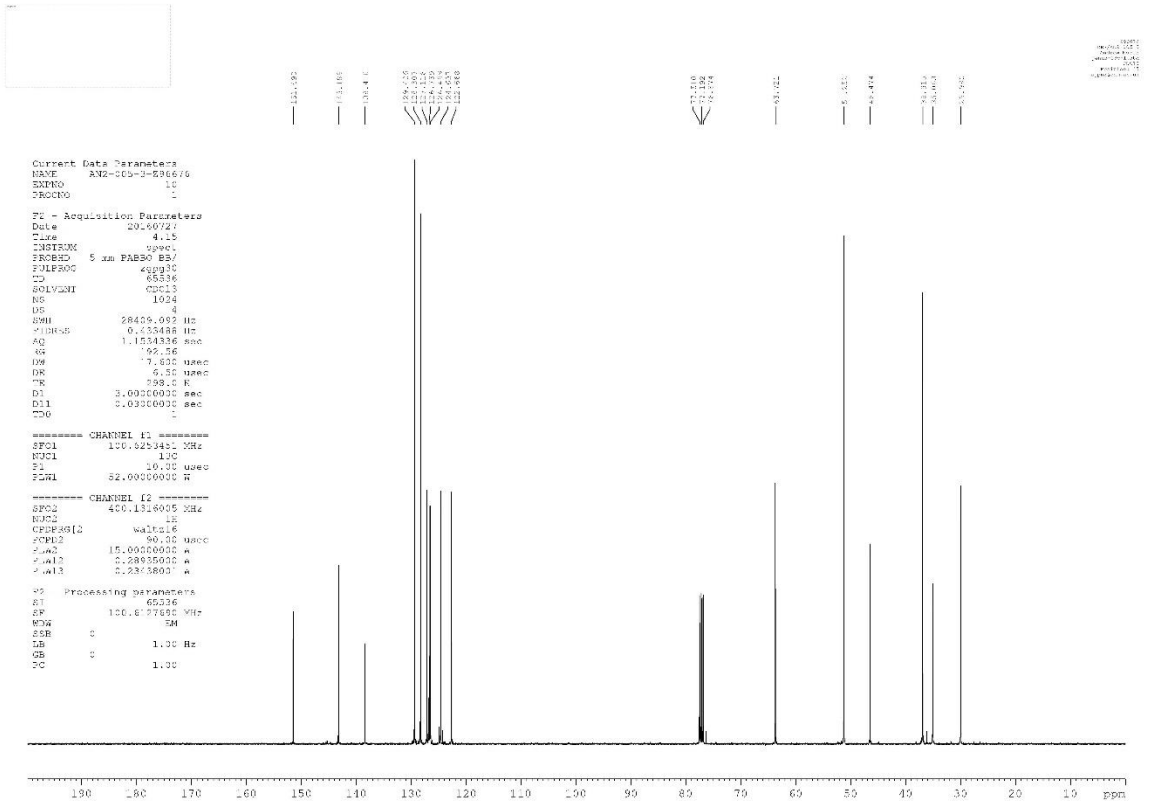

tert-Butyl spiro[indene-1,4′-piperidine]-1′-carboxylate, 102

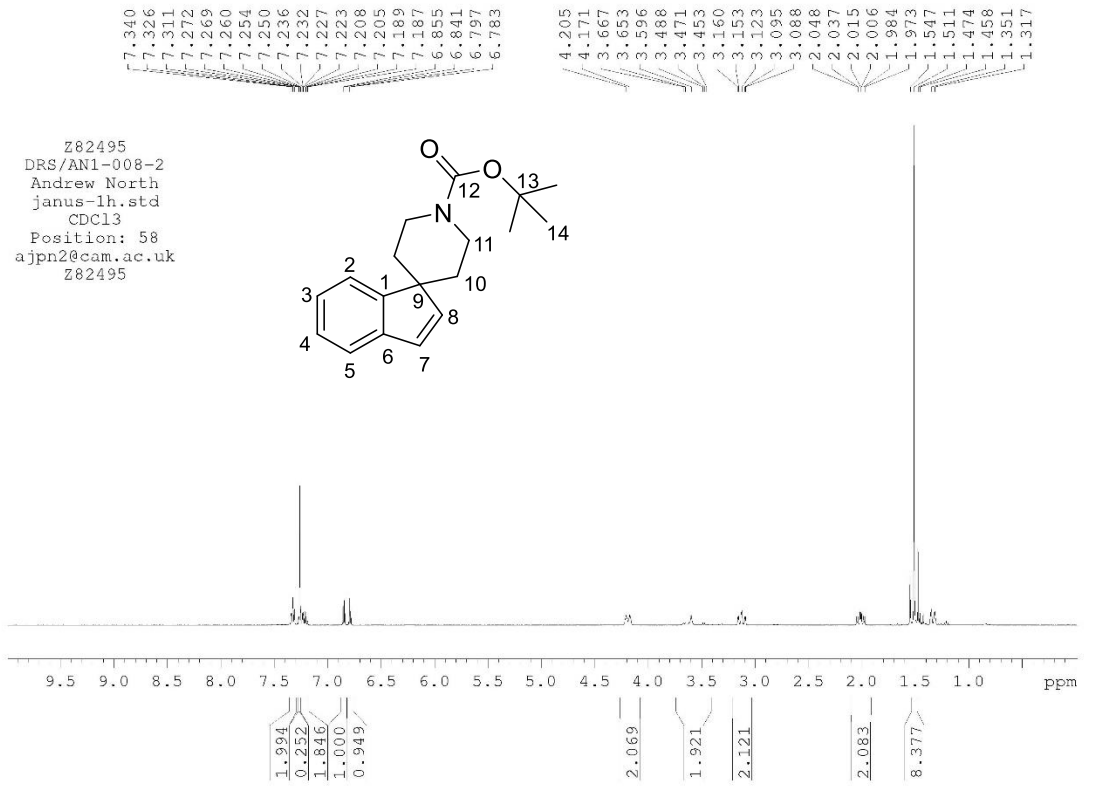

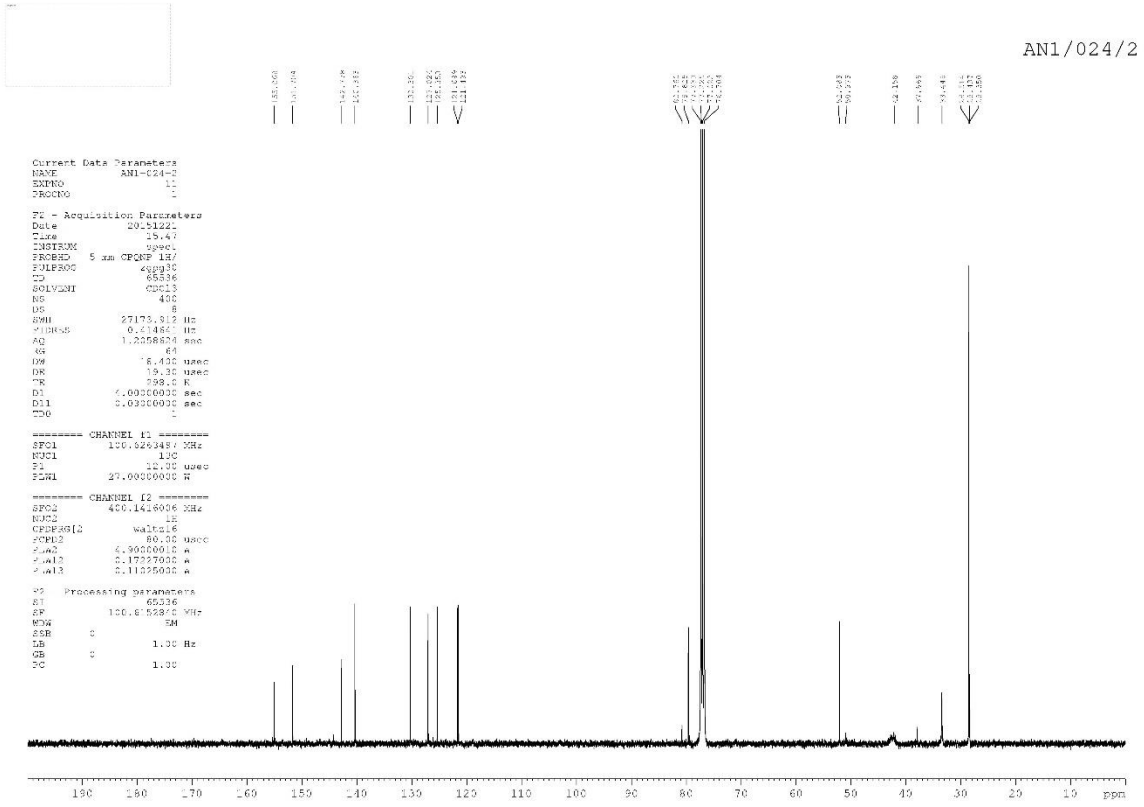

Spiro[indene-1,4′-piperidin]-1′-ium chloride, 103

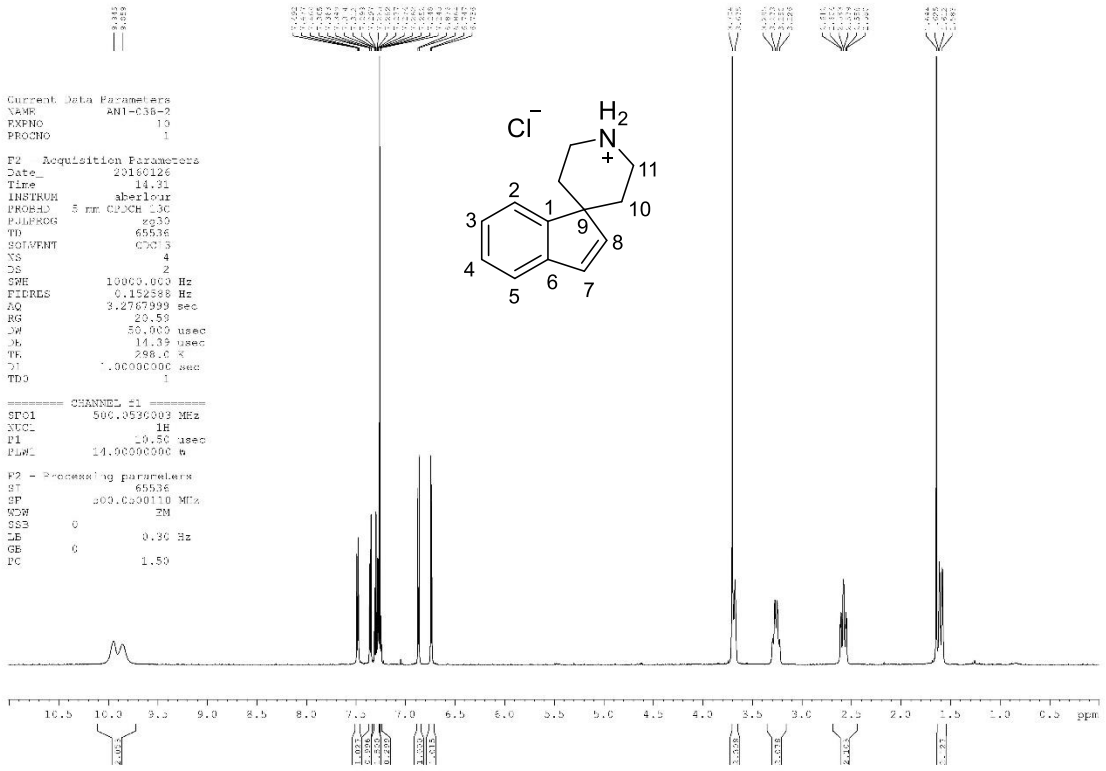

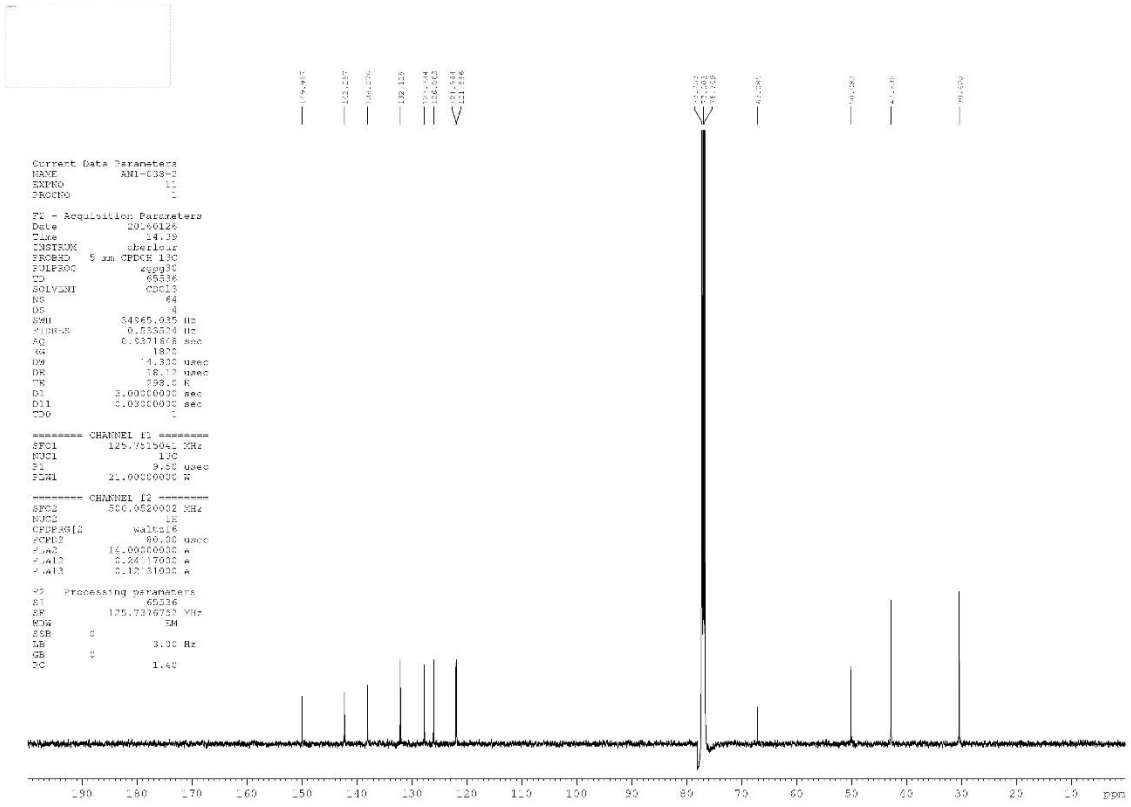

tert-Butyl 2-oxo-3,4-dihydroquinoline-1(2H)-carboxylate, 105

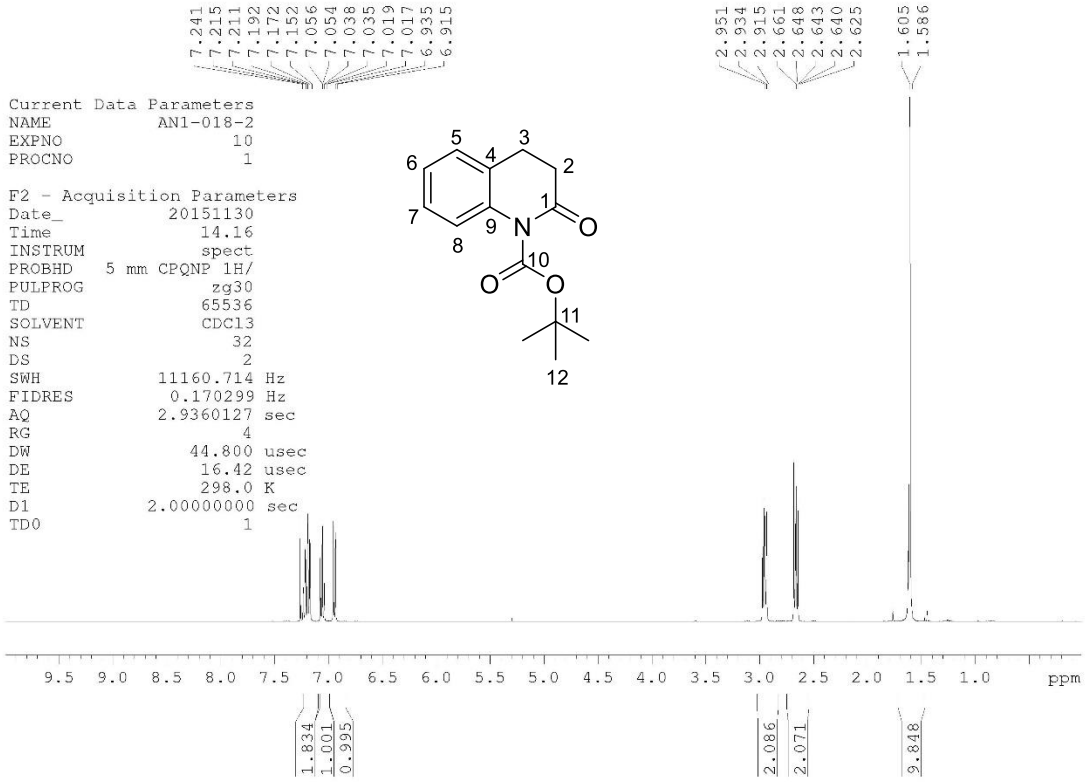

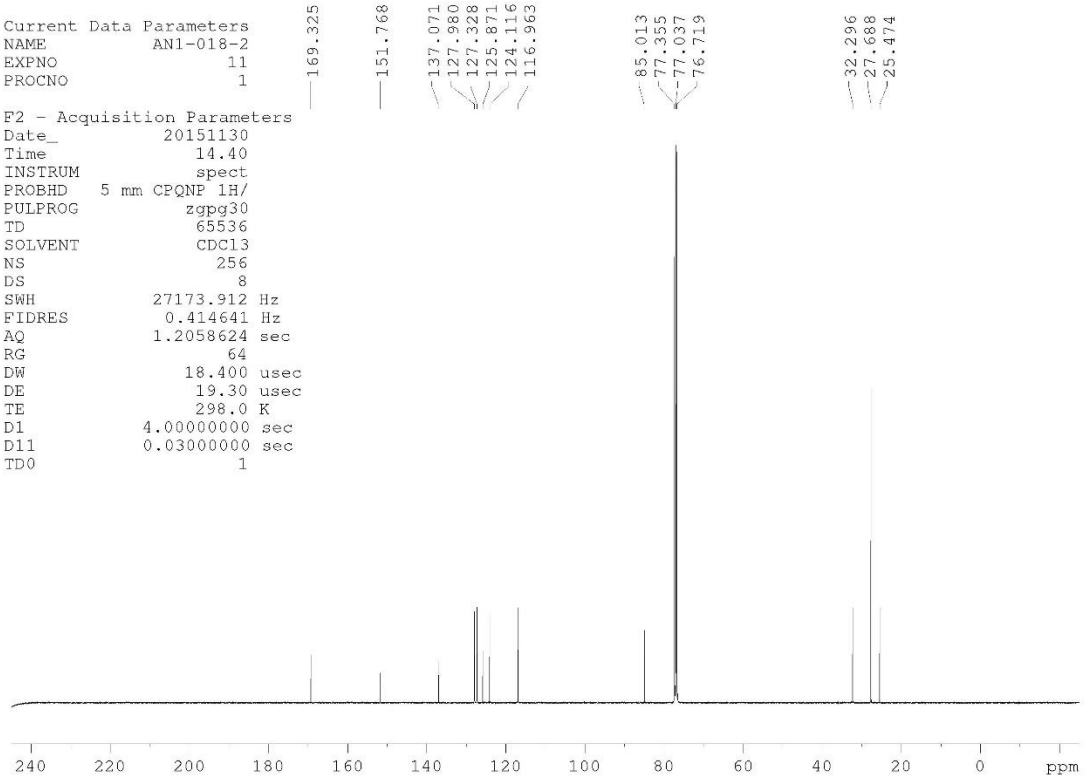

1-(*tert*-Butyl) 4-ethyl piperidine-1,4-dicarboxylate, 109

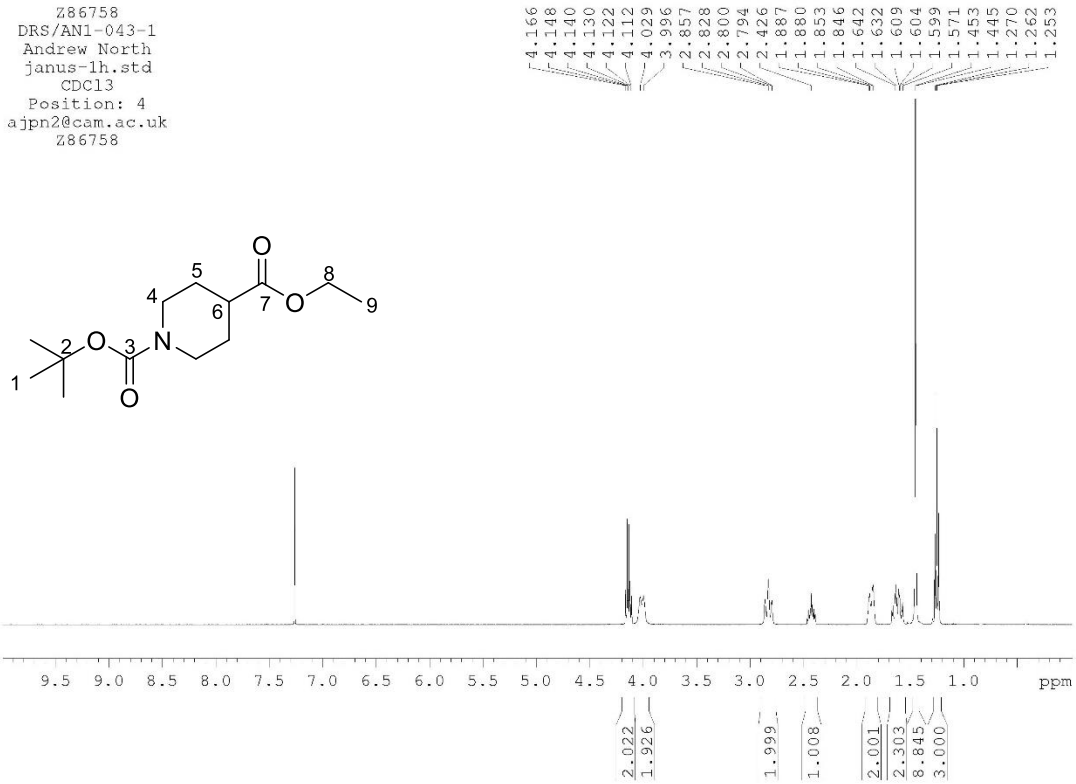

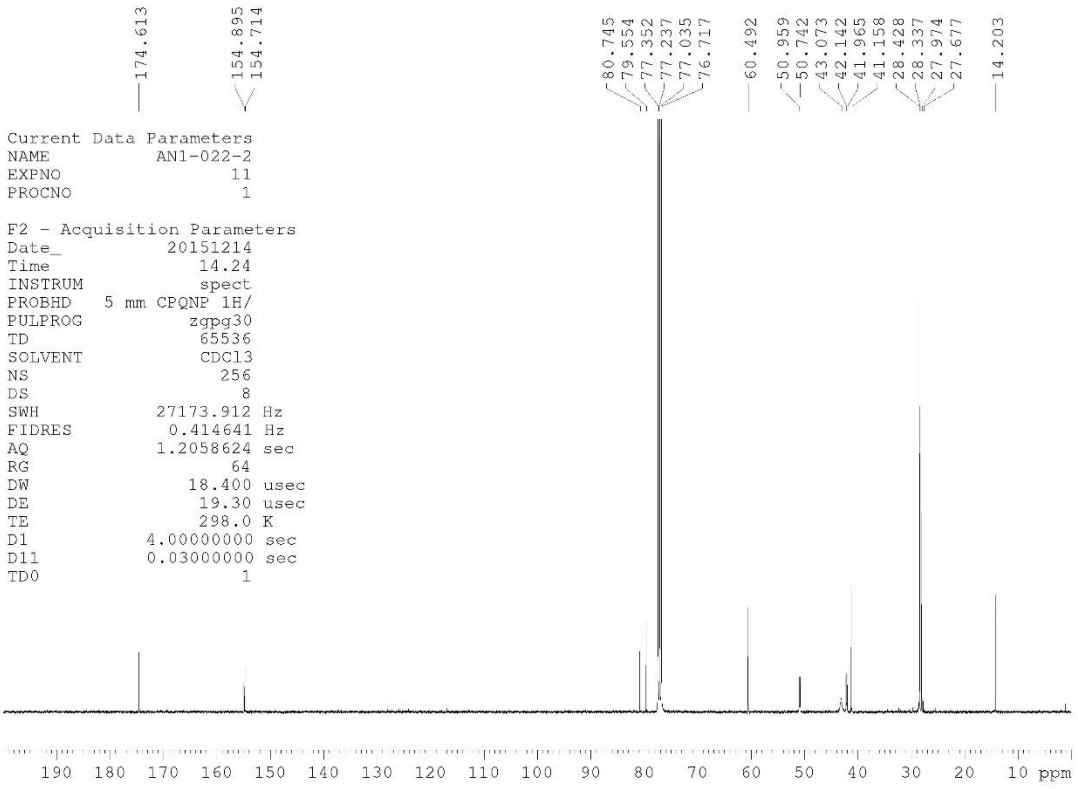

1-(*tert*-Butyl) 4-ethyl 4-(2-nitrobenzyl)piperidine-1,4-dicarboxylate, 111

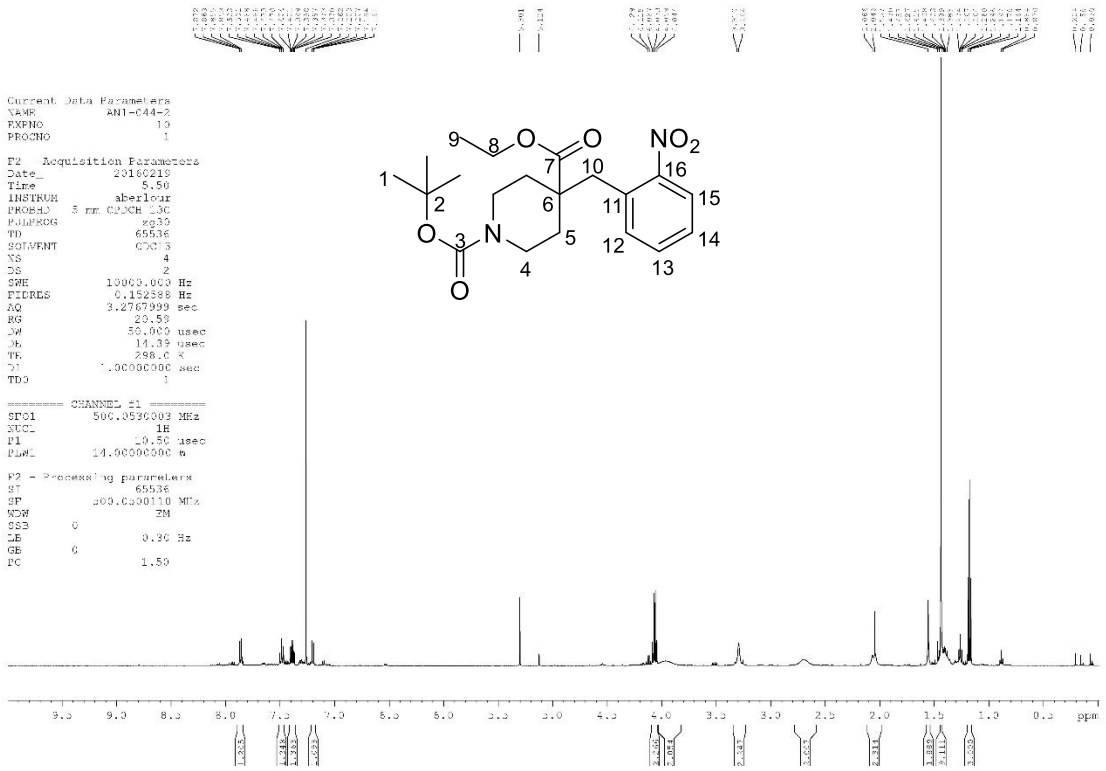

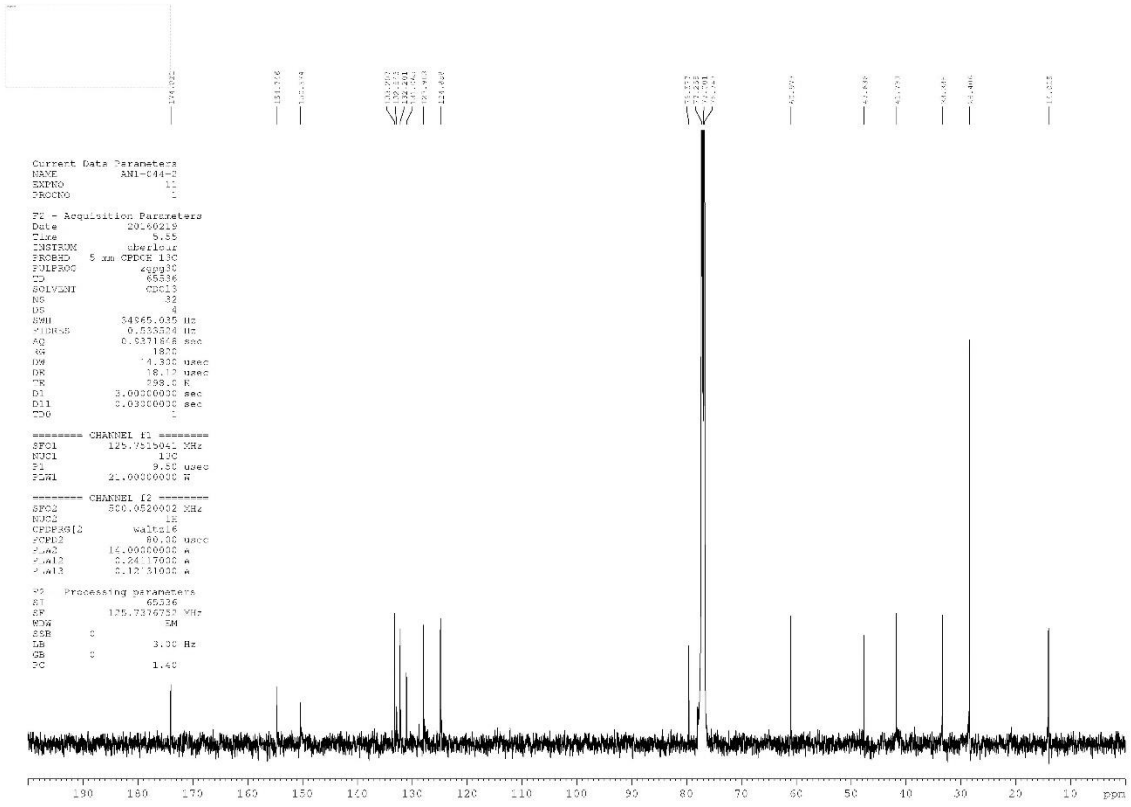

1-(*tert*-Butyl) 4-ethyl 4-(2-aminobenzyl)piperidine-1,4-dicarboxylate, 112

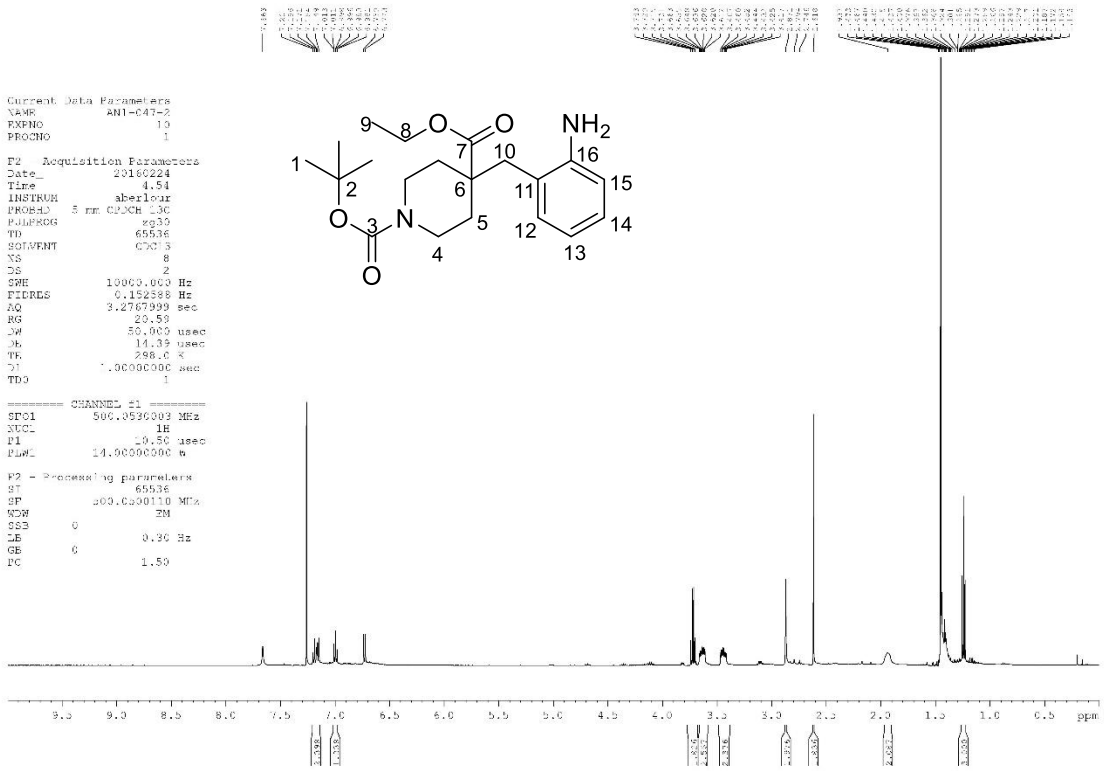

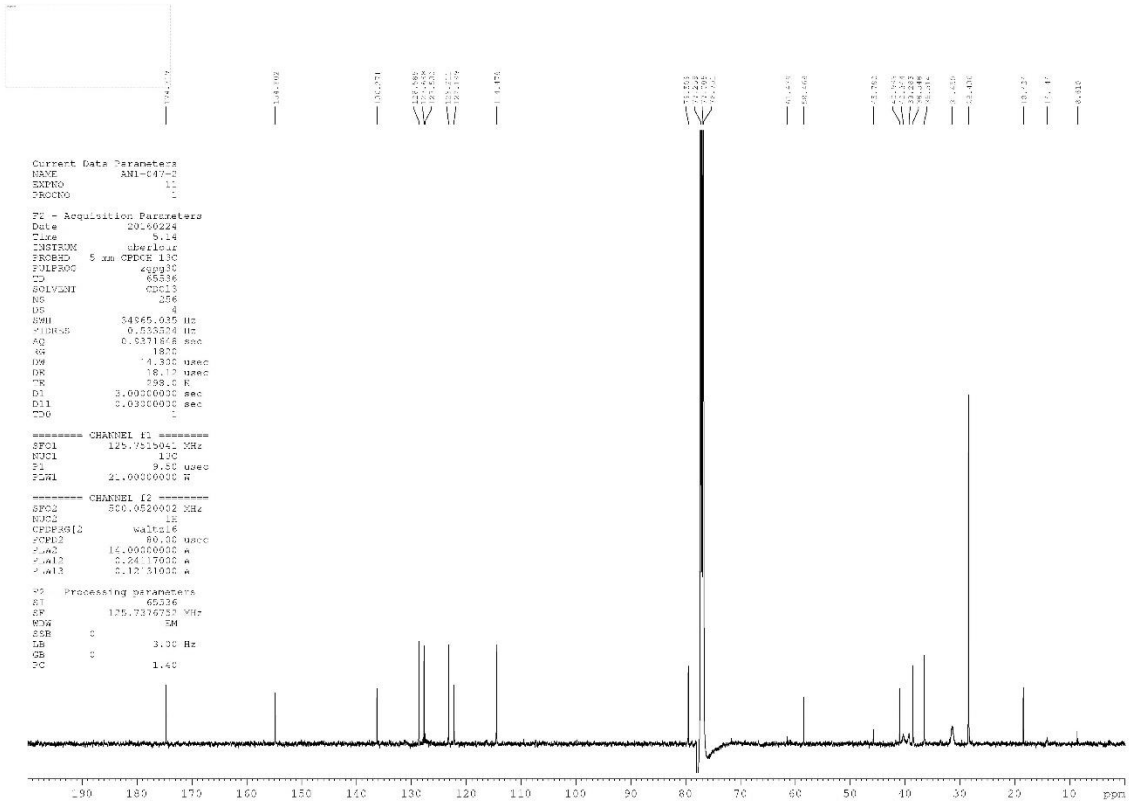

6-Chloro-1H-indene, 115

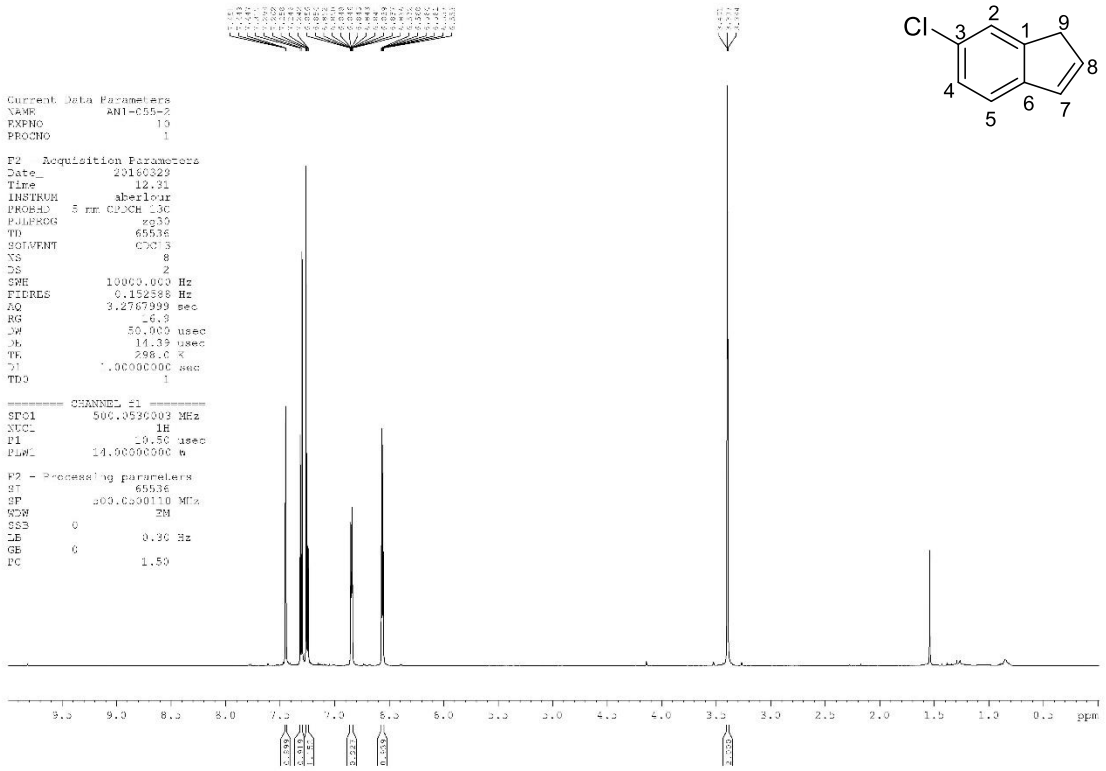

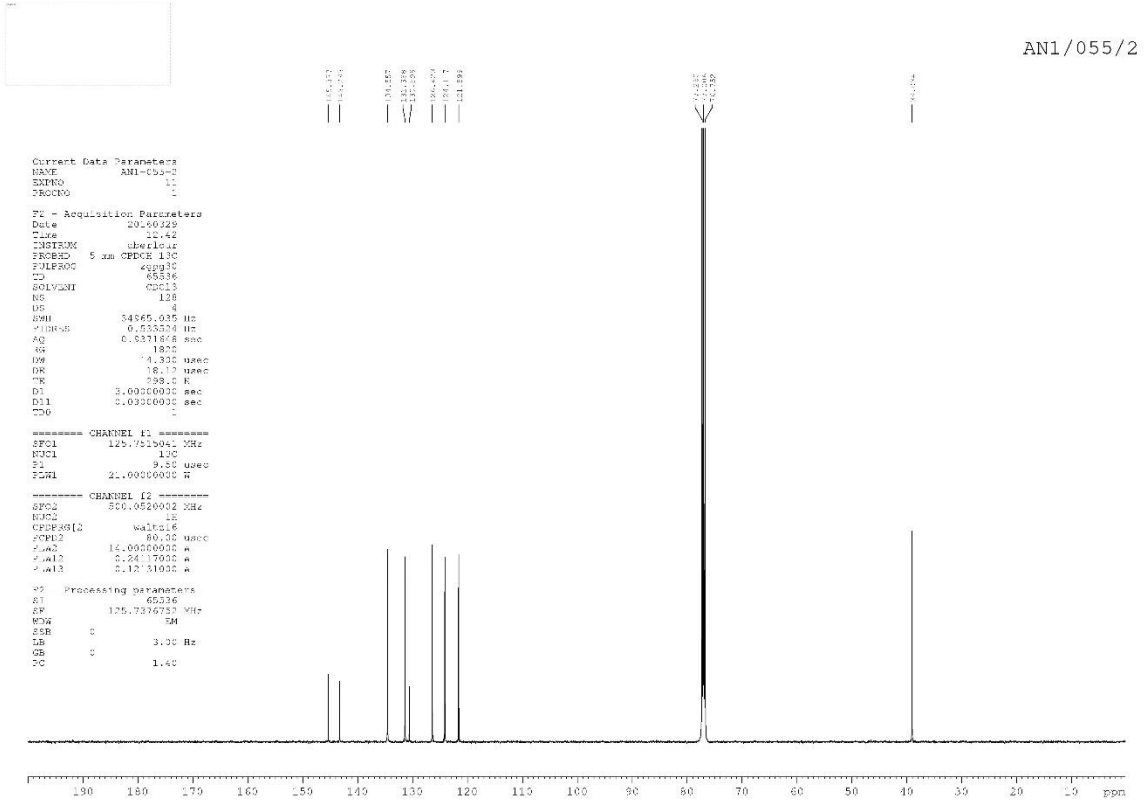

tert-Butyl 6-chlorospiro[indene-1,4′-piperidine]-1′-carboxylate, 116

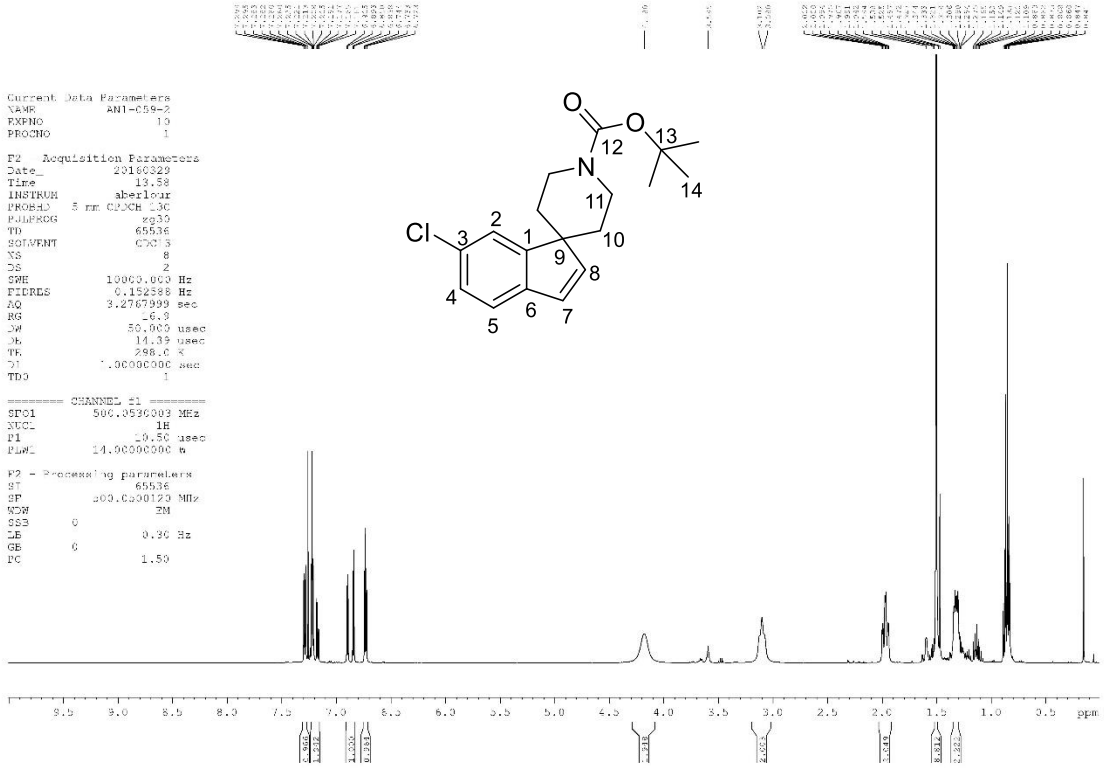

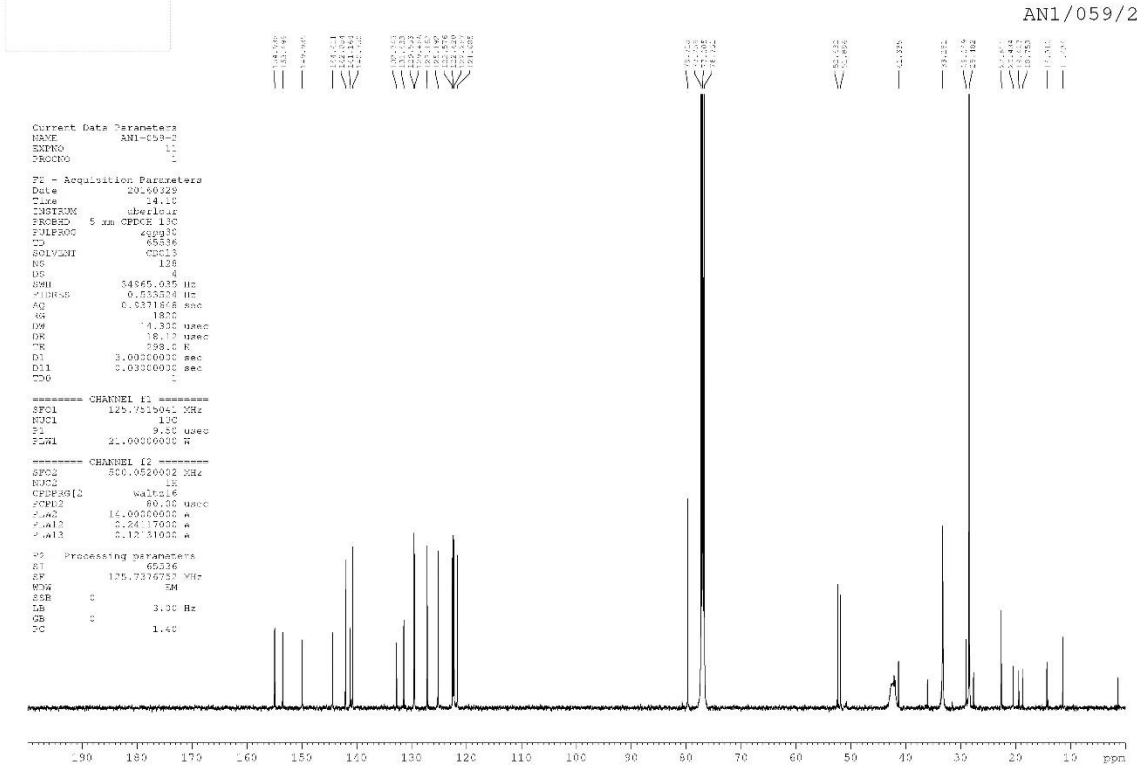

6-Chlorospiro[indene-1,4′-piperidin]-1′-ium chloride, 117

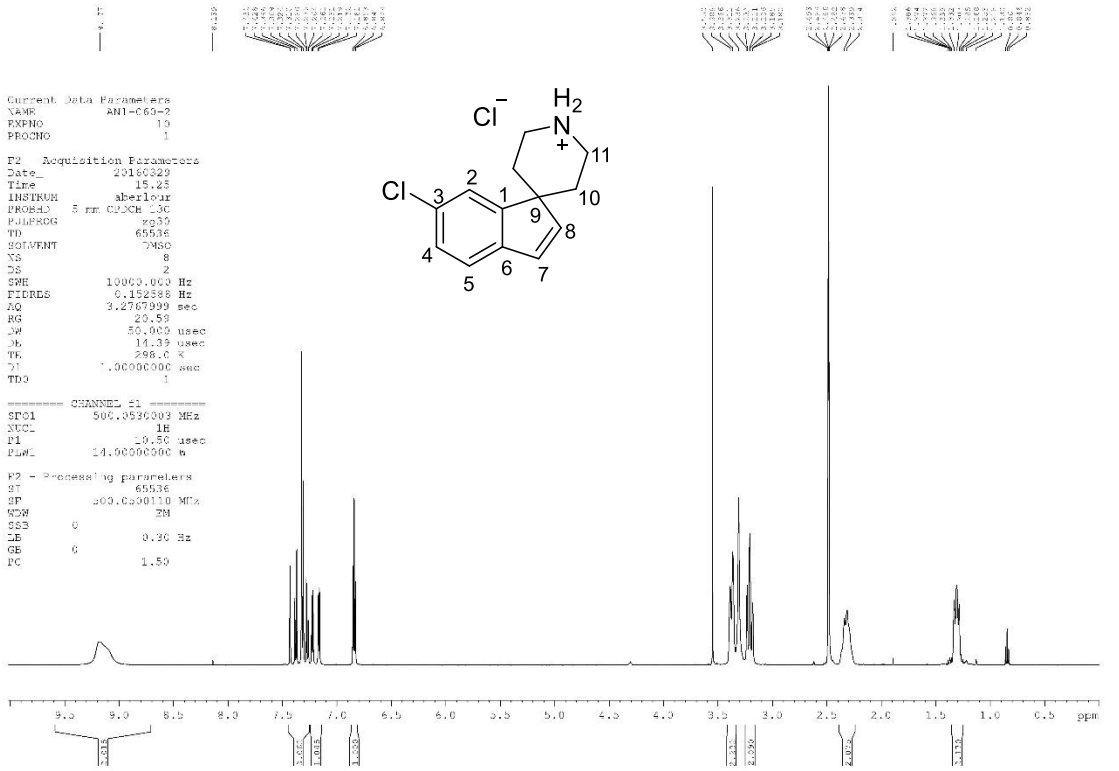

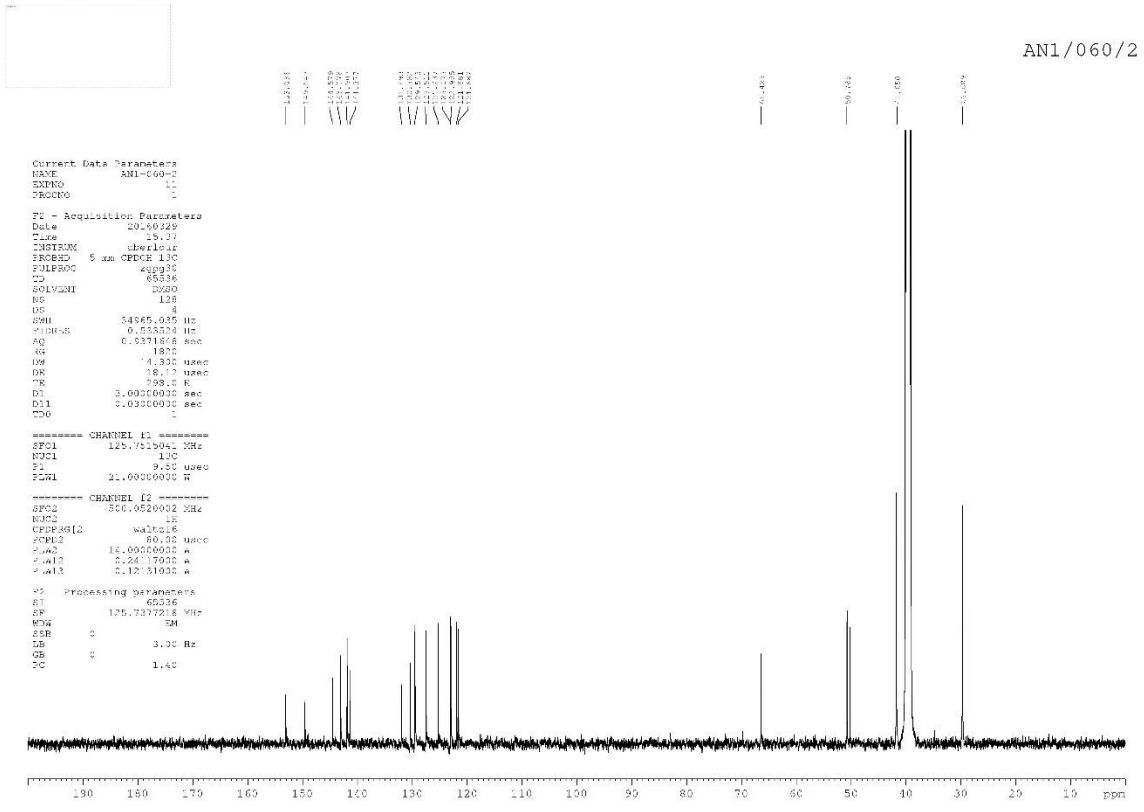

6-Chloro-2,3-dihydrospiro[indene-1,4′-piperidin]-1′-ium chloride, 118

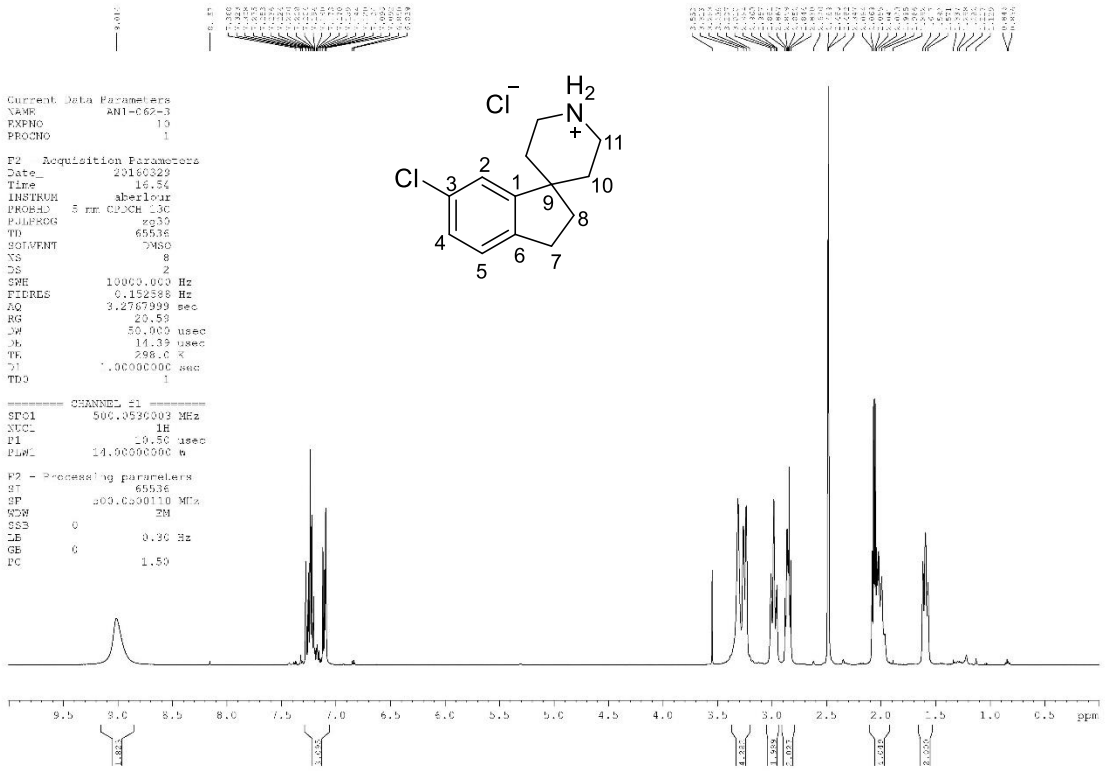

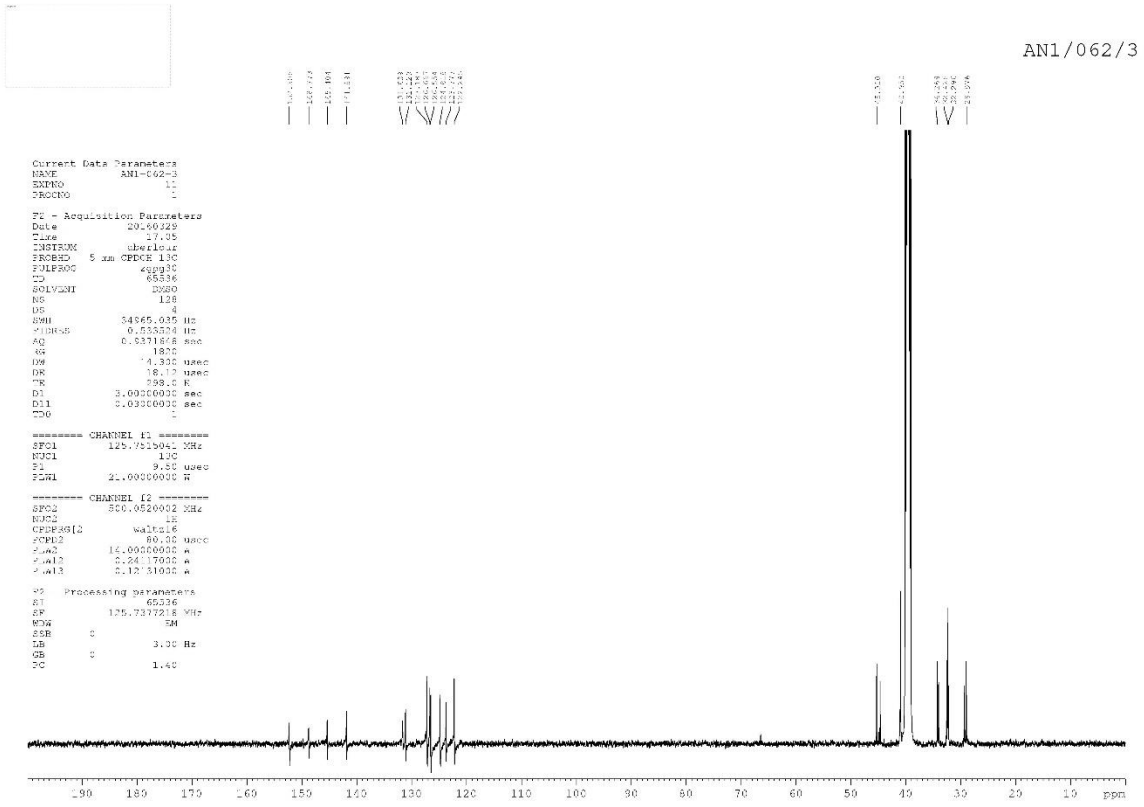

8-Chloro-2-(ethoxycarbonyl)-2,3,4,5-tetrahydro-1H-pyrido[4,3-b]indol-5-ium chloride, 121

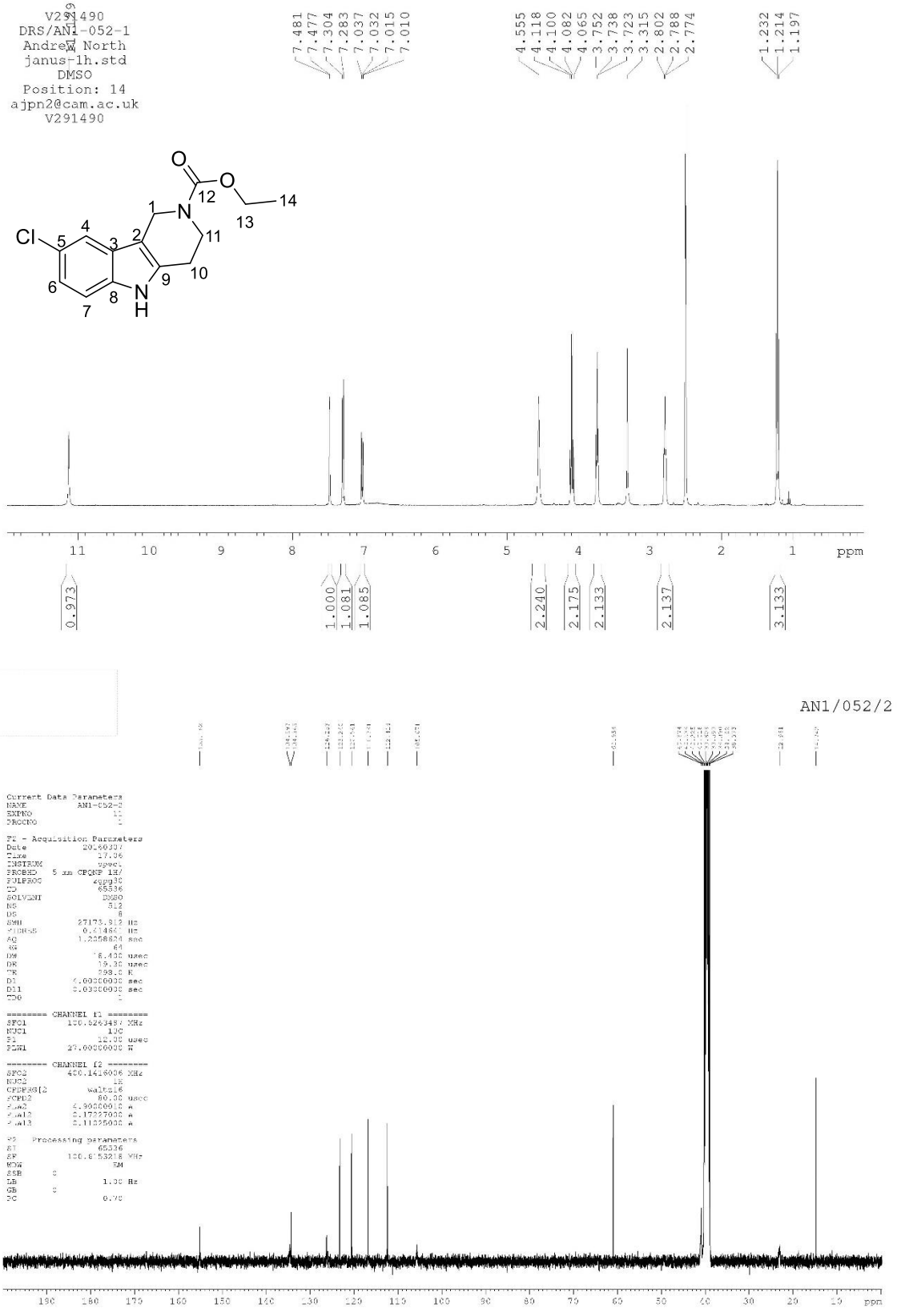

8-Chloro-2,3,4,5-tetrahydro-1H-pyrido[4,3-b]indol-2-ium chloride, 122

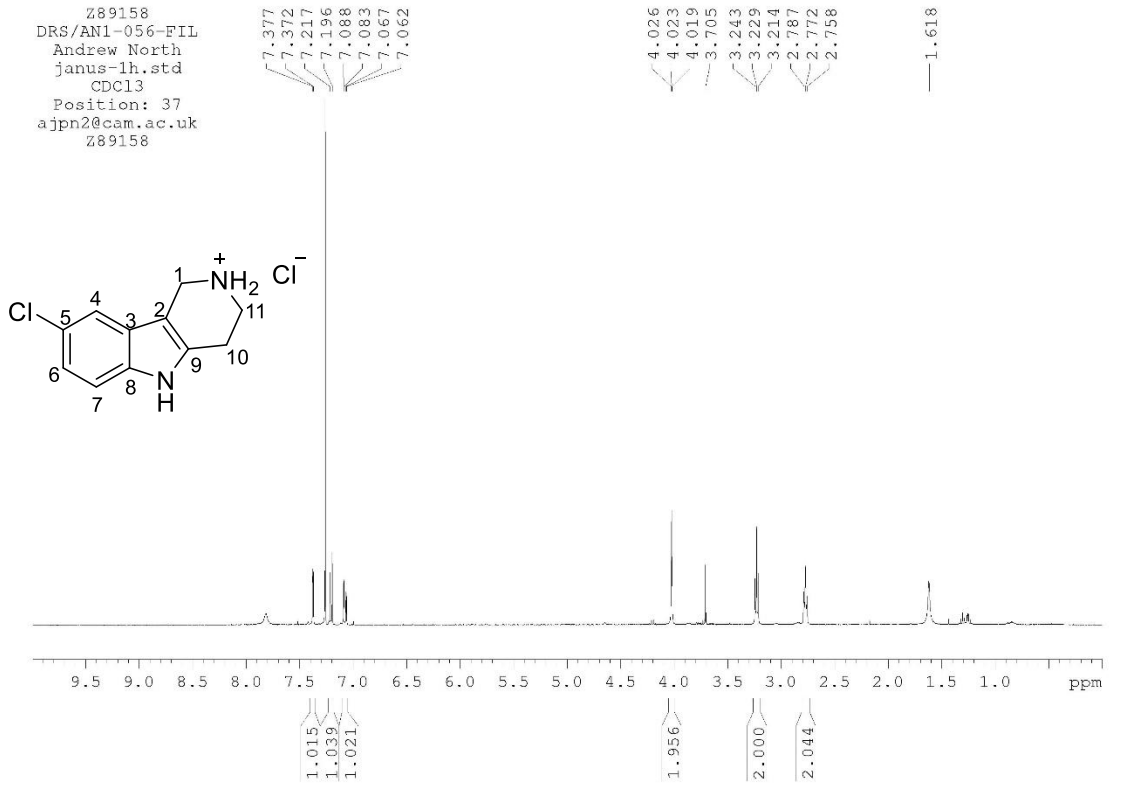

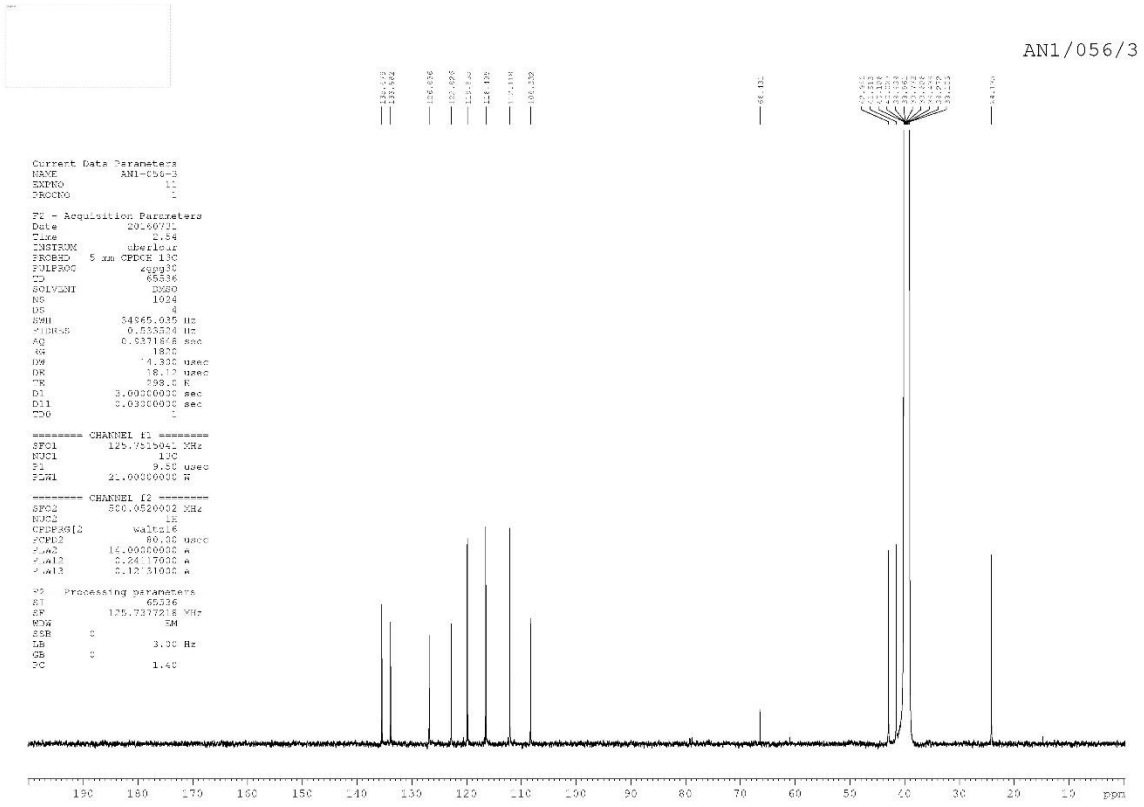

Ethyl (diphenylmethylene)glycinate, 140

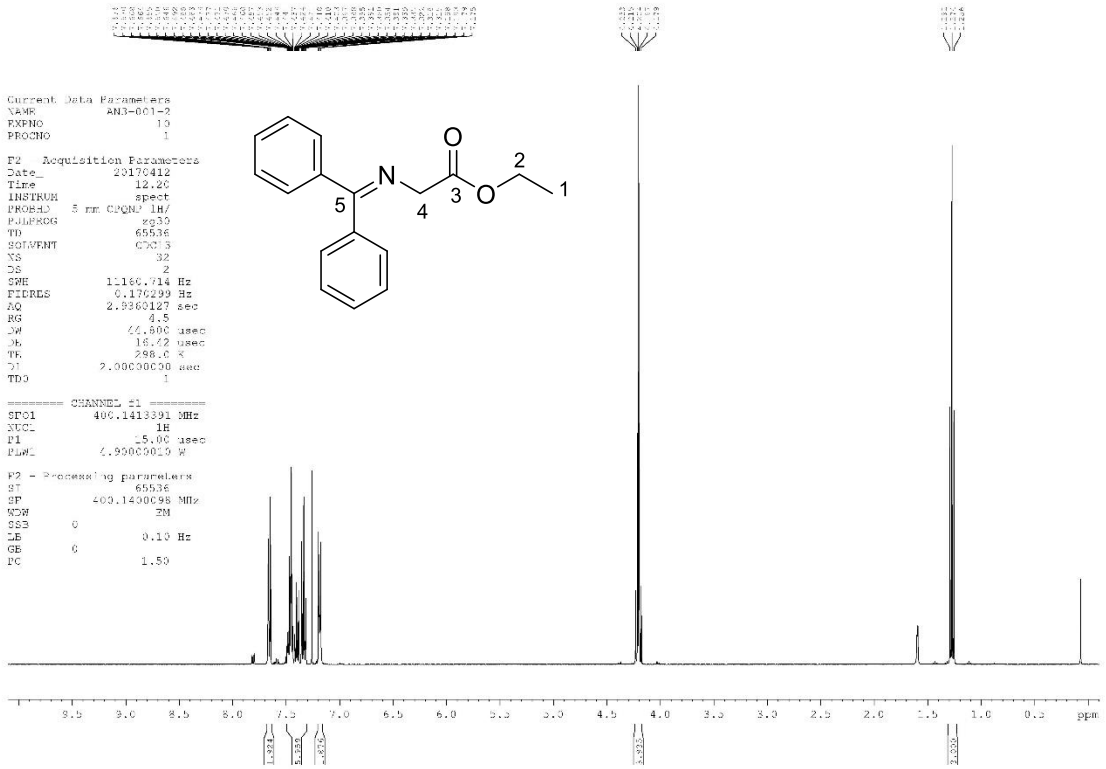

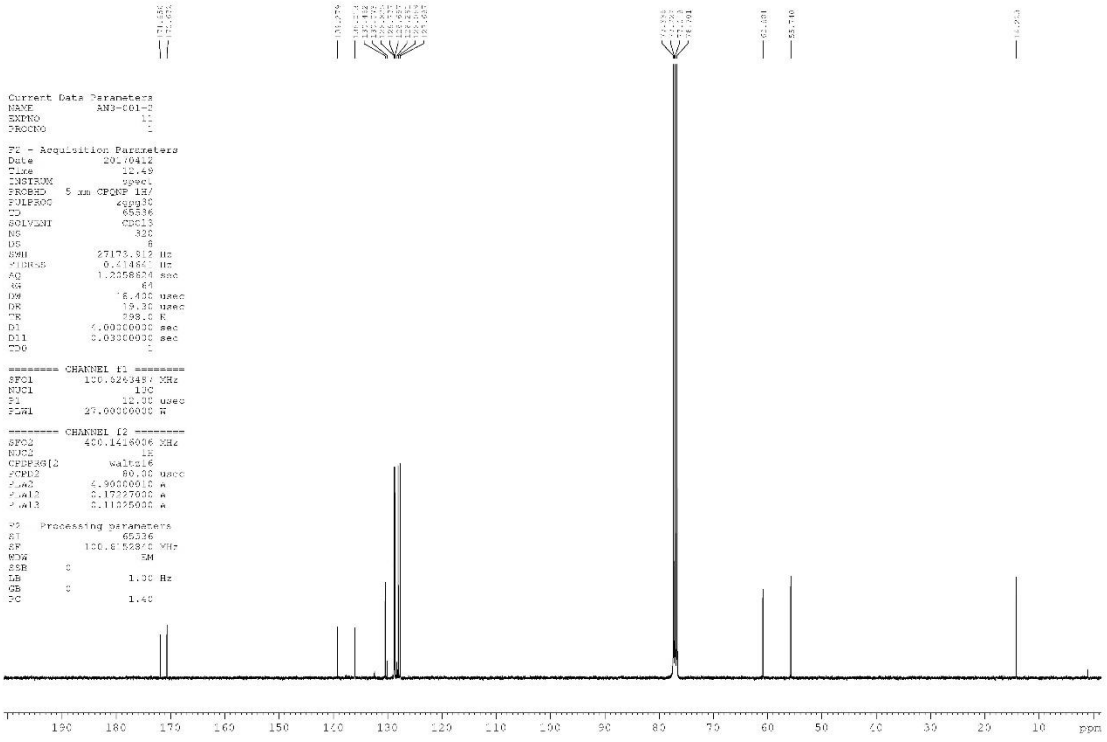

Ethyl 2-((diphenylmethylene)amino)hex-5-enoate, 141

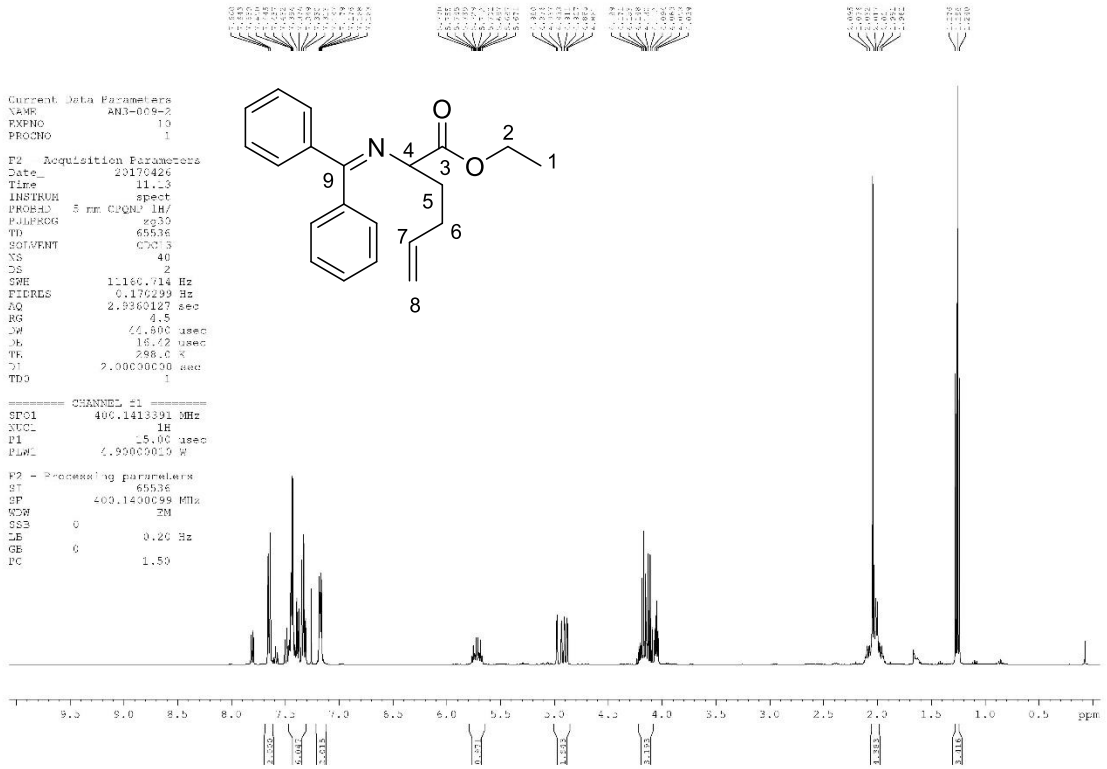

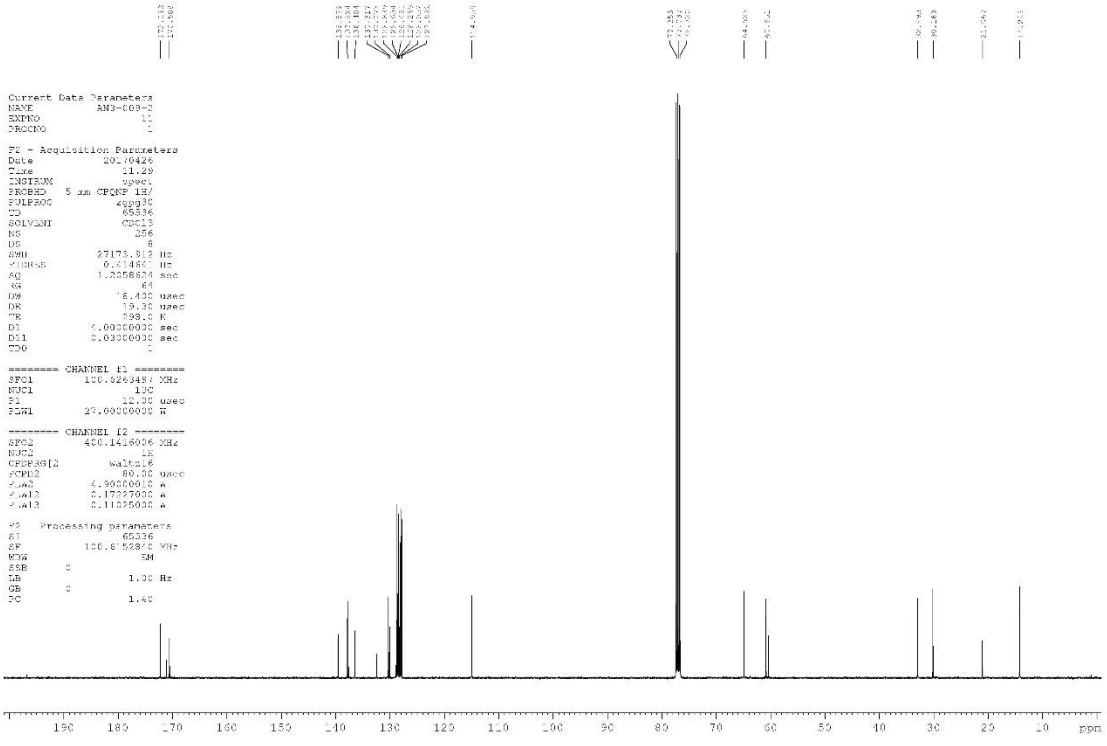

Ethyl 2-allyl-2-aminohex-5-enoate, 142

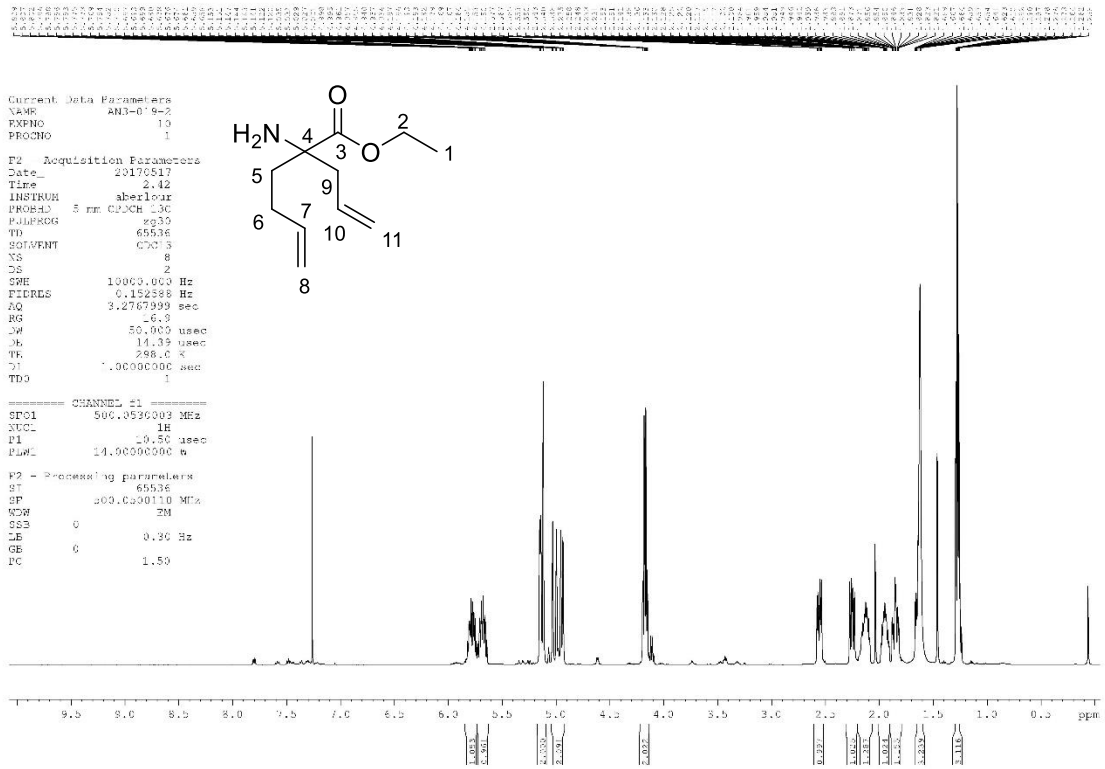

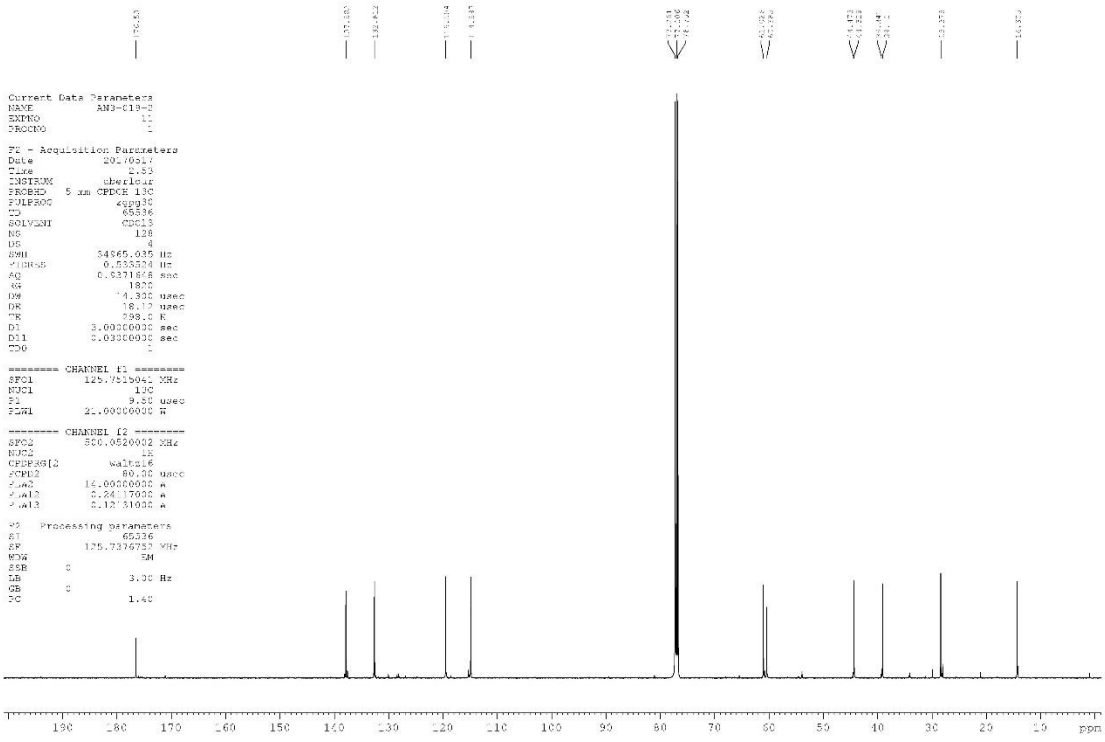

Ethyl 2-allyl-2-((*tert*-butoxycarbonyl)amino)hex-5-enoate, 143

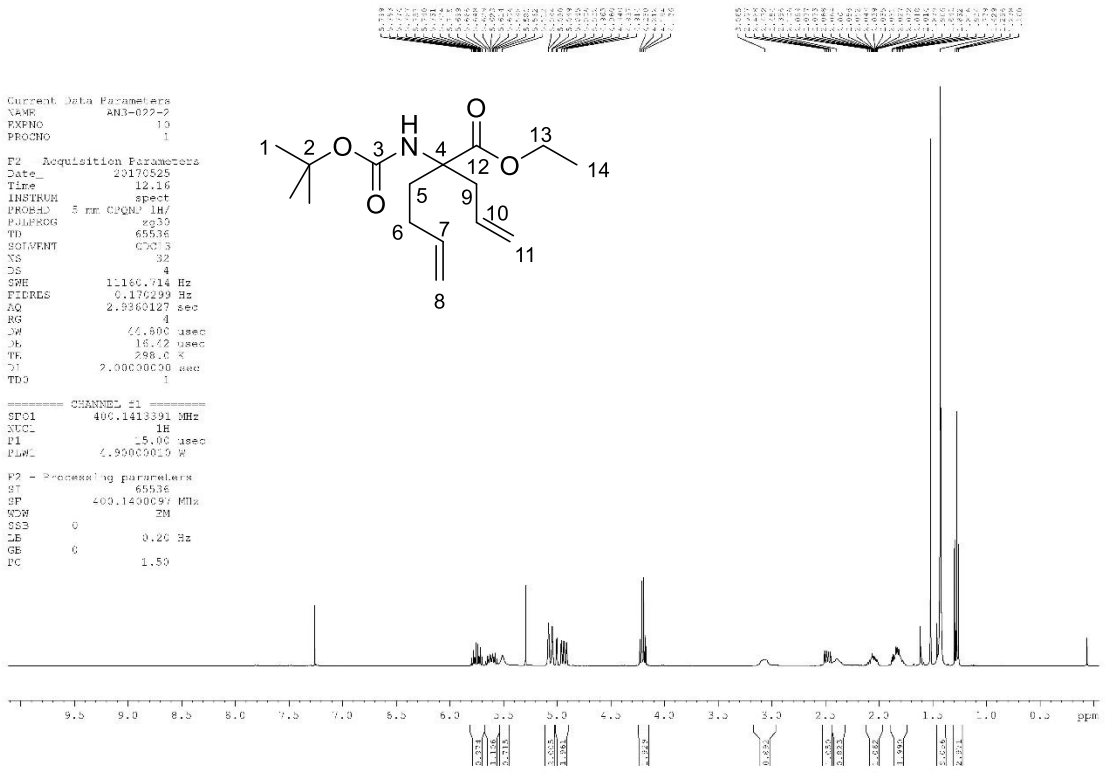

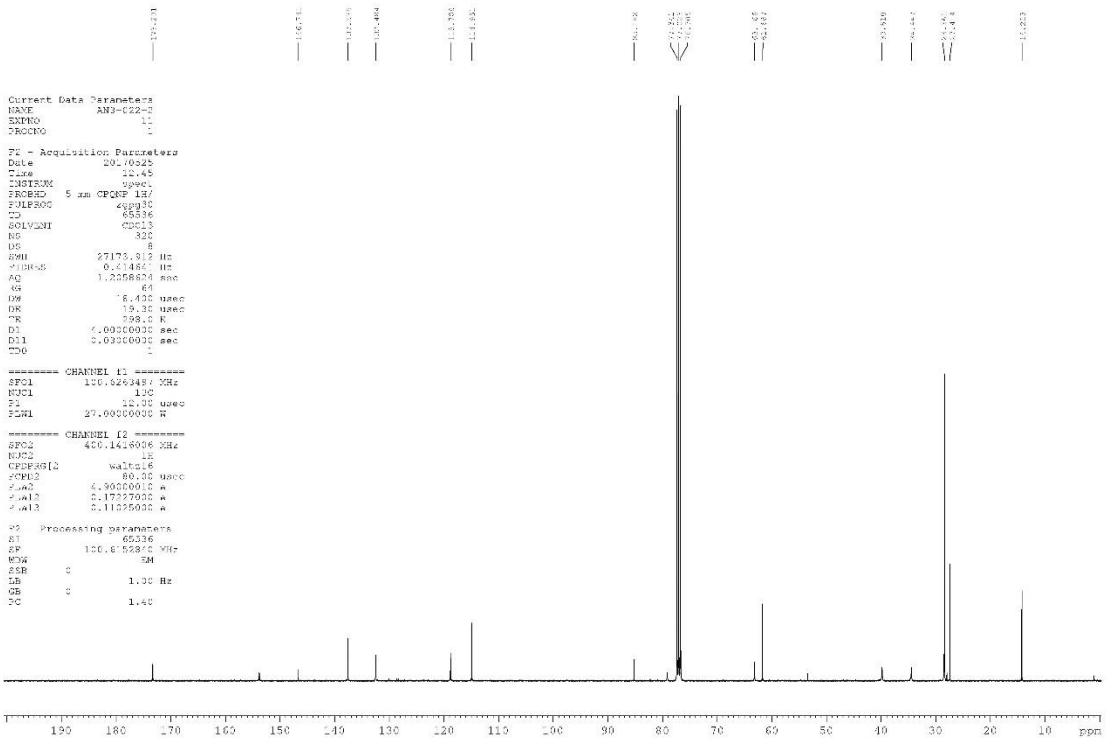

Ethyl 1-((*tert*-butoxycarbonyl)amino)cyclohex-3-ene-1-carboxylate, 144

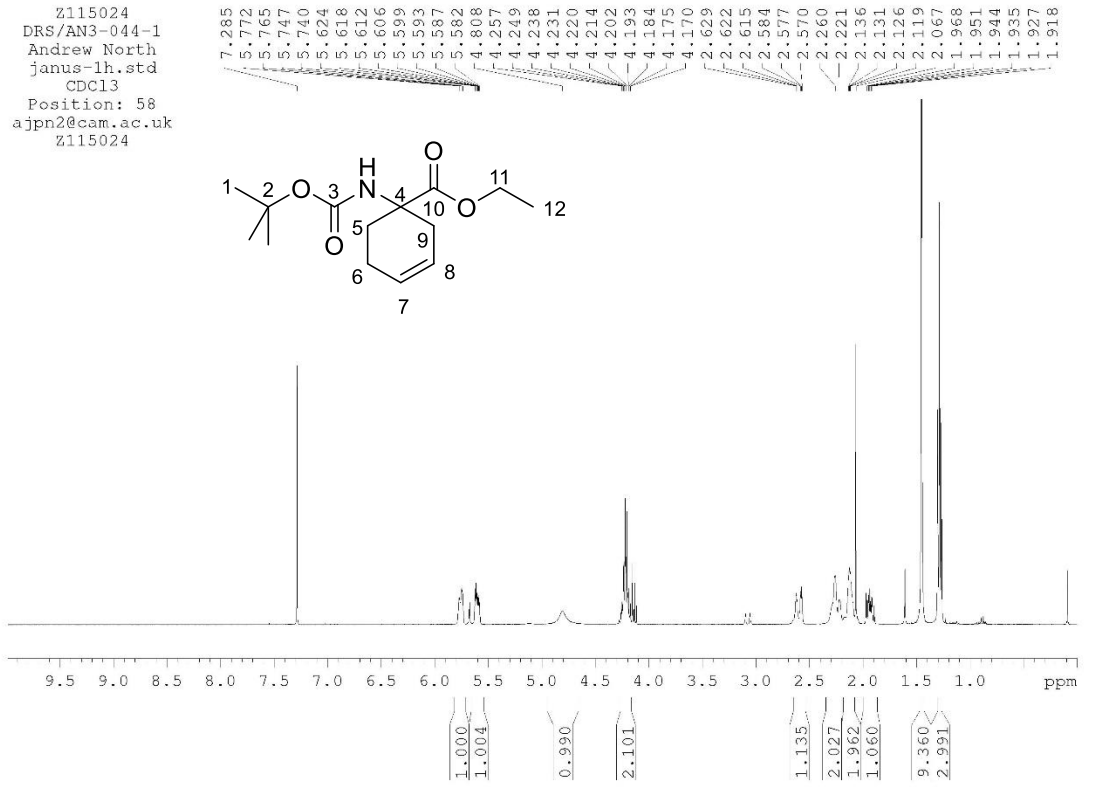

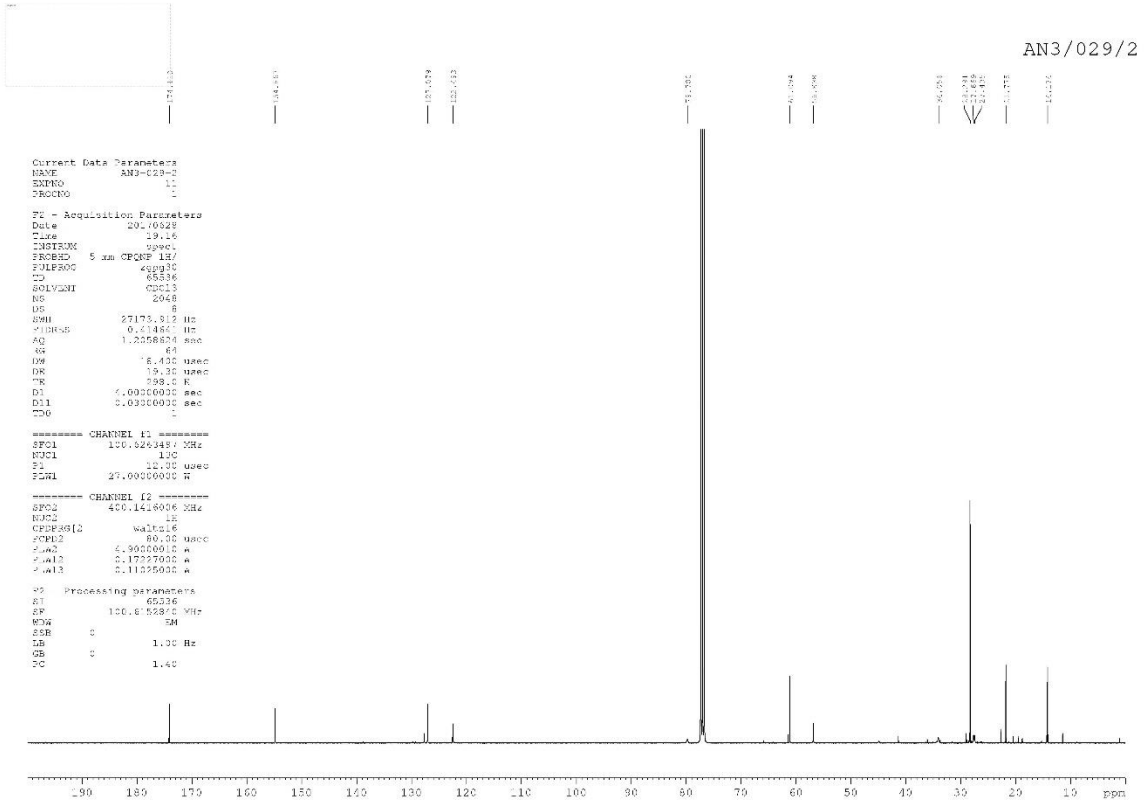

tert-Butyl (1-(hydroxymethyl)cyclohex-3-en-1-yl)carbamate, 145

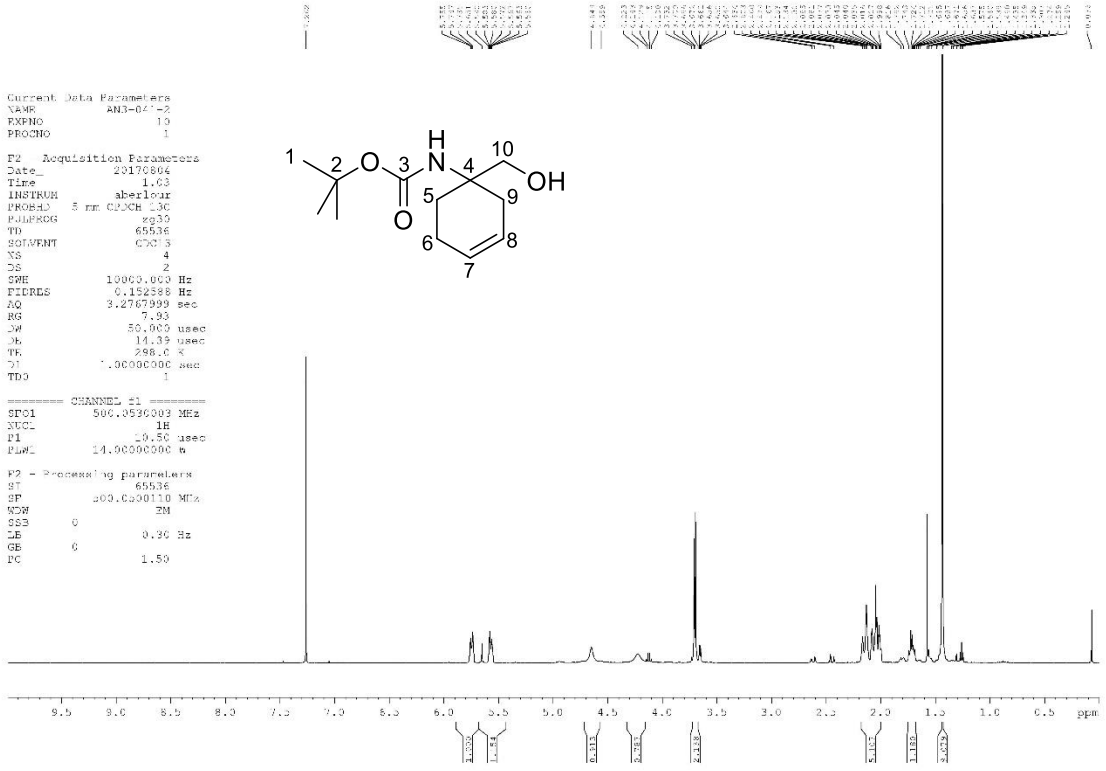

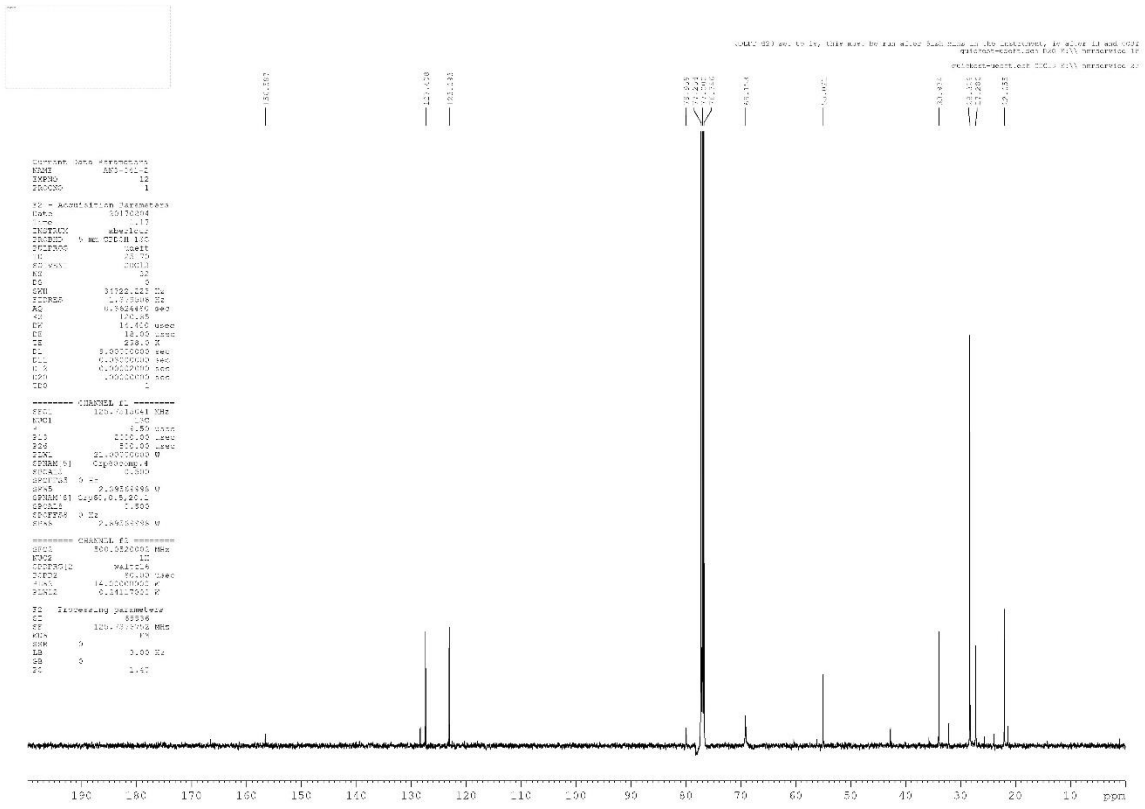

1-(Hydroxymethyl)cyclohex-3-en-1-aminium chloride, 146

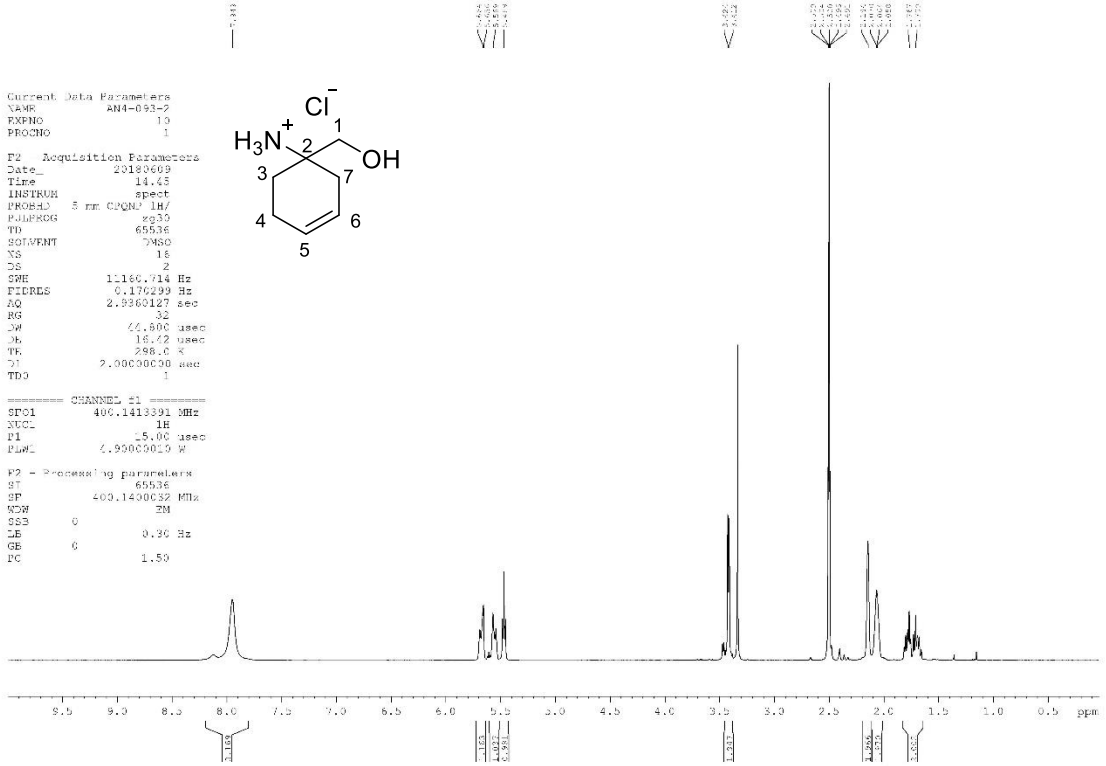

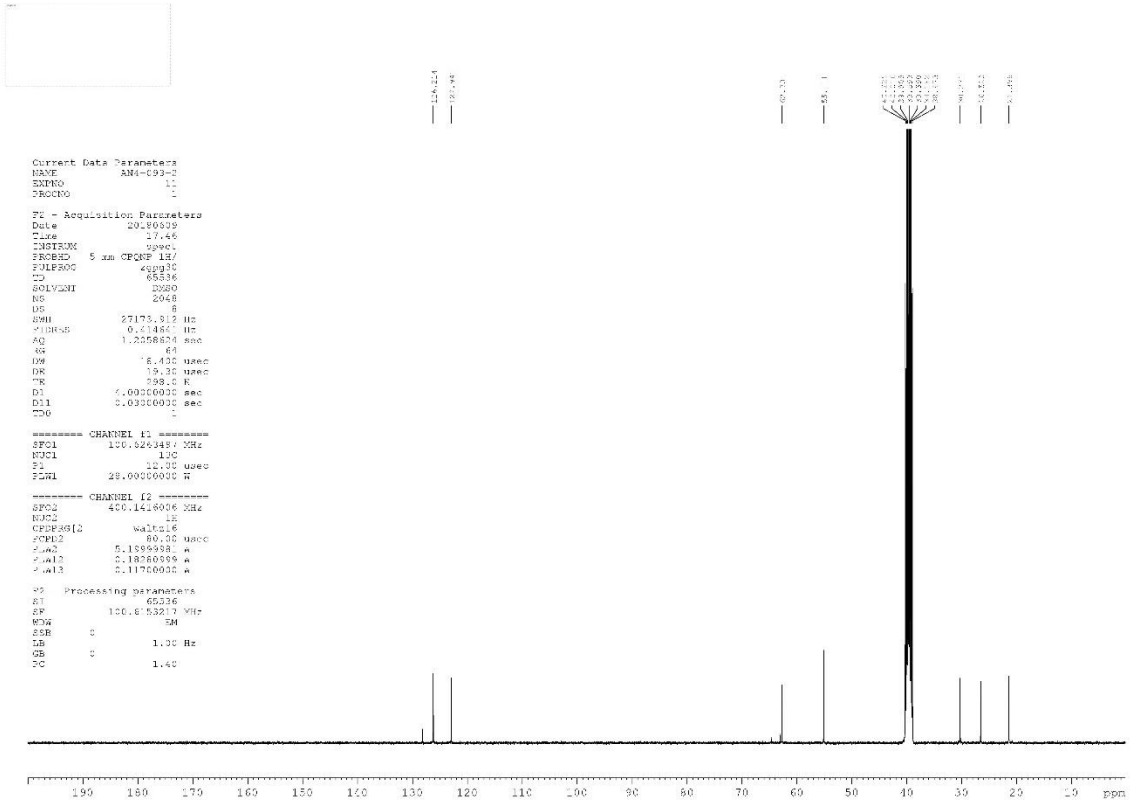

tert-Butyl (4-(hydroxymethyl)octa-1,7-dien-4-yl)carbamate, 147

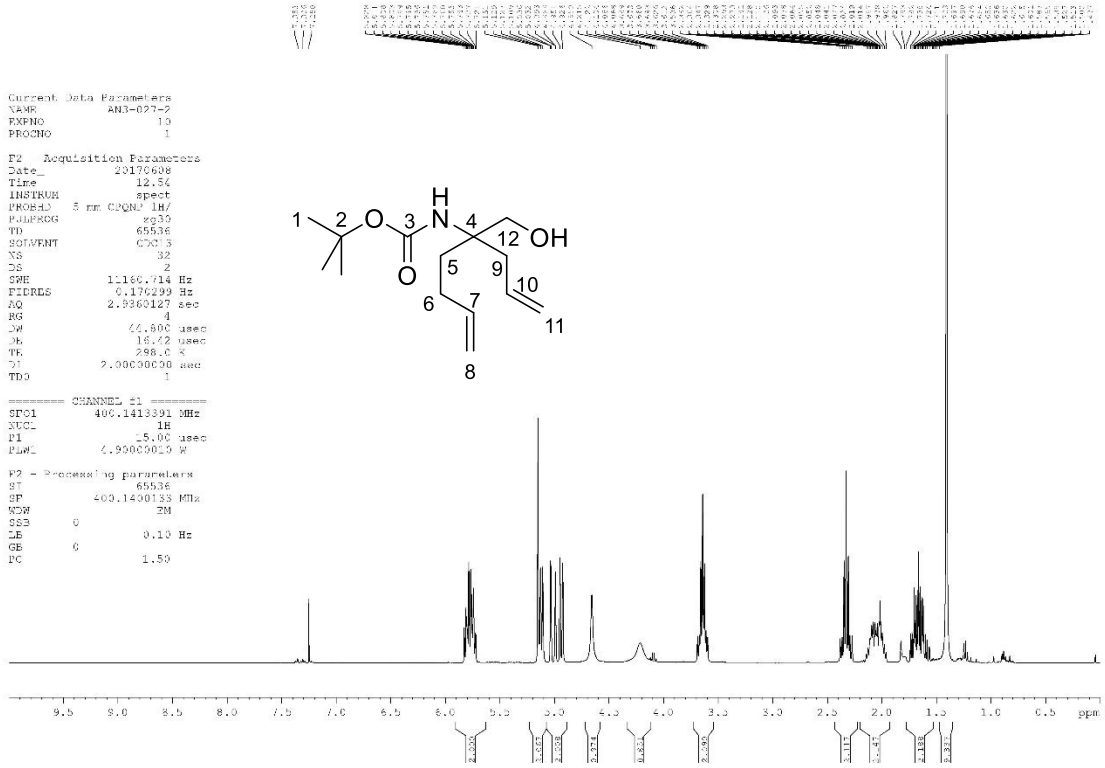

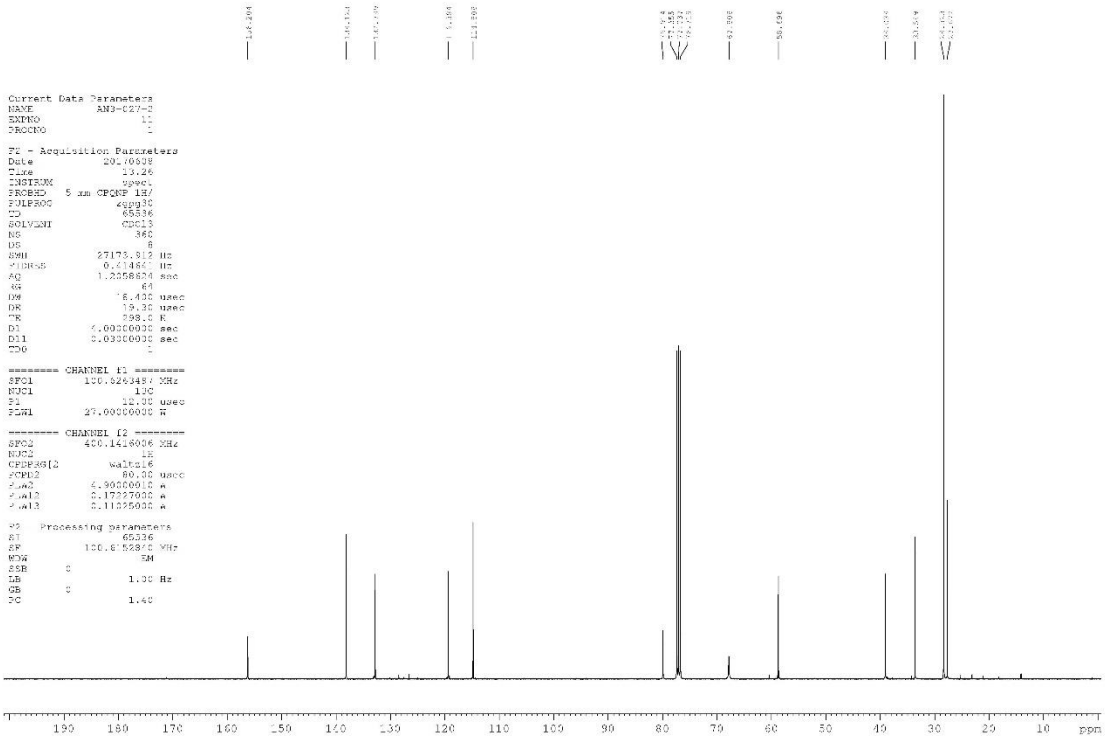

3-Oxa-1-azaspiro[4.5]dec-7-en-2-one, 148

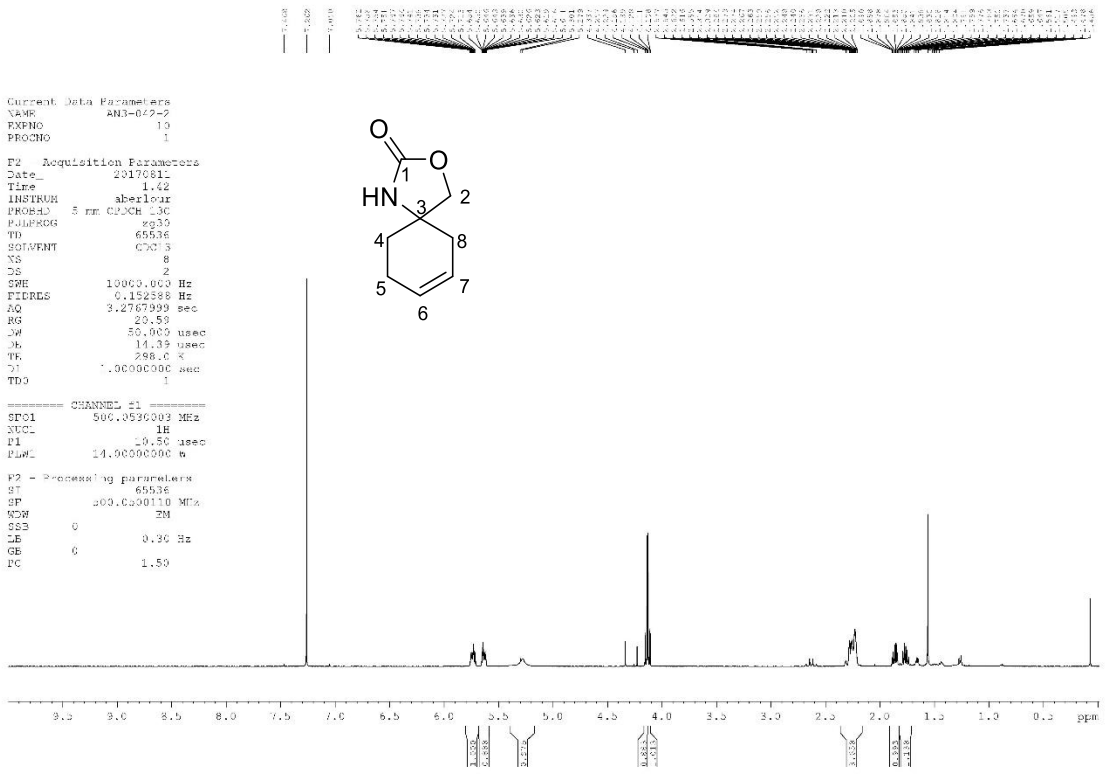

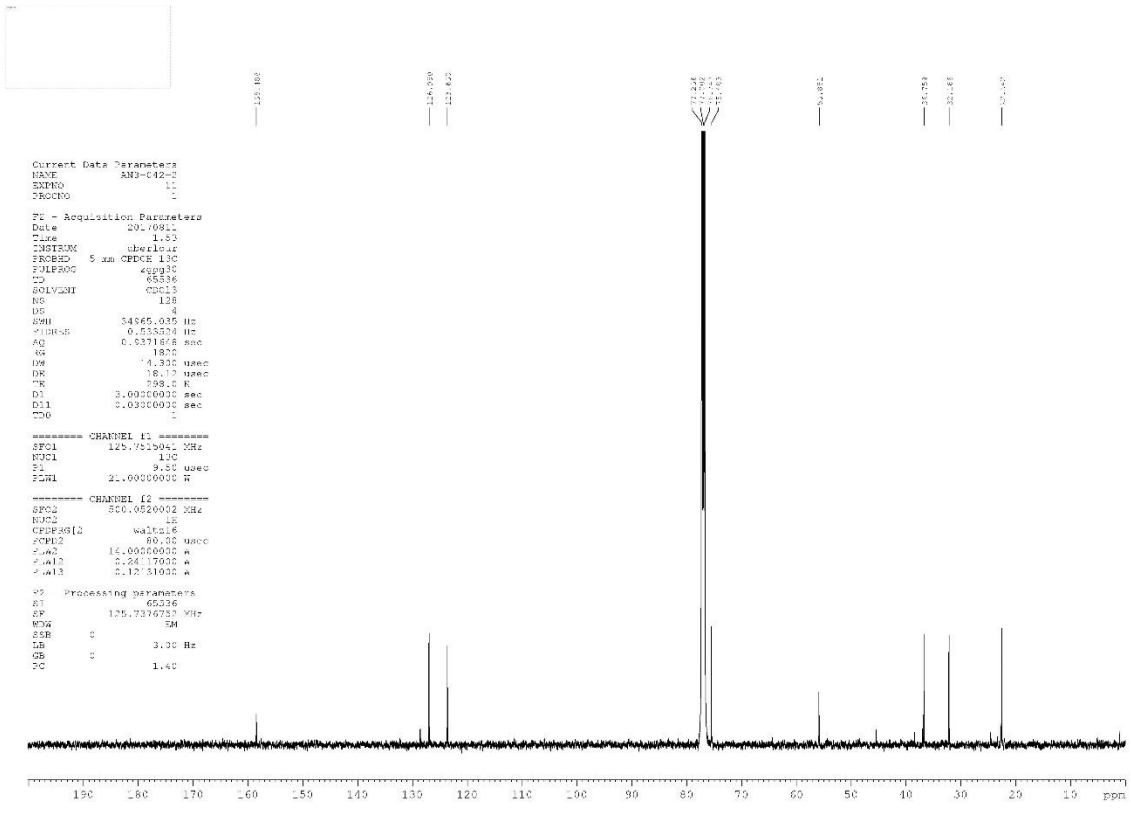

Ethyl benzimidate hydrochloride, 150

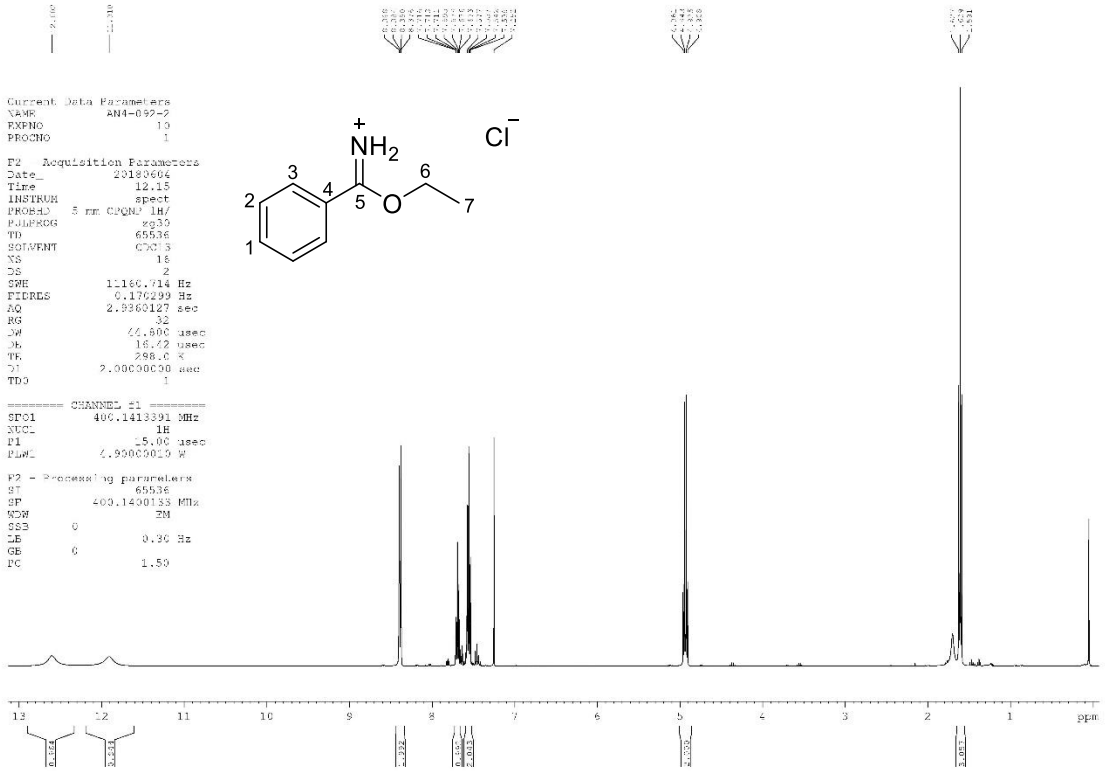

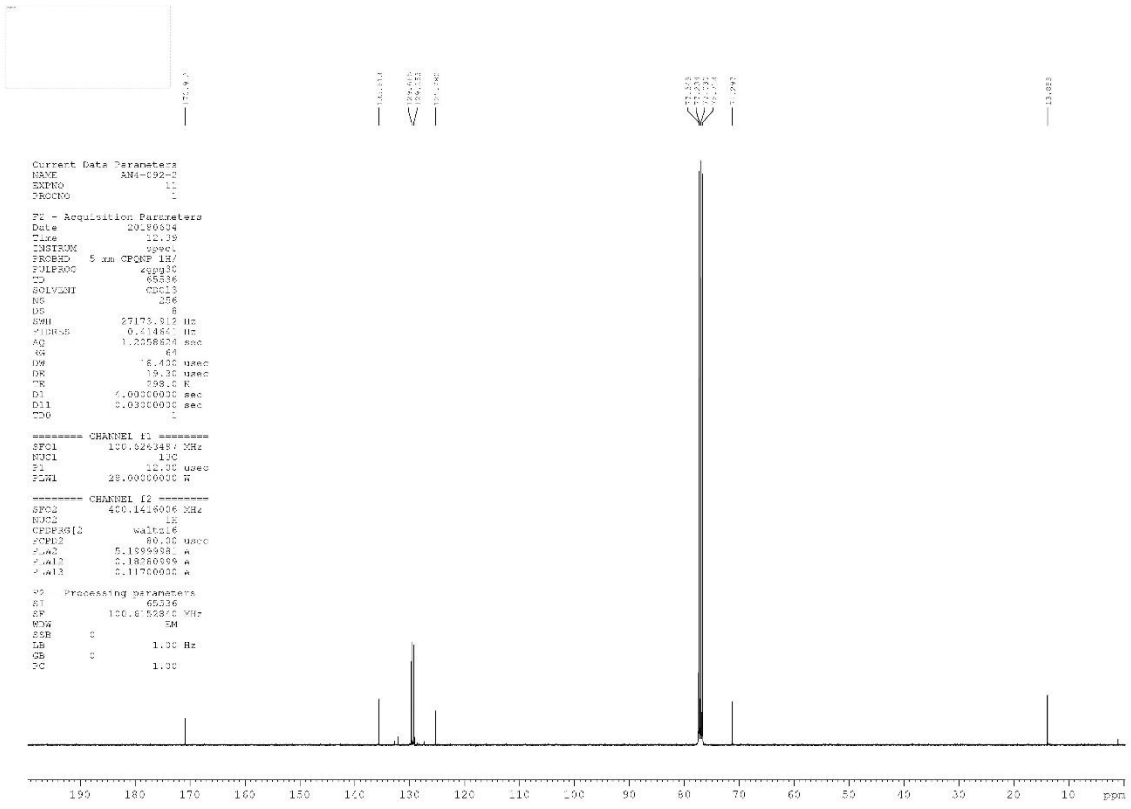

2-Phenyl-3-oxa-1-azaspiro[4.5]deca-1,7-diene, 151

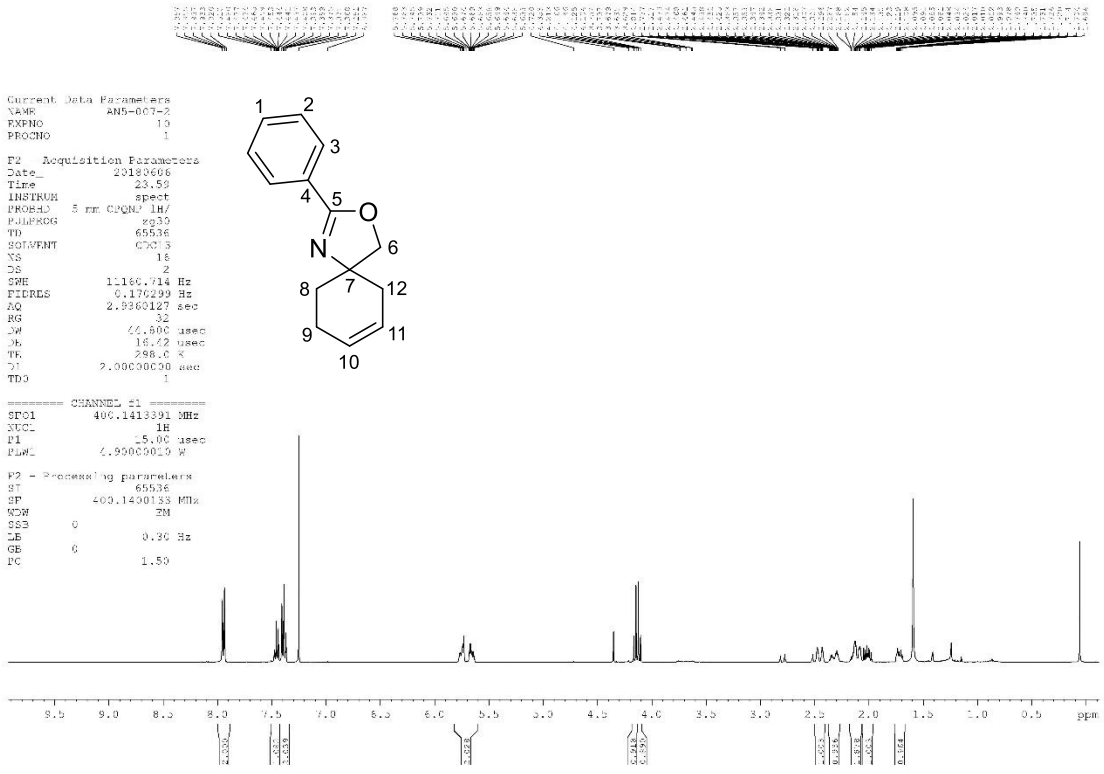

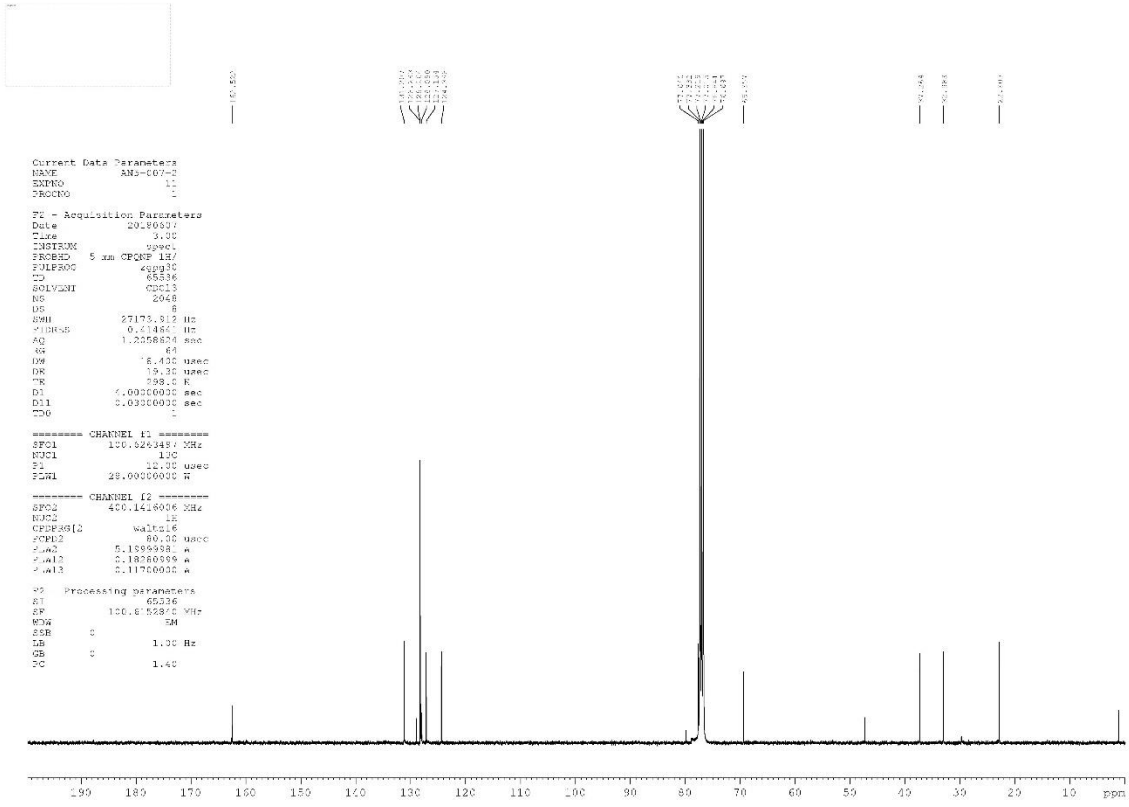

3-Oxa-1-azaspiro[4.5]deca-1,7-dien-2-amine, 152

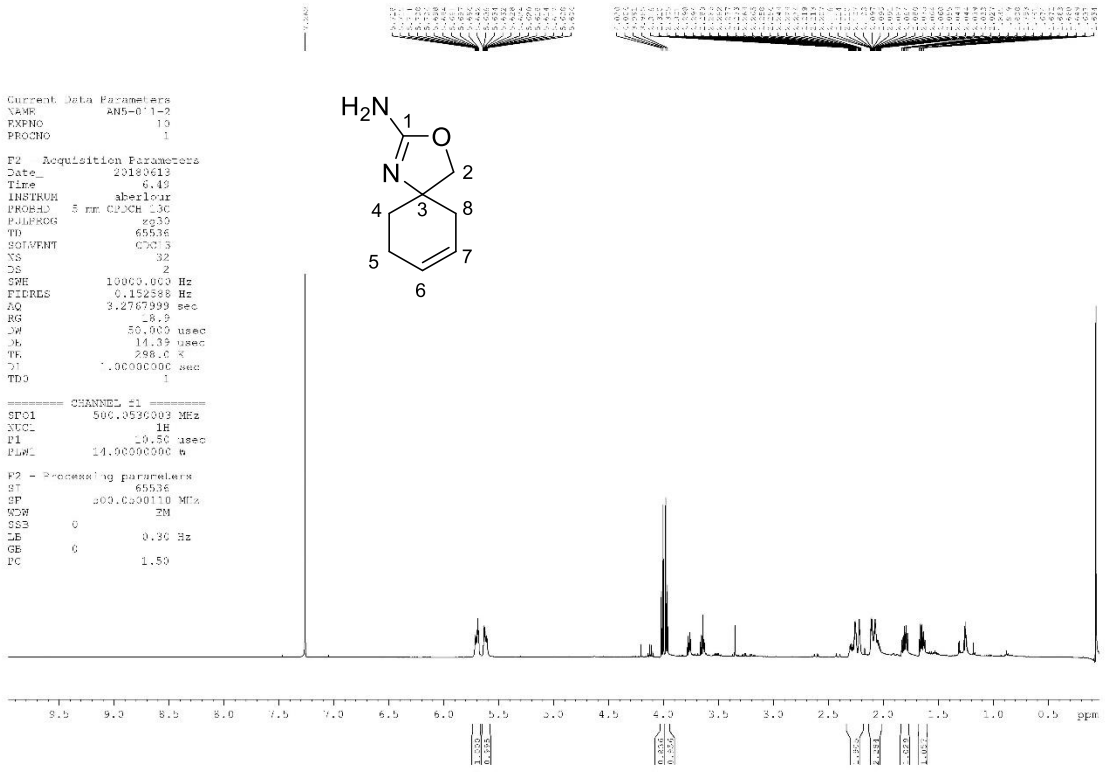

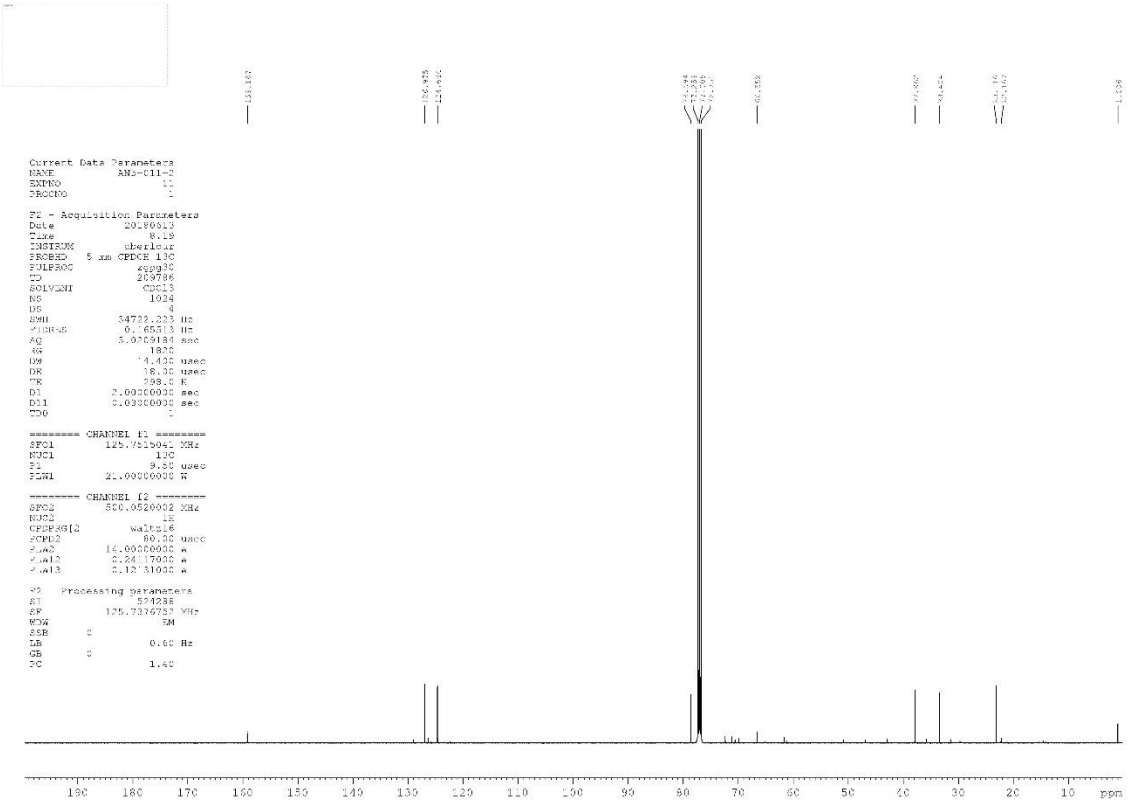

4-Oxa-1-azaspiro[5.5]undec-8-en-3-one, 158

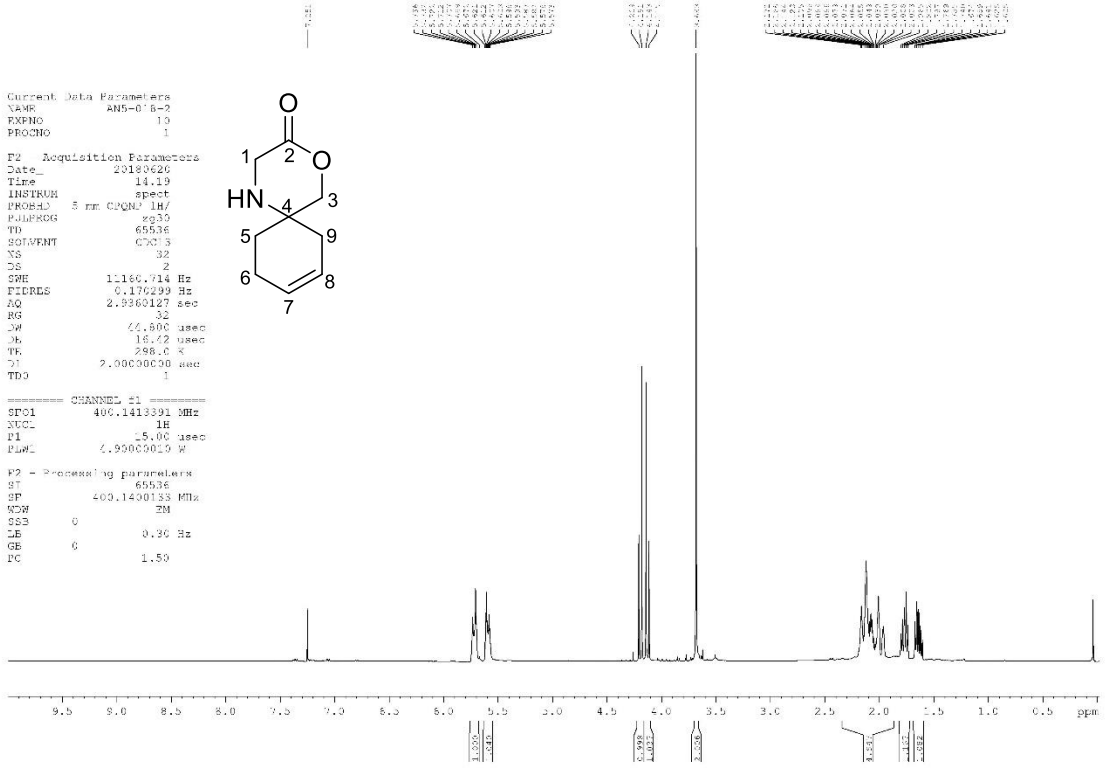

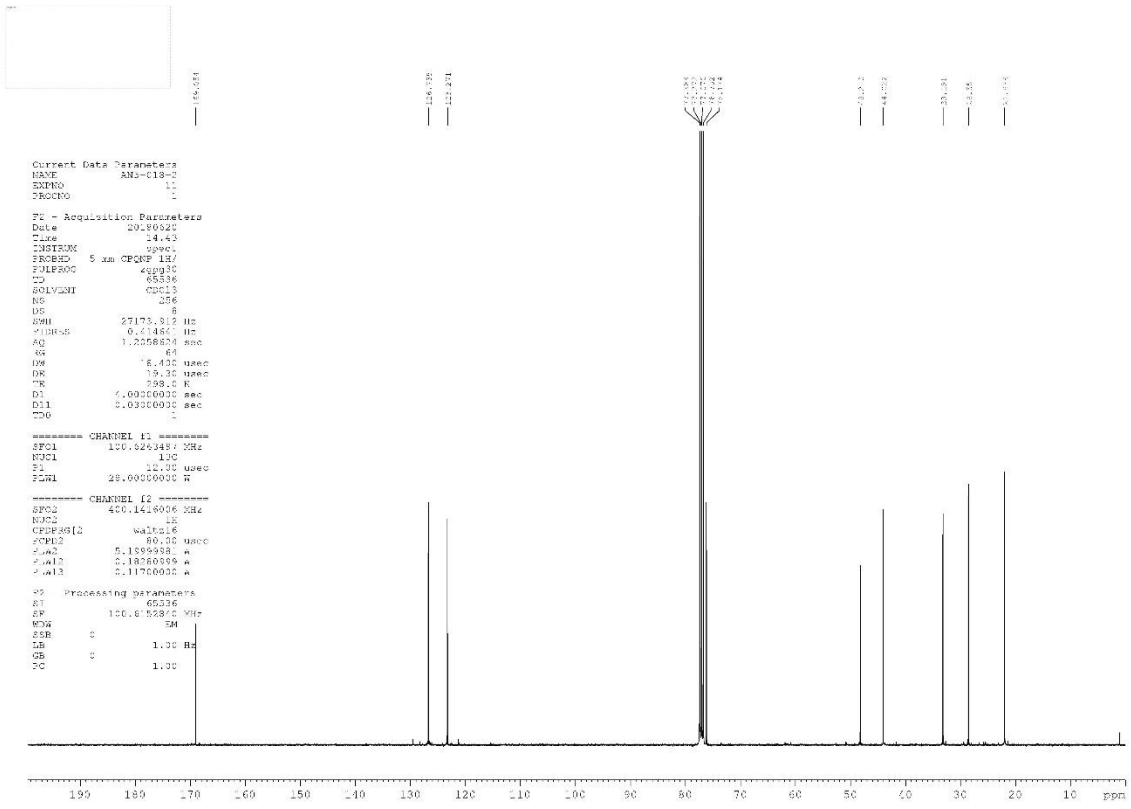

4-Oxa-1-azaspiro[5.5]undeca-1,8-dien-3-one, 159

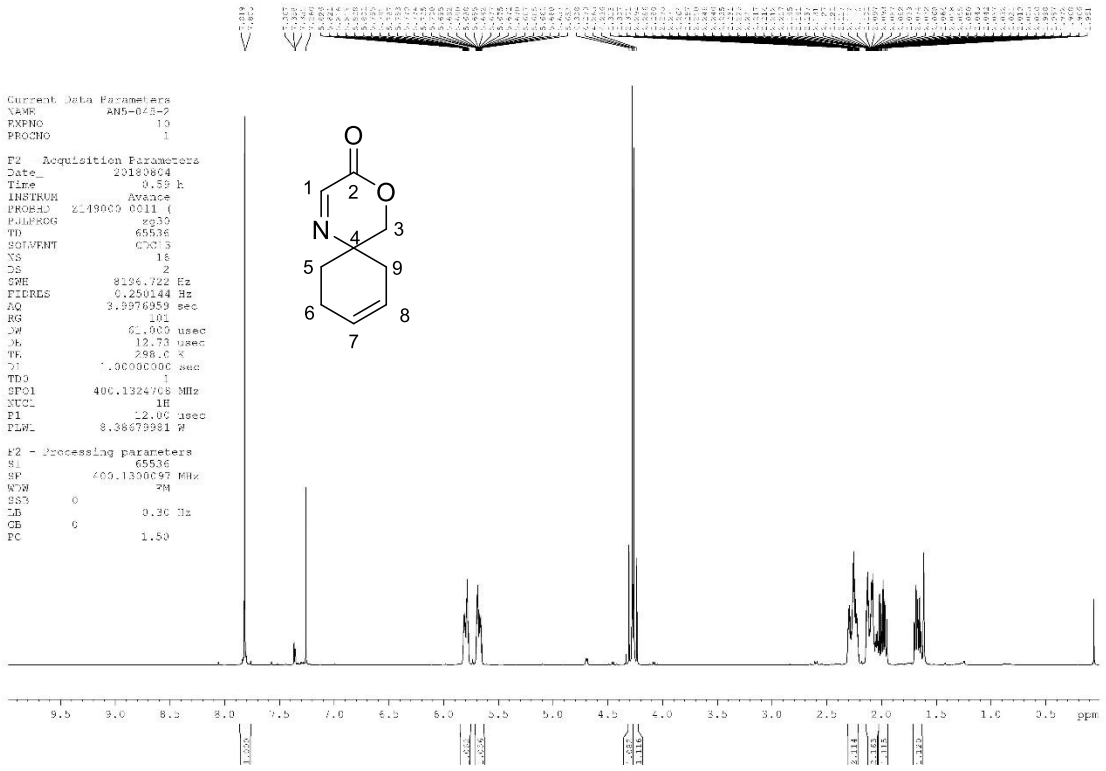

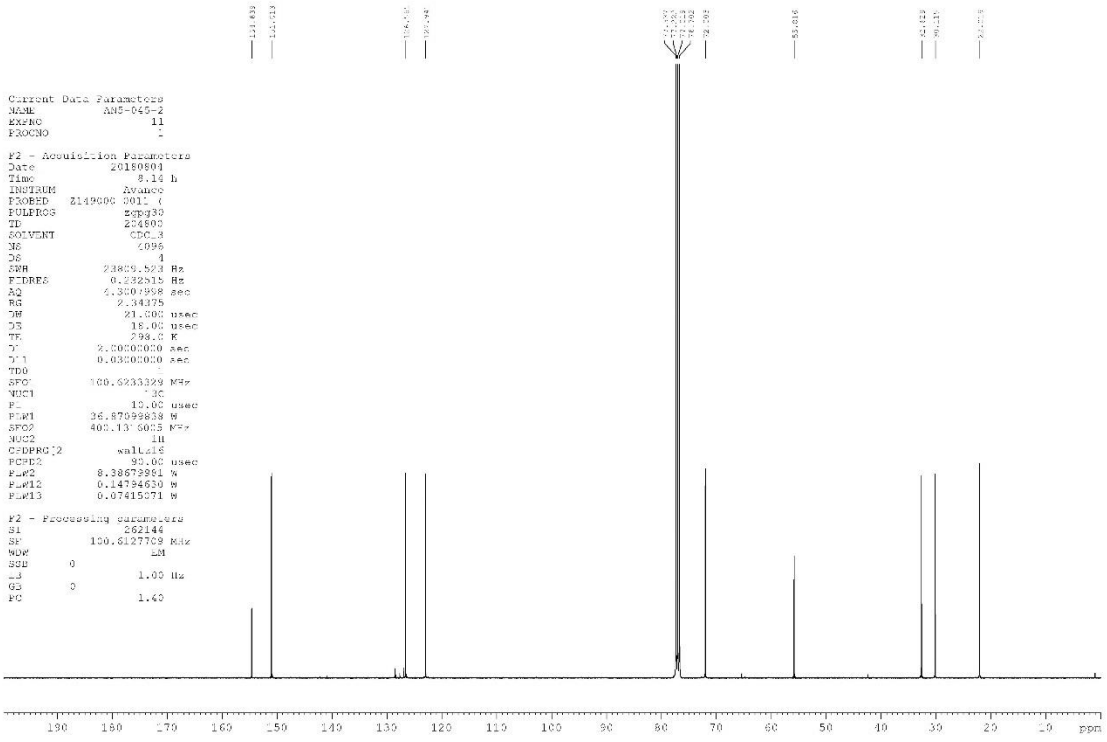

2-Chloro-N-(1-(hydroxymethyl)cyclohex-3-en-1-yl)acetamide, 160

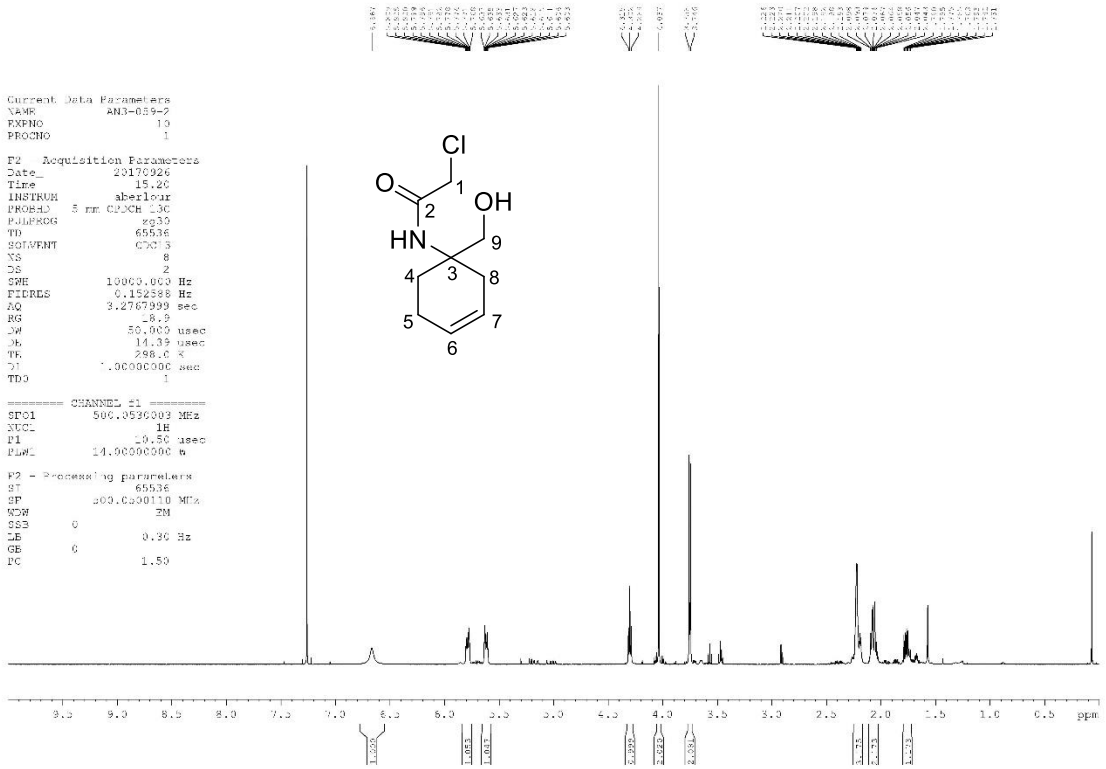

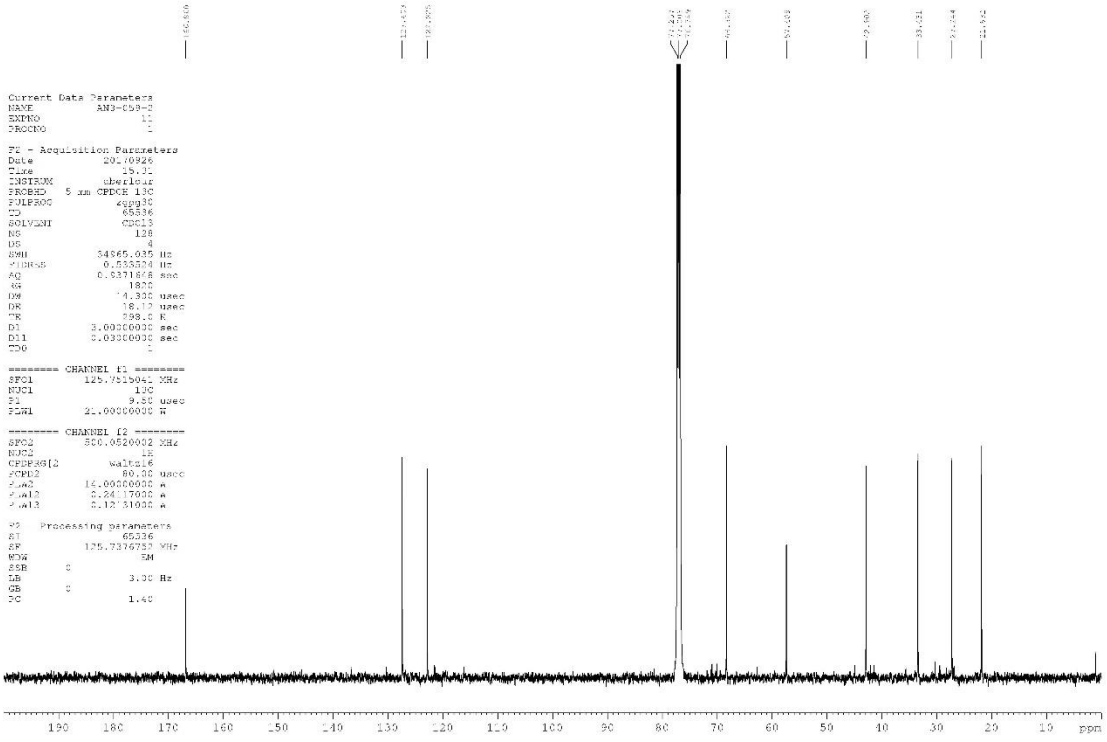

4-Oxa-1-azaspiro[5.5]undec-8-en-2-one, 161

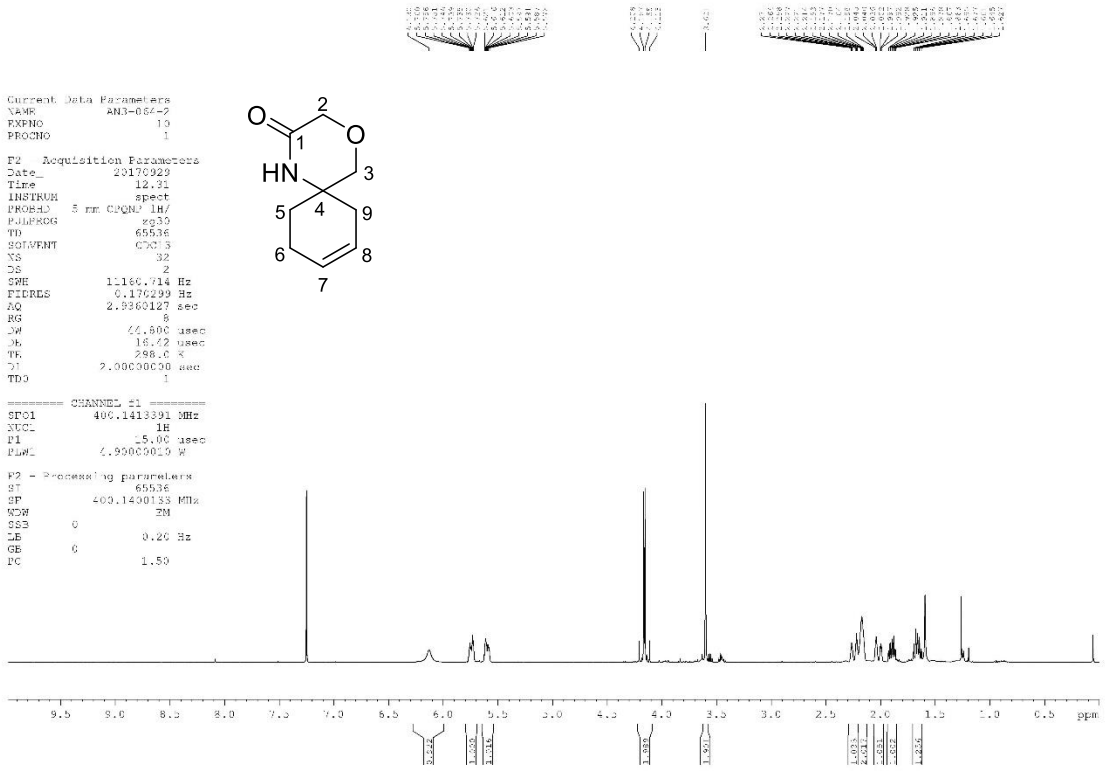

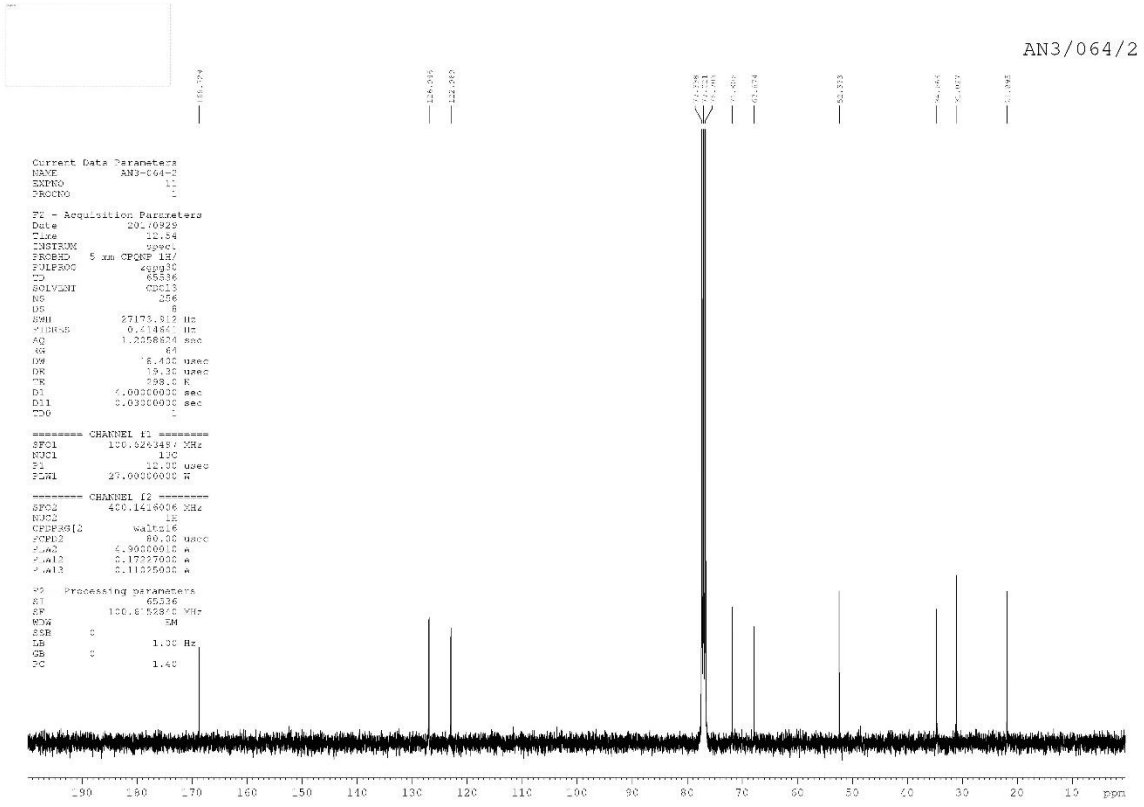

Ethyl 2-allyl-2-(3-ethoxy-3-oxopropanamido)hex-5-enoate, 165

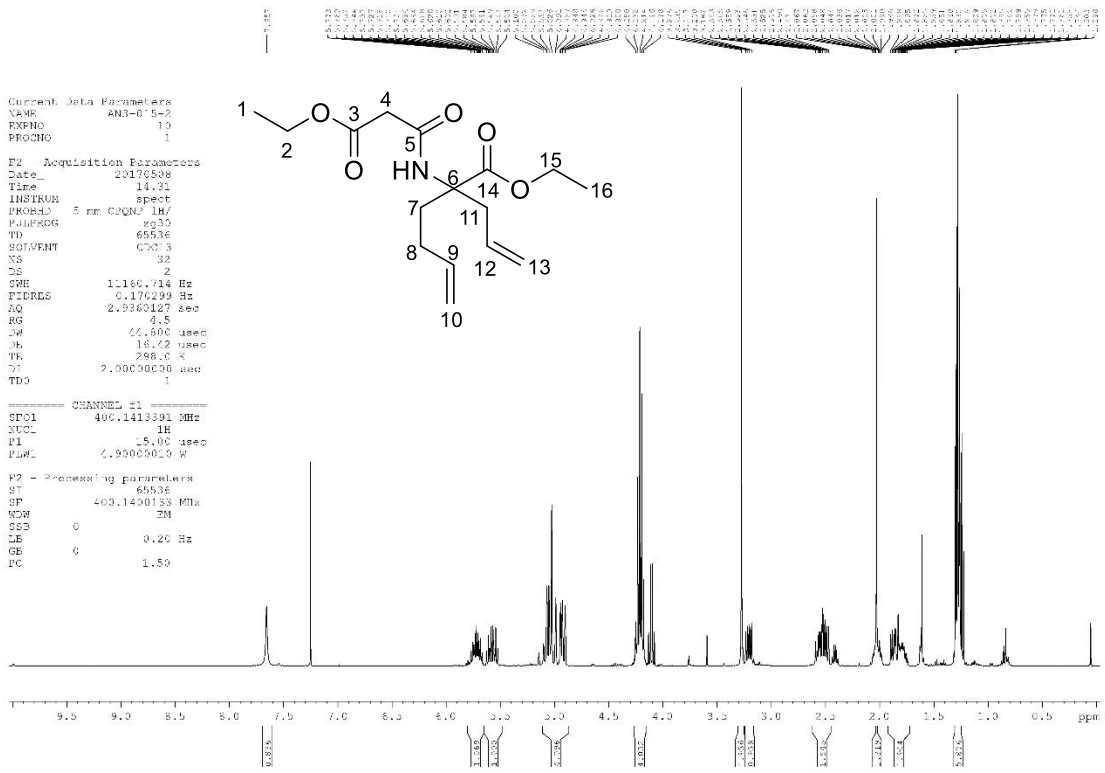

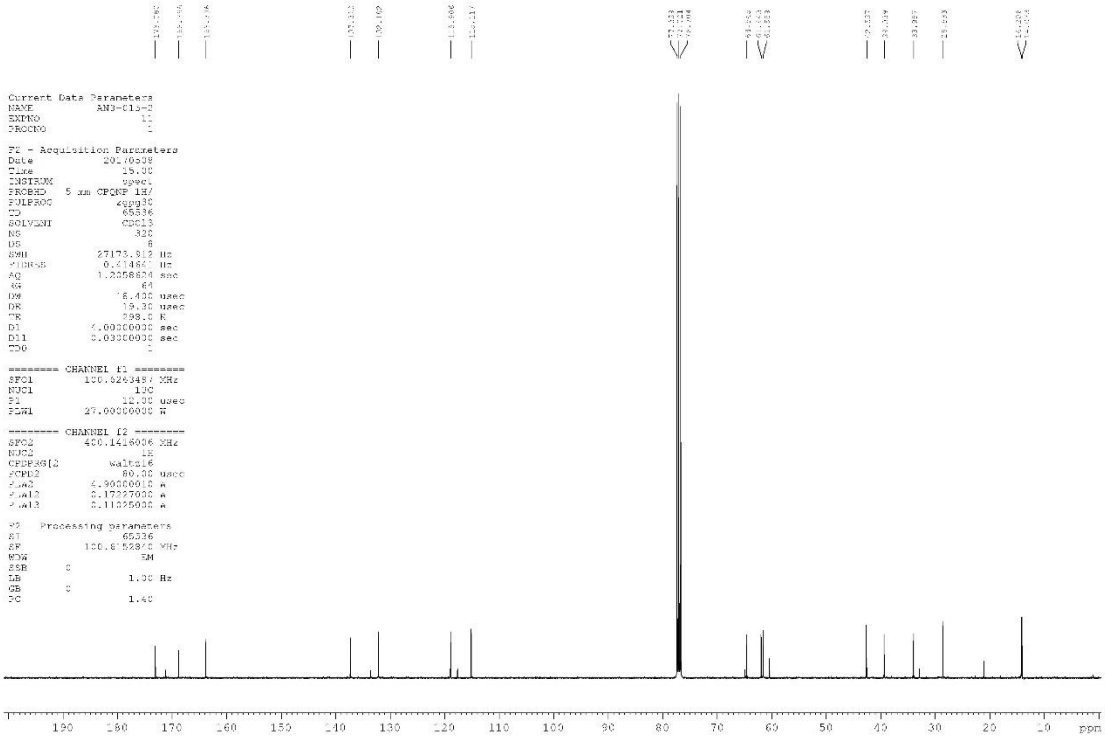

5-Allyl-5-(but-3-en-1-yl)pyrrolidine-2,4-dione, 167

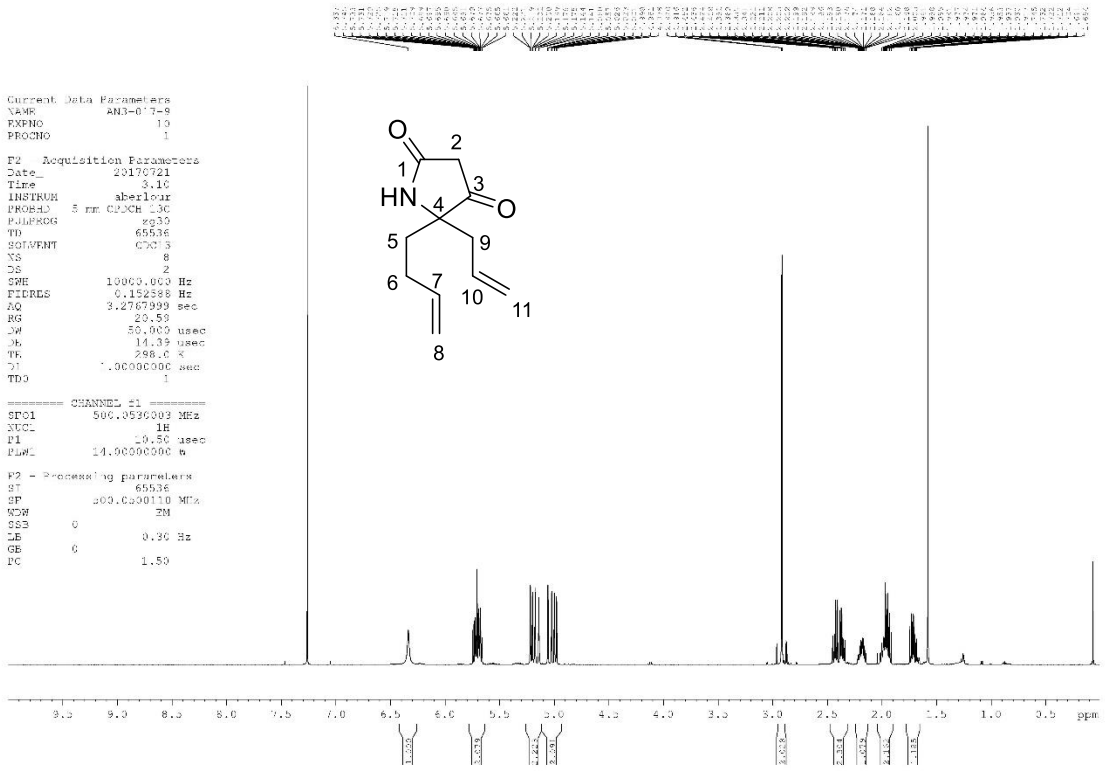

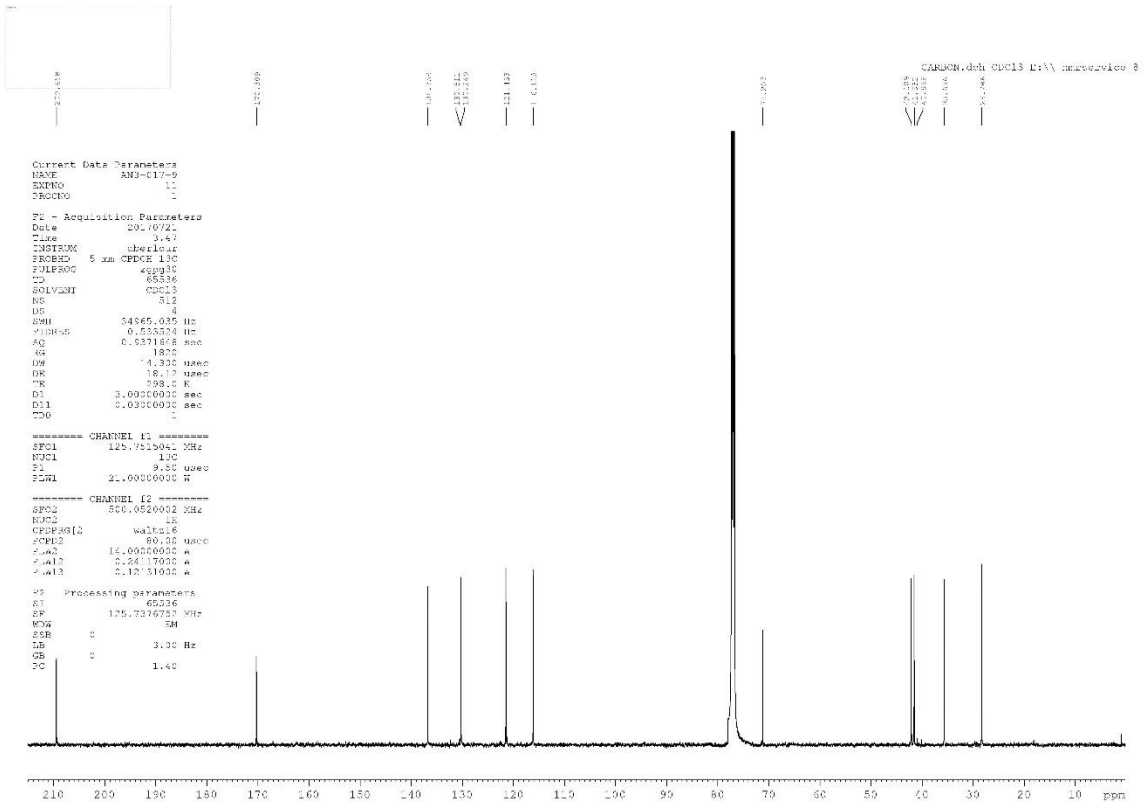

1-Azaspiro[4.5]dec-7-ene-2,4-dione, 168

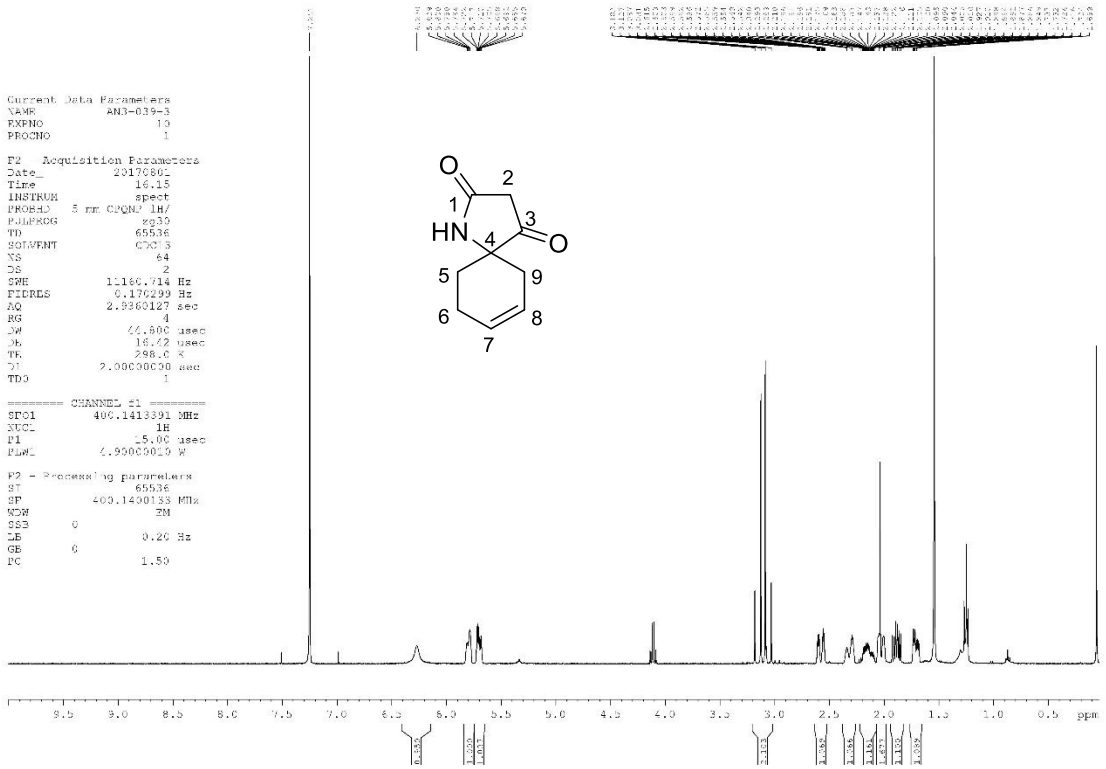

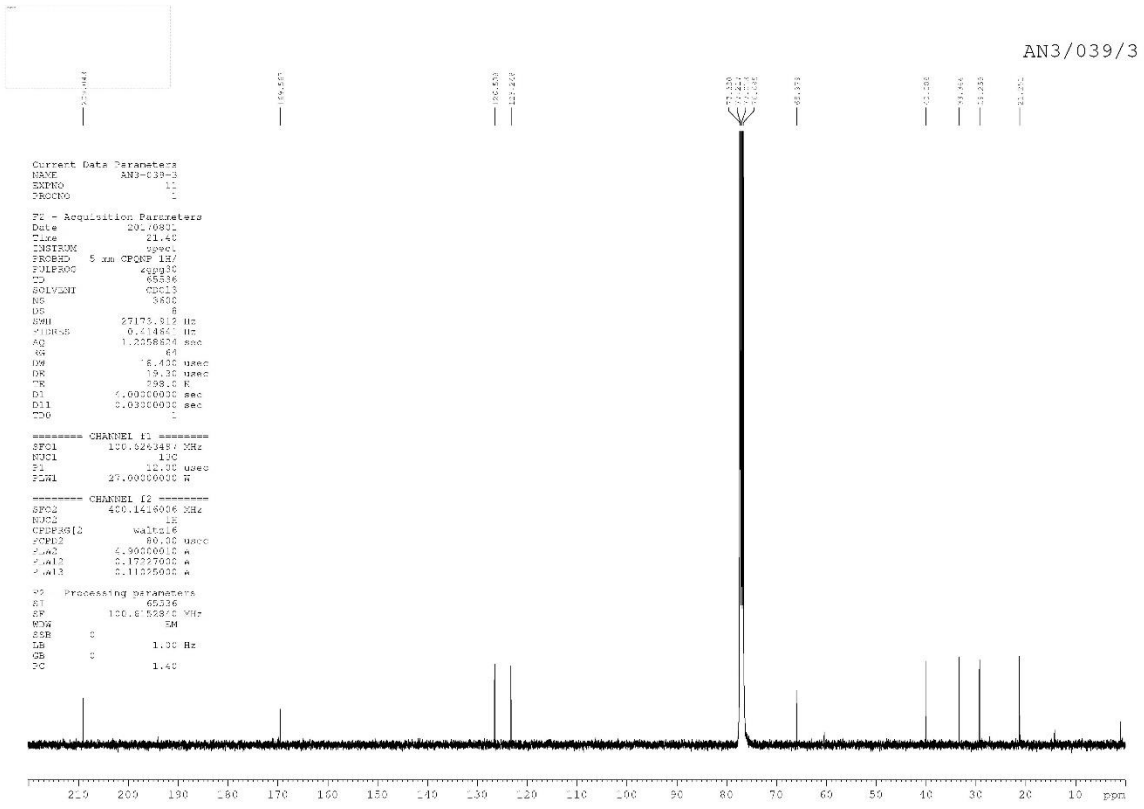

4-Ethoxy-1-azaspiro[4.5]deca-3,7-dien-2-one, 174

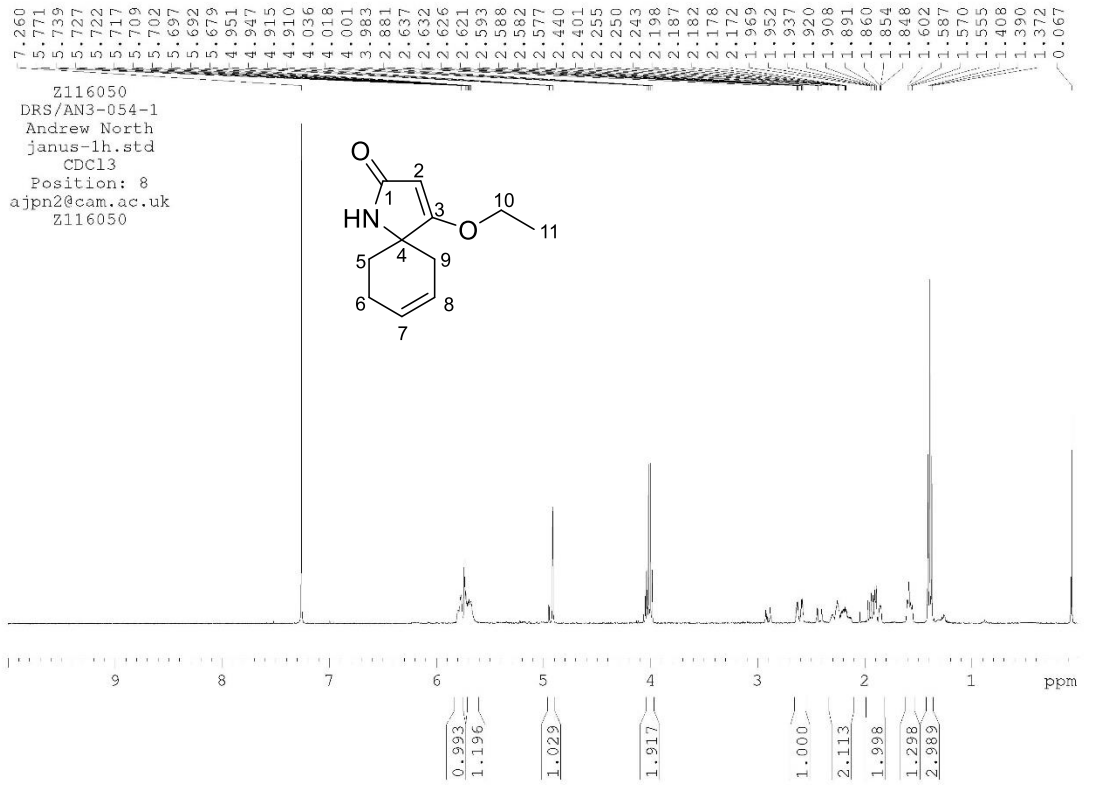

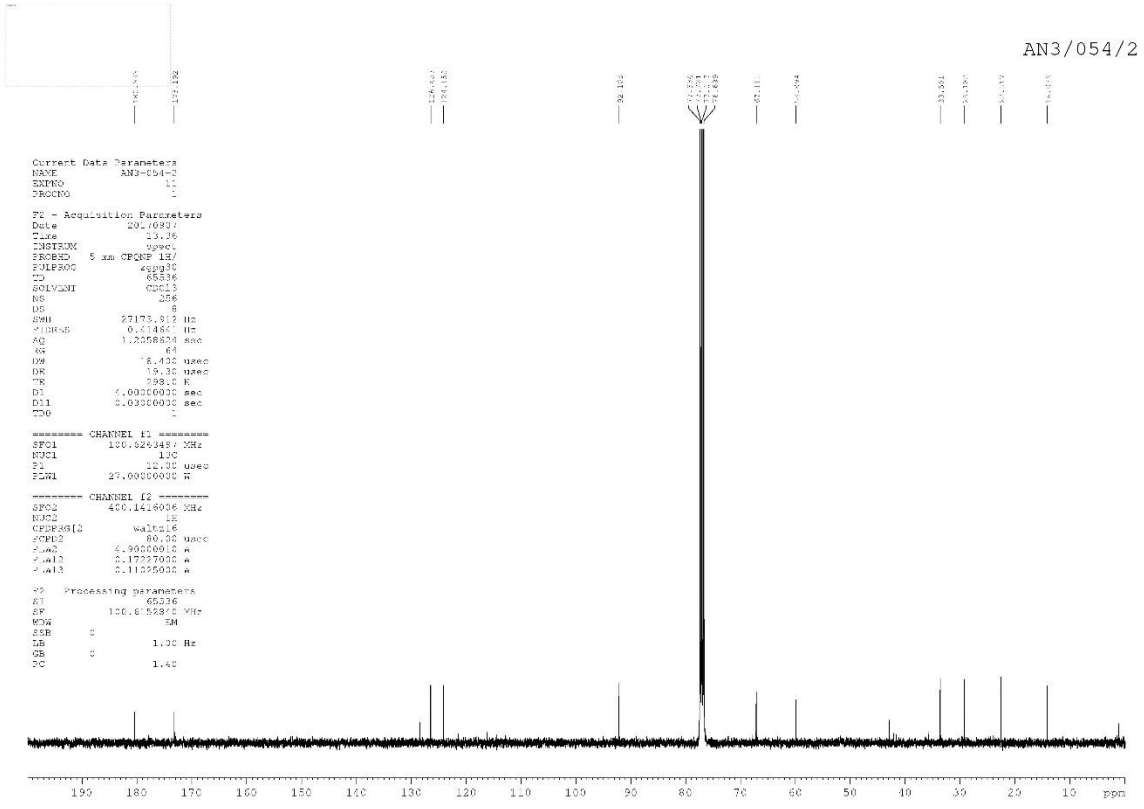

2-Oxo-1-azaspiro[4.5]deca-3,7-dien-4-yl trifluoromethanesulfonate, 175

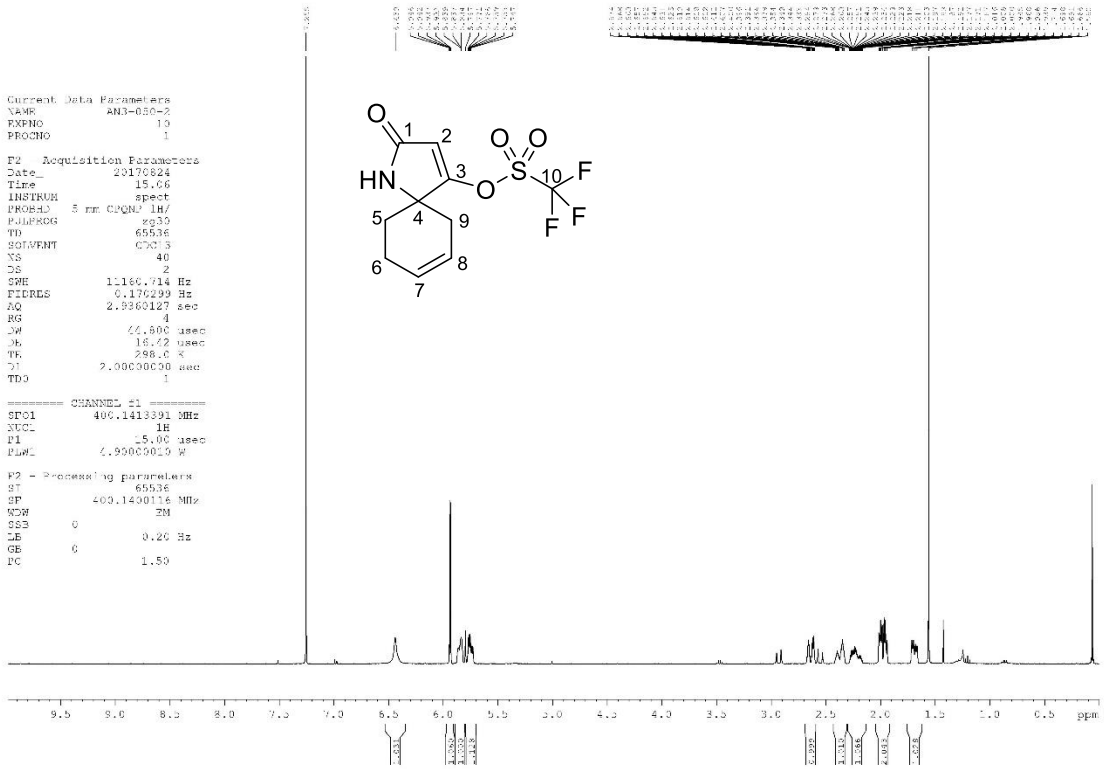

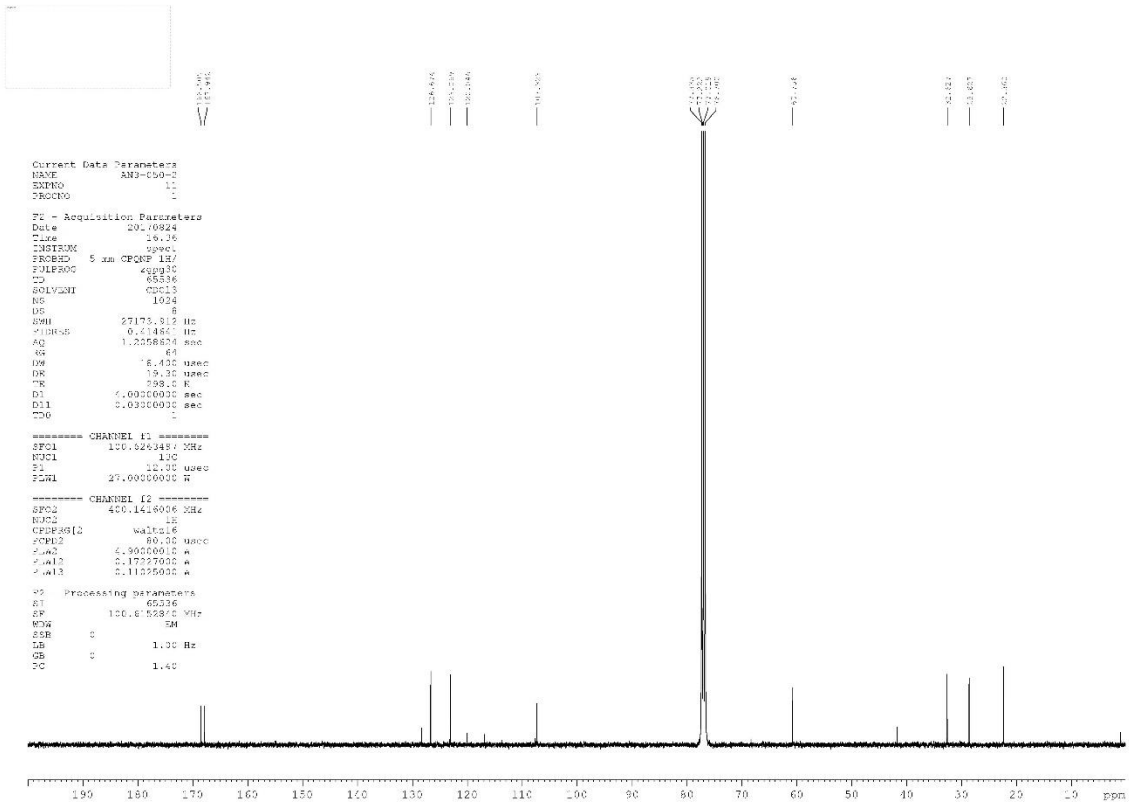

4-(4-Methoxyphenyl)-1-azaspiro[4.5]deca-3,7-dien-2-one, 176

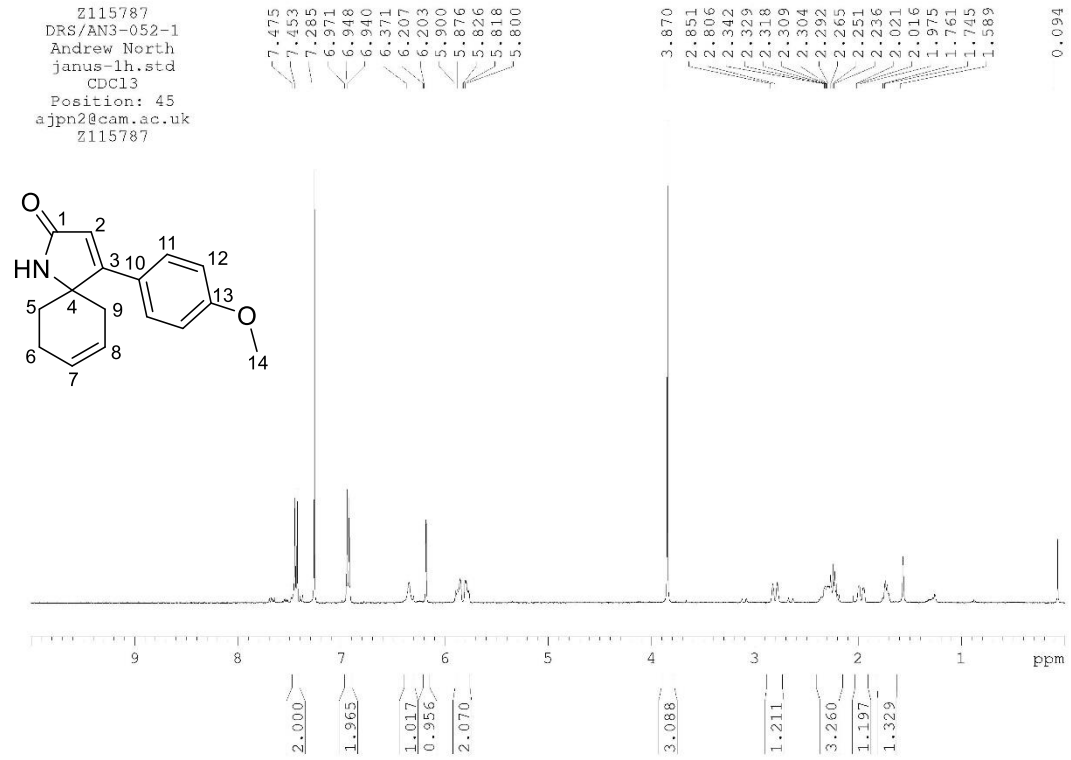

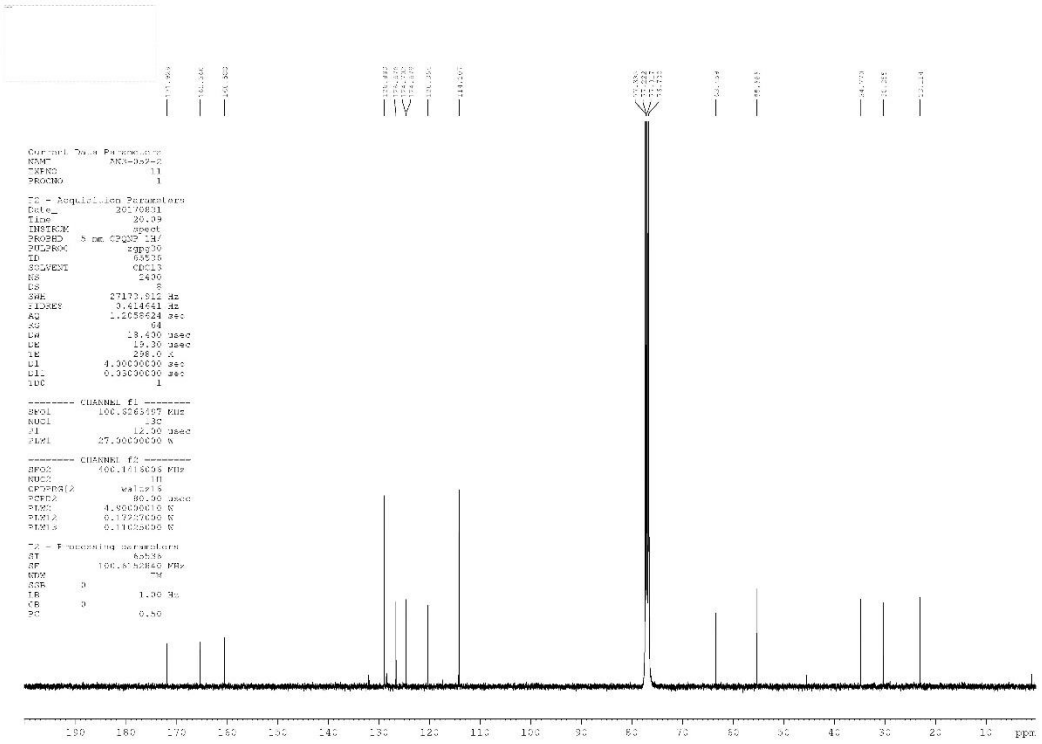

4-Hydroxy-1-azaspiro[4.5]dec-7-en-2-one, 177

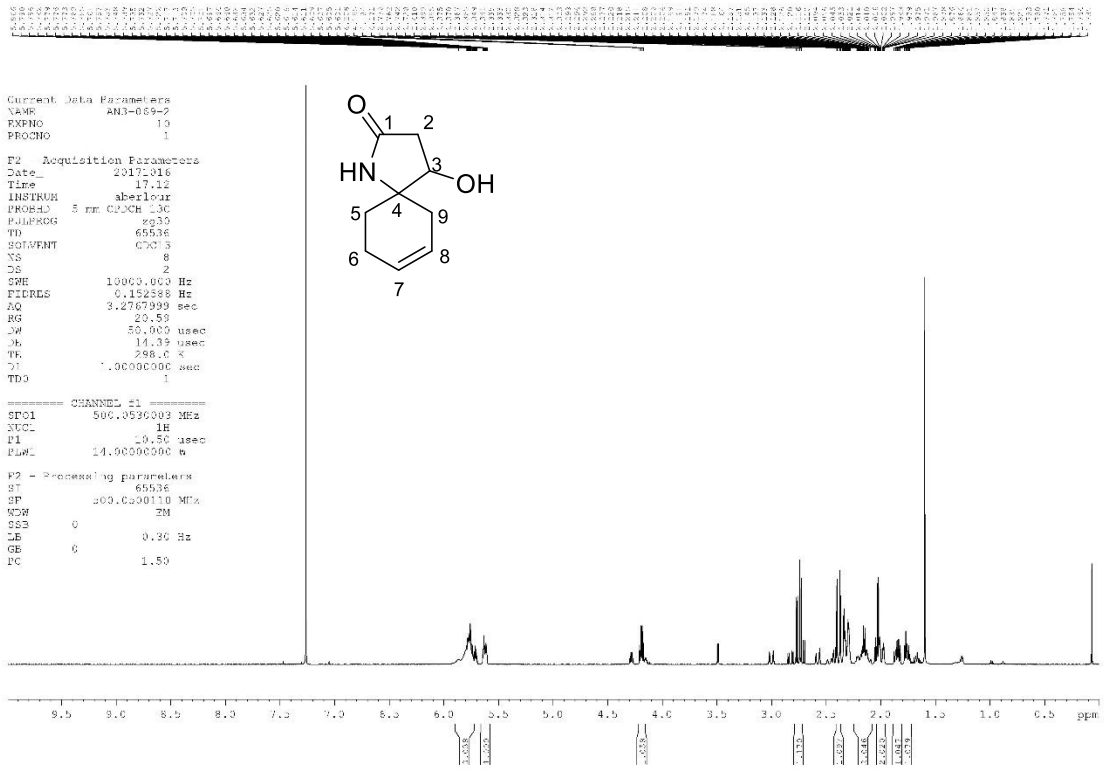

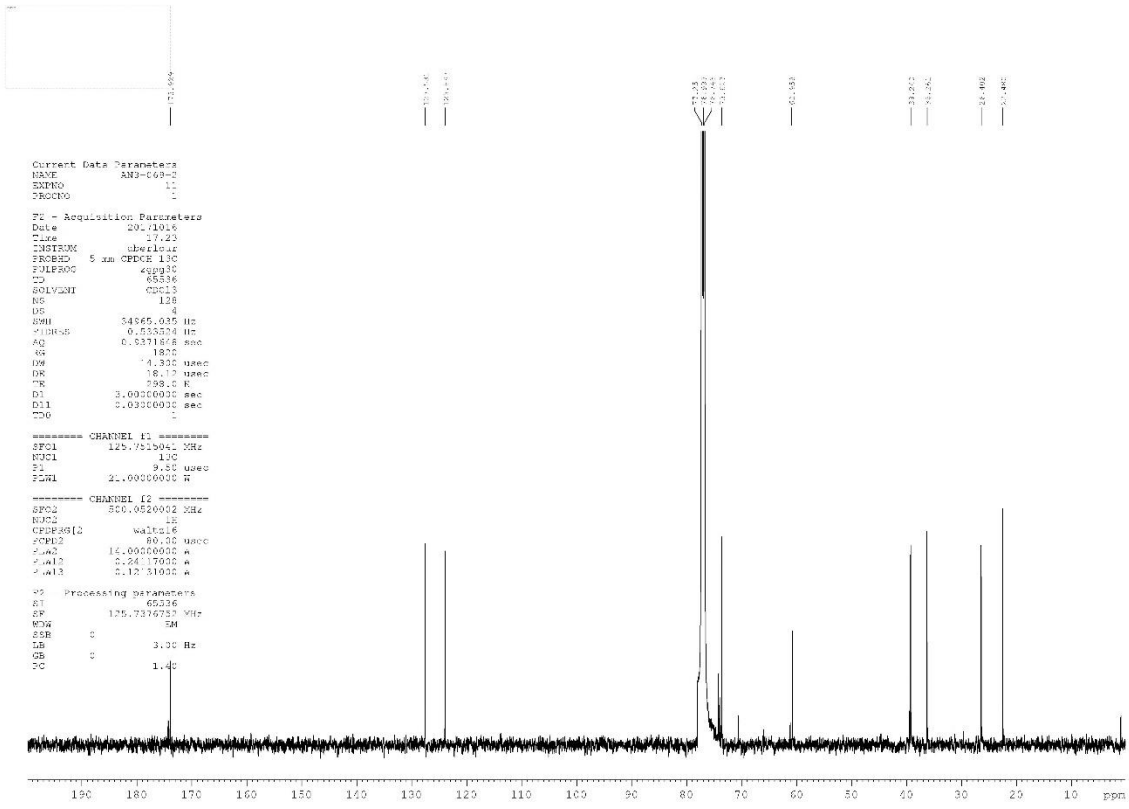

2-Oxo-1-azaspiro[4.5]dec-7-en-4-yl methanesulfonate, 178

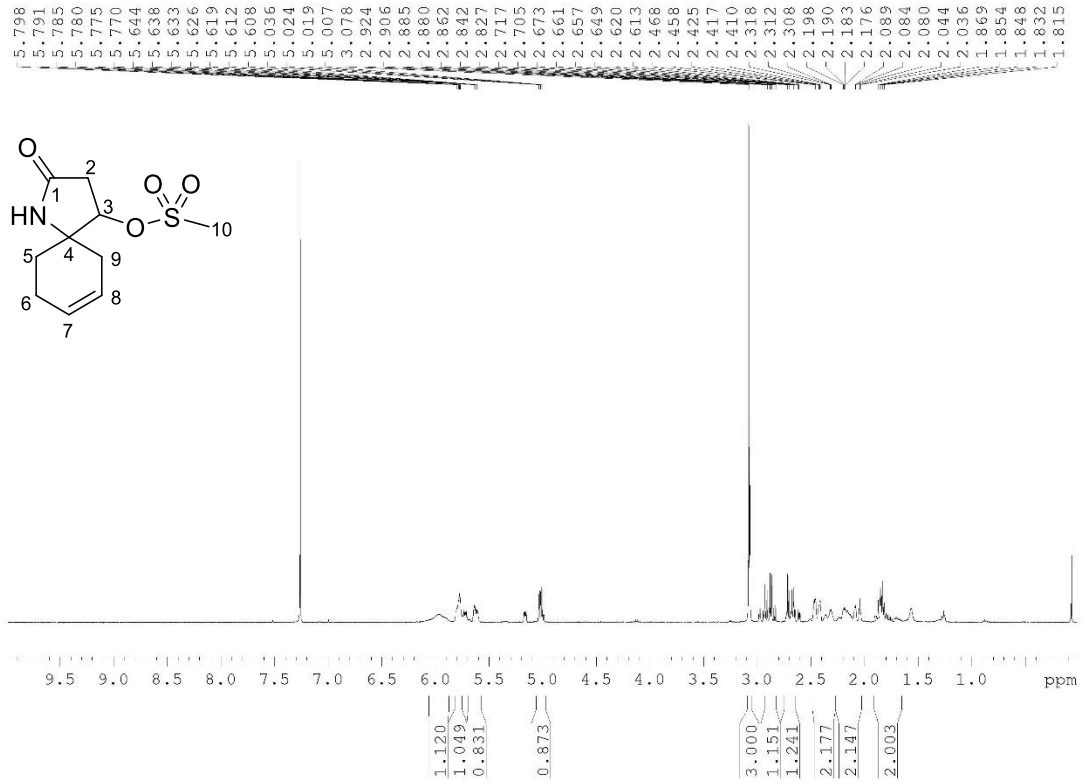

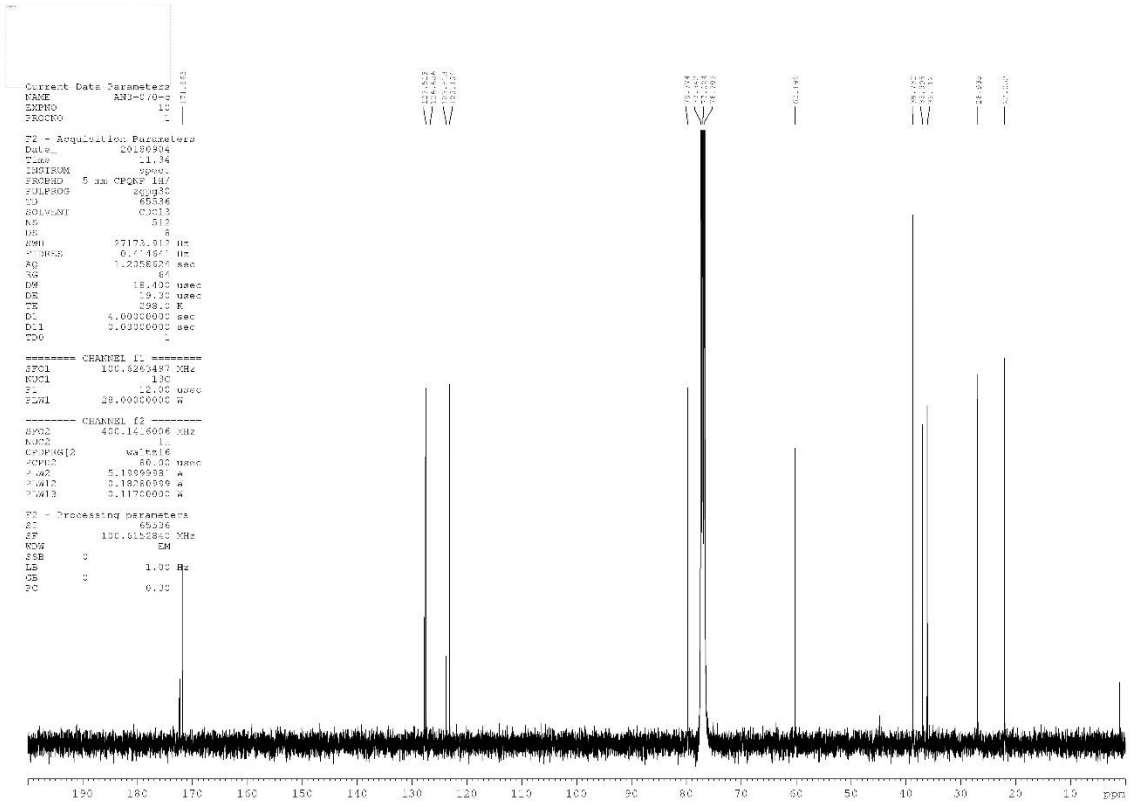

1-Azaspiro[4.5]deca-3,7-dien-2-one, 179

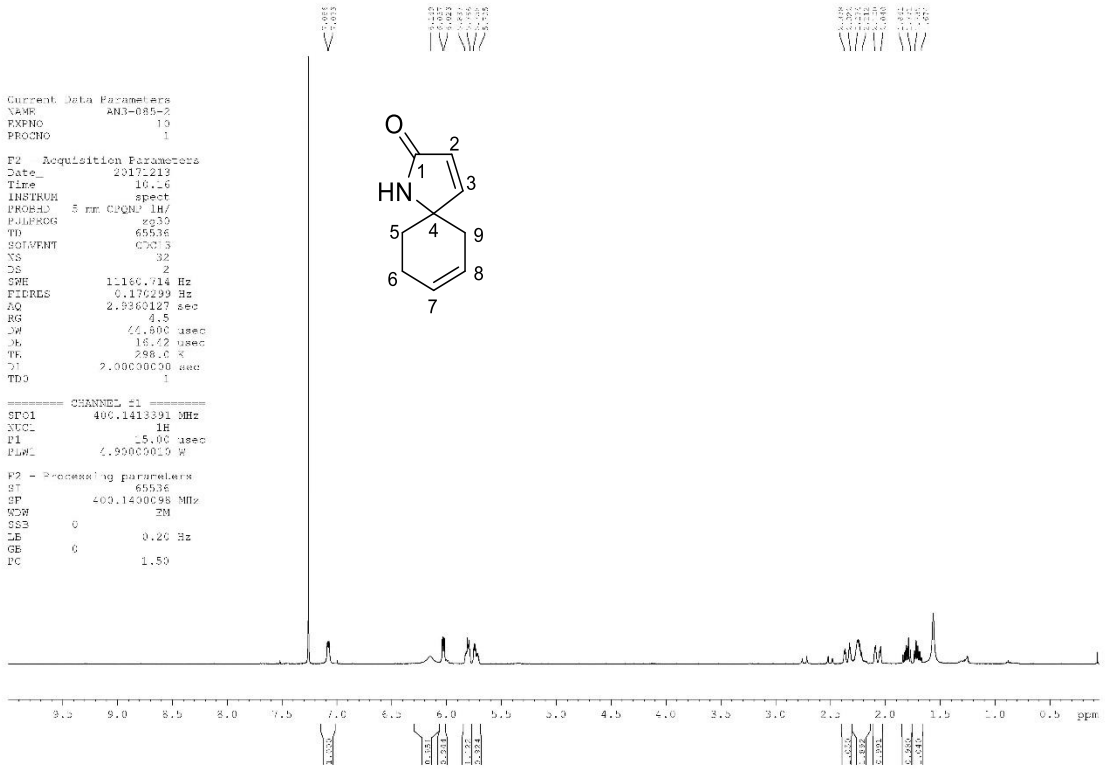

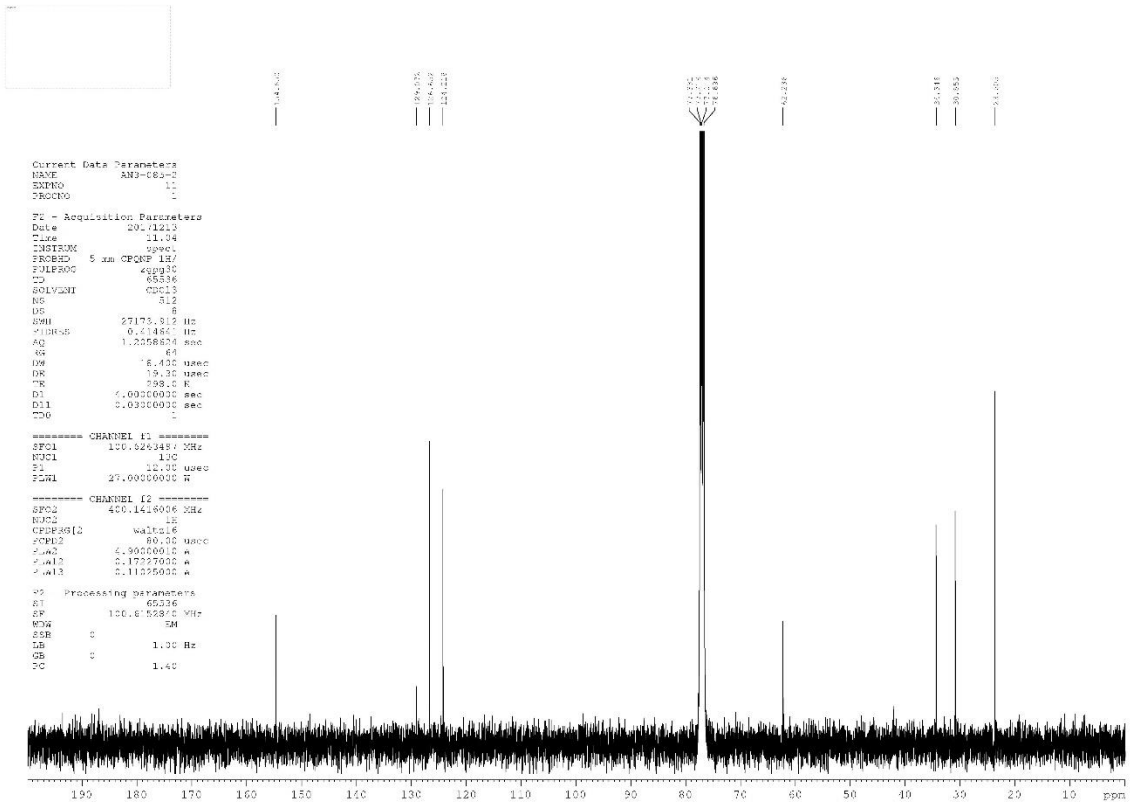

2-Allyl-2-((*tert*-butoxycarbonyl)amino)hex-5-enoic acid, 184

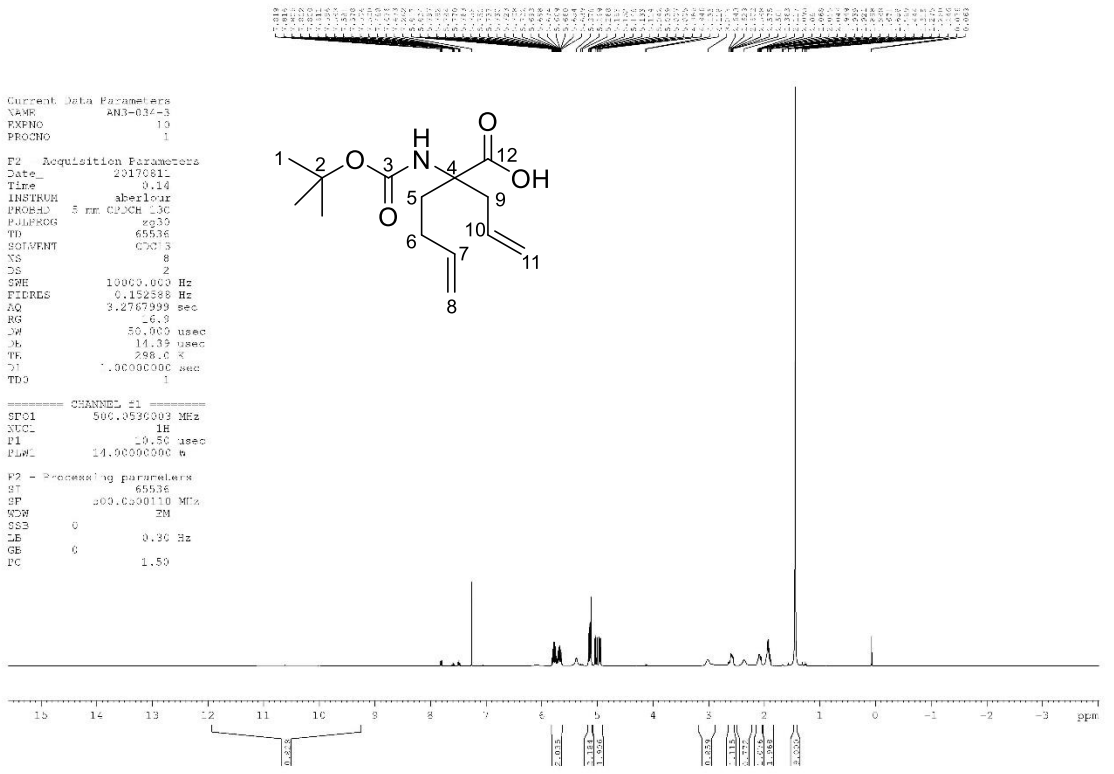

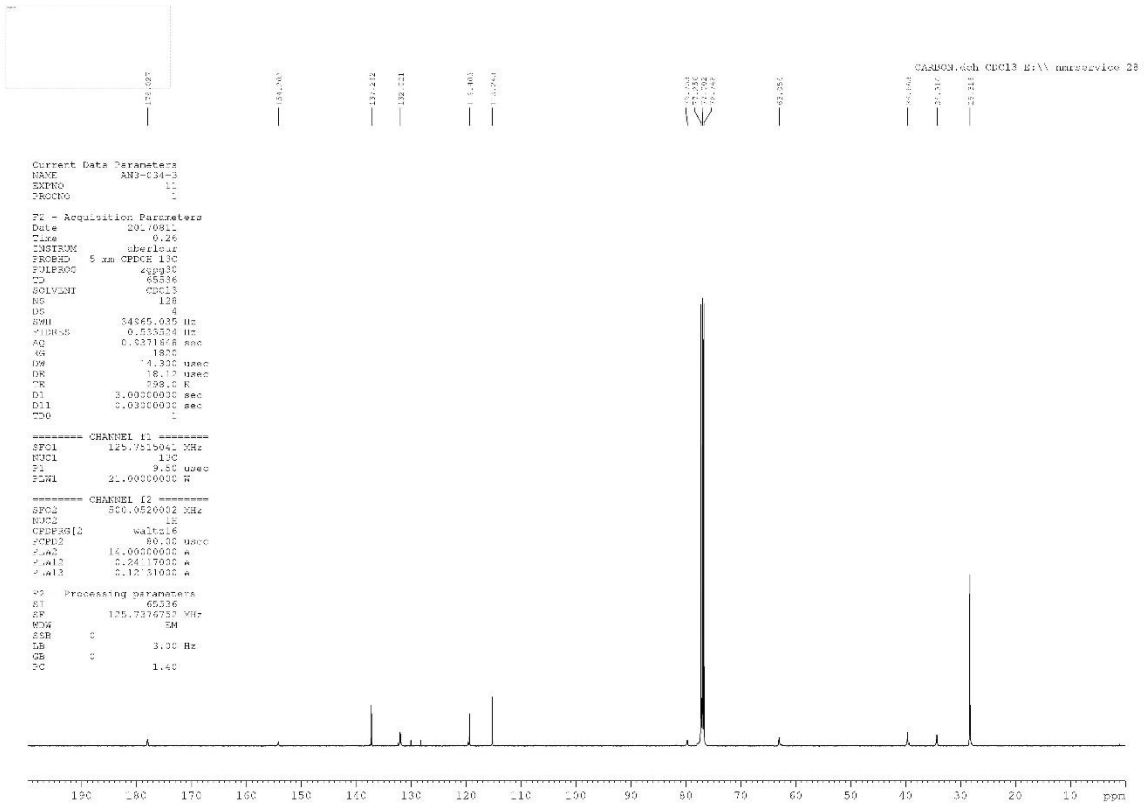

Ethyl (*tert*-butoxycarbonyl)-L-serinate, 201

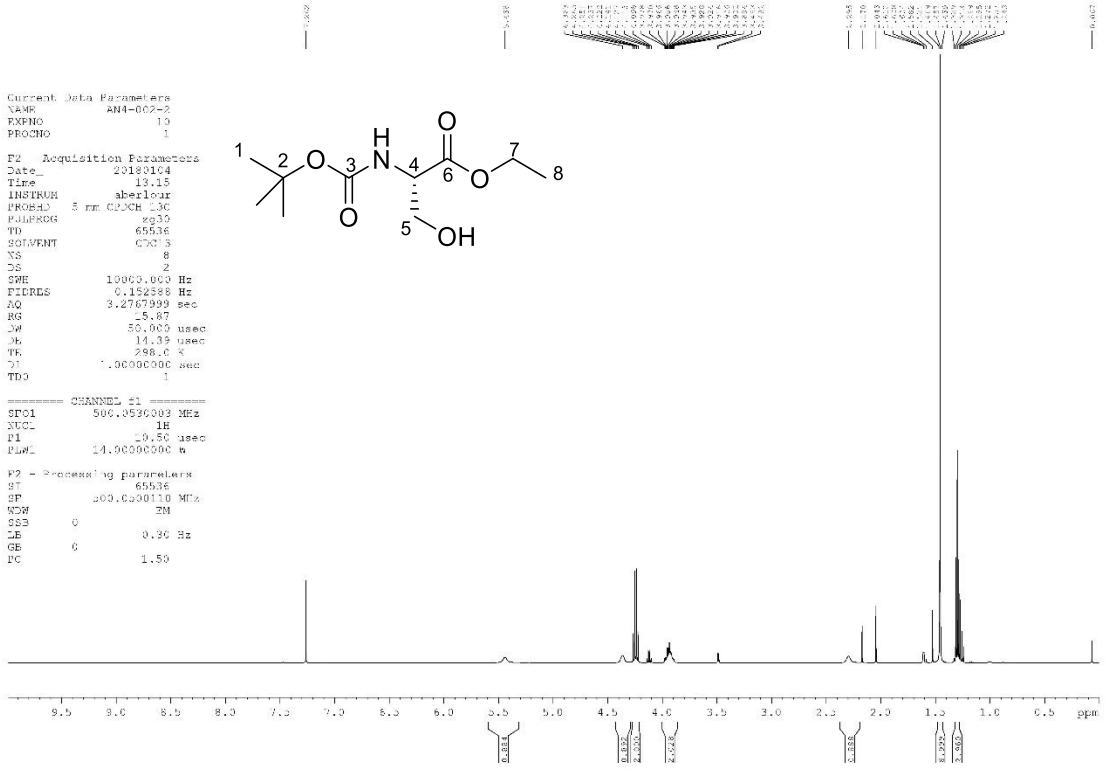

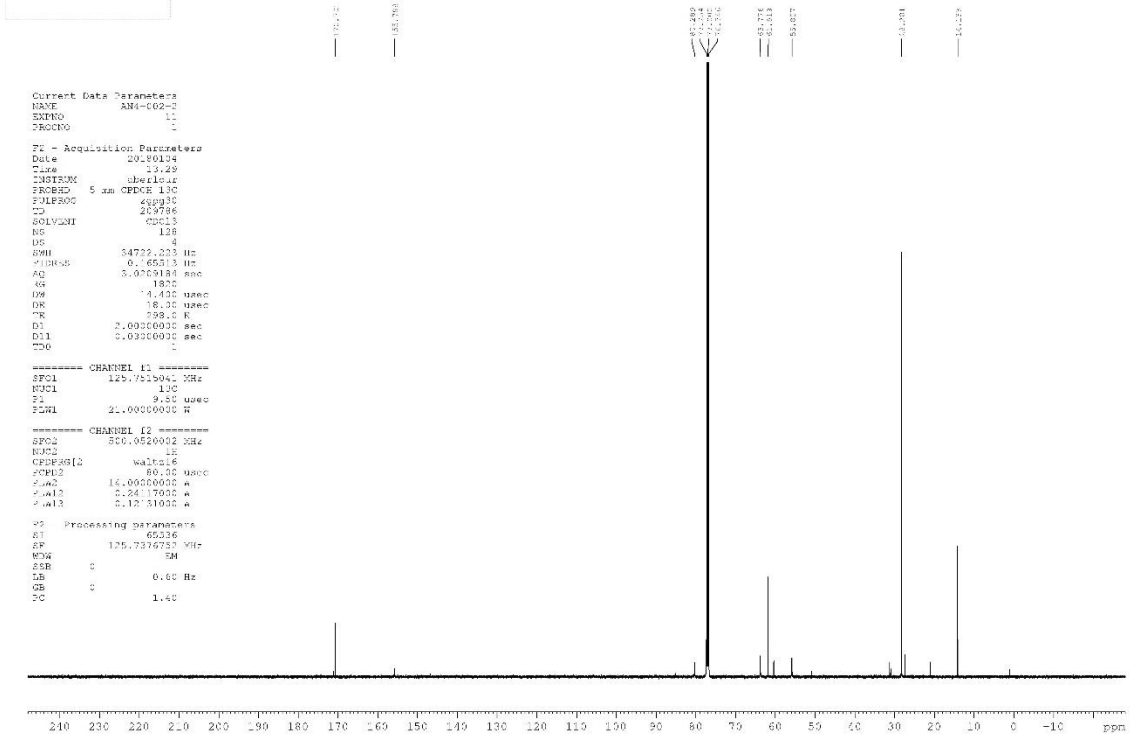

Ethyl 2-((*tert*-butoxycarbonyl)amino)acrylate, 202

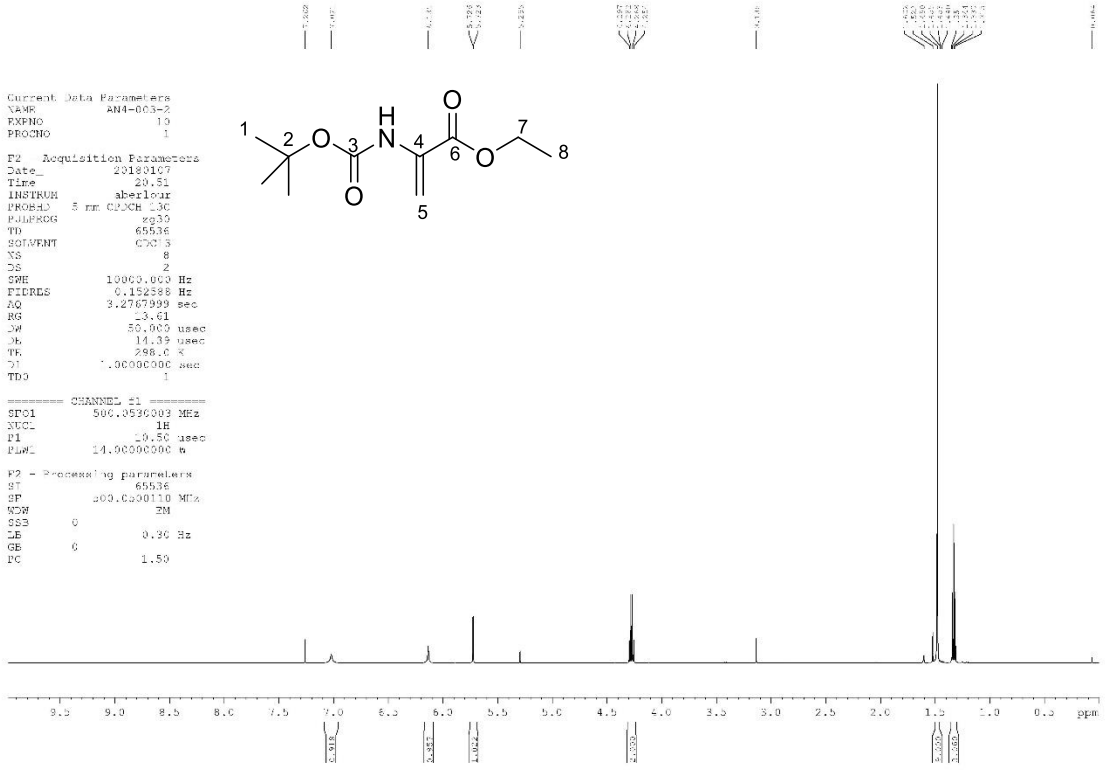

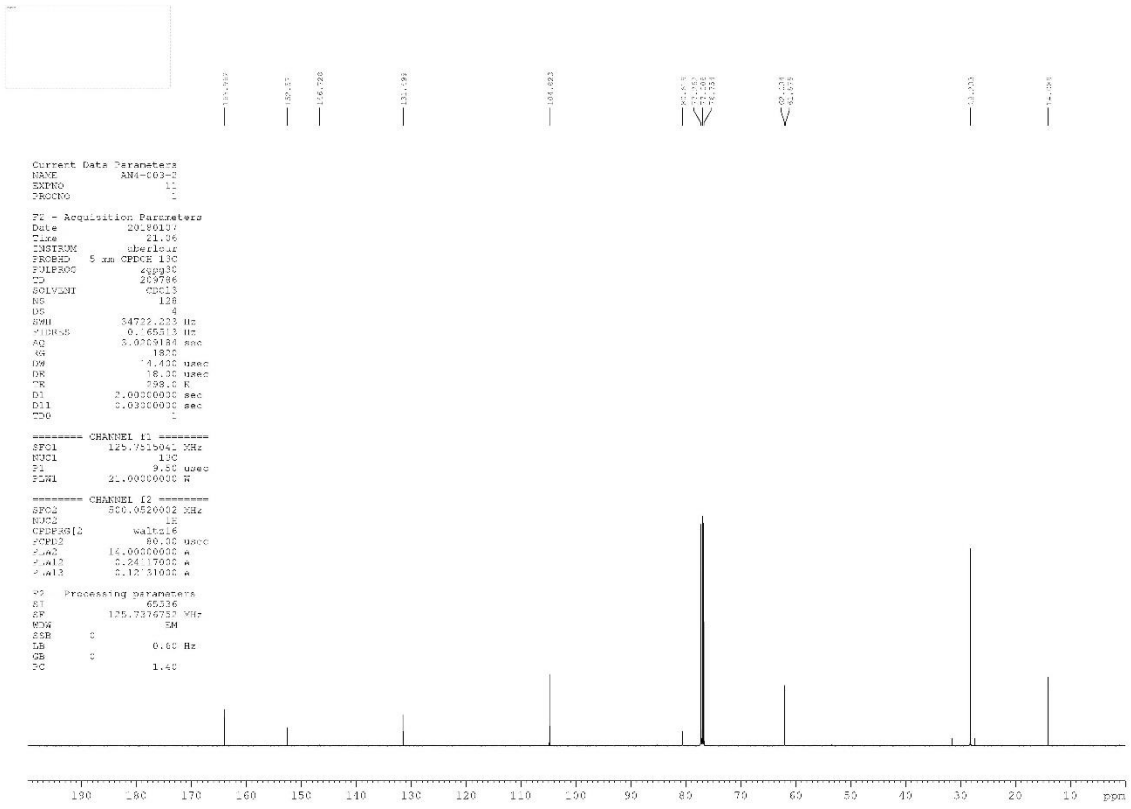

4-Methyloxazol-2(3H)-one, 204

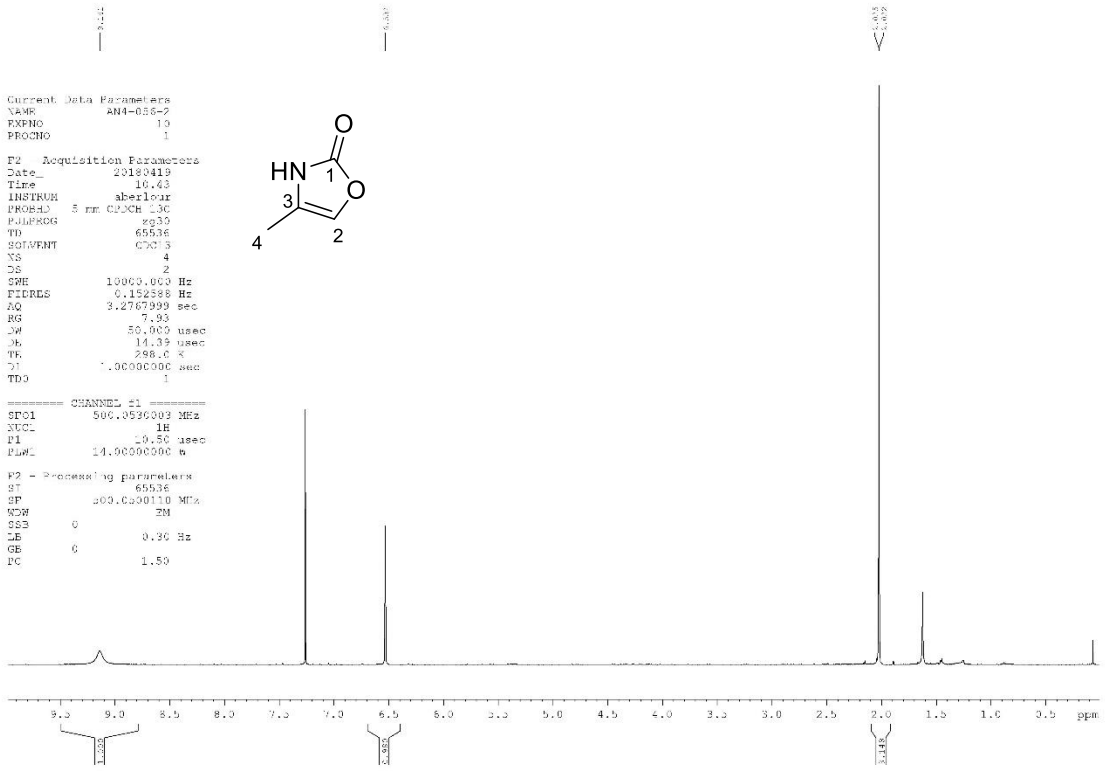

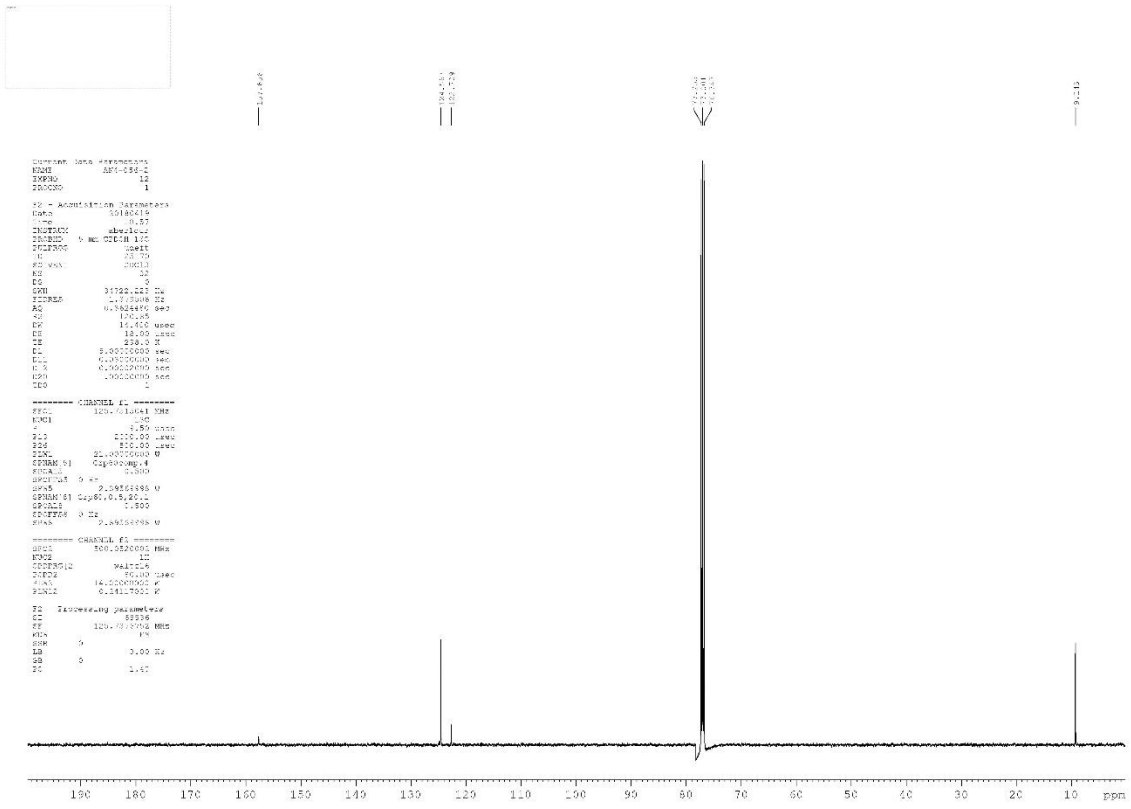

Ethyl 4-((*tert*-butoxycarbonyl)amino)-3-phenyl-4,5-dihydroisoxazole-4-carboxylate, 210

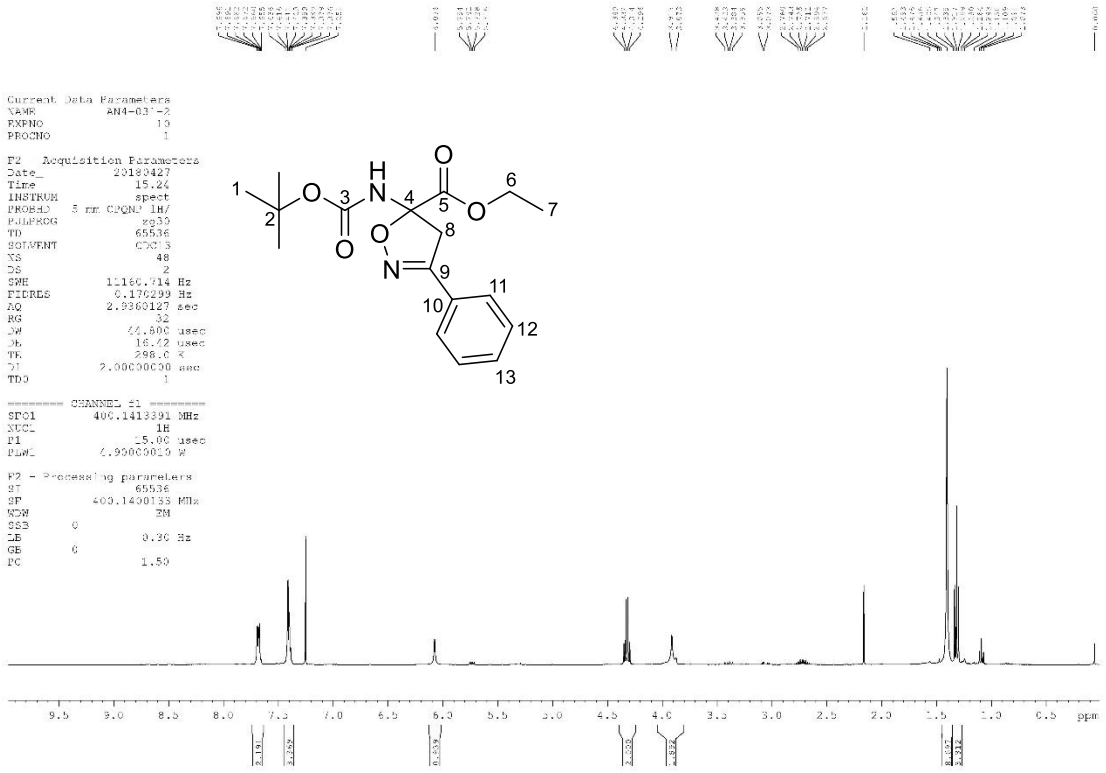

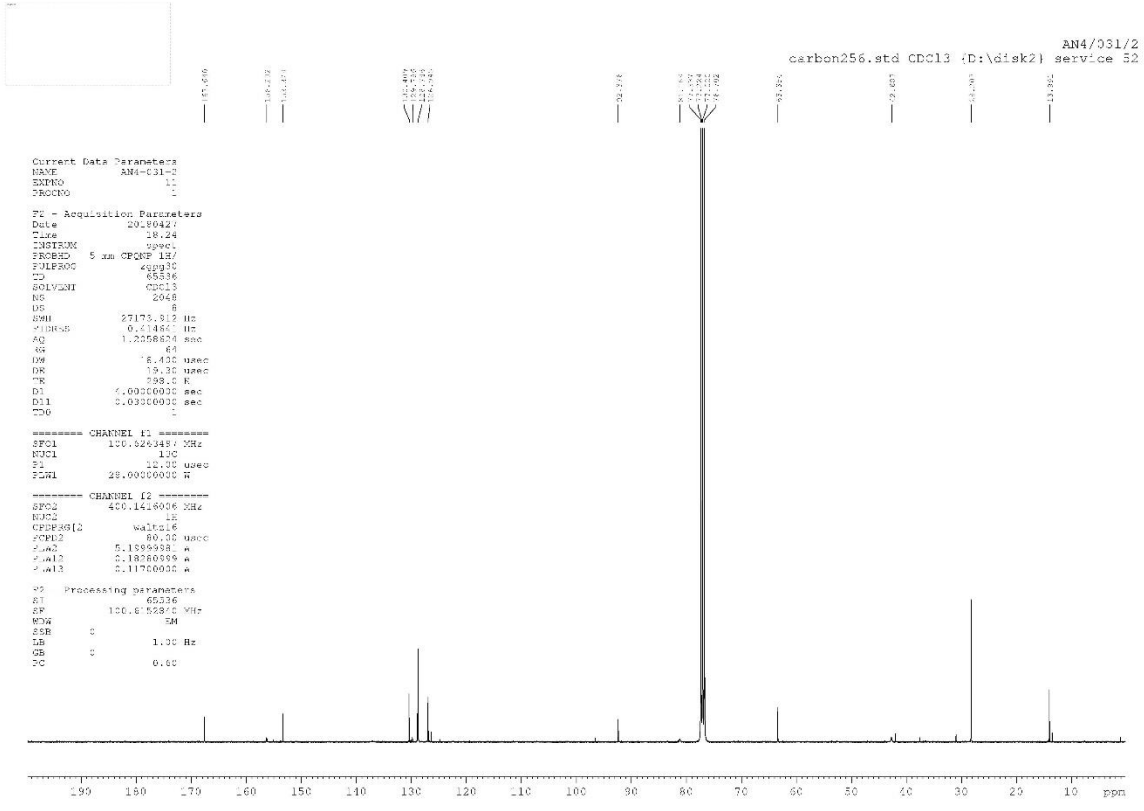

tert-Butyl (4-(hydroxymethyl)-3-phenyl-4,5-dihydroisoxazol-4-yl)carbamate, 211

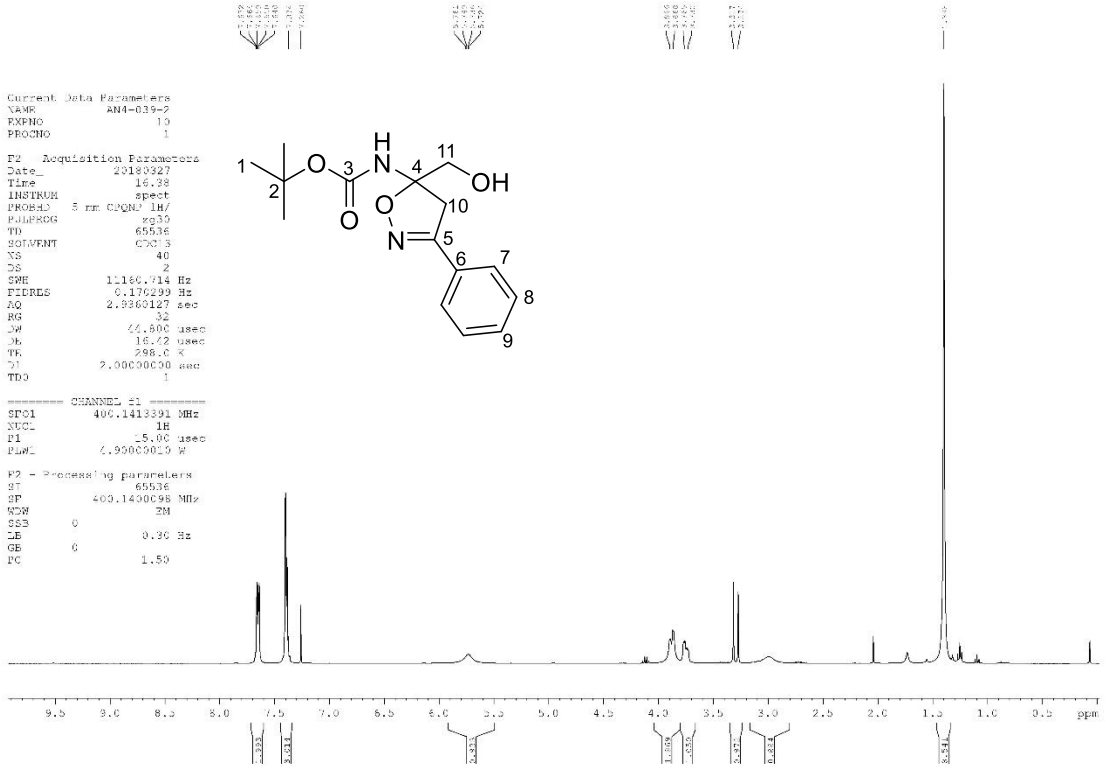

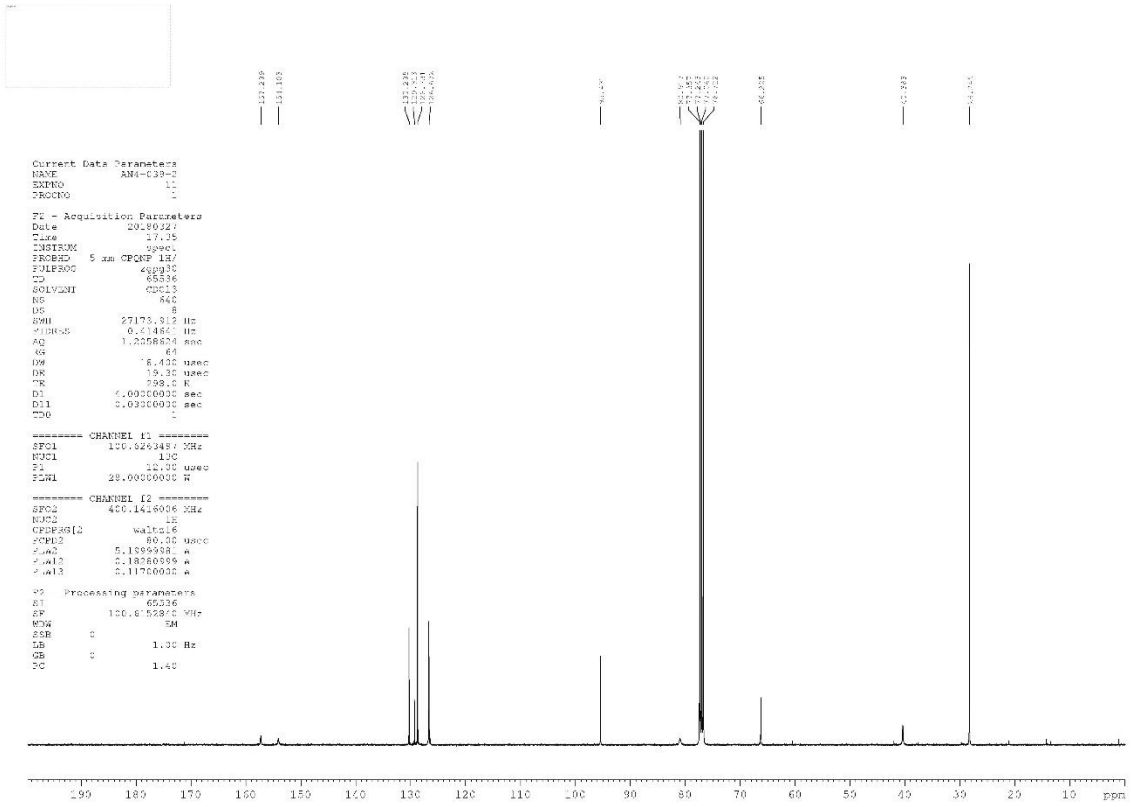

3-Phenyl-1,8-dioxa-2,6-diazaspiro[4.4]non-2-en-7-one, 212

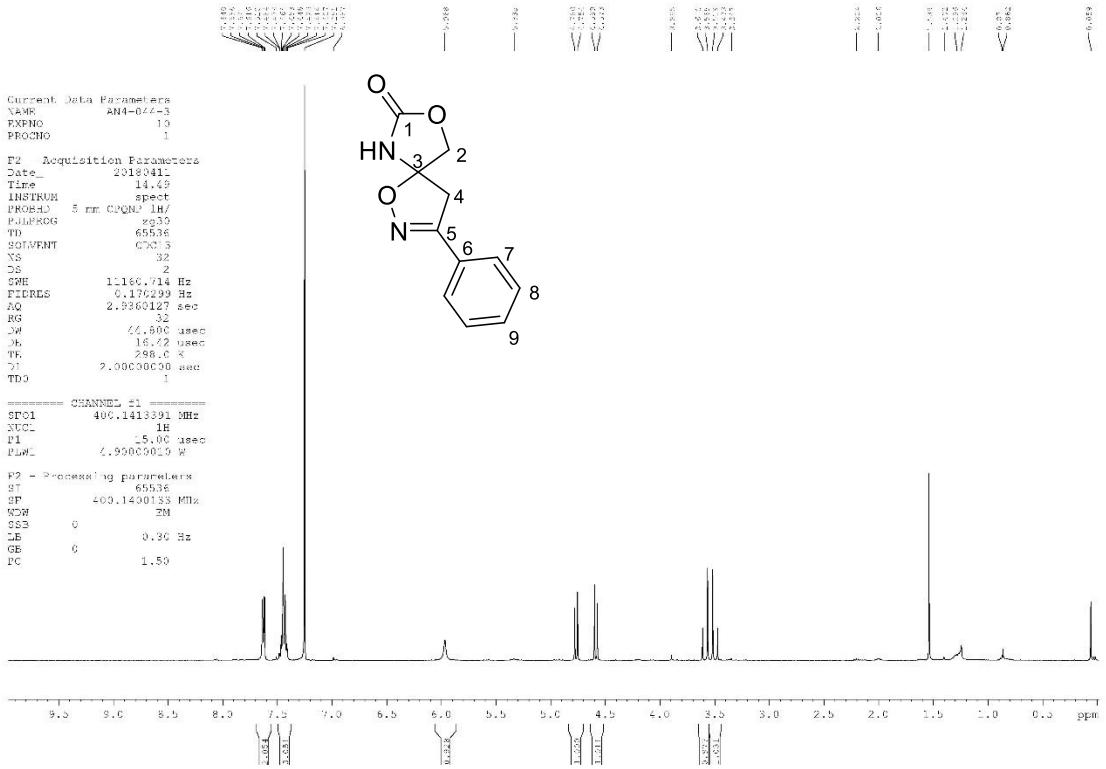

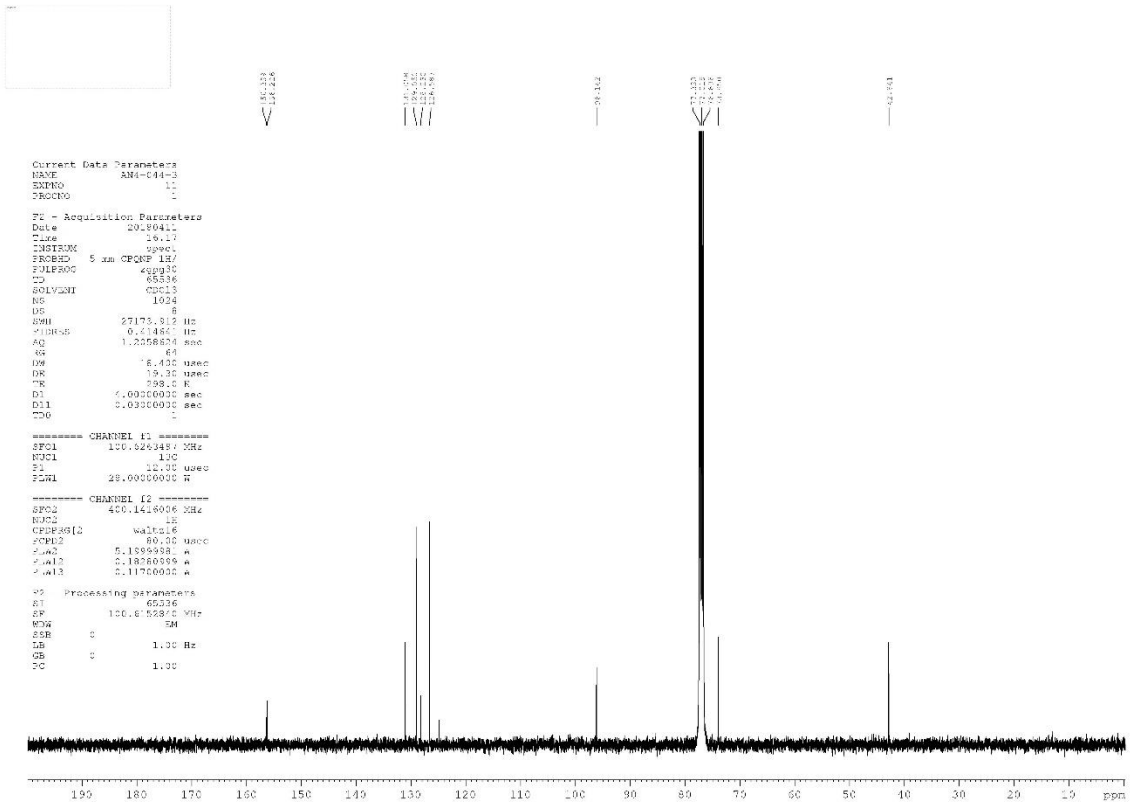

Ethyl (2-chloroacetyl)-l-serinate, 214

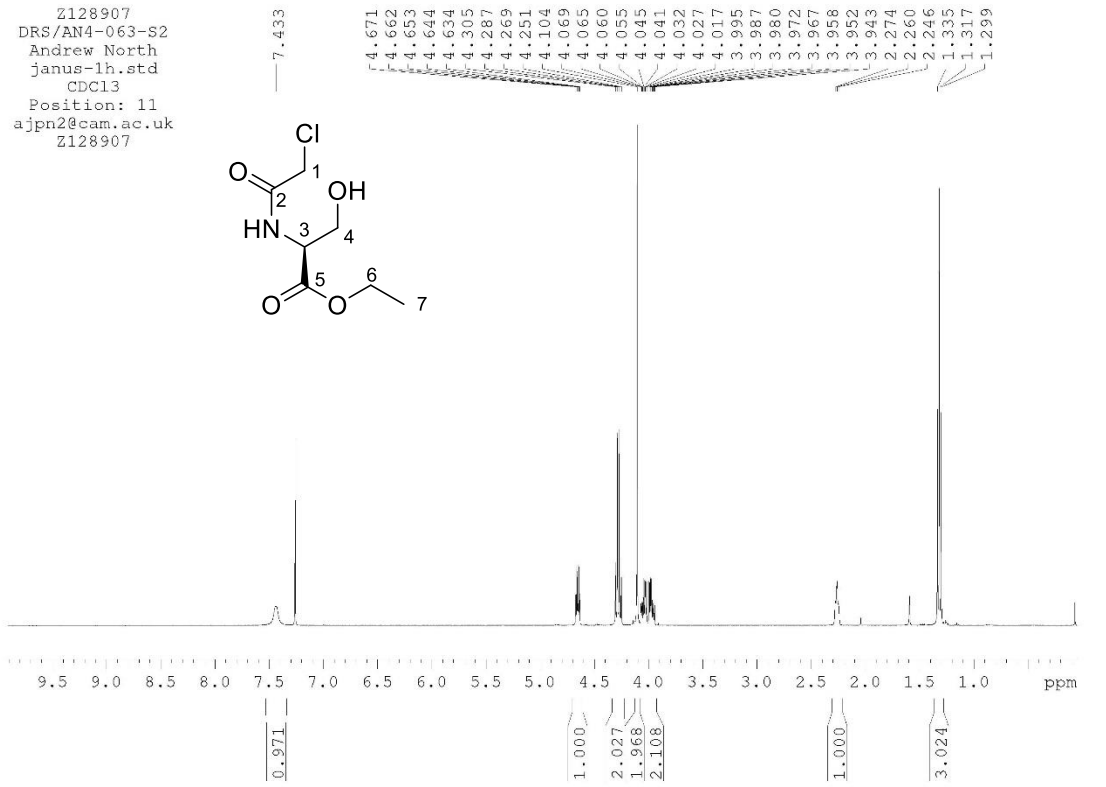

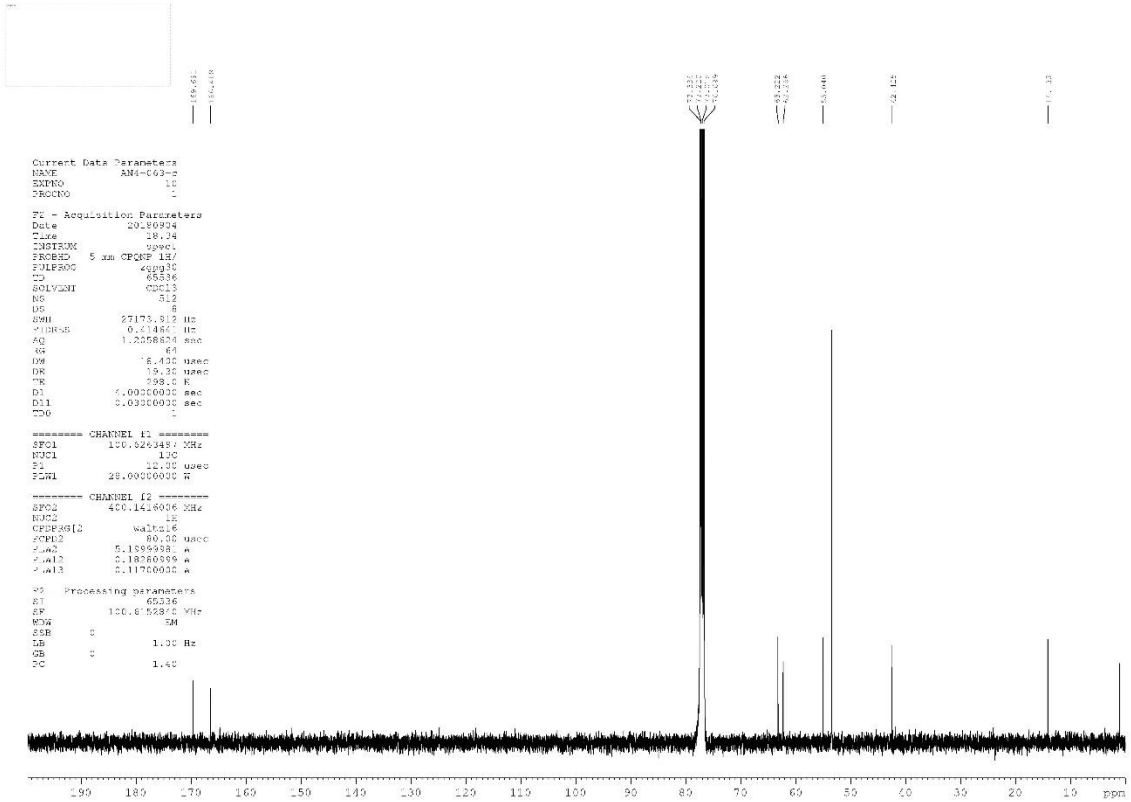

Ethyl *N*,*O*-bis(2-chloroacetyl)-L-serinate, 215

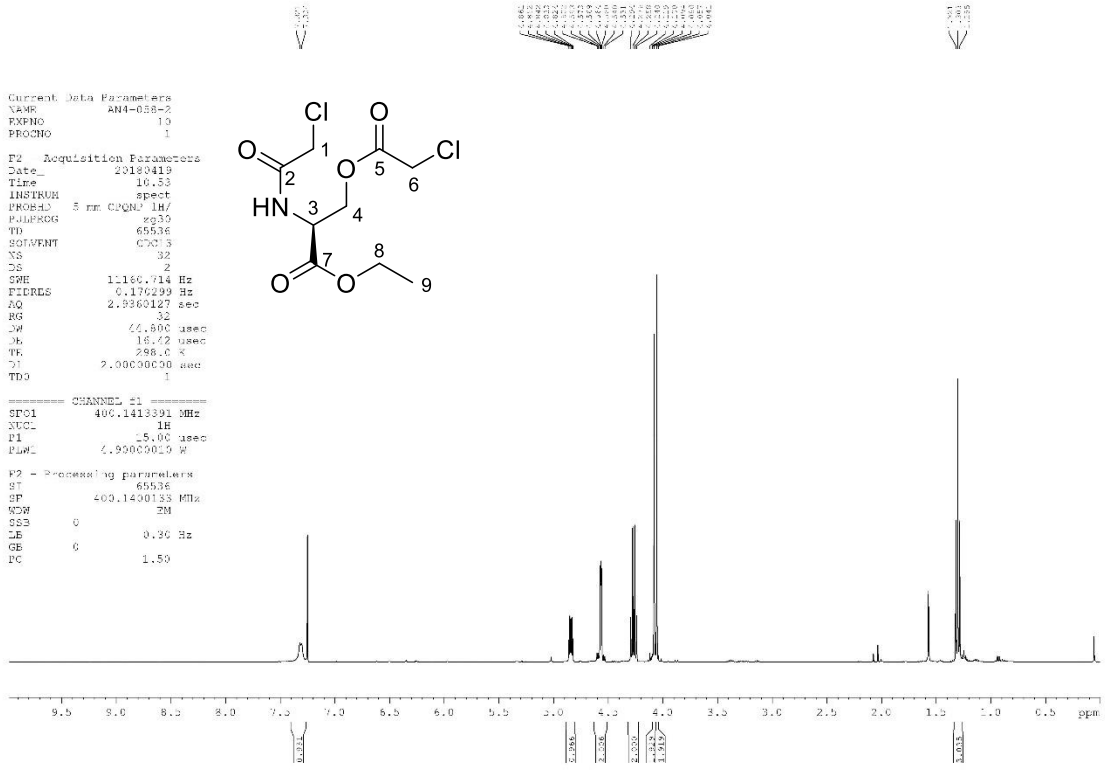

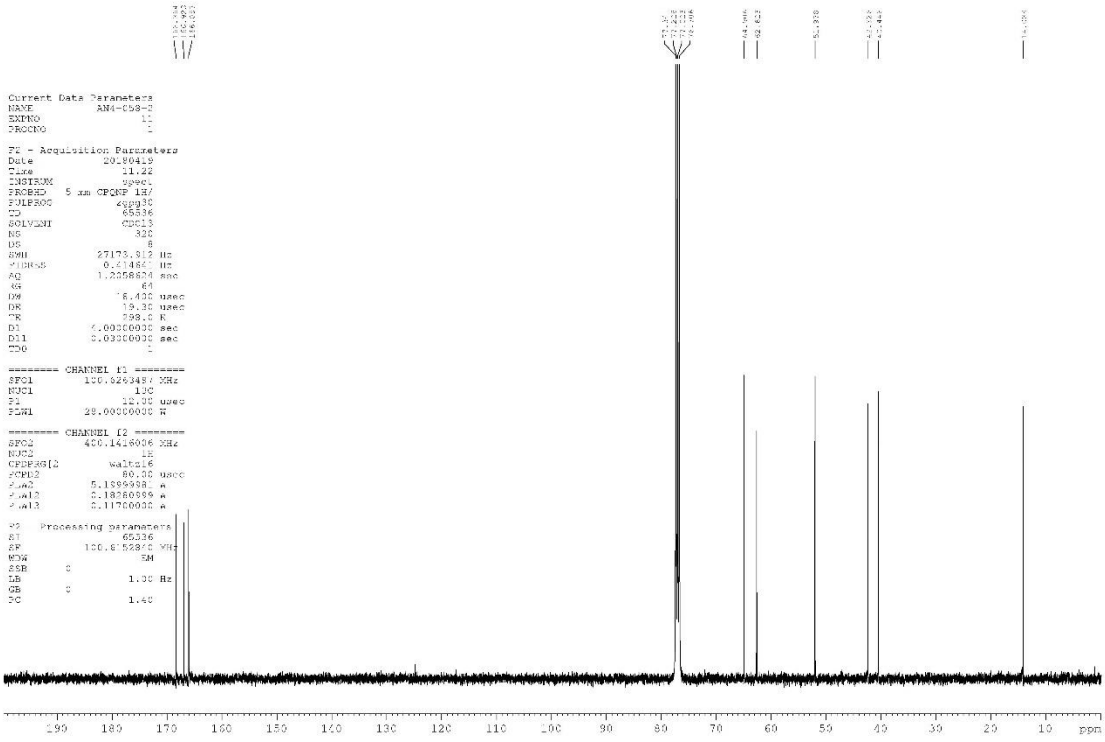

Ethyl (S)-2-oxooxazolidine-4-carboxylate, 219

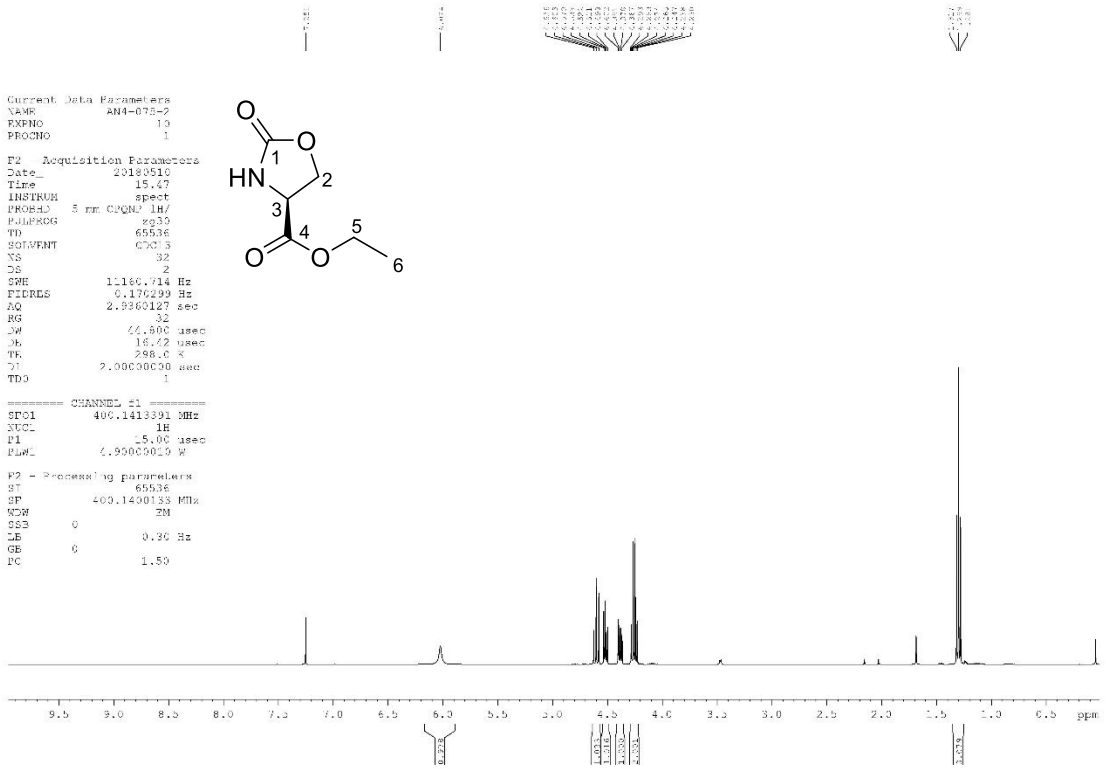

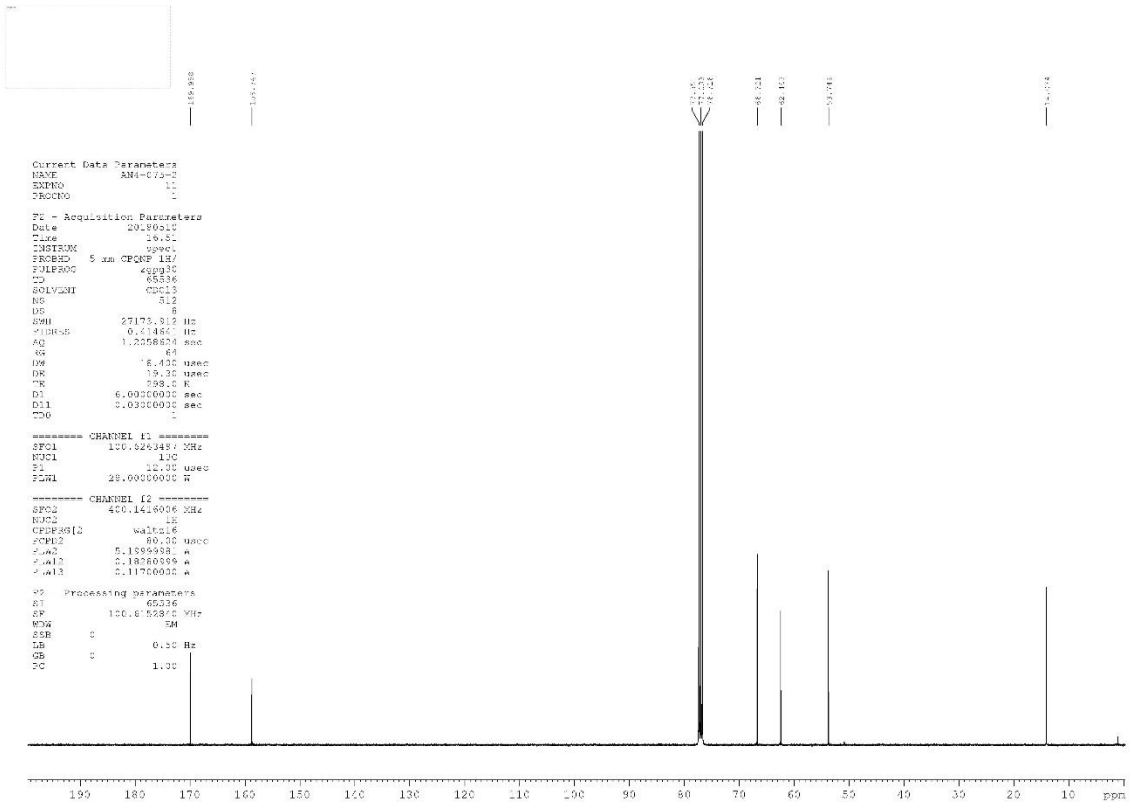

Ethyl (S)-2-phenyl-4,5-dihydrooxazole-4-carboxylate, 221

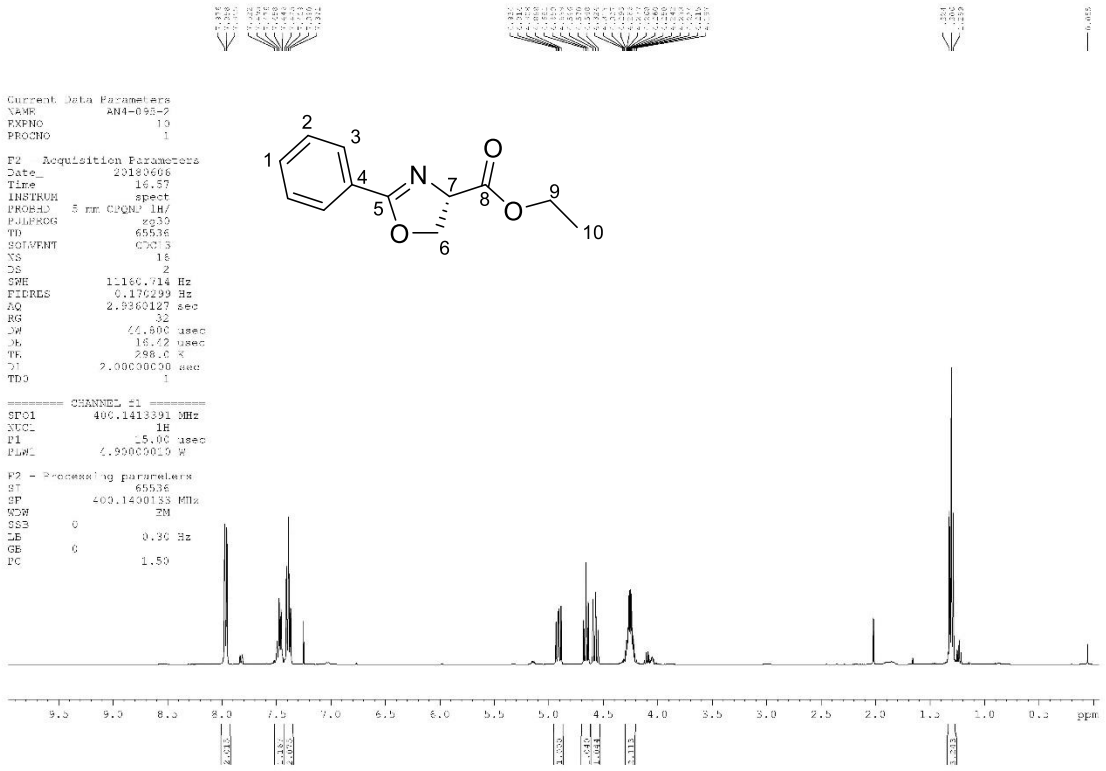

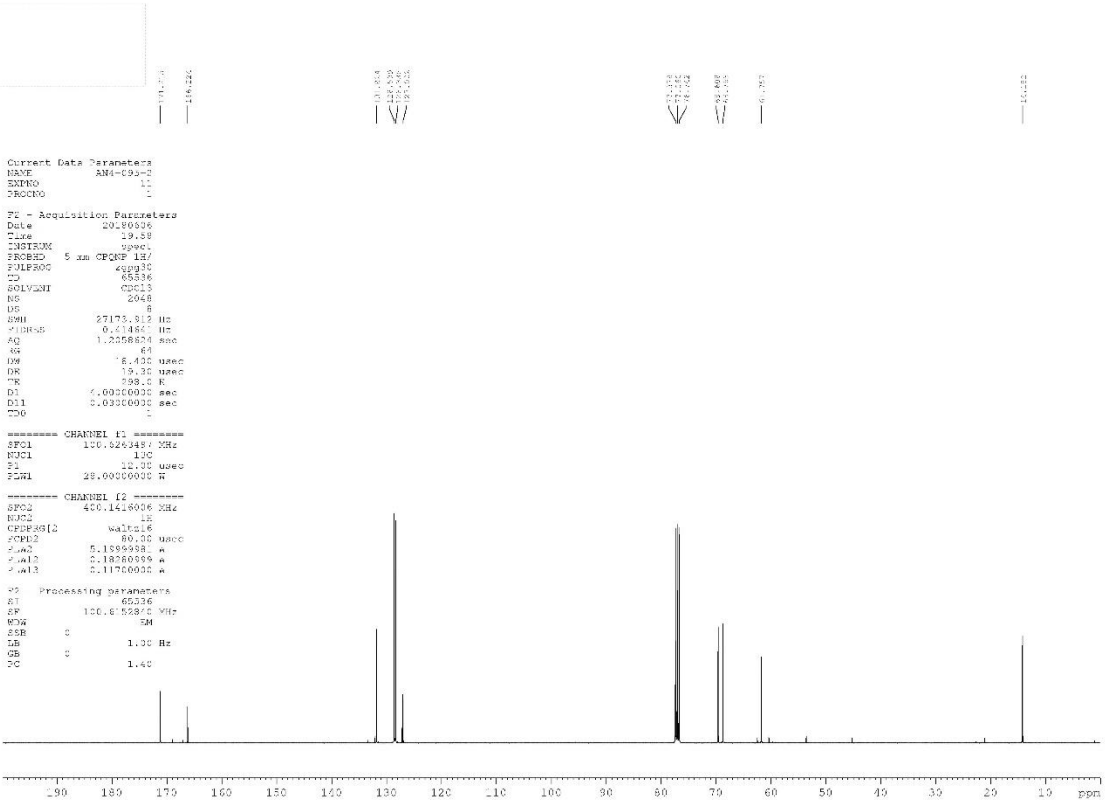

(R)-(2-Phenyl-4,5-dihydrooxazol-4-yl)methanol, 222

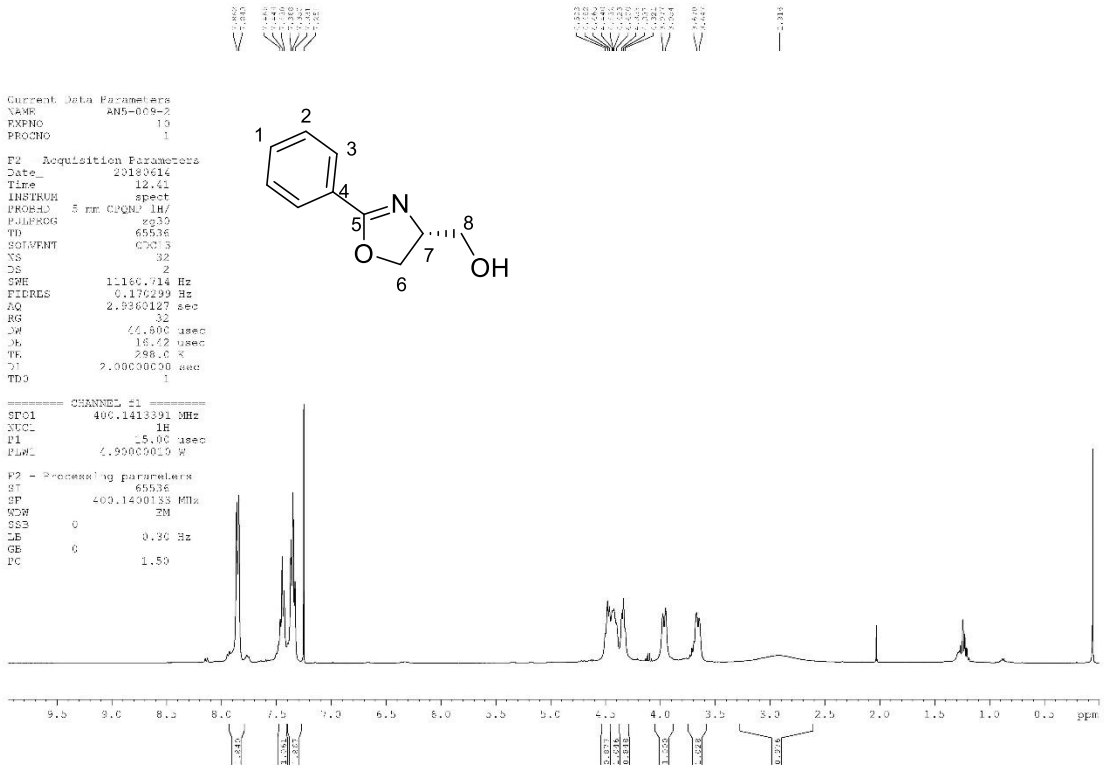

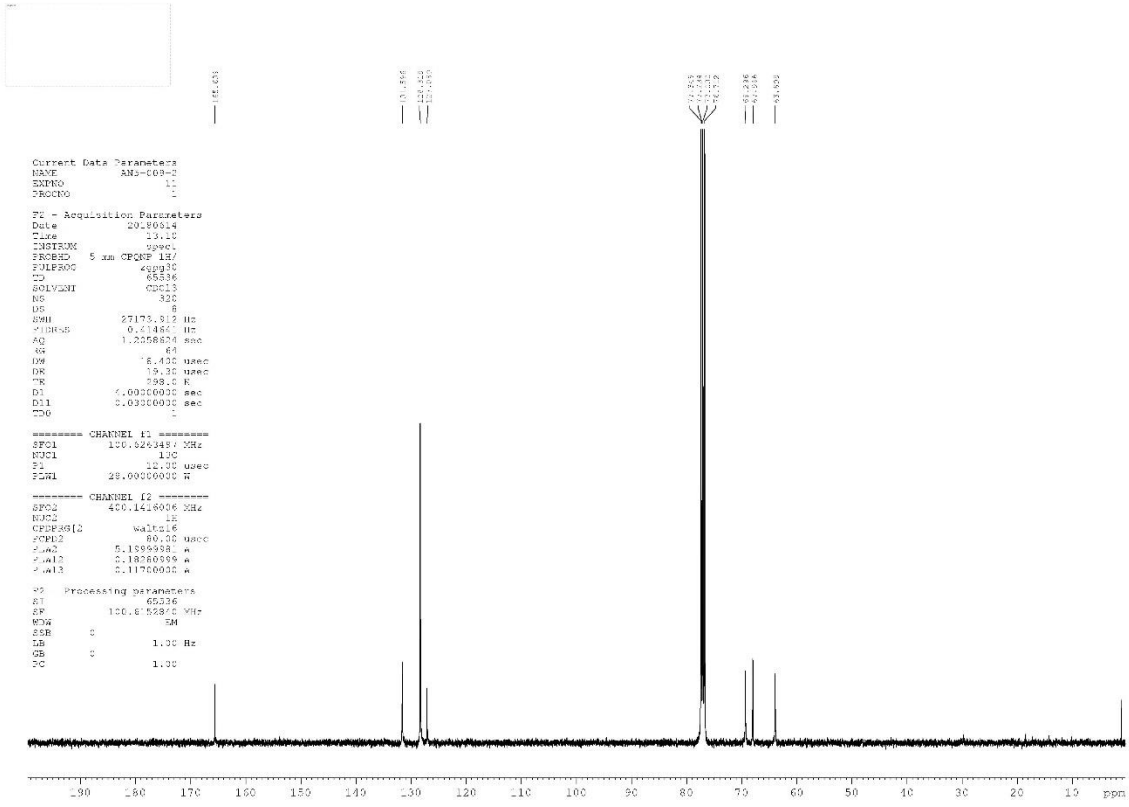

Ethyl O-(*tert*-butyldimethylsilyl)-l-serinate, 224

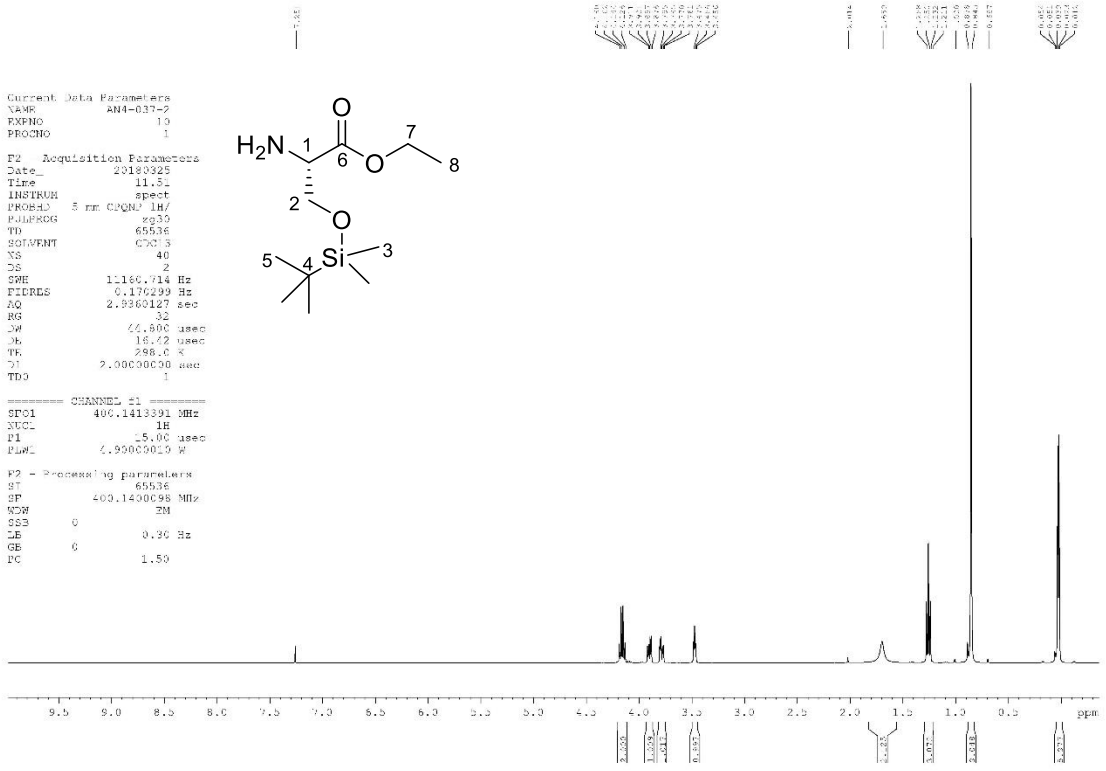

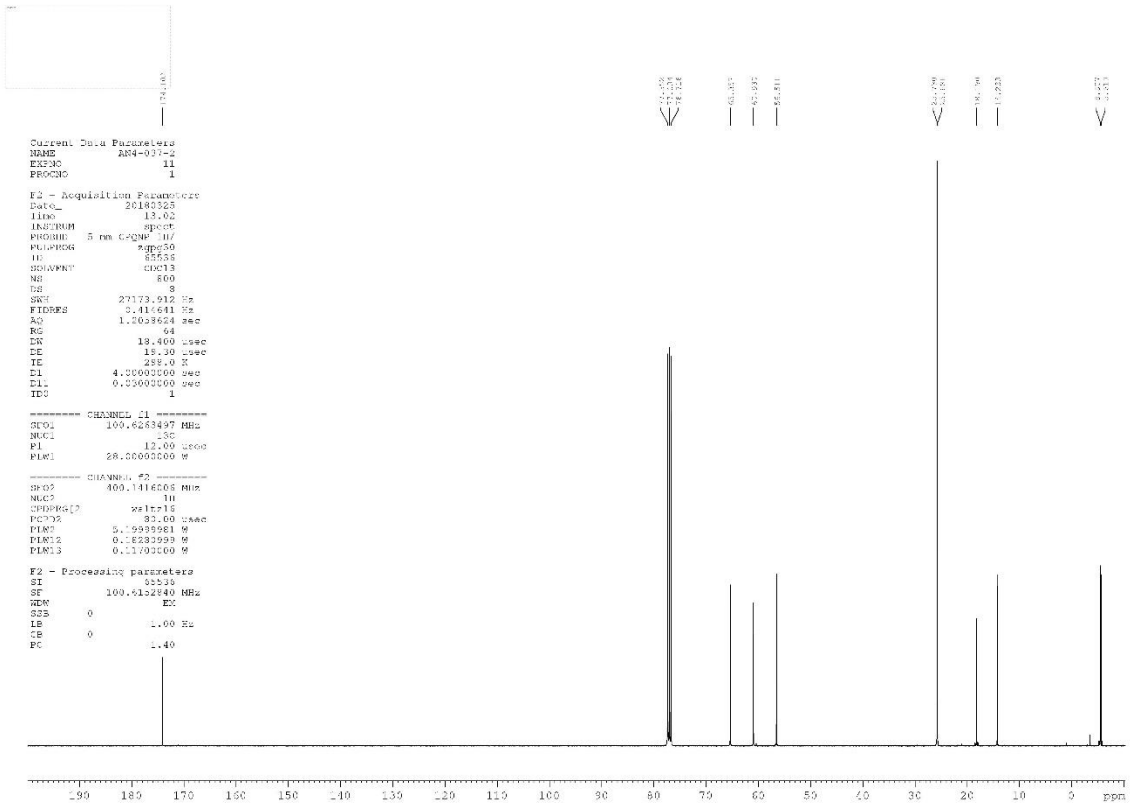

Ethyl O-(*tert*-butyldimethylsilyl)-N-(2-chloroacetyl)-l-serinate, 225

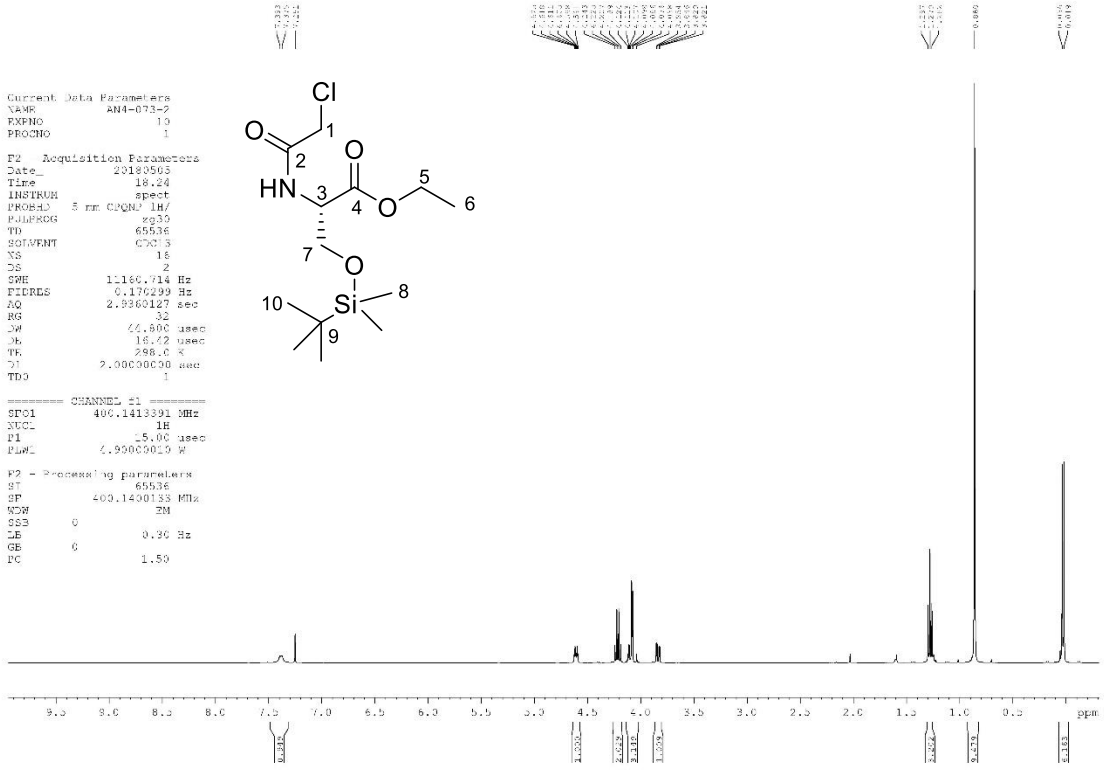

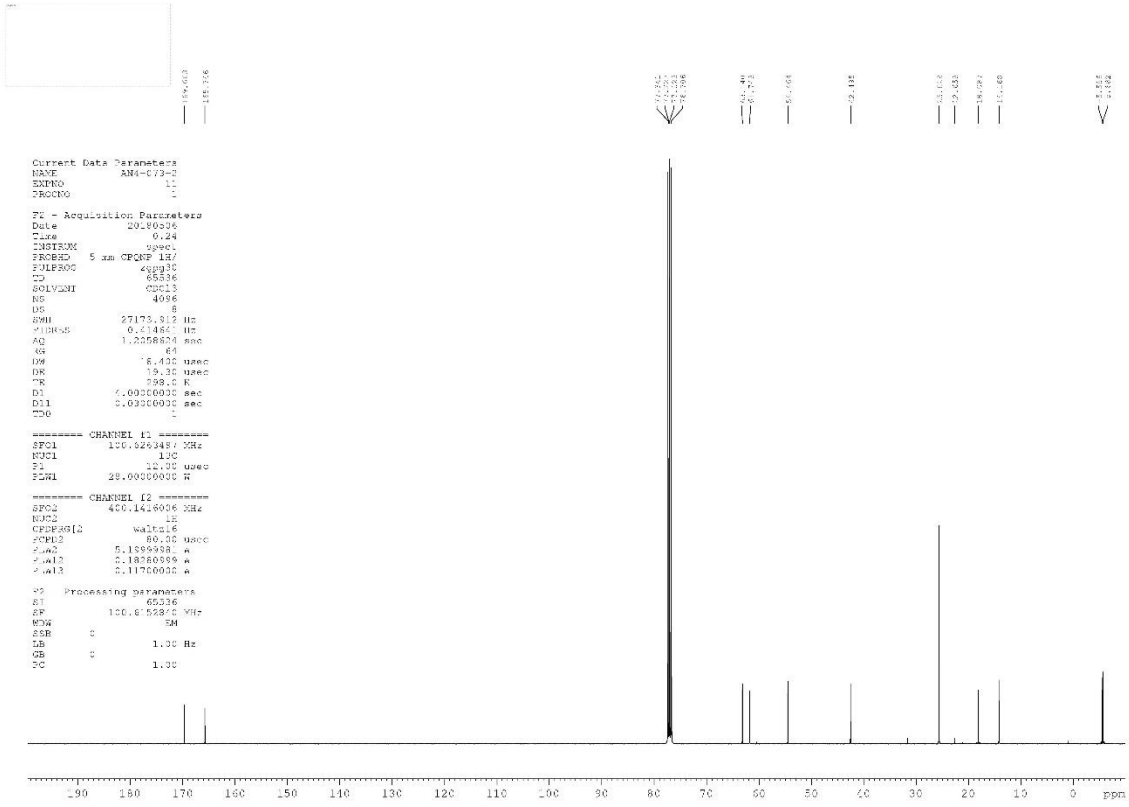

(R)-N-(1-((*tert*-Butyldimethylsilyl)oxy)-3-hydroxypropan-2-yl)-2-chloroacetamide, 226

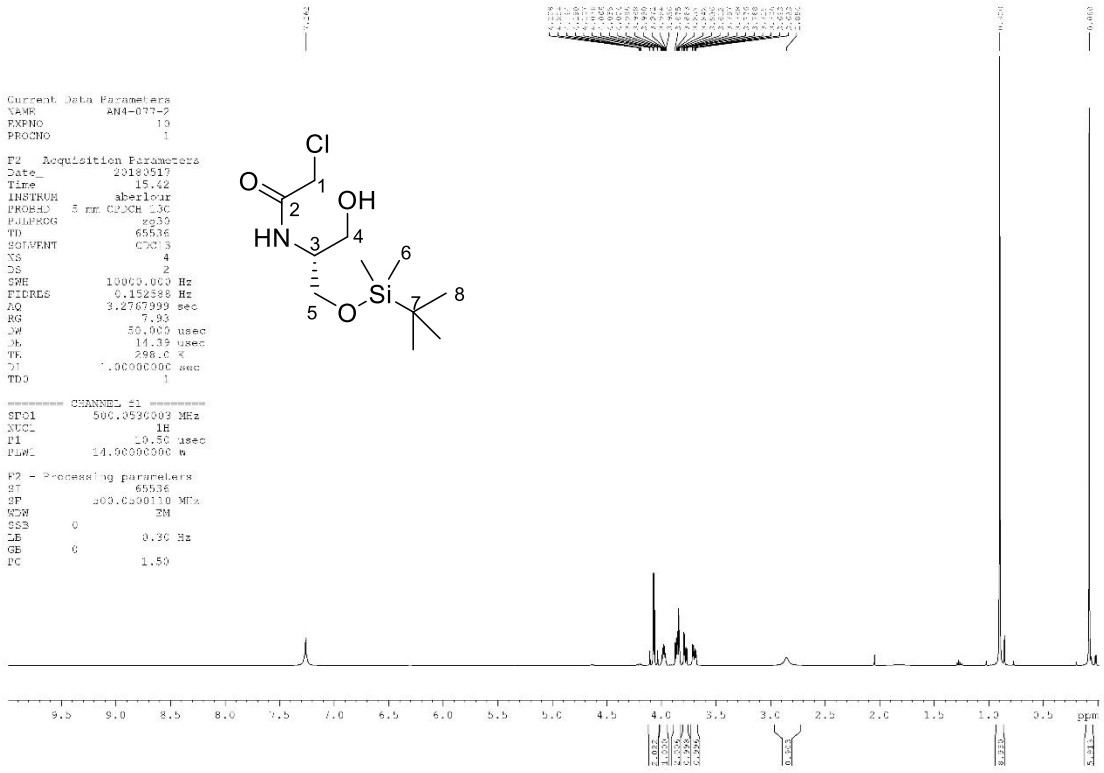

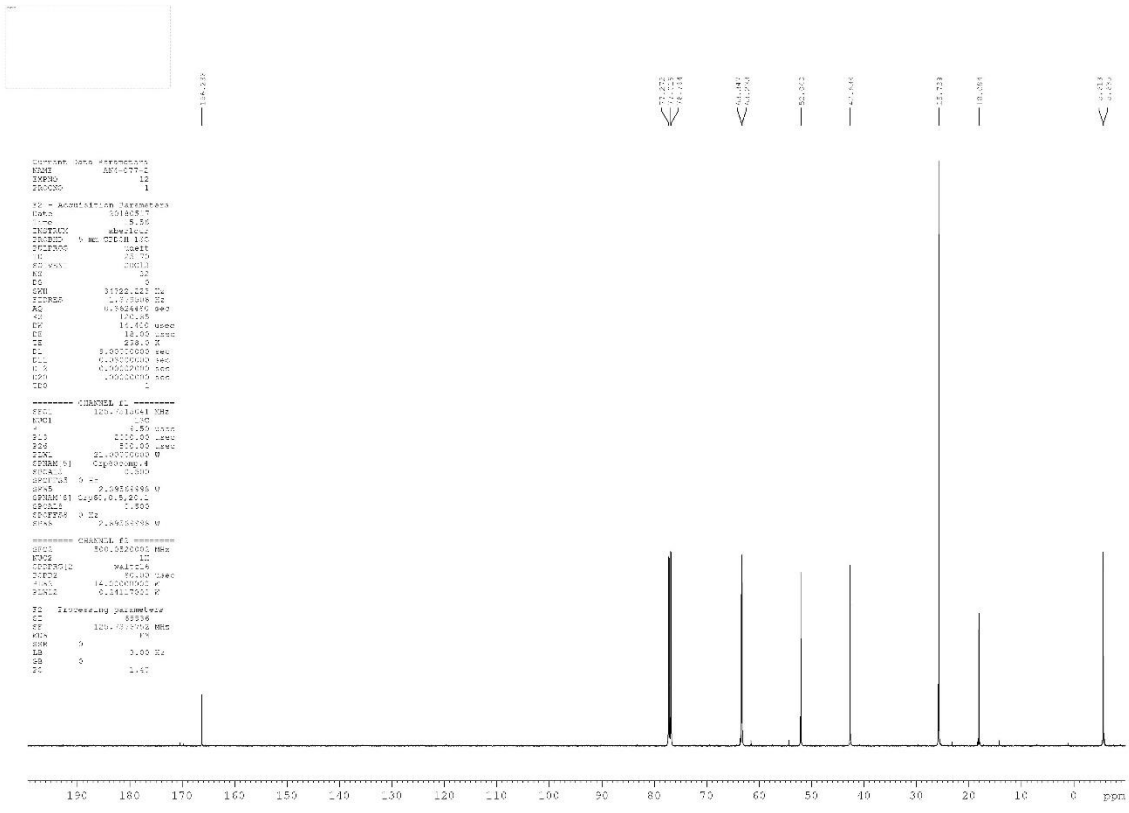

Ethyl O-(*tert*-butyldimethylsilyl)-N-(3-ethoxy-3-oxopropanoyl)-l-serinate, 228

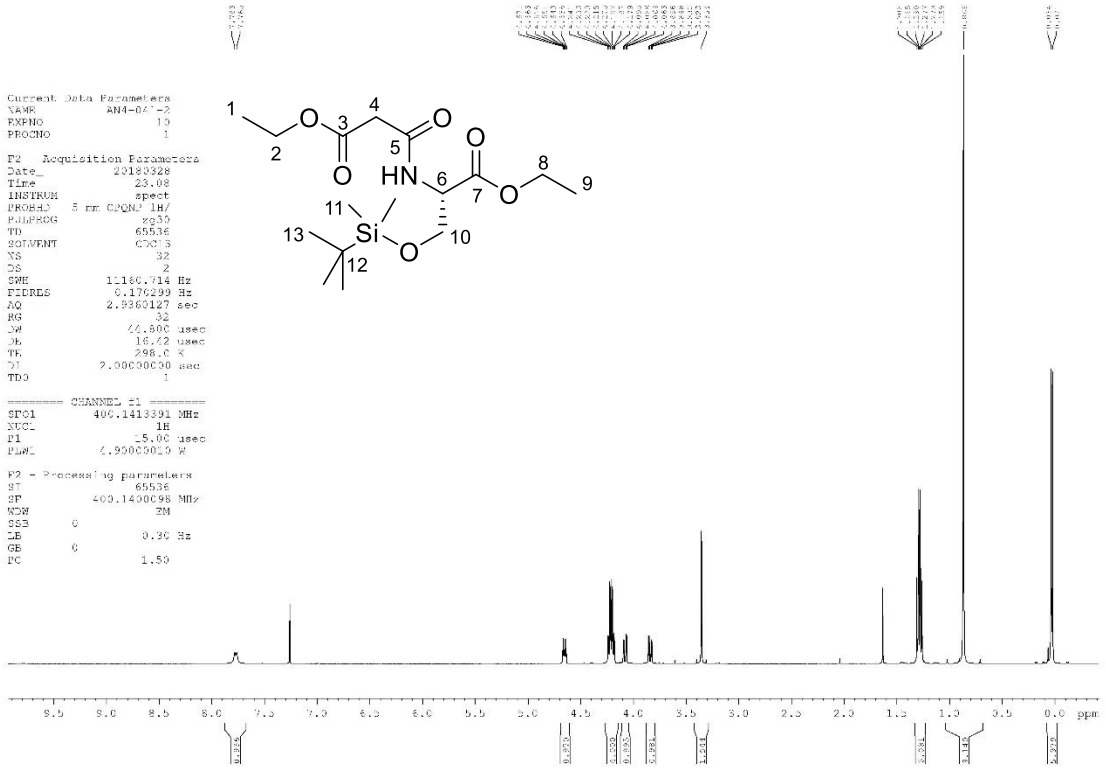

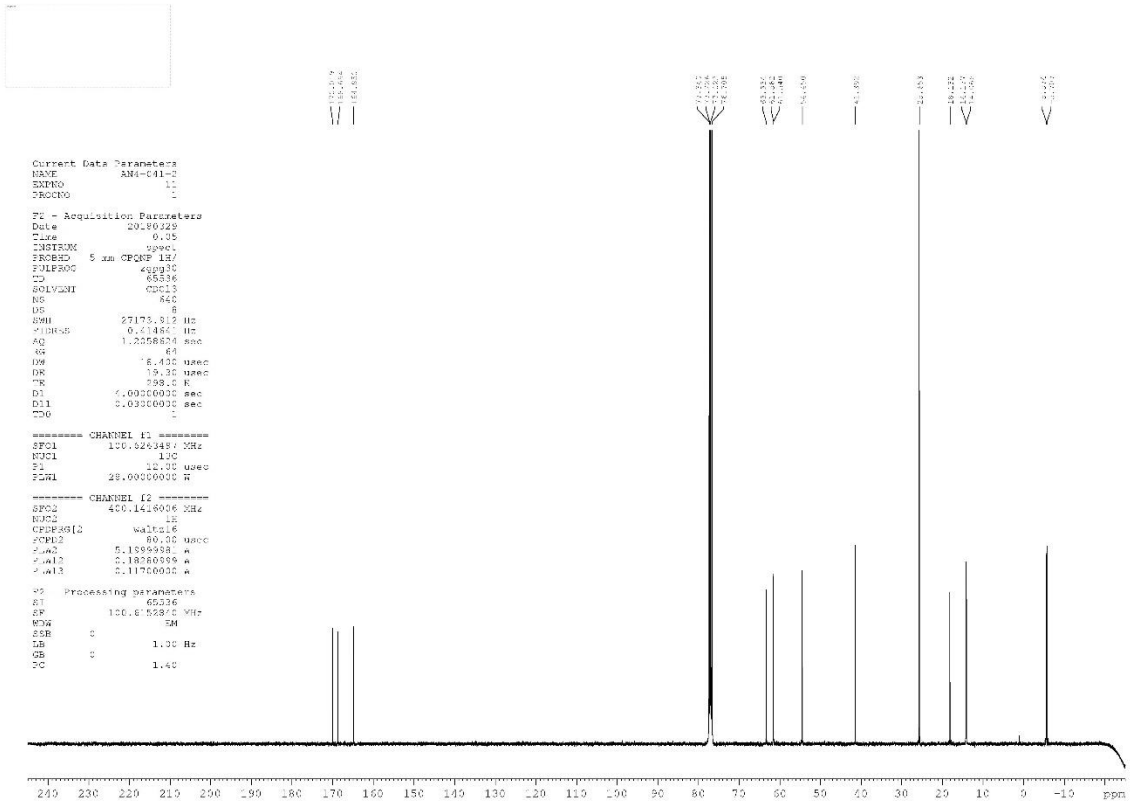

4-Ethoxy-5-methylene-1,5-dihydro-2H-pyrrol-2-one, 230

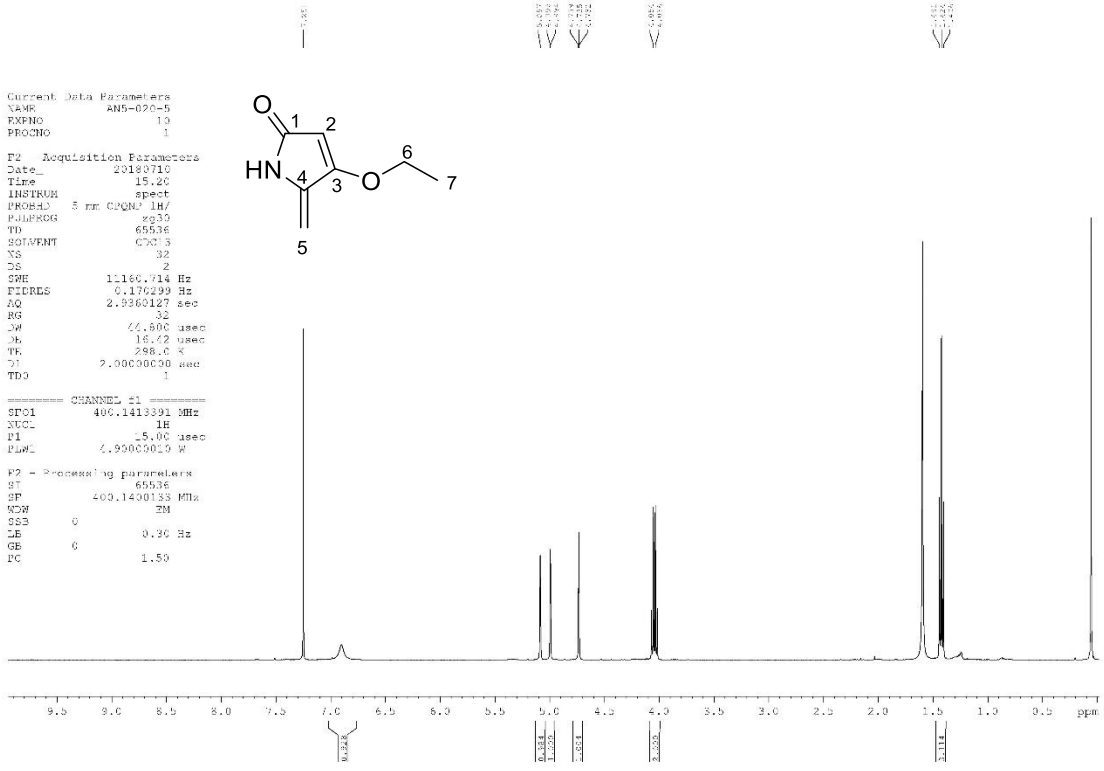

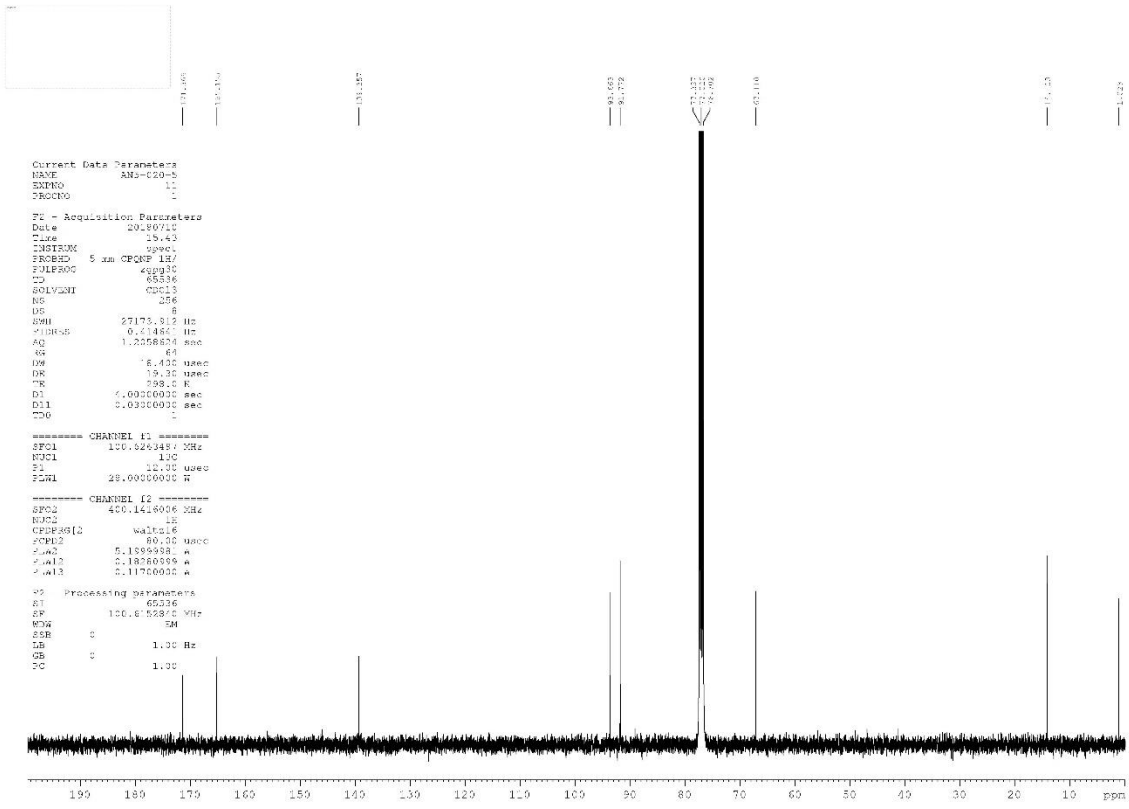

tert-Butyl 3-(2-ethoxy-2-oxoethylidene)azetidine-1-carboxylate, 236

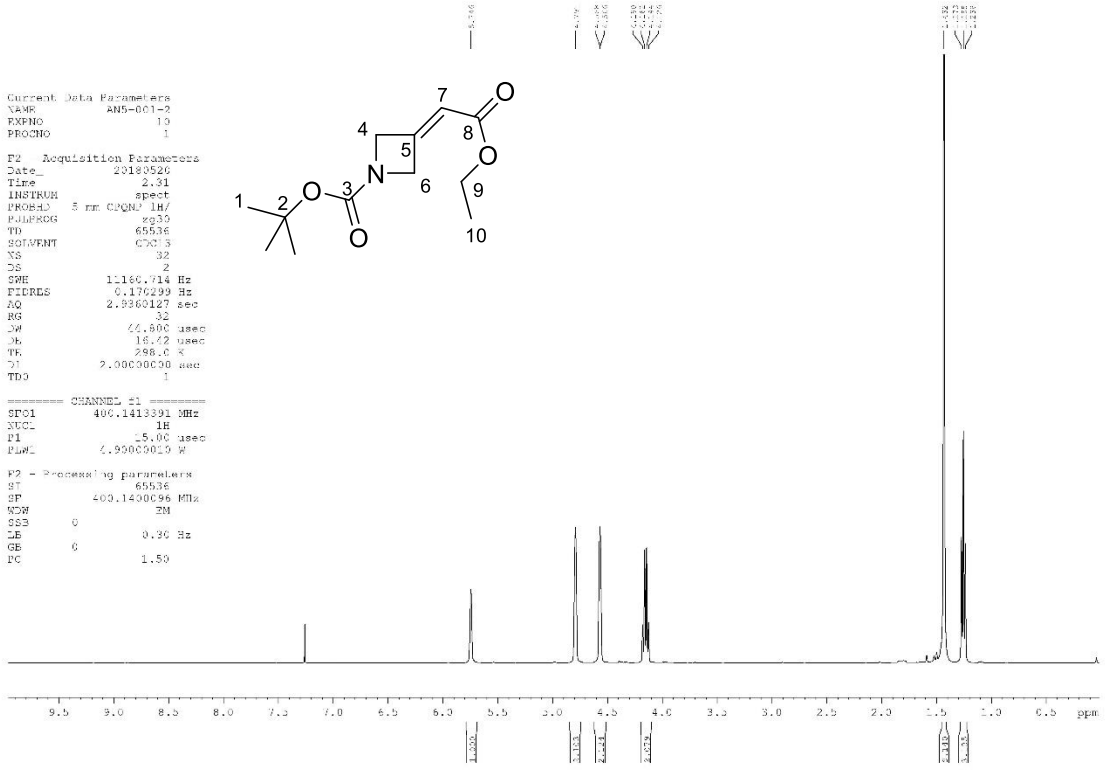

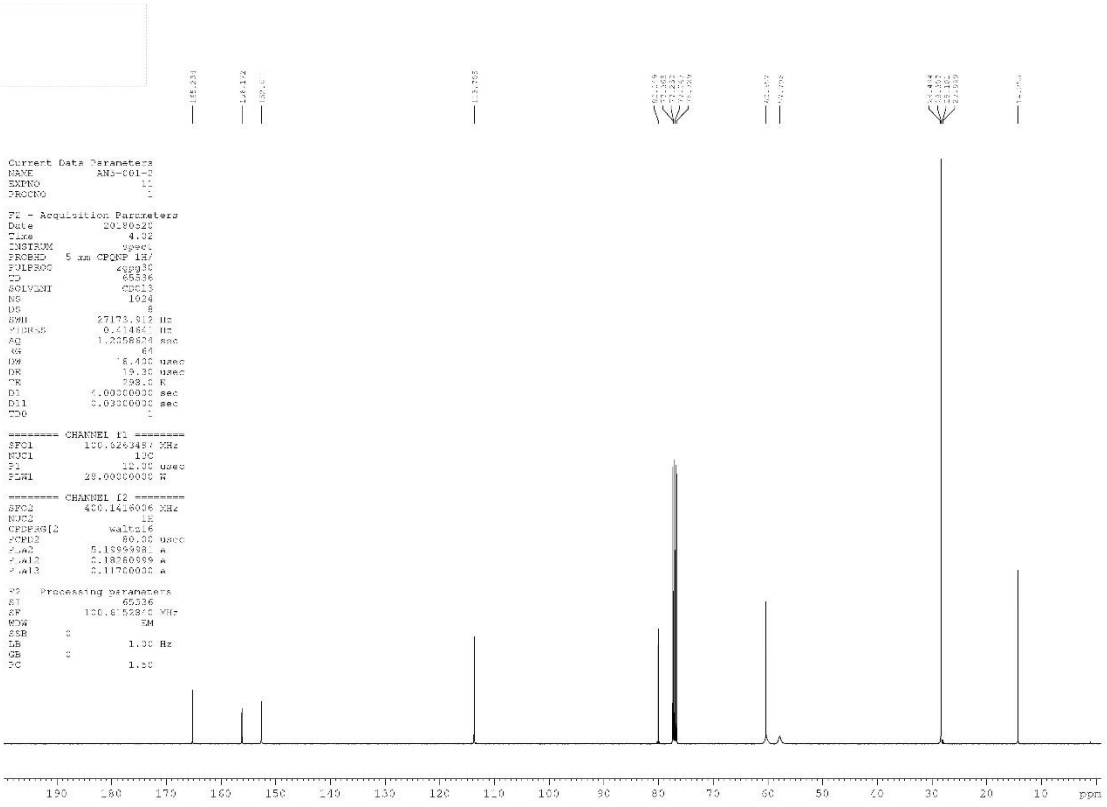

2-(*tert*-Butyl) 8-ethyl 7-phenyl-5-oxa-2,6-diazaspiro[3.4]oct-6-ene-2,8-dicarboxylate, 237

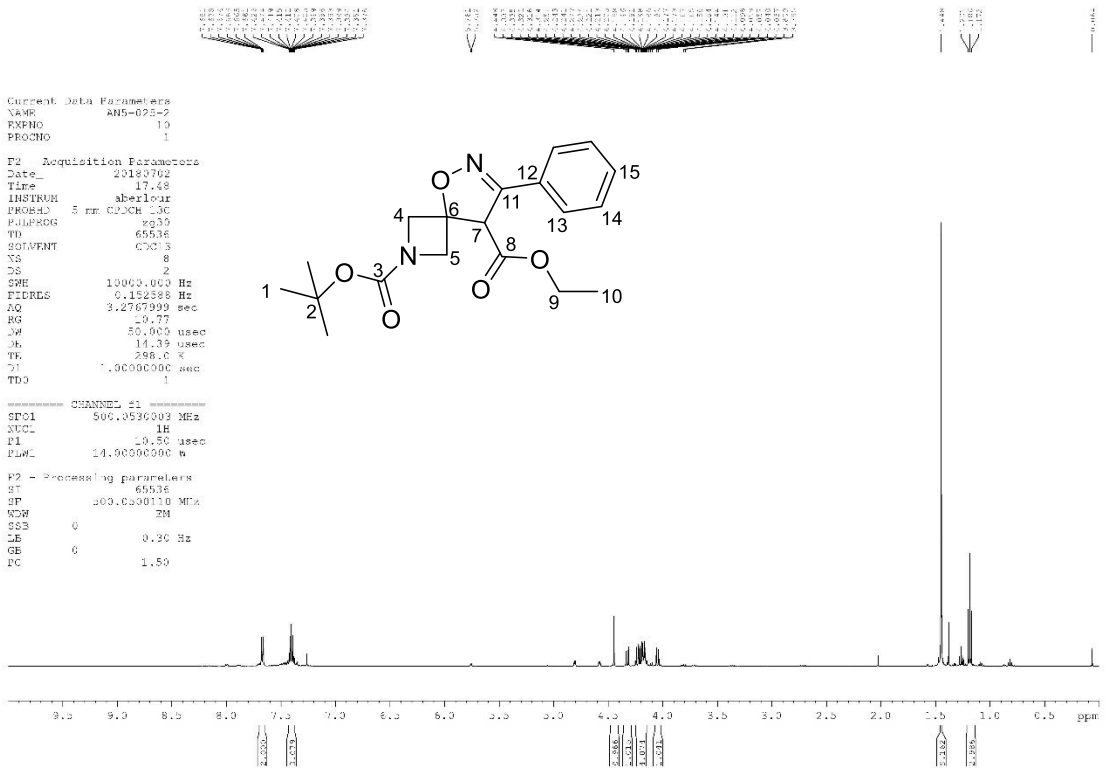

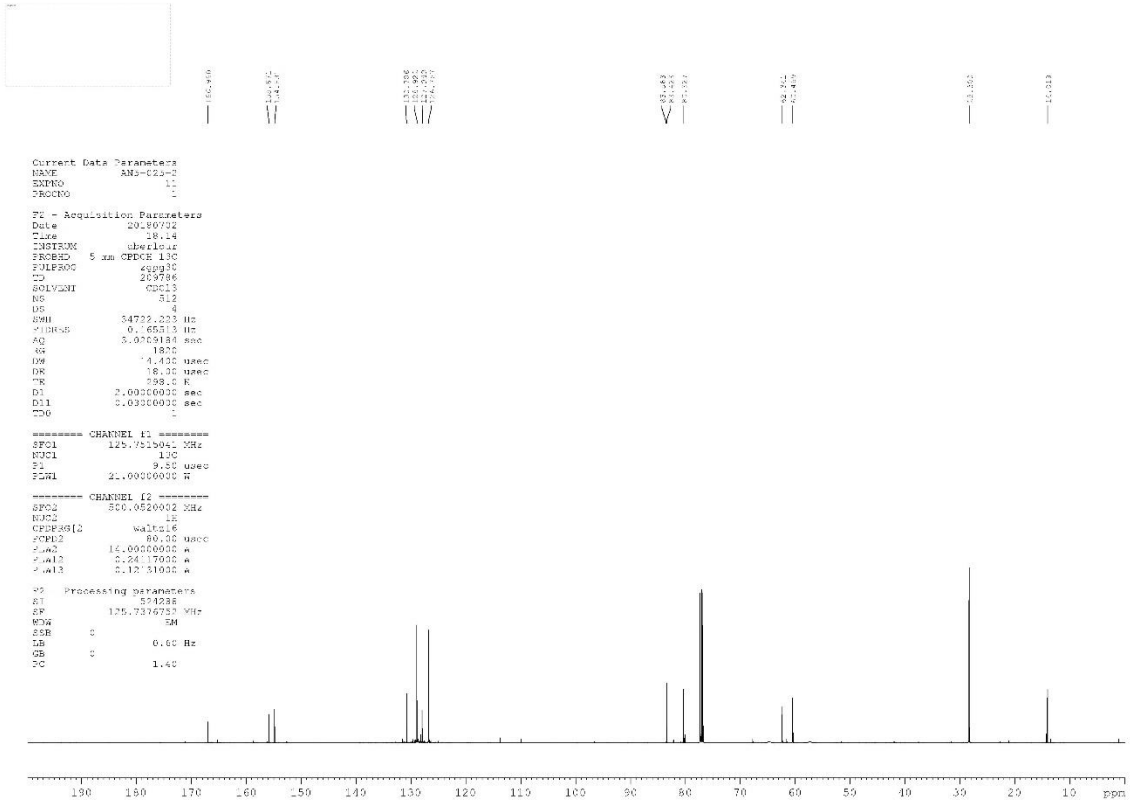

2-(*tert*-Butyl) 8-ethyl 7-benzyl-2,5,6,7-tetraazaspiro[3.4]oct-5-ene-2,8-dicarboxylate, 238

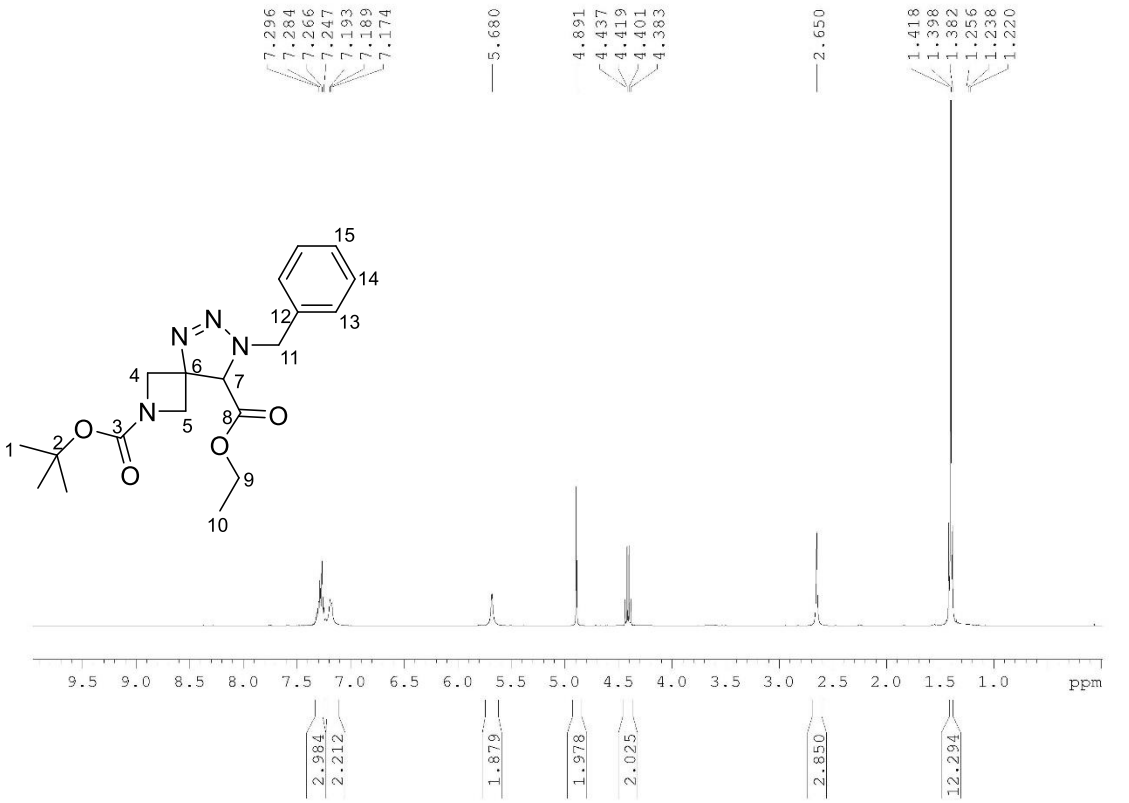

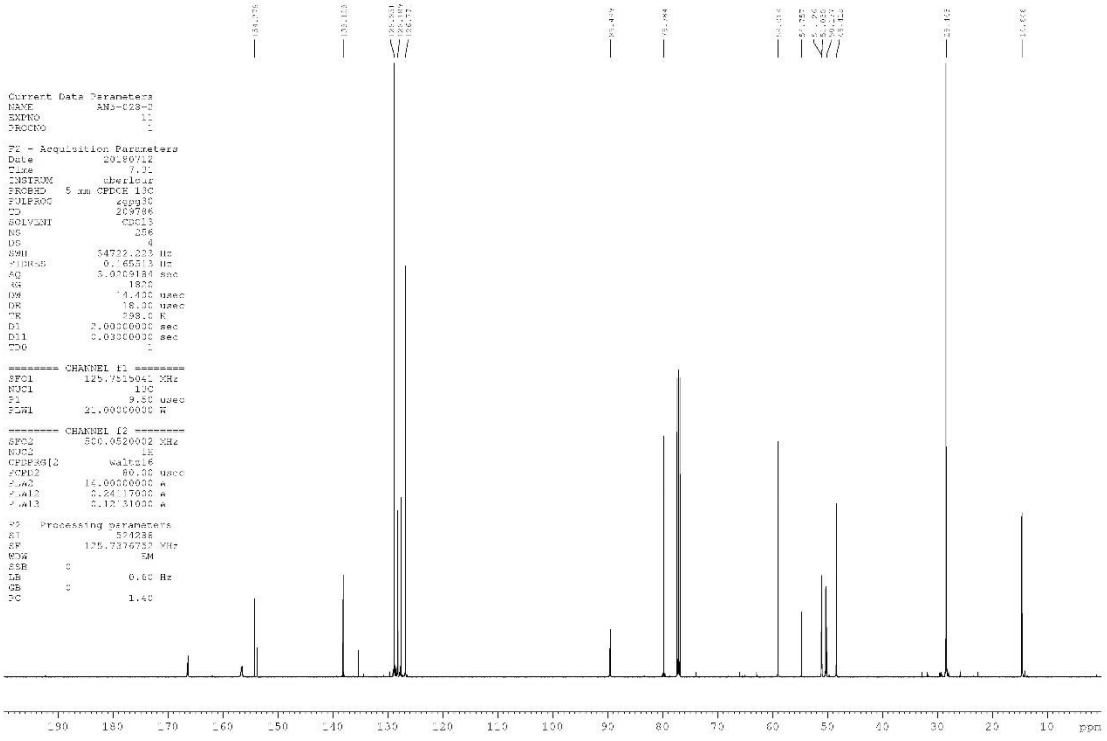

(2-Hydroxy-5-oxo-5,6-dihydro-2H-pyran-2-yl)methyl acetate, 242

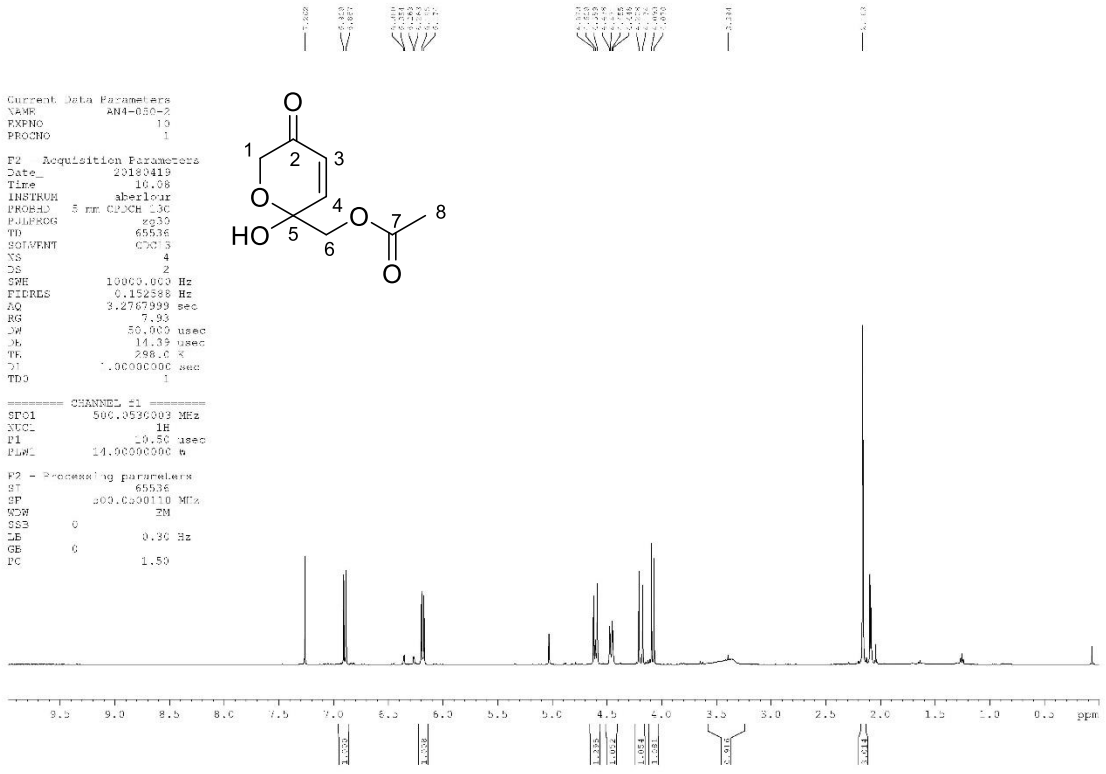

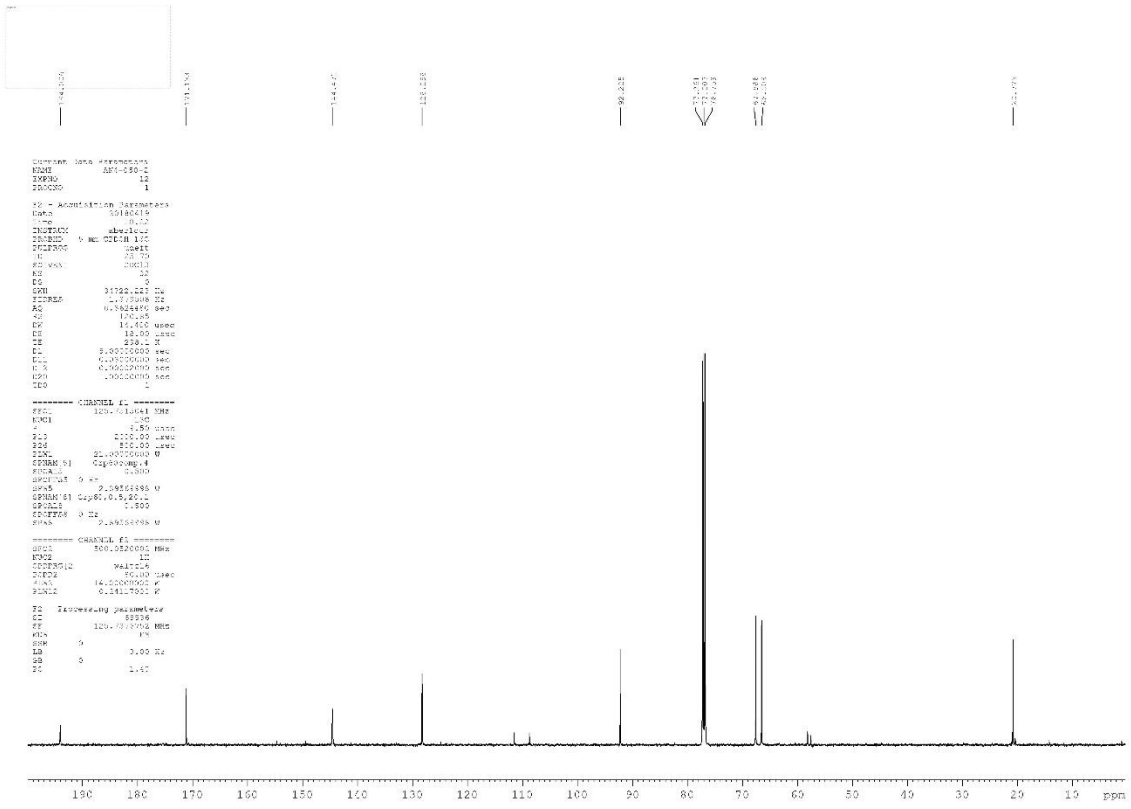

10,12-Dioxo-3,11-dioxatricyclo[5.3.1.12,6]dodeca-4,8-diene-4,7-diyl)bis(methylene) diacetate, 244

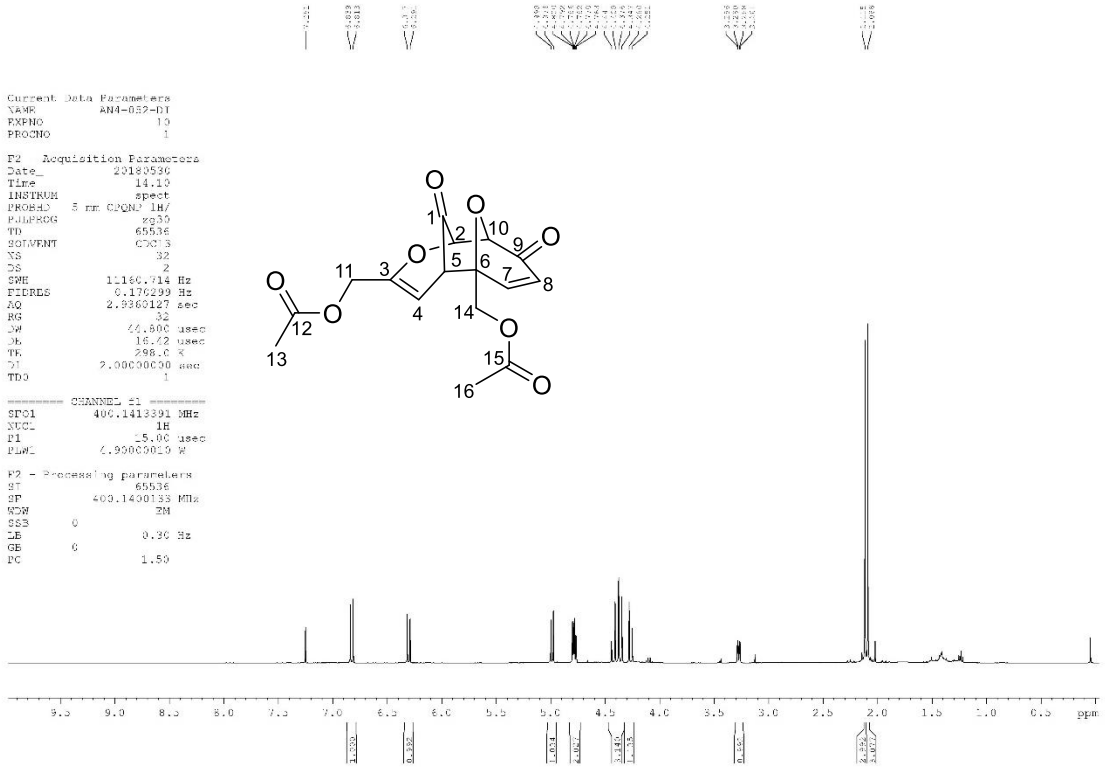

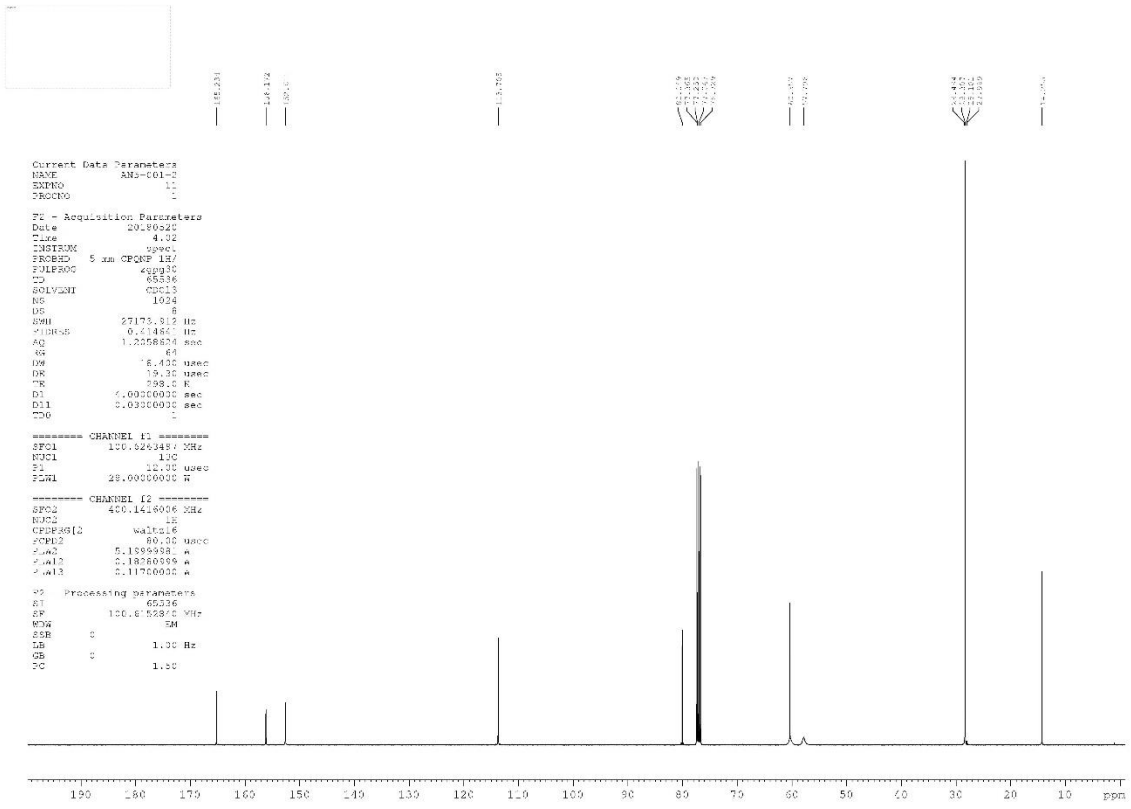

L-(+)-Prolinol, 254

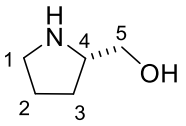

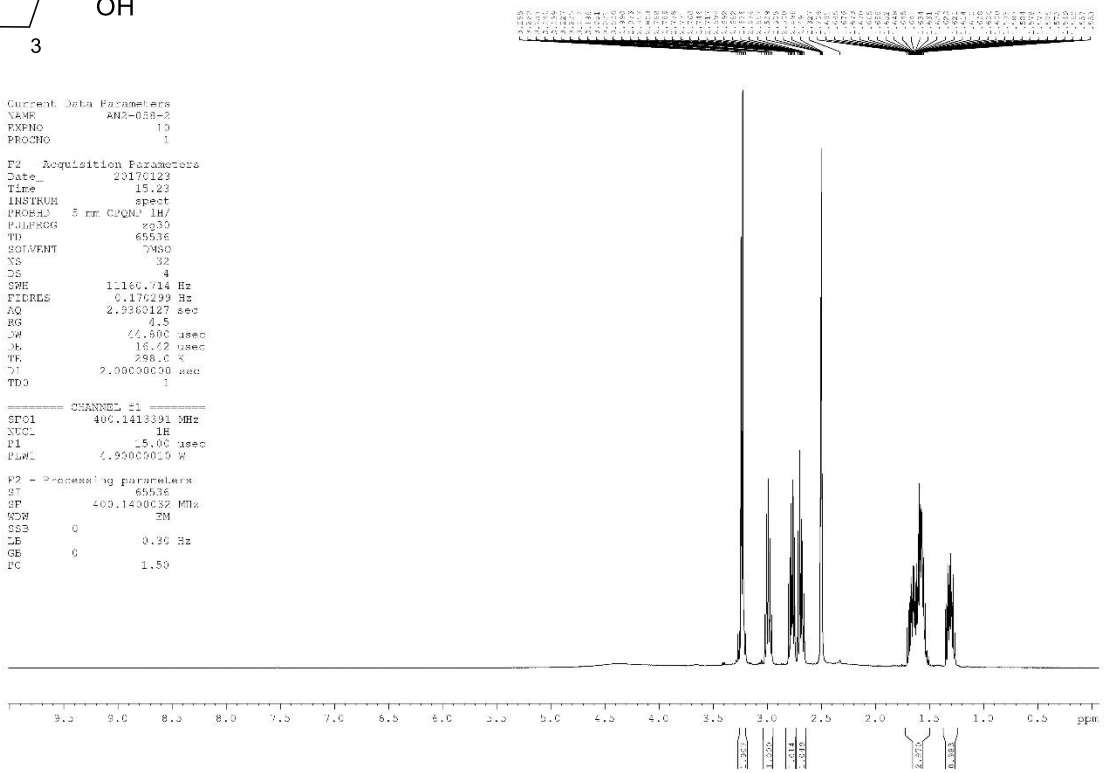

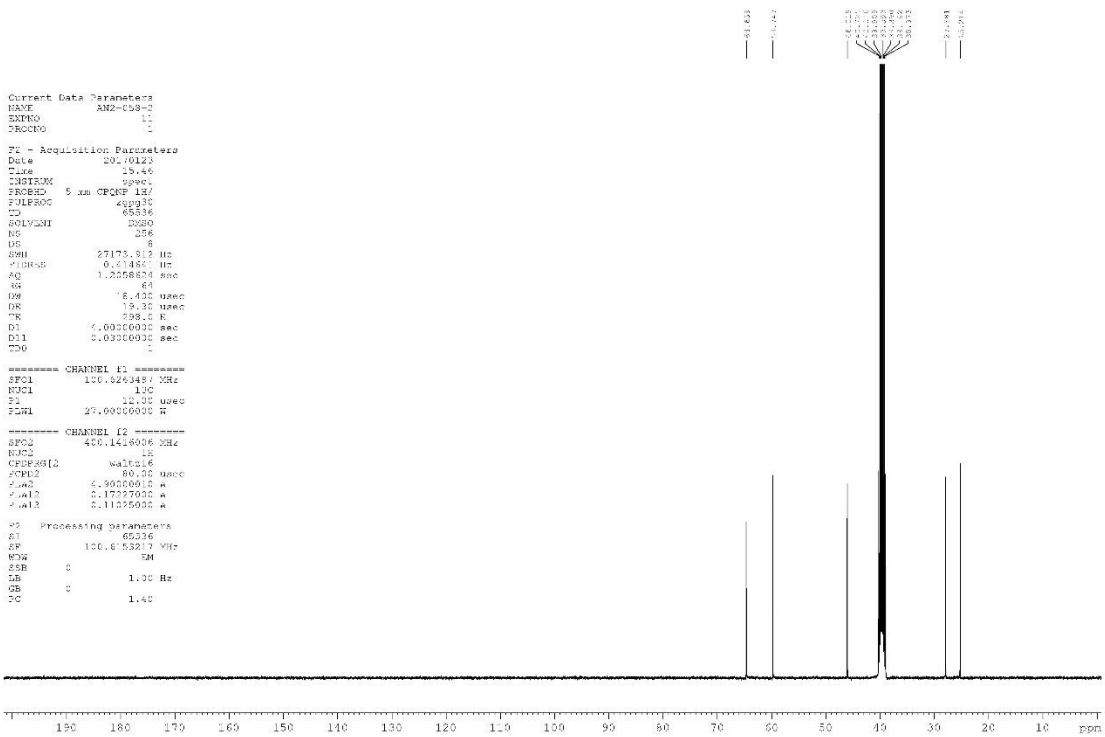

1,3-Diiodoacetone, 256

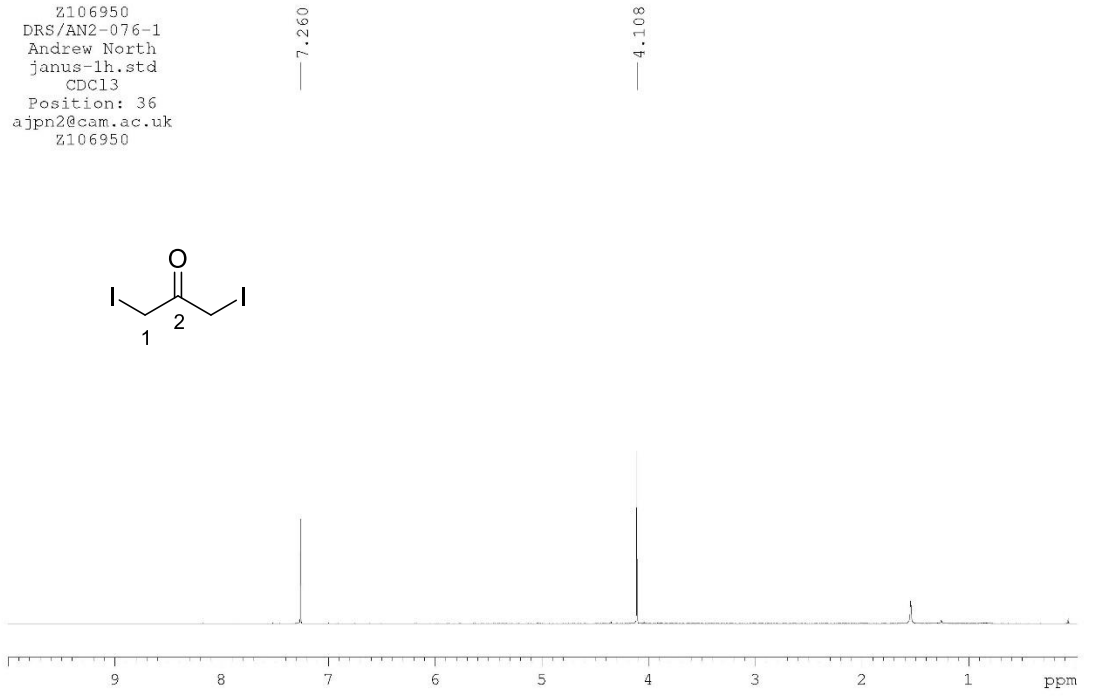

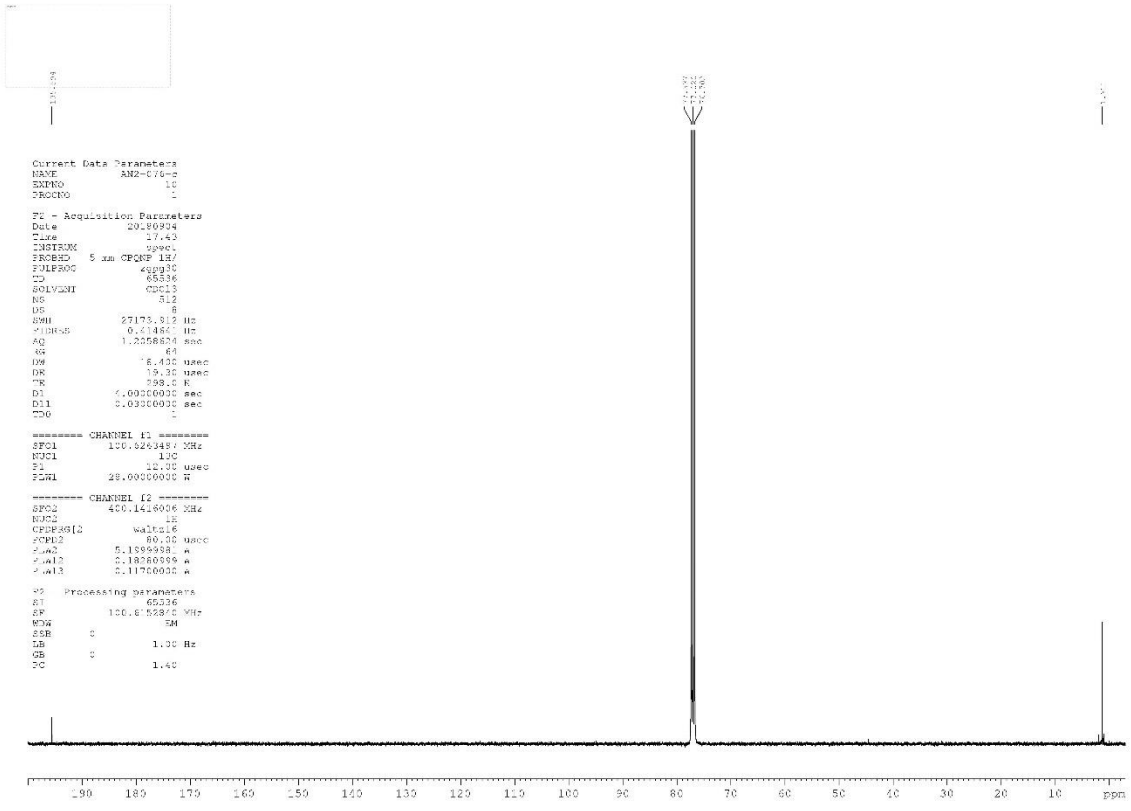

tert-Butyl((1,3-dichloropropan-2-yl)oxy)dimethylsilane, 262

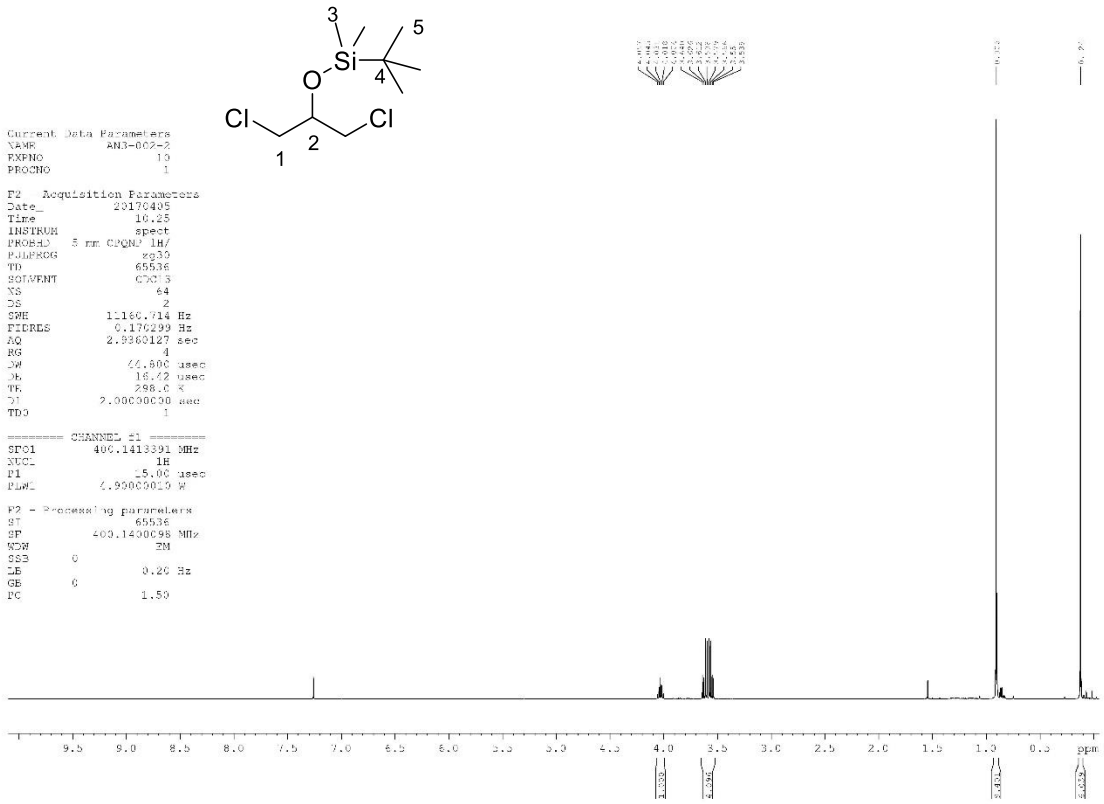

(S)-(+)-4-Methylenehexahydro-1H,3H-pyrrolo[2,1-c][1,4]oxazepane, 266

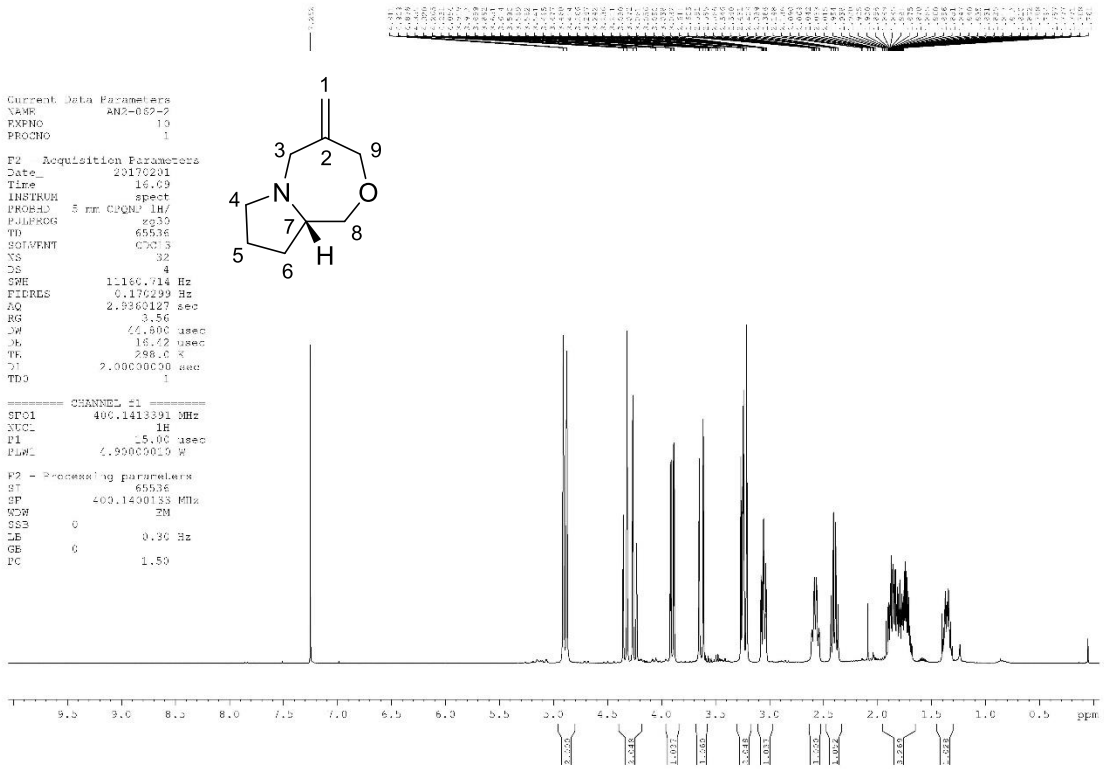

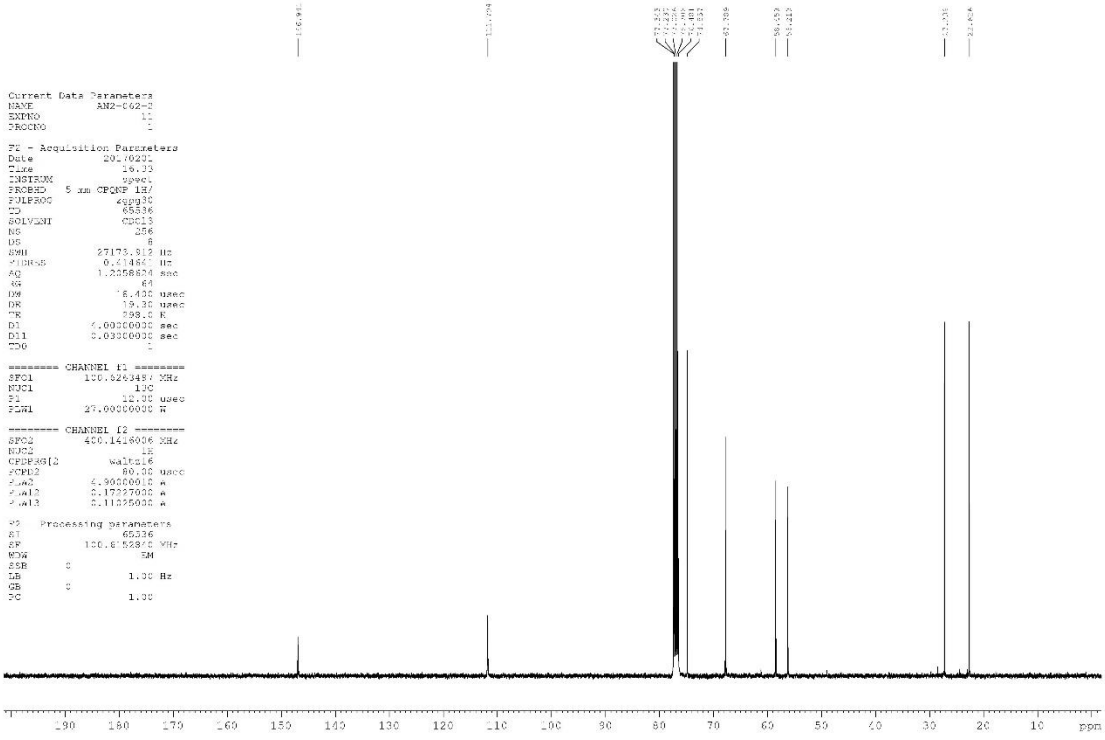

Appendix B

Crystallographic Data

4-(4-Methoxyphenyl)-1-azaspiro[4.5]deca-3,7-dien-2-one, 176

Identification code	DS_B1_0023	
Empirical formula	$C_{16}H_{17}NO_2$	
Formula weight	255.3170 $gmol^{-1}$	
Temperature	180 (2) K	
Crystal system	Triclinic	
Space group	$P\bar{1}$	
Unit cell dimensions	a = 5. 9870(3) Å	α = 71.715(3)°
	b = 9.9585(5) Å	β = 83.642(3)°
	c = 11.5405(6) Å	γ = 89.345(3)°
Volume	649.104 $Å^3$	

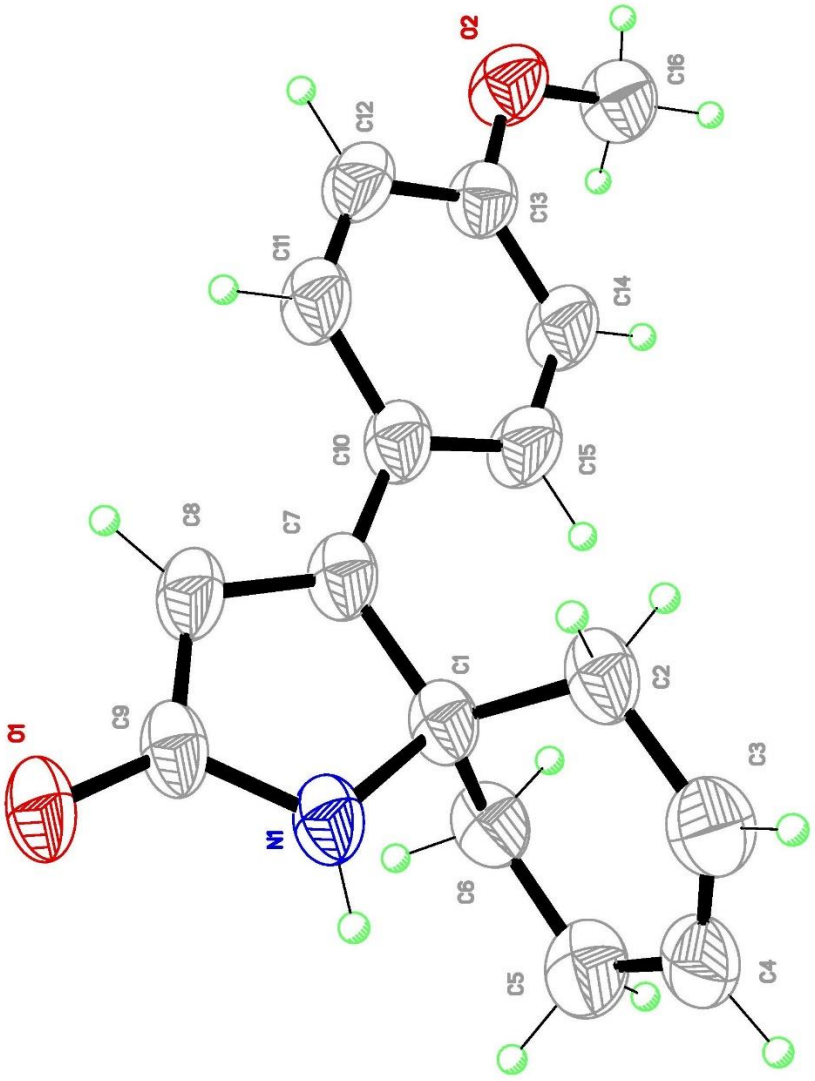
O2
C16
C12
C13
C11
C14
C10
C15
C8
C7
C1
C2
O1
C9
C3
N
C6
C5
C4

1-Azaspiro[4.5]deca-3,7-dien-2-one, 179

Identification code	DS_B1_0024	
Empirical formula	$C_9H_{11}NO$	
Formula weight	149.19 $gmol^{-1}$	
Temperature	180(2) K	
Crystal system	Orthorhombic	
Space group	$Pna2_2$	
Unit cell dimensions	a = 10.2930(5) Å	α = 90°
	b = 9.8937(5) Å	β = 90°
	c = 7.6125(4) Å	γ = 90°
Volume	775.25 $Å^3$	

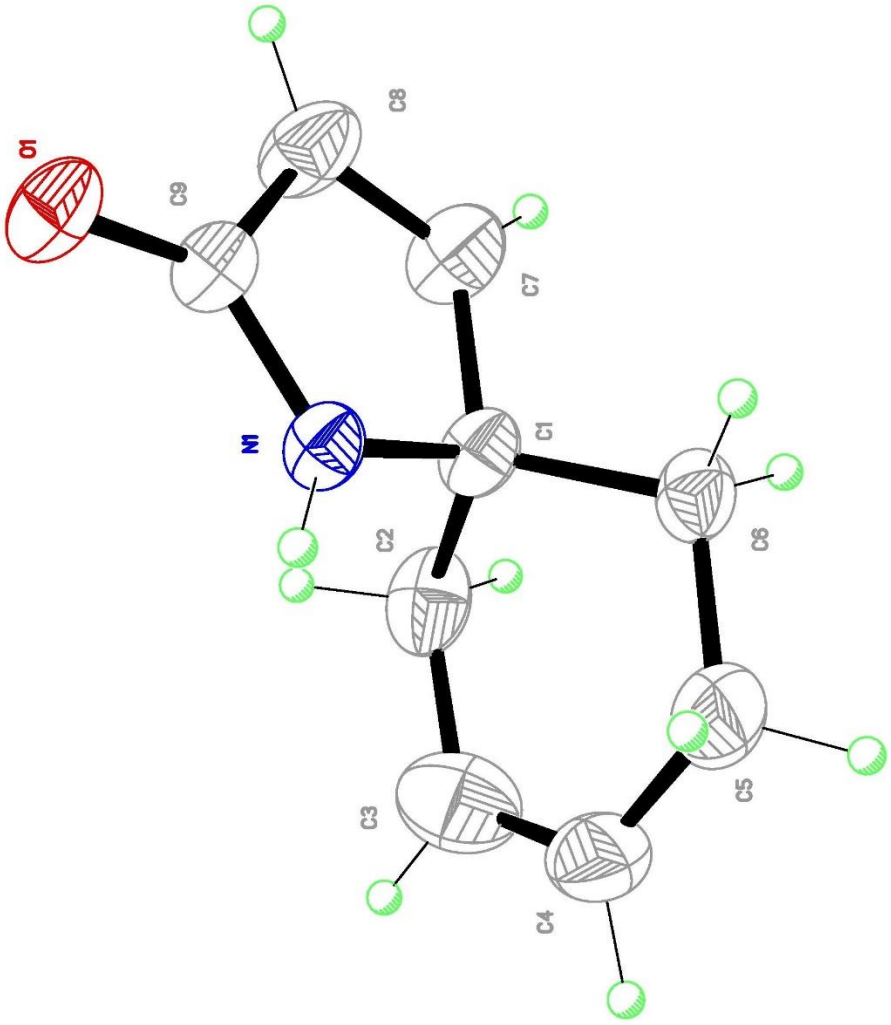
O
C9
C8
C7
N
C1
C2
C6
C3
C5
C4

3-Phenyl-1,8-dioxa-2,6-diazaspiro[4.4]non-2-en-7-one, 212

Identification code	DS_B1_0017	
Empirical formula	$C_{11}H_{10}N_2O_3$	
Formula weight	218.2120 $gmol^{-1}$	
Temperature	180(2) K	
Wavelength	1.54178 Å	
Crystal system	Triclinic	
Space group	$P\bar{1}(2)$	
Unit cell dimensions	a = 5.3405(3) Å	α = 78.073(4)°
	b = 8.0452(5) Å	β = 77.997(4)°
	c = 12.0561(7) Å	γ = 81.581(4)°
Volume	492.828 $Å^3$	
Z	2	
Density (calculated)	1.470 gcm^{-3}	
Absorption coefficient	0.914 mm^{-1}	
F(000)	228	
Crystal size	0.180 × 0.040 × 0.020 mm^3	
Theta range for data colletion	3.81–66.58°	
Index ranges	$-6 \le h \le 3$, $-9 \le k \le 9$, $-14 \le l \le 13$	
Reflections collected	4038	
Independent reflections	1723	
Completeness to theta = 66.58°	98.7%	
Absorption correction	Multi-scan	
Max. and min. transmission	0.7528 and 0.6366	
Refinement method	Full-matrix least-squares on F^2	
Data/restraints/parameters	1723/0/149	
Goodness-of-fit F^2	1.036	
Final R indices [I > 2σ(I)]	R1 = 0.0482, wR2 = 0.1032	
R indices (all data)	R1 = 0.0790, wR2 = 0.1153	
Largest diff. peak and hole	0.224 and –0.250 $eÅ^{-3}$	

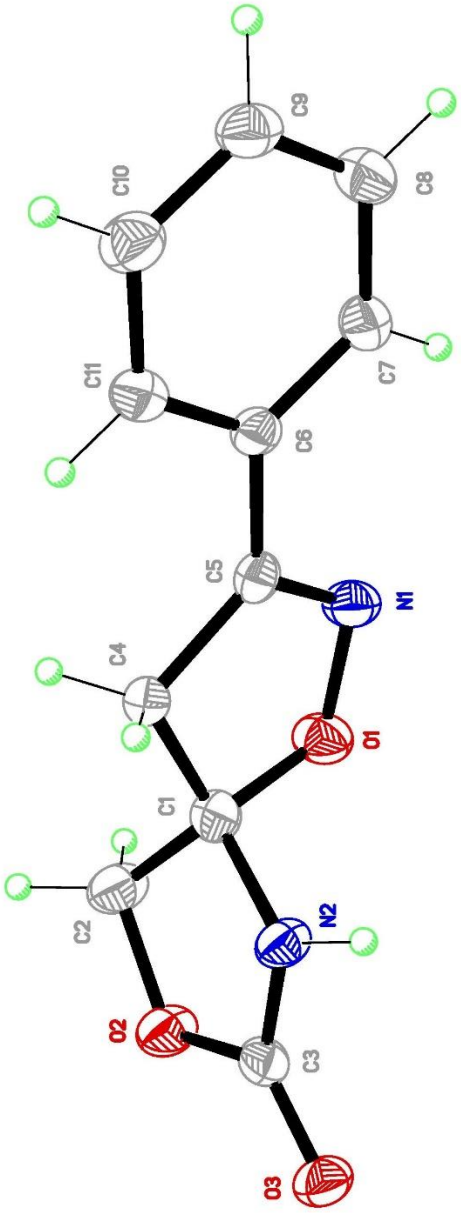
C9
C10
C8
C11
C7
C6
C5
N1
C4
O1
C1
C2
N2
O2
C3
O3

3-Oxa-1-azaspiro[4.5]deca-1,7-dien-2-amine, 152

Identification code	DS_B1_0020	
Empirical formula	$C_8H_{12}N_2O$	
Formula weight	152.1970 $gmol^{-1}$	
Temperature	180(2) K	
Wavelength	1.54056 Å	
Crystal system	Monoclinic	
Space group	$P2_1/c$	
Unit cell dimensions	a = 10.3028(8) Å	α = 90°
	b = 7.6579(5) Å	β = 91.728(5)°
	c = 10.3040(8) Å	γ = 90°
Volume	812.593 $Å^3$	
Z	4	
Density (calculated)	1.244 gcm^{-3}	
Absorption coefficient	0.678 mm^{-1}	
F(000)	328	
Crystal size	0.250 × 0.060 × 0.020 mm^3	
Theta range for data colletion	4.29–66.73°	
Index ranges	$-12 \leq h \leq 12$, $-9 \leq k \leq 9$, $-12 \leq l \leq 12$	
Reflections collected	9075	
Independent reflections	1443	
Completeness to theta = 66.73°	99.9%	
Absorption correction	Multi-scan	
Max. and min. transmission	0.987 and 0.849	
Refinement method	Full-matrix least-squares on F^2	
Data/restraints/parameters	1443/0/108	
Goodness-of-fit F^2	1.094	
Final R indices [I > 2σ(I)]	R1 = 0.0465, wR2 = 0.1122	
R indices (all data)	R1 = 0.0583, wR2 = 0.1185	
Largest diff. peak and hole	0.189 and –0.184 $eÅ^{-3}$	

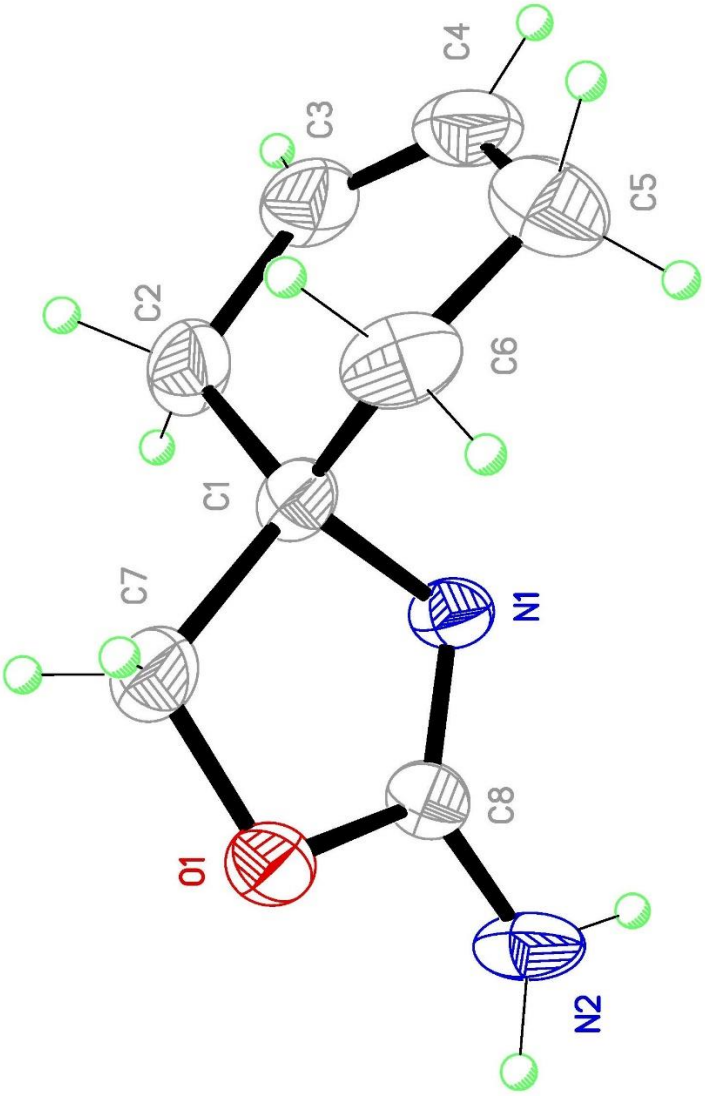
C4
C3
C5
C2
C6
C1
C7
N1
C8
O1
N2

Appendix C

Computational analysis

C.1. Reference Set

The following are the small molecule drugs from the top 50 best-selling drugs of 2013:

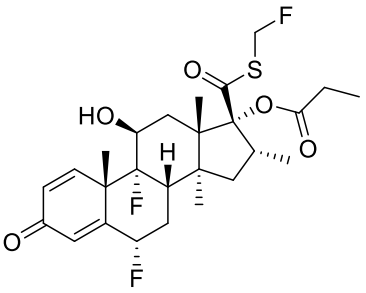

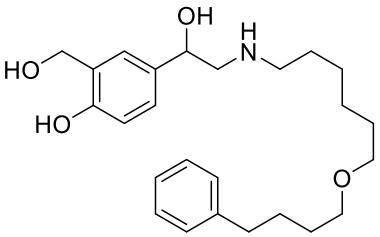

Seretide (Fluticasone + Salmeterol)

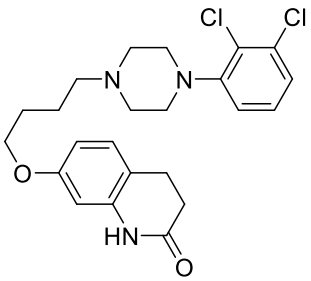

Abilify

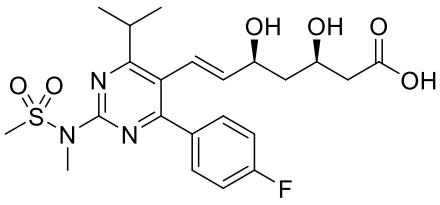

Crestor

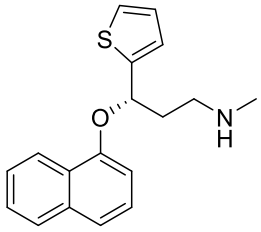

Cymbalta

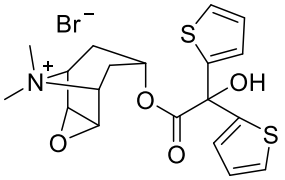

Spiriva

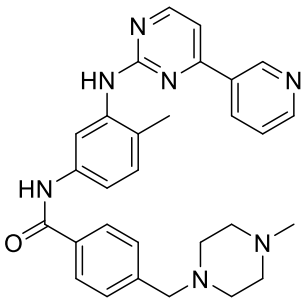

Gleevec

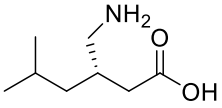

Lyrica

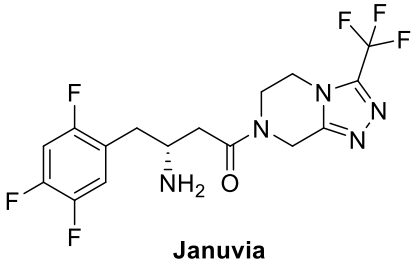

Januvia

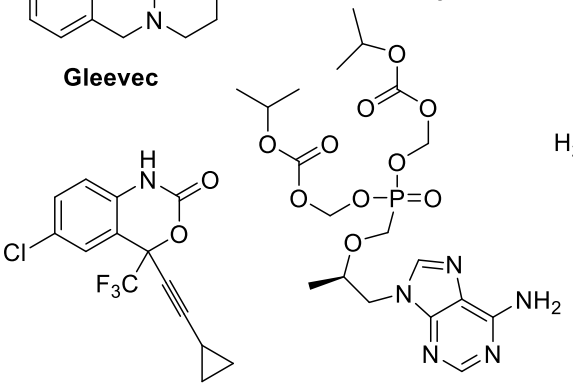

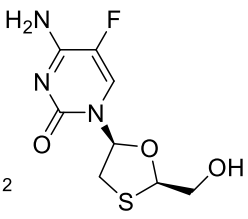

Atripla (Efavirenz + Tenofovir + Emtricitabine)

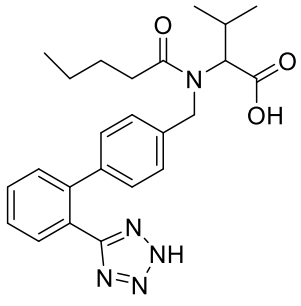

Diovan

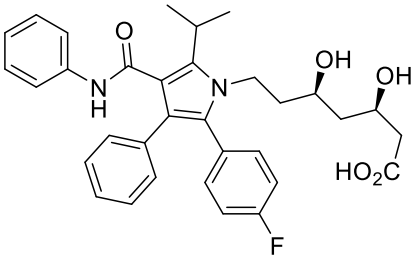

Lipitor

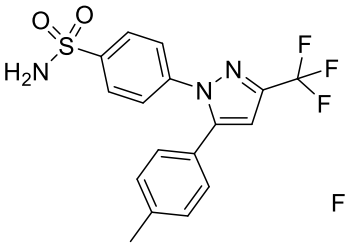

Celebrex

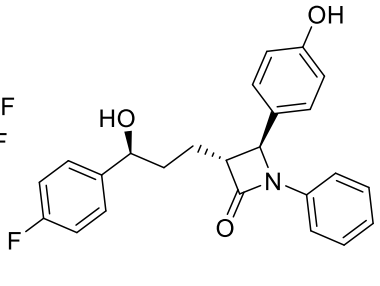

Zetia

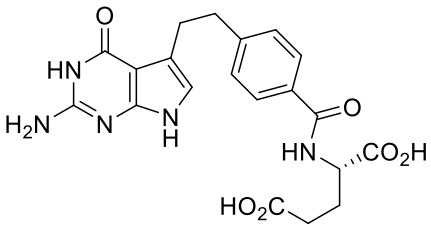

Alimta

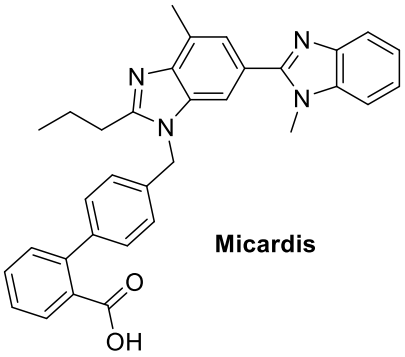

Micardis

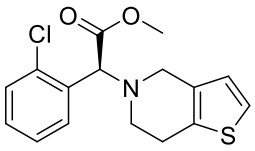

Palvix

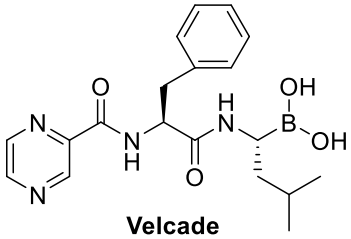

Velcade

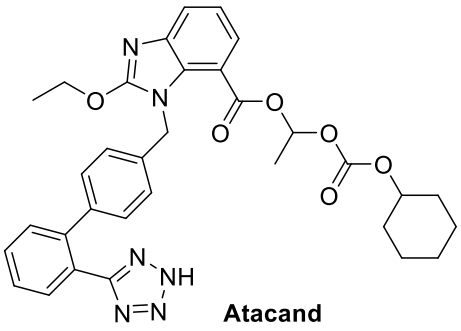

Atacand

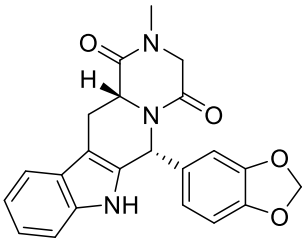

Cialis

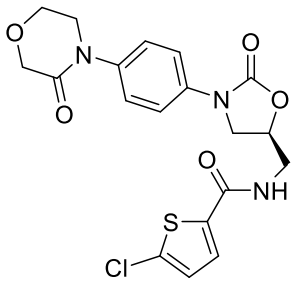

Xarelto

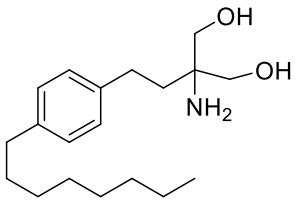

Gilenya

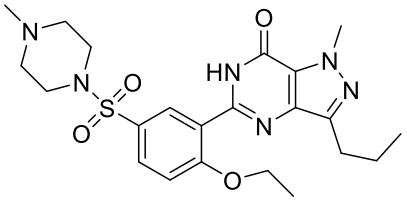

Viagra

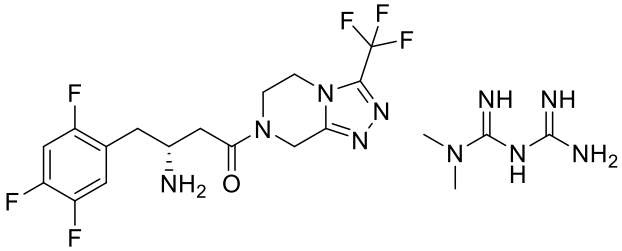

Janumet (Sitagliptin + Metformin)

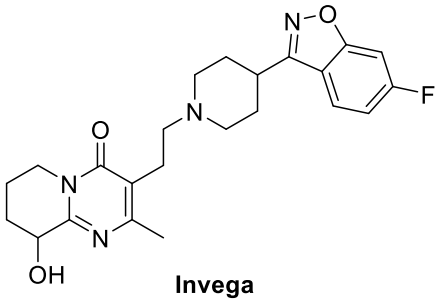

Invega

C.2. Principle Moment of Inertia

Using MOE 2018.0602 the following parameters were used in conformer searching:

Table C.1 Conformational search settings.

Force field	MMFF94x
Solvation	Born
Method	LowModeMD
Rejection Limit	100
RMS Gradient	0.005
Iteration Limit	10000
MM Iteration Limit	500
RMSD Limit	0.15
Energy Window	3
Conformation Limit	200

C.3. Principle Component Analysis

Using MOE 2018.0602 the following structural and physico-chemical parameters were used in PCA:

Table C.2 Structural and physcio-chemical parameters used in PCA.

Parameter	Description	2D or 3D
ASA_H	Total hydrophobic surface area	3D
ASA_P	Total polar surface area	3D
a_acc	Number of hydrogen bond acceptor atoms	2D
a_aro	Number of aromatic rings	2D
a_don	Number of hydrogen bond donor atoms	2D
a_nN	Number of nitrogen atoms	2D
a_nO	Number of oxygen atoms	2D
b_rotN	Number of rotatable bonds	2D
chiral	Number of chiral centres	2D
KierFlex	Molecular flexibility	2D
logS	Log solubility in water	2D
mr	Molar refractivity	2D
rings	Number of rings	2D
SlogP	Log octanol/water partition coefficient	2D
TPSA	Topological polar surface area ($Å^2$)	2D
vol	Van der Waals volume	3D
weight	Molecular weight	2D

The following settings were used in the principle component analysis:

Table C.3 Principle component settings.

Weight field	None
Prefix	PCA
Component limit	0
Minimum variance (%)	95
Condition limit	1e+006

C.4. LLAMA Parameters

The following reactions were used in the LLAMA program to elaborate the spirocyclic scaffolds

Table C.4 Reactions used in LLAMA elaboration.

Reductive amination
Buchwald-Hartwig amination
Sulfonamide formation
Urea formation
Alcohol alkylation
Carbamate formation
Secondary amide alkylation
Esterification
Secondary amide arylation
Amide formation
Alcohol arylation

Appendix D

Publication

Novel non-ATP competitive small molecules targeting the CK2 α/β interface

Paul Brear, Andrew North, Jessica Iegre, Kathy Hadje Georgiou, Alexandra Lubin, Laura Carro, William Green, Hannah F. Sore, Marko Hyvönen, David R. Spring

https://doi.org/10.1016/j.bmc.2018.05.011

This paper contains the research the Spring Group has done into elaborating NMR154 and NMR154L to find novel non-ATP competitive fragments which inhibit the interface site CK2.

I was given responsibility to write a publication bringing together all the group's work in this field. This first involved analysing the 144 molecules which had been synthesised to bind at the interface. These were then sorted into groups based on the vectors of NMR154 which had been elaborated, or if they were not NMR154 based. With the data in hand I wrote the entire manuscript, compiled the supplementary information, and synthesised a couple of compounds to record missing data.